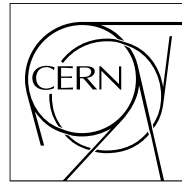


The Compact Muon Solenoid Experiment
Analysis Note

The content of this note is intended for CMS internal use and distribution only



23 February 2018 (v18, 13 June 2019)

Measurement of multi-differential cross sections for top quark pair production in the dilepton channel at $\sqrt{s} = 13$ TeV

Olaf Behnke, Mykola Savitskyi, Oleksandr Zenaiev

Abstract

Normalized multi-differential cross sections for top quark pair ($t\bar{t}$) production are measured in pp collisions at a center-of-mass energy of 13 TeV using the decay channels into two opposite-sign leptons. The analysed dataset was recorded in 2016 and corresponds to an integrated luminosity of 35.9 fb^{-1} . The $t\bar{t}$ cross section is measured as a function of the kinematic properties of the top quark, $t\bar{t}$ system and jet multiplicity. The measurements are presented at parton level in the full phase. The data are compared with Monte Carlo predictions and perturbative QCD calculations at next-to-leading-order. The impact of the measured cross sections on the gluon distribution in the proton and QCD parameters is demonstrated.

1 Contents

2	1	Introduction	3
3	2	Data and simulated samples	5
4	3	Event selection	10
5	3.1	Muon selection	10
6	3.2	Electron selection	11
7	3.3	Lepton pair selection	11
8	3.4	Jet selection	12
9	3.5	b jet selection	12
10	3.6	Missing transverse energy	13
11	3.7	Event yields and control distributions	13
12	4	Reconstruction of the top quark kinematics	22
13	4.1	Full kinematic reconstruction	22
14	4.2	Loose kinematic reconstruction	23
15	4.3	Comparison of full and loose kinematic reconstruction	28
16	4.4	Comparison of sensitivity of measured cross section to m_t	29
17	4.5	Selection of extra jets	33
18	5	Scaling factors and systematic uncertainties	38
19	5.1	Experimental uncertainties	38
20	5.2	Model uncertainties	44
21	6	Cross section definition and determination	46
22	6.1	Measured cross sections	46
23	6.2	Signal extraction	46
24	6.3	Unfolding	51
25	6.4	Closure tests	52
26	6.5	Cross section determination	64
27	7	Results of the measurement	79
28	7.1	Impact of statistical and systematic uncertainties	79
29	7.2	Comparison to MC models	84
30	8	Extraction of α_s and m_t^{pole} from measured $[N_{\text{jet}}, M(\text{t}\bar{t}), y(\text{t}\bar{t})]$ cross sections using external PDFs	92
31	8.1	Comparison of measured $[N_{\text{jet}}, M(\text{t}\bar{t}), y(\text{t}\bar{t})]$ cross sections to fixed-order calculations	92
32	8.2	Extraction of α_s and m_t^{pole} from $[N_{\text{jet}}, M(\text{t}\bar{t}), y(\text{t}\bar{t})]$ cross sections	97
33	8.3	Cross checks of α_s and m_t^{pole} extraction using different distributions	99
34	8.4	Comparison of NLO vs NLO+PS theoretical predictions	107
35	9	Simultaneous PDF, α_s and m_t^{pole} fit	110
36	9.1	Details of the PDF fit	110
37	9.2	Study of PDF parametrisation	111
38	9.3	α_s and m_t^{pole} extraction	112
39	9.4	Impact of the $\text{t}\bar{t}$ cross section measurements on PDFs	120
40	9.5	Cross check using MC method	121

43	10	Summary	129
44	A	Values of the measured cross sections	130
45	B	Closure tests: additional materials	131
46	B.1	Data tests	131
47	B.2	Toy tests	180
48	B.3	Reweighting tests	188
49	C	Study of m_t sensitivity of full kinematic reconstruction	194
50	D	Study of cross sections sensitivity to $p_T(t)$ reweighting	196
51	E	Study of scale choice for NLO calculations	197
52	F	NNLO corrections to the $M(t\bar{t})$ distribution	200
53	G	Study of scale variation in bins with different N_{jet}	202
54	H	Comparison of measured [$N_{jet}, M(t\bar{t}), y(t\bar{t})$] cross sections to fixed-order calculations: additional plots	204
55	I	Comparison of absolute cross sections to NLO predictions and extraction of α_s and m_t^{pole}	206
56	I.1	Comparison of unnormalised [$N_{jet}, M(t\bar{t}), y(t\bar{t})$] cross sections to fixed-order calculations	206
57	I.2	Extraction of α_s and m_t^{pole} from unnormalised [$N_{jet}, M(t\bar{t}), y(t\bar{t})$] cross sections	208
58	J	Full kinematic reconstruction: performance studies related to minimum $M(t\bar{t})$ choice	215
59	K	Values of the measured cross sections	217
60	L	Change Logs	258
61			
62			
63			
64			
65			

DRAFT

66 1 Introduction

67 Measurements of the top quark pair ($t\bar{t}$) production at the CERN LHC are fundamental for
 68 testing the standard model (SM) and searching for new phenomena. In particular, precise
 69 differential measurements of the $t\bar{t}$ production cross section as a function of $t\bar{t}$ kinematic ob-
 70 servables have become possible, which allow for the validation of the most-recent predictions
 71 of perturbative quantum chromodynamics (QCD). At the LHC, top quarks are predominantly
 72 produced via gluon-gluon fusion. Thus, using measurements of the production cross section
 73 in a global fit of the parton distribution functions (PDFs) can help to better determine the gluon
 74 distribution at large values of x , where x is the fraction of the proton momentum carried by
 75 a parton [1–3]. Furthermore, measurements of the cross section as function of the $t\bar{t}$ invariant
 76 mass, scanning over the mass threshold to much larger values, provide high sensitivity for con-
 77 straining the top quark pole mass. At the LHC energies, the fraction of $t\bar{t}$ events produced with
 78 additional hard jets in the final state is large. These reactions constitute important backgrounds
 79 for interesting but rare processes such as associated production of a Higgs boson with $t\bar{t}$ as well
 80 as for many new physics searches with $t\bar{t}$ and thus need to be understood. Within the SM con-
 81 text the processes with extra jets can be used to constrain the strong coupling strength at the
 82 scale of the top mass. Furthermore, the production of $t\bar{t}$ in association with extra jets provides
 83 an additional sensitivity to m_t^{pole} since gluon radiation depends on m_t^{pole} through threshold and
 84 cone effects [4].

85 Normalized differential cross sections for $t\bar{t}$ production have been measured previously in
 86 proton-antiproton collisions at the Tevatron at a centre-of-mass energy of 1.96 TeV [5, 6] and
 87 in pp collisions at the LHC at $\sqrt{s} = 7$ TeV [7–10], 8 TeV [10–12], and 13 TeV [13, 14]. A recent
 88 milestone was achieved in the analysis [15], where the $t\bar{t}$ production dynamics was probed in
 89 great detail with normalised double-differential cross sections. The analysis used data recorded
 90 at $\sqrt{s} = 8$ TeV by the CMS experiment in 2012, corresponding to an integrated luminosity of
 91 $19.7 \pm 0.5 \text{ fb}^{-1}$. The $e^\pm \mu^\mp$ decay mode ($e\mu$) of $t\bar{t}$ was selected, requiring two oppositely charged
 92 leptons and at least two jets. In this paper a new measurement is presented, following the pro-
 93 cedures from [15]. It is based on data taken by the CMS experiment in 2016 at $\sqrt{s} = 13$ TeV,
 94 corresponding to an integrated luminosity of $35.7 \pm 0.5 \text{ fb}^{-1}$. In addition to $e\mu$, the two other
 95 dilepton decay modes e^+e^- (ee) and $\mu^+\mu^-$ ($\mu\mu$) are also selected, roughly doubling the total
 96 number of expected $t\bar{t}$ signal events.

97 As in the previous paper [15], measurements of the normalized double-differential $t\bar{t}$ produc-
 98 tion cross section are performed. These measurements probe the details of the $t\bar{t}$ production
 99 dynamics, irrespective of other objects in the events. The cross section is measured as a func-
 100 tion of observables describing the kinematics of the top quark and $t\bar{t}$: the transverse momentum
 101 of the top quark, $p_T(t)$, the rapidity of the top quark, $y(t)$, the transverse momentum, $p_T(t\bar{t})$,
 102 the rapidity, $y(t\bar{t})$, and the invariant mass, $M(t\bar{t})$, of $t\bar{t}$, the pseudorapidity between the top
 103 quark and antiquark, $\Delta\eta(t, \bar{t})$, and the angle between the top quark and antiquark in the trans-
 104 verse plane, $\Delta\phi(t, \bar{t})$. In total, the double-differential $t\bar{t}$ cross section is measured as a function
 105 of six different pairs of kinematic variables. As demonstrated in [15], the different kinematic
 106 variable combinations are sensitive to specific aspects or ingredients of the theory calculations,
 107 representing the SM, that are compared to the data and detailed below.

108 In addition, for the first time, the triple-differential cross section is measured as a function of
 109 $M(t\bar{t})$, $y(t\bar{t})$ and N_{jet} , where N_{jet} is the number of extra jets. For this purpose a special kine-
 110 matic reconstruction is used, optimised to determine the invariant mass of the $t\bar{t}$ system in an
 111 unbiased way. As will be shown the triple-differential results provide a tight constraint on the
 112 parametrised gluon distribution in the PDF, the strong coupling strength and the top quark

113 pole mass.

114 The measurements are defined at parton level and thus are corrected for the effects of had-
115 ronization and detector resolutions and inefficiencies. A regularized unfolding process is per-
116 formed simultaneously in bins of the two or three variables in which the cross sections are
117 measured. The normalized differential $t\bar{t}$ cross section is determined by dividing by the mea-
118 sured total inclusive $t\bar{t}$ production cross section, where the latter is evaluated by integrating
119 over all bins in the respective observables.

120 The parton level results are compared to theoretical predictions obtained at NLO with several
121 PDF sets, as well as with the generators POWHEG (v. 2) [16, 17] and MG5_aMC@NLO(FxFx) [18],
122 interfaced to PYTHIA8 [19, 20] for parton evolution and hadronization, and multiple-parton
123 interactions.

124 The structure of the paper is as follows: details of the event simulation are given in Section 2.
125 The event selection, kinematic reconstruction, and comparisons between data and simulation
126 are described in Sections 3 and 4. The assessment of the systematic uncertainties is elucidated in
127 Section 5. The method to determine the differential cross sections is presented in Section 6. The
128 results of the measurement are discussed and compared to theoretical predictions in Section 7.
129 Section 8 presents the extraction of the strong coupling strength α_s and top quark pole mass
130 m_t^{pole} from the measured $t\bar{t}$ cross sections using external PDF sets, and Section 9 presents the
131 simultaneous fit of PDFs, α_s and m_t^{pole} . Finally, Section 10 provides a summary.

DRAFT

132 2 Data and simulated samples

133 The data sets, collected during the full LHC 2016 run at 13 TeV, used in this analysis are listed
 134 in Table 1. From these data sets, certified runs are selected by application of the certified good-
 135 run lists as given in [21]. As can be seen from Table 1, in this analysis the dilepton data streams
 136 (MuonEG, DoubleEG, and DoubleMuon) are used alongside single lepton ones (SingleMuon
 137 and SingleElectron). This is done in order to recover the dilepton events in the region of interest,
 138 which failed to pass the dilepton trigger requirements and thus are not available in the dilepton
 139 data streams. Usage of the single lepton data streams in this analysis recovers approximately
 140 10% of the dilepton events.

141 The total integrated luminosity of the complete data sample is $35.9 \text{ fb}^{-1} \pm 2.5\%$ [22].

142 The analysis has been carried out using the CMS event data model and the official software
 143 framework for event generation, simulation, and reconstruction (*03Feb2017 ReReco* data and
 144 *Summer16* Monte Carlo in CMSSW_8_0_X). Centrally provided MiniAODs (v2) generated with
 145 CMSSW_8_0_X are analyzed using release CMSSW_8_0_26_patch2.

146 Monte Carlo (MC) simulated data samples from the *Summer16* processing, comprising the
 147 $t\bar{t}$ signal and the relevant background processes, are used in the analysis. The signal pro-
 148 cesses in this analysis is the inclusive production of top quark pairs followed by top quark
 149 decays $t \rightarrow W^+ b$ and $\bar{t} \rightarrow W^- \bar{b}$, and subsequent leptonic W boson direct decays into muons
 150 or electrons. For the simulation of the reference $t\bar{t}$ signal sample, the next-to-leading-order
 151 (NLO) POWHEG (v. 2) [16, 23] event generator is used. The value of the top quark mass is
 152 fixed to $m_t = 172.5 \text{ GeV}$ and the proton structure is described by the parton density functions
 153 (PDF) NNPDF3.0 NLO set [24]. The renormalisation μ_r and factorisation μ_f scales are set to

154 $\mu_r = \mu_f = \sqrt{m_t^2 + p_{T,t\bar{t}}^2(t)}$, where $p_{T,t\bar{t}}(t)$ is the transverse momentum of the top (anti)quark
 155 in the $t\bar{t}$ rest frame. The generated events are subsequently processed with PYTHIA (v. 8.2) [20]
 156 (referred to as PYTHIA8 in the following) for parton showering and hadronization. The CMS
 157 detector response is simulated using GEANT4 (v. 9.4) [25].

158 In addition to the POWHEG+PYTHIA8 simulation, alternative samples of $t\bar{t}$ events obtained
 159 with the NLO MG5_aMC@NLO(FxFx) (v. 2.2.2) [18] generator including MADSPIN [26] are
 160 compared to the final results presented in Section 7. These samples are interfaced with PYTHIA8
 161 for parton showering and hadronization. The matching of matrix-element jets to parton show-
 162 ers is performed using the FxFx [27] prescription. The proton structure is described by the
 163 NNPDF3.0 NLO set. [TODO: specify scale choice] A sample of $t\bar{t}$ events generated with
 164 POWHEG (v. 2) and interfaced with HERWIG++ (v. 2.7.1) [28] is also used for data and the-
 165 ory comparison. In these alternative samples, the value of the top quark mass is set to $m_t =$
 166 172.5 GeV , as in the reference simulation.

167 Besides the $t\bar{t}$ signal process, dominant background contributions are also taken from MC sim-
 168 ulations. The background contributions stem from Z+jets, single top quark tW, W+jets and di-
 169 bosons (WW, WZ, and ZZ). The W+jets and Z+jets samples are simulated with MG5_aMC@NLO
 170 (MLM). POWHEG (v. 1) [17, 29] is used for single top quark production, while PYTHIA8 is used
 171 for diboson (WW, WZ, and ZZ) production. Parton showering and hadronization are also sim-
 172 ulated with PYTHIA8 in all the background samples. The PYTHIA8 CUETP8M2T4 tune [30, 31]
 173 is used in both the $t\bar{t}$ and single top samples, while the PYTHIA8 CUETP8M1 tune is applied
 174 for all other background samples.

175 For comparison with the measured distributions, the events yields in the simulated data sam-
 176 ples are normalized to the corresponding integrated luminosity of 35.9 fb^{-1} according to their

Table 1: Collision data samples used in the analysis.

Sample	Run range
/MuonEG/Run2016B-03Feb2017_ver2-v2	272007-275376
/MuonEG/Run2016C-03Feb2017-v1	275657-276283
/MuonEG/Run2016D-03Feb2017-v1	276315-276811
/MuonEG/Run2016E-03Feb2017-v1	276831-277420
/MuonEG/Run2016F-03Feb2017-v1	277772-278808
/MuonEG/Run2016G-03Feb2017-v1	278820-280385
/MuonEG/Run2016H-03Feb2017_ver2-v1	281613-284035
/MuonEG/Run2016H-03Feb2017_ver3-v1	284036-284044
/DoubleEG/Run2016B-03Feb2017_ver2-v2	272007-275376
/DoubleEG/Run2016C-03Feb2017-v1	275657-276283
/DoubleEG/Run2016D-03Feb2017-v1	276315-276811
/DoubleEG/Run2016E-03Feb2017-v1	276831-277420
/DoubleEG/Run2016F-03Feb2017-v1	277772-278808
/DoubleEG/Run2016G-03Feb2017-v1	278820-280385
/DoubleEG/Run2016H-03Feb2017_ver2-v1	281613-284035
/DoubleEG/Run2016H-03Feb2017_ver3-v1	284036-284044
/DoubleMuon/Run2016B-03Feb2017_ver2-v2	272007-275376
/DoubleMuon/Run2016C-03Feb2017-v1	275657-276283
/DoubleMuon/Run2016D-03Feb2017-v1	276315-276811
/DoubleMuon/Run2016E-03Feb2017-v1	276831-277420
/DoubleMuon/Run2016F-03Feb2017-v1	277772-278808
/DoubleMuon/Run2016G-03Feb2017-v1	278820-280385
/DoubleMuon/Run2016H-03Feb2017_ver2-v1	281613-284035
/DoubleMuon/Run2016H-03Feb2017_ver3-v1	284036-284044
/SingleMuon/Run2016B-03Feb2017_ver2-v2	272007-275376
/SingleMuon/Run2016C-03Feb2017-v1	275657-276283
/SingleMuon/Run2016D-03Feb2017-v1	276315-276811
/SingleMuon/Run2016E-03Feb2017-v1	276831-277420
/SingleMuon/Run2016F-03Feb2017-v1	277772-278808
/SingleMuon/Run2016G-03Feb2017-v1	278820-280385
/SingleMuon/Run2016H-03Feb2017_ver2-v1	281613-284035
/SingleMuon/Run2016H-03Feb2017_ver3-v1	284036-284044
/SingleElectron/Run2016B-03Feb2017_ver2-v2	272007-275376
/SingleElectron/Run2016C-03Feb2017-v1	275657-276283
/SingleElectron/Run2016D-03Feb2017-v1	276315-276811
/SingleElectron/Run2016E-03Feb2017-v1	276831-277420
/SingleElectron/Run2016F-03Feb2017-v1	277772-278808
/SingleElectron/Run2016G-03Feb2017-v1	278820-280385
/SingleElectron/Run2016H-03Feb2017_ver2-v1	281613-284035
/SingleElectron/Run2016H-03Feb2017_ver3-v1	284036-284044

Table 2: Summary of simulated nominal data samples used in this analysis, together with the cross section assigned to the process.

sample	σ [pb]
/TT_TuneCUETP8M2T4_13TeV-powheg-pythia8/ RunIIISummer16MiniaODv2-PUMoriond17_80X_mcRun2_asymptotic_2016_TrancheIV_v6-v1	831.76
/TT_TuneCUETP8M2T4_13TeV-powheg-pythia8/ RunIIISummer16MiniaODv2-PUMoriond17_backup_80X_mcRun2_asymptotic_2016_TrancheIV_v6-v1	831.76
/ST_tW_top_5f_inclusiveDecays_13TeV-powheg-pythia8_TuneCUETP8M2T4/ RunIIISummer16MiniaODv2-PUMoriond17_80X_mcRun2_asymptotic_2016_TrancheIV_v6-v1	35.85
/ST_tW_antitop_5f_inclusiveDecays_13TeV-powheg-pythia8_TuneCUETP8M2T4/ RunIIISummer16MiniaODv2-PUMoriond17_80X_mcRun2_asymptotic_2016_TrancheIV_v6-v1	35.85
/DYJetsToLL_M-50_TuneCUETP8M1_13TeV-madgraphMLM-pythia8/ RunIIISummer16MiniaODv2-PUMoriond17_80X_mcRun2_asymptotic_2016_TrancheIV_v6_ext1-v2	6025.2
/DYJetsToLL_M-50_TuneCUETP8M1_13TeV-madgraphMLM-pythia8/ RunIIISummer16MiniaODv2-PUMoriond17_80X_mcRun2_asymptotic_2016_TrancheIV_v6_ext2-v1	6025.2
/DYJetsToLL_M-10to50_TuneCUETP8M1_13TeV-madgraphMLM-pythia8/ RunIIISummer16MiniaODv2-PUMoriond17_80X_mcRun2_asymptotic_2016_TrancheIV_v6-v1	22635.1
/WJetsToLNu_TuneCUETP8M1_13TeV-madgraphMLM-pythia8/ RunIIISummer16MiniaODv2-PUMoriond17_80X_mcRun2_asymptotic_2016_TrancheIV_v6-v1	61526.7
/WJetsToLNu_TuneCUETP8M1_13TeV-madgraphMLM-pythia8/ RunIIISummer16MiniaODv2-PUMoriond17_80X_mcRun2_asymptotic_2016_TrancheIV_v6_ext2-v1	61526.7
/WW_TuneCUETP8M1_13TeV-pythia8/ RunIIISummer16MiniaODv2-PUMoriond17_80X_mcRun2_asymptotic_2016_TrancheIV_v6-v1	118.7
/WW_TuneCUETP8M1_13TeV-pythia8/ RunIIISummer16MiniaODv2-PUMoriond17_80X_mcRun2_asymptotic_2016_TrancheIV_v6_ext1-v1	118.7
/WZ_TuneCUETP8M1_13TeV-pythia8/ RunIIISummer16MiniaODv2-PUMoriond17_80X_mcRun2_asymptotic_2016_TrancheIV_v6-v1	47.13
/WZ_TuneCUETP8M1_13TeV-pythia8/ RunIIISummer16MiniaODv2-PUMoriond17_80X_mcRun2_asymptotic_2016_TrancheIV_v6_ext1-v1	47.13
/ZZ_TuneCUETP8M1_13TeV-pythia8/ RunIIISummer16MiniaODv2-PUMoriond17_80X_mcRun2_asymptotic_2016_TrancheIV_v6-v1	16.523
/ZZ_TuneCUETP8M1_13TeV-pythia8/ RunIIISummer16MiniaODv2-PUMoriond17_80X_mcRun2_asymptotic_2016_TrancheIV_v6_ext1-v1	16.523

¹⁷⁷ theoretically predicted cross sections. These are taken from next-to-next-to-leading-order (NNLO)
¹⁷⁸ (W+jets and Z+jets), approximate NNLO (single top quark tW channels [32]), and NLO (dibo-
¹⁷⁹ son [33]) calculations. For the simulated $t\bar{t}$ sample, the NNLO+NNLL calculation [34–39] is
¹⁸⁰ used, performed with the TOP++ 2.0 program [40].

¹⁸¹ The complete list of simulated samples used in this analysis is shown in Tables 2, 3 and 4
¹⁸² alongside the predicted cross sections used for these samples.

Table 3: Summary (Part 1) of simulated $t\bar{t}$ samples used in this analysis for the estimation of systematic uncertainties and comparisons, together with the cross section assigned to the process. The samples with the standalone simulation of dileptonic matrix elements are additionally scaled with the corresponding branching ratio.

sample	σ [pb]
/TT_TuneCUETP8M2T4_13TeV-powheg-fsrdown-pythia8/ RunIISummer16MiniAODv2-PUMoriond17_80X_mcRun2_asymptotic_2016_TrancheIV_v6-v1	831.76
/TT_TuneCUETP8M2T4_13TeV-powheg-fsrdown-pythia8/ RunIISummer16MiniAODv2-PUMoriond17_80X_mcRun2_asymptotic_2016_TrancheIV_v6_ext1-v1	831.76
/TT_TuneCUETP8M2T4_13TeV-powheg-fsrdown-pythia8/ RunIISummer16MiniAODv2-PUMoriond17_80X_mcRun2_asymptotic_2016_TrancheIV_v6_ext2-v1	831.76
/TT_TuneCUETP8M2T4_13TeV-powheg-fsrup-pythia8/ RunIISummer16MiniAODv2-PUMoriond17_80X_mcRun2_asymptotic_2016_TrancheIV_v6-v1	831.76
/TT_TuneCUETP8M2T4_13TeV-powheg-fsrup-pythia8/ RunIISummer16MiniAODv2-PUMoriond17_80X_mcRun2_asymptotic_2016_TrancheIV_v6_ext1-v1	831.76
/TT_TuneCUETP8M2T4_13TeV-powheg-fsrup-pythia8/ RunIISummer16MiniAODv2-PUMoriond17_80X_mcRun2_asymptotic_2016_TrancheIV_v6_ext2-v1	831.76
/TT_TuneCUETP8M2T4_13TeV-powheg-isrdown-pythia8/ RunIISummer16MiniAODv2-PUMoriond17_80X_mcRun2_asymptotic_2016_TrancheIV_v6-v1	831.76
/TT_TuneCUETP8M2T4_13TeV-powheg-isrdown-pythia8/ RunIISummer16MiniAODv2-PUMoriond17_80X_mcRun2_asymptotic_2016_TrancheIV_v6_ext1-v1	831.76
/TT_TuneCUETP8M2T4_13TeV-powheg-isrdown-pythia8/ RunIISummer16MiniAODv2-PUMoriond17_80X_mcRun2_asymptotic_2016_TrancheIV_v6_ext2-v1	831.76
/TT_TuneCUETP8M2T4_13TeV-powheg-isrup-pythia8/ RunIISummer16MiniAODv2-PUMoriond17_80X_mcRun2_asymptotic_2016_TrancheIV_v6_ext1-v1	831.76
/TT_TuneCUETP8M2T4_13TeV-powheg-isrup-pythia8/ RunIISummer16MiniAODv2-PUMoriond17_80X_mcRun2_asymptotic_2016_TrancheIV_v6_ext2-v1	831.76
/TT_TuneCUETP8M2T4down_13TeV-powheg-pythia8/ RunIISummer16MiniAODv2-PUMoriond17_80X_mcRun2_asymptotic_2016_TrancheIV_v6-v1	831.76
/TT_TuneCUETP8M2T4down_13TeV-powheg-pythia8/ RunIISummer16MiniAODv2-PUMoriond17_80X_mcRun2_asymptotic_2016_TrancheIV_v6_ext1-v1	831.76
/TTTo2L2Nu_TuneCUETP8M2T4down_13TeV-powheg-pythia8/ RunIISummer16MiniAODv2-PUMoriond17_80X_mcRun2_asymptotic_2016_TrancheIV_v6-v1	831.76×0.1049
/TT_TuneCUETP8M2T4up_13TeV-powheg-pythia8/ RunIISummer16MiniAODv2-PUMoriond17_80X_mcRun2_asymptotic_2016_TrancheIV_v6-v1	831.76
/TT_TuneCUETP8M2T4up_13TeV-powheg-pythia8/ RunIISummer16MiniAODv2-PUMoriond17_80X_mcRun2_asymptotic_2016_TrancheIV_v6_ext1-v1	831.76
/TTTo2L2Nu_TuneCUETP8M2T4up_13TeV-powheg-pythia8/ RunIISummer16MiniAODv2-PUMoriond17_80X_mcRun2_asymptotic_2016_TrancheIV_v6-v1	831.76×0.1049
/TT_hdampUP_TuneCUETP8M2T4_13TeV-powheg-pythia8/ RunIISummer16MiniAODv2-PUMoriond17_80X_mcRun2_asymptotic_2016_TrancheIV_v6-v1	831.76
/TT_hdampUP_TuneCUETP8M2T4_13TeV-powheg-pythia8/ RunIISummer16MiniAODv2-PUMoriond17_80X_mcRun2_asymptotic_2016_TrancheIV_v6_ext1-v1	831.76
/TTTo2L2Nu_hdampUP_TuneCUETP8M2T4_13TeV-powheg-pythia8/ RunIISummer16MiniAODv2-PUMoriond17_80X_mcRun2_asymptotic_2016_TrancheIV_v6-v1	831.76×0.1049
/TT_hdampDOWN_TuneCUETP8M2T4_13TeV-powheg-pythia8/ RunIISummer16MiniAODv2-PUMoriond17_80X_mcRun2_asymptotic_2016_TrancheIV_v6-v1	831.76
/TT_hdampDOWN_TuneCUETP8M2T4_13TeV-powheg-pythia8/ RunIISummer16MiniAODv2-PUMoriond17_80X_mcRun2_asymptotic_2016_TrancheIV_v6_ext1-v1	831.76
/TTTo2L2Nu_hdampDOWN_TuneCUETP8M2T4_13TeV-powheg-pythia8/ RunIISummer16MiniAODv2-PUMoriond17_80X_mcRun2_asymptotic_2016_TrancheIV_v6-v1	831.76×0.1049

Table 4: Summary (Part 2) of simulated $t\bar{t}$ samples used in this analysis for the estimation of systematic uncertainties and comparisons, together with the cross section assigned to the process. The samples with the standalone simulation of dileptonic matrix elements are additionally scaled with the corresponding branching ratio.

sample	σ [pb]
/TT_TuneCUETP8M2T4_mtop1695_13TeV-powheg-pythia8/	
RunIISummer16MiniAODv2-PUMoriond17_backup_80X_mcRun2_asymptotic_2016_TrancheIV_v6-v1	831.76
/TT_TuneCUETP8M2T4_mtop1695_13TeV-powheg-pythia8/	
RunIISummer16MiniAODv2-PUMoriond17_80X_mcRun2_asymptotic_2016_TrancheIV_v6_ext1-v1	831.76
/TT_TuneCUETP8M2T4_mtop1695_13TeV-powheg-pythia8/	
RunIISummer16MiniAODv2-PUMoriond17_80X_mcRun2_asymptotic_2016_TrancheIV_v6_ext2-v1	831.76
/TTTo2L2Nu_TuneCUETP8M2T4_mtop1695_13TeV-powheg-pythia8/	
RunIISummer16MiniAODv2-PUMoriond17_80X_mcRun2_asymptotic_2016_TrancheIV_v6-v1	831.76 $\times 0.1049$
/TT_TuneCUETP8M2T4_mtop1755_13TeV-powheg-pythia8/	
RunIISummer16MiniAODv2-PUMoriond17_80X_mcRun2_asymptotic_2016_TrancheIV_v6-v1	831.76
/TT_TuneCUETP8M2T4_mtop1755_13TeV-powheg-pythia8/	
RunIISummer16MiniAODv2-PUMoriond17_80X_mcRun2_asymptotic_2016_TrancheIV_v6_ext1-v1	831.76
/TT_TuneCUETP8M2T4_mtop1755_13TeV-powheg-pythia8/	
RunIISummer16MiniAODv2-PUMoriond17_80X_mcRun2_asymptotic_2016_TrancheIV_v6_ext2-v1	831.76
/TTTo2L2Nu_TuneCUETP8M2T4_mtop1755_13TeV-powheg-pythia8/	
RunIISummer16MiniAODv2-PUMoriond17_80X_mcRun2_asymptotic_2016_TrancheIV_v6-v1	831.76 $\times 0.1049$
/TT_TuneCUETP8M2T4_erdON_13TeV-powheg-pythia8/	
RunIISummer16MiniAODv2-PUMoriond17_80X_mcRun2_asymptotic_2016_TrancheIV_v6-v1	831.76
/TT_TuneCUETP8M2T4_erdON_13TeV-powheg-pythia8/	
RunIISummer16MiniAODv2-PUMoriond17_80X_mcRun2_asymptotic_2016_TrancheIV_v6_ext1-v1	831.76
/TTTo2L2Nu_TuneCUETP8M2T4_erdON_13TeV-powheg-pythia8/	
RunIISummer16MiniAODv2-PUMoriond17_80X_mcRun2_asymptotic_2016_TrancheIV_v6-v1	831.76 $\times 0.1049$
/TT_TuneCUETP8M2T4_GluonMoveCRTune_13TeV-powheg-pythia8/	
RunIISummer16MiniAODv2-PUMoriond17_80X_mcRun2_asymptotic_2016_TrancheIV_v6-v1	831.76
/TTTo2L2Nu_TuneCUETP8M2T4_GluonMoveCRTune_13TeV-powheg-pythia8/	
RunIISummer16MiniAODv2-PUMoriond17_80X_mcRun2_asymptotic_2016_TrancheIV_v6-v1	831.76 $\times 0.1049$
/TT_TuneCUETP8M2T4_QCDbasedCRTune_erdON_13TeV-powheg-pythia8/	
RunIISummer16MiniAODv2-PUMoriond17_80X_mcRun2_asymptotic_2016_TrancheIV_v6-v1	831.76
/TT_TuneCUETP8M2T4_QCDbasedCRTune_erdON_13TeV-powheg-pythia8/	
RunIISummer16MiniAODv2-PUMoriond17_80X_mcRun2_asymptotic_2016_TrancheIV_v6_ext1-v1	831.76
/TTTo2L2Nu_TuneCUETP8M2T4_QCDbasedCRTune_erdON_13TeV-powheg-pythia8/	
RunIISummer16MiniAODv2-PUMoriond17_80X_mcRun2_asymptotic_2016_TrancheIV_v6-v1	831.76 $\times 0.1049$
/TT_TuneEE5C_13TeV-powheg-herwigpp/	
RunIISummer16MiniAODv2-PUMoriond17_80X_mcRun2_asymptotic_2016_TrancheIV_v6-v1	831.76
/TT_TuneEE5C_13TeV-powheg-herwigpp/	
RunIISummer16MiniAODv2-PUMoriond17_80X_mcRun2_asymptotic_2016_TrancheIV_v6_ext2-v1	831.76
/TT_TuneEE5C_13TeV-powheg-herwigpp/	
RunIISummer16MiniAODv2-PUMoriond17_80X_mcRun2_asymptotic_2016_TrancheIV_v6_ext3-v1	831.76
/TTJets_Dilept_TuneCUETP8M2T4_13TeV-amcatnloFXFX-pythia8/	
RunIISummer16MiniAODv2-PUMoriond17_80X_mcRun2_asymptotic_2016_TrancheIV_v6-v1	831.76 $\times 0.1049$
/TTJets_Dilept_TuneCUETP8M2T4_13TeV-amcatnloFXFX-pythia8/	
RunIISummer16MiniAODv2-PUMoriond17_80X_mcRun2_asymptotic_2016_TrancheIV_v6_ext1-v1	831.76 $\times 0.1049$
/TTJets_TuneCUETP8M2T4_13TeV-amcatnloFXFX-pythia8/	
RunIISummer16MiniAODv2-PUMoriond17_80X_mcRun2_asymptotic_2016_TrancheIV_v6_ext3-v1	831.76

Table 5: Triggers used in different data periods for the three dilepton channels. The same trigger menu is configured for the use in MC.

channel	run	trigger
$\mu^+ \mu^-$	B-G	HLT_Mu17_TrkIsoVVL_Mu8_TrkIsoVVL_v*
	B-G	HLT_Mu17_TrkIsoVVL_TkMu8_TrkIsoVVL_v*
	H	HLT_Mu17_TrkIsoVVL_Mu8_TrkIsoVVL_DZ_v*
	H	HLT_Mu17_TrkIsoVVL_TkMu8_TrkIsoVVL_DZ_v*
	B-H	HLT_IsoMu24_v*
	B-H	HLT_IsoTkMu24_v*
$e^+ e^-$	B-H	HLT_Ele23_Ele12_CaloIdL_TrackIdL_IsoVL_DZ_v*
	B-H	HLT_Ele27_WPTight_Gsf_v*
$\mu^\pm e^\mp$	B-G	HLT_Mu23_TrkIsoVVL_Ele12_CaloIdL_TrackIdL_IsoVL_v*
	B-G	HLT_Mu8_TrkIsoVVL_Ele23_CaloIdL_TrackIdL_IsoVL_v*
	H	HLT_Mu23_TrkIsoVVL_Ele12_CaloIdL_TrackIdL_IsoVL_DZ_v*
	H	HLT_Mu8_TrkIsoVVL_Ele23_CaloIdL_TrackIdL_IsoVL_DZ_v*
	B-H	HLT_Ele27_WPTight_Gsf_v*
	B-H	HLT_IsoMu24_v*
	B-H	HLT_IsoTkMu24_v*

183 3 Event selection

184 Events are required to fulfill the good-run selection described above. Several dilepton triggers
 185 are used for the trigger selection in the data as detailed in Table 5. A logical “OR” between the
 186 different trigger terms is applied to select events in the dilepton channel.

187 The analysis is performed using the CMS software version CMSSW_8_0_26_patch2. The object
 188 reconstruction and identification follow the configuration settings recommended by the Top
 189 Physics Analysis Group for dilepton final states [41]. It is configured to perform a charged-
 190 hadron subtraction (`pfNoPileUP`) to remove pile-up. Because `pfNoPileUP` can only remove
 191 charged hadrons, the L1FastJet algorithm is applied to subtract the remaining neutral compo-
 192 nents. Events are accepted if the primary vertex fulfills a requirement of good quality: number
 193 of degrees of freedom (dof)>4, $|\rho| < 2$ cm and $|z| < 24$ cm.

194 The simulation is reweighted to describe the pile-up distributions in the data. The target pileup
 195 distribution is generated using the instantaneous luminosity per bunch crossing for each lumi-
 196 nosity section, stored in the LumiDB database, and the total pp inelastic cross section of 69.2
 197 mb. A Poisson smearing is applied to model statistical fluctuations. The distribution is taken
 198 from the PileupInfo collection which stores the true number of pileup events mixed with the
 199 particular hard interaction process in each MC event. A variation of $\pm 4.6\%$ on the minimum
 200 bias cross section is used to estimate the uncertainties due to pileup modeling [42].

201 The $t\bar{t}$ dilepton final state is characterized by the presence of two high- p_T isolated leptons with
 202 opposite electric charge, large missing transverse energy E_T^{miss} and at least two jets associated
 203 to b quarks from $t\bar{t}$. The reconstruction of the different objects is based on the particle-flow (PF)
 204 algorithm [43]. The event selection requirements [41] are described in the following.

205 3.1 Muon selection

206 Muon candidates are reconstructed using the PF algorithm and are required to have a trans-
 207 verse momentum $p_T > 25(20)$ GeV for leading (trailing) leptons within a pseudorapidity $|\eta| <$
 208 2.4. Candidates are required to fulfill the *tight ID* selection criteria, comprising the *GlobalMuon*
 209 and *PFMuon* conditions:

- 210 • number of matched stations > 1;

- number of valid pixel hits > 0;
- number of valid hits in the inner tracker > 5;
- number of muon hits > 0;
- $\chi^2/ndof < 10$ for the global muon fit (combination of tracker and muon detector hits);
- transverse impact parameter w.r.t. the beam spot < 0.2 cm and $dZ < 0.5$ cm, applied on the track from the inner tracker;

These requirements ensure prompt muons with high purity, suppressing fake muons or muons originating from decay-in-flight processes.

An isolation criterion is applied to remove contributions from leptons originating from QCD events. Muon candidates are selected if they fulfill the condition $I_{\text{Rel}}^{\text{PF}} < 0.15$, where $I_{\text{Rel}}^{\text{PF}}$ is defined as the sum of transverse energy deposits from charged and neutral hadrons and photons, relative to the p_{T} of the lepton, inside a cone in η - ϕ space of $\Delta R \equiv \sqrt{(\Delta\eta)^2 + (\Delta\phi)^2} < 0.4$ around the muon. Charged PF candidates from pile-up events are removed (PF charged subtraction). The $\Delta\beta$ corrections are applied to the muons.

3.2 Electron selection

Electron candidates are also reconstructed using the PF algorithm, but the four momentum of the electron is reconstructed using the Gaussian Sum Filter Electron (gsf) algorithm [41]. Electron candidates are required to have $p_{\text{T}} > 25(20)$ GeV for leading (trailing) leptons and $|\eta| < 2.4$. The gap between the barrel and endcap region of the ECAL ($1.4442 < |\eta_{\text{sc}}| < 1.5660$) is excluded, where η_{sc} is the detector pseudorapidity defined with respect to the origin of the coordinate system at the centre of the CMS detector.

To further ensure a high purity sample, the electron selection uses the cut-based *tight ID Summer16-25ns* working point (see Table 6), as detailed in Ref. [44]. Electron candidates originating from the conversion of photons are rejected. The electron isolation is based on photons, neutral hadrons, and charged hadrons as identified by the PF algorithm in a cone of $\Delta R < 0.3$ around the electron. The relative isolation is calculated as $I_{\text{Rel}}^{\text{PF}} = I_{\text{ch}} + \max(I_{\gamma} + I_{\text{nh}} - \rho A_{\text{eff}}, 0)$ and divided by the p_{T} of the electron. The term A_{eff} is an η dependent factor that is used in combination with ρ to subtract the energy deposition from pile-up interactions from the isolation. The energy deposition per area ρ due to unclustered objects is estimated from a fixed grid approach. This correction ensures that the isolation efficiency is nearly independent of the pile-up conditions.

3.3 Lepton pair selection

All leptons fulfilling the above selection cuts are considered for the definition of a lepton pair. In this way, the leading selected lepton is required to have $p_{\text{T}} > 25$ GeV. If more than two leptons are reconstructed in the event, the pair with the highest scalar sum of the p_{T} of the two leptons is chosen. The events with the dilepton system consisting out of the oppositely-charged leptons are accepted for the further consideration. The event is then unambiguously classified as e^+e^- , $\mu^{\pm}e^{\mp}$, or $\mu^+\mu^-$ depending on the type of the selected lepton pair (i.e. an event with three leptons, e.g. μ^+, μ^- , and e^+ , will be assigned either to the $\mu^{\pm}e^{\mp}$ or the $\mu^+\mu^-$ channel, but not to both). Finally, an event is discarded if there are additional leptons in the event, other than the two which enter the defined lepton pair. The invariant mass of the selected lepton pair is required to be larger than 20 GeV to suppress events from decays of heavy-flavour resonances and low-mass Drell-Yan processes.

	Barrel ($ \eta_{\text{sc}} < 1.4442$)	Endcap ($1.5660 < \eta_{\text{sc}} < 2.5$)
$ \Delta\eta_{In} $	0.00308	0.00605
$ \Delta\phi_{In} $	0.0816	0.0394
full $5 \times 5 \sigma_{I_\eta I_\eta}$	0.00998	0.0292
$\frac{h}{E}$	0.0414	0.0641
$ \Delta\theta $	0.05	0.10
$ \Delta z $	0.10	0.20
$\frac{1}{E} - \frac{1}{p}$	0.0129	0.0129
relative electron isolation	0.0588	0.0571
expected missing inner hits	1	1
pass conversion veto	yes	yes

Table 6: Electron identification requirements (Summer16-25ns tuning).

255 Moreover, in the $\mu^+\mu^-$ and e^+e^- decay channels, events are rejected if the dilepton invariant
 256 mass is within the region $76 \text{ GeV} < m_{\ell\ell} < 106 \text{ GeV}$, where background from Z boson produc-
 257 tion is dominant.

258 3.4 Jet selection

259 The $t\bar{t}$ signal is characterized by the presence of energetic hadronic jets corresponding to b jets
 260 and softer jets from initial- and final-state radiation (ISR and FSR, respectively). Most back-
 261 ground events are not expected to have such hadronic activity, therefore the requirement of jets
 262 in the event selection further suppresses the background contribution.

263 Jets are reconstructed using particle candidates from the PF algorithm after charge hadron sub-
 264 tracted [45]. The anti- k_T clustering algorithm (with clustering parameter equal to 0.4) is used
 265 for the jet identification and kinematics reconstruction. The latest set of jet energy scale correc-
 266 tions (Summer16_23Sep2016V4.MC and Summer16_23Sep2016V4.DATA) and jet energy res-
 267 olution corrections (Summer16_25nsV1) are applied. The momentum of the jets is corrected
 268 by application of the ‘L1FastJet’ corrections compatible with PFnoPU, ‘Level 2’, and ‘Level 3’
 269 corrections applied in both data and simulation; ‘L2L3Residual’ corrections are applied only
 270 on data. In addition, the following “loose” jet identification criteria are applied: fraction of
 271 charged hadronic energy ≥ 0 ; fraction of charged electromagnetic energy ≤ 0.99 ; fraction of
 272 neutral hadronic energy < 0.99 ; fraction of neutral electromagnetic fraction < 0.99 .

273 A jet-lepton cleaning is applied, which excludes jets overlapping with fully selected leptons
 274 (electron/muon) used in the analysis if $\Delta R(jet, lepton) < 0.4$.

275 The event selection requires the presence of at least two jets with $p_T > 30 \text{ GeV}$ and within
 276 $|\eta| < 2.4$.

277 3.5 b jet selection

278 A b-tagging algorithm is applied to all reconstructed jets in the event. In this analysis, the up-
 279 dated version of the Combined Secondary Vertex (CSV) [46] algorithm for 13 TeV data is used,
 280 the CSVv2. The CSVv2 algorithm uses secondary vertices and track-based lifetime information
 281 as an input for a Multivariate Analysis (MVA). The BTV POG defines 3 working points for each
 282 b-tagging algorithm according the b -jet mistag efficiency: $\sim 10\%$, $\sim 1\%$ and $\sim 0.1\%$ for loose
 283 (L), medium (M) and tight (T), respectively. In this analysis, a loose working point is selected:
 284 CSVv2L = 0.5426.

285 Due to the differences in the data and MC b-tagging algorithms efficiencies, the BTV POG derives data to MC corrections (referred to as scale factors, SF_{BTV}) using QCD multijet events [47].
 286 Additionally, to correct the possible difference in the b-tagging efficiency due to the different
 287 kinematics of the $t\bar{t}$ and QCD multijet events, the b-tagging efficiency (ε_{MC}) is estimated in this
 288 analysis using $t\bar{t}$ signal events.

290 In this measurement, the simulated events are reweighted using the scale factors and MC b-
 291 tagging efficiencies [48]. This method is chosen due to the fact that with such a logic only
 292 the selected MC events will be used later for the kinematic reconstruction of the top quark,
 293 since there is no migration of events between different b-jet multiplicity bins. Additionally,
 294 there is no re-shuffling of the b-tagging status between the jets of different flavours, which is
 295 disfavoured for the top quark kinematic reconstruction.

296 Accordingly to the mentioned above b-tagging scale factor application method and used design-
 297 nations, the probability P of a given configuration of jets in MC simulation and data is defined
 298 as:

$$P(MC) = \prod_{i=\text{tagged}} \varepsilon_i \prod_{j=\text{not tagged}} (1 - \varepsilon_j), \quad (1)$$

$$P(DATA) = \prod_{i=\text{tagged}} SF_i \varepsilon_i \prod_{j=\text{not tagged}} (1 - SF_j \varepsilon_j), \quad (2)$$

299 where ε_i and SF_i refer respectively to ε_{MC} and SF_{BTV} , which are functions of the jet flavor, jet
 300 p_T , and jet η . Afterwards, the event weight is computed accordingly to $w_{b\text{-tag}} = \frac{P(DATA)}{P(MC)}$.

301 Finally, the event is required to have at least 1 b-tagged jet, and is reweighted once it was
 302 selected using the $w_{b\text{-tag}}$ value.

303 3.6 Missing transverse energy

304 The missing transverse energy E_T^{miss} is defined as the magnitude of the projection, on the plane
 305 perpendicular to the beams, of the negative vector sum of the momenta of all reconstructed
 306 particles in an event using the particle-flow algorithm [49]:

$$E_{x,y} = - \sum_{\text{all reconstructed particles}} p_{x,y} \quad (3)$$

307 The calculation of the missing transverse energy E_T^{miss} is based on PF objects. A beam halo filter
 308 and filters against noise in hadronic or electron (endcap region) calorimeters are used to avoid
 309 a misreconstruction of E_T^{miss} [50].

310 Events in the $\mu^+\mu^-$ and e^+e^- channels are required to have $E_T^{\text{miss}} > 40 \text{ GeV}$. No requirement
 311 on E_T^{miss} is applied in the $\mu^\pm e^\mp$ channel.

312 3.7 Event yields and control distributions

313 The numbers of observed events in the data compared to the expected events from the simula-
 314 tion are given in Table 7 after each consecutive selection step described below.

- 315 • **2 leptons:** Events with exactly 2 oppositely-charged isolated leptons and $m_{\ell\ell} >$
 316 20 GeV , passing the trigger. The Z+jets background is removed by rejecting events in
 317 the Z boson mass region $76 \text{ GeV} < m_{\ell\ell} < 106 \text{ GeV}$. This requirement is only applied
 318 in the $\mu^+\mu^-$ and e^+e^- channels.

Table 7: Number of expected signal and background events, compared to the event yields in the data, after various selection steps and for various $t\bar{t}$ decay channels. Percentage event fractions of the MC predictions are given in brackets.

mm	2 leptons	2 jets	E_T^{miss}	b-tag	kin. rec. (loose)
$t\bar{t}$ signal	113221[6.2%]	82177[47.8%]	64896[65.9%]	59820[74.7%]	54900[77.1%] (56767[77.0%])
$t\bar{t}$ other via τ	17014[0.9%]	12284[7.1%]	9944[10.1%]	9138[11.4%]	8571[12.0%] (8722[11.8%])
$t\bar{t}$ other not via τ	1473[0.1%]	1179[0.7%]	863[0.9%]	690[0.9%]	578[0.8%] (597[0.8%])
tW	12816[0.7%]	4938[2.9%]	3883[3.9%]	3339[4.2%]	2273[3.2%] (2505[3.4%])
diboson	17769[1.0%]	1994[1.2%]	1090[1.1%]	352[0.4%]	193[0.3%] (213[0.3%])
W+jets	1508[0.1%]	212[0.1%]	186[0.2%]	163[0.2%]	77[0.1%] (77[0.1%])
Z+jets	1657927[91.0%]	69086[40.2%]	17675[17.9%]	6608[8.2%]	4589[6.4%] (4840[6.6%])
sum MC	1821728[100.0%]	171871[100.0%]	98537[100.0%]	80110[100.0%]	71182[100.0%] (73721[100.0%])
data	2032080	208732	104491	80359	70346 (72835)
em	2 leptons	2 jets	E_T^{miss}	b-tag	kin. rec. (loose)
$t\bar{t}$ signal	199005[57.2%]	145441[78.8%]	145441[78.8%]	134247[81.0%]	124422[82.0%] (127840[81.9%])
$t\bar{t}$ other via τ	30378[8.7%]	22020[11.9%]	22020[11.9%]	20262[12.2%]	19164[12.6%] (19444[12.5%])
$t\bar{t}$ other not via τ	2099[0.6%]	1697[0.9%]	1697[0.9%]	1382[0.8%]	1174[0.8%] (1212[0.8%])
tW	22816[6.6%]	8898[4.8%]	8898[4.8%]	7662[4.6%]	5486[3.6%] (5899[3.8%])
diboson	26640[7.7%]	2074[1.1%]	2074[1.1%]	684[0.4%]	406[0.3%] (444[0.3%])
W+jets	3943[1.1%]	457[0.2%]	457[0.2%]	121[0.1%]	50[0.0%] (100[0.1%])
Z+jets	63280[18.2%]	3883[2.1%]	3883[2.1%]	1366[0.8%]	1053[0.7%] (1081[0.7%])
sum MC	348160[100.0%]	184470[100.0%]	184470[100.0%]	165725[100.0%]	151755[100.0%] (156020[100.0%])
data	353773	184529	184529	164297	150410 (154444)
ee	2 leptons	2 jets	E_T^{miss}	b-tag	kin. rec. (loose)
$t\bar{t}$ signal	55219[7.4%]	40273[50.3%]	31730[68.0%]	29199[76.3%]	26573[78.8%] (27541[78.7%])
$t\bar{t}$ other via τ	7892[1.1%]	5753[7.2%]	4642[10.0%]	4256[11.1%]	3975[11.8%] (4048[11.6%])
$t\bar{t}$ other not via τ	341[0.0%]	274[0.3%]	201[0.4%]	169[0.4%]	144[0.4%] (147[0.4%])
tW	6319[0.9%]	2464[3.1%]	1970[4.2%]	1740[4.5%]	1146[3.4%] (1261[3.6%])
diboson	8171[1.1%]	1033[1.3%]	565[1.2%]	188[0.5%]	96[0.3%] (117[0.3%])
W+jets	1449[0.2%]	161[0.2%]	77[0.2%]	52[0.1%]	25[0.1%] (25[0.1%])
Z+jets	662424[89.3%]	30079[37.6%]	7455[16.0%]	2653[6.9%]	1754[5.2%] (1860[5.3%])
sum MC	741815[100.0%]	80036[100.0%]	46641[100.0%]	38257[100.0%]	33714[100.0%] (35000[100.0%])
data	867766	100137	51336	39984	34890 (36188)
ll	2 leptons	2 jets	E_T^{miss}	b-tag	kin. rec. (loose)
$t\bar{t}$ signal	367445[12.6%]	267891[61.4%]	242067[73.4%]	223267[78.6%]	205895[80.2%] (212147[80.1%])
$t\bar{t}$ other via τ	55284[1.9%]	40058[9.2%]	36607[11.1%]	33655[11.8%]	31710[12.4%] (32213[12.2%])
$t\bar{t}$ other not via τ	3913[0.1%]	3149[0.7%]	2761[0.8%]	2241[0.8%]	1896[0.7%] (1957[0.7%])
tW	41950[1.4%]	16301[3.7%]	14751[4.5%]	12741[4.5%]	8905[3.5%] (9665[3.7%])
diboson	52580[1.8%]	5101[1.2%]	3730[1.1%]	1225[0.4%]	695[0.3%] (774[0.3%])
W+jets	6901[0.2%]	829[0.2%]	719[0.2%]	335[0.1%]	153[0.1%] (203[0.1%])
Z+jets	2383631[81.9%]	103048[23.6%]	29012[8.8%]	10628[3.7%]	7396[2.9%] (7781[2.9%])
sum MC	2911703[100.0%]	436377[100.0%]	329648[100.0%]	284092[100.0%]	256650[100.0%] (264740[100.0%])
data	3253619	493398	340356	284640	255646 (263467)

- **2 jets:** Fully selected dilepton events with at least 2 jets fulfilling the jet p_T and η requirements.

- E_T^{miss} : Events surviving the full selection, including the requirement on the missing energy, in the $\mu^+\mu^-$ and e^+e^- channels.

- **b-tagging:** Events selected after all above cuts including b-tagging.

- **kinematic reconstruction (kin. rec.):** Events with physically meaningful solution for the kinematic reconstruction, either full or loose (see Section 4).

In Table 7, $t\bar{t}$ signal refers to the prompt dilepton $t\bar{t}$ decays. Contributions to $t\bar{t}$ event samples other than signal which originate from dilepton decays via a τ lepton and all other decays are presented separately.

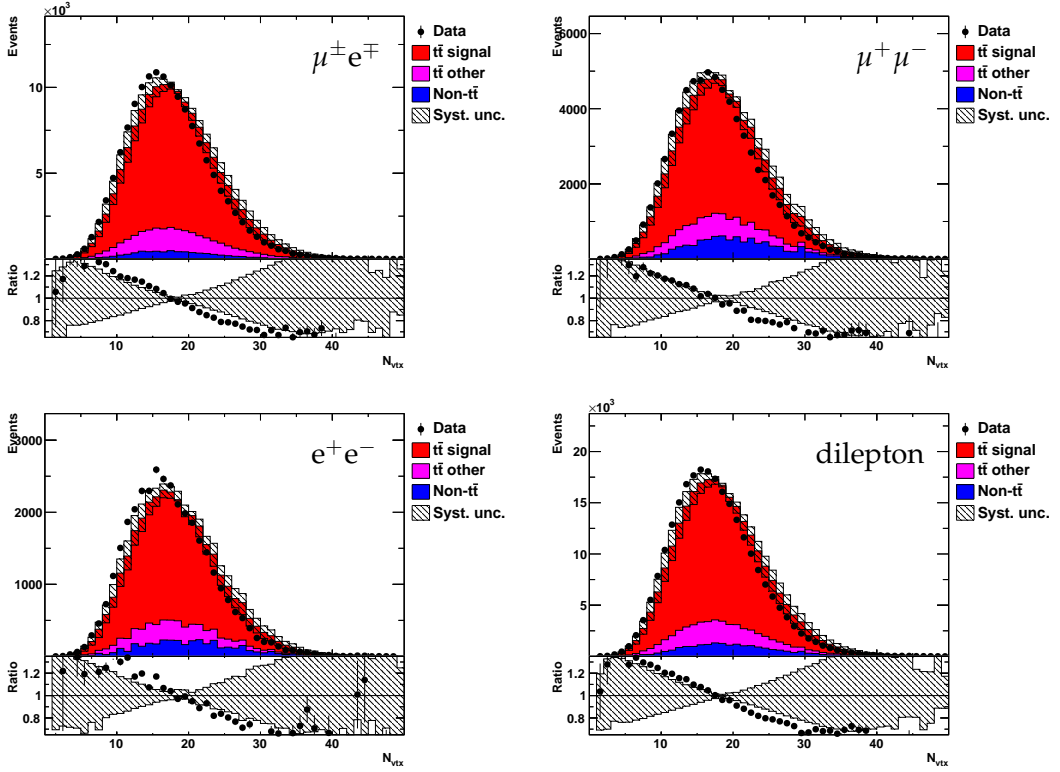


Figure 1: Distribution of the number of primary vertices in $\mu^\pm e^\mp$ (top left), $\mu^+ \mu^-$ (top right) $e^+ e^-$ (bottom left) and dilepton (bottom right) decay channels after pile-up reweighting. The hatched regions correspond to the estimated shape uncertainties in the signal and backgrounds (see Section 5).

In the following, the distributions in data are compared to those of the simulations for the separate decay channels after full event selection, including kinematic reconstruction described in Section 4. The shaded area corresponds to the shape uncertainties on the $t\bar{t}$ signal and background, described in Section 5. In Figure 1, the distribution of the number of primary vertices is shown. In Figure 2, the distribution of missing transverse energy is presented. Figures 3 and 4 show the distribution the transverse momentum of the leading and subleading lepton, respectively. Figures 5 and 6 show the distribution of the pseudorapidity of the leading and subleading lepton, respectively. In Figure 7, the distribution of the invariant mass of the lepton pair is presented. Figure 7 shows the distribution of the b-tagged jet multiplicity. Figures 9 to 12 present the distributions of the transverse momentum and pseudorapidity of the leading and subleading jets assigned to the $t\bar{t}$ decay in the kinematic reconstruction procedure, as detailed in Section 4. A good description of the data by the simulation is observed for all distributions within uncertainties.

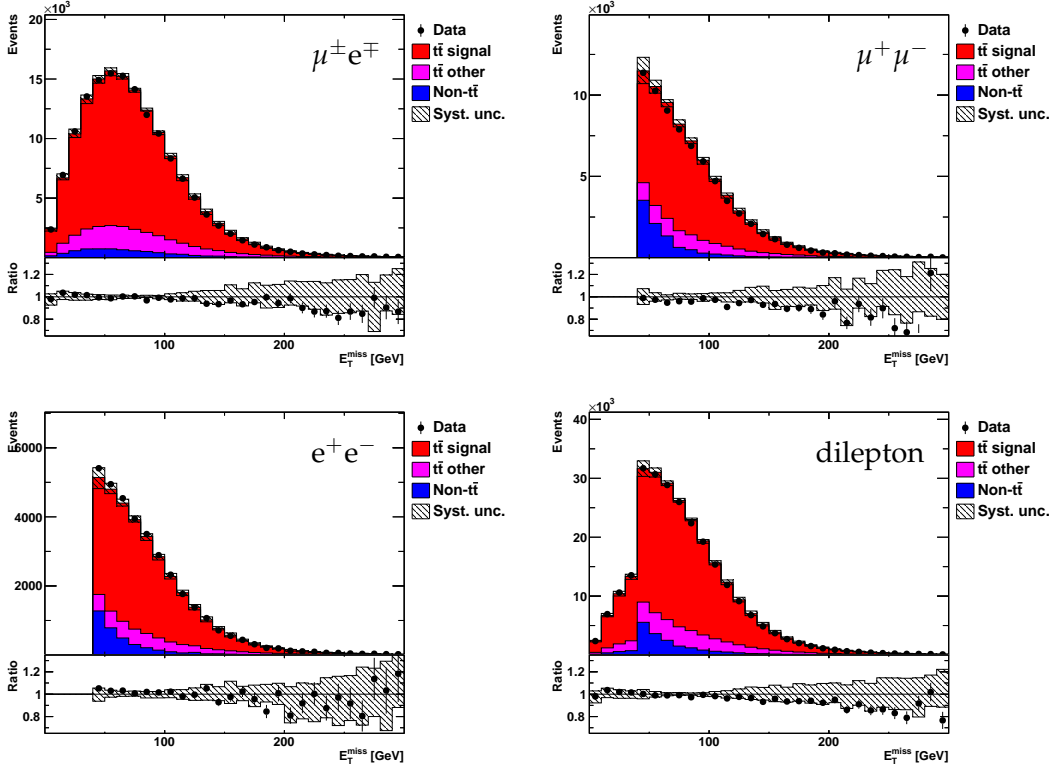


Figure 2: Distribution of E_T^{miss} in $\mu^\pm e^\mp$ (top left), $\mu^+ \mu^-$ (top right) $e^+ e^-$ (bottom left) and dilepton (bottom right) decay channels.

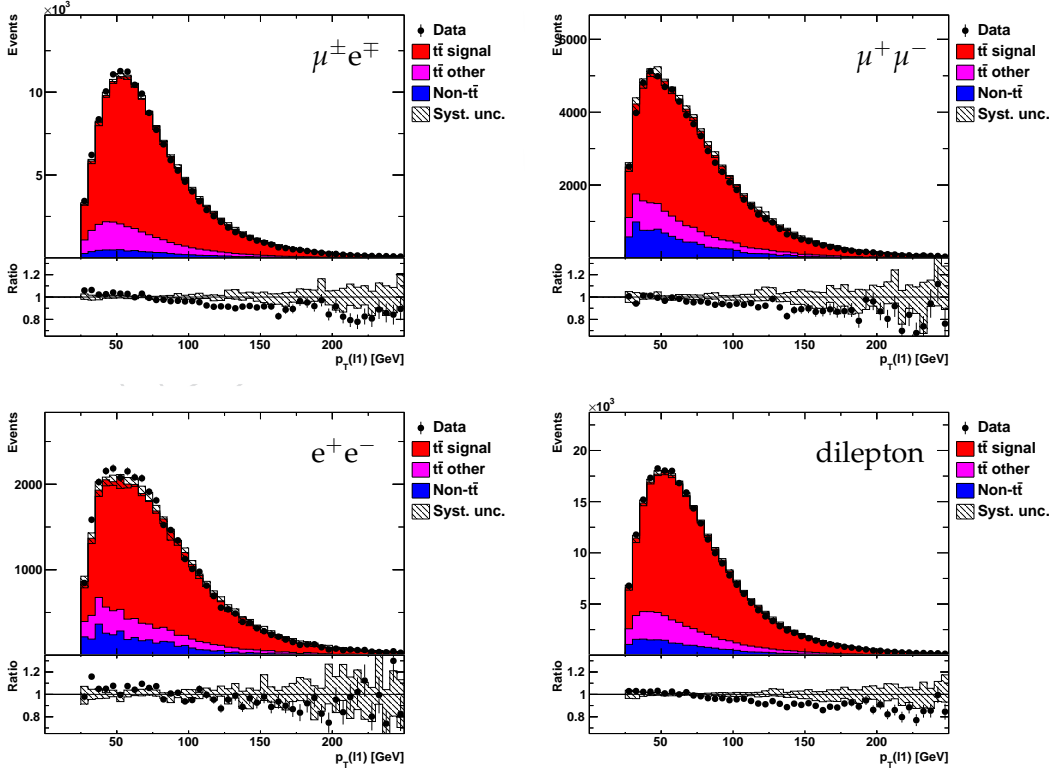


Figure 3: Distribution of leading lepton p_T in $\mu^\pm e^\mp$ (top left), $\mu^+ \mu^-$ (top right) $e^+ e^-$ (bottom left) and dilepton (bottom right) decay channels.

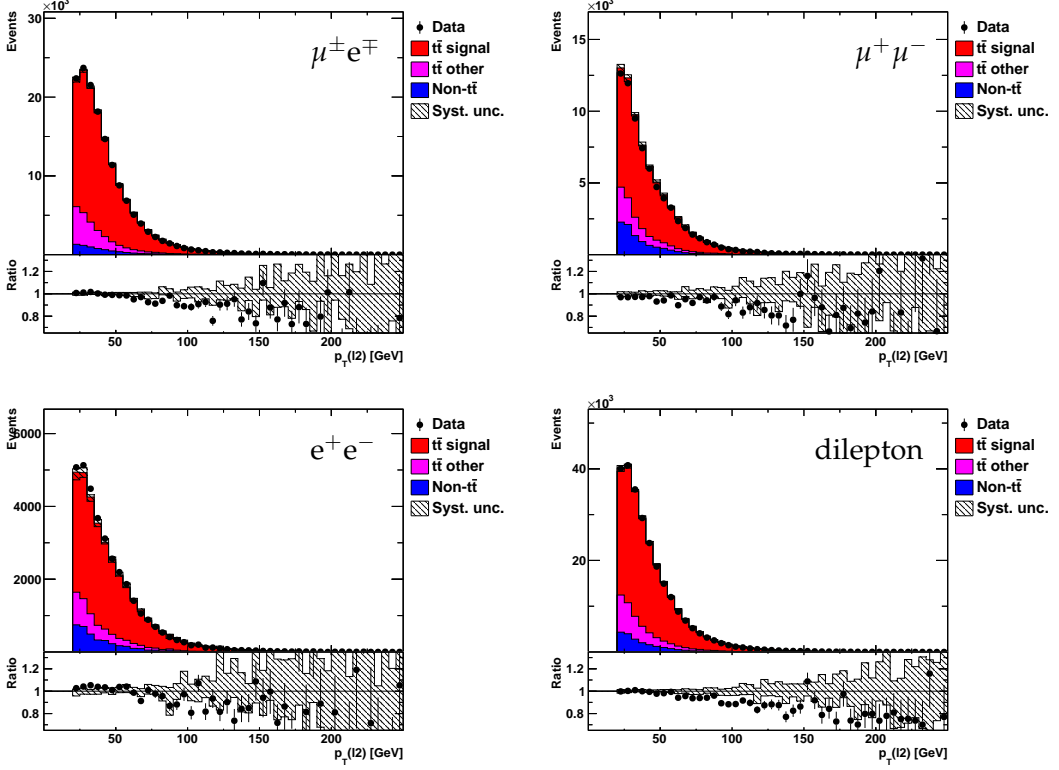


Figure 4: Distribution of subleading lepton p_T in $\mu^\pm e^\mp$ (top left), $\mu^+ \mu^-$ (top right) $e^+ e^-$ (bottom left) and dilepton (bottom right) decay channels.

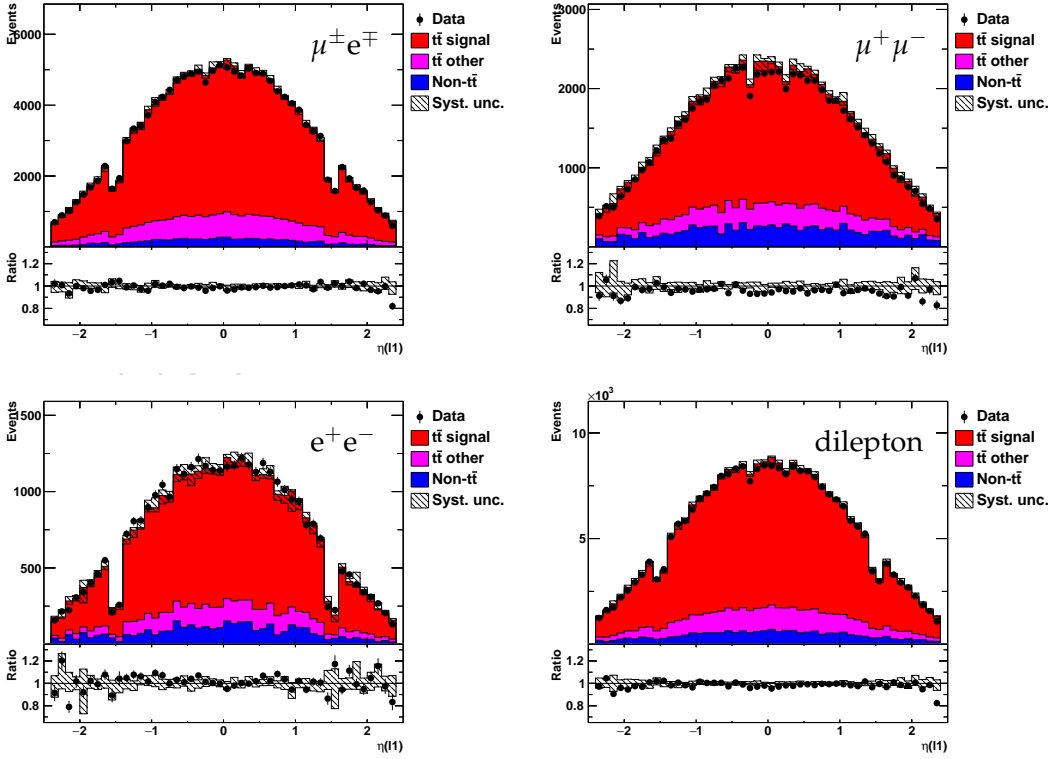


Figure 5: Distribution of leading lepton η in $\mu^\pm e^\mp$ (top left), $\mu^+ \mu^-$ (top right) $e^+ e^-$ (bottom left) and dilepton (bottom right) decay channels.

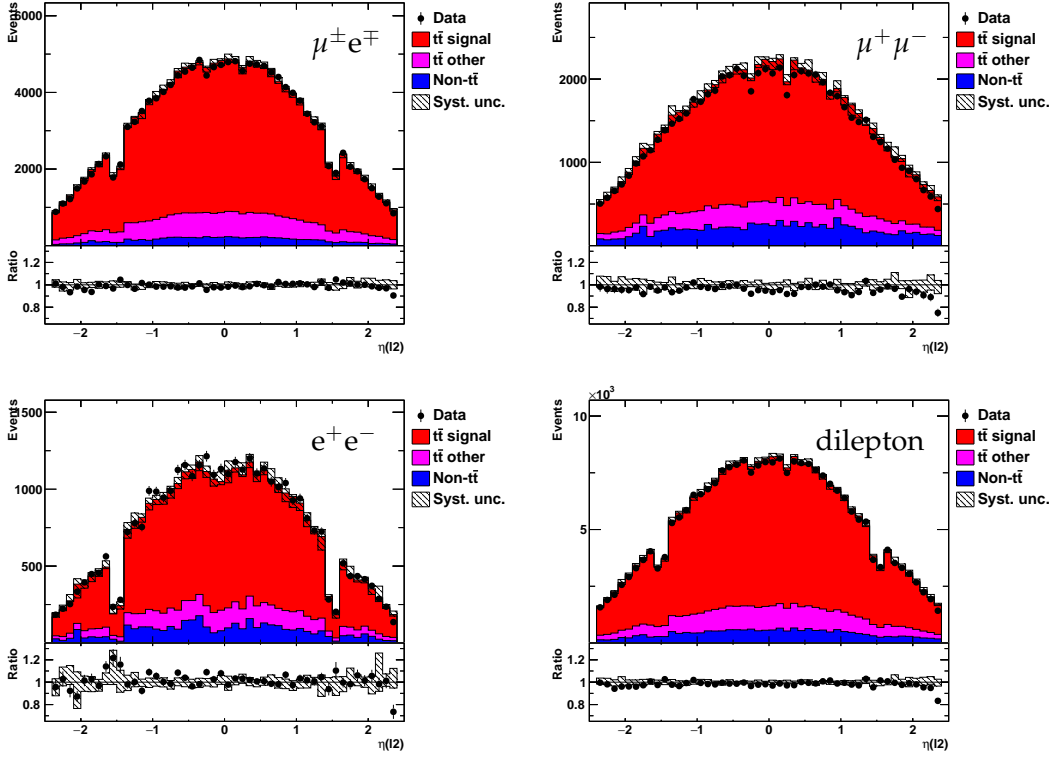


Figure 6: Distribution of subleading lepton η in $\mu^\pm e^\mp$ (top left), $\mu^+ \mu^-$ (top right) $e^+ e^-$ (bottom left) and dilepton (bottom right) decay channels.

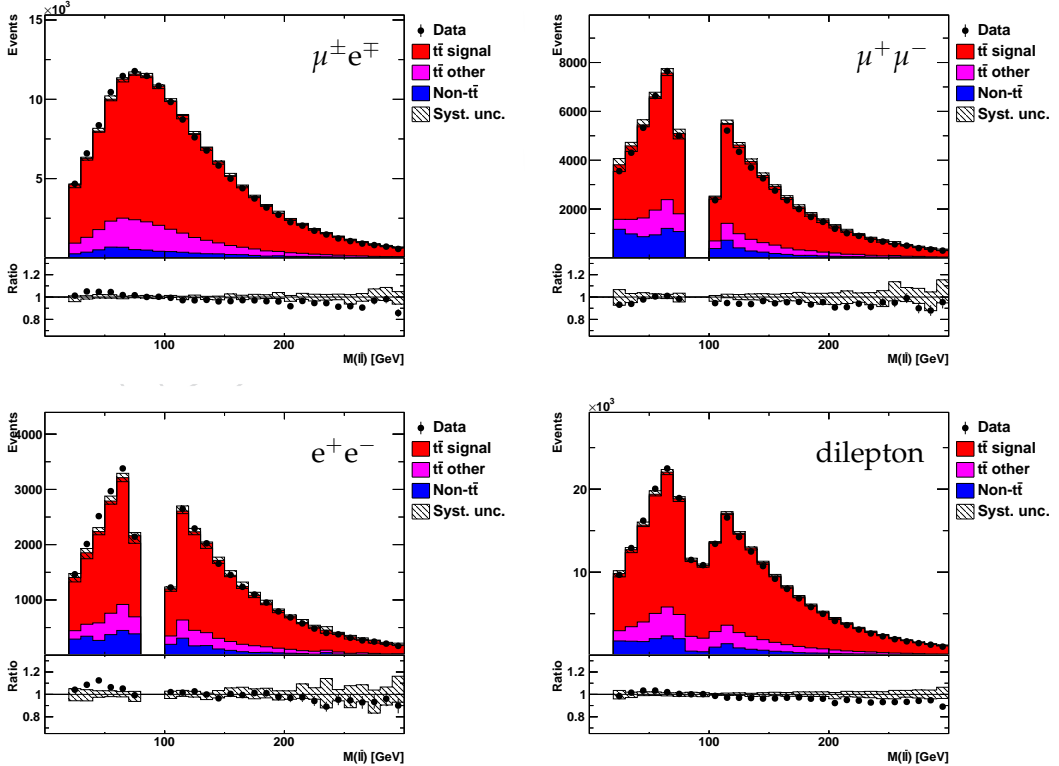


Figure 7: Distribution of the invariant mass of the lepton pair in $\mu^\pm e^\mp$ (top left), $\mu^+ \mu^-$ (top right) $e^+ e^-$ (bottom left) and dilepton (bottom right) decay channels.

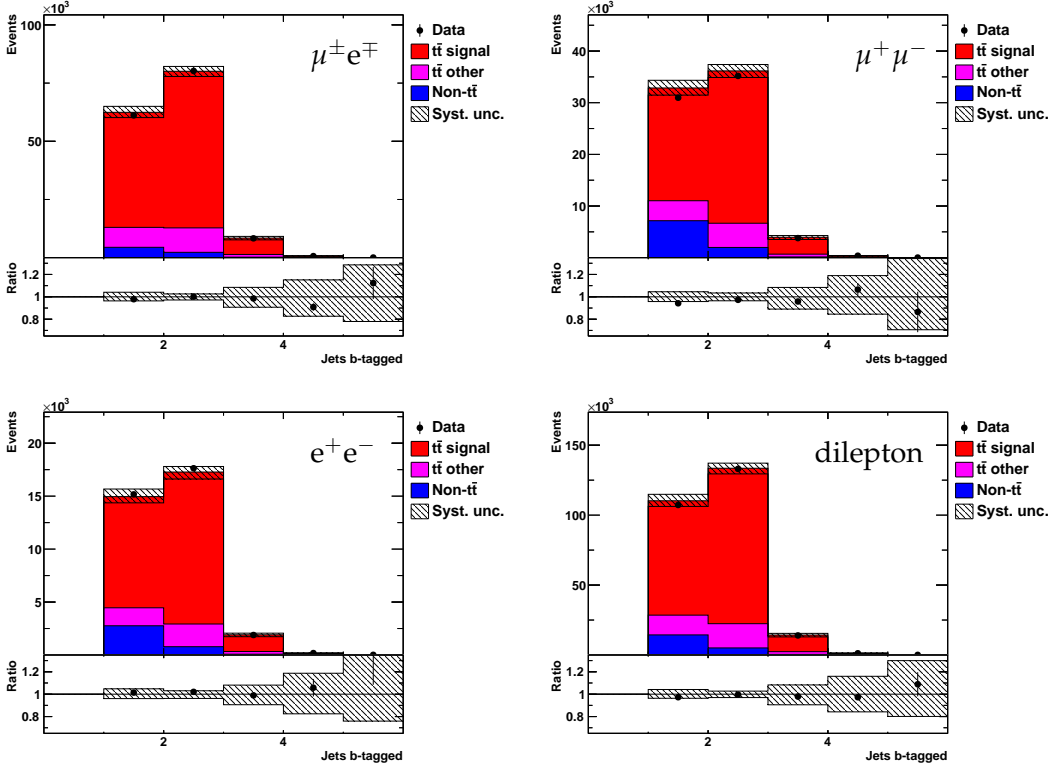


Figure 8: Distribution of b-tagged jet multiplicity in $\mu^\pm e^\mp$ (top left), $\mu^+ \mu^-$ (top right) $e^+ e^-$ (bottom left) and dilepton (bottom right) decay channels.

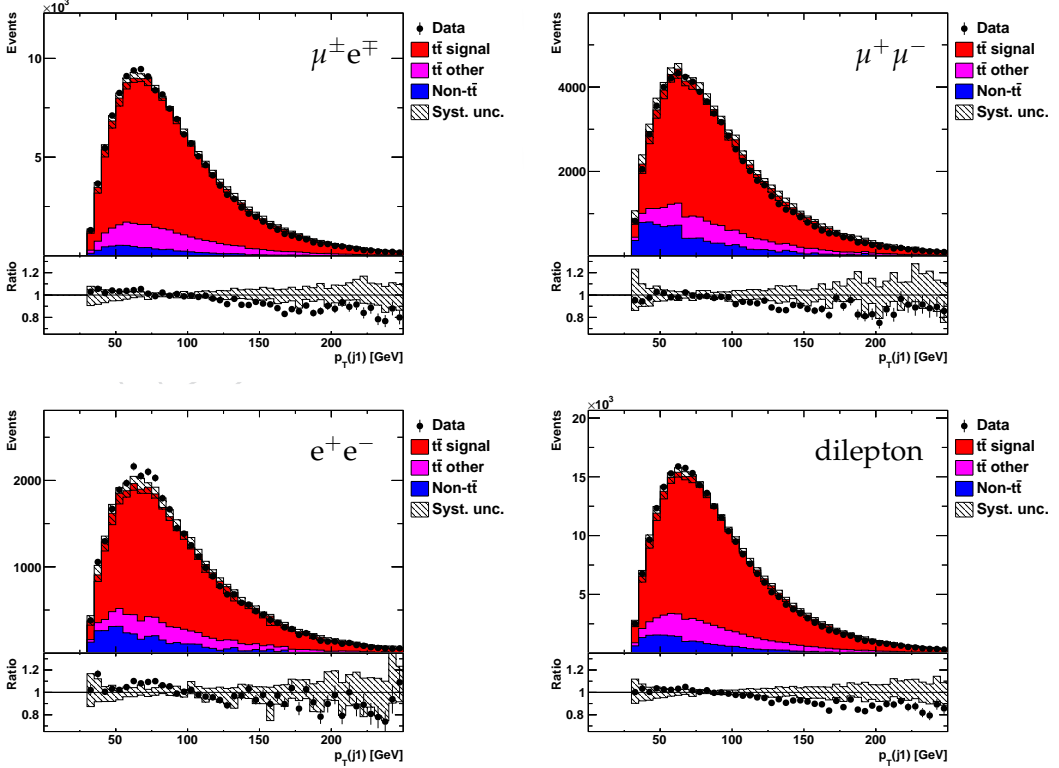


Figure 9: Distribution of leading jet from $t\bar{t}$ p_T in $\mu^\pm e^\mp$ (top left), $\mu^+ \mu^-$ (top right) $e^+ e^-$ (bottom left) and dilepton (bottom right) decay channels.

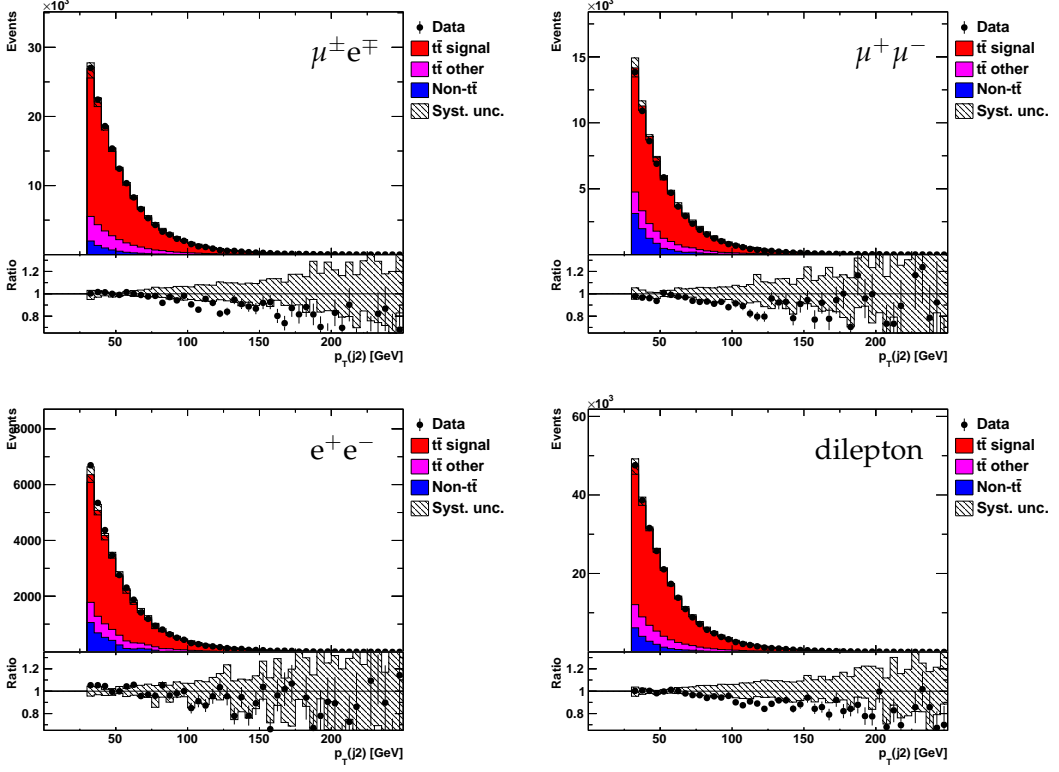


Figure 10: Distribution of subleading jet from $t\bar{t}$ p_T in $\mu^\pm e^\mp$ (top left), $\mu^+ \mu^-$ (top right) $e^+ e^-$ (bottom left) and dilepton (bottom right) decay channels.

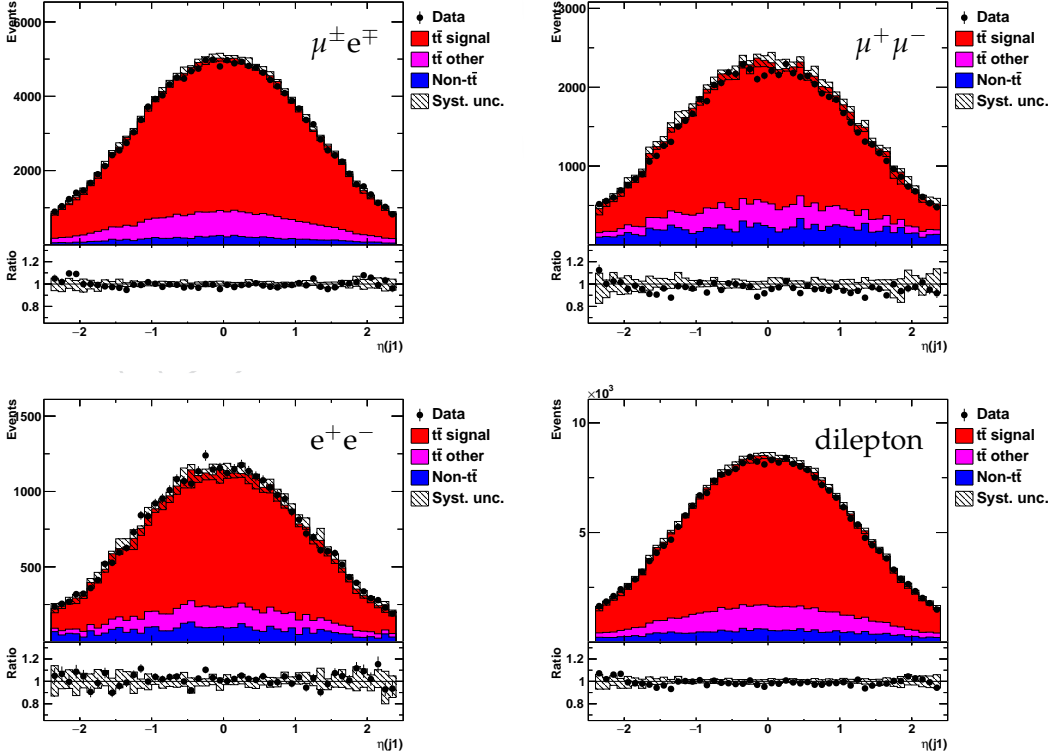


Figure 11: Distribution of leading jet from $t\bar{t}$ η in $\mu^\pm e^\mp$ (top left), $\mu^+ \mu^-$ (top right) $e^+ e^-$ (bottom left) and dilepton (bottom right) decay channels.

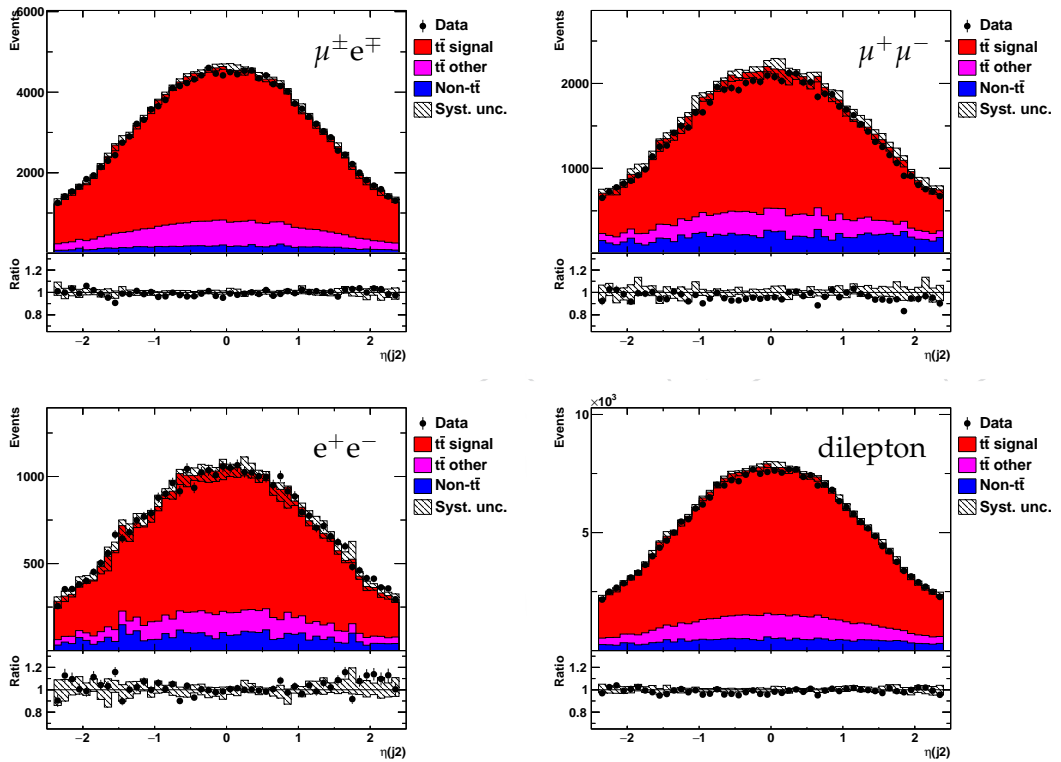


Figure 12: Distribution of subleading jet from $t\bar{t}$ η in $\mu^\pm e^\mp$ (top left), $\mu^+ \mu^-$ (top right) $e^+ e^-$ (bottom left) and dilepton (bottom right) decay channels.

342 4 Reconstruction of the top quark kinematics

343 4.1 Full kinematic reconstruction

344 For each event the kinematics of the top quark and of the antiquark are fully reconstructed
345 using the same algebraic method as in the $t\bar{t}$ differential cross section measurements [51, 52]
346 and [53] performed at 8 and 13 TeV, respectively. The six unknown quantities are the three-
347 momenta of the two neutrinos, which are reconstructed by imposing the following six kine-
348 matic constraints: p_T conservation in the event and the masses of the W bosons, top quark,
349 and top antiquark. The top quark and antiquark are required to have a mass of 172.5 GeV. It
350 is assumed that the p_T^{miss} in the event results from the two neutrinos in the top quark and anti-
351 quark decay chains. To resolve the ambiguity due to multiple algebraic solutions of the quartic
352 equations for the neutrino momenta, the solution with the smallest invariant mass of the $t\bar{t}$
353 system is taken. The reconstruction is performed 100 times, each time randomly smearing the
354 measured energies and directions of the reconstructed leptons and jets within their resolution.
355 This smearing recovers events that yielded no solution because of measurement fluctuations.
356 The three-momenta of the two neutrinos are determined as a weighted average over all the
357 smeared solutions. For each solution, the weight is calculated based on the expected invariant
358 mass spectrum of a lepton and a bottom jet as the product of two weights for the top quark
359 and antiquark decay chains. All possible lepton-jet combinations in the event are considered.
360 Combinations are ranked based on the presence of b-tagged jets in the assignments, i.e. a com-
361 bination with both leptons assigned to b-tagged jets is preferred over those with one or no
362 b-tagged jet. Among assignments with equal number of b-tagged jets, the one with the highest
363 average weight is chosen. Events with no solution after smearing are discarded. The method
364 yields an average reconstruction efficiency of $\approx 95\%$, which is determined in simulation as the
365 fraction of selected signal events (which include only direct $t\bar{t}$ decays via the $e^\pm e^\mp$, $\mu^\pm \mu^\mp$, $e^\pm \mu^\mp$
366 channels, i.e. excluding cascade decays via τ leptons) passing the kinematic reconstruction. The
367 overall difference in this efficiency between data and simulation is estimated to be $\approx 1\%$, and
368 a corresponding correction factor is applied to the simulation [54]. A more detailed descrip-
369 tion of the kinematic reconstruction procedure can be found in Ref. [54, 55].¹ In appendix J
370 some studies from [54] are shown, demonstrating that the minimum $M(t\bar{t})$ choice used in the
371 kinematic reconstruction provides good resolutions and small biases.

372 In this analysis, the energies and directions of the two jets and the two leptons are smeared.
373 The smearing factors are determined from the signal MC simulation for reconstructed b-jets
374 and leptons matched to the true b quarks and leptons from top quark decays. The smearing of
375 energies is implemented as a correction factor for the reconstructed energy sampled randomly
376 from the MC distribution of the ratio of the true energy on particle level divided by the re-
377 constructed energy. The shape of these distributions is found to be largely independent on the
378 true energy; thus the distribution obtained in the complete kinematic region of the analysis is
379 used for the sampling. The corresponding distributions for b jets and leptons are shown in Fig-
380 ure 13. For the directions, a random gaussian smearing is applied in a random direction around
381 the nominal direction. According to the MC simulation, the angular resolutions depend only
382 weakly on the b jet or lepton kinematics and thus the average resolutions were taken for the
383 gaussian smearing. Figure 14 shows the distributions from which the average resolutions were
384 obtained. One additional smearing is applied: the values of the W boson masses that were used
385 in the constraint are randomly sampled from a relativistic Breit-Wigner distribution, estimated
386 from the generator W boson mass distribution of the signal MC. This is shown in Figure 15
387 (left). The weights are calculated according to the expected (true) lepton-b-jet mass distribu-

¹This kinematic reconstruction procedure is often further referred to just as ‘kinematic reconstruction’.

tion in top quark decays after the kinematic selection requirements, estimated from the signal MC at particle level. Figure 15 (right) shows the true lepton-b-jet invariant mass distribution.

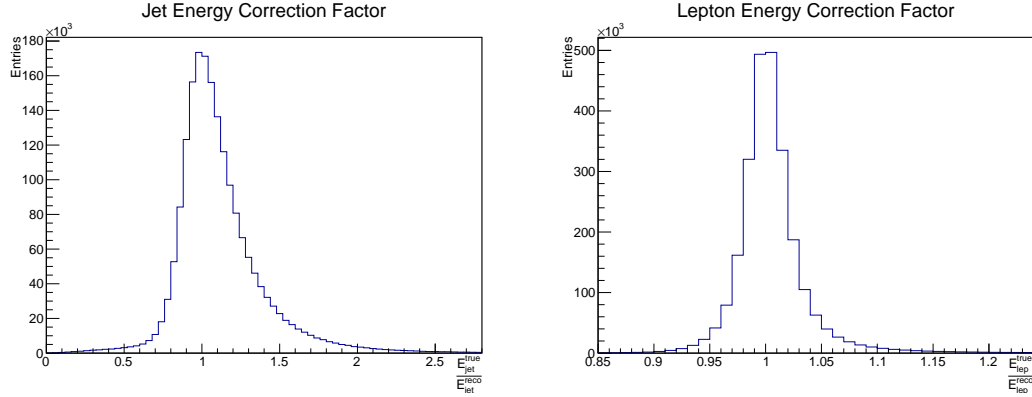


Figure 13: Distributions of the energy correction factors used for the energy smearing in the kinematic reconstruction of the top quark kinematics. The factors are shown (left) for the b quarks and (right) for the leptons.

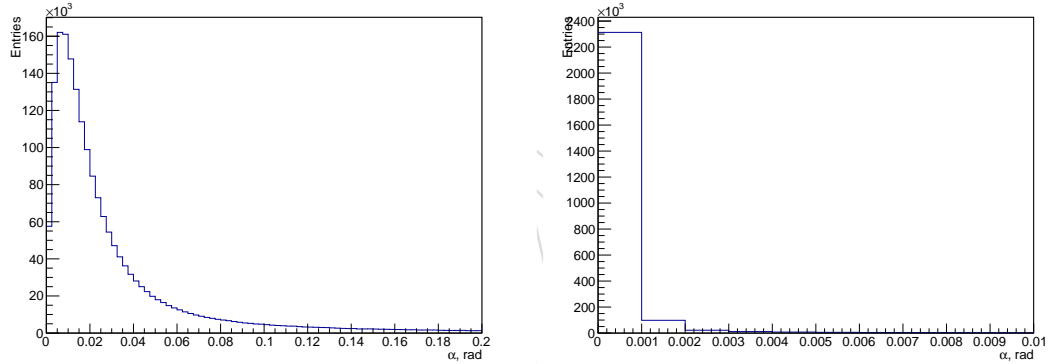


Figure 14: Distributions of the angle between the particle level direction and the detector level direction (left) for jets and (right) for leptons.

In Figures 16 to 20, the top quark and $t\bar{t}$ kinematic observables, as obtained from the kinematic reconstruction, are presented. A good description of the data by the simulation is observed within uncertainties.

4.2 Loose kinematic reconstruction

The $M(t\bar{t})$ distribution at detector level obtained using the full kinematic reconstruction described in the previous Section appears to be sensitive to the value of the top quark mass kinematic constraint and has little sensitivity to $M(t\bar{t})$ at generator level. Therefore, after unfolding to generator level, the unfolded $M(t\bar{t})$ cross section is sensitive to the top quark mass m_t used in MC to evaluate the response matrix (see Section 4.4 and Appendix C). Since one of the main objectives of the cross section measurement in this analysis is to extract m_t^{pole} exploiting the sensitivity of the predicted $M(t\bar{t})$ cross section to this parameter, in order to avoid the large sensitivity of the measured cross sections to m_t an alternative algorithm is employed which reconstructs $t\bar{t}$ kinematics only without using this constraint. This algorithm is referred to as a loose kinematic reconstruction.

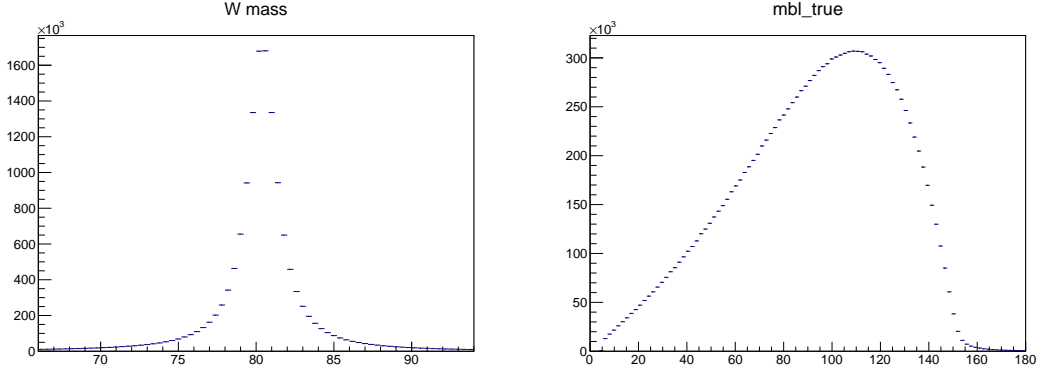


Figure 15: Distributions of the true W boson mass (left) and lepton-b-jet invariant mass distribution (right).

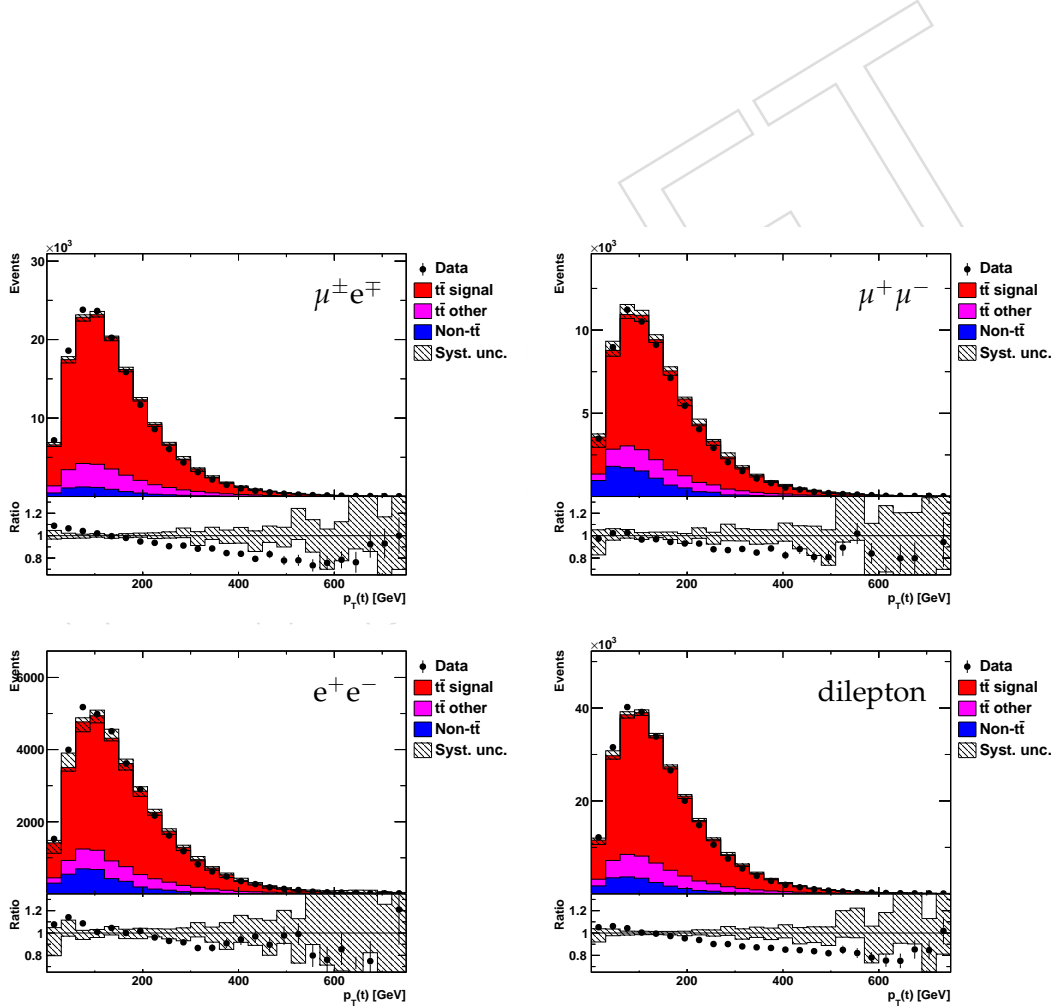


Figure 16: Distribution of top quark p_T in the $\mu^\pm e^\mp$ (top left), $\mu^+ \mu^-$ (top right) $e^+ e^-$ (bottom left) and dilepton (bottom right) decay channels.

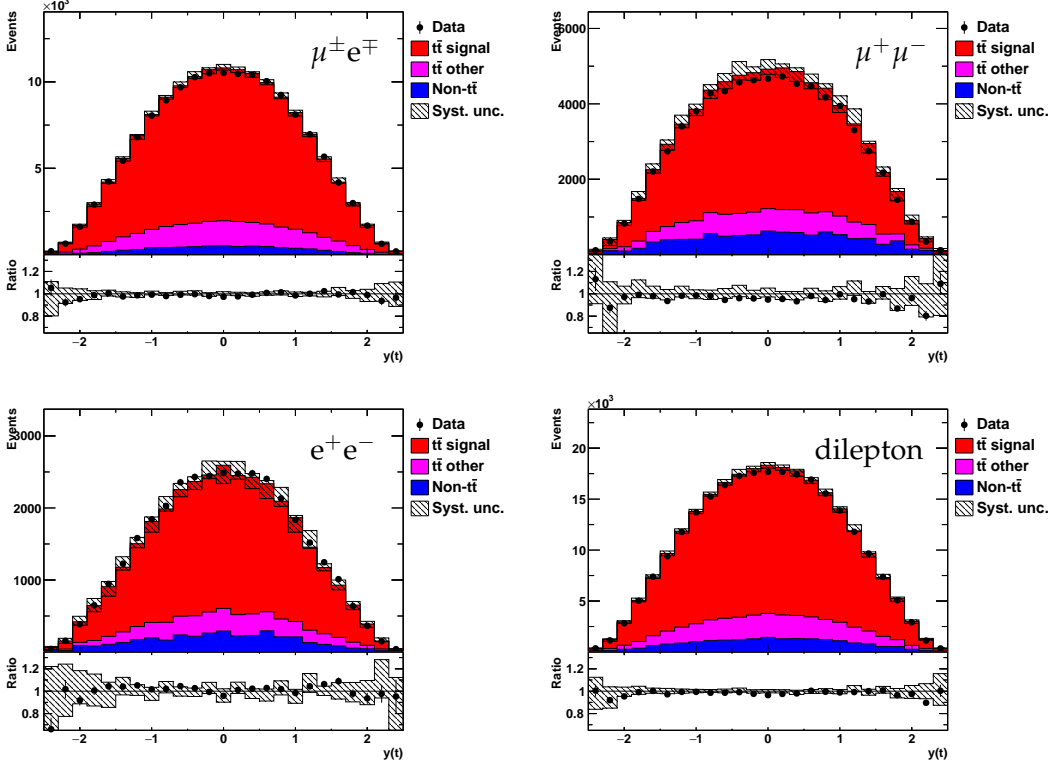


Figure 17: Distribution of top quark rapidity in the $\mu^\pm e^\mp$ (top left), $\mu^+ \mu^-$ (top right) $e^+ e^-$ (bottom left) and dilepton (bottom right) decay channels.

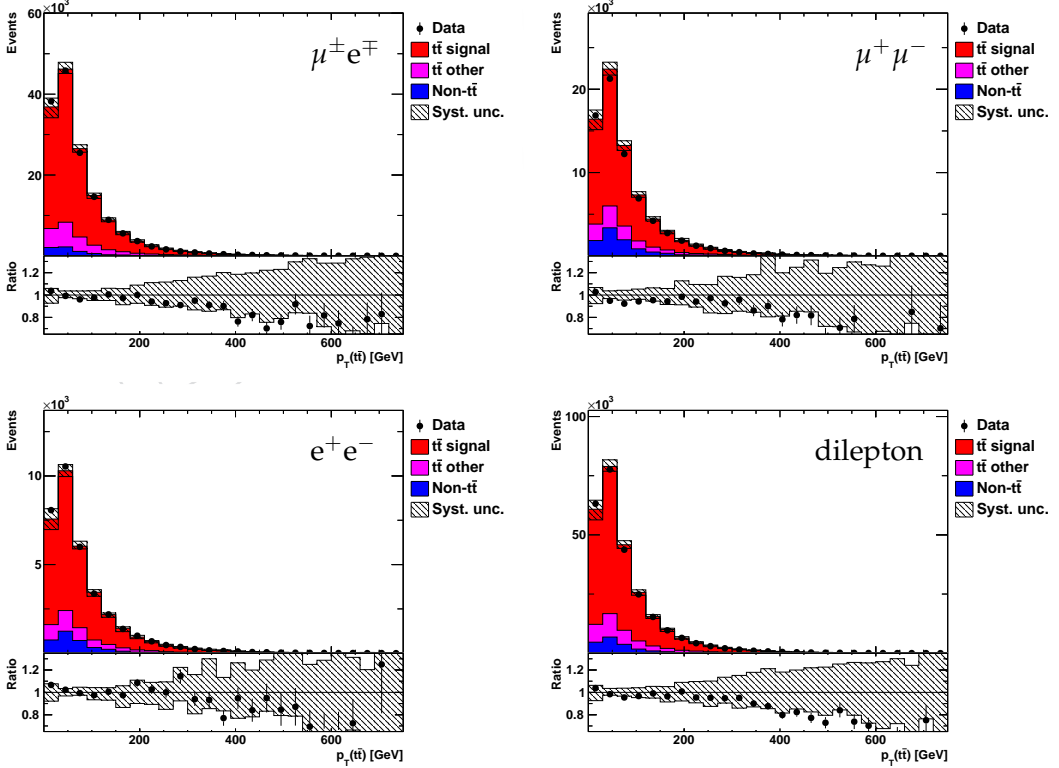


Figure 18: Distribution of $t\bar{t}$ p_T in the $\mu^\pm e^\mp$ (top left), $\mu^+ \mu^-$ (top right) $e^+ e^-$ (bottom left) and dilepton (bottom right) decay channels.

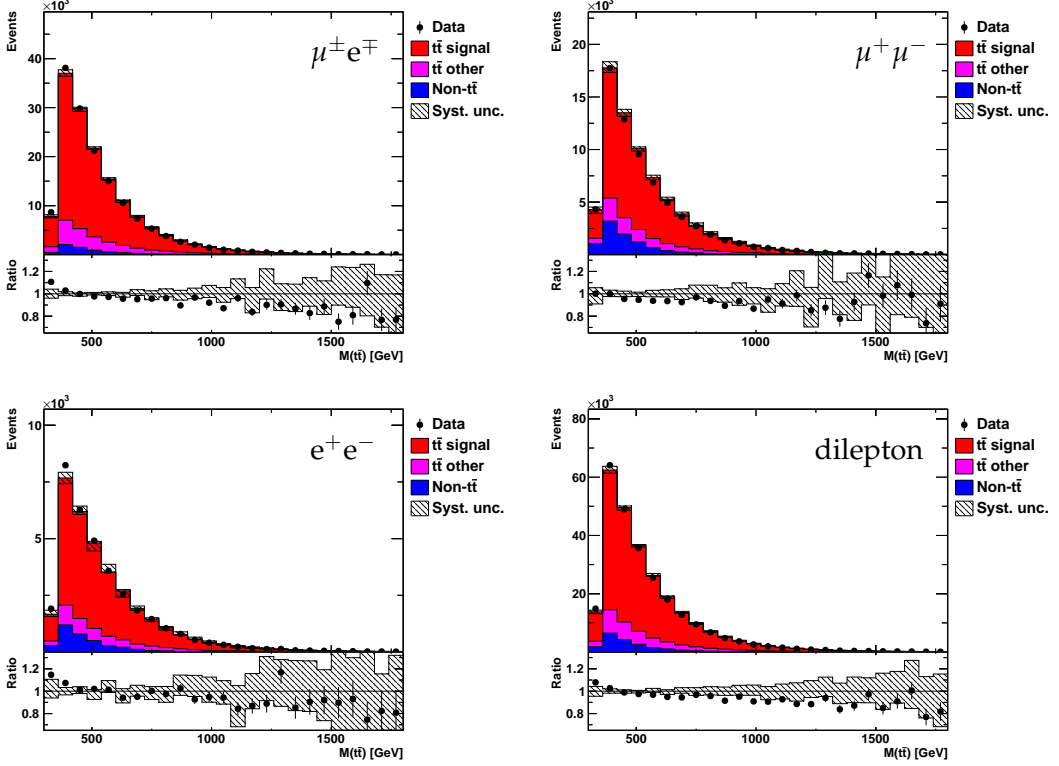


Figure 19: Distribution of $t\bar{t}$ invariant mass in the $\mu^\pm e^\mp$ (top left), $\mu^+ \mu^-$ (top right) $e^+ e^-$ (bottom left) and dilepton (bottom right) decay channels.

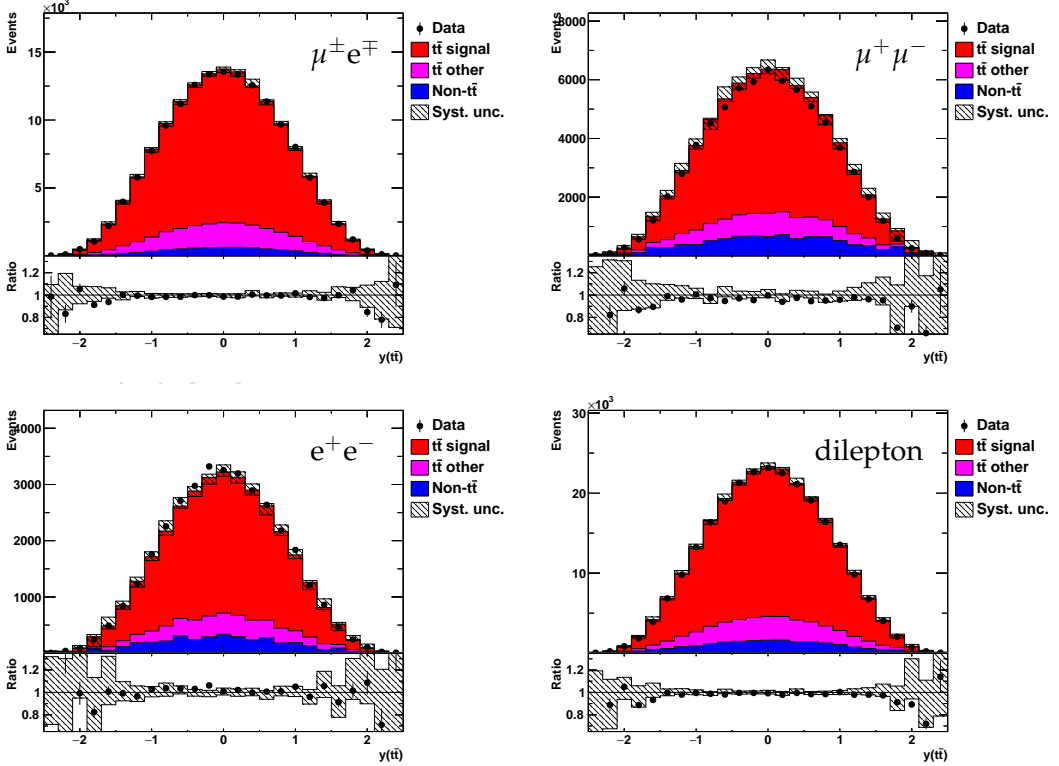


Figure 20: Distribution of $t\bar{t}$ rapidity in the $\mu^\pm e^\mp$ (top left), $\mu^+ \mu^-$ (top right) $e^+ e^-$ (bottom left) and dilepton (bottom right) decay channels.

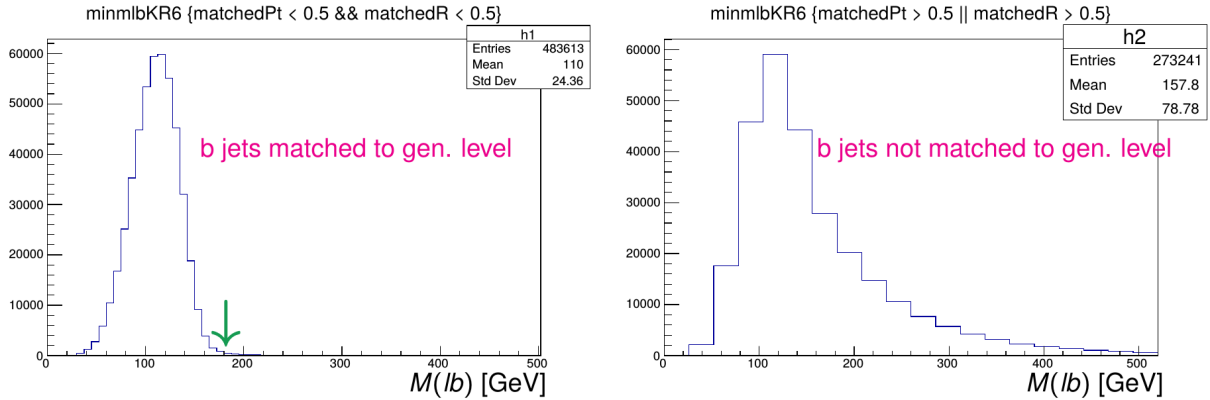


Figure 21: The M_{lb} distribution for jets matched to the true-level b jets (left) and not matched (right). The cut $M_{lb} < 180$ GeV is indicated.

404 As input for kinematic reconstruction, the algorithm uses the lepton pair, E_T^{miss} , and two b jets.
 405 While there is no ambiguity for the leptons, since there is only one lepton pair selected in the
 406 event (see Section 3.3), the two jets are selected in the following way:

- 407 1. only jets which satisfy $M_{lb} < 180$ GeV are considered,
- 408 2. b tagged jets are preferred over not b tagged jets,
- 409 3. in the same b tag category, jets are ranked in p_T .

410 The M_{lb} variable is determined for each pair of jets in the following way:

- 411 1. for each of two possible lepton and jet assignments, maximum $M(lb)$ of the two decay
 412 ‘legs’ (arising from the decays of top quark and top antiquark) are taken,
- 413 2. minimum $M(lb)$ over two jet-lepton assignments is taken.

414 Figure 21 presents the M_{lb} distribution for jets matched to the true-level b jets (left) and not
 415 matched (right). The requirement $M_{lb} > 180$ GeV rejects significant fraction of jets and thus
 416 rejects non-tt background and improves the performance of kinematic reconstruction consid-
 417 erably.

418 The transverse momenta of $\nu\bar{\nu}$ are set to E_T^{miss} , while the unknown longitudinal momentum and
 419 energy of $\nu\bar{\nu}$ are set to the longitudinal momentum and energy of the lepton pair. Additional
 420 requirements on the invariant mass of the neutrino pair $M(\nu\bar{\nu}) \geq 0$ and on the invariant mass
 421 of the W bosons $M(W^+W^-) \geq 2M_W$ are applied. The algorithm proceeds as follows:

- 422 1. set $(\nu\bar{\nu})_{X,Y} = (E_T^{\text{miss}})_{X,Y}$,
- 423 2. if $p_T(\nu\bar{\nu}) < E(l\bar{l})$, then set $(\nu\bar{\nu})_Z = (l\bar{l})_Z$, otherwise set $(\nu\bar{\nu})_Z = 0$,
- 424 3. if $p(\nu\bar{\nu}) < E(l\bar{l})$, then set $E(\nu\bar{\nu}) = E(l\bar{l})$, otherwise set $E(\nu\bar{\nu}) = p(\nu\bar{\nu})$,
- 425 4. the four-momentum of $l\bar{l}\nu\bar{\nu}$ is calculated as $l\bar{l}\nu\bar{\nu} = l + \bar{l} + \nu + \bar{\nu}$,
- 426 5. if $M(l\bar{l}\nu\bar{\nu}) < 2M_W$ where $M_W = 80.4$ GeV, then $l\bar{l}\nu\bar{\nu}$ is parametrised in terms of p_X, p_Y, y, M ,
 427 and M is set to $M(l\bar{l}\nu\bar{\nu}) = 2M_W$,

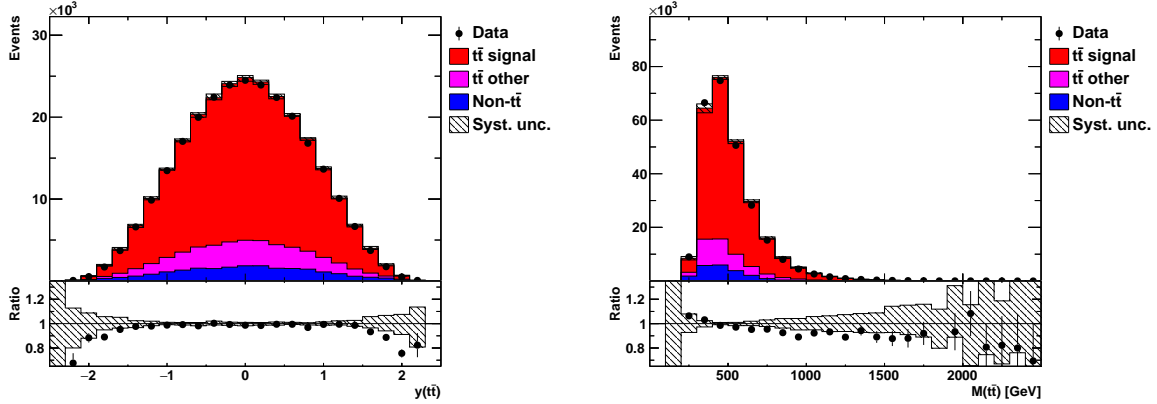


Figure 22: Distributions of $y(\bar{t}t)$ (right) and $M(\bar{t}t)$ (left) in selected events after the loose kinematic reconstruction.

428 6. the four-momentum of $\bar{t}t$ is calculated as $\bar{t}t = l\bar{l}\nu\bar{\nu} + b + \bar{b}$.

429 The additional requirements $M(\nu\bar{\nu}) \geq 0$ and $M(W^+W^-) \geq 2M_W$ have only minor effect on
430 the performance of the reconstruction. Notice that this algorithm reconstructs only the sum
431 $\nu\bar{\nu} = \nu + \bar{\nu}$ but not ν and $\bar{\nu}$ separately. Hence it reconstructs only $\bar{t}t$ but not the top quark
432 and antiquark and can be used to measure $\bar{t}t$ kinematic variables only, but not e.g. $p_T(t)$. In
433 this analysis, the loose kinematic reconstruction is used to measure triple-differential cross sec-
434 tions as a function of $M(\bar{t}t)$, $y(\bar{t}t)$ and extra jet multiplicity which are exploited to extract QCD
435 parameters and PDFs.

436 Figure 22 shows the distributions of the reconstructed $\bar{t}t$ invariant mass and rapidity using the
437 loose kinematic reconstruction. These distributinos are similar to the one obtained using the
438 full kinematic reconstruction (see Figs. 20, 19), and the data are reasonably well described by
439 the simulation within uncertainties.

440 4.3 Comparison of full and loose kinematic reconstruction

441 For benchmarking the following kinematic reconstruction algorithms are considered:

- 442 1. full kinematic reconstruction described in Section 4.1,
- 443 2. an algorithm which uses visible objects only, i.e. $\bar{t}t = l + \bar{l} + b + \bar{b} + E_T^{\text{miss}}$,
- 444 3. loose kinematic reconstruction described in Section 4.2.

445 Figure 23 show sensitivity of $M(\bar{t}t)$ distributions at generator and detector level to m_t . At gen-
446 erator level, this sensitivity is largest at low $M(\bar{t}t)$ where $M(\bar{t}t) \approx 2m_t^{\text{pole}}$, while the effect is
447 propagated to a higher $M(\bar{t}t)$ because of normalisation of the distribution. The detector level
448 distribution obtained using full kinematic reconstruction has little sensitivity to m_t (cf. the sen-
449 sitivity of generator level $M(\bar{t}t)$), instead it is sensitive to the top quark mass parameter used in
450 the reconstruction (top and antitop quark mass constraints). However, the $M(\bar{t}t)$ distributions
451 obtained using visible objects and loose kinematic reconstruction have significant sensitivity to
452 $M(\bar{t}t)$ (though smaller than $M(\bar{t}t)$ at generator level because of the detector smearing effects).
453 Therefore for the cross section measurement, after unfolding to generator level, the $M(\bar{t}t)$ cross
454 section obtained using the full kinematic reconstruction is expected to be biased towards the
455 generator-level $M(\bar{t}t)$ cross section.

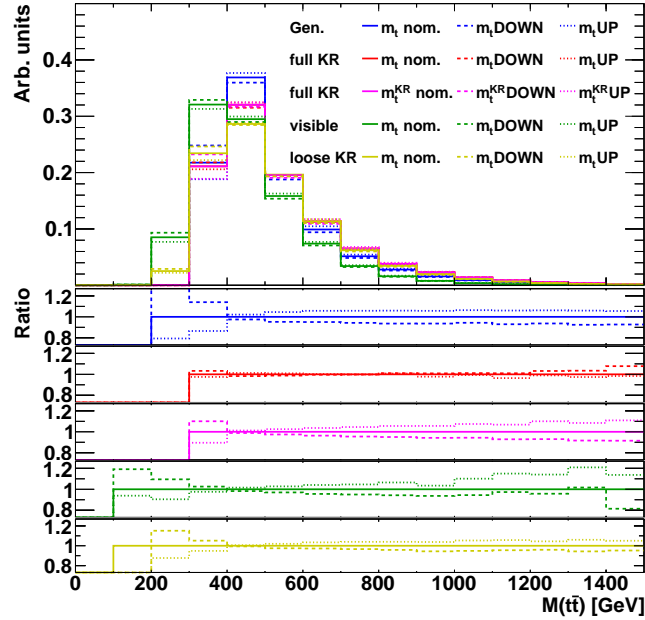


Figure 23: Distributions of $M(t\bar{t})$ at generator level and at detector level obtained using different kinematic reconstruction algorithms: full kinematic reconstruction ('full KR'), using visible decay objects only ('visible') and loose kinematic reconstruction ('loose KR'). The $M(t\bar{t})$ distributions are shown using nominal $m_t = 172.5$ GeV (m_t nom.) and variations $m_t = 173.5$ GeV (m_t UP), $m_t = 171.5$ GeV (m_t DOWN). For the full kinematic reconstruction, also the $M(t\bar{t})$ distributions obtained using the varied m_t parameters in the kinematic reconstruction are shown (m_t^{KR} UP for $m_t = 173.5$ GeV and m_t^{KR} DOWN for $m_t = 171.5$ GeV). The bottom panels show the ratios of $M(t\bar{t})$ distributions over the nominal ones.

456 Figures 24 and 25 show resolution of $M(t\bar{t})$ and $y(t\bar{t})$ distributions obtained at detector level
 457 using different kinematic reconstruction algorithms. It is presented as $M(t\bar{t})$ ($y(t\bar{t})$) at detector
 458 level vs the same quantity at generator level, and as the difference between $M(t\bar{t})$ ($y(t\bar{t})$) at
 459 generator and detector level in bins of the generator level quantity. The mean and RMS of the
 460 difference between $M(t\bar{t})$ ($y(t\bar{t})$) at generator and detector level are shown in Fig. 26. Similar
 461 results are obtained for the full and loose algorithms, while the visible reconstruction performs
 462 worse, as expected.² Note that the mean and RMS defined in this way reflects not only the gen-
 463 uine resolution of the algorithm, but they are affected also by the possible usage of wrong input
 464 jets and/or wrong jet to lepton assignment. The different kinematic reconstruction algorithms
 465 may use different b jets in the same events. The importance of input b jets selection is shown in
 466 Fig. 27, where also the performance of a loose kinematic reconstruction without $M(lb) < 180$
 467 GeV cut is shown. The cut on $M(lb)$ improves the resolution of loose kinematic reconstruction
 468 considerably, making it similar to the resolution of full kinematic reconstruction. The fractions
 469 of events with correct input b jets (matched to generator level b jets) were estimated using the
 470 nominal signal MC simulations and are given in Table 8. In addition, Fig. 28 shows resolution
 471 of $p_T(t)$, $y(t\bar{t})$, and $p_T(t\bar{t})$ distributions obtained using the full kinematic reconstruction, while
 472 the mean and RMS distributions are shown in Fig. 29.

473 4.4 Comparison of sensitivity of measured cross section to m_t

474 The impact of MC m_t on the generator and detector level $M(t\bar{t})$ distributions, and the mea-
 475 sured cross section as a function of $M(t\bar{t})$ is shown in Fig. 30. The cross sections are determined
 476 as described further in Section 6. A strong sensitivity of the measured cross sections to m_t is

²While the visible algorithm provides smallest RMS of $M(t\bar{t})$, $y(t\bar{t})$, at the same time their mean values are much larger, i.e. the reconstructed values are significantly biased).

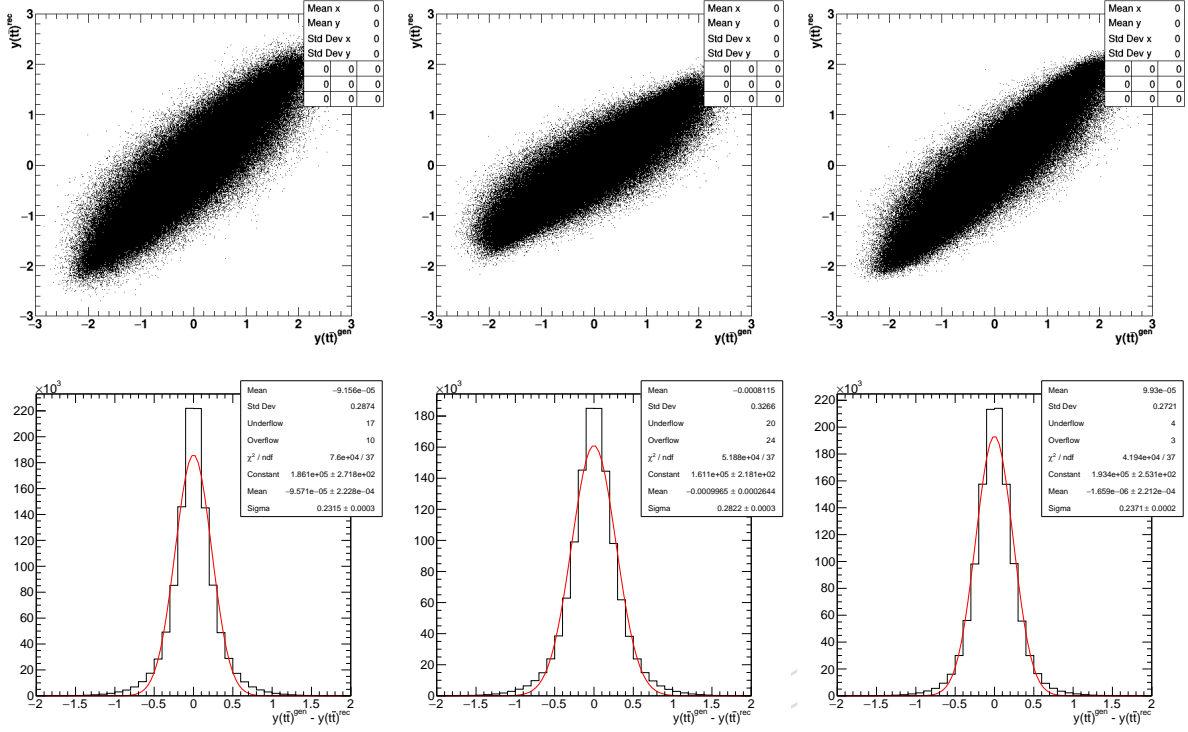


Figure 24: Top: $y(t\bar{t})$ at generator and detector level obtained using full (left), visible (middle) and loose (right) kinematic reconstruction. Bottom: the difference between $y(t\bar{t})$ at generator and detector level in bins of generator level $y(t\bar{t})$ (fitted with a Gaussian function for illustration).

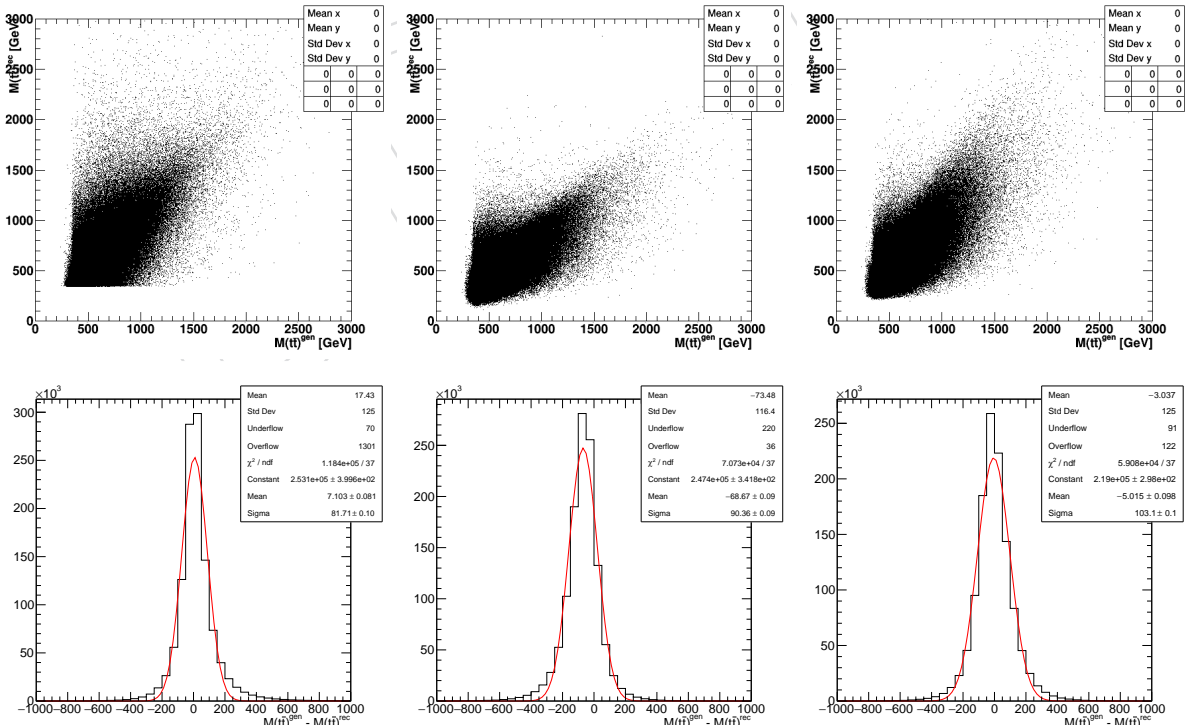


Figure 25: Top: $M(t\bar{t})$ at generator and detector level obtained using full (left), visible (middle) and loose (right) kinematic reconstruction. Bottom: the difference between $M(t\bar{t})$ at generator and detector level in bins of generator level $y(t\bar{t})$ (fitted with a Gaussian function for illustration).

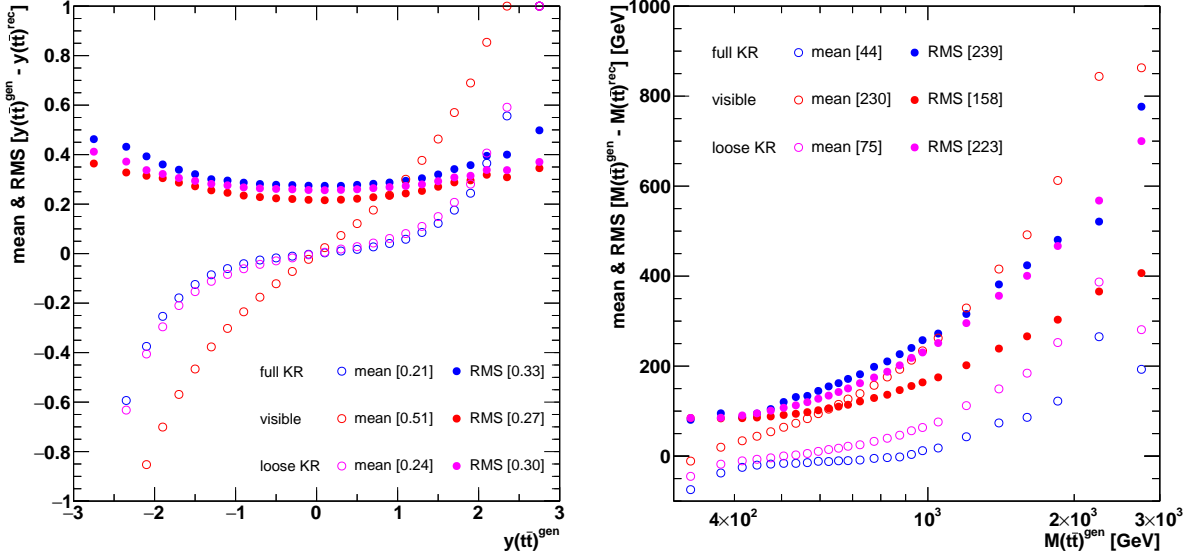


Figure 26: The mean and RMS of the difference between $y(t\bar{t})$ (left) and $M(t\bar{t})$ (right) at generator and detector level obtained using the full, visible and loose kinematic reconstruction algorithms. For the mean and RMS, their average values are given in brackets.

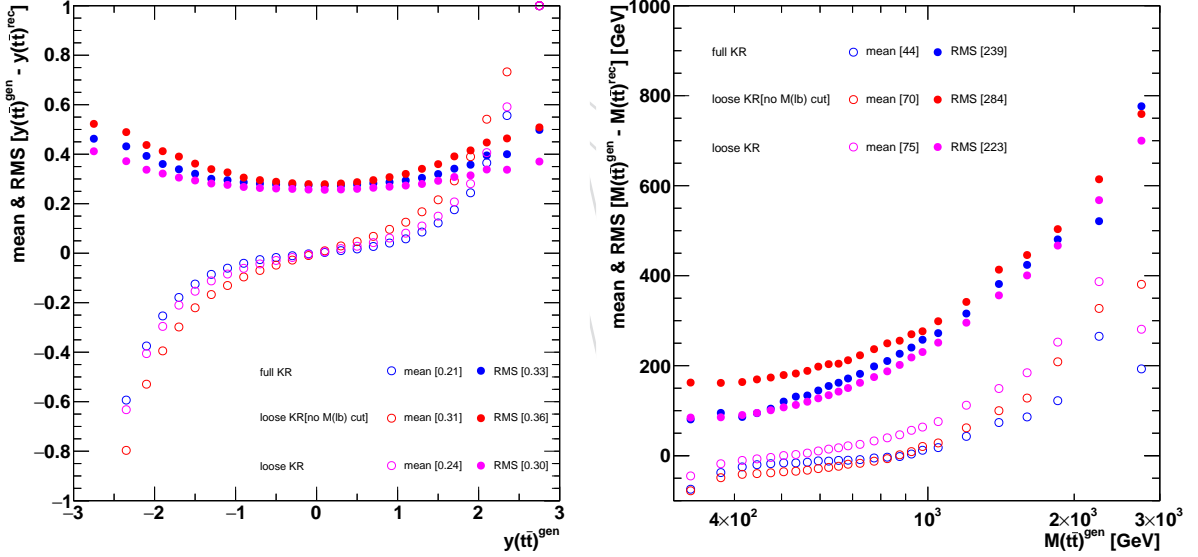


Figure 27: The mean and RMS of the difference between $y(t\bar{t})$ (left) and $M(t\bar{t})$ (right) at generator and detector level obtained using the full and loose kinematic reconstruction algorithms, as well as the loose reconstruction without the $M(lb) < 180$ GeV cut. For the mean and RMS, their average values are given in brackets.

Table 8: The fractions of events with correct input b jets (matched to generator level b jets) estimated using the nominal signal MC. As matching criteria, the difference between generator and reconstructed level jets in p_T is required $\frac{|p_T^{\text{gen}} - p_T^{\text{rec}}|}{p_T^{\text{gen}}} < 0.5$ and $\Delta R = \sqrt{\Delta\eta^2 + \Delta\phi^2}$ separation $|\Delta R^{\text{gen}} - \Delta R^{\text{rec}}| < 0.5$.

algorithm	correct $t\bar{t}$	correct t and \bar{t}
full KR	0.80	0.70
loose KR	0.69	n/a

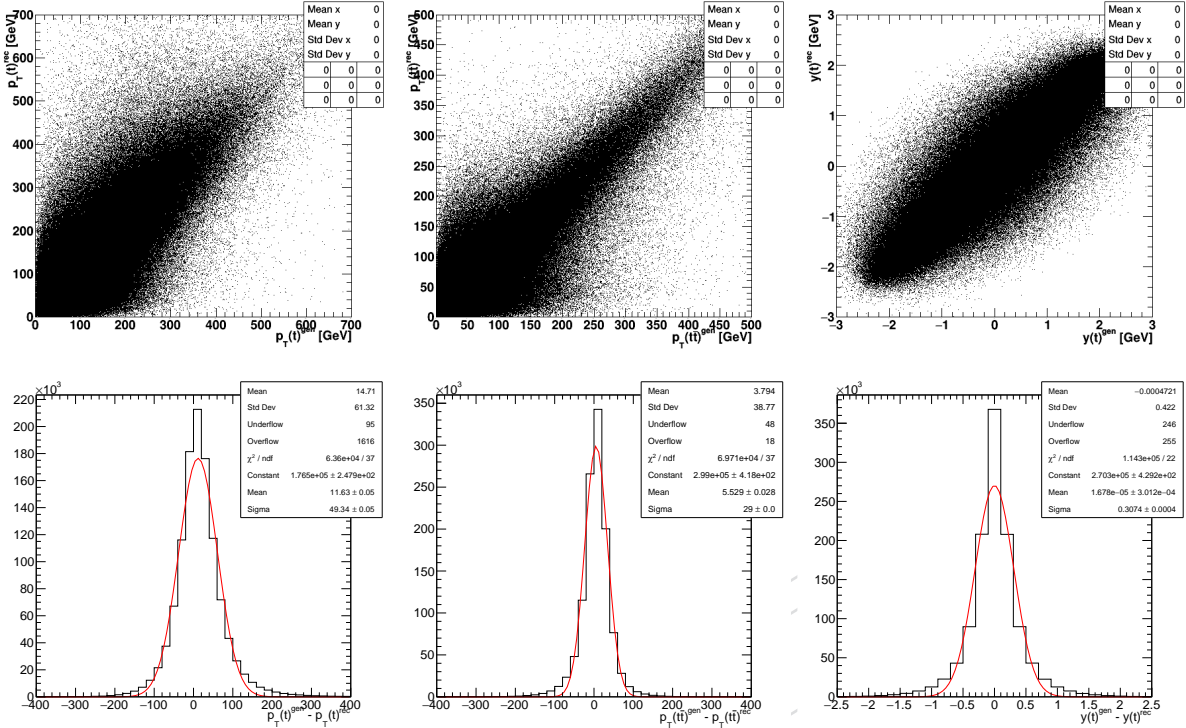


Figure 28: Top: $p_T(t)$ (left), $p_T(t\bar{t})$ (middle) and $y(t)$ (right) at generator and detector level obtained using full kinematic reconstruction. Bottom: the difference between these quantities at generator and detector level in bins of generator level quantities (fitted with a Gaussian function for illustration).

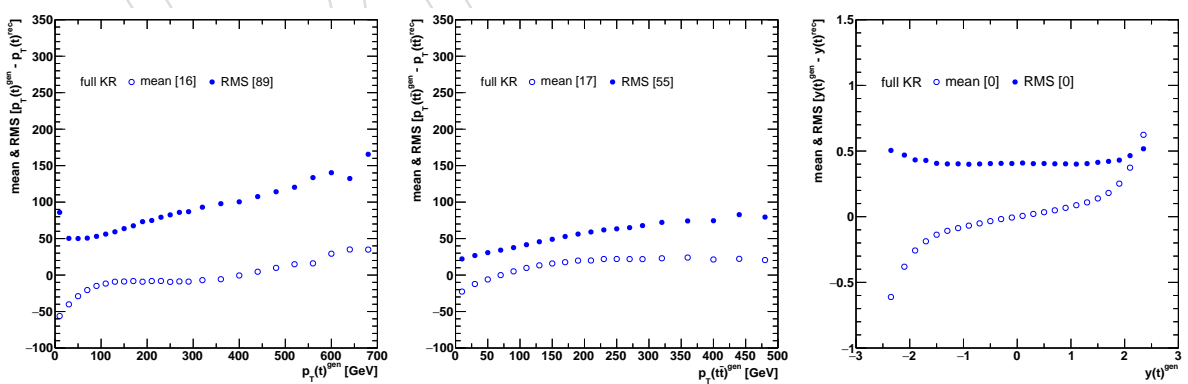


Figure 29: The mean and RMS of the difference between $p_T(t)$ (left), $p_T(t\bar{t})$ (middle) and $y(t)$ (right) at generator and detector level obtained using the full kinematic reconstruction. For the mean and RMS, their average values are given in brackets.

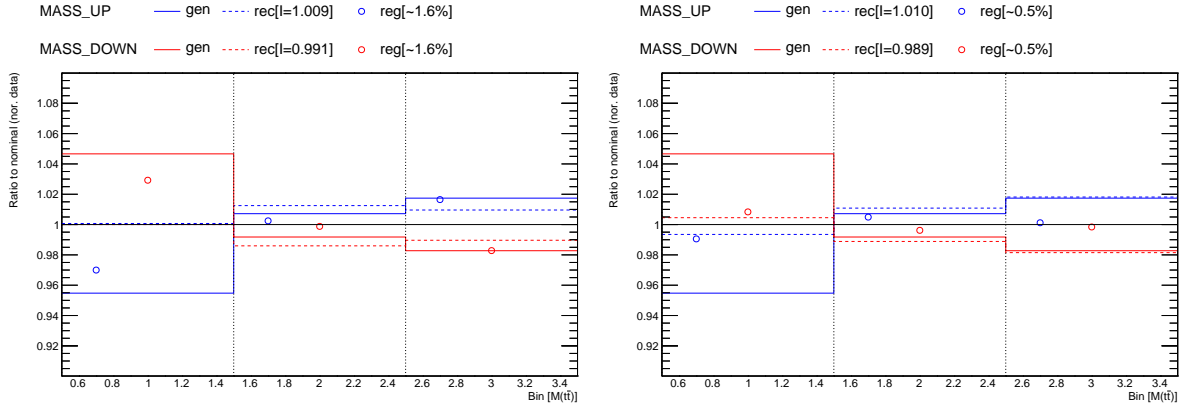


Figure 30: The impact of MC m_t variation by ± 1 GeV ('gen'), reconstructed level ('rec') and measured cross-section ('reg', for the regularised unfolding) as obtained using the full kinematic reconstruction (left) and loose kinematic reconstruction (right). For each variation, the average effect is reported in brackets. At true level, the distributions with m_t variations are normalised to the cross section of the nominal MC.

477 observed when using the full kinematic reconstruction (see also Appendix C), while it is neg-
478 ligible when using the loose kinematic reconstruction³. This justifies that the loose kinematic
479 reconstruction is preferable for the cross section measurement which is further used to extract
480 m_t . In this analysis, the loose kinematic reconstruction algorithm is employed to measure the
481 triple-differential cross section as a function of $M(t\bar{t})$, $y(t\bar{t})$ and N_{jet} , while the full kinematic
482 reconstruction is used for all other measured cross sections.

483 4.5 Selection of extra jets

484 In this analysis the $t\bar{t}$ production cross section is measured besides as a function of the extra
485 jet multiplicity, N_{jet} . Extra jets (also referred to as additional jets) are jets produced in the hard
486 scattering process but not originated from decays of the top quarks, thus they probe hard QCD
487 radiation. At reconstruction level the extra jets are defined in dilepton $t\bar{t}$ events as jets with
488 $p_T > 30 \text{ GeV}$, $|\eta| < 2.4$ reconstructed as described in Section 3.4 which are further required
489 to be isolated from the charged leptons and b jets originating from the top quark decays by
490 $\Delta R \equiv \sqrt{(\Delta\eta)^2 + (\Delta\phi)^2} > 0.4$, where $\Delta\eta = \eta_j - \eta_{l,b}$ and $\Delta\phi = \phi_j - \phi_{l,b}$ are the pseudorapidity
491 and azimuthal angle of the extra jets and charged leptons or b quarks, respectively. At generator
492 level the extra jets are defined as jets with $p_T > 30 \text{ GeV}$, $|\eta| < 2.4$ built of particles except
493 neutrinos and isolated from the charged leptons and b quarks originating from the top quark
494 decays by the same ΔR cut. The charged leptons and b quarks are taken directly after W and
495 top quark decays, respectively. Such definition of the extra jets provides a proxy to jets arising
496 primarily from hard QCD radiation and not from the top quark decays. Figure 31 shows the
497 distribution of the extra jet multiplicity. A good description of the data by the simulation is
498 observed within uncertainties, while the central MC prediction overestimates event rates with
499 high N_{jet} . Figure 32 shows resolution and mean and RMS of the N_{jet} distribution.

To compare the measured cross sections to the fixed-order QCD calculations, the latter cross sections involving the extra jet multiplicity are further corrected from parton to particle level. The fixed-order QCD calculations are provided for parton-level jets and stable top quarks, therefore the corrections (further referred to as non-perturbative, NP) are determined using

³Note that a small sensitivity of the measured $M(t\bar{t})$ cross section to m_t is expected when extrapolating to the full phase space because of the dependence of kinematic acceptance on m_t due to the cuts applied on the $t\bar{t}$ decay products.

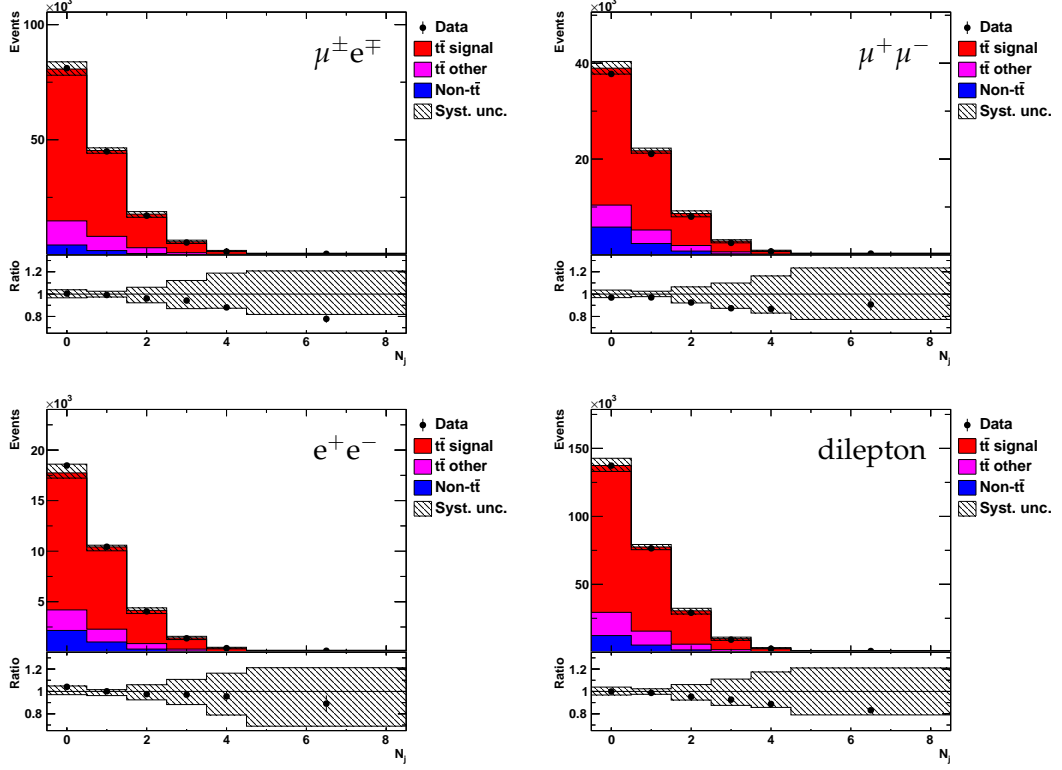


Figure 31: Distribution of extra jet multiplicity in $\mu^\pm e^\mp$ (top left), $\mu^+ \mu^-$ (top right) $e^+ e^-$ (bottom left) and dilepton (bottom right) decay channels.

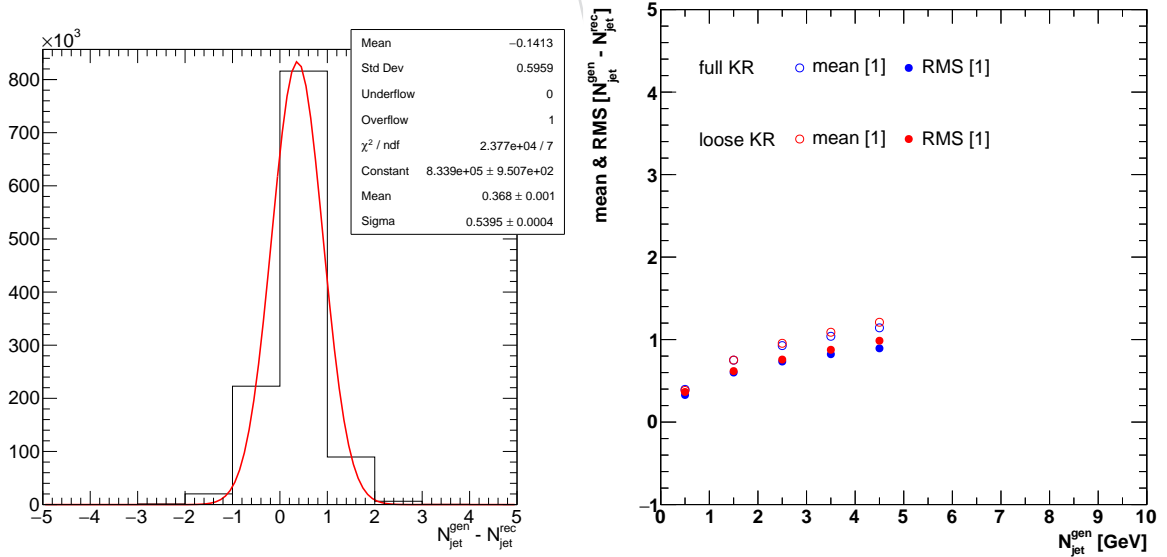


Figure 32: Top: the difference between N_{jet} at generator and detector level in bins of generator level quantity. Bottom: the mean and RMS of the difference between N_{jet} at generator and detector level.

the MC simulations with and without multiparton interactions (MPI), hadronisation and top quark decays, and defined as:

$$\mathcal{C}_{\text{NP}} = \frac{\sigma_{\text{isolated from } t \rightarrow l,b}^{\text{particle}}}{\sigma_{\text{no MPI, no had., no } t\bar{t} \text{ decays}}^{\text{parton}}}. \quad (4)$$

Here $\sigma_{\text{isolated from } t \rightarrow l,b}^{\text{particle}}$ is the cross section for jets built of particles excluding neutrinos and isolated from the charged leptons and b quarks from the top quark decays, and $\sigma_{\text{no MPI, no had., no } t\bar{t} \text{ decays}}^{\text{parton}}$ is the cross section for jets built of partons excluding t and \bar{t} . The \mathcal{C}_{NP} is used to multiply the NLO predictions to correct them to particle level. This correction can be thought as consisting of three factors: the correction for MPI, hadronisation and top quark decays, denoted as \mathcal{C}_{MPI} , \mathcal{C}_{had} and $\mathcal{C}_{\text{decays}}$, respectively:

$$\begin{aligned} \mathcal{C}_{\text{NP}} &\approx \mathcal{C}_{\text{MPI}} \mathcal{C}_{\text{had}} \mathcal{C}_{\text{decays}} \\ \mathcal{C}_{\text{MPI}} &= \frac{\sigma_{\text{isolated from } t \rightarrow l,b}^{\text{particle}}}{\sigma_{\text{no MPI, isolated from } t \rightarrow l,b}^{\text{particle}}}, \\ \mathcal{C}_{\text{had}} &= \frac{\sigma_{\text{isolated from } t \rightarrow l,b}^{\text{particle}}}{\sigma_{\text{no had., isolated from } t \rightarrow l,b}^{\text{parton}}}, \\ \mathcal{C}_{\text{decays}} &= \frac{\sigma_{\text{no MPI, no had., isolated from } t \rightarrow l,b}^{\text{parton}}}{\sigma_{\text{no MPI, no had., no } t\bar{t} \text{ decay}}^{\text{parton}}}. \end{aligned} \quad (5)$$

500 The NP corrections and their different components are shown in Fig. 33 for the cross section as
 501 a function of N_{jet} , $M(t\bar{t})$ and $y(t\bar{t})$. They are mostly independent of $M(t\bar{t})$ and $y(t\bar{t})$ and changes
 502 only with varying N_{jet} . The MPI increases N_{jet} because of extra particles in the final state, while
 503 hadronisation reduces N_{jet} because of out-of-cone effects, such that these two effects cancel to
 504 some extent. In the kinematic region of this analysis, the NP corrections are small. For the two
 505 N_{jet} bins, \mathcal{C}_{NP} and its components does not exceed 5%. For the three N_{jet} bins, \mathcal{C}_{NP} is within 5%,
 506 while its different components are within 10%.

507 The dependence of the NP corrections on MC modelling was studied by using MC samples
 508 with the varied hadronisation model and underlying event tune as detailed in Section 5.2. The
 509 results are shown in Fig. 34 for the N_{jet} cross sections (as for the nominal NP corrections, no
 510 dependence on $M(t\bar{t})$ and $y(t\bar{t})$ was observed). In addition, a possible dependence of the NP
 511 corrections on ISR, FSR scales and ME-PS scale was studied (Fig. 35), and on the factorisa-
 512 tion and renormalisation scales (Fig. 36). All these variations follow the description of model
 513 systematic uncertainties given in Section 5. All variations are negligible ($\lesssim 1\%$), therefore no
 514 uncertainties on the determined NP corrections are assigned.

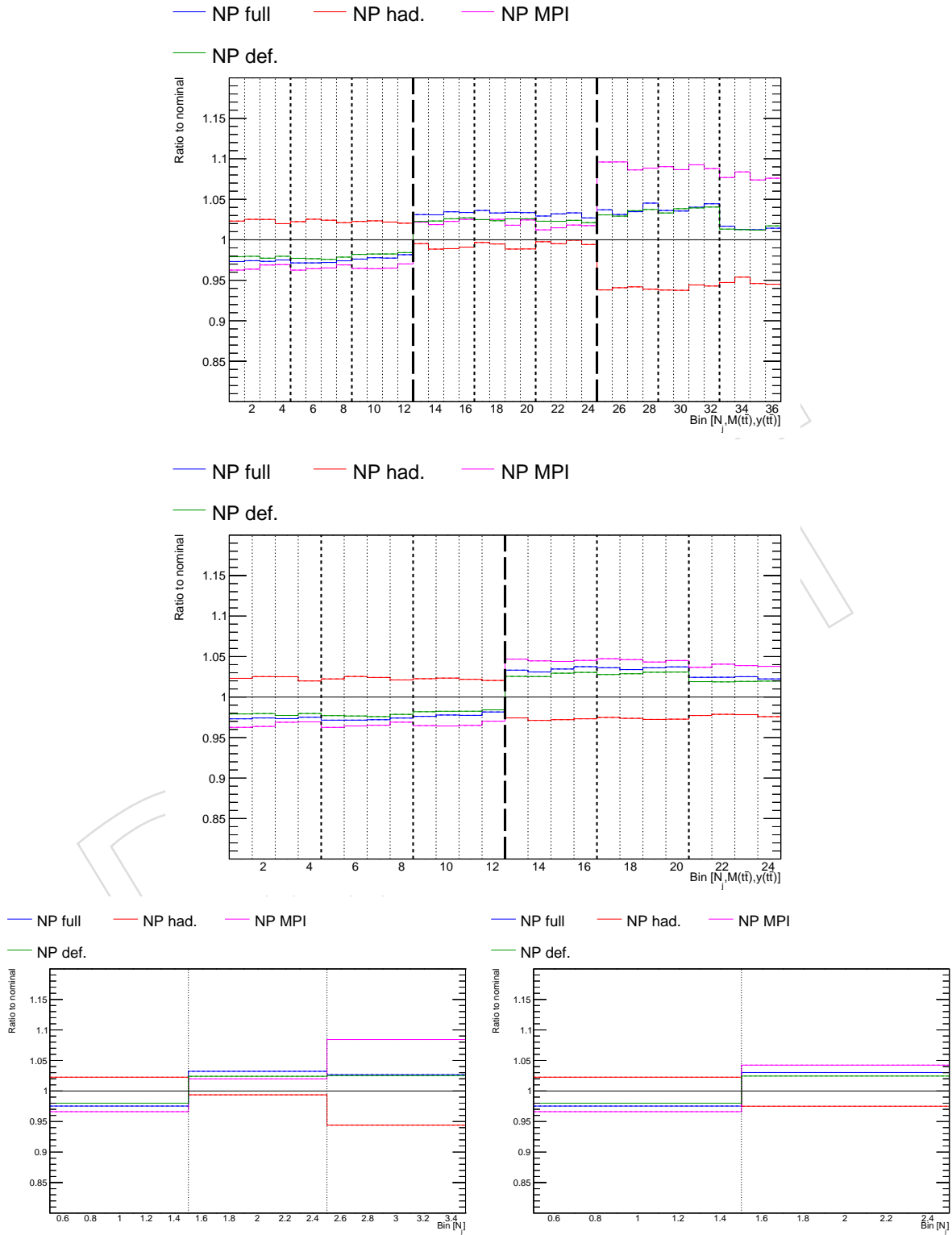


Figure 33: The NP corrections for the $[N_{\text{jet}}, M(t\bar{t}), y(t\bar{t})]$ cross sections with 3 (top) and 2 (middle) N_{jet} bins, and for the N_{jet} cross sections (bottom) with the same numbers of bins.

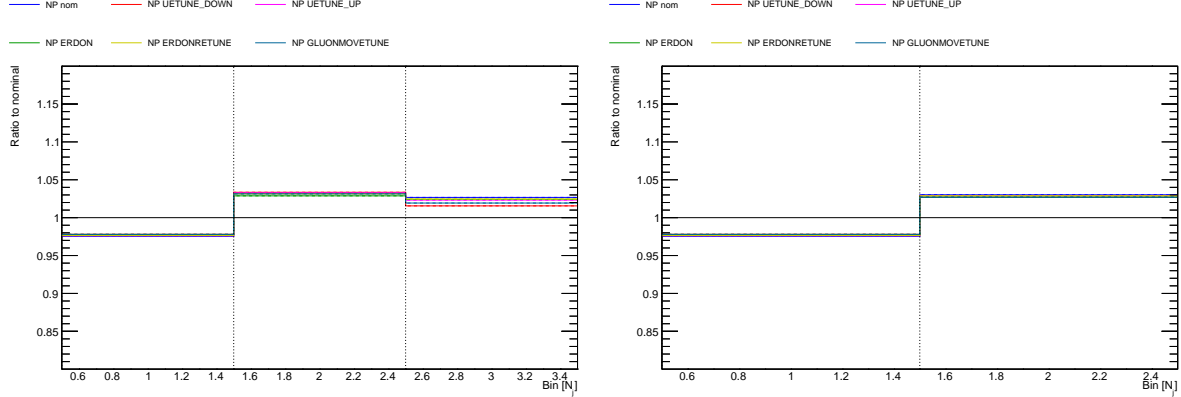


Figure 34: The variations of NP corrections due to the hadronisation model and underlying event tune for the N_{jet} cross sections with 3 (left) and 2 (right) N_{jet} bins.

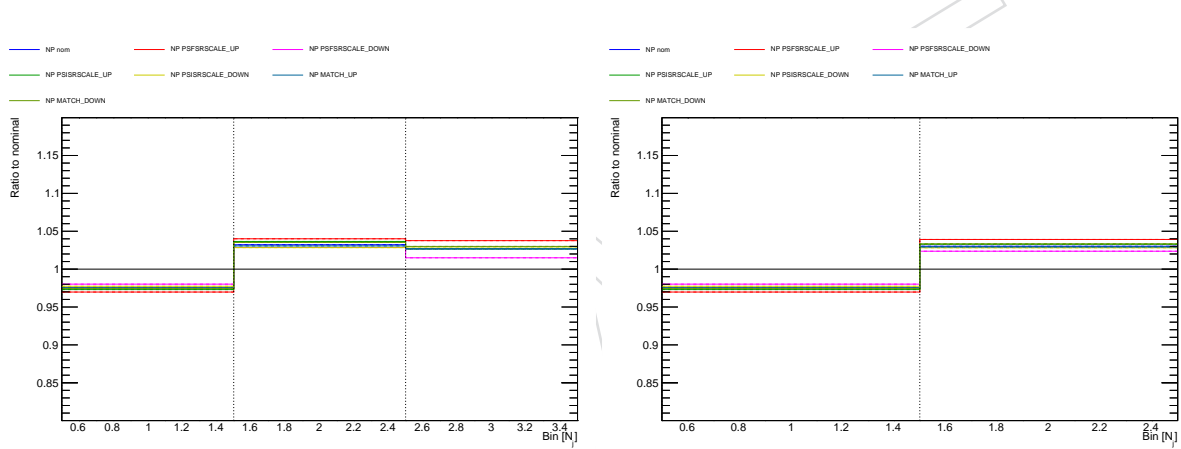


Figure 35: The variations of NP corrections due to the ISR, FSR and ME-PS scale variations for the N_{jet} cross sections with 3 (left) and 2 (right) N_{jet} bins.

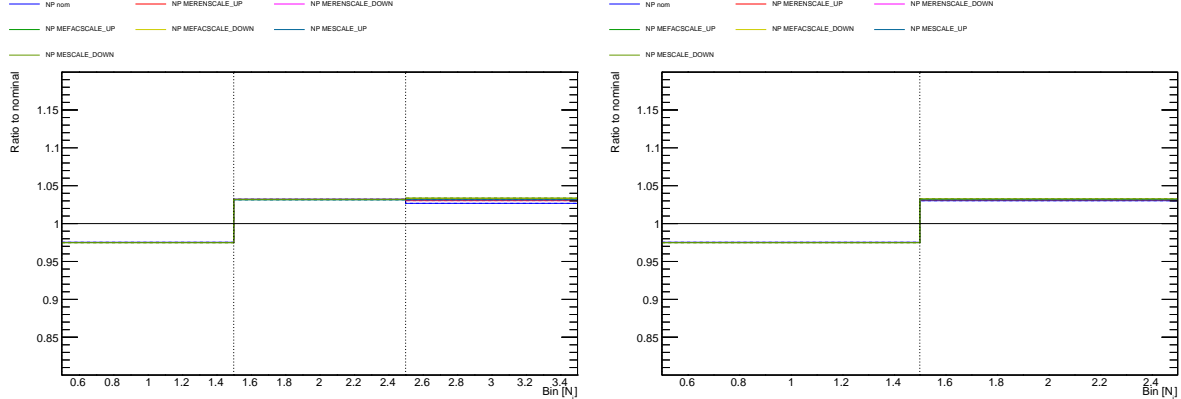


Figure 36: The variations of NP corrections due to the factorisation and renormalisation scale variations for the N_{jet} cross sections with 3 (left) and 2 (right) N_{jet} bins.

5 Scaling factors and systematic uncertainties

Scale factors $SF = \frac{\epsilon_{data}}{\epsilon_{MC}}$ are used where necessary to optimize the description of the data by the simulation. The scaling factors are generally applied as event weights to the simulation, unless stated differently. The measurement is affected by systematic uncertainties that originate from detector effects and from the modelling of the processes. Each source of systematic uncertainty is assessed individually by changing in the simulation the corresponding efficiency, resolution, or scale by its uncertainty. For each change made, the cross section determination is repeated, and the difference with respect to the nominal result in each bin is taken as the systematic uncertainty. Often experimental systematic uncertainties are evaluated by varying the scale factors within their uncertainties. In the following, the scale factors and systematic uncertainties are discussed in detail.

5.1 Experimental uncertainties

Trigger efficiency

The trigger efficiency is measured as a function of the lepton η using triggers that are only weakly correlated to the dilepton triggers (E_T^{miss} -based triggers), as described in Refs. [56, 57]. The trigger efficiency measured in data is then used to correct the MC predictions. Details on the trigger efficiency and its uncertainty can be found in [58].

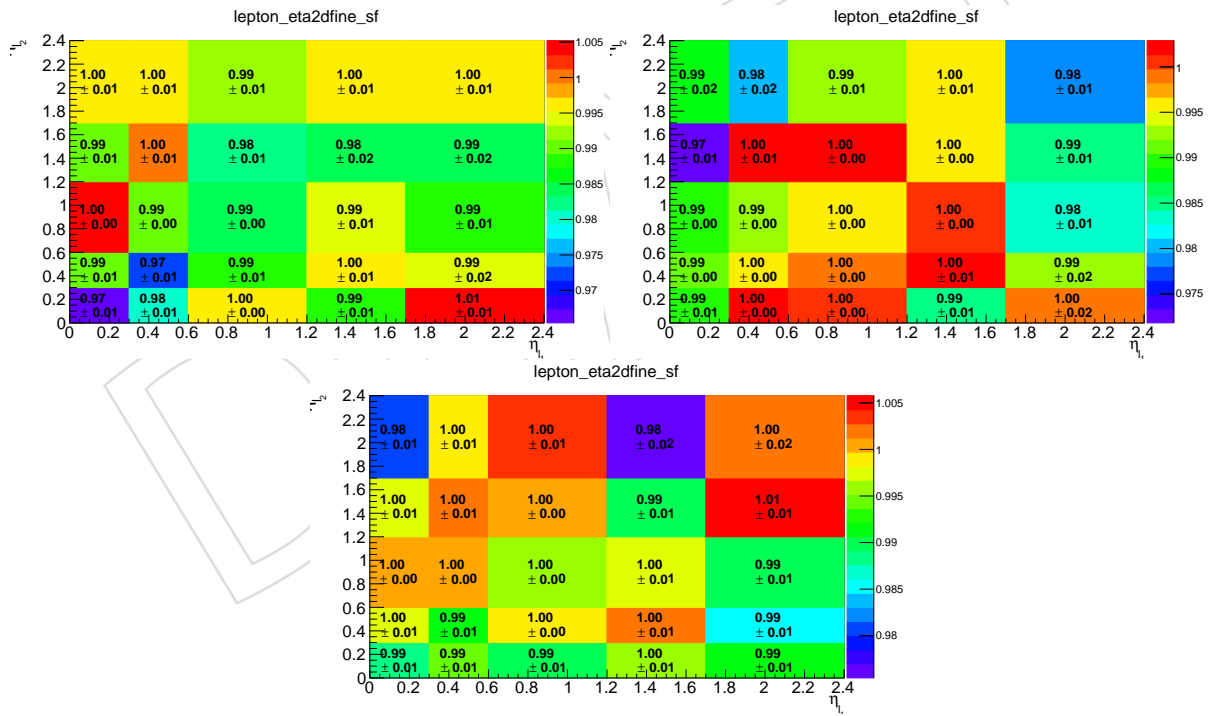


Figure 37: The trigger scale factors are measured differentially as a function of η for both leptons as is shown for e^+e^- (top left), $\mu^+\mu^-$ (top right) and $\mu^\pm e^\mp$ (bottom) channels. The results correspond to an integrated luminosity of 35.9 fb^{-1} . The given uncertainties correspond to the statistical uncertainty added in quadratures to the additional 0.3% systematic uncertainty on the measured value.

The trigger scale factors are measured differentially as a function of η for both leptons in the bins as shown in Figure 37. The measured scale factors are typically close to unity across all

535 bins.

536 For the estimation of the related uncertainties, two types of variations are considered. In first
 537 case, the scale factors are varied accordingly to their uncertainties as they are provided, which
 538 mostly affects the change in total rates with respect to nominal simulation. The second type of
 539 variation is an ad-hoc shape variation, when the scale factors are varied by the corresponding
 540 uncertainty antagonistically depending on the η of both leptons. The “up” variation is done in
 541 order to mimic a shape variation in the following way:

- 542 • lepton-1 in barrel, lepton-2 in barrel : $\varepsilon + 1.0 \cdot \sigma$
- 543 • lepton-1 in barrel, lepton-2 in endcap : $\varepsilon + 0.5 \cdot \sigma$
- 544 • lepton-1 in endcap, lepton-2 in barrel : $\varepsilon + 0.5 \cdot \sigma$
- 545 • lepton-1 in endcap, lepton-2 in endcap : $\varepsilon - 1.0 \cdot \sigma,$

546 where ε denotes trigger efficiency measured in the corresponding bin and σ corresponds to its
 547 total uncertainty as given in Figure 37. The “down” variation is performed in similar way, but
 548 multiplying coefficients before σ used for “up” variation by factor of “-1”.

549 Lepton selection

550 The identification and isolation efficiencies for muons or electrons are estimated using the “tag-
 551 and-probe” method with Z boson event samples as a function of p_T and η , as provided by the
 552 Muon and EGamma POGs (in this analysis, only for electrons, the id component is recalculated
 553 with a finer binning using the tools and recipes recommended by the EGamma POG for 2016)
 554 and as shown in Figure 38, and are found to be above 95% in all bins of the measurement for
 555 the muons, while efficiency scale factors for the electrons are mainly between 0.9 – 1.1 values.
 556 The muon efficiency is well described in the simulation, i.e. with residual scale factors being
 557 very close to unity.

558 b-Tagging

559 The data-to-simulation scale factors (SF_{BTV}) for the b-tagging efficiency of individual b-jets, c-
 560 jets and light-(l) jets (typically referred to as *mistag rate* for c- and l -jets) are measured by the
 561 BTV group [47] using muon-jet data samples. Further in the text of this section, the *BTV* sub-
 562 index is omitted. The SF are parameterized as a function of the jet p_T and η . For the CSVv2L
 563 tagger used in this analysis, the SF for b flavour jets is found to be between 0.92 and 1.00 with
 564 an error of up to 0.04% in the $p_T = 30\text{--}670\,\text{GeV}$ and $|\eta| < 2.4$ ranges.

565 The individual b-tagging efficiency (ϵ_{MC}) of b-jets, and mistag rate for c- and l -jets, is deter-
 566 mined from simulation. It does not only depend on the jet kinematic properties, but also on the
 567 analysis specific details. Results for this analysis are shown in Figure 39 as a function of the jet
 568 flavour, jet p_T and jet η .

569 The determination of the b-tagging uncertainty follows the recommendations of the BTV group,
 570 Ref. [59]. The variation of the scale factor depends also in the flavour of the original parton
 571 which originates the jet. The heavy flavour (b and c) jets are considered fully correlated, while
 572 the light jets fully uncorrelated to the b-jets.

573 Kinematic reconstruction efficiency

574 The kinematic reconstruction algorithm used to reconstruct the properties of the top quarks
 575 has been described in Section 4. For a fraction of events (about 9%) no physical result is found

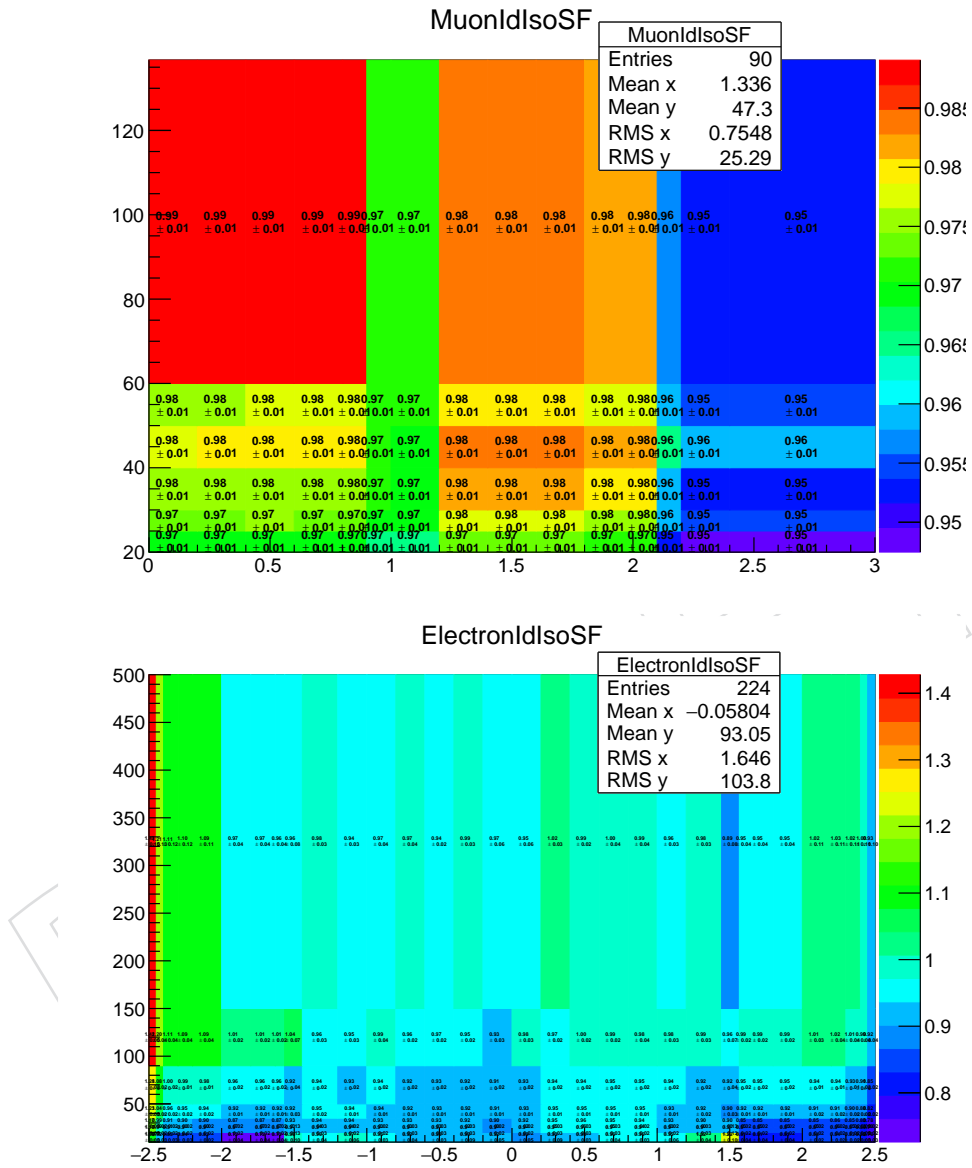


Figure 38: The identification and isolation efficiencies for muons (top) and electrons (bottom) as a function of p_T and η as recommended by the Muon and EGamma POGs (see text for more details) for 2016 data.

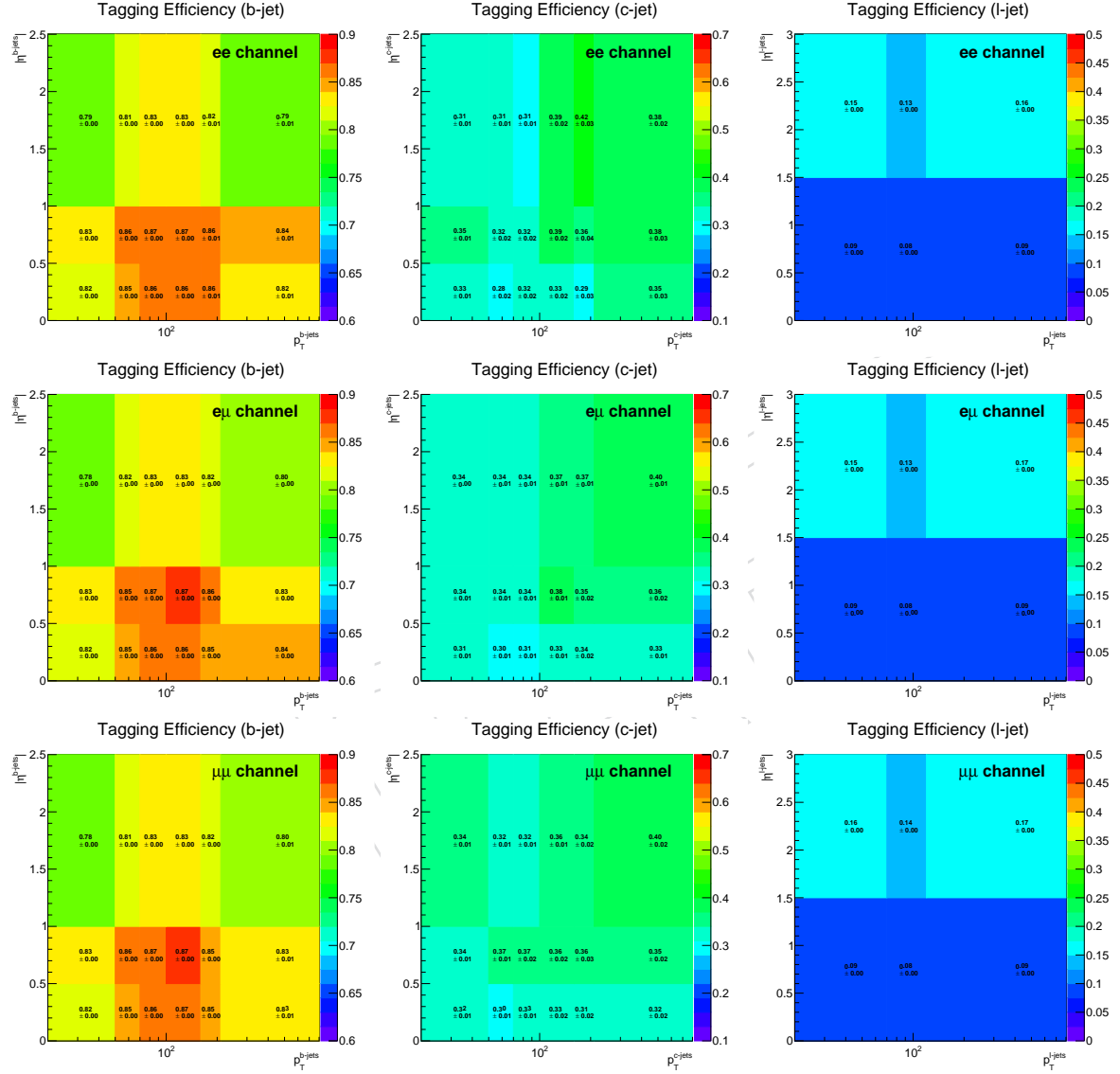


Figure 39: b-tagging efficiency of individual b-jets (left) and mistag rate for c-jets (middle) and l -jets (right) as function of jet p_T and η for e^+e^- (top), $\mu^\pm e^\mp$ (center) and $\mu^+\mu^-$ (bottom) channels, determined from the simulation.

and the events are rejected. The efficiency of the kinematic reconstruction algorithm has been studied in detail in Ref. [60].

The efficiencies of the kinematic reconstruction in the data and in the simulations are compared with respect to the lepton observables, the b jets and the E_T^{miss} distributions, and are shown in Figures 40 and 41 for the e^+e^- , $\mu^\pm e^\mp$ and $\mu^+\mu^-$ channels. The selection efficiency is calculated from the ratio of events before and after the kinematic event reconstruction. Scale factors are derived and also presented in these plots.

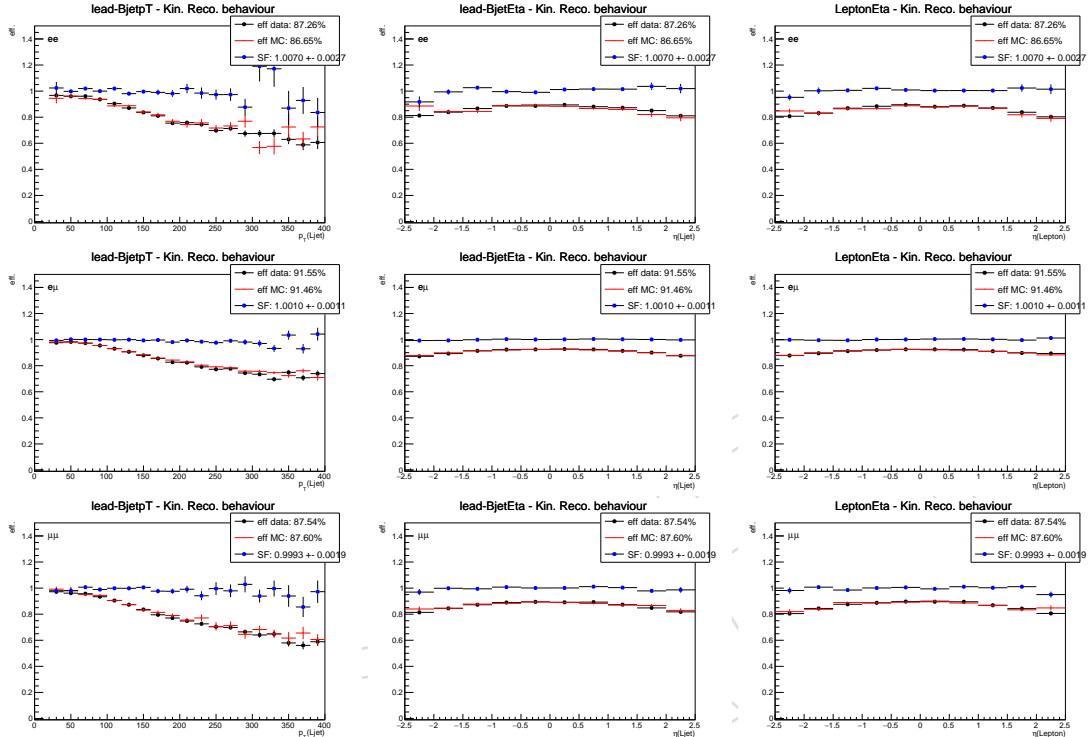


Figure 40: Efficiency of the kinematic reconstruction algorithm as a function of the leading jet p_T (left column), leading jet η (middle column) and lepton (right row) η , in the e^+e^- (top row), $\mu^\pm e^\mp$ (central row) and $\mu^+\mu^-$ (bottom row) channels both for data (black) and simulation (red). The corresponding scale factor is also shown (blue).

Backgrounds

The uncertainty due to background normalization is determined by variation of the backgrounds by $\pm 30\%$. The resulting uncertainties partially cancel for the normalised cross sections (see Section 7, Figs. 82–90).

Jet energy scale uncertainty

To determine the uncertainty due to the jet energy scale (JES) the p_T - and η -dependent JES uncertainties provided by the CMS Jet-MET POG [61] are used, which are of the order of few percent for high-energy jets. The uncertainty is calculated out of the 19 JES uncertainty sources, which are relevant for this analysis. The simulation is run with the jet four momenta being scaled up and down by the corresponding uncertainties. The vectorial changes of the jet momenta are propagated to the missing transverse energy. The selection efficiency is recalculated with the rescaled simulated samples and the difference with respect to the original samples is taken as systematic uncertainty from the relevant JES source.

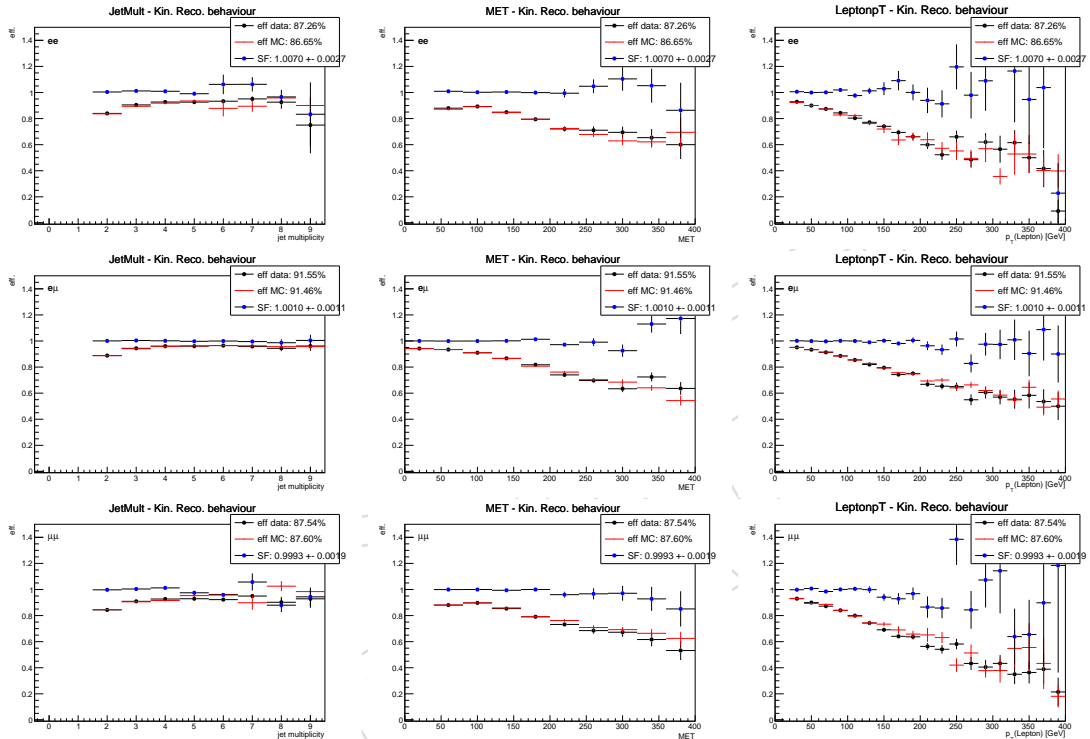


Figure 41: Efficiency of the kinematic reconstruction algorithm as a function of the jet multiplicity (left column), E_T^{miss} (central column) and lepton transverse momentum (right column), in the e^+e^- (top row), $\mu^\pm e^\mp$ (central row) and $\mu^+\mu^-$ (bottom row) channels both for data (black) and simulation (red). The corresponding scale factor is also shown (blue).

596 Jet energy resolution uncertainty

597 The uncertainty on the jet energy resolution (JER) is determined in the simulation by the variation
598 of the simulated JER by $\pm 1\sigma$ in different η regions according the prescription given by the
599 Jet/MET group [62].

600 Unclustered E_T^{miss}

601 In order to account for the unclustered missing energy, the E_T^{miss} 4-vector is recalculated varying
602 the deposited energy from the charged and neutral hadrons and photons according to the
603 corresponding energy resolutions.

604 Pile-up

605 To estimate the impact from pile-up on the signal selection efficiency, the simulated pile-up
606 distribution is varied by $\pm 4.6\%$ with respect to the nominal value, and the cross section is
607 recalculated.

608 Luminosity

609 The uncertainty on the integrated luminosity for the 2016 data sample is presently 2.5% [22].
610 This uncertainty cancels out for the normalized differential cross section measurement.

611 Decay branching fraction

612 This uncertainty cancels out for the normalized differential cross section measurement.

613 5.2 Model uncertainties

614 The impact of theoretical assumptions in the modelling is determined by repeating the analysis
615 and replacing the reference POWHEG+PYTHIA8 $t\bar{t}$ simulation by dedicated simulation samples
616 with altered parameters or by varying the reference simulation with a use of the source-related
617 weights.

618 Matrix element μ_R and μ_F scales

619 The uncertainty on modelling of the hard-production process is assessed through changes in
620 the renormalization and factorization scales (μ_r and μ_f respectively) in the matrix element in
621 the POWHEG sample via the use of weights. The following separate variations are computed
622 varying μ_r and μ_f with respect to their nominal values:

- 623 • μ_r fixed, μ_f varied by 2.0 (0.5) for up (down) variation,
- 624 • μ_f fixed, μ_r varied by 2.0 (0.5) for up (down) variation,
- 625 • μ_r and μ_f varied simultaneously by 2.0 (0.5) for up (down) variation,

626 The simultaneous μ_r , μ_f variation always gives the largest uncertainty, therefore it is taken to
627 assess the final systematic uncertainty corresponding to this source.

628 Variation of α_S in parton shower

629 In order to evaluate an impact of the choice of α_S value in the parton shower simulation, the
630 dedicated POWHEG+PYTHIA8 samples are used which are produced with a configuration done
631 by the TOP ModGen group. The uncertainties influenced by the initial or final state radiation
632 are estimated with the separate 2.0/0.5 (up/down) variations of the α_S^{ISR} or α_S^{FSR} parameter in
633 the dedicated samples respectively. This concludes into two sources of the uncertainties: α_S^{ISR}

634 or α_S^{FSR} dependent. Finally, the resulting uncertainty dependent from α_S^{FSR} is re-scaled to the
 635 $\sqrt{2} - 1/\sqrt{2}$ interval as is recommended by the TOP PAG.

636 Top quark mass

637 For the uncertainty of the top quark mass – which in the default sample is 172.5 GeV – two
 638 samples with a top mass of 175.5 GeV and 169.5 GeV are used to estimate the impact of the top
 639 mass uncertainty on the signal selection efficiency. The resulting variations are scaled linearly
 640 in order to mimic a variation of 1 GeV.

641 ME-PS matching

642 The uncertainty on the matching of the matrix element to parton shower calculations is eval-
 643 uated by means of the dedicated POWHEG+PYTHIA8 simulations with the up/down variation
 644 of the $hdamp$ parameter with respect to its nominal value, accordingly to $hdamp = 1.58_{-0.59}^{+0.66} m_t$.
 645 More details in [63].

646 Underlying event tune

647 The related uncertainty is estimated using the dedicated POWHEG+PYTHIA8 simulations with
 648 the up/down variations of the tuned parameters accordingly to their uncertainties that are
 649 determined by the tuning process. More details in [63].

650 Parton distribution function

651 The uncertainty arising from the parton distribution functions (PDF) is assessed by reweighting
 652 the $t\bar{t}$ signal sample according to the 56 eigenvectors in the CT14 NLO PDF set. Also, the
 653 separate variation of the α_S value used in the CT14 NLO PDF set is taken into account by
 654 reweighting.

655 Colour reconnection

656 The default colour reconnection (CP) model used in the reference $t\bar{t}$ simulation is a MPI-based
 657 scheme with the early resonance decays (ERD) switched off, as is implemented in PYTHIA8.
 658 Three more CR schemes are considered: MPI-based scheme with ERD switched on, gluon-
 659 move scheme and QCD-inspired scheme. The analysis results are recalculated using a dedi-
 660 cated $t\bar{t}$ sample corresponding to one or another CR scheme.

661 Fragmentation

662 Here, by a fragmentation is meant the momentum transfer from the b-quark to the B-hadron.
 663 The default fragmentation function used in the nominal $t\bar{t}$ simulation is the Bowler-Lund func-
 664 tion, where the Bowler-Lund parameter is set to 0.855 [63]. The effect from the up(down)-
 665 variation in the Bowler-Lund parameter is evaluated by the reweighting of the relevant transfer
 666 function at the generator level in the reference $t\bar{t}$ sample. In addition, an alternative fragmen-
 667 tation function is tested, the Peterson function, and the nominal $t\bar{t}$ simulation is reweighted
 668 correspondingly.

669 B semi-leptonic BR

670 The nominal $t\bar{t}$ sample is reweighted to account for an uncertainty in the branching ratios of
 671 the semi-leptonic B hadron decays to match the corresponding uncertainty as is given in PDG
 672 2017.

Table 9: The binning scheme used to measure the $[y(t), p_T(t)]$ cross sections.

$y(t)$	$p_T(t) [\text{GeV}^{-1}]$	bin
0.00–0.35	0–80	1
0.00–0.35	80–150	2
0.00–0.35	150–250	3
0.00–0.35	250–600	4
0.35–0.85	0–80	5
0.35–0.85	80–150	6
0.35–0.85	150–250	7
0.35–0.85	250–600	8
0.85–1.45	0–80	9
0.85–1.45	80–150	10
0.85–1.45	150–250	11
0.85–1.45	250–600	12
1.45–2.50	0–80	13
1.45–2.50	80–150	14
1.45–2.50	150–250	15
1.45–2.50	250–600	16

6 Cross section definition and determination

6.1 Measured cross sections

In this analysis, normalised differential cross sections are measured as a function of the following variables:

1. double-differential cross sections as a function of pair of variables:

- $y(t)$ and $p_T(t)$,
- $M(t\bar{t})$ and $y(t)$,
- $M(t\bar{t})$ and $y(\bar{t}\bar{t})$,
- $M(t\bar{t})$ and $\Delta\eta(t, \bar{t})$,
- $M(t\bar{t})$ and $\Delta\phi(t, \bar{t})$,
- $M(t\bar{t})$ and $p_T(t\bar{t})$,
- $M(t\bar{t})$ and $p_T(t)$,

2. triple-differential cross sections as a function of N_{jet} , $M(t\bar{t})$ and $y(t\bar{t})$. This cross section is measured separately using two and three bins of N_{jet} ,

such that in total nine cross sections are measured. The binning schemes which are used to measure these cross sections are given in Tables 9–17. The bin numbers reported in these tables are often used in the further description when multi-differential cross sections have to be presented in one-dimensional plots.

6.2 Signal extraction

The number of signal events, N_i^{sig} , is extracted from the data in the i th bin of the reconstructed observables using

$$N_i^{\text{sig}} = N_i^{\text{sel}} - N_i^{\text{bkg}}, \quad 1 \leq i \leq n, \quad (6)$$

Table 10: The binning scheme used to measure the $[M(t\bar{t}), y(t)]$ cross sections.

$M(t\bar{t}) [\text{GeV}^{-1}]$	$y(t)$	bin
300–400	0.00–0.35	1
300–400	0.35–0.85	2
300–400	0.85–1.45	3
300–400	1.45–2.50	4
400–500	0.00–0.35	5
400–500	0.35–0.85	6
400–500	0.85–1.45	7
400–500	1.45–2.50	8
500–650	0.00–0.35	9
500–650	0.35–0.85	10
500–650	0.85–1.45	11
500–650	1.45–2.50	12
650–1500	0.00–0.35	13
650–1500	0.35–0.85	14
650–1500	0.85–1.45	15
650–1500	1.45–2.50	16

Table 11: The binning scheme used to measure the $[M(t\bar{t}), y(t\bar{t})]$ cross sections.

$M(t\bar{t}) [\text{GeV}^{-1}]$	$y(t\bar{t})$	bin
300–400	0.00–0.35	1
300–400	0.35–0.75	2
300–400	0.75–1.15	3
300–400	1.15–2.50	4
400–500	0.00–0.35	5
400–500	0.35–0.75	6
400–500	0.75–1.15	7
400–500	1.15–2.50	8
500–650	0.00–0.35	9
500–650	0.35–0.75	10
500–650	0.75–1.15	11
500–650	1.15–2.50	12
650–1500	0.00–0.35	13
650–1500	0.35–0.75	14
650–1500	0.75–1.15	15
650–1500	1.15–2.50	16

Table 12: The binning scheme used to measure the $[M(t\bar{t}), \Delta\eta(t, \bar{t})]$ cross sections.

$M(t\bar{t}) [\text{GeV}^{-1}]$	$\Delta\eta(t, \bar{t})$	bin
300–400	0.0–0.4	1
300–400	0.4–1.2	2
300–400	1.2–6.0	3
400–500	0.0–0.4	4
400–500	0.4–1.2	5
400–500	1.2–6.0	6
500–650	0.0–0.4	7
500–650	0.4–1.2	8
500–650	1.2–6.0	9
650–1500	0.0–0.4	10
650–1500	0.4–1.2	11
650–1500	1.2–6.0	12

Table 13: The binning scheme used to measure the $[M(t\bar{t}), \Delta\phi(t, \bar{t})]$ cross sections.

$M(t\bar{t}) [\text{GeV}^{-1}]$	$\Delta\phi(t, \bar{t}) [\text{rad}^{-1}]$	bin
300–400	0.00–2.20	1
300–400	2.20–2.95	2
300–400	2.95–3.14	3
400–500	0.00–2.20	4
400–500	2.20–2.95	5
400–500	2.95–3.14	6
500–650	0.00–2.20	7
500–650	2.20–2.95	8
500–650	2.95–3.14	9
650–1500	0.00–2.20	10
650–1500	2.20–2.95	11
650–1500	2.95–3.14	12

Table 14: The binning scheme used to measure the $[M(t\bar{t}), p_T(t\bar{t})]$ cross sections.

$M(t\bar{t}) [\text{GeV}^{-1}]$	$p_T(t\bar{t}) [\text{GeV}^{-1}]$	bin
300–400	0–30	1
300–400	30–75	2
300–400	75–150	3
300–400	150–500	4
400–500	0–30	5
400–500	30–75	6
400–500	75–150	7
400–500	150–500	8
500–650	0–30	9
500–650	30–75	10
500–650	75–150	11
500–650	150–500	12
650–1500	0–30	13
650–1500	30–75	14
650–1500	75–150	15
650–1500	150–500	16

Table 15: The binning scheme used to measure the $[M(t\bar{t}), p_T(t)]$ cross sections.

$M(t\bar{t}) [\text{GeV}^{-1}]$	$p_T(t) [\text{GeV}^{-1}]$	bin
300–450	0–100	1
300–450	100–180	2
300–450	180–600	3
450–600	0–100	4
450–600	100–180	5
450–600	180–600	6
600–1500	0–100	7
600–1500	100–180	8
600–1500	180–600	9

Table 16: The binning scheme used to measure the $[N_{\text{jet}}, M(t\bar{t}), y(t\bar{t})]$ (2 N_{jet} bins) cross sections.

N_j	$M(t\bar{t}) [\text{GeV}^{-1}]$	$y(t\bar{t})$	bin
-0.5–0.5	300–400	0.00–0.35	1
-0.5–0.5	300–400	0.35–0.75	2
-0.5–0.5	300–400	0.75–1.15	3
-0.5–0.5	300–400	1.15–2.50	4
-0.5–0.5	400–500	0.00–0.35	5
-0.5–0.5	400–500	0.35–0.75	6
-0.5–0.5	400–500	0.75–1.15	7
-0.5–0.5	400–500	1.15–2.50	8
-0.5–0.5	500–1500	0.00–0.35	9
-0.5–0.5	500–1500	0.35–0.75	10
-0.5–0.5	500–1500	0.75–1.15	11
-0.5–0.5	500–1500	1.15–2.50	12
0.5–8.5	300–400	0.00–0.35	13
0.5–8.5	300–400	0.35–0.75	14
0.5–8.5	300–400	0.75–1.15	15
0.5–8.5	300–400	1.15–2.50	16
0.5–8.5	400–500	0.00–0.35	17
0.5–8.5	400–500	0.35–0.75	18
0.5–8.5	400–500	0.75–1.15	19
0.5–8.5	400–500	1.15–2.50	20
0.5–8.5	500–1500	0.00–0.35	21
0.5–8.5	500–1500	0.35–0.75	22
0.5–8.5	500–1500	0.75–1.15	23
0.5–8.5	500–1500	1.15–2.50	24

Table 17: The binning scheme used to measure the $[N_{\text{jet}}, M(t\bar{t}), y(t\bar{t})]$ (3 N_{jet} bins) cross sections.

N_j	$M(t\bar{t}) [\text{GeV}^{-1}]$	$y(t\bar{t})$	bin
-0.5–0.5	300–400	0.00–0.35	1
-0.5–0.5	300–400	0.35–0.75	2
-0.5–0.5	300–400	0.75–1.15	3
-0.5–0.5	300–400	1.15–2.50	4
-0.5–0.5	400–500	0.00–0.35	5
-0.5–0.5	400–500	0.35–0.75	6
-0.5–0.5	400–500	0.75–1.15	7
-0.5–0.5	400–500	1.15–2.50	8
-0.5–0.5	500–1500	0.00–0.35	9
-0.5–0.5	500–1500	0.35–0.75	10
-0.5–0.5	500–1500	0.75–1.15	11
-0.5–0.5	500–1500	1.15–2.50	12
0.5–1.5	300–400	0.00–0.35	13
0.5–1.5	300–400	0.35–0.75	14
0.5–1.5	300–400	0.75–1.15	15
0.5–1.5	300–400	1.15–2.50	16
0.5–1.5	400–500	0.00–0.35	17
0.5–1.5	400–500	0.35–0.75	18
0.5–1.5	400–500	0.75–1.15	19
0.5–1.5	400–500	1.15–2.50	20
0.5–1.5	500–1500	0.00–0.35	21
0.5–1.5	500–1500	0.35–0.75	22
0.5–1.5	500–1500	0.75–1.15	23
0.5–1.5	500–1500	1.15–2.50	24
1.5–8.5	300–400	0.00–0.35	25
1.5–8.5	300–400	0.35–0.75	26
1.5–8.5	300–400	0.75–1.15	27
1.5–8.5	300–400	1.15–2.50	28
1.5–8.5	400–500	0.00–0.35	29
1.5–8.5	400–500	0.35–0.75	30
1.5–8.5	400–500	0.75–1.15	31
1.5–8.5	400–500	1.15–2.50	32
1.5–8.5	500–1500	0.00–0.35	33
1.5–8.5	500–1500	0.35–0.75	34
1.5–8.5	500–1500	0.75–1.15	35
1.5–8.5	500–1500	1.15–2.50	36

where n denotes the total number of bins, N_i^{sel} is the number of selected events in the i th bin, and N_i^{bkg} corresponds to the expected number of background events in this bin, except for $t\bar{t}$ final states other than the signal. The latter are dominated by events in which one or both of the intermediate W bosons decay into τ leptons with subsequent decay into an electron or muon. Since these events arise from the same $t\bar{t}$ production process as the signal, the normalisation of this background is fixed to that of the signal. The expected signal fraction is defined as the ratio of the number of selected $t\bar{t}$ signal events to the total number of selected $t\bar{t}$ events (i.e. the signal and all other $t\bar{t}$ events) in simulation. This procedure avoids the dependence on the total inclusive $t\bar{t}$ cross section used in the normalization of the simulated signal sample.

6.3 Unfolding

The signal yields N_i^{sig} , determined in each i th bin of the reconstructed kinematic variables, may contain entries that were originally produced in other bins and have migrated because of the imperfect resolutions. This effect can be described as

$$M_i^{\text{sig}} = \sum_{j=1}^m A_{ij} M_j^{\text{unf}}, \quad 1 \leq i \leq n, \quad (7)$$

where m denotes the total number of bins in the true distribution, and M_j^{unf} is the number of events in the j th bin of the true distribution from data. The quantity M_i^{sig} is the expected number of events at detector level in the i th bin, and A_{ij} is a matrix of probabilities describing the migrations from the j th bin of the true distribution to the i th bin of the detector-level distribution, including acceptance and detector efficiencies. In this analysis, the migration matrix A_{ij} is defined such that the true level corresponds to the full phase space (with no kinematic restrictions) for $t\bar{t}$ production at parton level. At the detector level a binning is chosen in the same kinematic ranges as at the true level, but with the total number of bins typically a few times larger. The kinematic ranges of all variables are chosen such that the fraction of events that migrate into the regions outside the measured range is very small. It was checked that the inclusion of overflow bins outside the kinematic ranges does not significantly alter the unfolded results. The migration matrix A_{ij} is taken from the signal simulation. The observed event counts N_i^{sig} may be different from M_i^{sig} owing to statistical fluctuations.

The estimated value of M_j^{unf} , designated as \hat{M}_j^{unf} , is found using the TUnfold algorithm [64]. The unfolding of multidimensional distributions is performed by mapping the multidimensional arrays to one-dimensional arrays internally [64]. The unfolding is realized by a χ^2 minimization and includes an additional χ^2 term representing the Tikhonov regularization [65]:

$$\chi^2 = (\mathbf{M}^{\text{sig}} - \mathbf{A}\mathbf{M}^{\text{unf}})^T \mathbf{Cov}_{\mathbf{M}^{\text{sig}}\mathbf{M}^{\text{sig}}}^{-1} (\mathbf{M}^{\text{sig}} - \mathbf{A}\mathbf{M}^{\text{unf}}) + \tau^2 (\mathbf{M}^{\text{unf}} - \mathbf{M}^{\text{unf}0})^T (\mathbf{L}^T \mathbf{L}) (\mathbf{M}^{\text{unf}} - \mathbf{M}^{\text{unf}0}). \quad (8)$$

Bold symbols are used for vector and matrix quantities. Here τ is the regularisation strength, \mathbf{L} is the matrix of regularisation conditions, and $\mathbf{M}^{\text{unf}0}$ is the bias vector. For a given observed event counts $\mathbf{M}^{\text{sig}} = \mathbf{N}^{\text{sig}}$ with their covariances $\mathbf{M}^{\text{unf}} = \mathbf{Cov}_{\mathbf{N}^{\text{sig}}\mathbf{N}^{\text{sig}}}$, the solution of the problem is $\hat{\mathbf{M}}^{\text{unf}} = \hat{\mathbf{M}}^{\text{unf}}(\mathbf{N}^{\text{sig}}, \mathbf{Cov}_{\mathbf{N}^{\text{sig}}\mathbf{N}^{\text{sig}}}, \mathbf{M}^{\text{unf}0})$ with its covariance matrix $\mathbf{Cov}_{\hat{\mathbf{M}}^{\text{unf}}\hat{\mathbf{M}}^{\text{unf}}}$. In this analysis, only mutually exclusive bins are used at detector level, such that $\mathbf{Cov}_{\mathbf{N}^{\text{sig}}\mathbf{N}^{\text{sig}}}$ is always diagonal with its diagonal elements equal to the event yields \mathbf{N}^{sig} according to Poisson statistics. The regularization reduces the effect of the statistical fluctuations present in N_i^{sig} on the high-frequency content of \hat{M}_j^{unf} . From the available options in TUnfold, the regularisation of the second derivatives (curvature) is chosen, and the bias vector is set to the MC prediction.

724 The regularization strength is chosen such that the global correlation coefficient is minimal [66].
725 For the measurements presented here, this choice results in a small contribution from the reg-
726 ularization term to the total χ^2 , on the order of 1%. Also the area constraint is used, such that
727 the normalisation of the unfolded cross section, corrected for acceptance and detector efficien-
728 cies, is enforced to match the total event count, although a possible bias in normalisation is
729 not propagated to the normalised cross sections, and this constraint has a tiny impact (< 0.1%)
730 on the normalised cross sections measured in this analysis. A more detailed description of the
731 unfolding procedure can be found in Refs. [54, 55].

732 **6.4 Closure tests**

733 In order to validate the unfolding procedure described in the previous section, closure tests
734 were carried out. These are exercises with pseudodata unfolded and compared to the truth
735 in order to quantify the level of possible bias. The tests aim to verify the absence of bias and
736 motivate the choice for the unfolding setup used in this analysis by comparing to alternative
737 approaches.

738 The following closure tests were carried out [66]:

- 739 1. ‘Data test’ consists of folding of the unfolded distribution with the migration matrix and
740 comparing it to the detector-level distribution. In terms of χ^2 , one expects it to follow the
741 χ^2 distribution with *dof* equal to the difference of the numbers of bins at detector and
742 true level, if the MC model describes the data and the binning is fine enough (it relies
743 on good description of the distribution shape using fine detector-level bins within each
744 coarse generator-level bin). This can be thought of as a sanity check.
- 745 2. ‘Truth test’ consists of folding and unfolding of the given truth distribution and compar-
746 ing it to the original truth. This is a trivial check, and any reasonable unfolding algorithm
747 is expected to pass it.
- 748 3. ‘Toy test’ consists of generating a number of toys from the given truth distributions, fold-
749 ing and unfolding them, thus getting an independent determination of the average and
750 variance, and comparing them to the ones returned bu the unfolding algorithm. This test
751 validates the statistical properties of the estimator.
- 752 4. ‘Reweighting test’ consists of folding and unfolding a given truth distribution, but us-
753 ing a biased (reweighted) model to estimate the migration matrix and bias vector, and
754 comparing the result to the original truth. The test aims to assess the senisitvity of the
755 unfolding to the MC model and quantify the possible bias.

756 For an adequate unfolding algorithm, the data and pseudo tests are required to be passed.
757 In the toy test it is required that the mean and variance returned by the unfolding algorithm
758 match the ones estimated using toys. Once this requirement is satisfied, a decent algorithm
759 which provides a smaller variance is preferred. In the reweighting test it is required that the
760 observed bias falls within the variance, given the present statistical uncertainties. The latter test
761 requires as input the assumption by how much the MC models may deviate from the truth.

762 Three unfolding approaches are compared:

- 763 1. Bin-by-bin unfolding (‘BBB’) solves the problem of Eq. 8 by using $\tau = 0$ and diagonal
764 migration matrix, i.e. neglecting migrations, with the same number of bins at detector
765 and generator level.

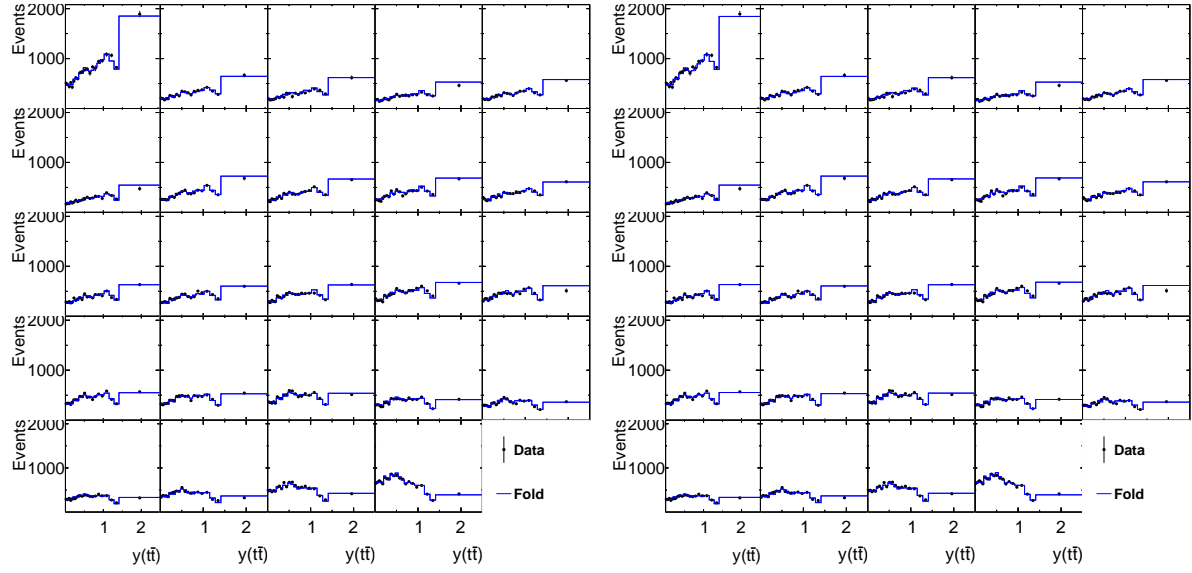


Figure 42: The folded $[M(t\bar{t}), y(t)]$ cross section compared to the data for the unregularised (left) and regularised (right) unfolding.

- 766 2. Unregularised unfolding ('NoReg') uses $\tau = 0$, thus it is expected to find the most unbiased result, which can be affected only by the finite bin widths of \mathbf{A} , but may contain large
 767 bin-to-bin correlations, known as high-frequency components, arising from the statistical
 768 fluctuations.
 769
- 770 3. Regularised unfolding ('Reg', also denoted as 'MinRhoAvg' reflecting the choice of τ) is the nominal approach of this analysis which uses the value of τ which minimises the
 771 global correlation coefficient. The regularisation is supposed to damp the high-frequency
 772 components but introduces a bias. It is important to verify that the size of this bias is
 773 sufficiently small.
 774

775 The closure tests are performed for each of the measured cross sections (see Section 7) using
 776 the signal data events (after subtraction of background) and nominal signal MC simulation
 777 (POWHEGv2 + PYTHIA8). The data events are used only in order to give the statistical un-
 778 certainties which are used when generating the toys. The background is subtracted from data
 779 before doing closure tests.

780 6.4.1 Data test

781 The χ^2 values for the different distributions obtained in the data tests of the unregularised
 782 and regularised unfolding are summarised in Table 18. Typically, the values $\chi^2/dof \approx 2$ are
 783 observed, reflecting a non-perfect agreement between the data and MC. An exemplary compar-
 784 ision of the folded measured cross section and data for the $[M(t\bar{t}), y(t\bar{t})]$ distribution is shown
 785 in Fig. 42, while the same plots for all distributions are provided in appendix (Figs. 143-159)
 786 Both regularised and unregularised unfolding are considered to pass this test. No data test can
 787 be done for the bin-by-bin unfolding because of $dof = 0$.

788 Table 18 reports also the χ^2 contribution of the regularisation term in Eq. 8 and the value of τ .
 789 For all measured distributions, the τ values are of the order of 10^{-4} and the χ^2 contribution
 790 from regularisation ranges from 0.3% to 2%.

Table 18: The χ^2 values obtained in the data tests of the unregularised and regularised unfolding. For the latter, the contributions from the two terms of Eq. 8 are quoted separately, and the τ value is given.

Cross section	dof	Unregularised unfolding	Regularised	unfolding
$[y(t), p_T(t)]$	383	456.5	$459.7 + 6.0$	$8.11\text{e-}05$
$[M(t\bar{t}), y(t)]$	463	511.0	$513.7 + 6.5$	$7.50\text{e-}05$
$[M(t\bar{t}), y(\bar{t})]$	487	569.5	$574.2 + 8.6$	$9.31\text{e-}05$
$[M(t\bar{t}), \Delta\eta(t, \bar{t})]$	299	452.6	$462.6 + 10.9$	$6.04\text{e-}05$
$[M(t\bar{t}), \Delta\phi(t, \bar{t})]$	251	294.9	$299.2 + 6.9$	$6.04\text{e-}05$
$[M(t\bar{t}), p_T(t\bar{t})]$	559	627.4	$644.1 + 26.0$	$7.45\text{e-}05$
$[M(t\bar{t}), p_T(t)]$	89	110.4	$123.3 + 12.1$	$9.31\text{e-}05$
$[N_{\text{jet}}, M(t\bar{t}), y(t\bar{t})] (2 N_{\text{jet}} \text{ bins})$	371	504.3	$507.7 + 4.9$	$9.31\text{e-}05$
$[N_{\text{jet}}, M(t\bar{t}), y(t\bar{t})] (3 N_{\text{jet}} \text{ bins})$	359	455.7	$463.1 + 8.5$	$1.02\text{e-}04$

6.4.2 Truth test

In this test the detector-level MC distributions are unfolded and compared to the known true-level distributions. The results of the truth test are shown in Figs. 43–51. The level of agreement with the truth is estimated by calculating χ^2 between the unfolded and true distribution taking into bin-by-bin correlations of the unfolded distribution. All three unfolding algorithms are able to pass this trivial test, though the bin-by-bin unfolding gives a non-zero χ^2 which indicates deviations from the truth. However those are within the statistical uncertainties.

6.4.3 Toy test

The test using toys is crucial in revealing properties of the different unfolding approaches and choosing the most appropriate one. Using the data distribution, 1000 toy distributions are generated by smearing the MC event yields according to the size of the statistical uncertainties of the data in bins at true and detector level assuming Poisson statistics. Each toy is unfolded, and the average and covariance of the unfolded results in each bin is calculated:

$$\hat{\mathbf{M}}_{\text{avg}}^{\text{unf}} = \langle \hat{\mathbf{M}}^{\text{unf}} \rangle, \\ (\text{Cov}_{\hat{\mathbf{M}}_{\text{avg}}^{\text{unf}} \hat{\mathbf{M}}_{\text{avg}}^{\text{unf}}})_{ij} = \langle (\hat{\mathbf{M}}_i^{\text{unf}} - \hat{\mathbf{M}}_{\text{avg},i}^{\text{unf}})(\hat{\mathbf{M}}_j^{\text{unf}} - \hat{\mathbf{M}}_{\text{avg},j}^{\text{unf}}) \rangle. \quad (9)$$

Here $\langle \dots \rangle$ denotes averaging over the set of toys. The average is compared to the true distribution from MC, and the covariance is compared to the averaged covariances reported by the unfolding algorithm, both in the individual bins and for all bins in the distribution in terms of χ^2 . For a valid unfolding approach, one expects agreement in these comparisons, and the smaller are the (co)variances, the better is the unfolding algorithm.

In Fig. 52 the differences between the averaged cross sections and the truth (residuals) in individual bins and their RMS are shown for the $[y(t), p_T(t)]$ distribution. The same Figure also show the mean and RMS values of the pull distribution in each bin, i.e. the residuals divided by their uncertainties, and the χ^2 distribution for cross sections in all bins. All three unfolding are able to pass this test, however while the regularised and unregularised unfolding have negligible deviations from expectation in all bins, the bin-by-bin approach produces differences of the order of the statistical uncertainties in some bins. The width of residuals are smallest for the bin-by-bin approach, followed by regularised unfolding with the width being larger by

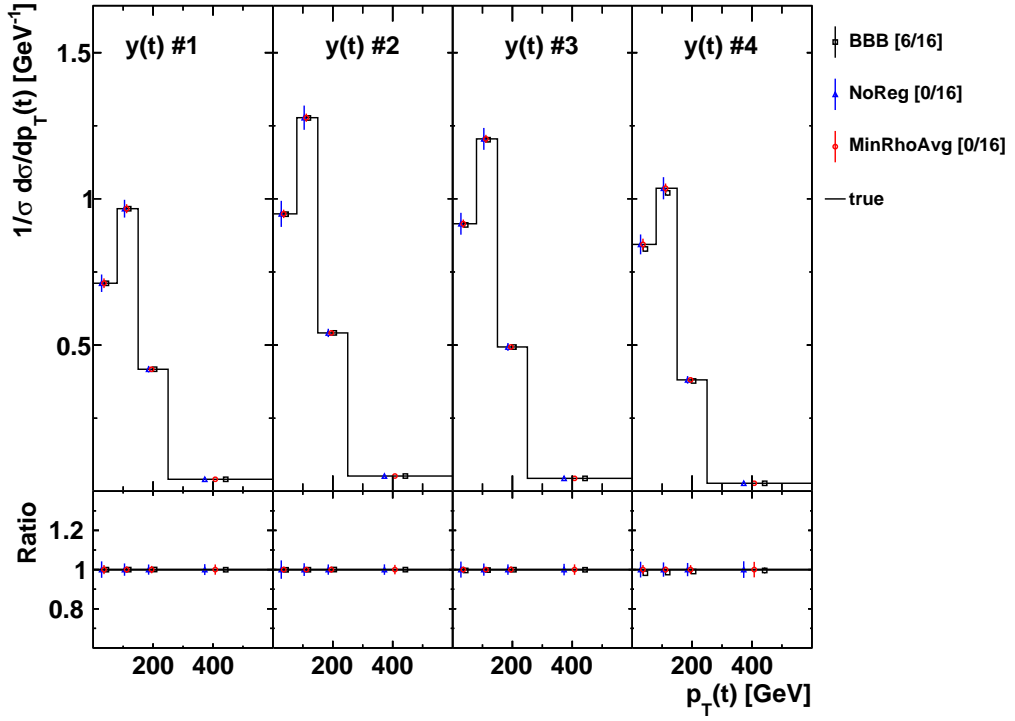


Figure 43: The unfolded $[y(t), p_T(t)]$ cross section compared to the truth using three unfolding approaches. The value of χ^2/dof is reported (in quadratic brackets) for each algorithm.

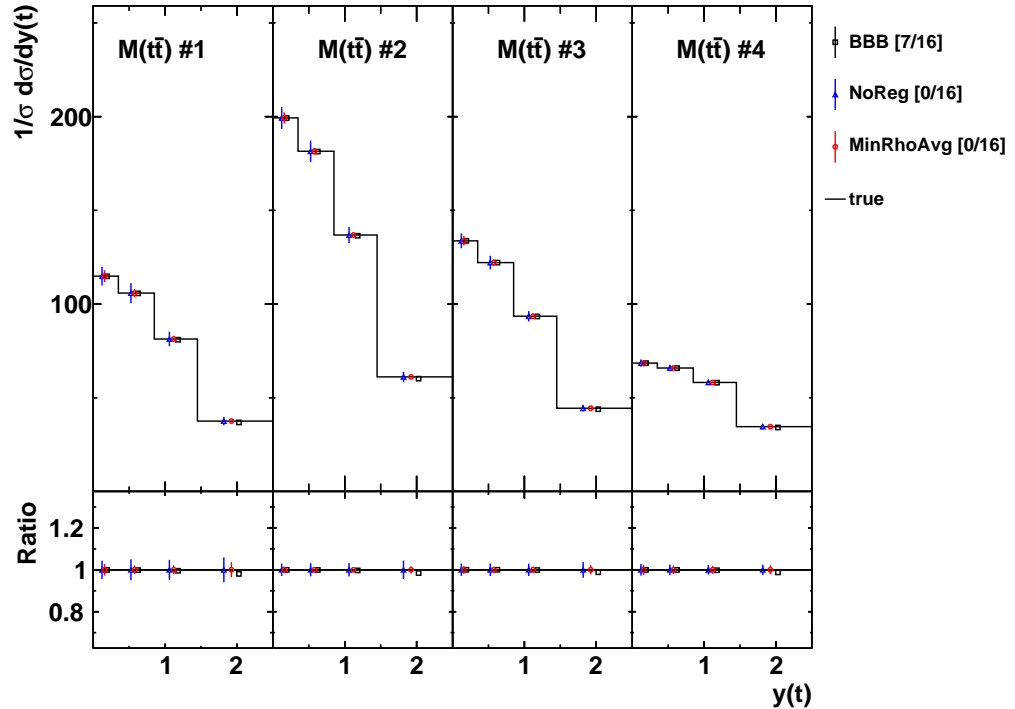


Figure 44: The unfolded $[M(t\bar{t}), y(t)]$ cross section compared to the truth using three unfolding approaches. See Fig. 43 for further details.

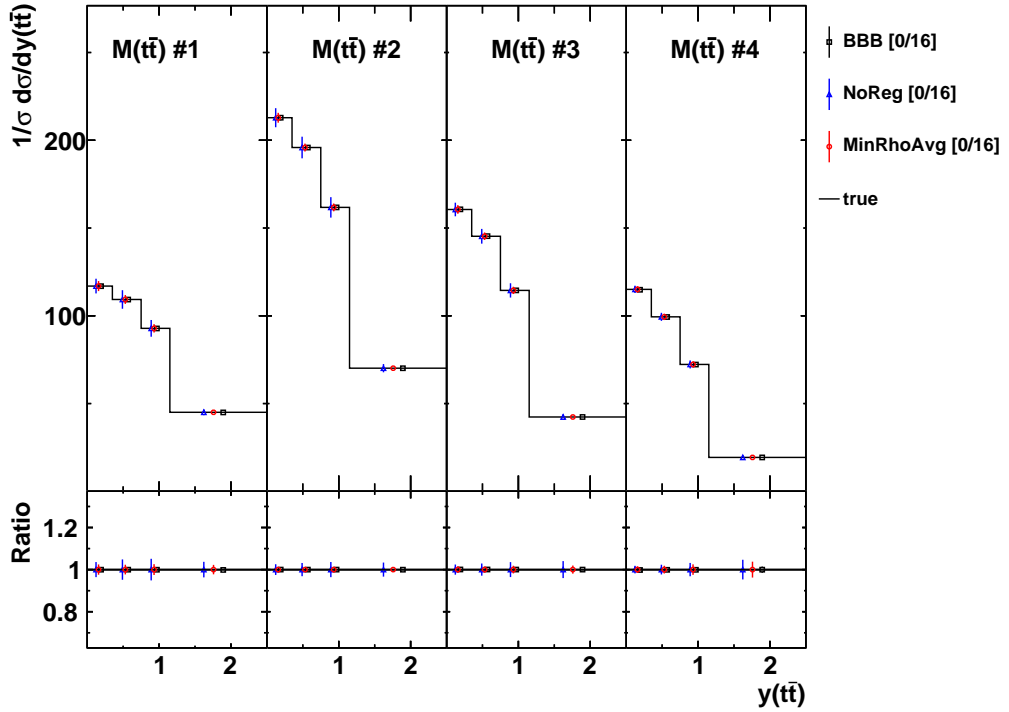


Figure 45: The unfolded $[M(t\bar{t}), y(t\bar{t})]$ cross section compared to the truth using three unfolding approaches. See Fig. 43 for further details.

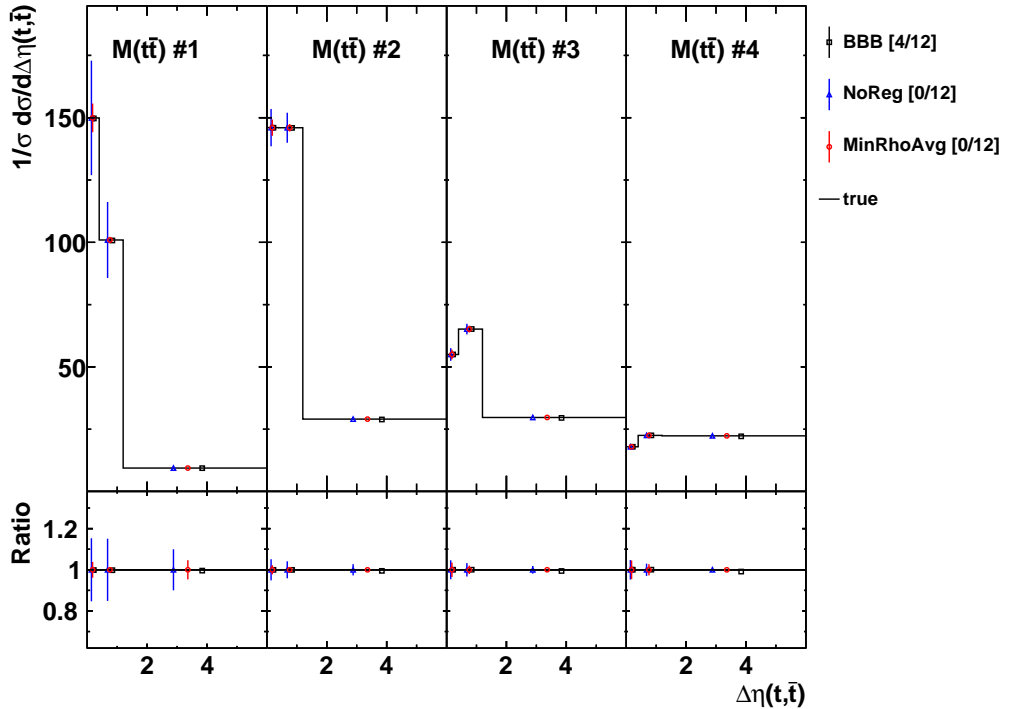


Figure 46: The unfolded $[M(t\bar{t}), \Delta\eta(t, t\bar{t})]$ cross section compared to the truth using three unfolding approaches. See Fig. 43 for further details.

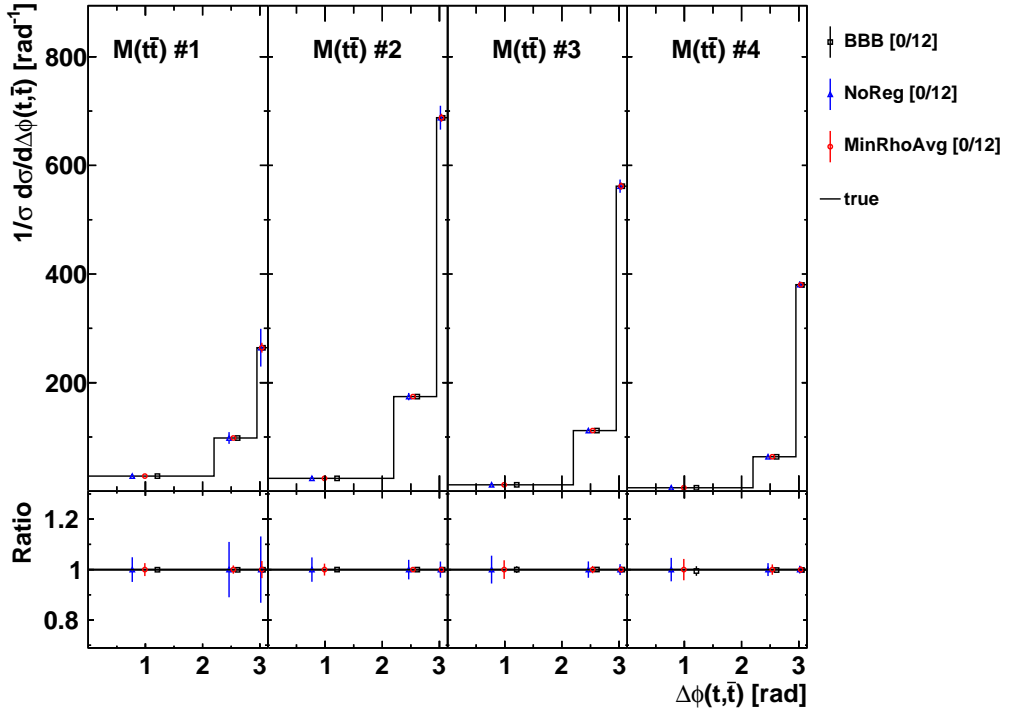


Figure 47: The unfolded $[M(t\bar{t}), \Delta\phi(t, \bar{t})]$ cross section compared to the truth using three unfolding approaches. See Fig. 43 for further details.

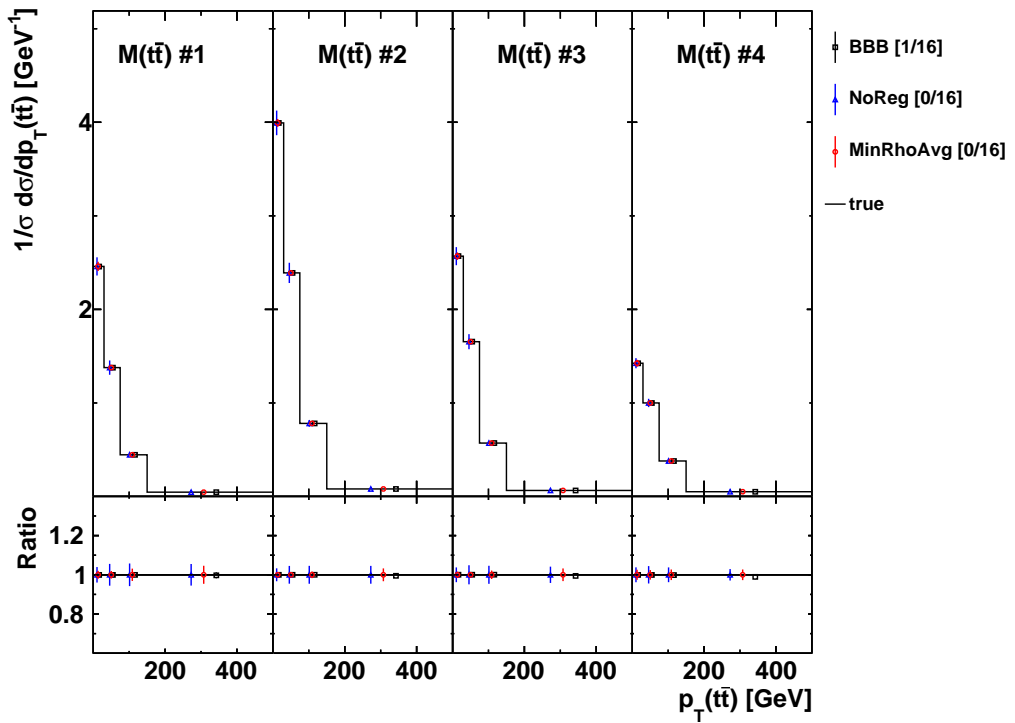


Figure 48: The unfolded $[M(t\bar{t}), p_T(t\bar{t})]$ cross section compared to the truth using three unfolding approaches. See Fig. 43 for further details.

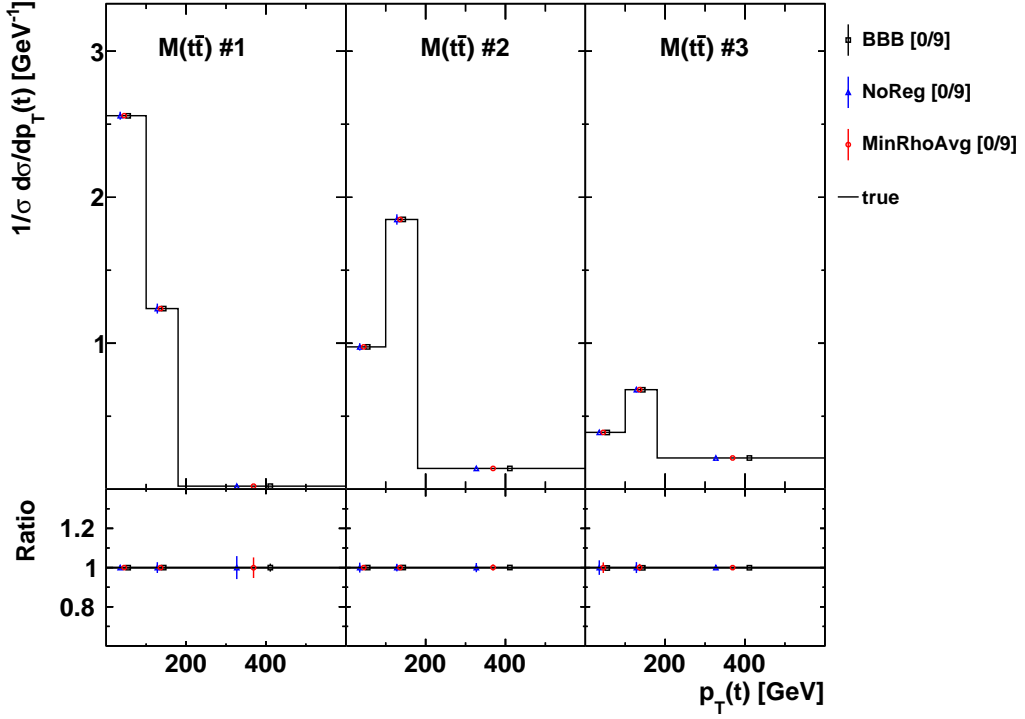


Figure 49: The unfolded $[M(t\bar{t}), p_T(t)]$ cross section compared to the truth using three unfolding approaches. See Fig. 43 for further details.

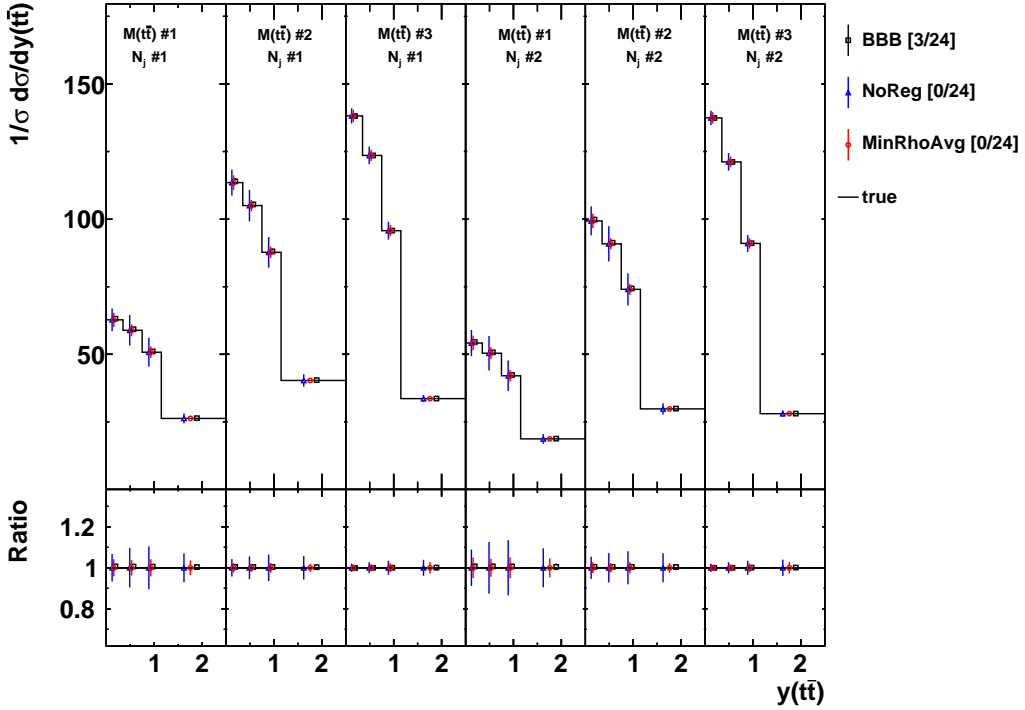


Figure 50: The unfolded $[N_{jet}, M(t\bar{t}), y(t\bar{t})]$ cross section (2 N_{jet} bins) compared to the truth using three unfolding approaches. See Fig. 43 for further details.

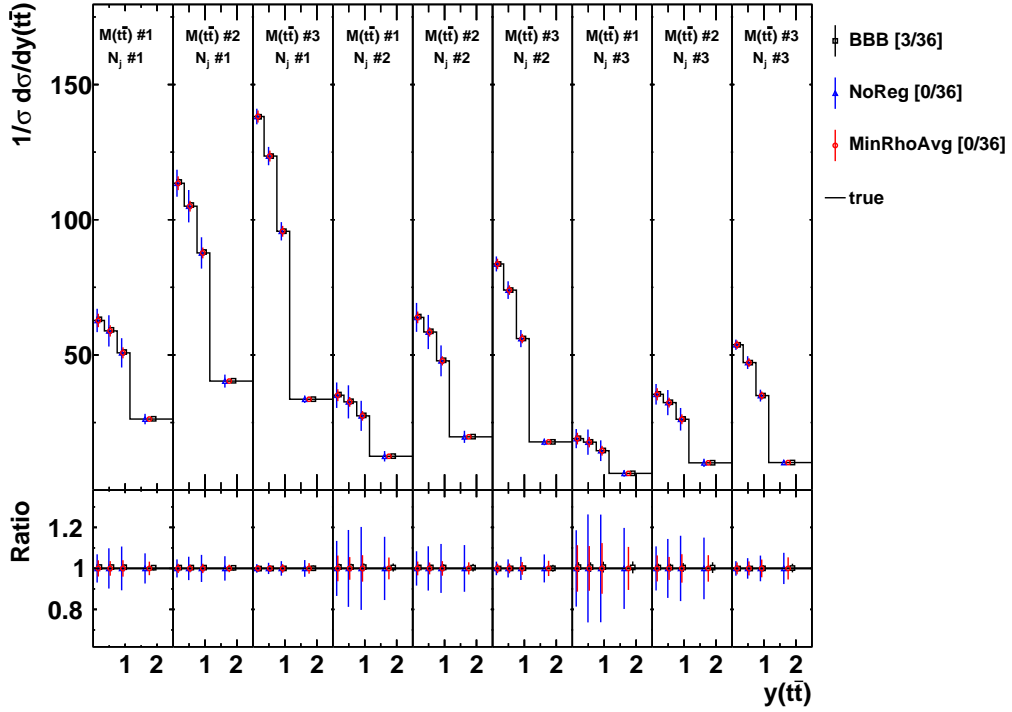


Figure 51: The unfolded $[N_{jet}, M(t\bar{t}), y(t\bar{t})]$ cross section (3 N_{jet} bins) compared to the truth using three unfolding approaches. See Fig. 43 for further details.

about factor of 2, in turn followed by unregularised unfolding with the width increased by another factor of 2. However contrary to the distributions of residuals and pulls which take into account only diagonal elements of covariance matrix $\text{Cov}_{\hat{M}^{\text{unf}} \hat{M}^{\text{unf}}}$, the comparison in terms of χ^2 which takes into account bin-to-bin correlations reveals that unregularised and regularised unfolding are very similar. This indicates that the high-frequency components which affect the results obtained using unregularised unfolding and expand their (co)variances, have only small impact on χ^2 once the correlations are taken into account.

The correlation coefficients returned by the unfolding algorithms were also checked by comparing them to the ones estimated from the set of toys. An exemplary result is shown in Fig. 61, while the same comparison for all measured cross section is available in appendix in Figs. 161–173. For all algorithms, there is a good agreement for the correlations between the bins of unfolded cross sections.

6.4.4 Reweighting test

All previous closure tests were carried out assuming that the MC simulation, which is used to produce the migration matrix and as the bias vector in regularised unfolding, is the truth. The last closure test aims to estimate how large is the bias if the MC model deviates from the truth. To yield these different distributions, the nominal MC is reweighted as a function of each variable y by using the generic functional form:

$$w = Ax^B(1-x)^C(1+Dx+Ex^2), x = \frac{y - y_{\min}}{y_{\max} - y_{\min}}, \quad (10)$$

where y_{\min} and y_{\max} are the minimum and maximum values of y , respectively. The parameters B, C, D and E are chosen freely, while the A parameter is chosen to preserve normalisation of

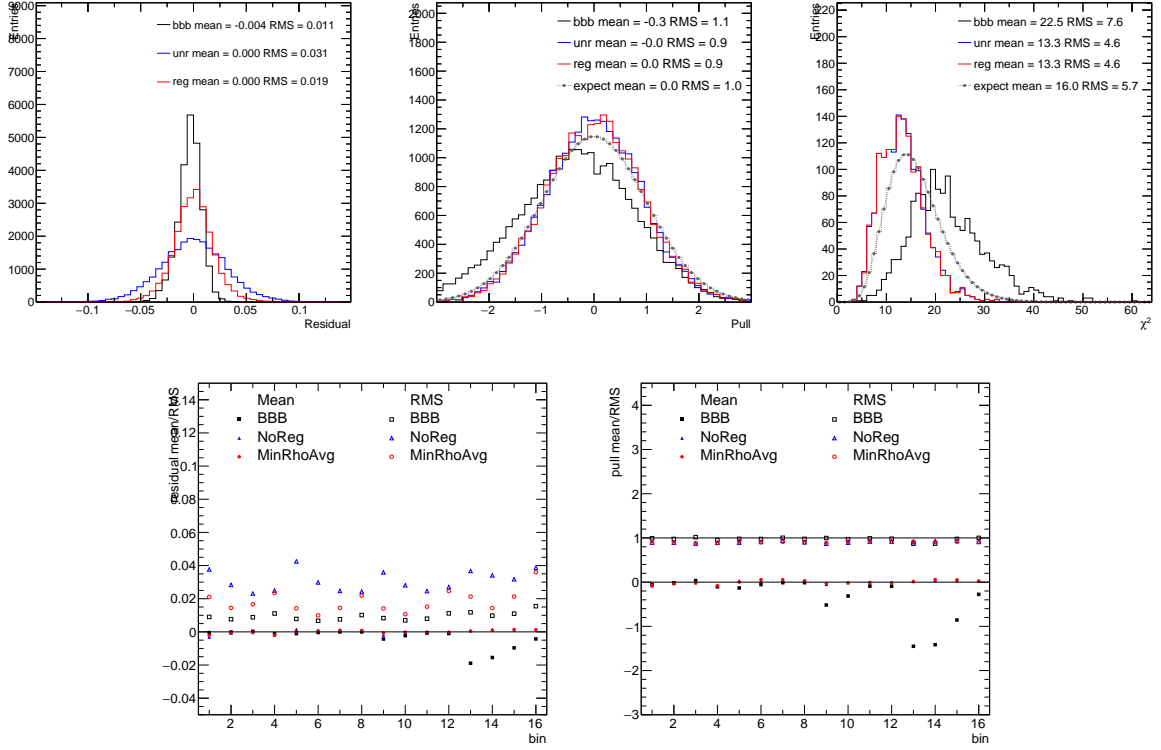


Figure 52: The residual (top left), pull (top middle) and χ^2 distributions (top right) for all bins, and the mean and RMS of the residuals (bottom left) and pulls (bottom right) for the individual bins of the $[y(t), p_T(t)]$ cross sections in the toy test using three unfolding approaches.

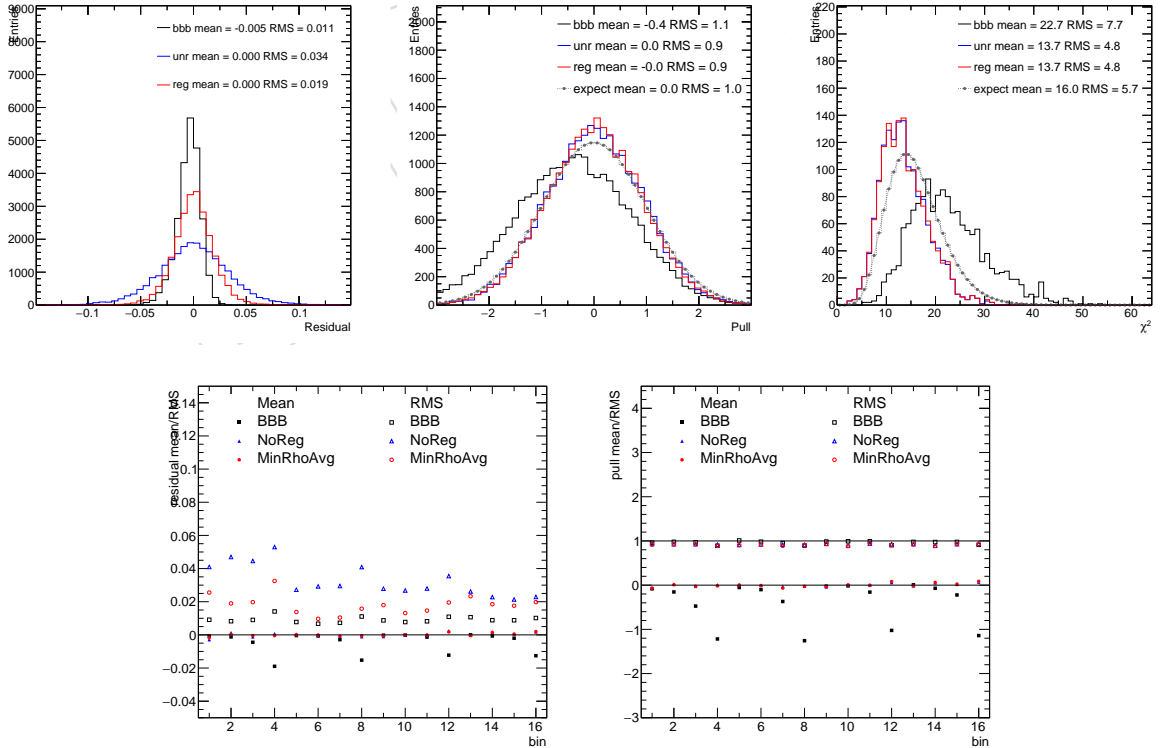
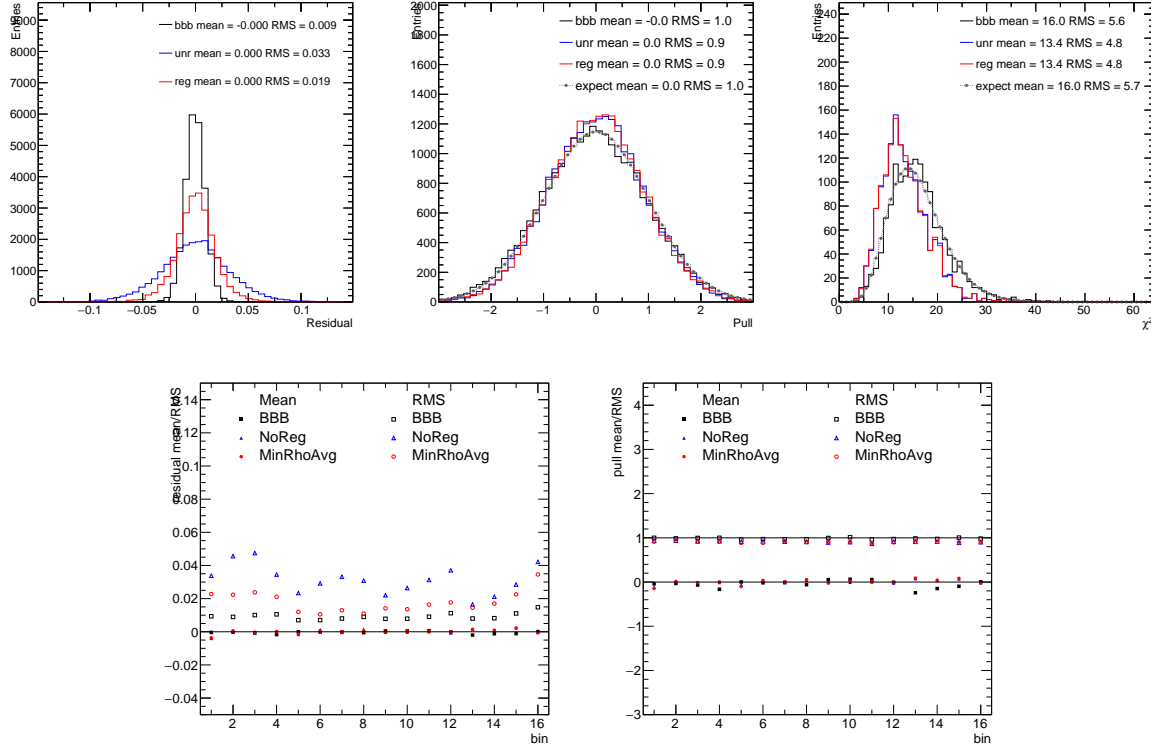
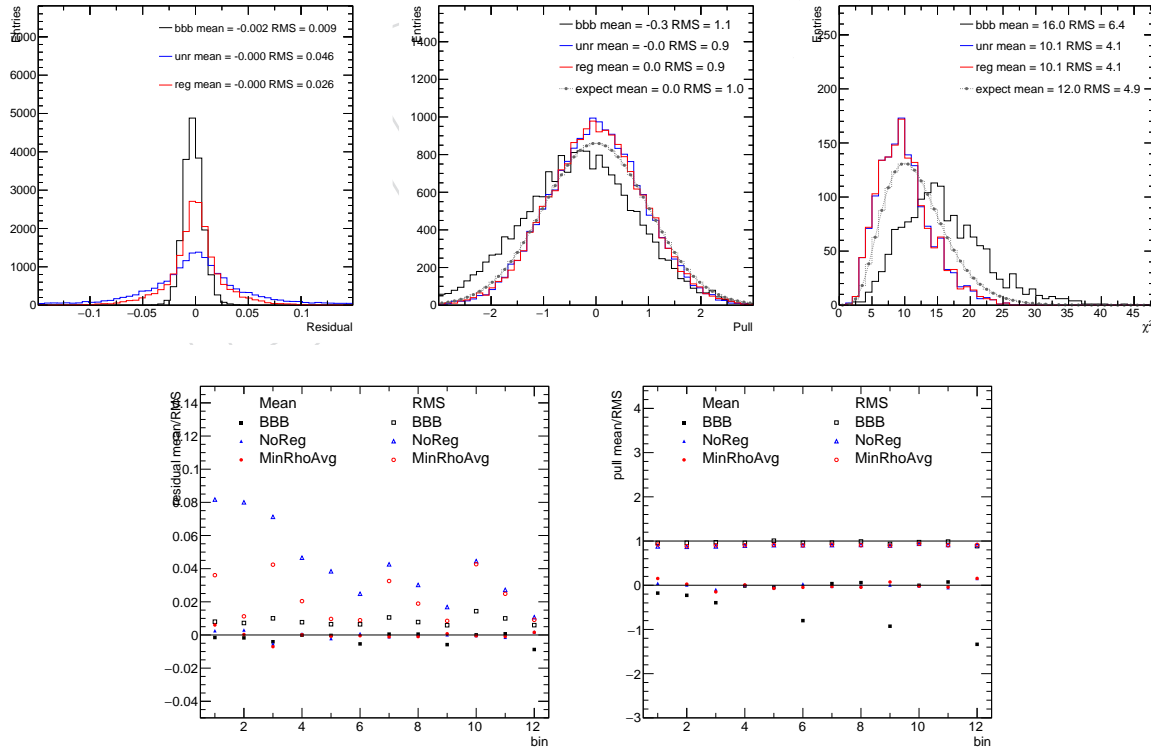


Figure 53: Same as in Fig. 52 for the $[M(t\bar{t}), y(t)]$ cross sections.

Figure 54: Same as in Fig. 52 for the $[M(t), y(t)]$ cross sections.Figure 55: Same as in Fig. 52 for the $[M(\bar{t}), \Delta\eta(t, \bar{t})]$ cross sections.

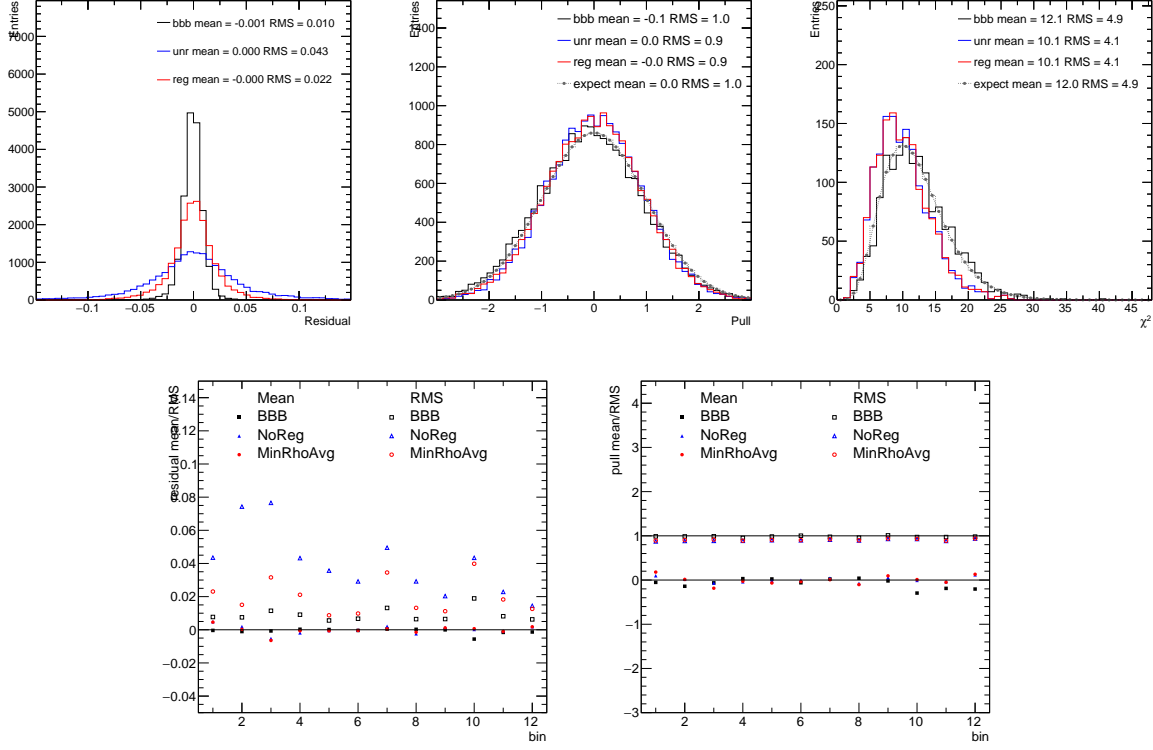


Figure 56: Same as in Fig. 52 for the $[M(t\bar{t}), \Delta\phi(t, \bar{t})]$ cross sections.

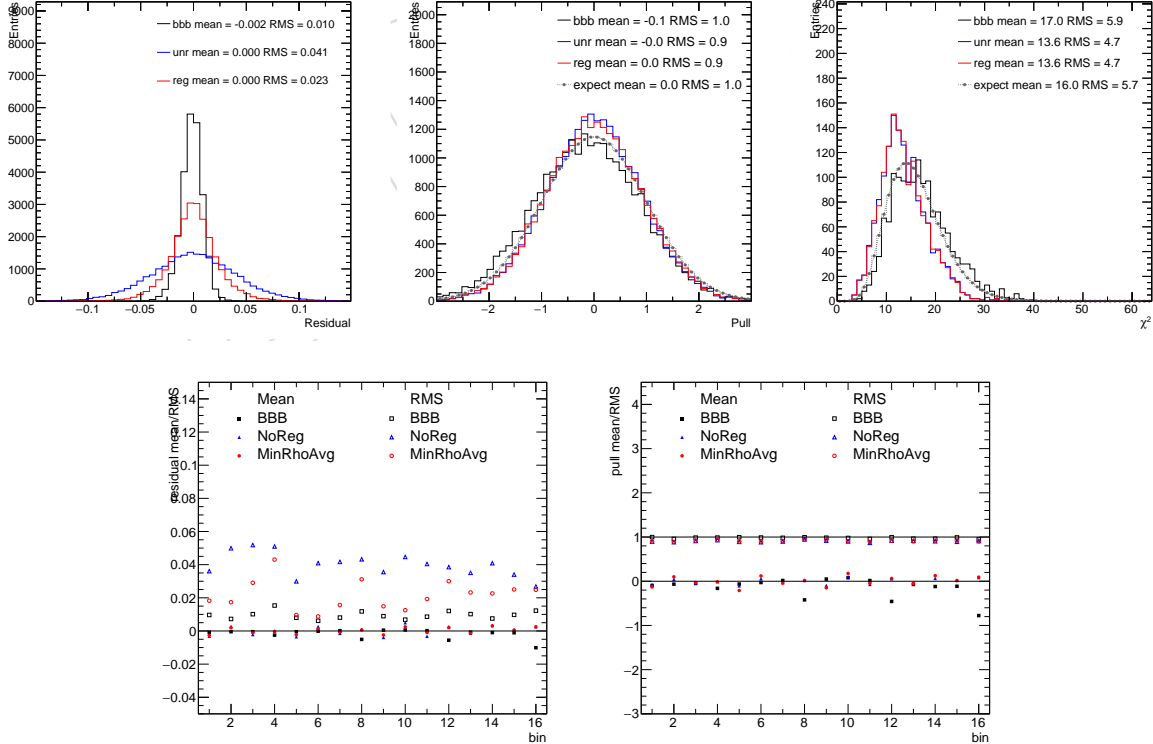
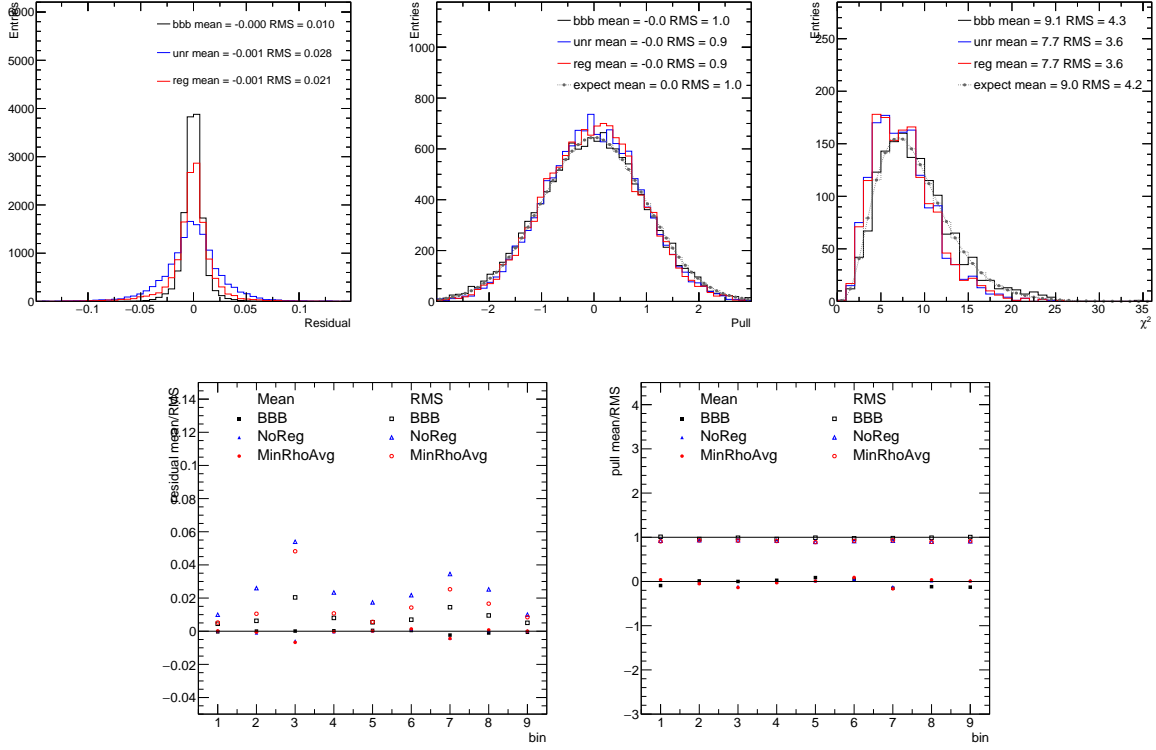
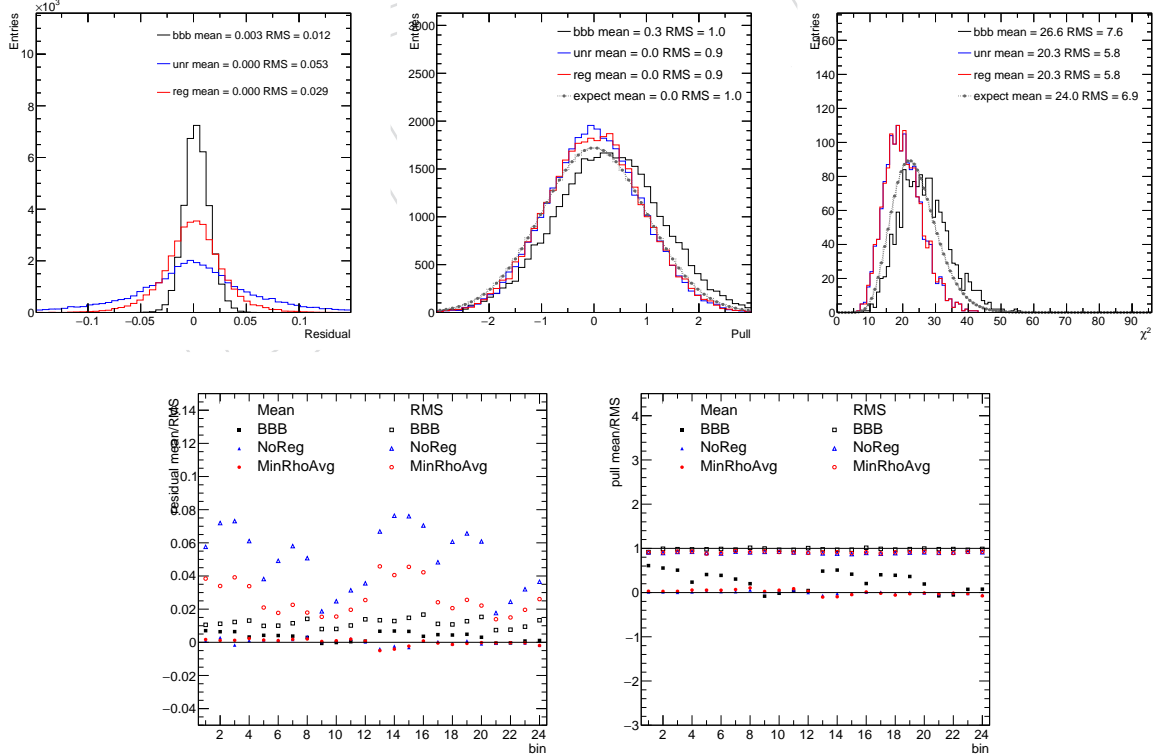


Figure 57: Same as in Fig. 52 for the $[M(t\bar{t}), p_T(t\bar{t})]$ cross sections.

Figure 58: Same as in Fig. 52 for the $[M(t), p_T(t)]$ cross sections.Figure 59: Same as in Fig. 52 for the $[N_{\text{jet}}, M(t), y(t)]$ (2 N_{jet} bins) cross sections.

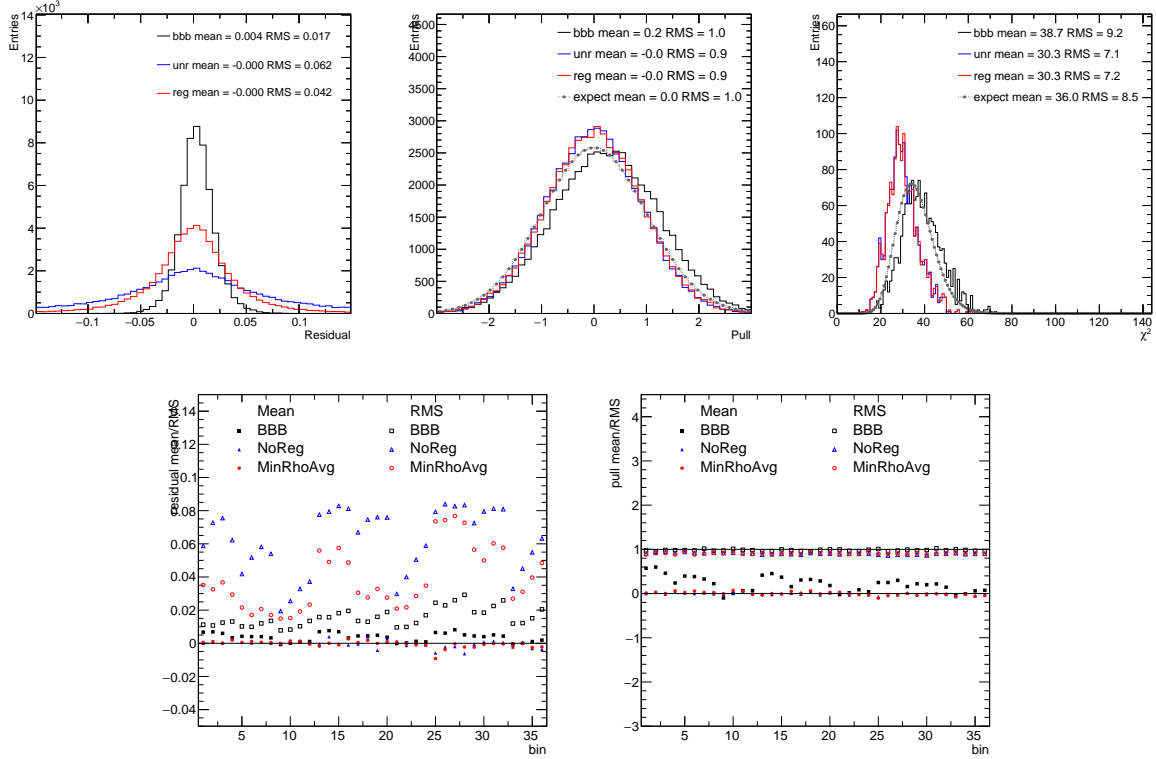


Figure 60: Same as in Fig. 52 for the $[N_{\text{jet}}, M(\bar{t}t), y(t)]$ (3 N_{jet} bins) cross sections.

the reweighted cross section. Four different scenarios are considered using different values of B , C , D and E , such that the changes of the cross sections in individual bins varies from small values of $\sim 5\%$ to very large distortions $\gtrsim 100\%$. Exemplary results for the $[M(\bar{t}t), y(\bar{t}t)]$ are shown in Figs. 62 and 63, while the results for all cross sections can be found in appendix in Figs. 174–182 and demonstrate similar results. The bin-by-bin approach fails to pass the test even when the lowest distortions of $\sim 5\%$ are applied. Regularised unfolding is able to recover the truth if the distortions are within $\sim 25\%$ (see Fig. 62 bottom), while for larger distortions the biases exceed the statistical uncertainties. Unregularised unfolding recovers the truth with negligible bias even for the largest considered distortions (see Fig. 63 bottom). Since the nominal MC modelling do not deviate from data by typically more than 25% in all kinematic regions of different observables (see control distributions in Figs. 1–20), the regularised unfolding can be safely utilised in this analysis.

6.4.5 Summary

The closure tests are summarised in Table 19. Regularised unfolding is chosen in this analysis, since it produces the smallest uncertainties and passes all tests. The main difference to using unregularised unfolding is expected to be only in the size of uncertainties in the individual bins, while for a comparison to predictions at level of χ^2 the impact of regularisation is expected to be very small.

6.5 Cross section determination

The normalized double-differential cross sections of $\bar{t}t$ production are measured in the full $\bar{t}t$ kinematic phase space at parton level. The number of unfolded signal events \hat{M}^{unf} in bins i of variables x_i is used to define the normalized multi-differential cross sections of the $\bar{t}t$ production

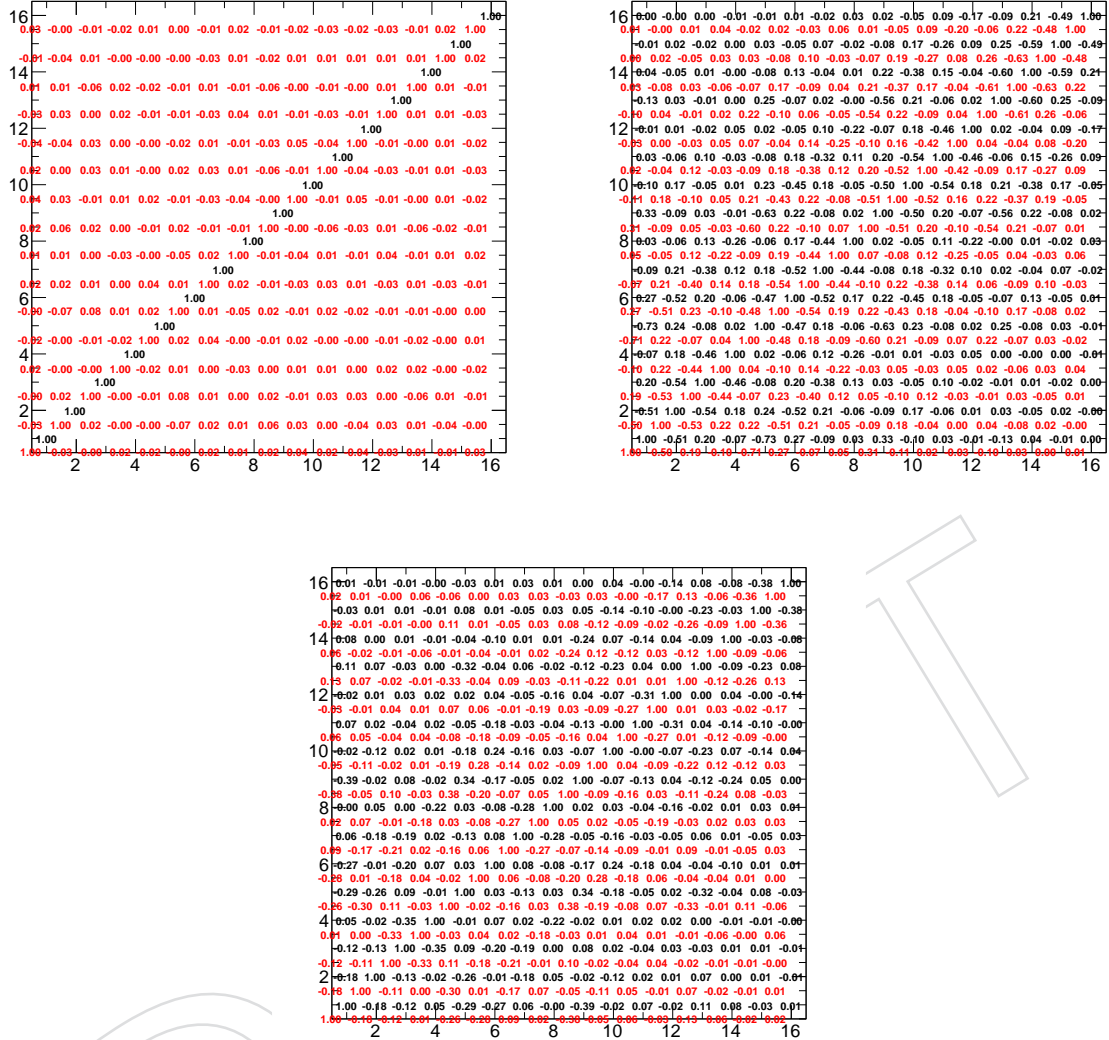


Figure 61: The correlation matrices for the unfolded $[y(t), p_T(t)]$ cross sections using the bin-by-bin (top left), unregularised (top right) and regularised (bottom) unfolding. Black numbers show the values of $\langle (\hat{M}_{avg}^{unf})_{ij} \rangle$, while red numbers (displaced for each element to the bottom right for better visibility) show the values of $\langle (\hat{M}_i^{unf} - \hat{M}_{avg,i}^{unf})(\hat{M}_j^{unf} - \hat{M}_{avg,j}^{unf}) \rangle$ (see text for further details). No black off-diagonal numbers are shown for the bin-by-bin unfolding, because all such elements are 0.

Table 19: Summary of the performed closure tests for all measured cross sections.

Test \ Unfolding	bin-by-bin	Unregularised	Regularised
Data test	n/a	passed	passed
Truth test	passed	passed	passed
Toy test	smallest unc., bias within unc.	largest unc., no bias	moderate unc., no bias
Reweighting test	always fails	always passed	passed if reweighting $\lesssim 25\%$

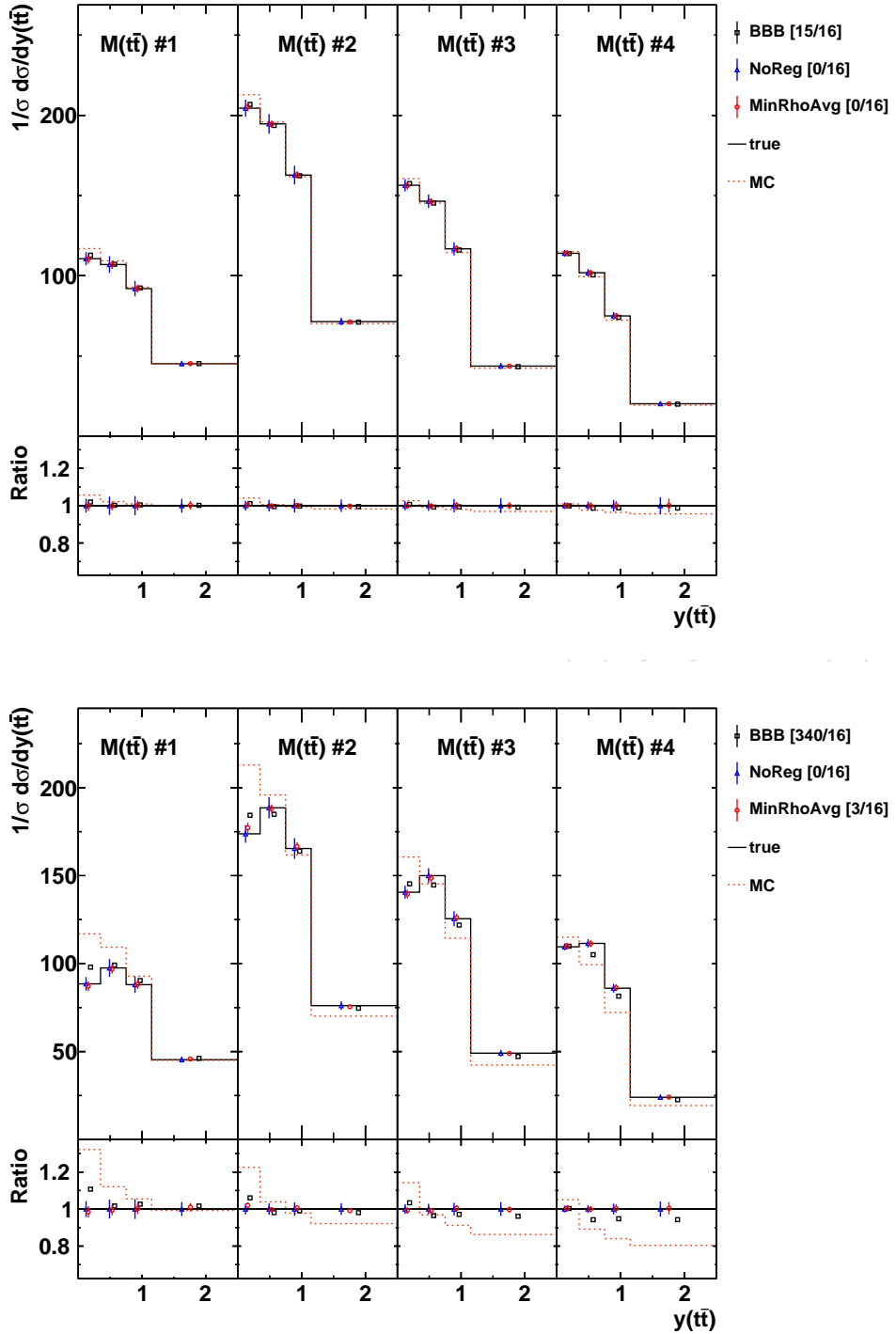


Figure 62: The unfolded $[M(t\bar{t}), y(t\bar{t})]$ cross sections obtained using differently reweighted MC models compared to the truth. The value of χ^2/dof is reported (in quadratic brackets) for each algorithm.

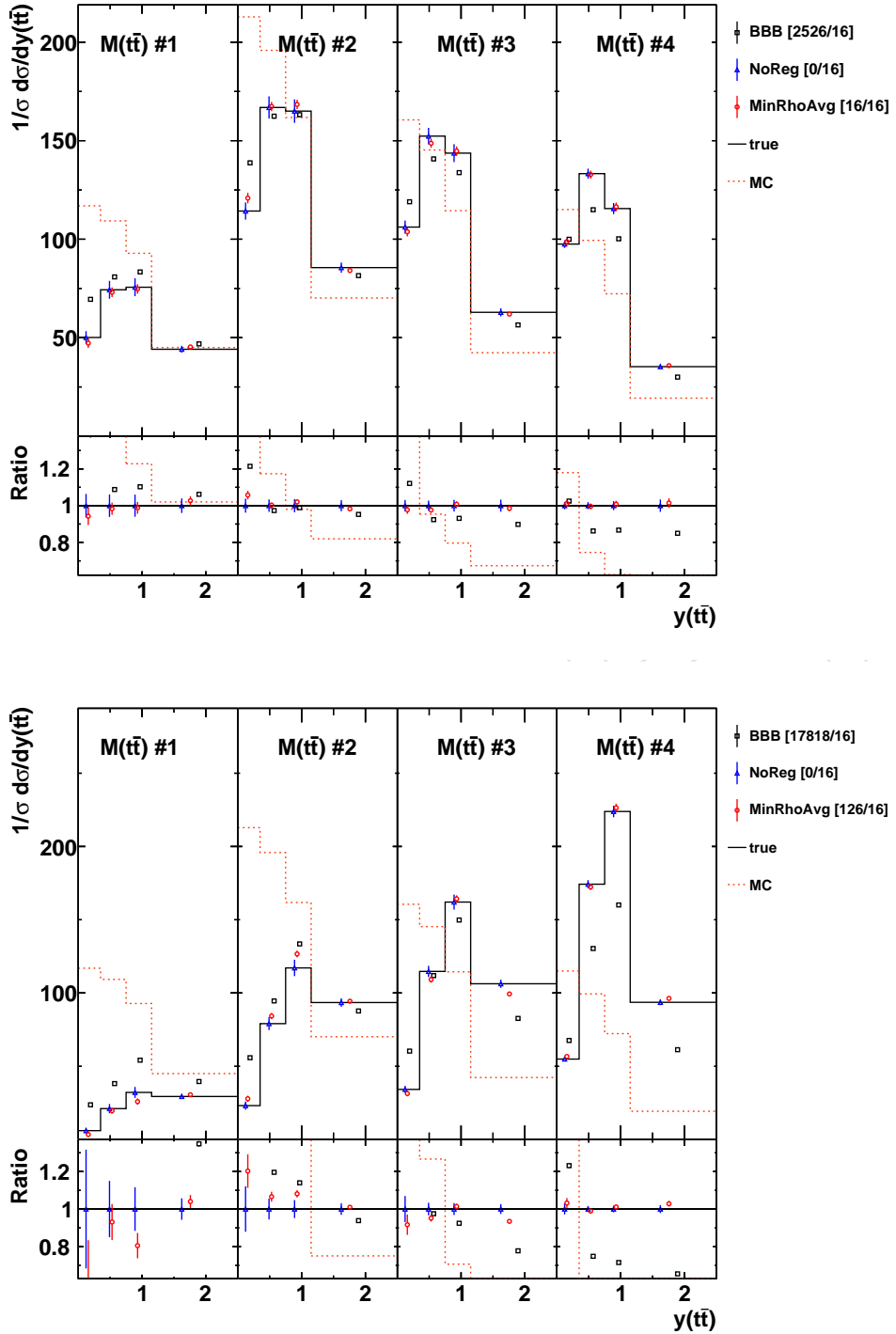


Figure 63: The unfolded $[M(\bar{t}), y(\bar{t})]$ cross sections obtained using differently reweighted MC models compared to the truth. The value of χ^2/dof is reported (in quadratic brackets) for each algorithm.

process,

$$\frac{1}{\sigma} \frac{d\sigma}{\prod dx_i} = \frac{1}{\sigma} \frac{1}{\prod \Delta x_i} \frac{\hat{M}^{\text{unf}}}{\mathcal{B} \mathcal{L}}, \quad (11)$$

where σ is the total cross section, which is evaluated by integrating $\frac{d\sigma}{\prod dx_i}$ over all bins. The branching fraction of $t\bar{t}$ into $e\mu$ final state is taken to be $\mathcal{B} = 2.3\%$ [67], and \mathcal{L} is the integrated luminosity of the data sample. The bin widths of the x variables are denoted by Δx_i . The bin widths are chosen based on the resolution, such that the purity and the stability of each bin is generally above 20%. For a given bin, the purity is defined as the fraction of events in the $t\bar{t}$ signal simulation that are generated and reconstructed in the same bin with respect to the total number of events reconstructed in that bin. To evaluate the stability, the number of events in the $t\bar{t}$ signal simulation that are generated and reconstructed in a given bin are divided by the total number of reconstructed events generated in the bin. Another important characteristics is efficiency which is supposed to reflect the probability of the generated event to appear at reconstruction level, taking into account both detector efficiency and acceptance, but being independent of the bin sizes. Thus it is directly related to the migration matrix, however, once migrations of events take place the migration matrix is non-diagonal and there is no unambiguous definition of efficiency in a given bin can be constructed. The two definitions of efficiency are used: the first one defining it as the number of events that are generated in this bin and reconstructed in any bin over the number of events reconstructed in the bin (denoted as ‘Efficiency’ in the Figures), and another one as the number of events that are reconstructed in the bin over the total number of events that are generated in this bin (denoted as ‘Efficiency (R/G)'). These two values would be equal if there are no migrations of events between bins. The values of purity, stability and efficiency for all measured distributions are shown in Figs. 64–72. The efficiency ranges from 5% to 30%, depending on the kinematic region. The migration matrices for the generator-level binning are shown in Figs. 73–81 (note that these are not the migration matrices used in the unfolding which have a finer binning at detector level). These matrices show the expected structure with the main diagonal and several sub-diagonal: the diagonal elements show the (high) probability for events to be reconstructed in the same bin where they are generated, while the sub-diagonal show the probability for events at detector level to migrate to the next bin of the 2nd (or 3rd in the case of $[N_{\text{jet}}, M(t\bar{t}), y(t\bar{t})]$) variable (notice that the bins are grouped such that first all bins of the 1st variable are plotted for the 1st bin of the 2nd variable, then all bins of the 1st variable are plotted for the 2nd bin of the 2nd variable etc.).

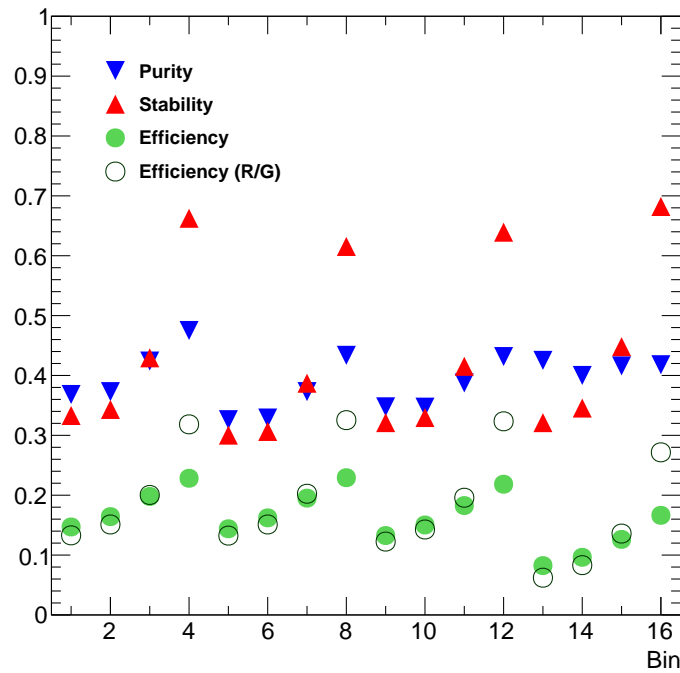


Figure 64: Purity, stability and efficiency for the $[y(t), p_T(t)]$ cross sections (see text for further details).

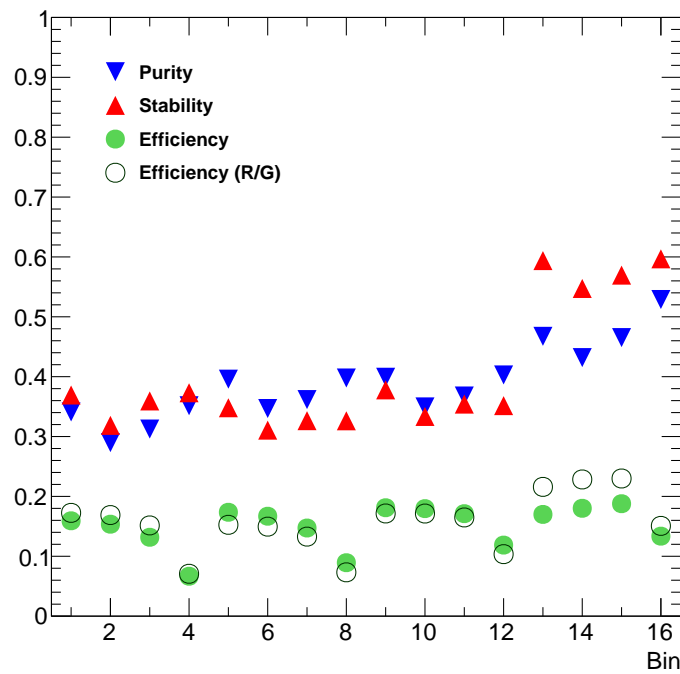


Figure 65: Purity, stability and efficiency for the $[M(t\bar{t}), y(t)]$ cross sections (see text for further details).

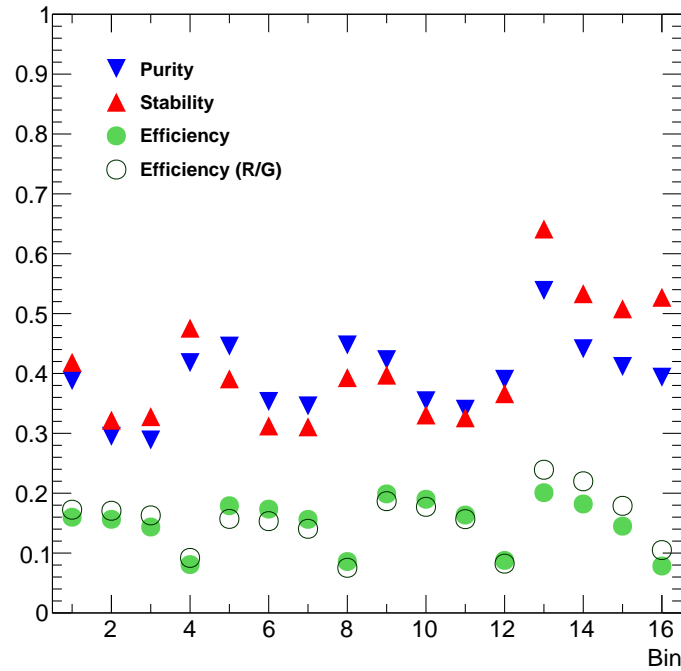


Figure 66: Purity, stability and efficiency for the $[M(t\bar{t}), y(t\bar{t})]$ cross sections (see text for further details).

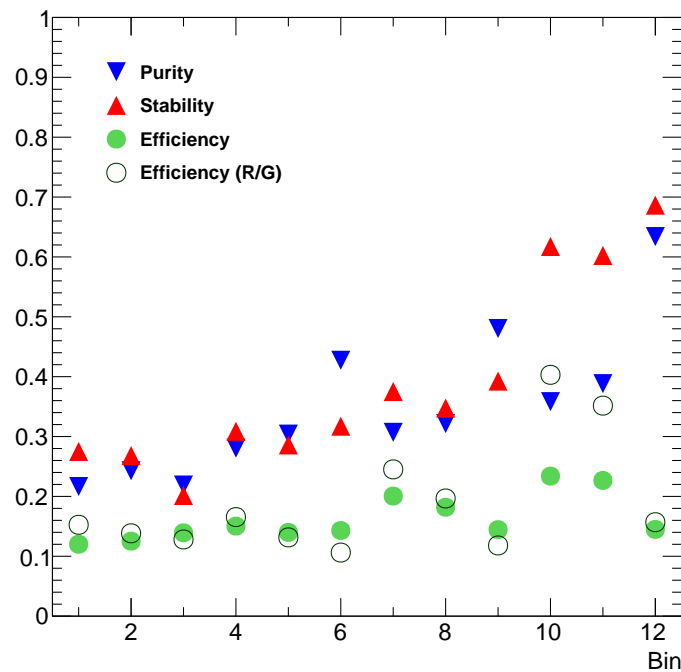


Figure 67: Purity, stability and efficiency for the $[M(t\bar{t}), \Delta\eta(t, \bar{t})]$ cross sections (see text for further details).

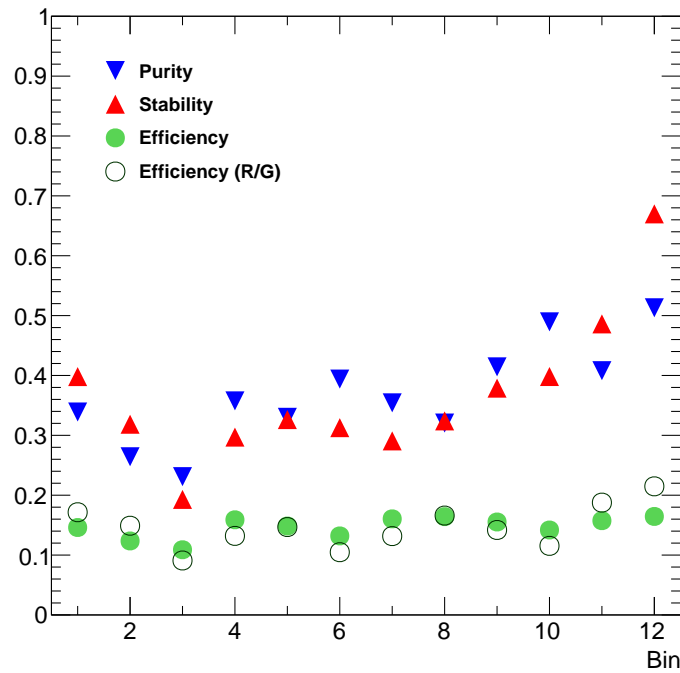


Figure 68: Purity, stability and efficiency for the $[M(t\bar{t}), \Delta\phi(t, \bar{t})]$ cross sections (see text for further details).

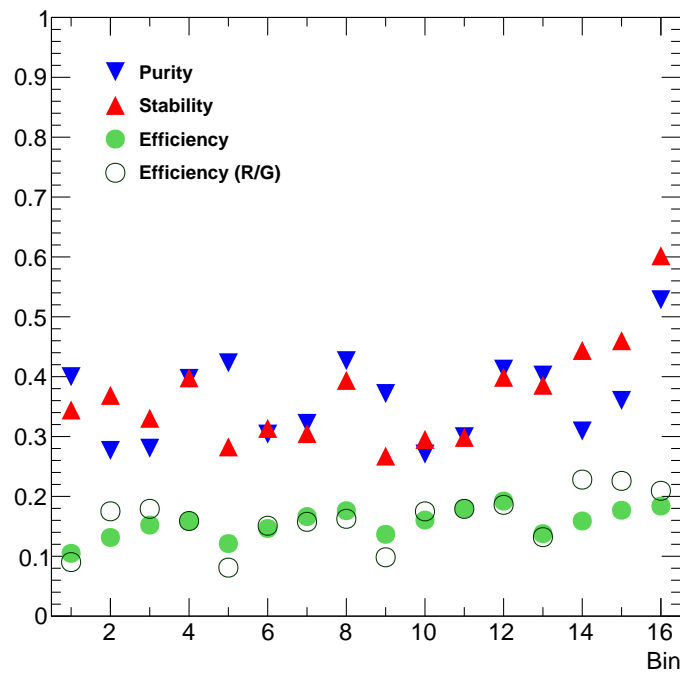


Figure 69: Purity, stability and efficiency for the $[M(t\bar{t}), p_T(t\bar{t})]$ cross sections (see text for further details).

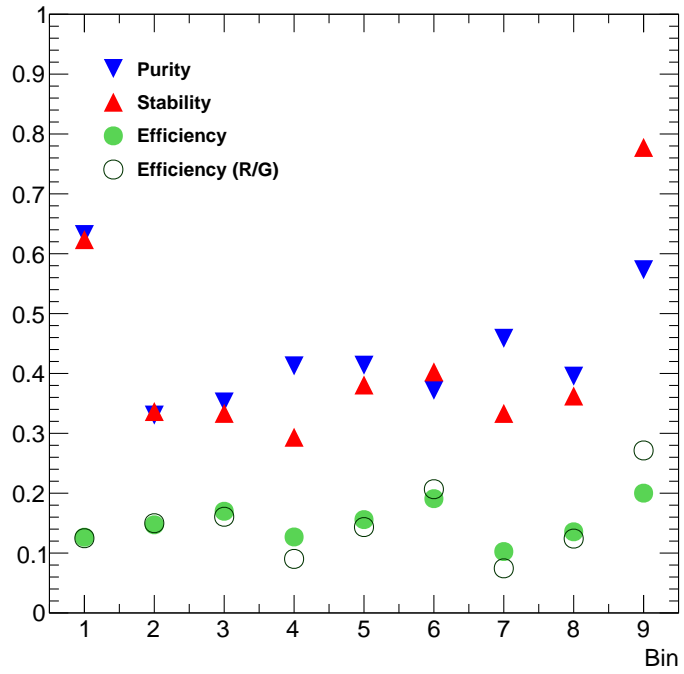


Figure 70: Purity, stability and efficiency for the $[M(t\bar{t}), p_T(t)]$ cross sections (see text for further details).

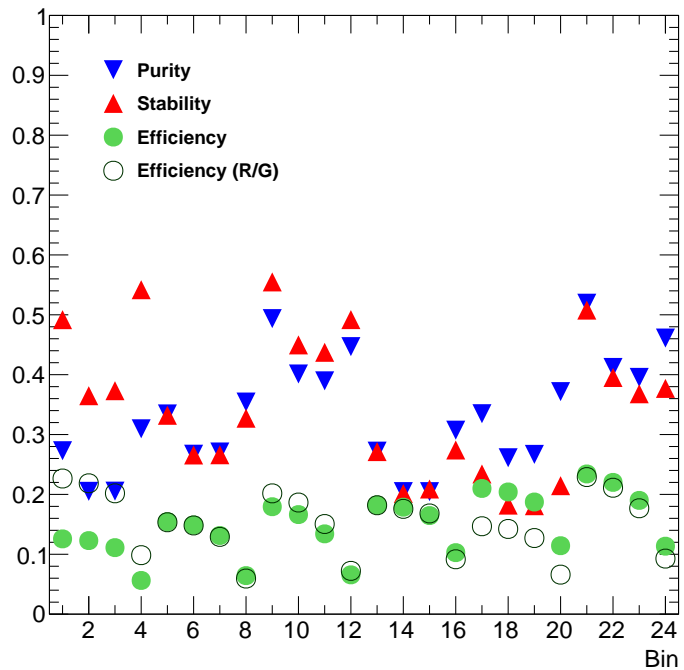


Figure 71: Purity, stability and efficiency for the $[N_{jet}, M(t\bar{t}), y(t\bar{t})]$ cross sections (with 2 N_{jet} bins).

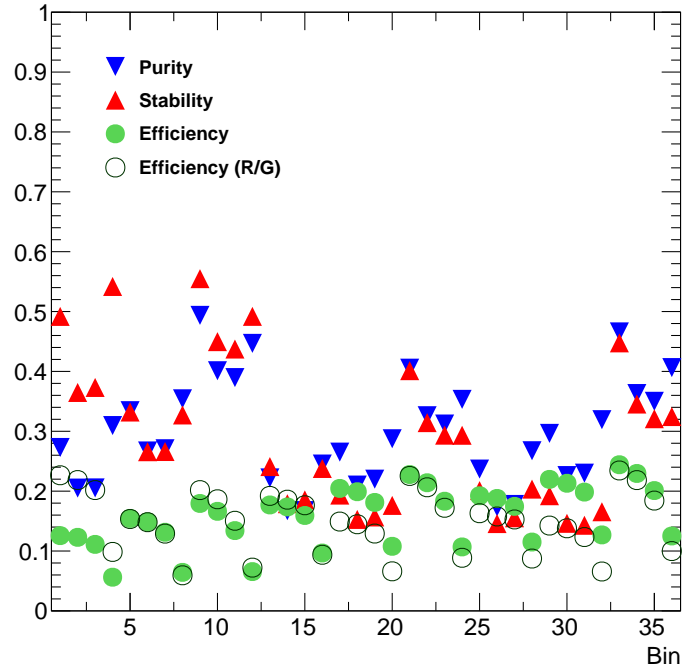


Figure 72: Purity, stability and efficiency for the $[N_{\text{jet}}, M(\bar{t}), y(\bar{t})]$ cross sections (with 3 N_{jet} bins).

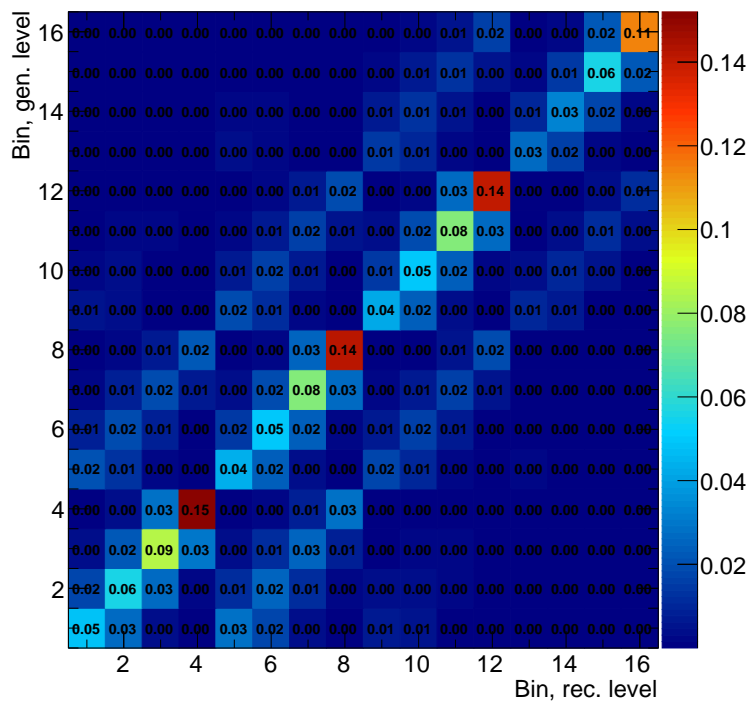


Figure 73: The migration matrix for the $[y(t), p_T(t)]$ cross sections for the generator-level bins.

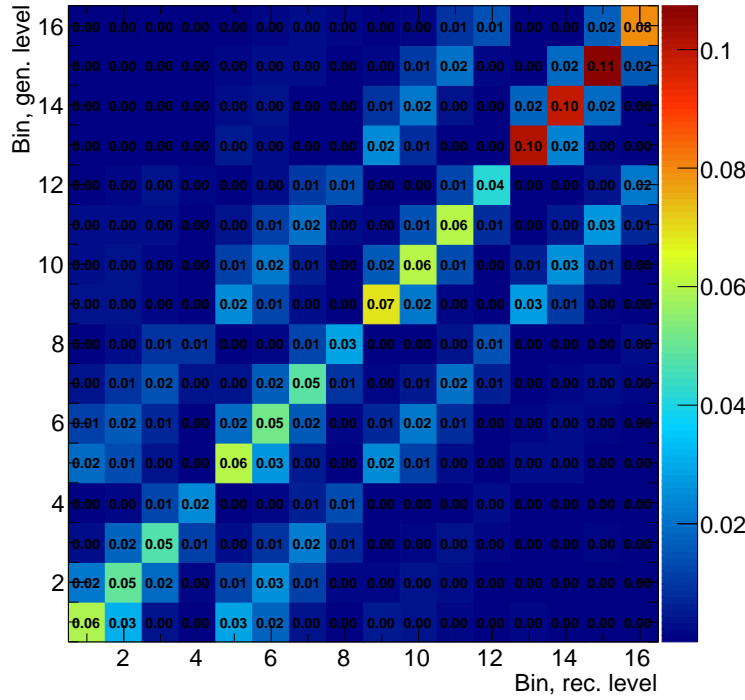


Figure 74: The migration matrix for the $[M(\bar{t}\bar{t}), y(t)]$ cross sections for the generator-level bins.

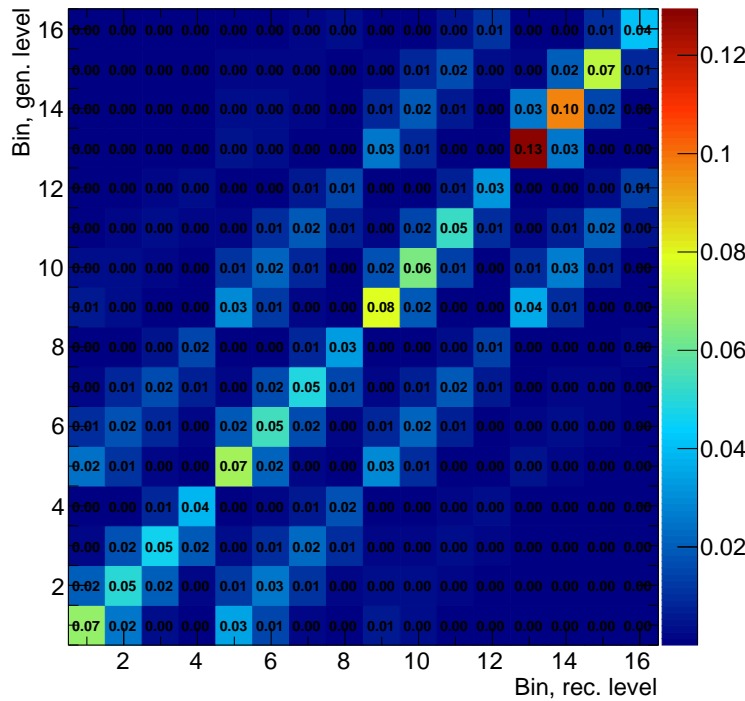


Figure 75: The migration matrix for the $[M(\bar{t}\bar{t}), y(\bar{t}\bar{t})]$ cross sections for the generator-level bins.

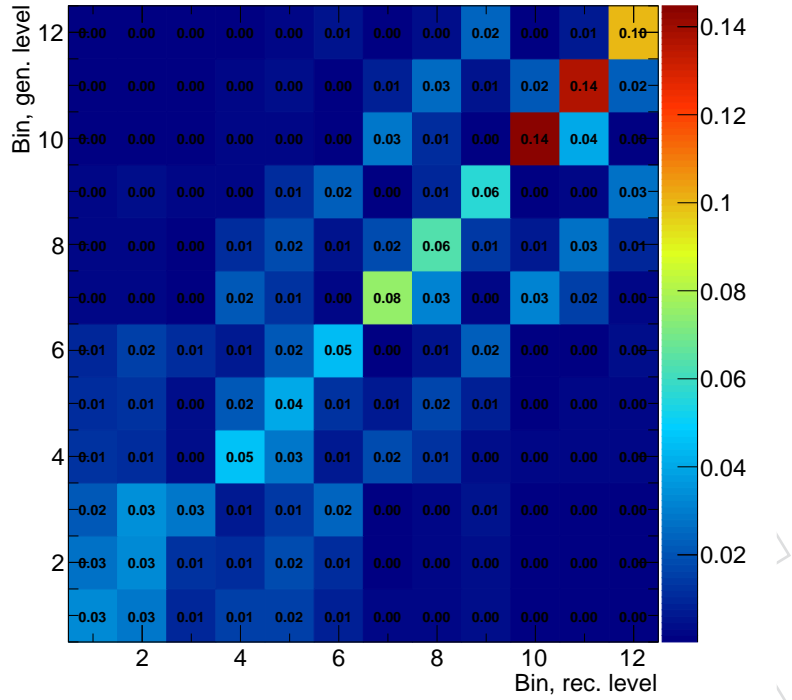


Figure 76: The migration matrix for the $[M(\bar{t}), \Delta\eta(t, \bar{t})]$ cross sections for the generator-level bins.

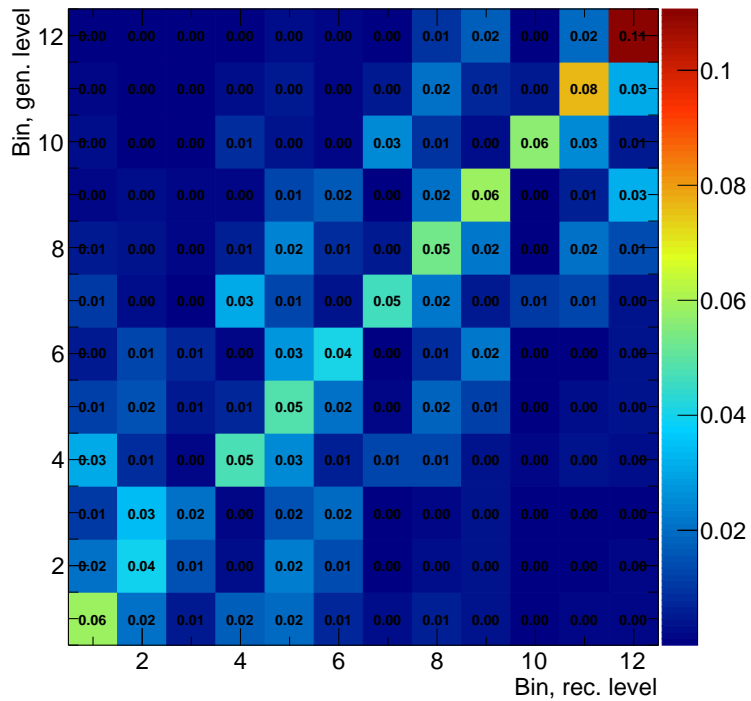


Figure 77: The migration matrix for the $[M(\bar{t}), \Delta\phi(t, \bar{t})]$ cross sections for the generator-level bins.

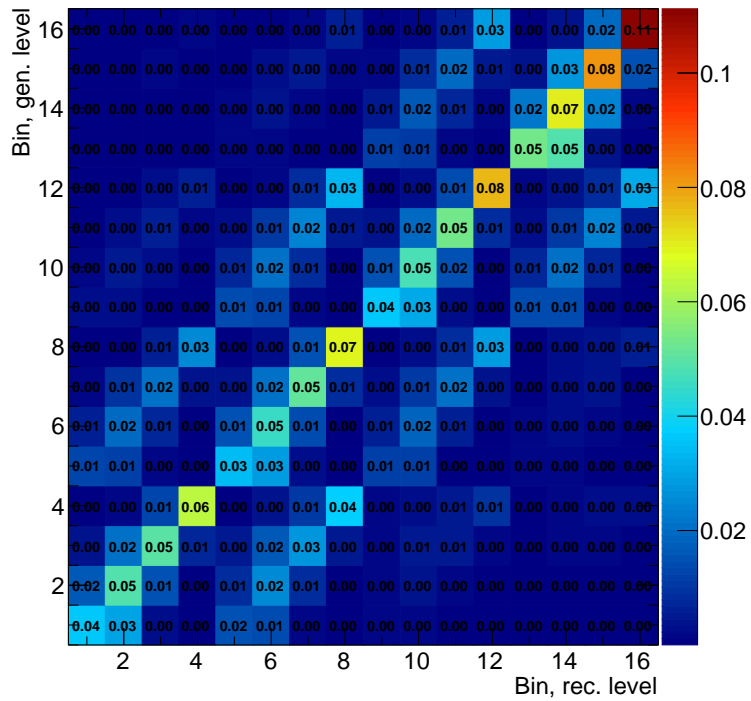


Figure 78: The migration matrix for the $[M(t\bar{t}), p_T(t\bar{t})]$ cross sections for the generator-level bins.

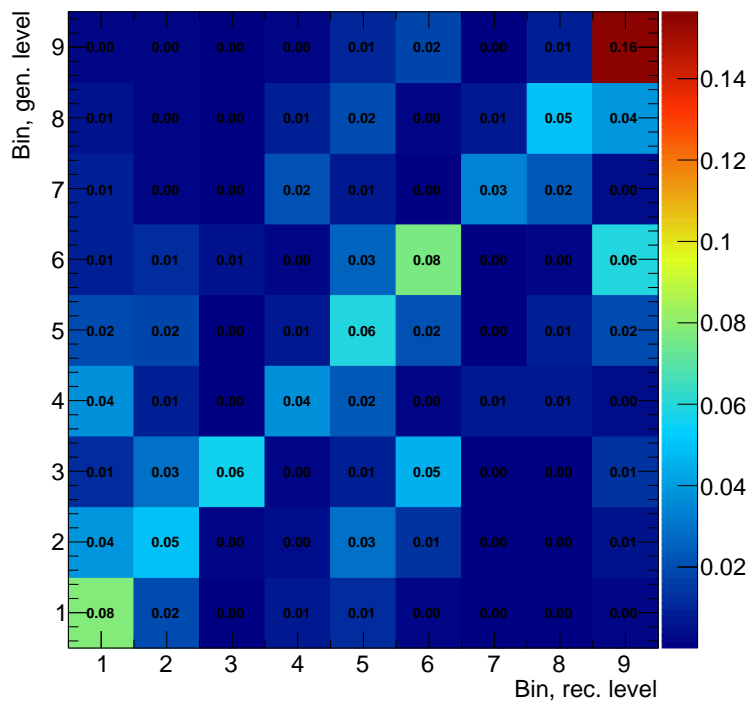


Figure 79: The migration matrix for the $[M(t\bar{t}), p_T(t)]$ cross sections for the generator-level bins.

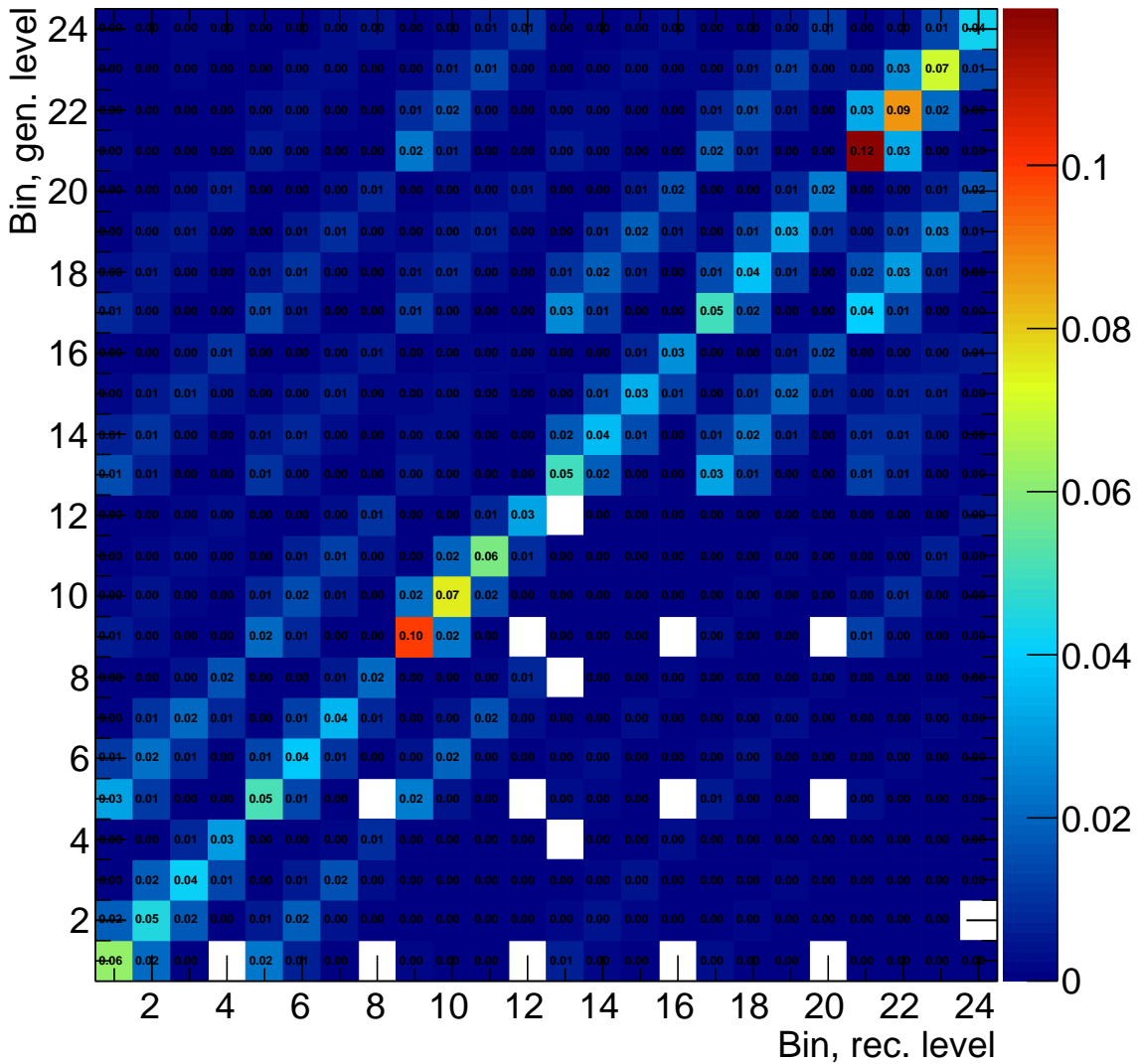


Figure 80: The migration matrix for the $[N_{\text{jet}}, M(t\bar{t}), y(t\bar{t})]$ cross sections (2 N_{jet} bins) for the generator-level bins.

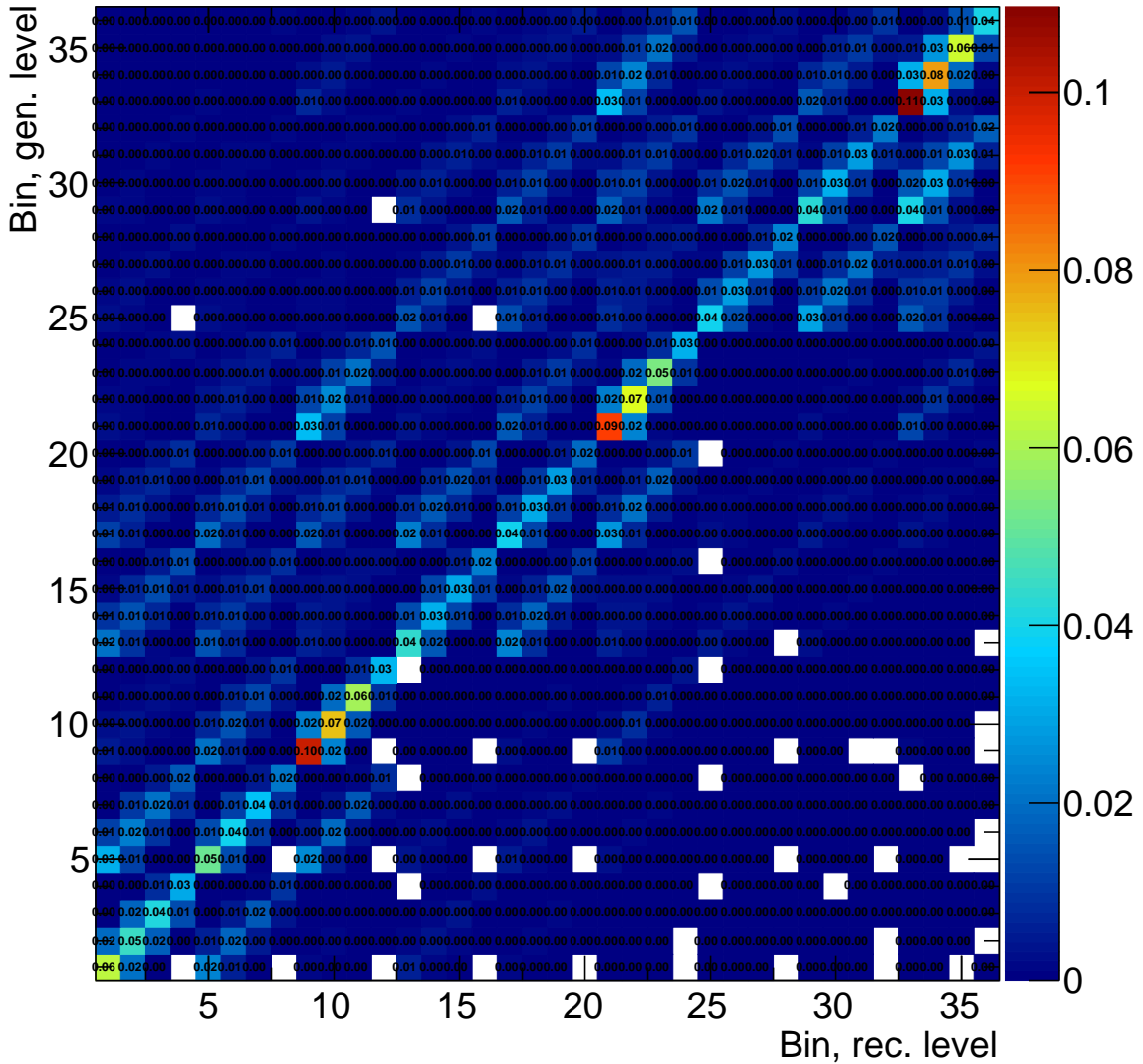


Figure 81: The migration matrix for the $[N_{\text{jet}}, M(t\bar{t}), y(t\bar{t})]$ cross sections (3 N_{jet} bins) for the generator-level bins.

875 7 Results of the measurement

876 The normalised differential⁴ cross sections are measured in the full phase space at parton level
 877 for the following variables:

878 1. double-differential cross sections as a function of pair of variables:

- 879 • $y(t)$ and $p_T(t)$,
- 880 • $M(t\bar{t})$ and $y(t)$,
- 881 • $M(t\bar{t})$ and $y(\bar{t}\bar{t})$,
- 882 • $M(t\bar{t})$ and $\Delta\eta(t, \bar{t})$,
- 883 • $M(t\bar{t})$ and $\Delta\phi(t, \bar{t})$,
- 884 • $M(t\bar{t})$ and $p_T(\bar{t}\bar{t})$,
- 885 • $M(t\bar{t})$ and $p_T(t)$,

886 2. triple-differential cross sections as a function of N_{jet} , $M(t\bar{t})$ and $y(t\bar{t})$. This cross section is
 887 measured separately using two and three bins of N_{jet} .

888 7.1 Impact of statistical and systematic uncertainties

889 The statistical⁵ and systematic uncertainties for all measured cross sections are shown in Figs. 82–
 890 90. For all distributions, the bins for the last dimension variable are grouped in ranges of the
 891 first (first and second) variable for double-differential (triple-differential) cross sections (these
 892 ranges are separated by bold dotted vertical lines on the plots, while the bins for the last dimen-
 893 sion variable are separated by ordinary dotted vertical lines). Separately are shown contribu-
 894 tions from the statistical and systematic uncertainties. The systematic uncertainties are further
 895 splitted into three contributions: experimental systematic uncertainties ('exp'), model system-
 896 atic uncertainties which are estimated by using weights ('mod (w)') and model systematic un-
 897 certainties which are estimated using independent MC samples ('mod (i)'). Furthermore, the
 898 breakdown of the individual systematic uncertainties is shown for each of the three contribu-
 899 tions. For each uncertainty component, its average size over all bins is estimated and reported
 900 on the plot.

901 The numerical values of the measured cross sections and their uncertainties are provided in
 902 Appendix K. On average, the total uncertainties constitute 5–10% for all measured cross sec-
 903 tions, but reach 20% and more in some phase-space corners, such as e.g. the last N_{jet} bin of
 904 the $[N_{jet}, M(t\bar{t}), y(t\bar{t})]$ cross section with three bins of N_{jet} . The total uncertainties are domi-
 905 nated by the systematic uncertainties receiving similar contributions from the experimental and
 906 independent-MC based systematic sources, while the weight-based systematic sources provide
 907 a smaller contribution. Further, the experimental systematic uncertainties are dominated by the
 908 JES variations, while the independent-MC based systematic uncertainties receive about equal
 909 contributions from almost all sources. For most of the sources, the latter is consistent with be-
 910 ing driven by the statistical fluctuations arising from the limited MC statistics, as estimated by
 911 taking into account the number of generated MC events in the nominal MC simulation and in
 912 each systematic variation ($\approx 160M$) and comparing to the number of reconstructed events in
 913 the data and MC (see Tab. 7). Also the JES uncertainties receive contributions arising due to the
 914 limited MC statistics, because each JES variation results in a different event sample.

⁴For presentation purposes, all measured multi-differential cross sections are reported as single-differential in different ranges, i.e. the cross sections are divided by the bin width of one of the variables only.

⁵The quoted statistical uncertainties include also a small contribution (which increases them by $\approx 10\%$) arising from the limited statistics of the nominal MC simulation.

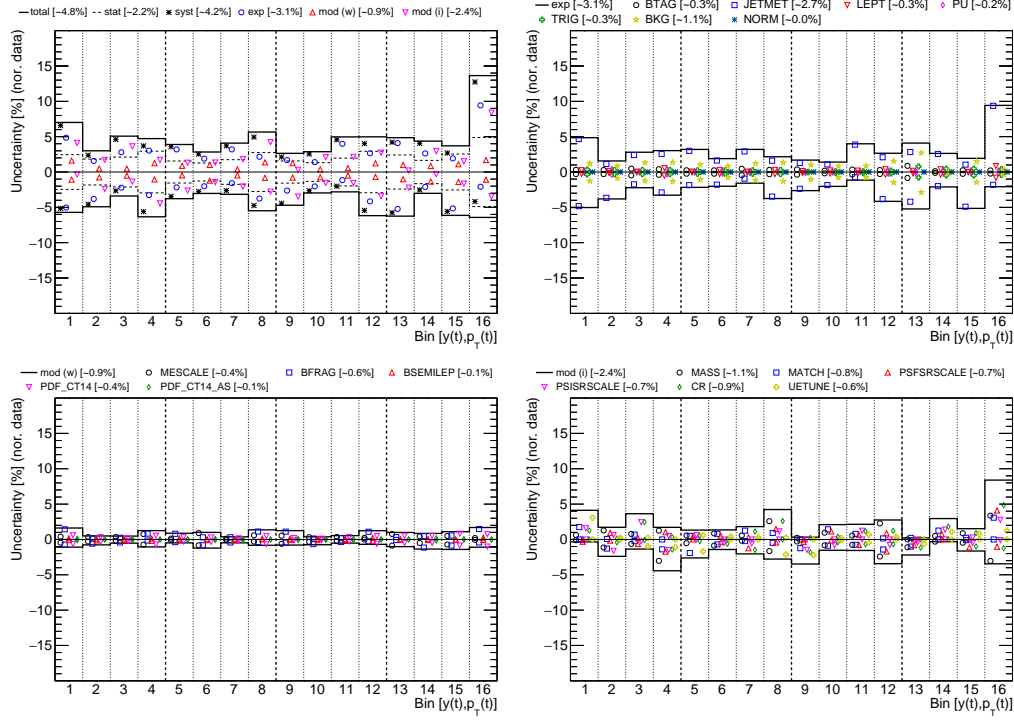


Figure 82: The statistical and systematic uncertainties of the measured $[y(t), p_T(t)]$ cross sections (see text for further details).

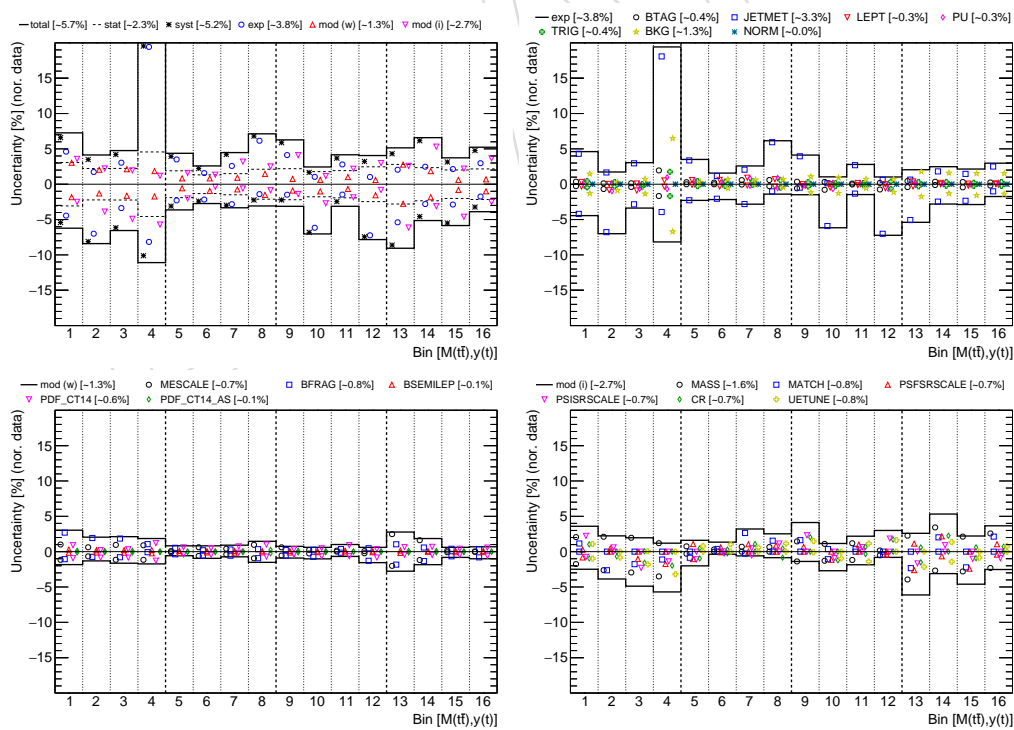


Figure 83: The statistical and systematic uncertainties of the measured $[M(t), y(t)]$ cross sections (see text for further details).

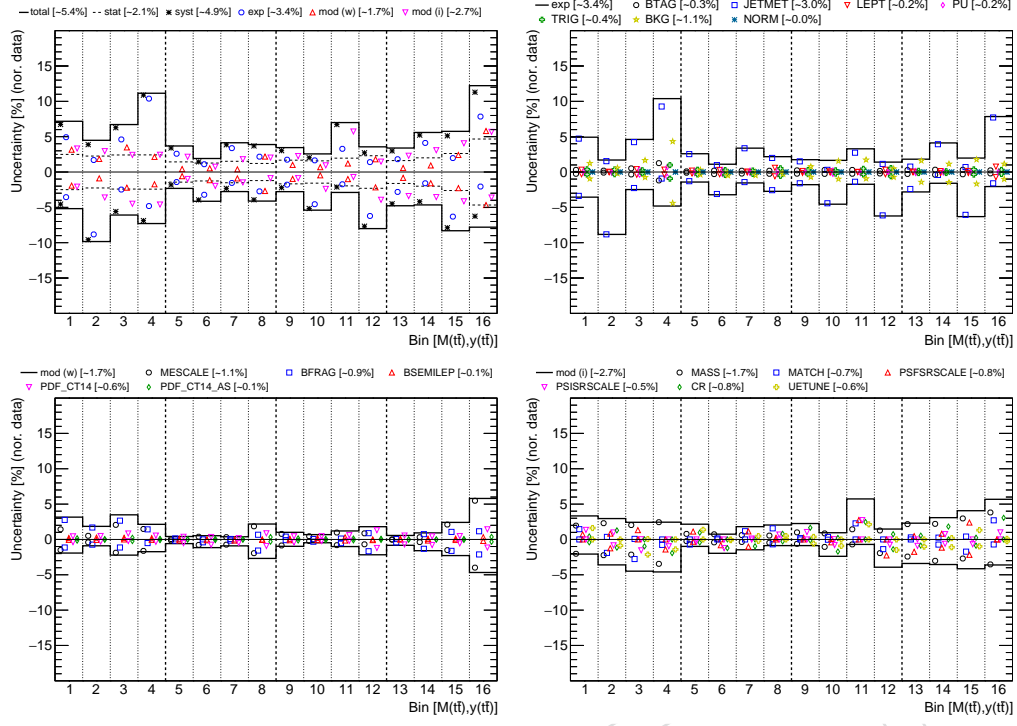


Figure 84: The statistical and systematic uncertainties of the measured $[M(t\bar{t}), y(t\bar{t})]$ cross sections (see text for further details).

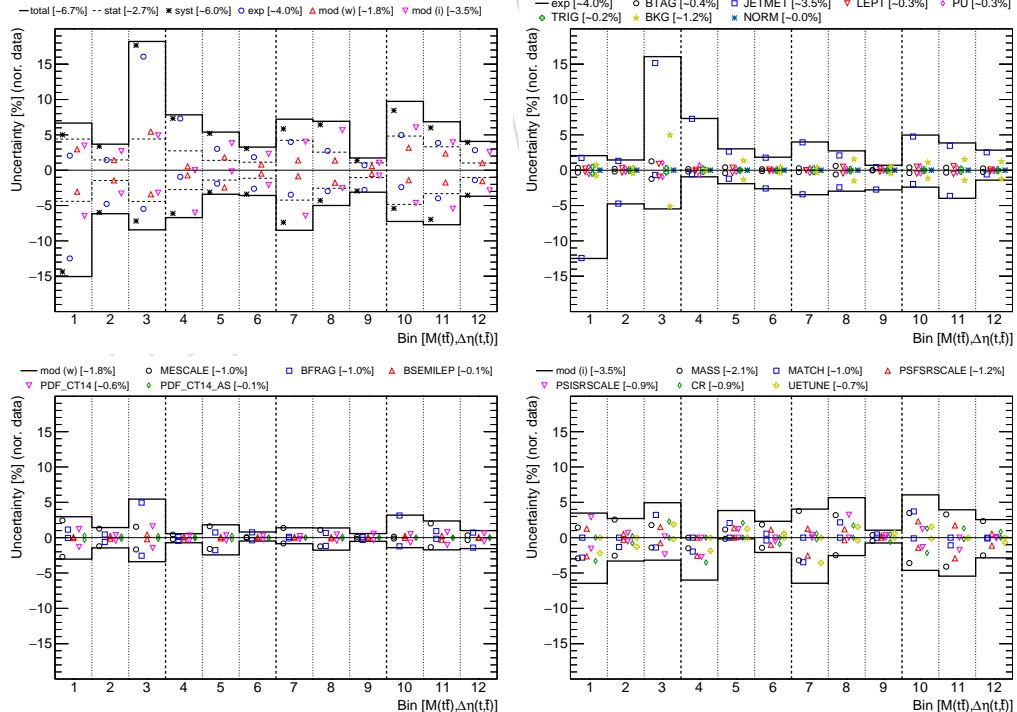


Figure 85: The statistical and systematic uncertainties of the measured $[M(t\bar{t}), \Delta\eta(t, \bar{t})]$ cross sections (see text for further details).

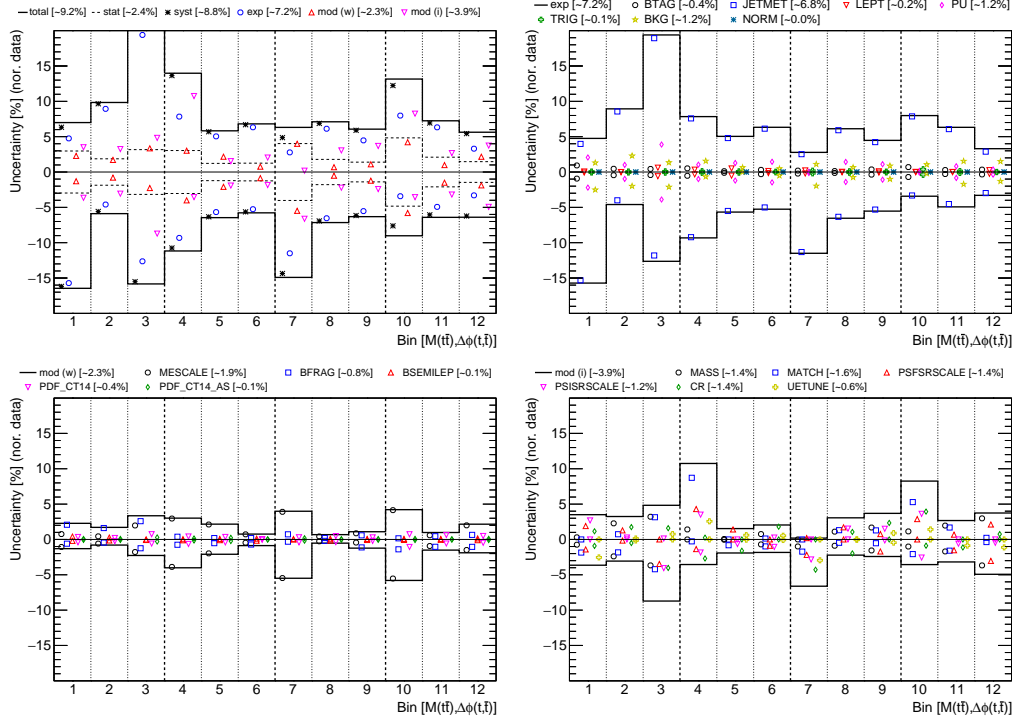


Figure 86: The statistical and systematic uncertainties of the measured $[M(t\bar{t}), \Delta\phi(t, \bar{t})]$ cross sections (see text for further details).

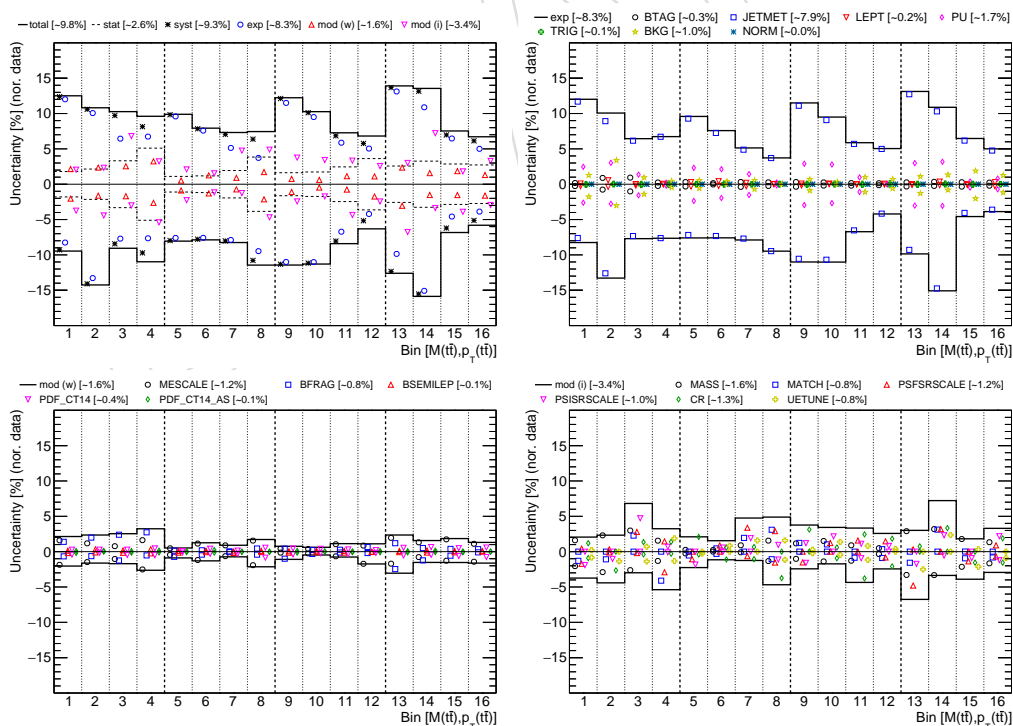


Figure 87: The statistical and systematic uncertainties of the measured $[M(t\bar{t}), p_T(t\bar{t})]$ cross sections (see text for further details).

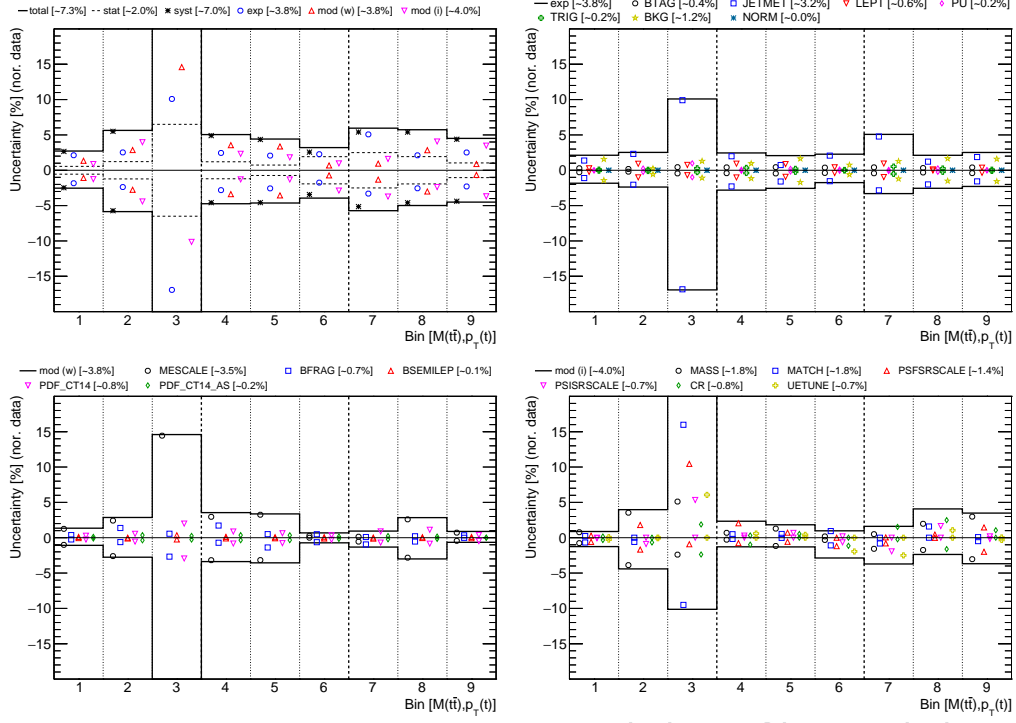


Figure 88: The statistical and systematic uncertainties of the measured $[M(\bar{t}), p_T(t)]$ cross sections (see text for further details).

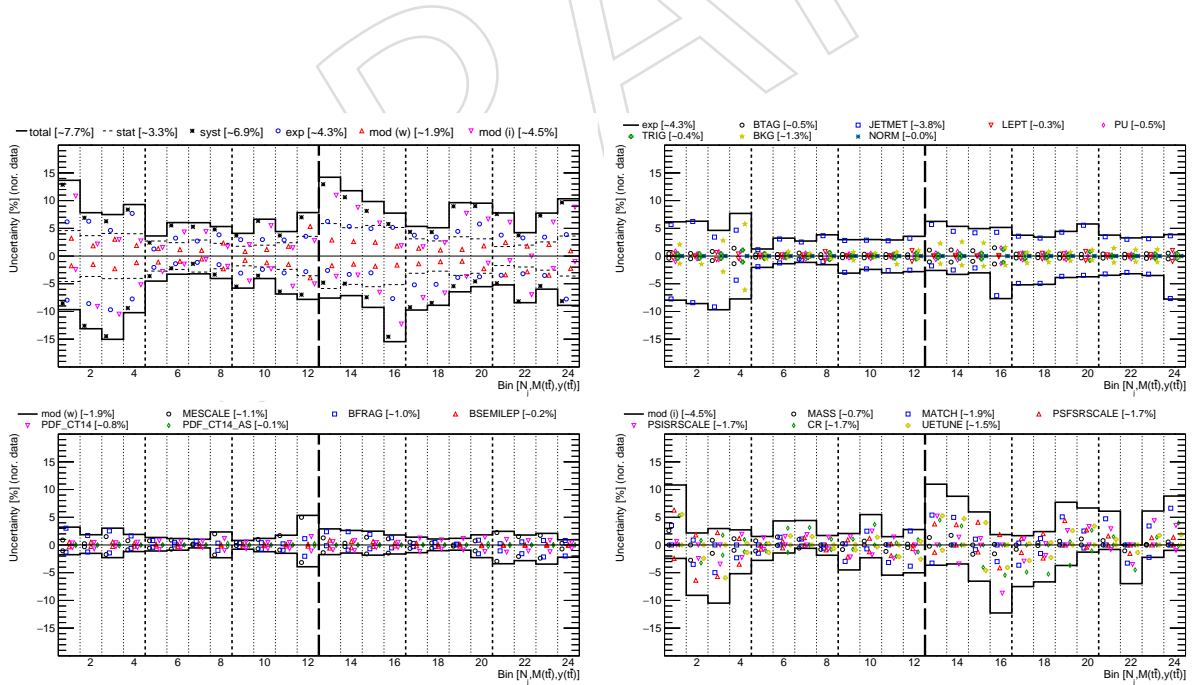


Figure 89: The statistical and systematic uncertainties of the measured $[N_{jet}, M(\bar{t}), y(\bar{t})]$ cross sections (see text for further details).

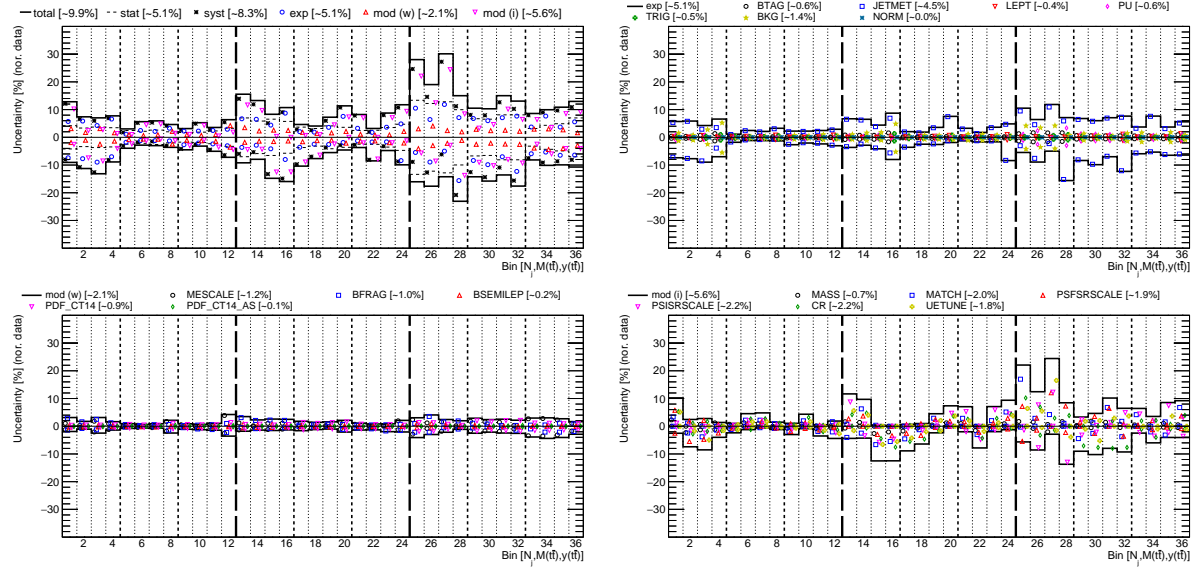


Figure 90: The statistical and systematic uncertainties of the measured $[N_{\text{jet}}, M(\text{t}\bar{t}), y(\text{t}\bar{t})]$ cross sections (see text for further details).

915 7.2 Comparison to MC models

In Figs. 91–99 the measured cross sections are compared to three MC simulations: POWHEGv2 + PYTHIA8, POWHEGv2 + HERWIG++, and MG5_aMC@NLO($FxFx$) + PYTHIA8. For each comparison, χ^2 is reported which is calculated taking into account the statistical and systematic data uncertainties. The χ^2 values are calculated as follows:

$$\chi^2 = \mathbf{R}_{N-1}^T \mathbf{Cov}_{N-1}^{-1} \mathbf{R}_{N-1}, \quad (12)$$

where \mathbf{R}_{N-1} is the column vector of the residuals calculated as the difference of the measured cross sections and the corresponding predictions obtained by discarding one of the N bins, and \mathbf{Cov}_{N-1} is the $(N-1) \times (N-1)$ submatrix obtained from the full covariance matrix by discarding the corresponding row and column. The matrix \mathbf{Cov}_{N-1} obtained in this way is invertible, while the original covariance matrix \mathbf{Cov} is singular. This is because for normalized cross sections one loses one degree of freedom, as can be deduced from Eq. (11). The covariance matrix \mathbf{Cov} is calculated as:

$$\mathbf{Cov} = \mathbf{Cov}^{\text{unf}} + \mathbf{Cov}^{\text{syst}}, \quad (13)$$

where $\mathbf{Cov}^{\text{unf}}$ and $\mathbf{Cov}^{\text{syst}}$ are the covariance matrices accounting for the statistical uncertainties from the unfolding, and the systematic uncertainties, respectively. The systematic covariance matrix $\mathbf{Cov}^{\text{syst}}$ is calculated as:

$$\mathbf{Cov}_{ij}^{\text{syst}} = \sum_{k,l} \frac{1}{N_k} C_{j,k,l} C_{i,k,l}, \quad 1 \leq i \leq N, \quad 1 \leq j \leq N, \quad (14)$$

916 where $C_{i,k,l}$ stands for the systematic uncertainty from variation l of source k in the i th bin, and
 917 N_k is the number of variations for source k . The sums run over all sources of the systematic un-
 918 certainty and all corresponding variations. Most of the systematic uncertainty sources in this
 919 analysis consist of positive and negative variations and thus have $N_k = 2$, whilst several model
 920 uncertainties (the model of color reconnection and the b quark fragmentation function) consist
 921 of more than two variations which is accounted for in Eq. 14. All systematic uncertainties are
 922 treated as additive, i.e. the relative uncertainties are used to scale the corresponding measured

value in the construction of $\mathbf{Cov}^{\text{syst}}$. This treatment is consistent with the cross section normalization. The cross section measurements for different pairs of observables are statistically and systematically correlated. No attempt is made to quantify the correlations between bins from different double-differential distributions. Thus, quantitative comparisons between theoretical predictions and the data can only be made for individual distributions.

In Fig. 91, the $p_T(t)$ distribution is compared in different ranges of $|y(t)|$ to predictions from POWHEGV2 + PYTHIA8, POWHEGV2 + HERWIG++, and MG5_aMC@NLO(FxFx) + PYTHIA8. The data distribution is softer than that of the MC expectation over the entire $y(t)$ range. Only POWHEGV2 + HERWIG++ describes the data well, while the other two simulations predict a harder $p_T(t)$ distribution than measured in the data over the entire $y(t)$ range. The disagreement level is the strongest for POWHEGV2 + PYTHIA8.

Figures 92 and 93 illustrate the distributions of $|y(t)|$ and $|y(\bar{t})|$ in different $M(t\bar{t})$ ranges compared to the same set of MC models. The shape of the $y(t)$ and $y(\bar{t})$ distribution is well modelled by all MC, while the $M(t\bar{t})$ distribution is softer in the data than in MC. The latter trend is the strongest for POWHEGV2 + PYTHIA8, being consistent with the disagreement for the $p_T(t)$ distribution (see Fig. 91). The best agreement for both $[M(t\bar{t}), y(t)]$ and $[M(t\bar{t}), y(\bar{t})]$ cross sections is provided by POWHEGV2 + HERWIG++.

In Fig. 94, the $\Delta\eta(t, \bar{t})$ distribution is compared in the same $M(t\bar{t})$ ranges to the MC predictions. For all generators there is a discrepancy between the data and simulation for the medium and high $M(t\bar{t})$ bins, where the predicted $\Delta\eta(t, \bar{t})$ values are too low. The disagreement is the strongest for MG5_aMC@NLO(FxFx) + PYTHIA8.

Figures 95 and 96 illustrate the comparison of the distributions of $\Delta\phi(t, \bar{t})$ and $p_T(t\bar{t})$ in the same $M(t\bar{t})$ ranges to the MC models. Both these cross sections are sensitive to radiation. All MC models describe the data well within uncertainties, except MG5_aMC@NLO(FxFx) + PYTHIA8 and the $[M(t\bar{t}), p_T(t\bar{t})]$ cross sections, which predicts a too hard $p_T(t\bar{t})$ distribution in the last $M(t\bar{t})$ bin.

In Fig. 97, the $p_T(t)$ distribution is compared in different $M(t\bar{t})$ ranges to the MC predictions. None of the simulations is able to describe the data, generally predicting a too hard $p_T(t)$ distribution. The disagreement is the strongest for POWHEGV2 + PYTHIA8. While the POWHEGV2 + HERWIG++ simulation was found to be able to reasonably describe the $p_T(t)$ distribution in the entire range of $y(t\bar{t})$ (see Fig. 91), it does not provide a good description in all ranges of $M(t\bar{t})$, in particular predicting a too hard distribution at high $M(t\bar{t})$.

Figures 98 and 99 illustrate the triple-differential cross sections as a function of $y(t\bar{t})$ in different $M(t\bar{t})$ and N_{jet} ranges, measured using two and three bins of N_{jet} . For the measurement with two N_{jet} bins, all MC models describe the data well. For the measurement with three N_{jet} bins, only POWHEGV2 + PYTHIA8 is in satisfactory agreement with the data.

All obtained χ^2 values, together with the corresponding numbers of degrees of freedom (dof), are listed in Table 20. The corresponding p -values are visualised in Fig. 100. From these values one can conclude that none of the considered MC generators is able to correctly describe all distributions. In particular, for $[M(t\bar{t}), \Delta\eta(t, \bar{t})]$ and $[M(t\bar{t}), p_T(t)]$ the χ^2 values are relatively large for all MC generators. In total, the best agreement with the data is provided by POWHEGV2 + PYTHIA8 and POWHEGV2 + HERWIG++, with POWHEGV2 + HERWIG++ better describing the measurements involving probing the p_T distribution and POWHEGV2 + PYTHIA8 better describing the ones with extra jet multiplicity, while MG5_aMC@NLO(FxFx) + PYTHIA8 describes the data worse.

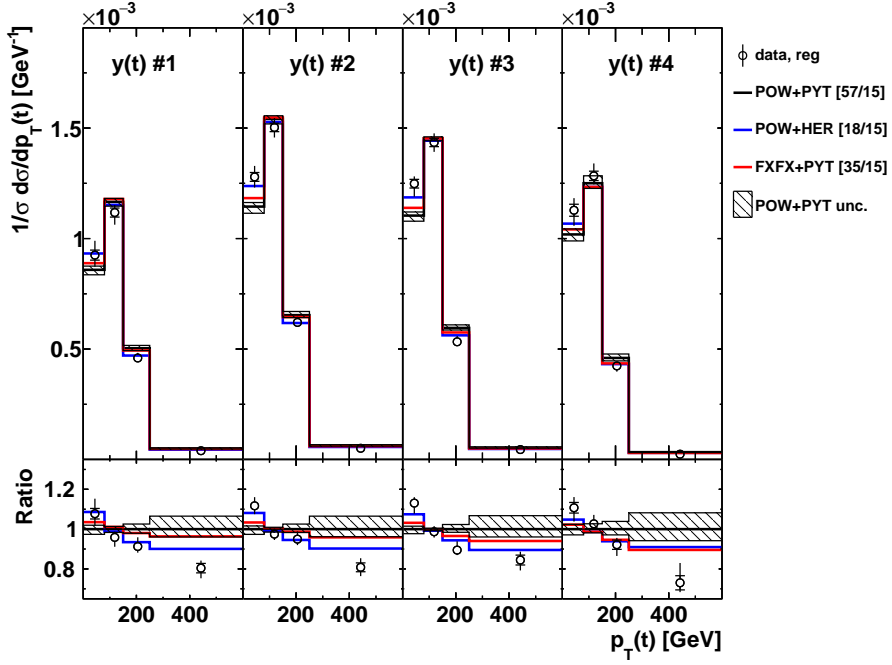


Figure 91: Comparison of the measured $[y(t), p_T(t)]$ cross sections to MC predictions calculated using POWHEGv2 + PYTHIA8 ('POW-PYT'), POWHEGv2 + HERWIG++ ('POW-HER'), and MG5_aMC@NLO($FxFx$) + PYTHIA8 ('FXFX-PYT'). The inner vertical bars on the data points represent the statistical uncertainties and the full bars include also the systematic uncertainties added in quadrature. For each MC model, χ^2/dof is reported in brackets. The hatched regions correspond to the estimated uncertainties in POWHEGv2 + PYTHIA8 (see Section 5). In the bottom panel, the ratios of the data and other simulations to the POWHEGv2 + PYTHIA8 predictions are shown.

Table 20: The χ^2 values (taking into account data uncertainties only) and dof of the measured cross sections with respect to the various MC predictions.

Cross section variables	dof	χ^2		
		POW-PYT	POW-HER	FXFX-PYT
$[y(t), p_T(t)]$	15	57	18	35
$[M(t\bar{t}), y(t)]$	15	26	18	36
$[M(t\bar{t}), y(\bar{t})]$	15	28	17	23
$[M(t\bar{t}), \Delta\eta(t, \bar{t})]$	11	66	68	124
$[M(t\bar{t}), \Delta\phi(t, \bar{t})]$	15	14	18	10
$[M(t\bar{t}), p_T(t\bar{t})]$	15	21	22	29
$[M(t\bar{t}), p_T(t)]$	15	77	34	68
$[N_{\text{jet}}, M(t\bar{t}), y(t\bar{t})]$ (2 N_{jet} bins)	23	34	31	34
$[N_{\text{jet}}, M(t\bar{t}), y(t\bar{t})]$ (3 N_{jet} bins)	35	50	66	63

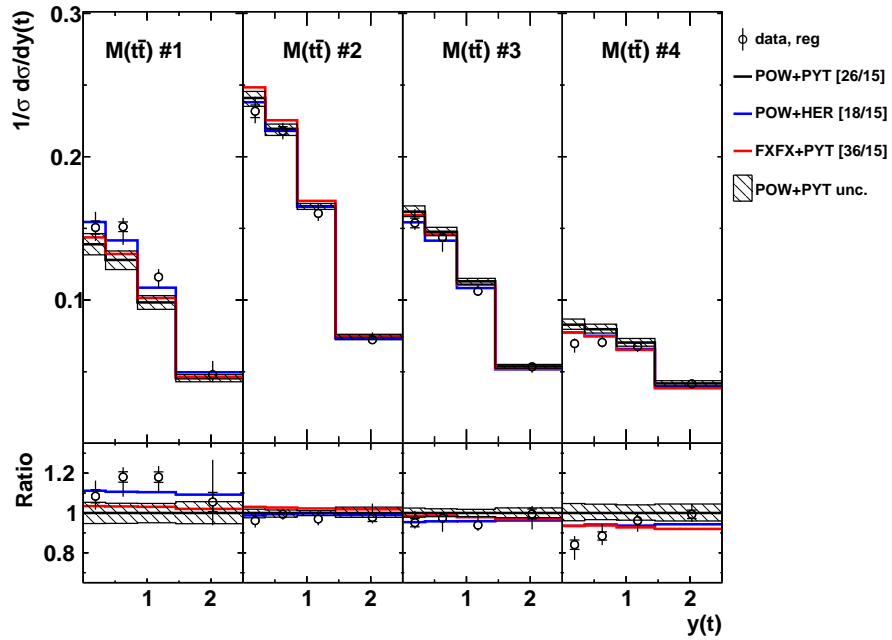


Figure 92: Comparison of the measured $[M(t\bar{t}), y(t)]$ cross sections to MC predictions (see Fig. 91 for further details).

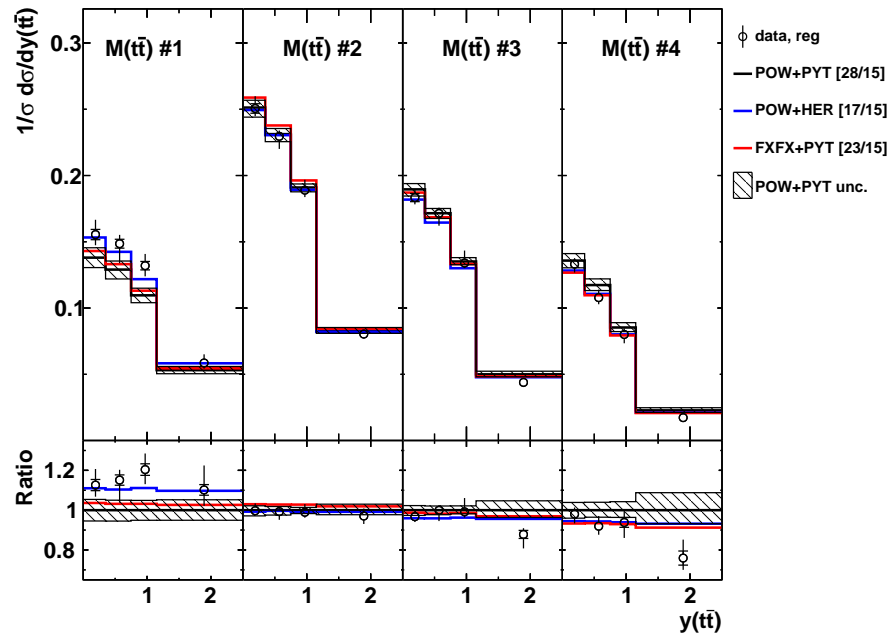


Figure 93: Comparison of the measured $[M(t\bar{t}), y(t\bar{t})]$ cross sections to MC predictions (see Fig. 91 for further details).

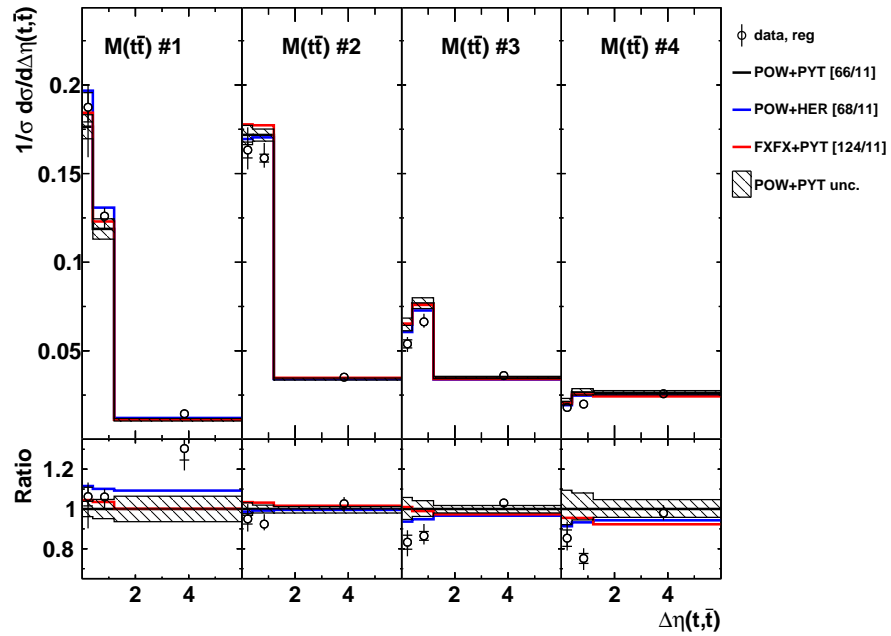


Figure 94: Comparison of the measured $[M(\bar{t}), \Delta\eta(t, \bar{t})]$ cross sections to MC predictions (see Fig. 91 for further details).

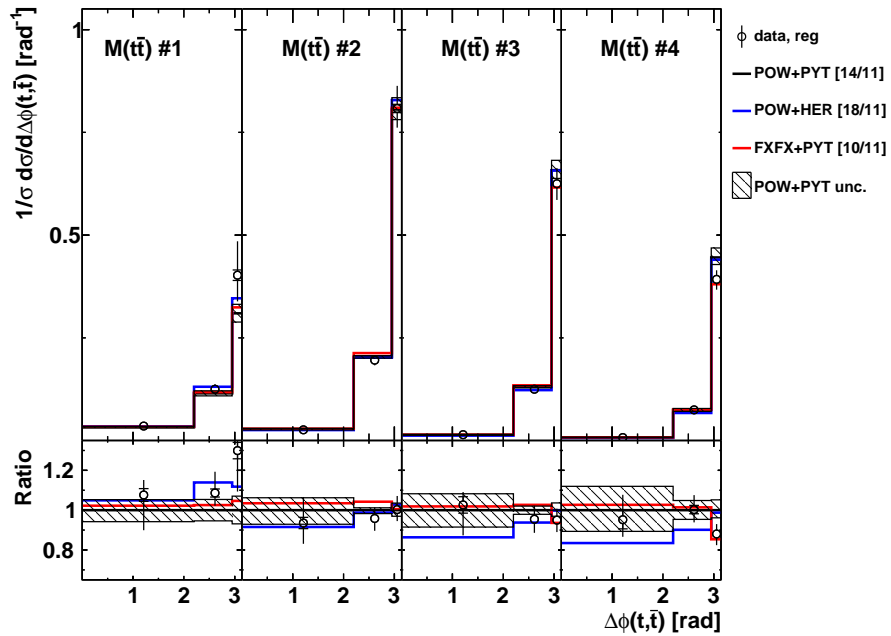


Figure 95: Comparison of the measured $[M(\bar{t}), \Delta\phi(t, \bar{t})]$ cross sections to MC predictions (see Fig. 91 for further details).

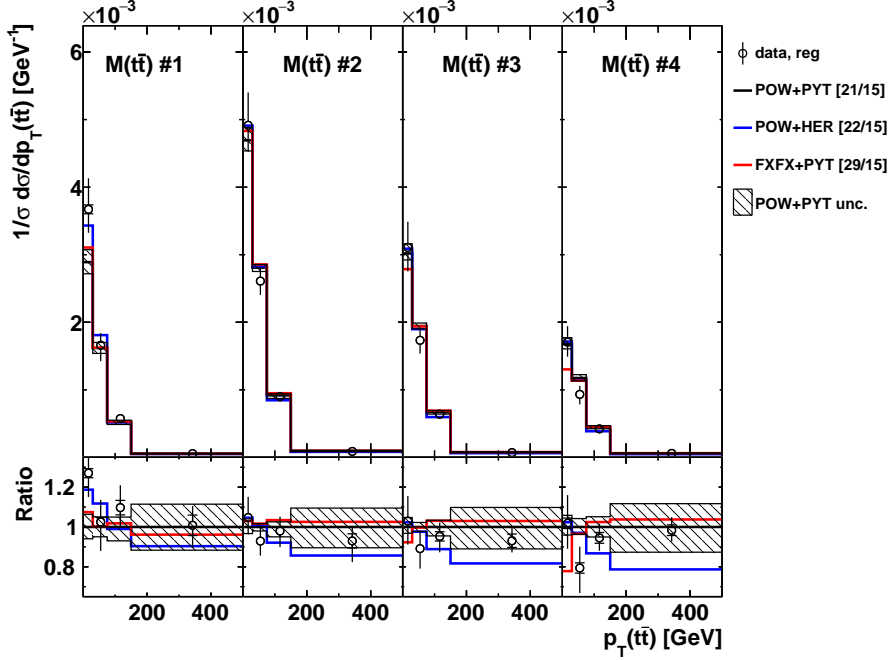


Figure 96: Comparison of the measured $[M(t\bar{t}), p_T(t\bar{t})]$ cross sections to MC predictions (see Fig. 91 for further details).

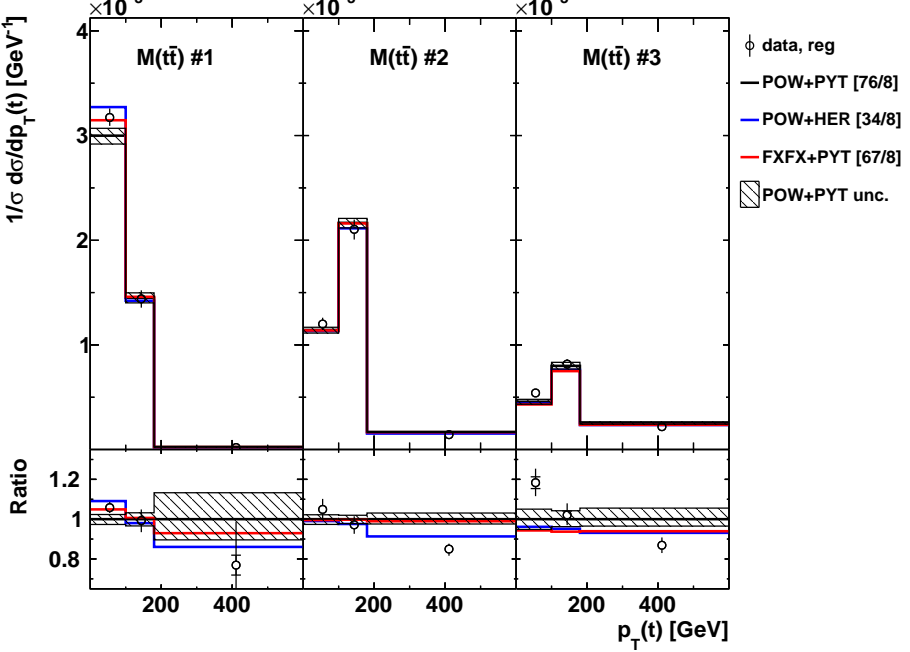


Figure 97: Comparison of the measured $[M(t\bar{t}), p_T(t)]$ cross sections to MC predictions (see Fig. 91 for further details).

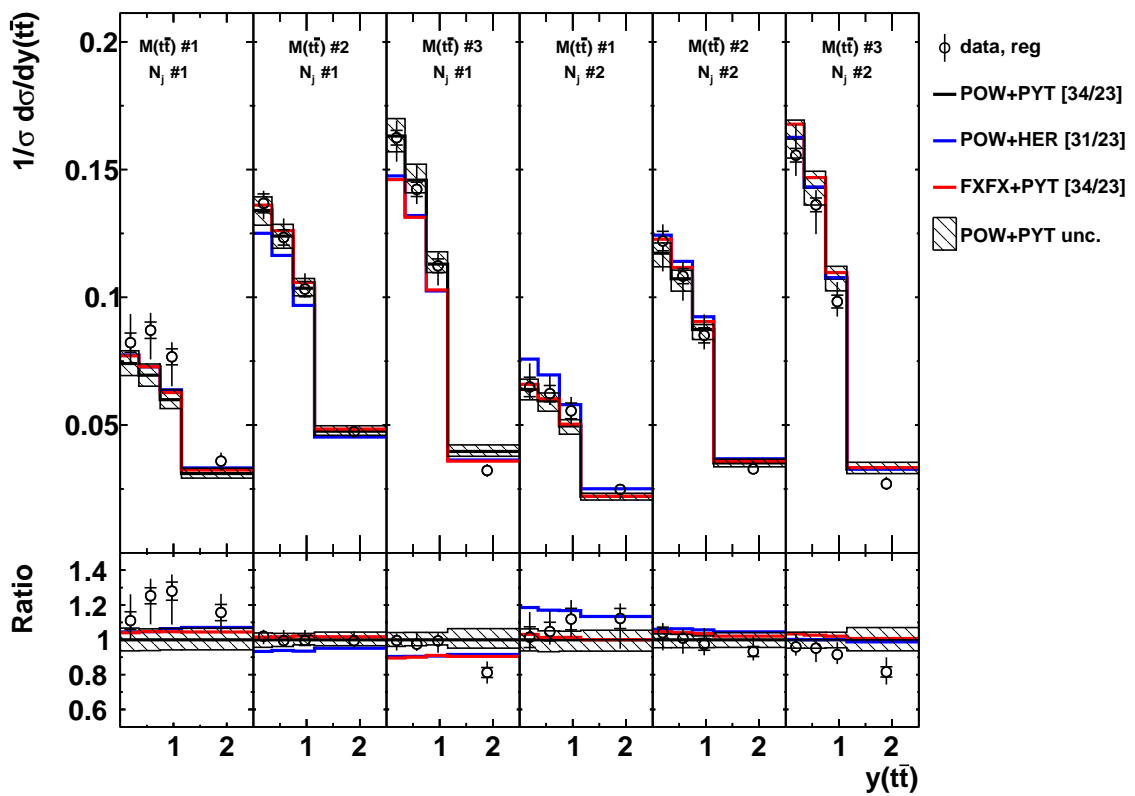


Figure 98: Comparison of the measured $[N_{\text{jet}}, M(t\bar{t}), y(t\bar{t})]$ cross sections to MC predictions (see Fig. 91 for further details).

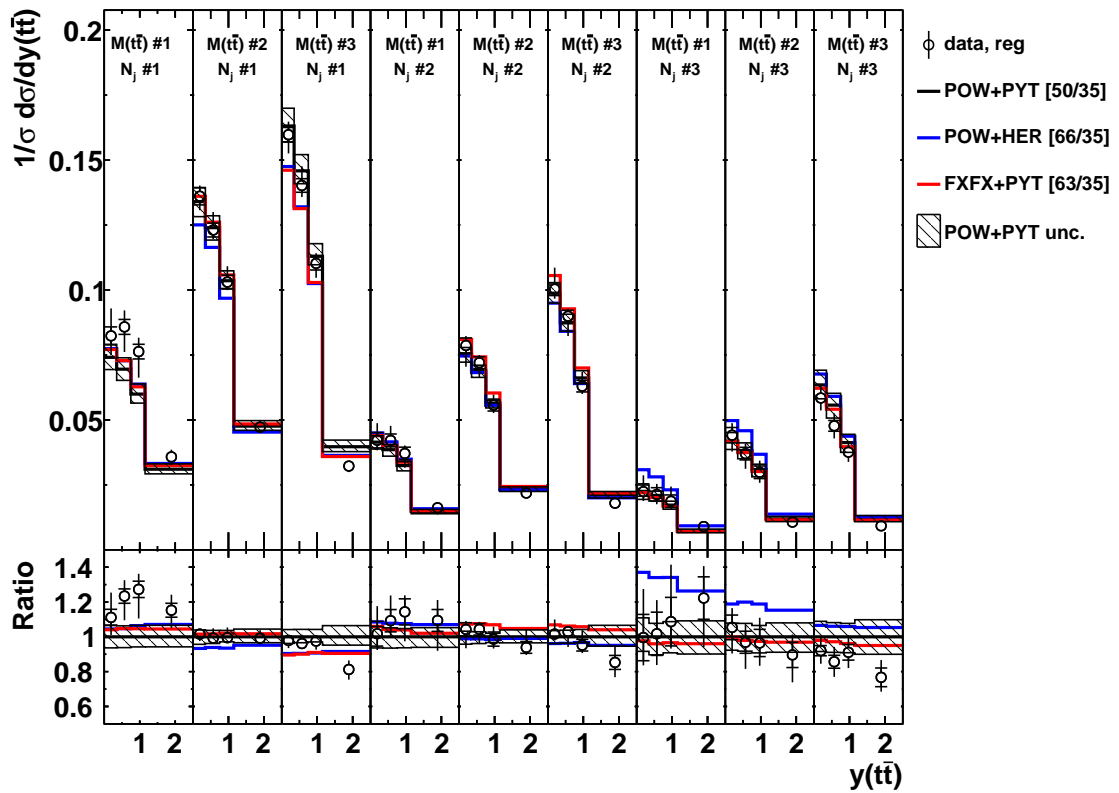


Figure 99: Comparison of the measured $[N_{\text{jet}}, M(t\bar{t}), y(t\bar{t})]$ cross sections to MC predictions (see Fig. 91 for further details).

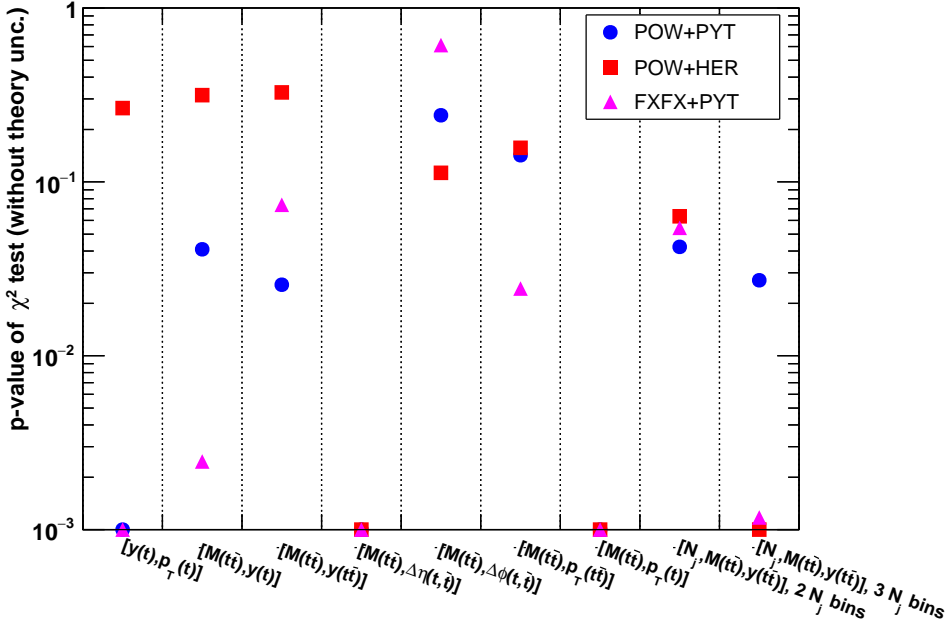


Figure 100: The p -values (taking into account data uncertainties only) of the measured cross sections with respect to the various MC predictions. Points with $p \leq 0.001$ are shown at $p = 0.001$.

968 8 Extraction of α_s and m_t^{pole} from measured $[N_{jet}, M(t\bar{t}), y(t\bar{t})]$ cross 969 sections using external PDFs

970 To extract α_s and m_t^{pole} , the measured cross sections are compared to fixed-order (NLO) predictions,
971 which do not have tunable parameters, except factorisation and renormalisation scales,
972 and thus allow a more rigorous assessment of theoretical uncertainties than predictions of MC
973 event generators that complement fixed-order computations with parton showers, hadronisation,
974 and multiple-parton interactions. Furthermore, for PDF determination using these data
975 fast computation techniques have to be used which are currently available only for fixed-order
976 calculations.

977 8.1 Comparison of measured $[N_{jet}, M(t\bar{t}), y(t\bar{t})]$ cross sections to fixed-order 978 calculations

979 Fixed-order theoretical calculations for fully differential cross sections in inclusive $t\bar{t}$ production
980 are publicly available at NLO $O(\alpha_s^3)$ in the fixed-flavour number scheme [68], where α_s is the
981 strong coupling strength. NLO calculations are also available for inclusive $t\bar{t}$ production with
982 1 [69], 2 [70, 71] or 3 [72] additional jets. The exact fully differential NNLO $O(\alpha_s^4)$ calculations
983 for inclusive $t\bar{t}$ production have recently appeared in the literature [73, 74].

984 The measured $[N_{jet}, M(t\bar{t}), y(t\bar{t})]$ cross sections are compared to NLO predictions obtained using
985 different PDF sets, α_s and m_t^{pole} values to assess their sensitivity to their input values. The
986 NLO predictions are obtained using the MG5_aMC@NLO framework. The cross sections for
987 the $N_{jet} = 0(1)$ bin are obtained as the difference of the inclusive $t\bar{t}$ ($t\bar{t} + 1$ jet) and $t\bar{t} + 1$ jet
988 ($t\bar{t} + 2$ jets) cross sections. A number of the latest proton PDF sets determined at NLO are used,
989 namely: ABMP16 [75], CJ15 [76], CT14 [77], HERAPDF2.0 [78], JR14 [79], MMHT2014 [80], and

NNPDF3.1 [81], available via the LHAPDF interface (version 6.1.5) [82]. The number of active flavours is set to $n_f = 5$, the top quark pole mass $m_t = 172.5 \text{ GeV}$ is used and α_s is set to the value used for the corresponding PDF extraction. The renormalization and factorization scales are chosen to be $\mu_r = \mu_f = H'/2, H' = \sum_i m_{T,i}$ with the sum running over all final-state partons (t, \bar{t} and up to three light partons in the $\bar{t}\bar{t} + 2$ jet calculations) and m_T is transverse mass $m_T = \sqrt{m^2 + p_T^2}$. The theoretical uncertainty is estimated by varying μ_r and μ_f independently up and down by a factor of 2, subject to the additional restriction that the ratio μ_r/μ_f be between 0.5 and 2 [83]. Additionally, an alternative scale choice is considered: $\mu_r = \mu_f = H/2, H = \sum_i m_{T,i}$ with the sum running over t and \bar{t} [74]. A more detailed study of the scale variations is provided in Appendix E. The final uncertainty is determined as an envelope of all scale variations. This uncertainty is referred to hereafter as a scale uncertainty and is supposed to estimate the missing higher-order corrections. The PDF uncertainties are taken into account in the theoretical predictions for each PDF set. The PDF uncertainties of CJ15 [76] and CT14 [77], evaluated at 90% CL, are rescaled to the 68% CL. The uncertainties in the normalized $\bar{t}\bar{t}$ cross sections originating from α_s and m_t are estimated by varying them $\alpha_s = 0.118 \pm 0.001$ and $m_t^{\text{pole}} = 172.5 \pm 1 \text{ GeV}$, respectively.

At the LHC Run-II $\bar{t}\bar{t}$ production proceeds predominantly via gluon-gluon splitting ($\sim 90\%$), thus the predicted cross sections are expected to be mostly sensitive to the gluon PDF. The gluon distribution with its uncertainty bands of several modern PDF sets is compared in Fig. 101 at the scale $\mu_f^2 = 30\,000 \text{ GeV}^2 \simeq m_t^2$ relevant for $\bar{t}\bar{t}$ production. There are significant differences between the PDF sets, especially at high $x \gtrsim 0.1$ values, observed for both the central values and the size of uncertainties. Because of lack of experimental data included in these fits which are able to constrain the gluon distribution in this kinematic range, its determination appears to be sensitive to many assumptions which need to be done in global PDF fits. Since $\bar{t}\bar{t}$ production at the LHC proceeds predominantly via gluon-gluon fusion it is expected to observe similar differences in the predicted cross sections obtained using different PDF sets.

The theoretical uncertainties for the $[N_{\text{jet}}, M(\bar{t}\bar{t}), y(\bar{t}\bar{t})]$ cross sections with 2 and 3 N_{jet} bins are shown in Fig. 102. The CT14 PDF set with $\alpha_s(M_Z) = 0.118$, $m_t^{\text{pole}} = 172.5 \text{ GeV}$ is used. The contributions arising from the PDF, $\alpha_s \pm 0.005$ and $m_t^{\text{pole}} \pm 1 \text{ GeV}$ uncertainties are shown separately. On average, the total theory uncertainties are 5–10%. They receive similar contribution from PDF, α_s , m_t^{pole} and scale variations. This shows that the measured $[N_{\text{jet}}, M(\bar{t}\bar{t}), y(\bar{t}\bar{t})]$ cross sections can be used for reliable and precise extraction of the PDFs and QCD parameters. In this analysis PDF, α_s and m_t^{pole} are extracted from the $[N_{\text{jet}}, M(\bar{t}\bar{t}), y(\bar{t}\bar{t})]$ cross sections with 2 N_{jet} bins. These results are considered as nominal and are checked by repeating the analysis using the $[N_{\text{jet}}, M(\bar{t}\bar{t}), y(\bar{t}\bar{t})]$ cross sections with 3 N_{jet} bins.

Further investigation of the theoretical uncertainties is shown in Figs. 103 and 104, which present the individual scale variations and the PDF uncertainties obtained using different PDF sets, respectively. The plot with the individual scale variations shows that all variations which use the same functional form for the scales tend to be in the same direction, predicting a lower multiplicity of extra jets, while the alternative scale choice $\mu_{r,f} = H/2$ results in the variation in the opposite direction (see also Appendix E). The largest uncertainties arise when varying μ_r and μ_f simultaneously, or using the alternative functional form. The plot with different PDF uncertainties shows that the latter can have very different size (by several times) depending on the PDF set used. The largest and smallest PDF uncertainties are obtained when using the CT14 and JR14 PDF sets, respectively, consistently with Fig. 101.

The sensitivity of the $[N_{\text{jet}}, M(\bar{t}\bar{t}), y(\bar{t}\bar{t})]$ cross sections with 2 N_{jet} bins to the different PDFs,

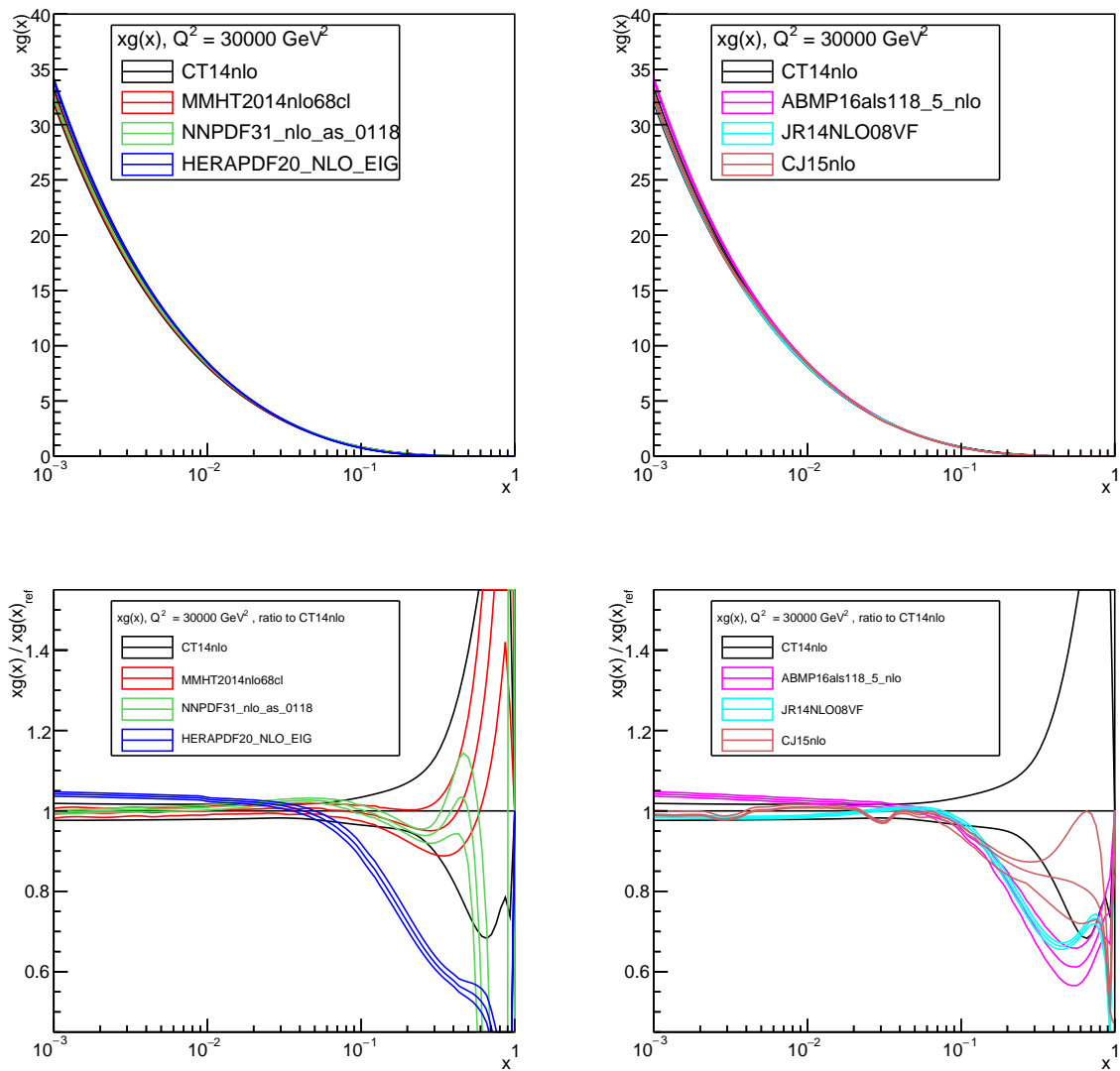


Figure 101: The gluon distribution with its uncertainty bands in different PDFs (top) and their ratios to CT14 (bottom).

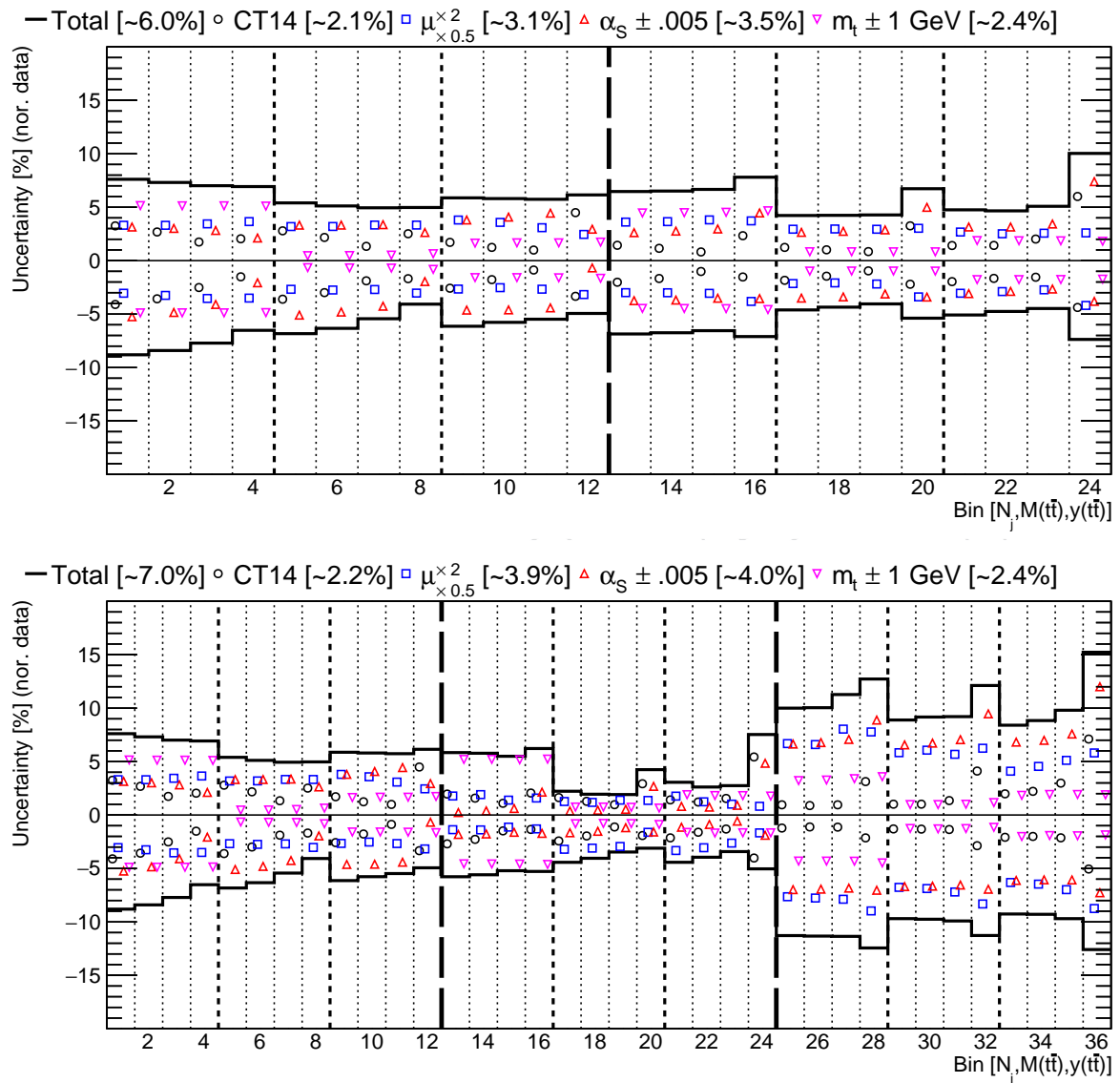


Figure 102: The theoretical uncertainties for the $[N_{\text{jet}}, M(\text{t}\bar{\text{t}}), y(\text{t}\bar{\text{t}})]$ cross sections with 2 (top) and 3 (bottom) N_{jet} bins.

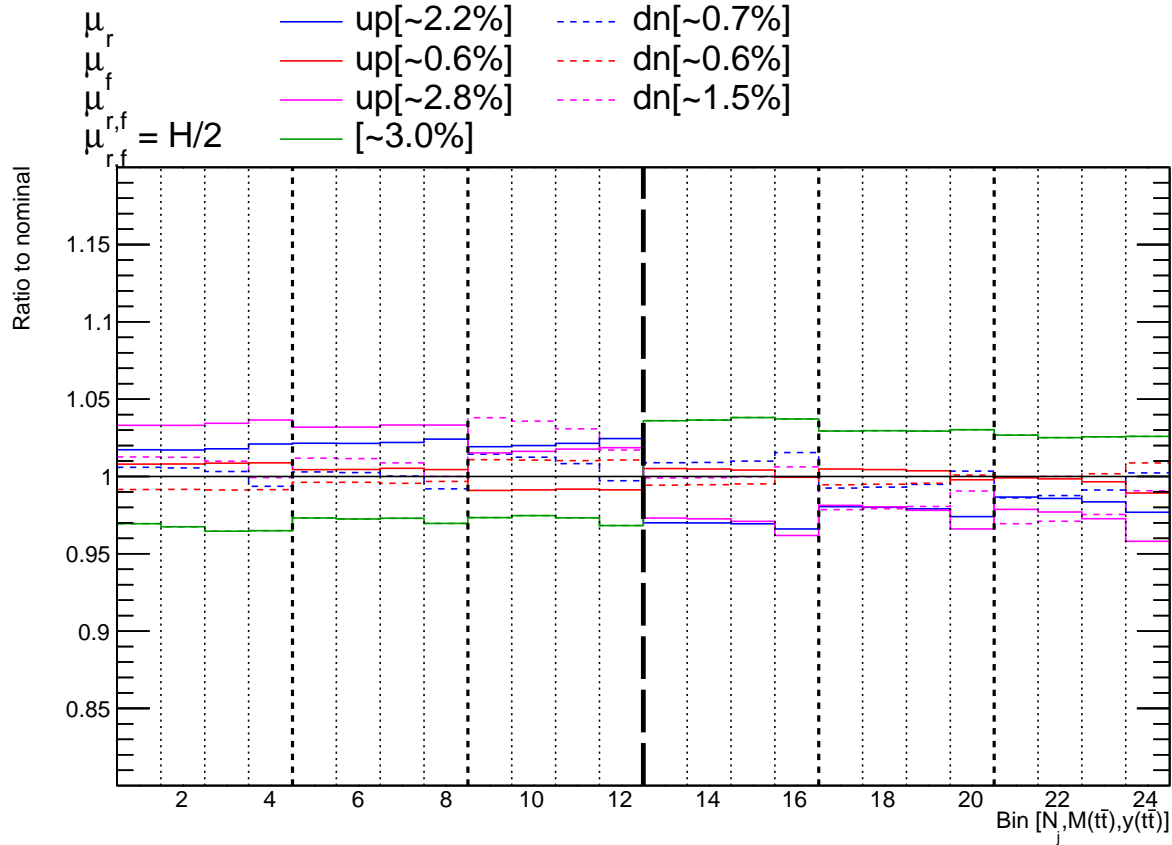


Figure 103: The individual scale variations for the $[N_{\text{jet}}, M(\text{t}\bar{t}), y(\text{t}\bar{t})]$ cross sections with 2 N_{jet} bins.

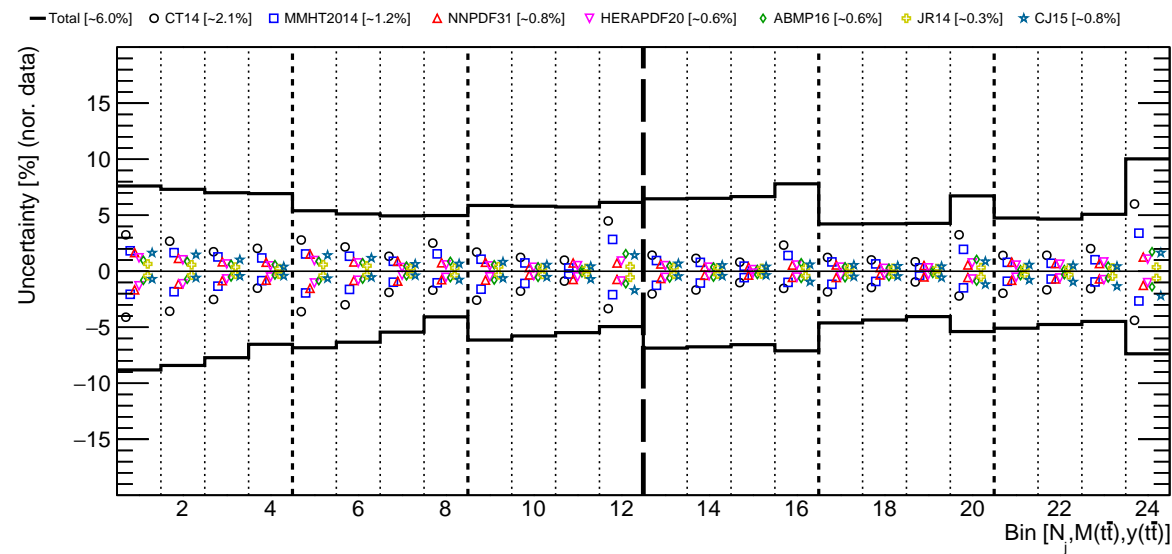


Figure 104: The PDF uncertainties obtained using different PDF sets for the $[N_{\text{jet}}, M(\text{t}\bar{t}), y(\text{t}\bar{t})]$ cross sections with 2 N_{jet} bins.

¹⁰³⁶ α_s and m_t^{pole} values is further demonstrated by comparing the measured cross sections to the
¹⁰³⁷ predictions obtained with their altered values. In Fig. 105 the data are compared to the pre-
¹⁰³⁸ dictions calculated using various PDF sets, α_s and m_t^{pole} . For each comparison, χ^2 is calcu-
¹⁰³⁹ lated which takes into account data only or data and PDF uncertainties, i.e. Eq. (13) becomes
¹⁰⁴⁰ $\mathbf{Cov} = \mathbf{Cov}^{\text{unf}} + \mathbf{Cov}^{\text{syst}} + \mathbf{Cov}^{\text{PDF}}$, where $\mathbf{Cov}^{\text{PDF}}$ is a covariance matrix that accounts for the
¹⁰⁴¹ PDF uncertainties. Theoretical uncertainties from scale, α_s and m_t^{pole} variations are not included
¹⁰⁴² in this χ^2 calculation. The impact of different PDF sets on the χ^2 value is very different indicat-
¹⁰⁴³ ing the different size of the corresponding PDF uncertainties. The best description is provided
¹⁰⁴⁴ by the predictions using the ABMP16 PDFs. Also the comparison illustrates that the data prefer
¹⁰⁴⁵ lower α_s and m_t^{pole} value than in the nominal calculation.

¹⁰⁴⁶ 8.2 Extraction of α_s and m_t^{pole} from $[N_{\text{jet}}, M(t\bar{t}), y(t\bar{t})]$ cross sections

¹⁰⁴⁷ The values of α_s and m_t^{pole} are extracted from the comparison of the data and NLO predictions
¹⁰⁴⁸ calculated using different input values of α_s and m_t^{pole} . For each such comparison, the χ^2 value
¹⁰⁴⁹ is calculated taking into account the data and PDF uncertainties and plotted as a function of
¹⁰⁵⁰ the input α_s or m_t^{pole} value. The resulting dependence of χ^2 on α_s or m_t^{pole} is approximated with
¹⁰⁵¹ a parabola. The minimum of the parabola is taken as the extracted α_s or m_t^{pole} value, while its
¹⁰⁵² uncertainty is estimated from the $\chi^2 + 1$ variation. Such extraction is performed separately us-
¹⁰⁵³ ing different PDF sets⁶, as well as different scale values. Furthermore, to assess the correlation
¹⁰⁵⁴ between α_s and m_t^{pole} , the extraction of α_s (m_t^{pole}) is performed for different m_t^{pole} (α_s) values.

¹⁰⁵⁵ The α_s scans for different PDF sets are shown in Fig. 106.⁷ The extracted α_s values are reported
¹⁰⁵⁶ on the plots. Furthermore, the α_s scans performed using altered scale and m_t^{pole} settings and
¹⁰⁵⁷ CT14, HERAPDF2.0 and ABMP16 PDF sets are shown in Fig. 107. Independent of the input
¹⁰⁵⁸ PDF set, the impact of the scale variations is moderate and there is a weak positive correlation
¹⁰⁵⁹ ($\sim 25\%$) of α_s and m_t^{pole} .

¹⁰⁶⁰ The extracted α_s values are compared in Fig. 108. The contributions to the total uncertainty
¹⁰⁶¹ arising from the data, PDF, scale and m_t^{pole} uncertainties are shown separately. The total un-
¹⁰⁶² certainty receive comparable contributions from the data, scale and PDF uncertainties with the
¹⁰⁶³ size of the latter varying significantly for different input PDFs. The results highly depend on
¹⁰⁶⁴ the input PDFs because of the strong correlation of the α_s and the gluon distribution. This il-
¹⁰⁶⁵ lustrates that precise and reliable α_s extraction from the measured data can be obtained only in
¹⁰⁶⁶ the simultaneous PDF and α_s fit.

¹⁰⁶⁷ Similarly, the m_t^{pole} scans for different PDF sets are shown in Fig. 109. The extracted m_t^{pole} values
¹⁰⁶⁸ are reported on the plots. Furthermore, the m_t^{pole} scans performed using altered scale and α_s
¹⁰⁶⁹ settings and CT14, HERAPDF2.0 and ABMP16 PDF sets are shown in Fig. 110. Independent of
¹⁰⁷⁰ the input PDF set, the impact of the scale variations is moderate and there is a weak positive
¹⁰⁷¹ correlation ($\sim 25\%$) of α_s and m_t^{pole} .

¹⁰⁷² The extracted m_t^{pole} values are compared in Fig. 111. The contributions to the total uncertainty
¹⁰⁷³ arising from the data, PDF, scale and α_s uncertainties are shown separately. The total un-
¹⁰⁷⁴ certainty is dominated by the data uncertainties.

⁶ Among available PDF sets, only CT14, HERAPDF2.0 and ABMP16 provide PDF sets for enough different α_s values and are suitable for α_s extraction.

⁷The α_s scans using also the MMHT2014 and NNPDF3.1 sets are available in Appendix H, Fig. 190.

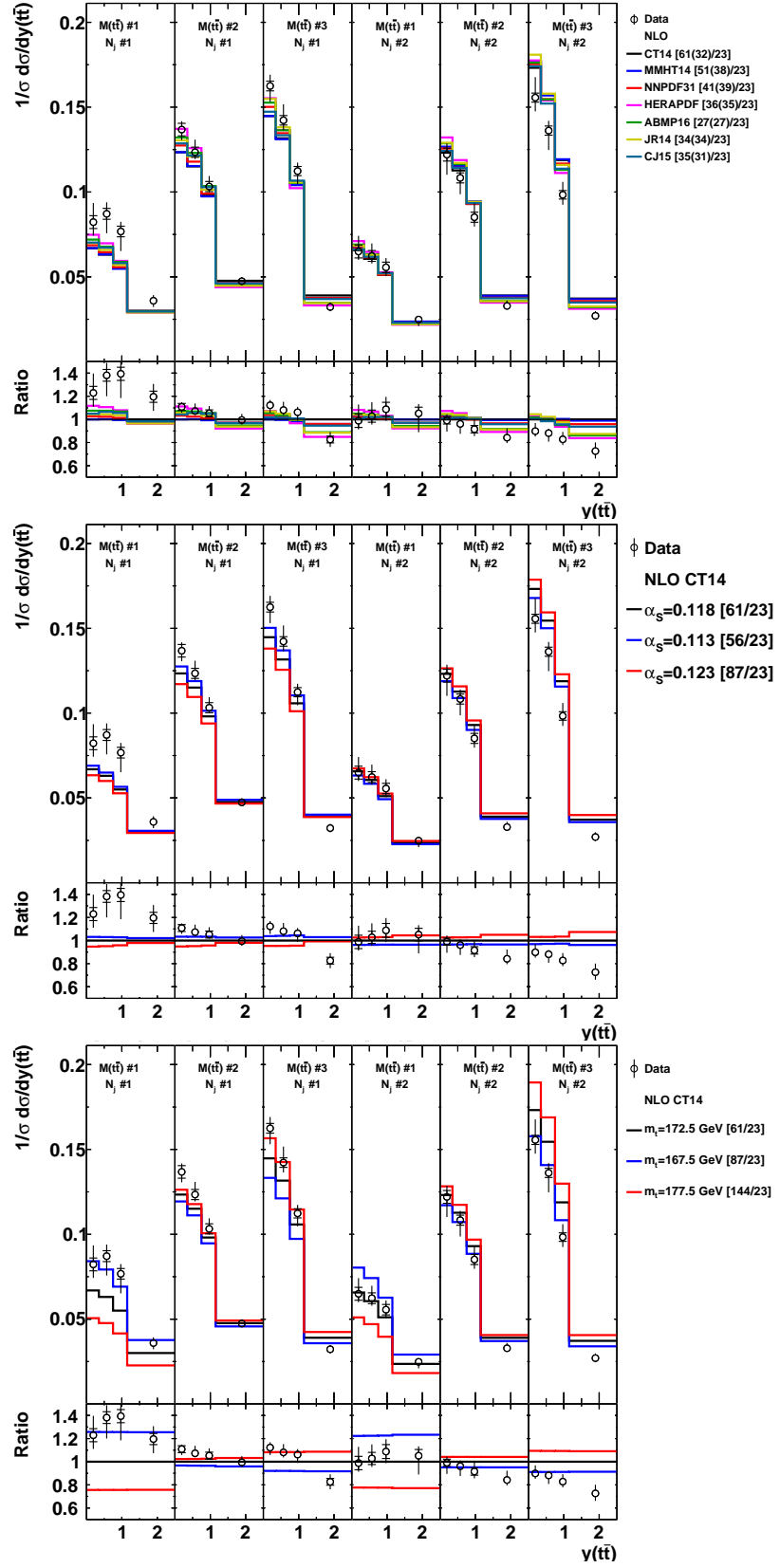


Figure 105: Comparison of the measured $[N_{jet}, M(t\bar{t}), y(t\bar{t})]$ cross sections to NLO predictions obtained using different PDF sets (top), α_s (middle) and m_t^{pole} (bottom) values.

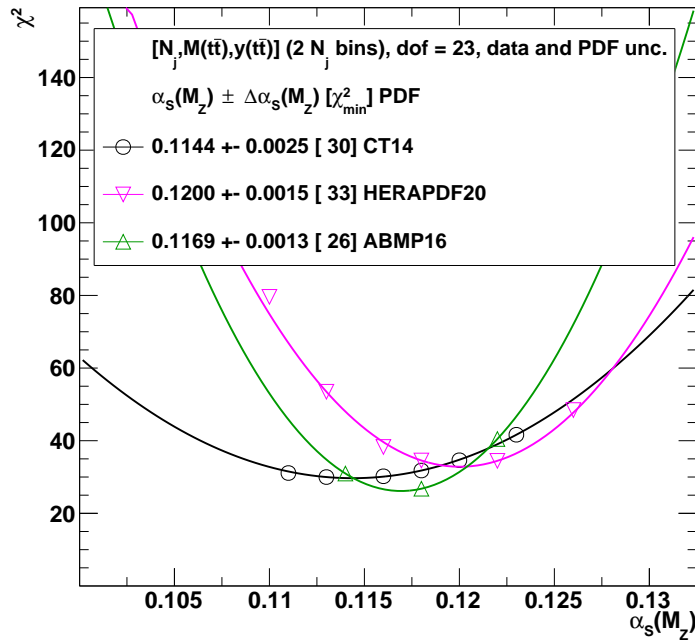


Figure 106: The α_s extraction from the measured $N_{\text{jet}}, M(\text{t}\bar{t}), y(\text{t}\bar{t})$ cross sections with 2 N_{jet} bins using different PDF sets. The extracted α_s values are reported for each PDF set, and the estimated minimum χ^2 value is shown in brackets. See text for further details.

For the m_t^{pole} extraction, it is relevant that near the mass threshold the perturbation serie needs to be improved with all order soft gluon resummation which however is not available in the tools used to obtain theoretical predictions in this work. In Ref. [84] these effects were found to be relevant only very close to the threshold (up to a few GeV) and give a correction about +1% to the total $\text{t}\bar{t}$ cross section. Attributing such correction to the first $M(\text{t}\bar{t})$ bin and assuming it is independent of $y(\text{t}\bar{t})$ and N_{jet} in this analysis it would result in about +0.7 GeV shift for the extracted m_t^{pole} which is comparable to the total uncertainty. This shows that including such effects in the theoretical calculations in the future is needed for an accurate m_t^{pole} extraction from differential $\text{t}\bar{t}$ cross sections. Furthermore, the impact of the parton shower was discussed in Ref. [4], where the predictions for inclusive $\text{t}\bar{t} + 1$ jet production obtained at NLO and using POWHEG NLO calculations matched with the PYTHIA8 parton shower have been compared (see Fig. 1 in Ref. [4]) and agreement between different approaches was found to be within 0.5 GeV for the extracted m_t^{pole} .

8.3 Cross checks of α_s and m_t^{pole} extraction using different distributions

The α_s and m_t^{pole} extraction described in the previous section is checked by repeating the procedure:

1. using single-differential $N_{\text{jet}}, M(\text{t}\bar{t}), y(\text{t}\bar{t})$ cross sections,
2. using triple-differential $[N_{\text{jet}}, M(\text{t}\bar{t}), y(\text{t}\bar{t})]$ cross section with 3 N_{jet} bins,
3. using triple-differential $[p_T(\text{t}\bar{t}), M(\text{t}\bar{t}), y(\text{t}\bar{t})]$ cross section with 2 $p_T(\text{t}\bar{t})$ bins.

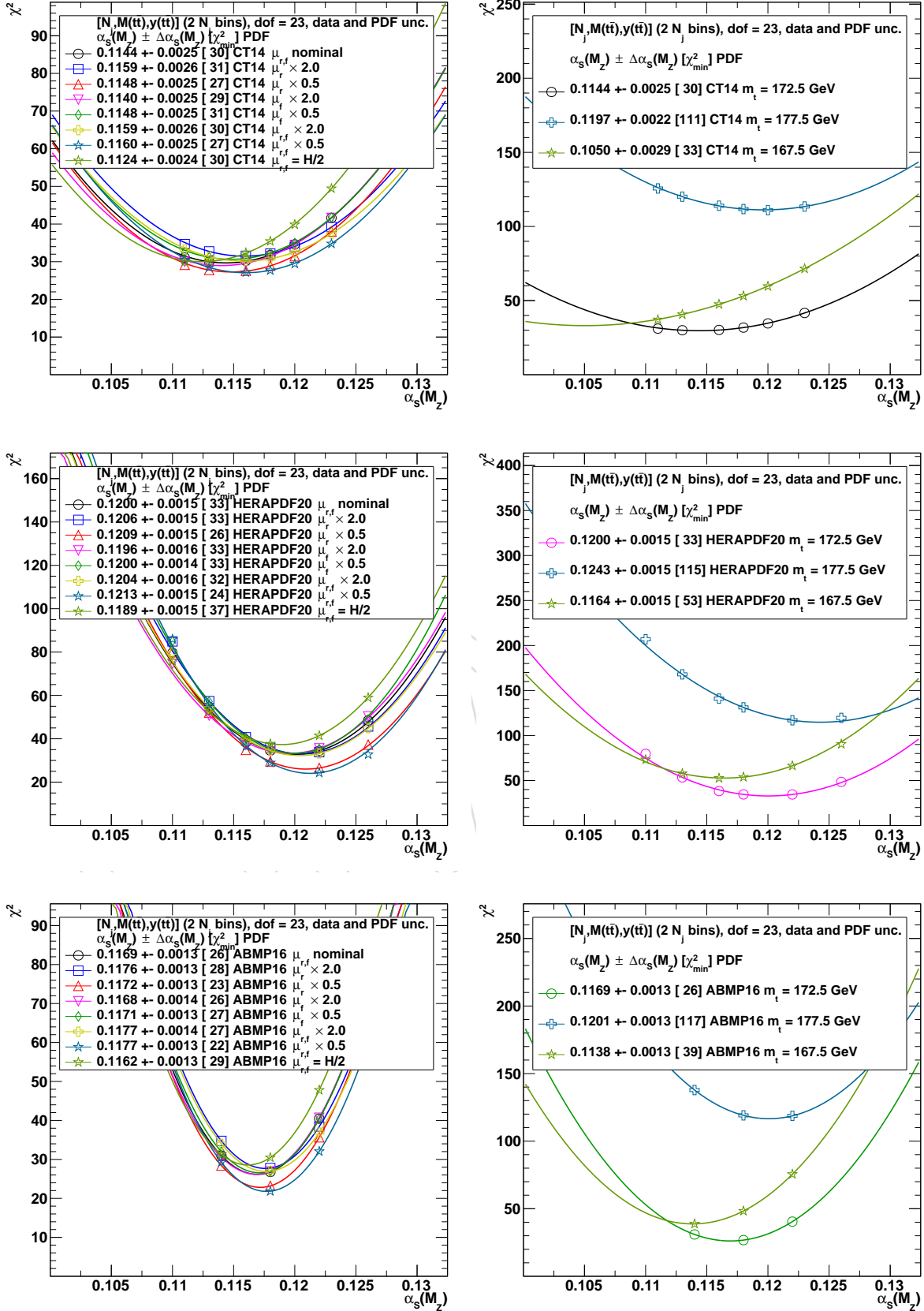


Figure 107: The α_s extraction from the measured $N_{\text{jet}}, M(\bar{t}), y(\bar{t})$ cross sections with 2 N_{jet} bins using varied scale and m_t^{pole} settings and CT14 (top), HERAPDF2.0 (middle) and ABMP16 (bottom) PDF sets.

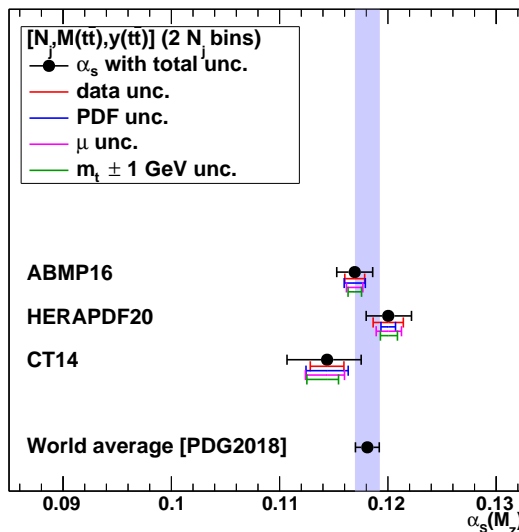


Figure 108: The α_s values extracted using different PDFs. The contributions to the total uncertainty arising from the data, PDF, scale and m_t^{pole} uncertainties are shown separately. The world average α_s value is also shown.

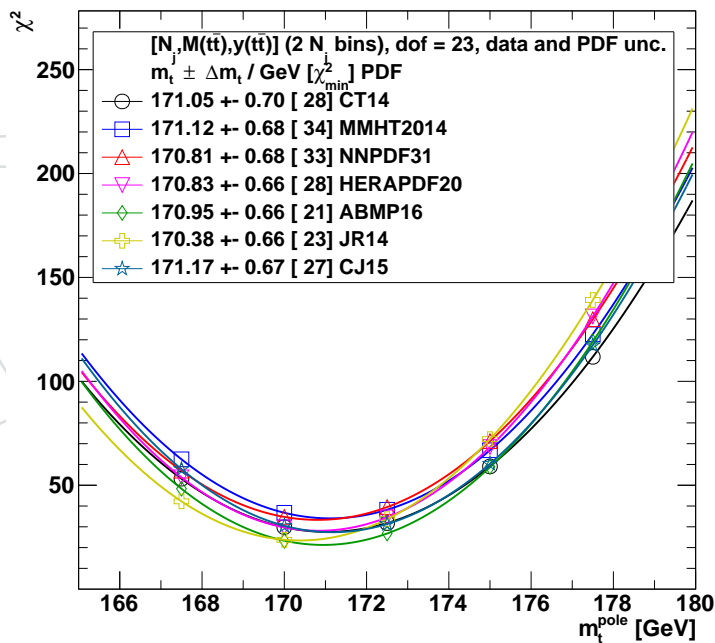


Figure 109: The m_t^{pole} extraction from the measured $N_{\text{jet}}, M(t\bar{t}), y(t\bar{t})$ cross sections with 2 N_{jet} bins using different PDF sets. The extracted m_t^{pole} values are reported for each PDF set, and the estimated minimum χ^2 value is shown in brackets. See text for further details.

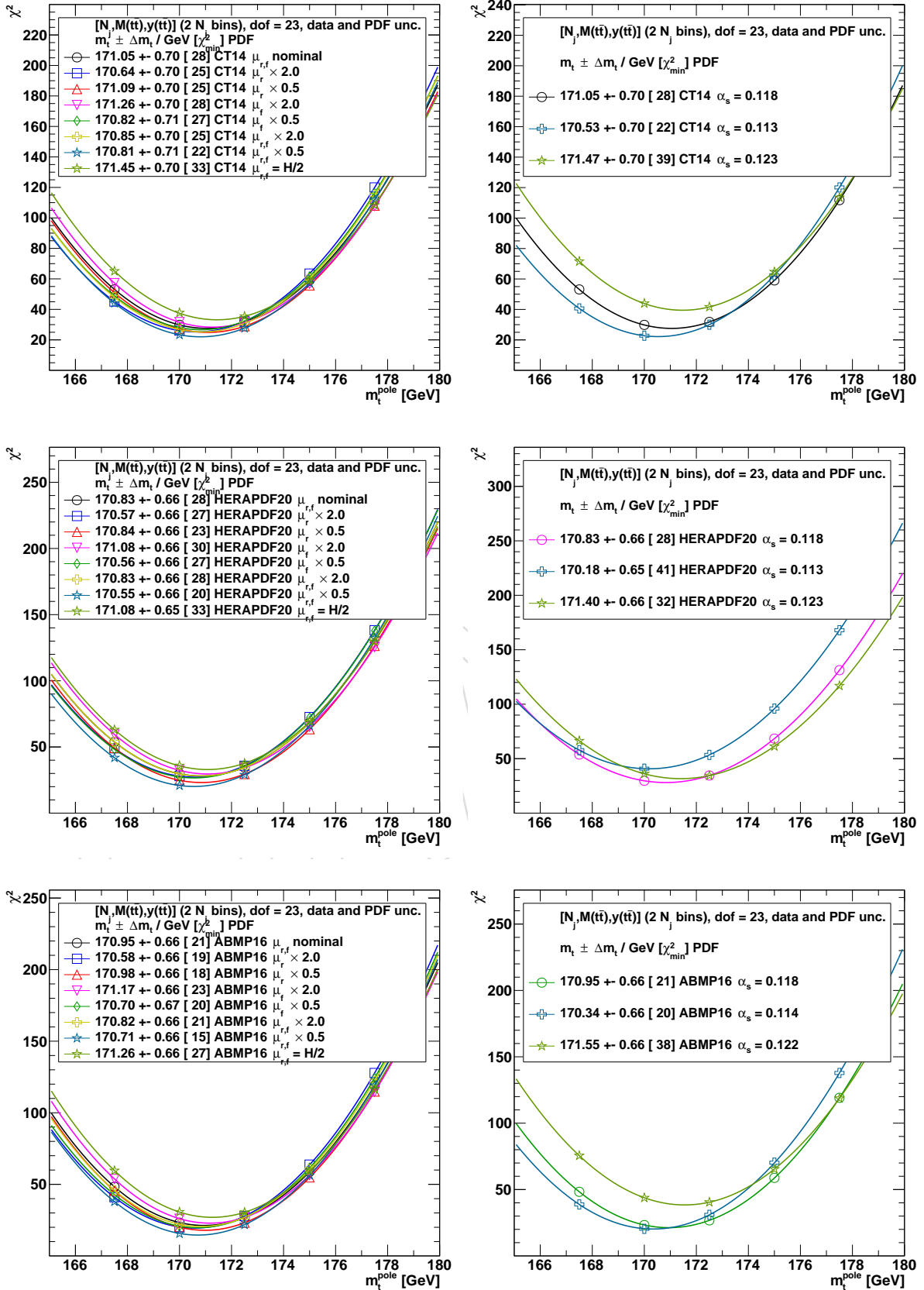


Figure 110: The m_t^{pole} extraction from the measured $N_j, M(t\bar{t}), y(t\bar{t})$ cross sections with 2 N_j bins using varied scale and α_s settings and CT14 (top), HERAPDF2.0 (middle) and ABMP16 (bottom) PDF sets.

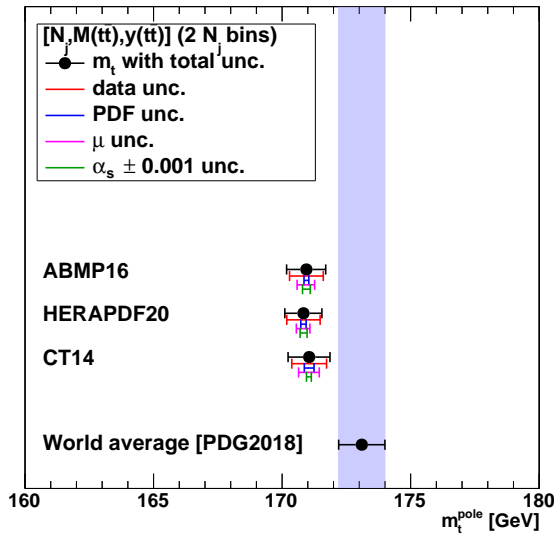


Figure 111: The m_t^{pole} values extracted using different PDFs. The contributions to the total uncertainty arising from the data, PDF, scale and α_s uncertainties are shown separately. The value $m_t^{\text{pole}} = 172.5 \pm 1$ GeV is also shown as a reference.

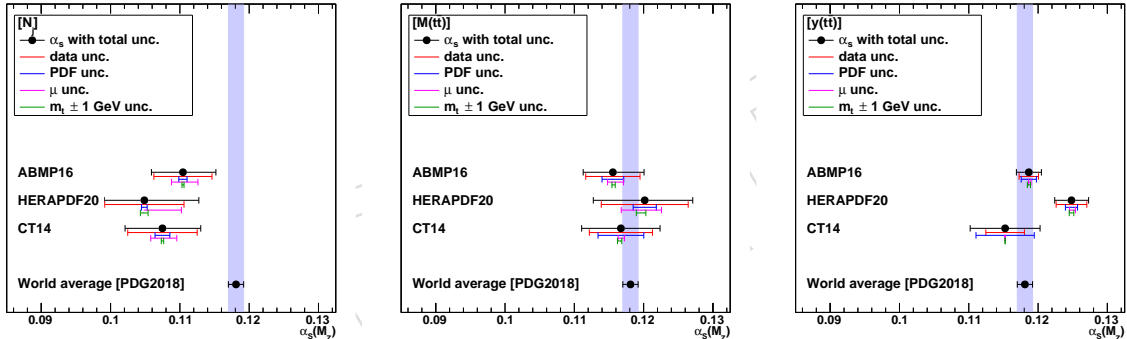


Figure 112: The α_s values extracted using different single-differential cross sections.

1094 8.3.1 α_s and m_t^{pole} extraction from single-differential N_{jet} , $M(\text{tt})$, $y(\text{tt})$ cross sections.

1095 The results of α_s and m_t^{pole} extraction from single-differential N_{jet} , $M(\text{tt})$, $y(\text{tt})$ cross sections
 1096 are shown in Figs 112 and 113. The largest sensitivity to α_s is observed when using the $y(\text{tt})$
 1097 cross sections, though it is strongly PDF dependent. The N_{jet} distribution provides a smaller α_s
 1098 sensitivity, but with little dependence on the PDFs. For m_t^{pole} , the largest sensitivity is observed
 1099 when using the $M(\text{tt})$ cross sections. In fact, almost no sensitivity to m_t^{pole} is present in $y(\text{tt})$ or
 1100 N_{jet} single-differential cross sections.

1101 8.3.2 α_s and m_t^{pole} extraction from $[N_{\text{jet}}, M(\text{tt}), y(\text{tt})]$ cross sections with 3 N_{jet} bins.

1102 The results of α_s and m_t^{pole} extraction from triple-differential $[N_{\text{jet}}, M(\text{tt}), y(\text{tt})]$ cross sections
 1103 with 3 N_{jet} bins are shown in Figs. 114 and 115. The extracted α_s and m_t^{pole} values are consistent
 1104 with the nominal ones obtained using 2 N_{jet} bins (see Figs. 108, 111) and have similar precision
 1105 with slightly different uncertainty decomposition: smaller data uncertainties but larger scale
 1106 uncertainties are present when using 3 N_{jet} bins. It is expected, since the more N_{jet} bins provide

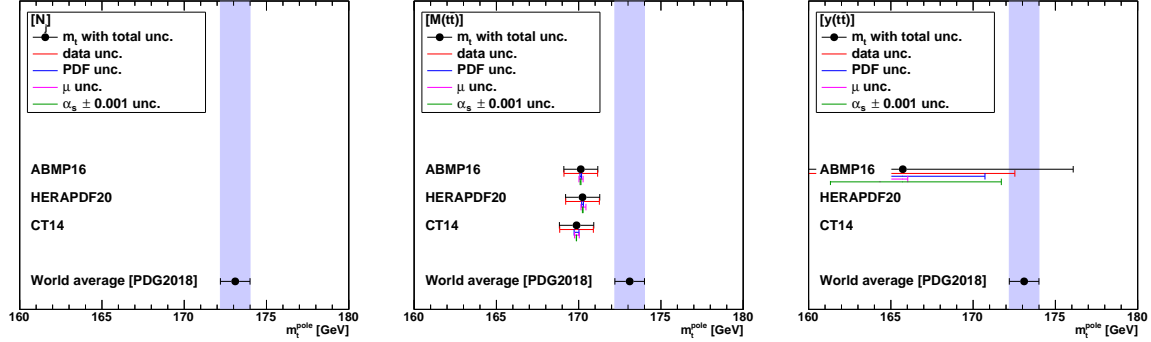


Figure 113: The m_t^{pole} values extracted using different single-differential cross sections. For central values outside the displayed m_t^{pole} range, no result is shown.

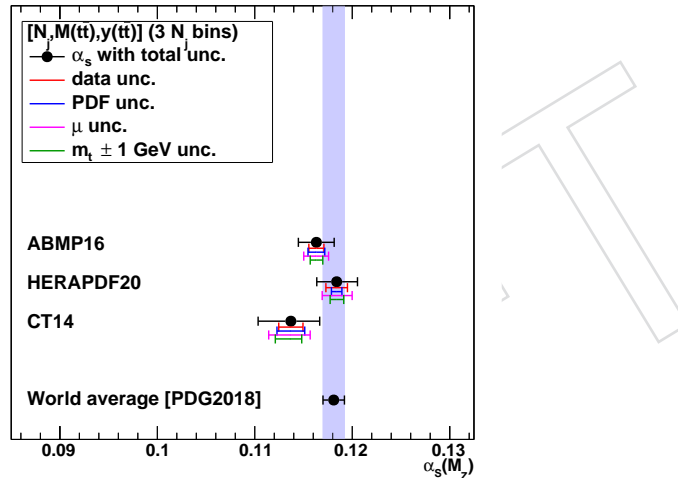


Figure 114: The α_s values extracted using $[N_{\text{jet}}, M(\bar{t}\bar{t}), y(\bar{t}\bar{t})]$ cross sections with $3 N_{\text{jet}}$ bins.

more sensitivity to α_s , however the NLO theoretical prediction for the last N_{jet} bins (2 or more extra jets) have larger scale uncertainties compared to the other bins (see Fig. 102).

These results show two important points:

1. NLO QCD predictions are able to describe $t\bar{t}$ data with up to 2 hard extra jets,
2. higher-order calculations are desirable to match experimental precision in order to achieve ultimate precision using these data to extract α_s and m_t^{pole} .

8.3.3 α_s and m_t^{pole} extraction from $[N_{\text{jet}}, M(\bar{t}\bar{t}), y(\bar{t}\bar{t})]$ and m_t^{pole} cross sections with $3 N_{\text{jet}}$ bins.

The results of α_s and m_t^{pole} extraction are also cross checked using triple-differential $[p_T(\bar{t}\bar{t}), M(\bar{t}\bar{t}), y(\bar{t}\bar{t})]$ cross sections with 2 $p_T(\bar{t}\bar{t})$ bins. Such distribution can be consistently described at NLO using calculations for inclusive $t\bar{t}$ production and inclusive $t\bar{t}$ with one extra jet production by choosing appropriate jet p_T threshold. Because the final state of the NLO calculation for $t\bar{t}$ and at least one jet consists of maximum two light partons, there can be up to two jets built of these partons, which balance the transverse momentum of $t\bar{t}$. Therefore e.g. for $p_T(\bar{t}\bar{t}) > 100$ GeV there is at least one jet with $p_T > 50$ GeV in the NLO calculation, and one can use the calcula-

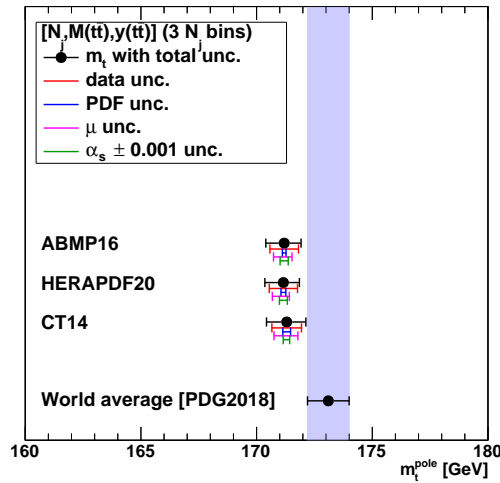


Figure 115: The m_t^{pole} values extracted using $[N_{\text{jet}}, M(\text{t}\bar{t}), y(\text{t}\bar{t})]$ cross sections with 3 N_{jet} bins.

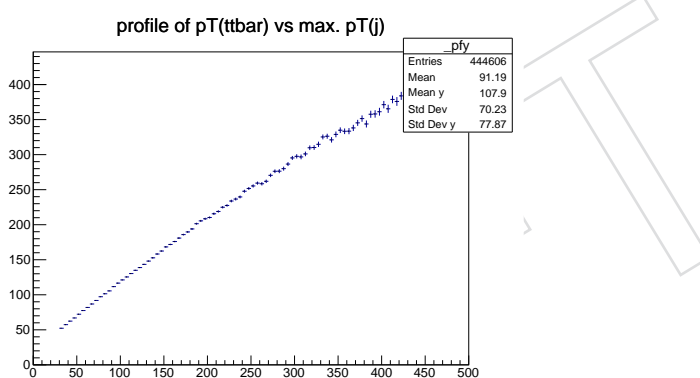


Figure 116: The dependence of the mean values of $p_T(\text{t}\bar{t})$ on jet p_T as predicted by the nominal MC.

tion requiring $p_T(\text{t}\bar{t}) > 100$ GeV without any requirement of the extra jet (if the jet p_T threshold is not larger than 50 GeV).

In this analysis, the jet $p_T > 30$ GeV was found to correspond approximately to $p_T(\text{t}\bar{t}) = 50$ GeV (see Fig. 116), therefore the boundary of 50 GeV was chosen to split the data into two $p_T(\text{t}\bar{t})$ bins. The minimum jet p_T of 15 GeV was used in the NLO calculation for inclusive $\text{t}\bar{t}$ and one jet production (no cut on jet $|\eta|$), and the predicted events were required to have $p_T(\text{t}\bar{t}) > 50$ GeV. This calculation was used for the bin with $p_T(\text{t}\bar{t}) > 50$ GeV, while for the bin with $p_T(\text{t}\bar{t}) < 50$ GeV the difference of the predictions for inclusive $\text{t}\bar{t}$ production and inclusive $\text{t}\bar{t}$ and one jet production was used.

The results of α_s and m_t^{pole} extraction from triple-differential $[p_T(\text{t}\bar{t}), M(\text{t}\bar{t}), y(\text{t}\bar{t})]$ cross sections are shown in Fig 117. The extracted α_s and m_t^{pole} values are consistent with the nominal ones (see Fig. 108) but have slightly larger uncertainties. The experimental, PDF and scale uncertainty components are increased compared to the nominal results using the $[N_{\text{jet}}, M(\text{t}\bar{t}), y(\text{t}\bar{t})]$ cross sections. Nevertheless, these results present an important cross check, because the $[p_T(\text{t}\bar{t}), M(\text{t}\bar{t}), y(\text{t}\bar{t})]$ cross sections are provided at parton level and do not require non-perturbative corrections, which have to be applied for distributions involving N_{jet} .

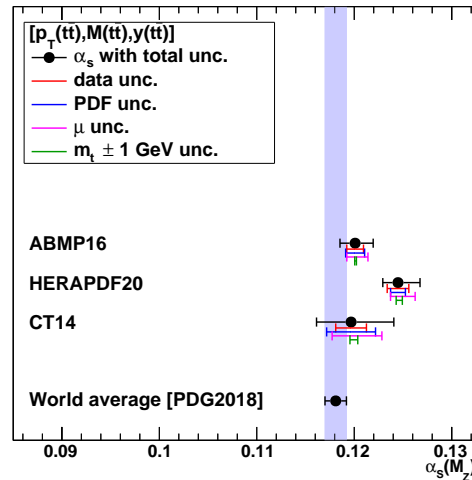


Figure 117: The α_s values extracted using $[p_T(t\bar{t}), M(t\bar{t}), y(t\bar{t})]$ cross sections with the $p_T(t\bar{t})$ threshold of 50 GeV.

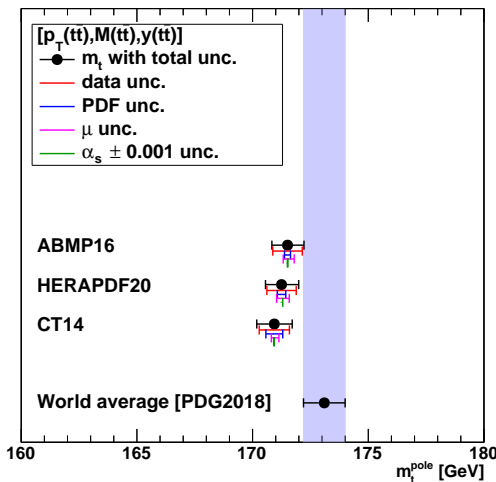


Figure 118: The m_t^{pole} values extracted using $[p_T(t\bar{t}), M(t\bar{t}), y(t\bar{t})]$ cross sections with the $p_T(t\bar{t})$ threshold of 50 GeV.

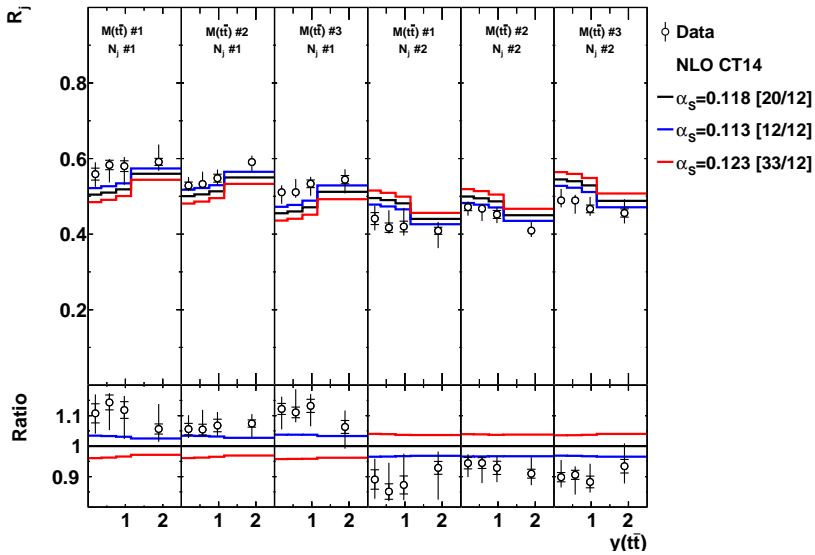


Figure 119: Comparison of the ratio cross sections to NLO predictions obtained using different PDF sets (top), α_s (middle) and m_t^{pole} (bottom) values.

8.3.4 α_s extraction from ratio cross sections

The extraction is performed using the cross section ratios calculated in each bin of $M(t\bar{t})$ and $y(t\bar{t})$, i.e. the cross section for $N_{\text{jet}} > 0$ is divided by the cross section for $N_{\text{jet}} = 0$ in each $M(t\bar{t})$, $y(t\bar{t})$ bin instead of the total cross section, referred further as ratio cross sections and denoted as R_j . The sensitivity of the ratio cross sections to the α_s variations is shown in Fig. 119, and the results of the α_s extraction are shown in Figs. 120 and 121. The extracted values are consistent with the nominal results withing the larger uncertainties. This demostrates that the ratio observables have reduced sensitivity to the PDFs and α_s than the nominal noramlised cross sections because they do not carry information about the $y(t\bar{t})$ and $M(t\bar{t})$ shapes.

8.3.5 α_s and m_t^{pole} extraction from unnormalised $[N_{\text{jet}}, M(t\bar{t}), y(t\bar{t})]$ cross sections

This check is described in detail in Appendix I. The results extracted using the unnormalised cross sections are in agreement with those extracted using the normalised cross sections, but have substantially larger experimental and scale uncertainties, which are due to the increased scale dependence of the NLO predictions for the unnormalised cross sections and uncancelled normalisation uncertainties of the measured cross sections.

8.4 Comparison of NLO vs NLO+PS theoretical predictions

In order to see the possible impact of resummation for the considered observables, in Fig. 122 the data are compared to the NLO predictions obtained using NNPDF3.1 and $m_t^{\text{pole}} = 172.5$ GeV (multiplied with the NP corrections) and to the FXFX+PYT predictions which have accuracy of NLO+PS for all bins of N_{jet} (these are the predictions which are shown on Figs. 98 and 105 top). The two predictions do not differ by more than $\approx 10\%$.

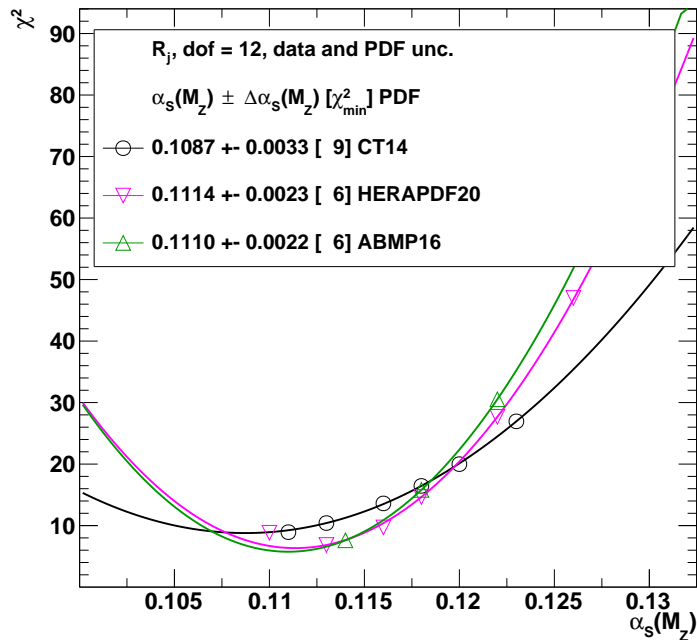


Figure 120: The α_s extraction from the ratio cross sections. The extracted α_s values are reported for each PDF set, and the estimated minimum χ^2 value is shown in brackets. See text for further details.

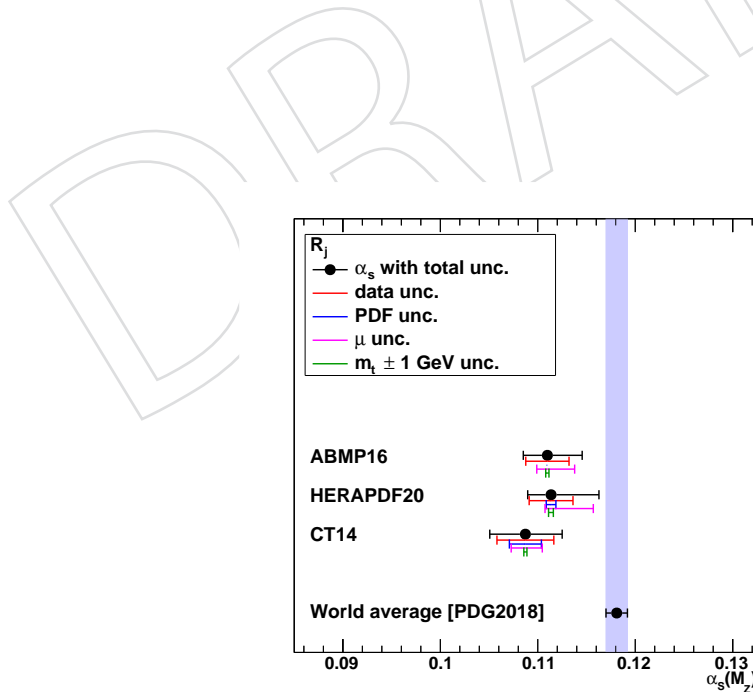


Figure 121: The α_s values extracted using the ratio cross sections.

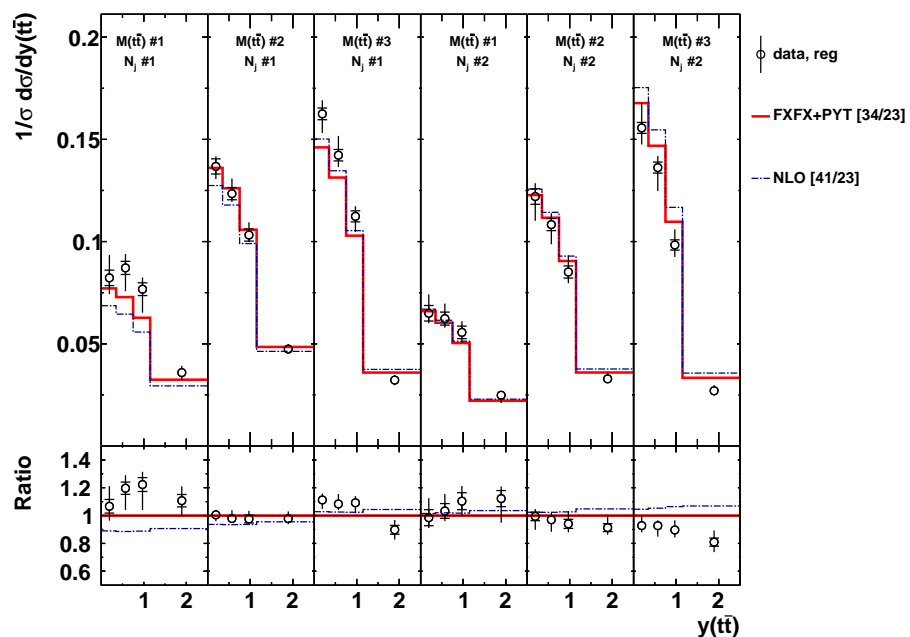


Figure 122: Comparison of the measured $[M(\tau\bar{\tau}), y(\tau\bar{\tau}), N_{jet}]$ cross sections to the NLO and FXFX+PYT predictions.

1159 9 Simultaneous PDF, α_s and m_t^{pole} fit

1160 The triple-differential normalized $t\bar{t}$ cross sections as a function of N_{jet} , $M(t\bar{t})$ and $y(t\bar{t})$ with 2
 1161 N_{jet} bins are used in a simultaneous PDF, α_s and m_t^{pole} fit at NLO (also referred to as a QCD
 1162 analysis), together with the combined HERA inclusive deep inelastic scattering (DIS) data [78].
 1163 The xFITTER program (version 2.0.0) [85], an open-source QCD fit framework for PDF determi-
 1164 nation, is used. The precise HERA DIS data, obtained from the combination of individual H1
 1165 and ZEUS results, are directly sensitive to the valence and sea quark distributions and probe
 1166 the gluon distribution through scaling violations. Therefore, these data form the core of all
 1167 PDF fits. The measured $t\bar{t}$ cross sections are included in the fit to constrain α_s and the gluon
 1168 distribution at high x values. The typical probed x values can be estimated using the LO kine-
 1169 matic relation $x = (M(t\bar{t})/\sqrt{s}) \exp [\pm y(t\bar{t})]$. Therefore, the present measurement is expected
 1170 to be mostly sensitive to x values in the region $0.01 \lesssim x \lesssim 0.1$, as estimated using the highest
 1171 or lowest $|y(t\bar{t})|$ or $M(t\bar{t})$ bins and taking the low or high bin edge where the cross section is
 1172 largest.

1173 9.1 Details of the PDF fit

1174 The scale evolution of partons is calculated through DGLAP equations [86–92] at NLO, as
 1175 implemented in the QCDCNUM program [93] (version 17.01.14). The Thorne–Roberts [94–96]
 1176 variable-flavour number scheme at NLO is used for the treatment of the heavy-quark con-
 1177 tributions. The number of flavours is set to 5, with c and b quark mass parameters $M_c =$
 1178 1.47 GeV and $M_b = 4.5 \text{ GeV}$ [78]. For the DIS data μ_r and μ_f are set to Q , which denotes
 1179 the four-momentum transfer. The theoretical predictions for the $t\bar{t}$ cross sections are calcu-
 1180 lated as described in Section I.1 and included in the fit using the MG5_aMC@NLO (version
 1181 2.6.0) [18] framework, interfaced with the AMCFAST (version 1.3.0) [97] and APPLGRID (ver-
 1182 sion 1.4.70) [98] programs. The strong coupling strength α_s and pole top quark mass m_t^{pole} are
 1183 left free in the fit.⁸ The Q^2 range of the HERA data is restricted to $Q^2 > Q_{\min}^2 = 3.5 \text{ GeV}^2$ [78].

The procedure for the determination of the PDFs follows the approach of HERAPDF2.0 [78]. The parametrized PDFs are the gluon distribution $xg(x)$, the valence quark distributions $xu_v(x)$ and $xd_v(x)$, and the u- and d-type antiquark distributions $x\bar{U}(x)$ and $x\bar{D}(x)$. At the initial QCD evolution scale $\mu_{f0}^2 = 1.9 \text{ GeV}^2$, the PDFs are parametrized as:

$$\begin{aligned} xg(x) &= A_g x^{B_g} (1-x)^{C_g} (1+E_g x^2) - A'_g x^{B'_g} (1-x)^{C'_g}, \\ xu_v(x) &= A_{u_v} x^{B_{u_v}} (1-x)^{C_{u_v}} (1+D_{u_v} x), \\ xd_v(x) &= A_{d_v} x^{B_{d_v}} (1-x)^{C_{d_v}}, \\ x\bar{U}(x) &= A_{\bar{U}} x^{B_{\bar{U}}} (1-x)^{C_{\bar{U}}} (1+D_{\bar{U}} x), \\ x\bar{D}(x) &= A_{\bar{D}} x^{B_{\bar{D}}} (1-x)^{C_{\bar{D}}}, \end{aligned} \quad (15)$$

1184 assuming the relations $x\bar{U}(x) = x\bar{u}(x)$ and $x\bar{D}(x) = x\bar{d}(x) + x\bar{s}(x)$. Here, $x\bar{u}(x)$, $x\bar{d}(x)$,
 1185 and $x\bar{s}(x)$ are the up, down, and strange antiquark distributions, respectively. The sea quark
 1186 distribution is defined as $x\Sigma(x) = x\bar{u}(x) + x\bar{d}(x) + x\bar{s}(x)$. The normalization parameters A_{u_v} ,
 1187 A_{d_v} , and A_g are determined by the QCD sum rules. The B and B' parameters determine the

⁸Technically, ApplGrid tables have been produced for fixed values of m_t^{pole} , while the theoretical predictions as a function of m_t^{pole} were obtained by linear interpolation between two predictions using m_t^{pole} values $m_t^{\text{pole}} = 167.5 \text{ GeV}$ and $m_t^{\text{pole}} = 175 \text{ GeV}$. It was checked that the results do not depend significantly on which particular m_t^{pole} values are used for linear interpolation.

1188 PDFs at small x , and the C parameters describe the shape of the distributions as $x \rightarrow 1$. The
 1189 parameter C'_g is fixed to 25 [99]. Additional constraints $B_{\bar{U}} = B_{\bar{D}}$ and $A_{\bar{U}} = A_{\bar{D}}(1 - f_s)$ are
 1190 imposed to ensure the same normalization for the $x\bar{u}$ and $x\bar{d}$ distributions as $x \rightarrow 0$. The
 1191 strangeness fraction $f_s = x\bar{s}/(x\bar{d} + x\bar{s})$ is fixed to $f_s = 0.4$ as in the HERAPDF2.0 analysis [78].
 1192 This value is consistent with the determination of the strangeness fraction when using the CMS
 1193 measurements of $W + c$ production [100].

1194 The parameters in Eq. (15) are selected by first fitting with all D and E parameters set to zero,
 1195 and then including them independently one at a time in the fit. The improvement in the χ^2 of
 1196 the fit is monitored and the procedure is stopped when no further improvement is observed.
 1197 This leads to an 15-parameter fit. The χ^2 definition used for the HERA DIS data follows that
 1198 of Eq. (32) in Ref. [78]. It includes an additional logarithmic term that is relevant when the
 1199 estimated statistical and uncorrelated systematic uncertainties in the data are rescaled during
 1200 the fit [101]. For the $t\bar{t}$ data presented here a χ^2 definition without such a logarithmic term is
 1201 employed. The full covariance matrix representing the statistical and uncorrelated systematic
 1202 uncertainties of the data is used in the fit. The correlated systematic uncertainties are treated
 1203 through nuisance parameters. For each nuisance parameter a penalty term is added to the χ^2 ,
 1204 representing the prior knowledge of the parameter. The treatment of the experimental uncer-
 1205 tainties for the HERA DIS data follows the prescription given in Ref. [78]. The treatment of the
 1206 experimental uncertainties in the $t\bar{t}$ double-differential cross section measurements follows the
 1207 prescription given in Section I.1.

1208 The PDF uncertainties are estimated according to the general approach of HERAPDF2.0 [78] in
 1209 which the fit, model, and parametrisation uncertainties are taken into account. Fit uncertain-
 1210 tainties are determined using the tolerance criterion of $\Delta\chi^2 = 1$. Model uncertainties arise from
 1211 the variations in the values assumed for the b and c quark mass parameters of $4.25 \leq M_b \leq$
 1212 4.75 GeV and $1.41 \leq M_c \leq 1.53 \text{ GeV}$, the strangeness fraction $0.3 \leq f_s \leq 0.5$, and the value of
 1213 Q_{\min}^2 imposed on the HERA data. The latter is varied within $2.5 \leq Q_{\min}^2 \leq 5.0 \text{ GeV}^2$, follow-
 1214 ing Ref. [78]. The parametrisation uncertainty is estimated by varying the functional form in
 1215 Eq. (15) of all parton distributions with parameters D and E added or removed one at a time,
 1216 as described in detail in the next section. Furthermore, μ_{f0}^2 is changed to 1.6 GeV^2 and 2.2 GeV^2 .
 1217 The parametrisation uncertainty is constructed as an envelope at each x value, built from the
 1218 maximal differences between the PDFs resulting from the central fit and all parametrisation
 1219 variations. This uncertainty is valid in the x range covered by the PDF fit to the data. The
 1220 total PDF uncertainty is obtained by adding the fit, model, and parametrisation uncertainties
 1221 in quadrature. In the following, the quoted uncertainties correspond to 68% CL.

1222 9.2 Study of PDF parametrisation

1223 The nominal PDF fit is performed using the 15-parameter functional form of Eq. 15. The χ^2
 1224 values obtained when using more rigid (with 13 or 14 parameters) or more flexible (with 16
 1225 parameters) parametrisation are provided in Table 21. The fits which do not converge to a min-
 1226 imum with a positive definite error matrix (as reported by the HESSE algorithm) are marked.
 1227 The resulting PDFs are shown in Figs. 123, 124, 125, 126, 127, 128. Since none of the converged
 1228 fits improves χ^2 significantly (i.e. by a few units, $\Delta\chi^2 \gg 1$), the 15-parametrisation form is
 1229 considered as the one which provides the best description of the data. Moreover, none of the
 1230 16-parametrisation converged fits provides significantly different PDFs (see Figs. 123, 124, 126,
 1231 127), therefore these fit variants do not contribute to the parametrisation uncertainties. The
 1232 two variants of the fits with more rigid parameterisation, namely those with $A_g = 0$ (note
 1233 that setting A_g to 0 eliminates also B_g and reduces the number of parameters by 2), and E_g

Table 21: The χ^2 values obtained in the fits with nominal (15p) and alternative PDF parametrisation. Results marker with * are minima with an error matrix which is not positive-definite as reported by HESSE.

Data	15p	$A'_g = 0$	$E_g = 0$	$D_{u_n} = 0$	$D_{\bar{U}} = 0$	D_g	E_{u_n}	D_{d_n}	E_{d_n}	$E_{\bar{U}}$	$D_{\bar{D}}$	$E_{\bar{D}}$
HERA DIS	1341.3	1343.0	1341.7	1404.0	1376.0	1337.2*	1339.2	1341.1	1340.5	1341.2	1341.3	1341.1
HERA DIS + $t\bar{t}$	1364.5	1368.7	1368.6	1428.6	1429.5	1355.9*	1363.2	1364.1	1363.7	1364.4	1364.5	1364.1

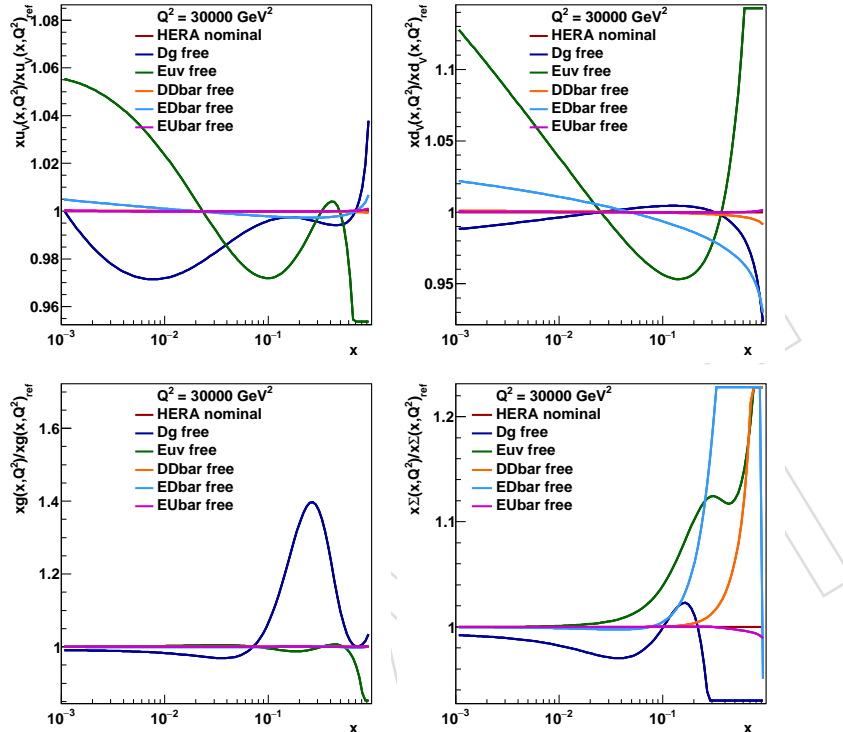


Figure 123: The PDFs obtained in the fits with more flexible (16-parameterisation) form using the HERA DIS data only.

(see Figs. 125, 128), have the χ^2 which are only a few units worse than that with the released parameters, therefore these fit variants are included in the parametrisation uncertainties.

As can be drawn from Table 21, the $t\bar{t}$ data in the fit improves its stability greatly, such that more fits converge to a well defined minimum compared to the fits using the HERA DIS data only. The $t\bar{t}$ data strongly impact the gluon distribution and prefer its more flexible parametrisation at the starting scale (cf. the change in χ^2 when setting $E_g = 0$ to 0 in the HERA DIS fit, and with the $t\bar{t}$ data). Furthermore, in the 16-parameter fit with D_g released the $t\bar{t}$ data significantly constrain the variation of the gluon distribution compared to the HERA DIS fit (cf. Figs. 123 and 126).

9.3 α_s and m_t^{pole} extraction

The extracted values of α_s and m_t^{pole} are:

$$\begin{aligned} \alpha_s(M_Z) &= 0.1135 \pm 0.0016(\text{fit})^{+0.0002}_{-0.0004}(\text{mod})^{+0.0008}_{-0.0001}(\text{par})^{+0.0011}_{-0.0005}(\text{scale}) = 0.1135^{+0.0021}_{-0.0017}(\text{total}), \\ m_t^{\text{pole}} &= 170.5 \pm 0.7(\text{fit})^{+0.1}_{-0.1}(\text{mod})^{+0.0}_{-0.1}(\text{par})^{+0.3}_{-0.3}(\text{scale}) \text{ GeV} = 170.5 \pm 0.8(\text{total}) \text{ GeV}. \end{aligned} \quad (16)$$

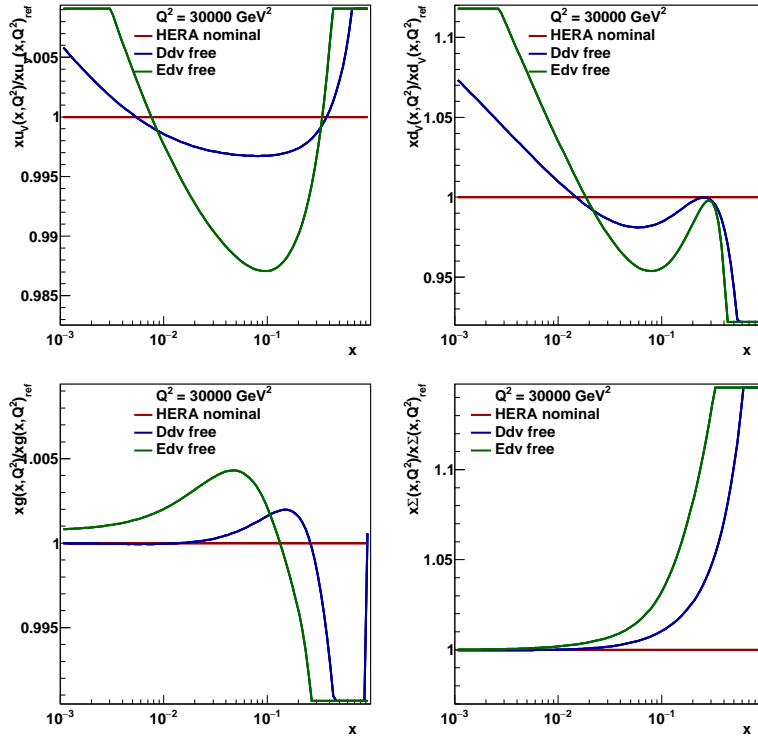


Figure 124: The PDFs obtained in the fits with more flexible (16-parameterisation) form using the HERA DIS data only.

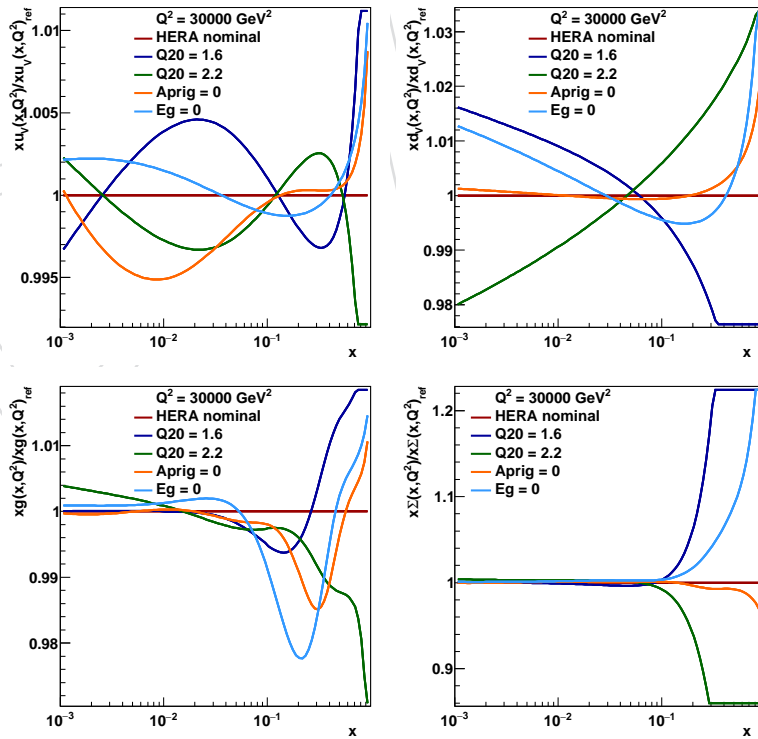


Figure 125: The PDF parameterisation variations: the PDFs obtained in the fits with more rigid (14- or 15-parameterisation) form using the HERA DIS data only. Also shown are PDFs obtained in the fits with the varied parameterisation scale Q_0^2 .

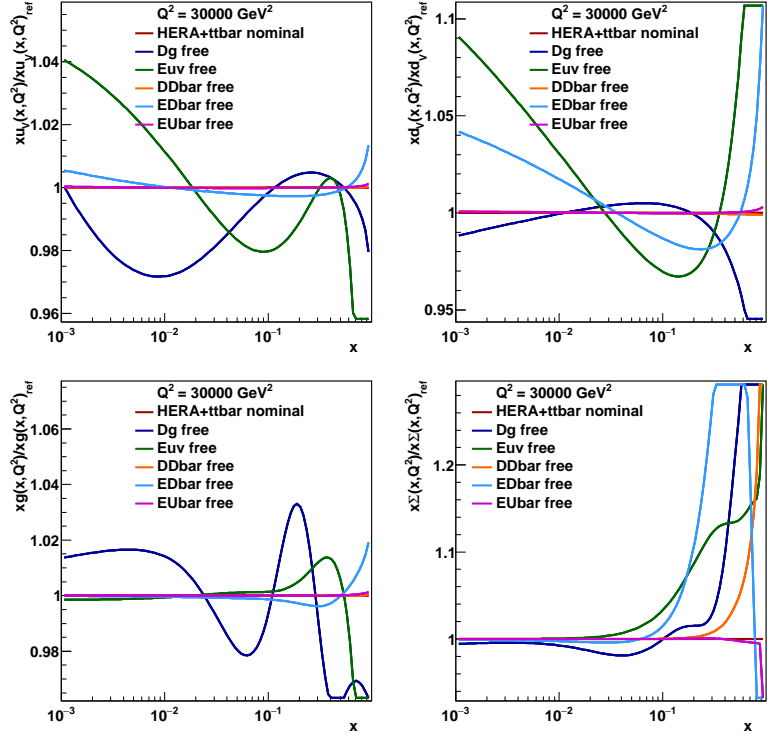


Figure 126: The PDFs obtained in the fits with more flexible (16-parameterisation) form using the HERA DIS and $t\bar{t}$ data.

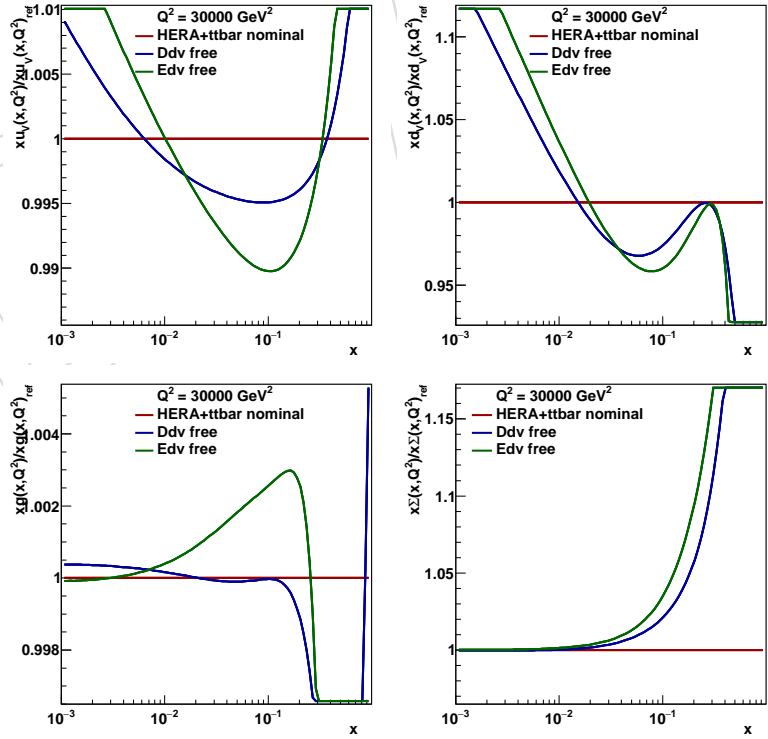


Figure 127: The PDFs obtained in the fits with more flexible (16-parameterisation) form using the HERA DIS and $t\bar{t}$ data.

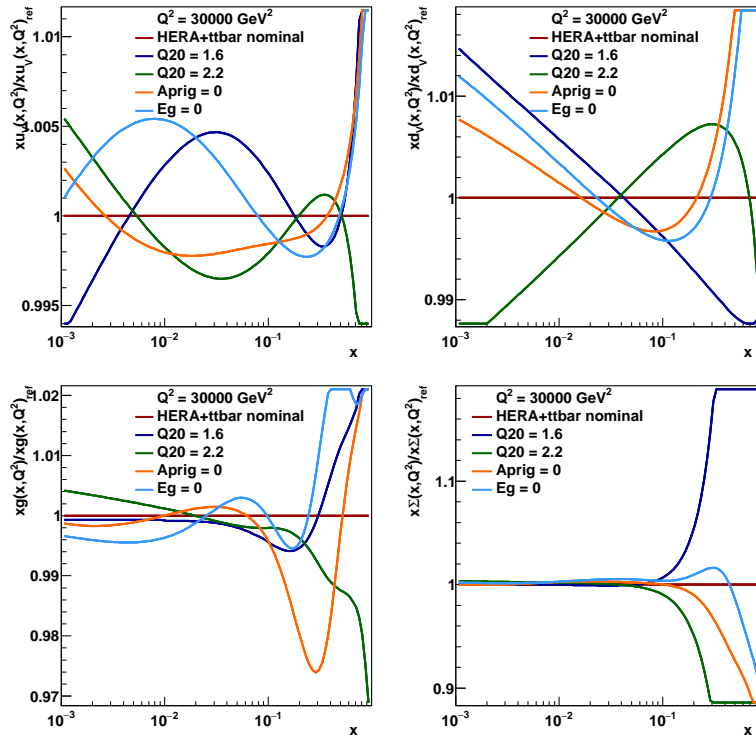


Figure 128: The PDF parameterisation variations: the PDFs obtained in the fits with more rigid (14- or 15-parameterisation) form using the HERA DIS and $t\bar{t}$ data. Also shown are PDFs obtained in the fits with the varied parameterisation scale Q_0^2 .

The uncertainties arising from the scale variations are estimated by repeating the fit with altered values of the scales as described in Section I.1 and taking the differences with respect to the nominal result. The individual contributions to the uncertainties are listed in Table 22. The extracted α_s and m_t^{pole} values have only weak positive correlation $\rho(\alpha_s, m_t^{\text{pole}}) = 0.3$. This manifests that the two SM parameters can be simultaneously determined from these data to high precision with only weak correlation between them.

The global and partial χ^2 values are listed in Table 23, illustrating the consistency among the input data. The DIS data show χ^2/dof values slightly larger than unity. This is similar to what is observed and investigated in Ref. [78]. For the $t\bar{t}$ data, the full χ^2 (including uncorrelated and correlated data uncertainties) is 25 for 23 dof. The $t\bar{t}$ cross sections are compared to the NLO predictions obtained after the fit in Fig. 129.

9.3.1 Scan of χ^2 vs. $\alpha_s(M_Z)$

PDF fits were performed for a series of $\alpha_s(M_Z)$ values ranging from $\alpha_s(M_Z) = 0.100$ to $\alpha_s(M_Z) = 0.130$ using only HERA DIS data, or HERA and $t\bar{t}$ data. The results are shown in Fig. 130. A shallow χ^2 dependence on $\alpha_s(M_Z)$ is present when using only the HERA DIS data, similar to the findings of the HERAPDF2.0 analysis [78]. Once the $t\bar{t}$ data are included in the fit, a distinct minimum in χ^2 is observed which coincides with the one found in the simultaneous PDF and $\alpha_s(M_Z)$ fit (Eq. 16). Therefore the performed $\alpha_s(M_Z)$ scans serve as a cross check of the simultaneous PDF and $\alpha_s(M_Z)$ fit.

Table 22: Central values and list of uncertainties for α_s and m_t^{pole} determination.

Parameter	Variation	$\alpha_s(M_Z)$	m_t^{pole} [GeV]
Central value			
		0.1135	170.5
Fit uncertainty			
Total	$\Delta\chi^2 = 1$	± 0.0016	± 0.7
Model uncertainty			
f_s	$f_s = 0.5$	+0.0001	+0.0
f_s	$f_s = 0.3$	-0.0000	-0.0
Q_{\min}^2	$Q_{\min}^2 = 5.0 \text{ GeV}^2$	+0.0002	+0.1
Q_{\min}^2	$Q_{\min}^2 = 2.5 \text{ GeV}^2$	-0.0004	-0.1
m_c	$m_c = 1.49 \text{ GeV}$	+0.0001	+0.0
m_c	$m_c = 1.37 \text{ GeV}$	-0.0000	-0.0
Total		+0.0002 -0.0004	+0.1 -0.1
PDF parameterisation uncertainty			
$\mu_{f,0}^2$	$\mu_{f,0}^2 = 2.2 \text{ GeV}^2$	-0.0001	-0.0
$\mu_{f,0}^2$	$\mu_{f,0}^2 = 1.6 \text{ GeV}^2$	+0.0002	+0.0
A'_g	set to 0	+0.0002	-0.1
E_g	set to 0	+0.0008	-0.0
Total		+0.0008 -0.0001	+0.0 -0.1
Scale uncertainty			
μ_r variation	$\mu_r \times 2.0$	+0.0004	-0.2
μ_r variation	$\mu_r \times 0.5$	+0.0007	+0.1
μ_f variation	$\mu_f \times 2.0$	-0.0002	+0.3
μ_f variation	$\mu_f \times 0.5$	+0.0001	-0.3
$\mu_{r,f}$ variation	$\mu_{r,f} \times 2.0$	+0.0004	+0.1
$\mu_{r,f}$ variation	$\mu_{r,f} \times 0.5$	+0.0011	-0.2
alternative $\mu_{r,f}$	$\mu_{r,f} = H/2$	-0.0005	+0.1
Total		+0.0011 -0.0005	+0.3 -0.3

Table 23: The global and partial χ^2/dof values for all variants of the PDF fit. The variant of the fit that uses the HERA DIS only is denoted as ‘Nominal fit’. For the HERA measurements, the energy of the proton beam, E_p , is listed for each data set, with the electron energy being $E_e = 27.5 \text{ GeV}$. CC and NC stand for charged and neutral current, respectively. The correlated χ^2 and the log-penalty χ^2 entries refer to the χ^2 contributions from the nuisance parameters and from the logarithmic term, respectively, as described in the text.

Data sets	χ^2/dof	
	Nominal fit	+ [$N_{\text{jet}}, y(\bar{t}\bar{t}), M(\bar{t}\bar{t})$]
CMS $t\bar{t}$		10/23
HERA CC $e^- p$, $E_p = 920 \text{ GeV}$	55/42	55/42
HERA CC $e^+ p$, $E_p = 920 \text{ GeV}$	38/39	39/39
HERA NC $e^- p$, $E_p = 920 \text{ GeV}$	218/159	217/159
HERA NC $e^+ p$, $E_p = 920 \text{ GeV}$	438/377	448/377
HERA NC $e^+ p$, $E_p = 820 \text{ GeV}$	70/70	71/70
HERA NC $e^+ p$, $E_p = 575 \text{ GeV}$	220/254	222/254
HERA NC $e^+ p$, $E_p = 460 \text{ GeV}$	219/204	220/204
Correlated χ^2	82	90
Log-penalty χ^2	+2	-7
Total χ^2/dof	1341/1130	1364/1151

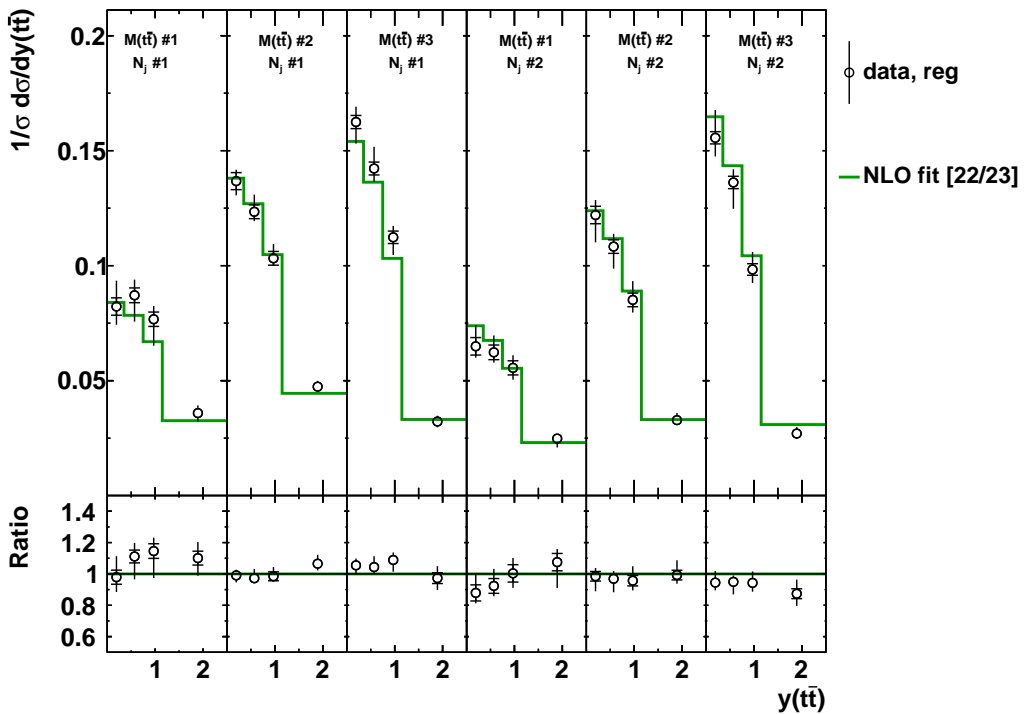


Figure 129: Comparison of the measured $[N_{\text{jet}}, M(\bar{t}\bar{t}), y(\bar{t}\bar{t})]$ cross sections to the NLO predictions from the simultaneous PDF, α_s and m_t^{pole} fit. The inner vertical bars on the data points represent the statistical uncertainties and the full bars include also the systematic uncertainties added in quadrature. A χ^2/dof is reported in brackets.

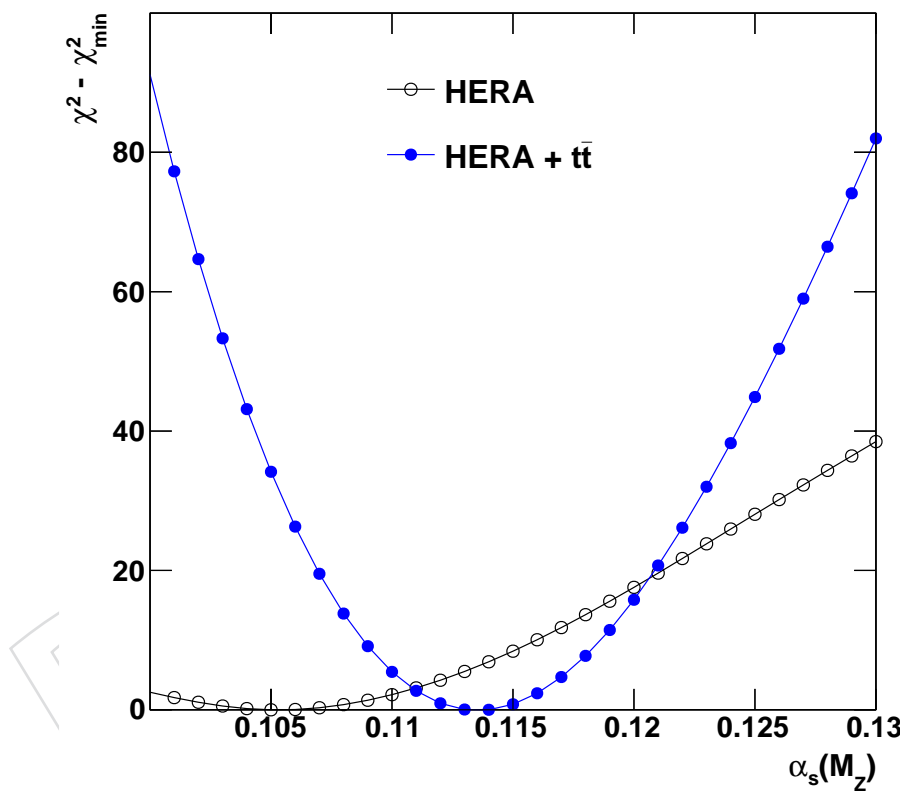


Figure 130: $\Delta\chi^2 = \chi^2 - \chi^2_{\min}$ as a function of $\alpha_s(M_Z)$ in the PDF fit using the HERA DIS data only, or HERA and $t\bar{t}$ data.

Table 24: The $\alpha_s(M_Z)$ values with their fit uncertainties extracted in the fits using different cuts on Q_{\min}^2 .

$Q_{\min}^2 [\text{GeV}^2]$	$\alpha_s(M_Z)$	
	HERA DIS	HERA DIS + $t\bar{t}$
2.5	0.1034 ± 0.0022	0.1131 ± 0.0015
3.5	0.1053 ± 0.0027	0.1135 ± 0.0015
5.0	0.1082 ± 0.0010	0.1137 ± 0.0016
7.5	0.1118 ± 0.0045	0.1143 ± 0.0008
10.0	0.1127 ± 0.0064	0.1130 ± 0.0020
15.0	0.1147 ± 0.0050	0.1132 ± 0.0018
20.0	0.1157 ± 0.0044	0.1125 ± 0.0019
30.0	0.1195 ± 0.0009	0.1128 ± 0.0020

9.3.2 Dependence of extracted $\alpha_s(M_Z)$ on Q_{\min}^2

The extracted $\alpha_s(M_Z)$ value is determined by both $t\bar{t}$ HERA DIS data in the fit: while the constraints from the $t\bar{t}$ data seem to be dominant, the residual dependence of $\alpha_s(M_Z)$ on the HERA DIS data may remain non-negligible. There is no way to assess the latter quantitatively because the HERA DIS data can not be removed from the PDF fit. However, as was investigated in the HERAPDF2.0 analysis [78], when using only the HERA DIS the minima are strongly dependent on the Q_{\min}^2 cut. As a cross check, the extraction of $\alpha_s(M_Z)$ was repeated for a larger cut variation $2.5 \leq Q_{\min}^2 \leq 30.0 \text{ GeV}^2$ (cf. the $2.5 \leq Q_{\min}^2 \leq 5.0 \text{ GeV}^2$ range used to estimate the model uncertainties). The results are given in Table 24.⁹ The extracted values of $\alpha_s(M_Z)$ show no systematic dependence on Q_{\min}^2 and are consistent with the nominal result of Eq. 16 within the total uncertainty.

9.3.3 Correlation between $\alpha_s(M_Z)$ and gluon distribution

PDF evolution involves $\alpha_s(M_Z)$, therefore PDFs always depend on the $\alpha_s(M_Z)$ assumed during their extraction. However, the exact dependence of different quark and gluon PDFs on $\alpha_s(M_Z)$ might be non-trivial because it is a net effect of several factors. E.g. with increasing $\alpha_s(M_Z)$ one expects the gluon distribution to decrease at low x because of more gluons splitting into quark-antiquark pairs, but at the same time at larger x values more gluons are radiated by the valence quarks resulting in the increase of the gluon distribution. Eventually one might expect a pivot x point where the gluon distribution does not change with changing $\alpha_s(M_Z)$, but this point may be different at different scales. In the PDF fits these effects are reflected in changes of the PDFs at the starting scale, taking into account also the momentum sum rule, therefore they may be partially compensated at higher scales, but in addition the dependence of the predictions for fitted data on $\alpha_s(M_Z)$ in the matrix elements plays a role.

PDFs extracted in this analysis assuming different values of $\alpha_s(M_Z)$ are shown at the typical scale of top quark production in Fig. 131 using the HERA data only, and in Fig. 132 using both HERA and $t\bar{t}$ data. The largest dependence on $\alpha_s(M_Z)$ is observed for the gluon distribution. As expected, there is the pivot point at $0.01 \lesssim x \lesssim 0.1$ where the dependence of the gluon distribution on $\alpha_s(M_Z)$ changes its sign. However, the overall dependence is greatly reduced once the $t\bar{t}$ data are included into the fit, because these data provide constraints on both the gluon distribution and $\alpha_s(M_Z)$ reducing their correlation. This is illustrated further in Fig. 133

⁹The fits with $Q_{\min}^2 = 5 \text{ GeV}$ and $Q_{\min}^2 = 30 \text{ GeV}$ using the HERA DIS data only, and $Q_{\min}^2 = 7.5 \text{ GeV}^2$ using the HERA DIS and $t\bar{t}$ data have minima with an error matrix which is not positive-definite as reported by HESSE. As a result of the error matrix being forced to be positive-definite, the reported α_s uncertainties are smaller than in the fits with other Q_{\min}^2 .

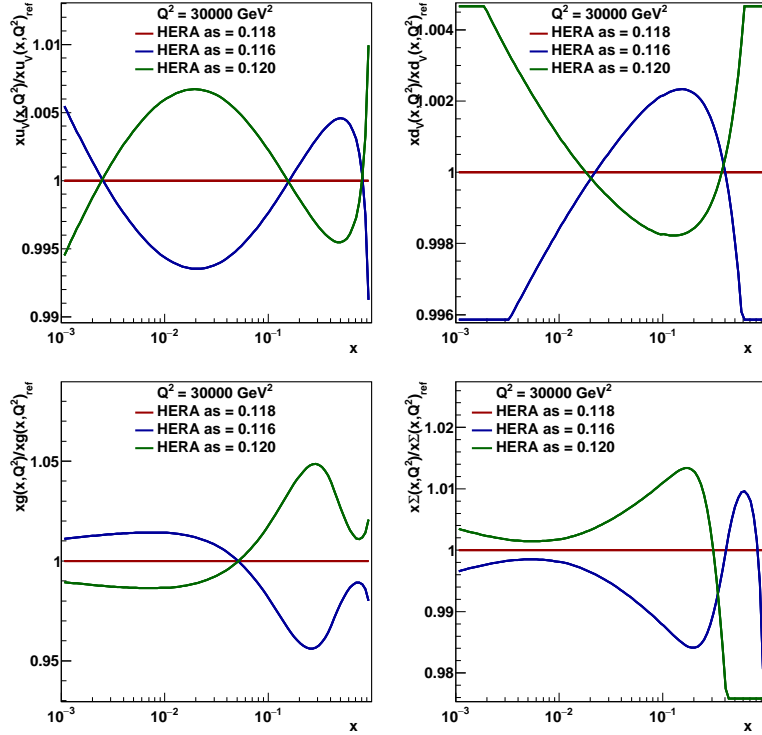


Figure 131: The PDFs at the scale $\mu_f^2 = 30000 \text{ GeV}^2$ for the fits with three values of $\alpha_s(M_Z)$ using the HERA DIS data. The results are normalised to the PDFs obtained with $\alpha_s(M_Z) = 0.118$.

1293 by plotting the gluon distribution at two different values $x = 0.01$ and $x = 0.1$ as a function of
 1294 $\alpha_s(M_Z)$ for the two variants of the fit. The chosen values of x represent the estimated bound-
 1295 boundaries of the sensitivity region of the $t\bar{t}$ data. The $t\bar{t}$ data greatly reduced the correlation between
 1296 the gluon distribution and $\alpha_s(M_Z)$, especially at high x .

1297 9.4 Impact of the $t\bar{t}$ cross section measurements on PDFs

1298 To demonstrate the added value of the $t\bar{t}$ cross sections, the PDF fit is first performed using only
 1299 the HERA DIS data. In this fit α_s is fixed to the value extracted from the fit using the $t\bar{t}$ data
 1300 $\alpha_s = 0.1135$ and its fit uncertainty $\alpha_s = 0.1135 \pm 0.0016$ is added to the PDF fit uncertainties.
 1301 Then the $[N_{\text{jet}}, M(t\bar{t}), y(t\bar{t})]$ measurement is added to the fit. The global and partial χ^2 values
 1302 for all variants of the fit are listed in Table 23.

1303 The PDFs from the two variants of the fit are compared in Fig. 134. The largest impact of the $t\bar{t}$
 1304 data is observed at $x \gtrsim 0.1$. In this region the gluon distribution lacks direct constraints in the
 1305 fit using the HERA DIS data only.

1306 In Figs. 135 and 136 the different PDF uncertainty components are compared in the fits using
 1307 the HERA DIS data only, and the HERA and $t\bar{t}$ data, respectively. In both fits, on average the
 1308 dominant uncertainties are the fit ones for all PDF distributions, however at high x the model
 1309 uncertainties are largest for the gluon PDF in the fit using the HERA data only. This uncertainty
 1310 is strongly reduced once the $t\bar{t}$ data are included in the fit.

1311 In Fig. 137 the fit PDF uncertainties are compared in the fits using the HERA DIS data only,
 1312 and HERA DIS and $t\bar{t}$ data. Reduction of uncertainties is observed for the gluon distribution,
 1313 especially at $x \sim 0.1$ where the included $t\bar{t}$ data are expected to provide constraints, while
 1314 the improvement at $x \lesssim 0.1$ originates from the reduced correlation between $\alpha_s(M_Z)$ and the

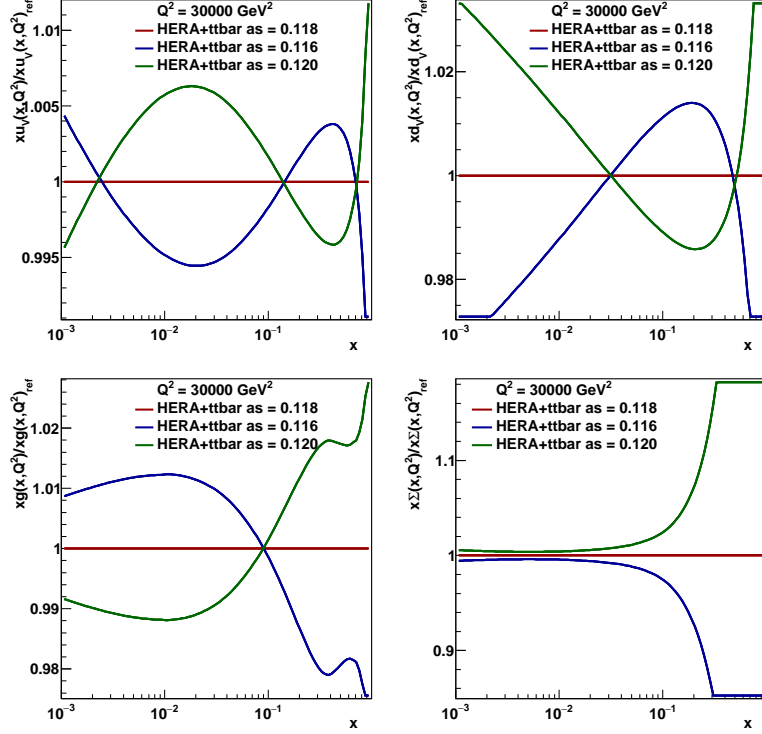


Figure 132: The PDFs at the scale $\mu_f^2 = 30000 \text{ GeV}^2$ for the fits with three values of $\alpha_s(M_Z)$ using the HERA DIS and $t\bar{t}$ data. The results are normalised to the PDFs obtained with $\alpha_s(M_Z) = 0.118$.

1315 gluon (see Fig. 133). A smaller uncertainty reduction is observed for other PDFs also, which
 1316 is expected because of the correlations between the different distributions in the fit arising
 1317 in the PDF evolution and from the momentum sum rule. Furthermore, in Fig. 138 the total
 1318 PDF uncertainties are compared in the two variants of the fits revealing similar reduction of
 1319 uncertainties after the inclusion of the $t\bar{t}$ data into the fit.

1320 9.4.1 Impact of variations of perturbative scales

1321 The PDFs extracted in the fits using varied μ_r and μ_f for $t\bar{t}$ production are shown in Figs. 139
 1322 and 140. The uncertainties arising when varying μ_r are larger than those arising when varying
 1323 μ_f . The dominant total uncertainties arise from the simultaneous μ_r and μ_f variation. These
 1324 uncertainties are well within the total PDF uncertainties.

1325 9.5 Cross check using MC method

1326 A cross check is performed using the Monte Carlo method [102, 103]. It is based on analysing a
 1327 large number of pseudo datasets called replicas. For this cross check, 1000 replicas are created
 1328 by taking the combined data and fluctuating the values of the reduced cross sections randomly
 1329 within their statistical and systematic uncertainties taking into account correlations. All un-
 1330 certainties are assumed to follow a Gaussian distribution. The central values for the fitted pa-
 1331 rameters and their uncertainties are estimated using the mean and RMS values over the fitted
 1332 replicas. Only converged fits of replicas are considered. In order to comply with multiplicative
 1333 treatment of data uncertainties for HERA data sets, data uncertainties in replicas are multiplied
 1334 by factor $\sqrt{2}$. The fits are performed with the free α_s , both when using the HERA DIS data only,
 1335 or the HERA DIS and $t\bar{t}$ data, in order to obtain uncertainties which can be directly compared,

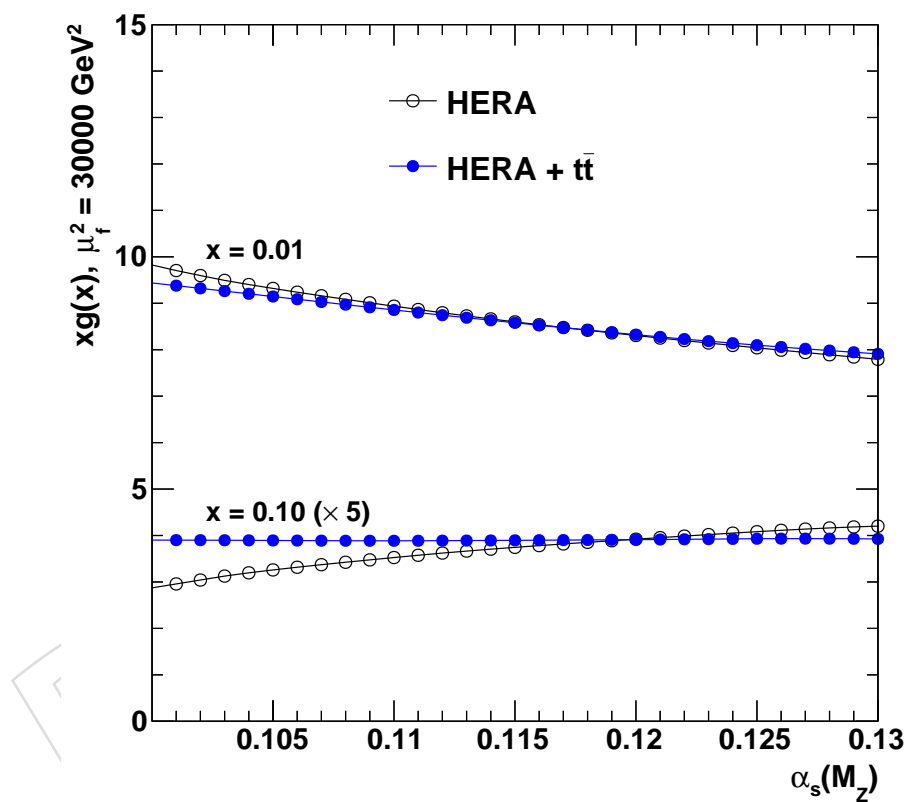


Figure 133: The gluon distribution $xg(x)$ at the scale $\mu_f^2 = 30000 \text{ GeV}^2$ for two values of $x = 0.01$ and $x = 0.15$ (the latter is scaled by factor 5 for better visibility) as a function of $\alpha_s(M_Z)$ in the PDF fit using the HERA DIS data only, or HERA and $t\bar{t}$ data.

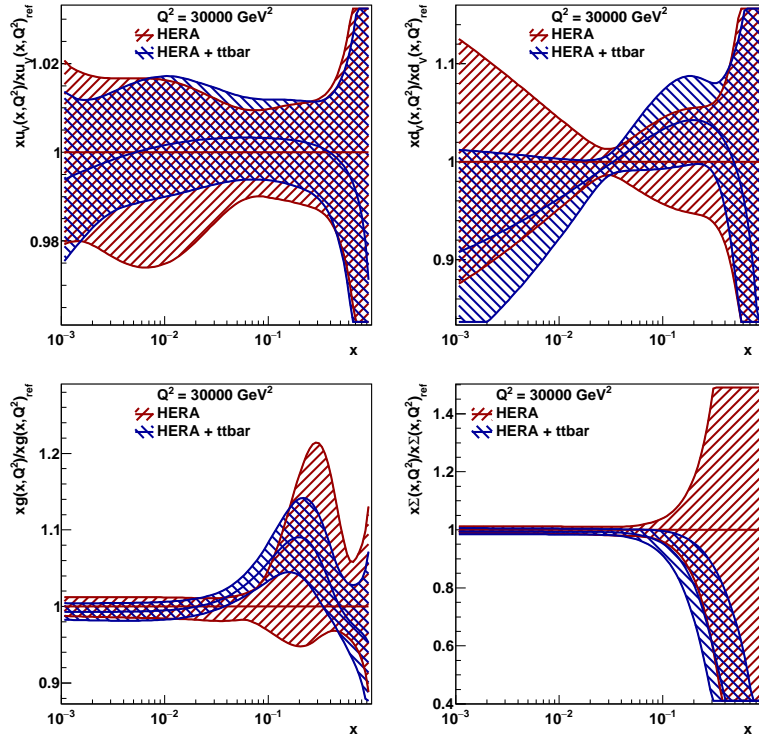


Figure 134: The PDFs with their total uncertainties in the fit using the HERA DIS data only, and the HERA DIS and $t\bar{t}$ data. The results are normalised to the PDFs obtained using the HERA DIS data only.

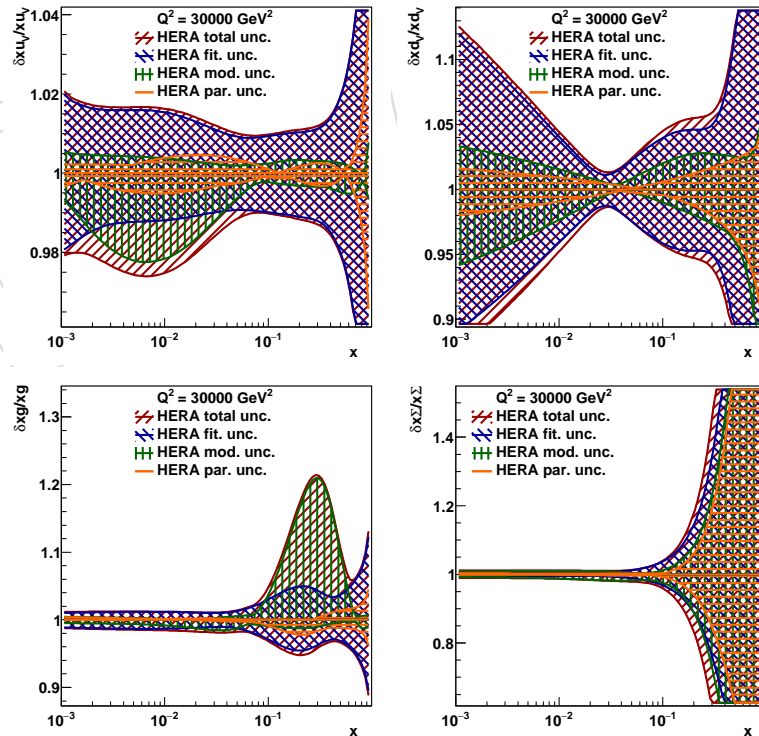


Figure 135: The PDF uncertainty components in the fit using the HERA DIS data only.

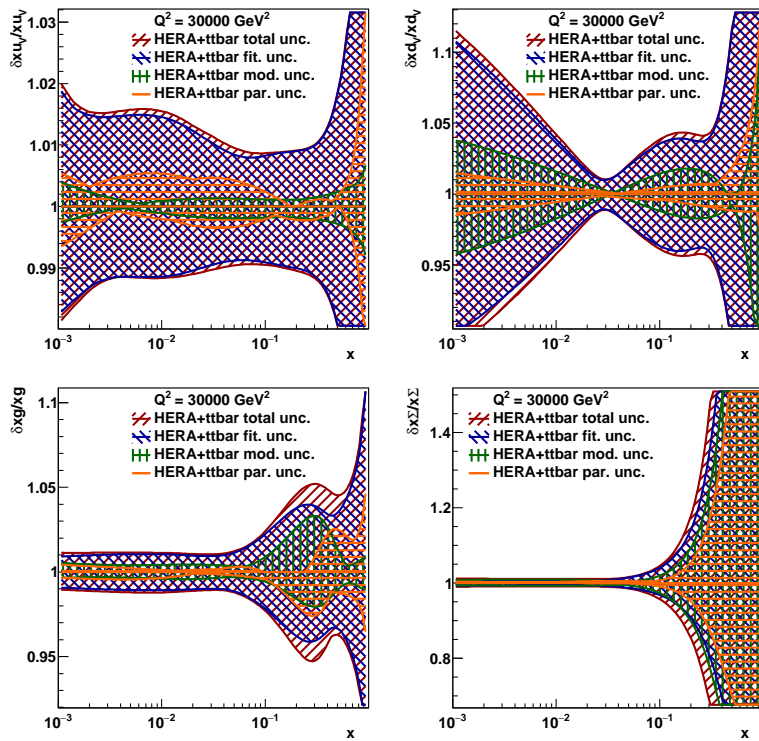


Figure 136: The PDF uncertainty components in the fit using the HERA DIS and $t\bar{t}$ data.

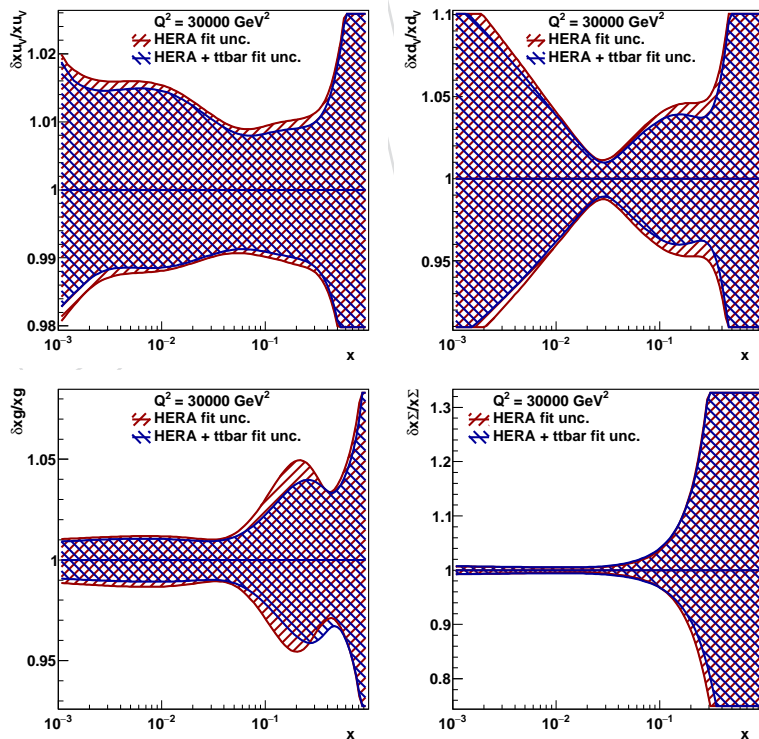


Figure 137: The total relative fit PDF uncertainties in the fit using the HERA DIS data only, and the HERA DIS and $t\bar{t}$ data.

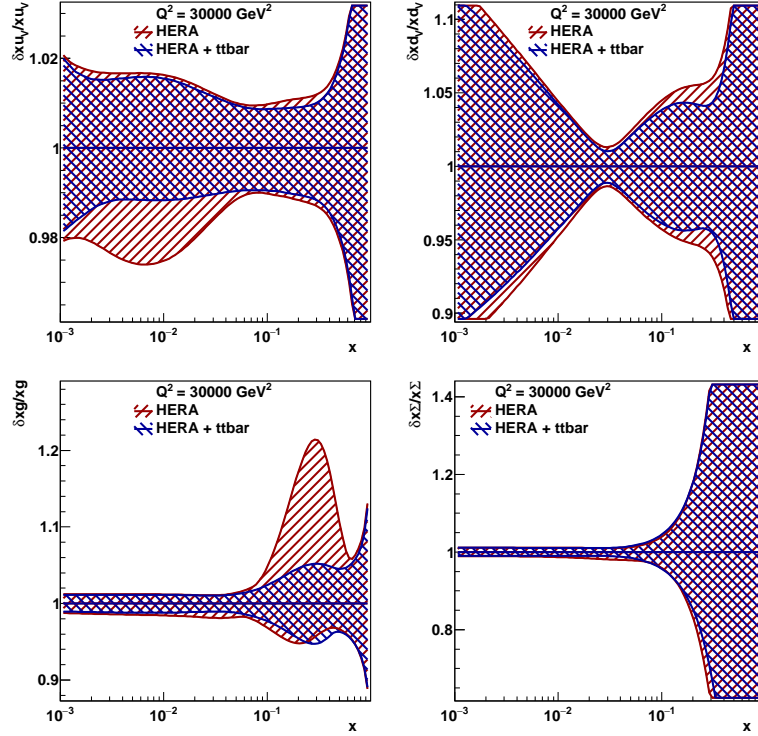


Figure 138: The relative total PDF uncertainties in the fit using the HERA DIS data only, and the HERA DIS and $t\bar{t}$ data.

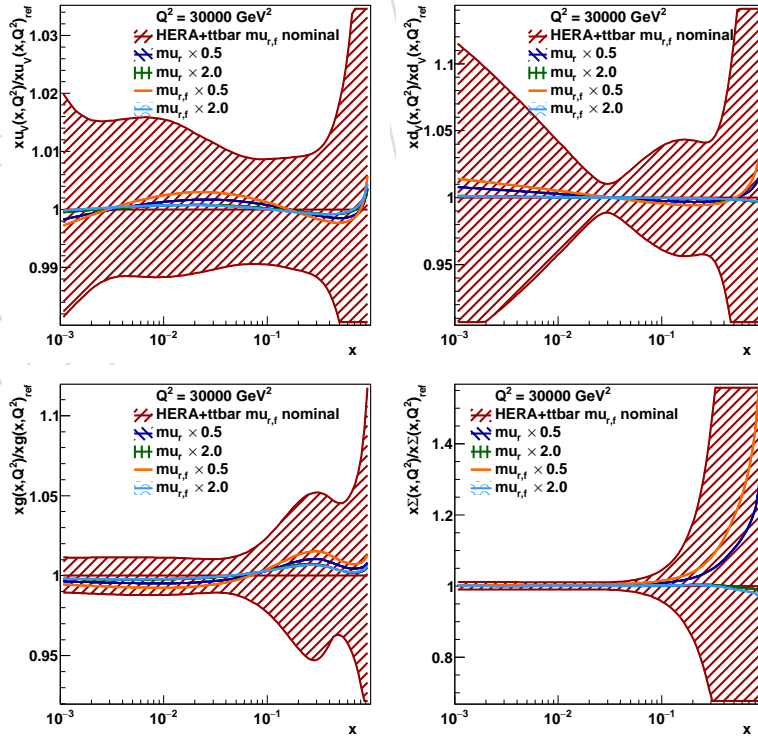


Figure 139: The PDFs obtained in the fits with varied scales for $t\bar{t}$ production using the HERA DIS and $t\bar{t}$ data.

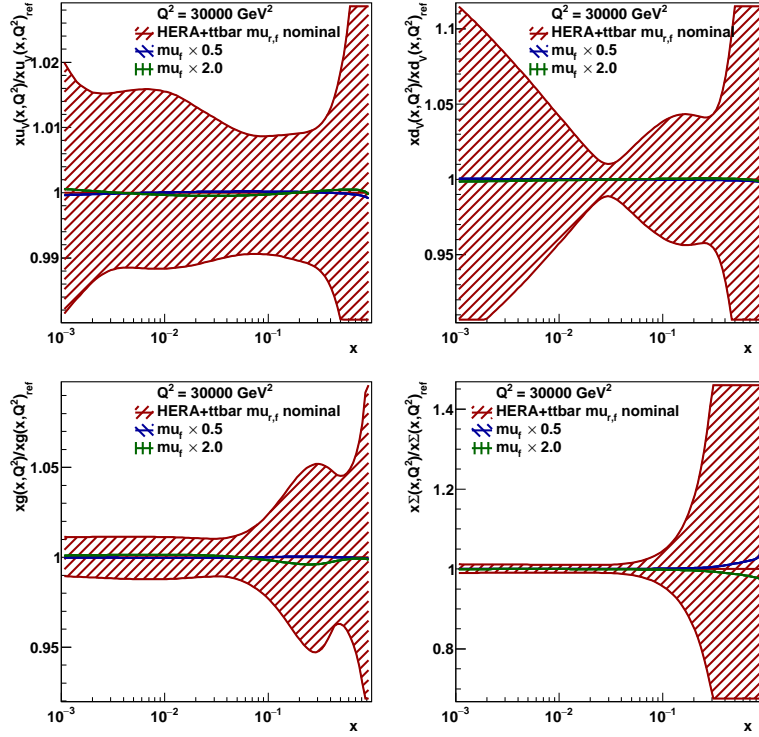


Figure 140: The PDFs obtained in the fits with varied scales for $t\bar{t}$ production using the HERA DIS and $t\bar{t}$ data.

1336 because α_s variations cannot be added to the determined MC uncertainties uncertainties as
1337 additional eigenvectors, contrary to the nominal approach.

1338 The obtained PDFs in the variants of the fit using the HERA DIS and $t\bar{t}$ data are shown in
1339 Fig. 141, while their relative uncertainties are compared in Fig. 142. All PDFs agree well as
1340 determined using the hessian and MC approaches. The MC uncertainties are on average larger
1341 than those obtained using the nominal hessian approach. This is expected, because the MC
1342 method is able to take into account multiple closely sitting minima and non-linearities, while
1343 in the hessian approach a single minimum and linearity of the problem has to be assumed. The
1344 increase of the PDF uncertainties is especially significant for the gluon PDF in the fit using the
1345 HERA DIS data only. All fit parameters with their fit uncertainties are provided in Table 25. It
1346 becomes obvious that the fit with free α_s using the HERA DIS data only might be not physical
1347 with the free E_g parameter, since its negative value results in the negative gluon distribution at
1348 the starting scale. This feature does not show up in the fit with the $t\bar{t}$ data included. The fitted
1349 parameters, including α_s and m_t^{pole} , are in good agreement obtained in the fit using the HESSE
1350 and MC methods.

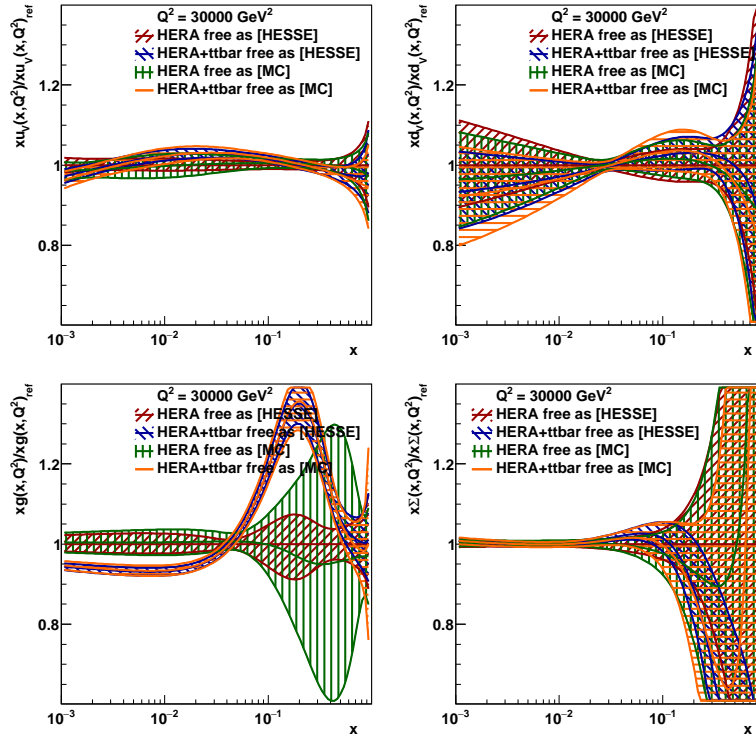


Figure 141: The PDFs obtained in the fits with varied scales for $t\bar{t}$ production using the HERA DIS and $t\bar{t}$ data.

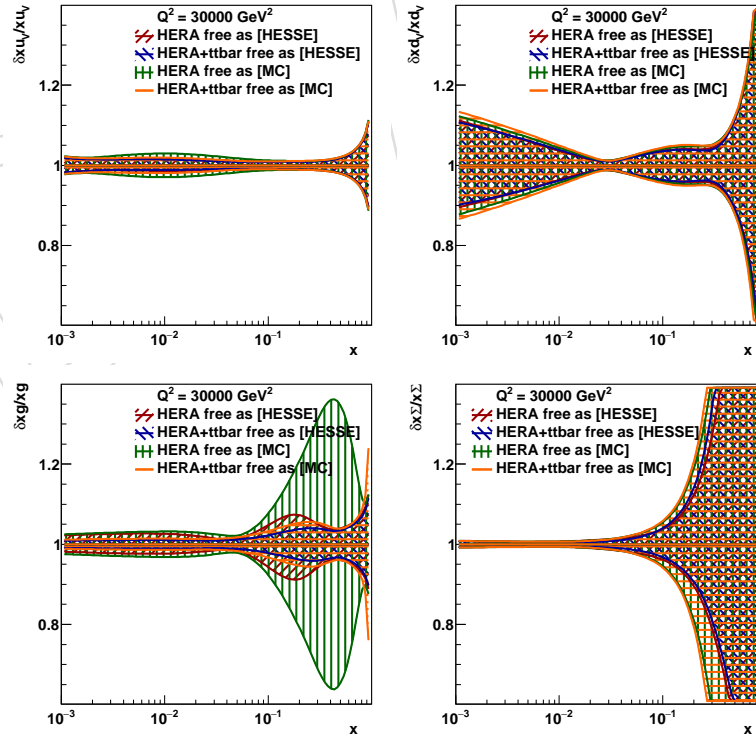


Figure 142: The PDFs obtained in the fits with varied scales for $t\bar{t}$ production using the HERA DIS and $t\bar{t}$ data.

Table 25: The fit parameters with their fit uncertainties determined using the hessian and MC approaches, for both fit variants using the HERA DIS data only, and the HERA DIS and $t\bar{t}$ data.

Parameter	HERA [HESSE]	HERA+ttbar [HESSE]	HERA [MC]	HERA+ttbar [MC]
'Bg'	-0.119 ± 0.050	0.024 ± 0.046	-0.114 ± 0.075	0.011 ± 0.042
'Cg'	15.0 ± 1.3	11.6 ± 1.1	14.3 ± 1.8	11.5 ± 1.1
'Eg'	-1.8 ± 7.2	16.6 ± 6.6	-2 ± 12	16.1 ± 4.0
'Aprig'	2.31 ± 0.72	0.143 ± 0.055	2.1 ± 1.4	0.143 ± 0.056
'Bprig'	-0.216 ± 0.044	-0.340 ± 0.047	-0.228 ± 0.066	-0.352 ± 0.040
'Buv'	0.390 ± 0.025	0.429 ± 0.028	0.395 ± 0.052	0.435 ± 0.042
'Cuv'	4.205 ± 0.069	4.097 ± 0.057	4.222 ± 0.066	4.122 ± 0.059
'Duv'	17.9 ± 2.4	17.4 ± 2.5	18.7 ± 5.3	17.6 ± 4.1
'Bdv'	0.915 ± 0.071	1.021 ± 0.077	0.948 ± 0.079	1.042 ± 0.094
'Cdv'	4.84 ± 0.36	4.86 ± 0.36	5.01 ± 0.38	5.01 ± 0.42
'Cubar'	15.44 ± 0.70	15.64 ± 0.65	15.37 ± 0.83	15.83 ± 0.72
'Dubar'	48.3 ± 5.7	41.0 ± 3.9	46.8 ± 6.0	41.9 ± 4.8
'ADbar'	0.1648 ± 0.0093	0.1670 ± 0.0093	0.171 ± 0.010	0.170 ± 0.011
'BDbar'	-0.1701 ± 0.0070	-0.1726 ± 0.0070	-0.1667 ± 0.0078	-0.1704 ± 0.0079
'CDbar'	6.0 ± 1.0	7.5 ± 1.5	7.0 ± 1.8	8.8 ± 2.9
'alphas'	0.1053 ± 0.0030	0.1135 ± 0.0015	0.1052 ± 0.0034	0.1132 ± 0.0020
'mtFit'	n/a	170.51 ± 0.72	n/a	170.52 ± 0.90
Fit status	converged	converged	MC-replica	MC-replica
Uncertainties	iterate	iterate	mean \pm rms	mean \pm rms

1351 10 Summary

1352 A measurement of normalized multi-differential $t\bar{t}$ production cross sections in pp collisions
 1353 at $\sqrt{s} = 8$ TeV has been presented. The measurement is performed using the decay channels
 1354 into two opposite-sign leptons, using data collected with the CMS detector at the LHC, corre-
 1355 sponding to an integrated luminosity of 35.9 fb^{-1} . The normalized $t\bar{t}$ cross section is measured
 1356 in the full phase space as a function of different pairs of kinematic variables describing the top
 1357 quark or $t\bar{t}$ system. None of the tested MC models is able to correctly describe all the distri-
 1358 butions. The data exhibit a softer transverse momentum $p_T(t)$ distribution, compared to the
 1359 Monte Carlo predictions, as was reported in previous single-differential and double-differential
 1360 $t\bar{t}$ cross section measurements.

1361 The measured cross sections as a function of N_{jet} , $M(t\bar{t})$ and $y(t\bar{t})$ have been incorporated into a
 1362 simultaneous PDF, α_s and m_t fit, together with the data from HERA. Including the $t\bar{t}$ data, one
 1363 observes a significant reduction in the uncertainties in the gluon distribution at large values of
 1364 parton momentum fraction x . In addition the extraction of α_s and m_t was carried out. These
 1365 two SM parameters have been simultaneously determined from the measured data to high
 1366 precision with only weak correlation between them. This strongly suggests the use the multi-
 1367 differential $t\bar{t}$ measurements in global PDF fits, and for determination of α_s and m_t .

DRAFT

1368 A Values of the measured cross sections

1369 Tables 75 to 121 provide the measured cross sections, including their correlation matrices of
 1370 statistical uncertainties and detailed breakdown of systematic uncertainties.

Table 26: The measured $[y(t), p_T(t)]$ cross sections, along with their relative statistical and systematic uncertainties.

$y(t)$	$p_T(t)$ [GeV]	$\frac{1}{\sigma(\text{t}\bar{\text{t}})} \frac{d\sigma}{dp_T(t)}$ [GeV $^{-1}$]	stat. [%]	syst. [%]	bin
0.00–0.35	0–80	9.251×10^{-4}	2.5	+6.6 −5.2	1
0.00–0.35	80–150	1.118×10^{-3}	1.8	+2.4 −4.6	2
0.00–0.35	150–250	4.596×10^{-4}	2.1	+4.6 −2.7	3
0.00–0.35	250–600	3.993×10^{-5}	2.9	+3.7 −5.6	4
0.35–0.85	0–80	1.279×10^{-3}	1.6	+3.6 −3.4	5
0.35–0.85	80–150	1.503×10^{-3}	1.3	+2.5 −2.8	6
0.35–0.85	150–250	6.206×10^{-4}	1.7	+3.7 −2.6	7
0.35–0.85	250–600	5.097×10^{-5}	2.8	+4.9 −4.7	8
0.85–1.45	0–80	1.248×10^{-3}	1.6	+2.1 −4.4	9
0.85–1.45	80–150	1.435×10^{-3}	1.3	+2.6 −2.7	10
0.85–1.45	150–250	5.328×10^{-4}	2.0	+4.6 −2.0	11
0.85–1.45	250–600	4.516×10^{-5}	2.9	+4.0 −5.4	12
1.45–2.50	0–80	1.128×10^{-3}	2.4	+4.2 −5.8	13
1.45–2.50	80–150	1.284×10^{-3}	1.6	+4.0 −2.5	14
1.45–2.50	150–250	4.238×10^{-4}	2.5	+2.7 −5.6	15
1.45–2.50	250–600	2.430×10^{-5}	4.9	+12.7 −4.2	16

1371 B Closure tests: additional materials

1372 B.1 Data tests

1373 Figures 143–159 present the results of data tests (see Section 6.4.1) for all distributions.

Table 27: The correlation matrix of statistical uncertainties for the measured $[y(t), p_T(t)]$ cross sections. The values are expressed as percentages. For bin indices see Table 75.

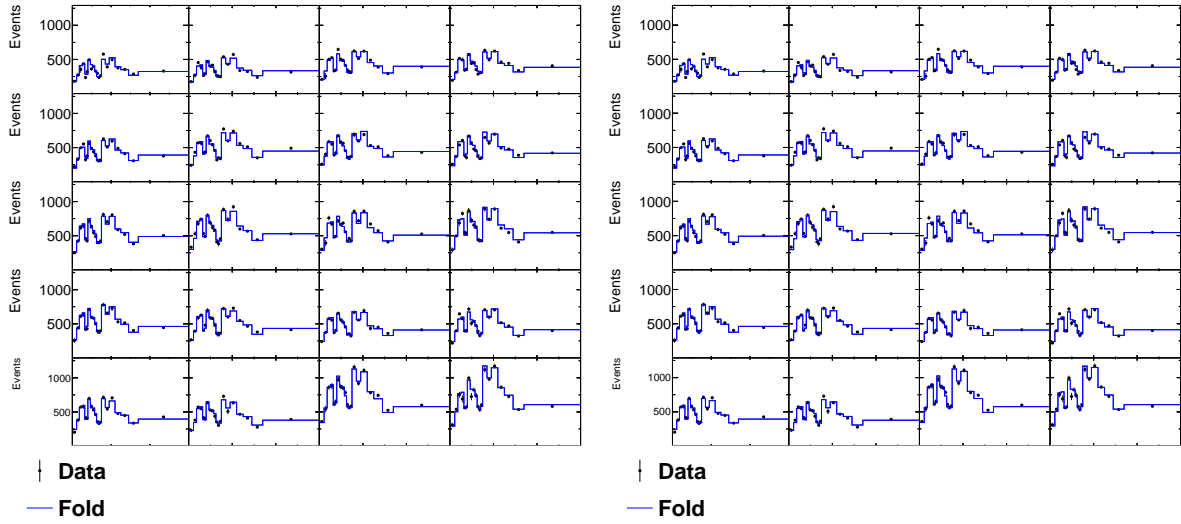


Figure 143: The folded $[y(t), p_T(t)]$ cross sections compared to the data for the unregularised (left) and regularised (right) unfolding shown as a function of $p_T(t)$ in different $y(t)$ ranges.

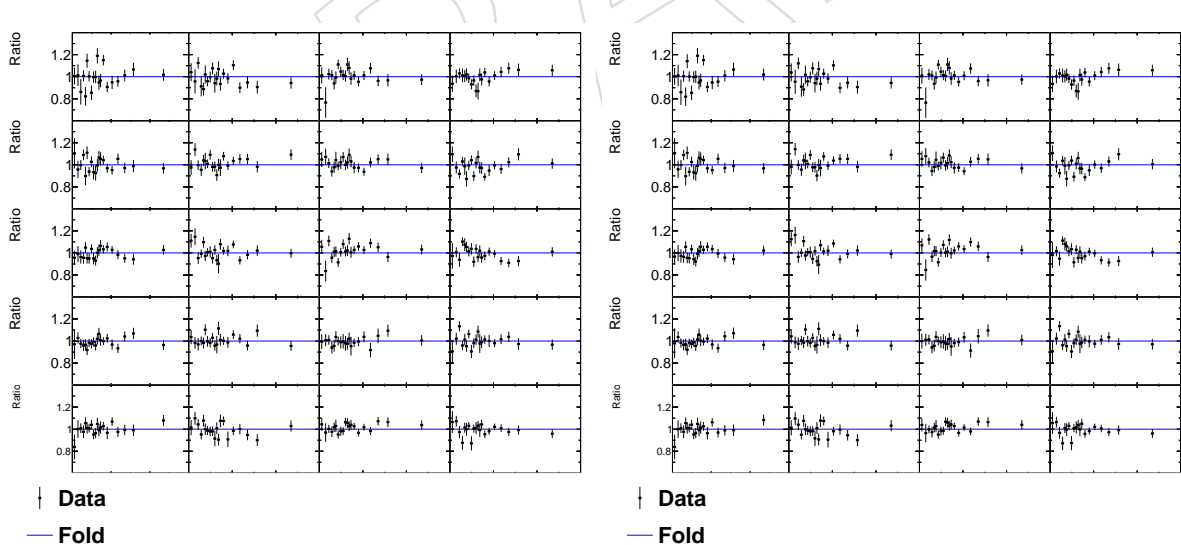


Figure 144: Ratio of the folded $[y(t), p_T(t)]$ cross sections to the data for the unregularised (left) and regularised (right) unfolding shown as a function of $p_T(t)$ in different $y(t)$ ranges.

Table 28: Sources and values of the relative systematic uncertainties in percent of the measured $[y(t), p_T(t)]$ cross sections. For bin indices see Table 75.

source / bin	1	2	3	4	5	6	7	8	9	10	11	12	13	14	15	16
JER	+0.4	-0.9	-0.3	+0.0	+0.1	+0.2	+0.2	-0.5	-0.7	-0.1	+0.4	-0.7	+0.7	+0.4	-0.2	-0.3
	+0.7	-0.3	-0.2	+0.8	+0.2	+0.1	+0.3	-0.2	-0.6	-0.1	+0.7	-0.1	-0.9	+0.3	-0.3	+1.0
JESAbsoluteMPFBias	+0.6	-0.3	+0.2	+0.2	+0.3	-0.0	+0.0	-0.3	+0.0	+0.1	+0.1	-0.0	-1.2	+0.3	+0.1	+0.8
	+1.0	-0.5	+0.1	-0.1	+0.7	-0.4	+0.3	+0.0	-0.6	+0.1	+0.4	-0.4	-0.9	+0.3	-0.1	+0.2
JESAbsoluteScale	-0.5	-0.5	+0.4	+0.0	+0.7	-0.1	+0.1	-0.1	+0.4	-0.5	+0.1	-0.5	+0.2	+0.1	-0.9	+2.1
	-0.0	-0.2	+0.2	-0.3	+0.2	-0.2	+0.4	-0.2	-0.4	-0.1	+0.4	+0.2	+0.3	-0.0	-0.5	+1.7
JESAbsoluteStat	+1.2	-0.1	-0.8	-0.2	+0.1	+0.0	+0.1	-0.8	+0.3	-0.0	-0.3	-0.1	+0.1	-0.3	-0.8	-0.5
	-2.1	+0.5	+0.1	+0.6	-0.4	+0.2	+0.8	+0.4	-0.2	-0.2	+0.4	+0.1	+0.6	+0.2	-0.3	+1.5
JESFlavourQCD	+0.4	-0.2	+0.3	+0.7	+0.5	-0.3	-0.1	+0.6	-0.3	-0.2	+0.5	+0.8	-1.1	+0.3	+0.2	+0.7
	+0.4	+0.2	+0.3	-1.5	-0.3	+0.3	+0.3	-0.8	-0.6	+0.2	+0.0	-1.5	-0.1	+0.3	+0.1	-0.8
JESFragmentation	-0.4	-0.4	+0.6	-0.0	+0.0	+0.2	+0.6	-0.8	-0.2	+0.2	-0.3	+0.7	+0.2	-0.1	-0.5	+1.0
	-0.3	-0.3	+0.4	-0.0	+0.5	-0.3	+0.2	-0.5	+0.1	-0.2	+0.4	-0.4	+0.1	+0.4	-0.9	+0.7
JESPileUpDataMC	-0.5	+0.4	+0.3	+0.4	-1.0	-0.2	-0.1	+0.0	-0.1	-0.1	+0.2	+0.1	+0.8	+0.4	-0.3	+2.5
	+0.8	-0.3	+0.4	-0.4	-0.4	+0.2	+0.4	-0.6	-0.1	-0.1	+0.3	-1.0	+0.3	-0.4	-0.5	+0.9
JESPileUpPtBB	+0.5	-0.6	+0.2	+0.1	+0.4	-0.4	+0.0	+0.3	-0.1	-0.3	+0.6	+0.0	+0.3	-0.3	-0.3	+1.2
	+1.0	-0.5	+0.1	-0.3	+0.1	-0.2	-0.1	-0.6	-0.1	-0.1	+0.3	-0.2	+0.8	-0.7	-0.4	+0.4
JESPileUpPtEC1	+0.8	+0.1	+0.5	+0.0	+0.4	+0.4	+0.9	+0.3	-0.4	+0.2	-0.1	+0.7	-1.7	-0.6	-0.3	+1.2
	-0.1	-0.9	-0.2	-0.6	+0.1	-0.0	-0.3	-0.5	+0.3	+0.2	-0.1	-0.1	+0.9	-0.2	+0.4	-0.8
JESPileUpPtEC2	-0.0	+0.0	-0.0	+0.0	+0.0	+0.0	-0.0	+0.0	+0.0	+0.0	+0.0	+0.0	-0.0	+0.0	+0.0	+0.0
	+0.0	+0.0	-0.0	+0.0	+0.0	+0.0	-0.0	+0.0	-0.0	+0.0	+0.0	+0.0	+0.0	+0.0	+0.0	+0.0
JESPileUpPtHF	+0.0	-0.0	-0.0	+0.0	-0.0	-0.0	-0.0	-0.0	-0.0	+0.0	+0.0	+0.0	+0.0	+0.0	+0.0	-0.0
	+0.0	+0.0	+0.0	+0.0	+0.0	+0.0	+0.0	+0.0	+0.0	+0.0	+0.0	+0.0	+0.0	+0.0	+0.0	+0.0
JESPileUpPtRef	+0.6	-0.8	+0.3	+0.2	+0.4	-0.2	+0.8	-0.0	+0.1	-0.5	+1.4	-0.2	-1.0	-0.1	+0.0	+1.4
	-0.3	+0.3	-0.7	+0.4	+0.2	+0.1	+0.0	-1.1	-0.0	-0.4	+0.8	-0.9	+0.4	+0.1	-0.6	+0.4
JESRelativeBal	+0.1	-0.7	-0.1	+0.9	+1.1	+0.1	+0.2	+0.1	-0.2	-0.0	+0.4	-0.2	+0.1	-0.4	-1.7	+1.9
	-0.5	-0.6	+0.1	-0.5	+0.1	+0.0	-0.0	-0.5	-0.3	+0.2	+0.4	-1.0	+0.1	+0.7	-0.0	+1.7
JESRelativeFSR	-1.1	-0.3	+0.5	-0.0	+0.4	+0.1	+0.0	-0.4	-0.3	+0.2	+0.2	-0.4	-0.1	+0.7	-0.5	+1.1
	+1.4	-0.9	+0.3	-0.3	+0.2	-0.2	-0.1	+0.6	-0.5	-0.1	+1.0	-0.6	+0.2	-0.3	-1.0	+2.6
JESRelativeJEREC1	-0.6	-0.1	+0.1	-0.2	+0.2	+0.3	+0.0	+0.0	-0.0	-0.3	-0.1	-0.0	-0.0	+0.4	-0.1	+0.4
	-0.2	-0.2	+0.2	-0.3	+0.3	+0.3	-0.1	-0.1	+0.2	+0.1	+0.0	+0.2	-0.1	-0.5	-0.3	+1.0
JESRelativeJEREC2	-0.0	+0.0	-0.0	+0.0	+0.0	+0.0	-0.0	+0.0	+0.0	+0.0	+0.0	+0.0	-0.0	+0.0	+0.0	+0.0
	+0.0	-0.0	-0.0	+0.0	-0.0	-0.0	-0.0	-0.0	-0.0	+0.0	+0.0	+0.0	+0.0	+0.0	+0.0	-0.0
JESRelativeJERHF	-0.0	+0.0	-0.0	+0.0	+0.0	+0.0	-0.0	+0.0	+0.0	+0.0	+0.0	+0.0	-0.0	+0.0	+0.0	+0.0
	+0.0	+0.0	-0.0	+0.0	+0.0	+0.0	-0.0	+0.0	-0.0	+0.0	+0.0	+0.0	+0.0	+0.0	+0.0	+0.0
JESRelativePtBB	+1.2	-0.4	+0.2	-0.2	-0.2	-0.7	+0.1	-0.2	-0.3	-0.3	+1.2	-0.3	+0.3	+0.0	-0.4	+0.7
	-0.6	+0.1	+0.5	+0.0	+0.2	+0.2	-0.2	-0.1	+0.2	+0.0	+0.1	-0.2	-0.4	+0.1	-0.6	+2.2
JESRelativePtEC1	-0.1	-0.1	+0.4	-0.1	+0.4	+0.3	+0.7	-0.1	+0.3	-0.4	+0.1	+0.2	-0.2	-0.5	-1.2	+0.0
	-0.2	-0.2	-0.3	-0.5	+0.3	+0.0	-0.1	-0.1	-0.3	+0.3	-0.0	+0.1	-0.3	+0.3	+0.5	+0.7
JESRelativePtEC2	-0.0	+0.0	-0.0	+0.0	+0.0	+0.0	-0.0	+0.0	+0.0	+0.0	+0.0	+0.0	-0.0	+0.0	+0.0	+0.0
	+0.0	+0.0	+0.0	+0.0	+0.0	+0.0	-0.0	+0.0	-0.0	+0.0	+0.0	+0.0	+0.0	+0.0	+0.0	+0.0
JESRelativePtHF	-0.0	+0.0	-0.0	+0.0	+0.0	+0.0	-0.0	+0.0	+0.0	+0.0	+0.0	+0.0	-0.0	+0.0	+0.0	+0.0
	-0.0	+0.0	-0.0	+0.0	+0.0	+0.0	-0.0	+0.0	-0.0	+0.0	+0.0	+0.0	-0.0	+0.0	+0.0	+0.0
JESRelativeStatEC	-0.3	+0.2	-0.0	-0.4	+0.4	+0.0	+0.5	-0.2	-0.1	-0.5	-0.1	+0.2	-0.1	+0.4	-0.4	-0.1
	-0.7	-0.4	+0.2	-0.4	+0.5	+0.1	+0.1	-0.0	+0.4	+0.1	+0.2	-0.2	-0.5	-0.1	+0.2	+0.4
JESRelativeStatFSR	-1.1	+0.1	+0.1	+0.2	+0.0	-0.1	+0.1	-0.4	+0.1	-0.1	+0.5	-0.4	+0.4	+0.3	-0.5	+0.8
	+0.6	-0.8	+0.5	+0.2	+0.5	-0.3	-0.3	-0.2	-0.5	+0.2	+0.3	-0.1	-0.1	+0.6	-1.1	+1.5
JESRelativeStatHF	+0.0	-0.0	-0.0	+0.0	-0.0	-0.0	-0.0	-0.0	-0.0	+0.0	+0.0	+0.0	+0.0	+0.0	+0.0	-0.0
	-0.0	+0.0	-0.0	+0.0	+0.0	+0.0	-0.0	+0.0	+0.0	+0.0	+0.0	+0.0	-0.0	+0.0	+0.0	+0.0
JESSinglePionECAL	+0.1	-0.2	-0.1	-0.5	+0.4	-0.0	-0.0	-0.3	-0.1	-0.1	-0.5	+0.2	+0.2	-0.2	-0.2	+0.5
	-1.6	-0.0	+0.0	+0.4	+0.6	+0.6	-0.1	+0.4	+0.2	+0.3	+0.4	-0.1	-0.9	-0.2	+0.1	+0.6

Table 29: Table 77 continued.

source / bin	1	2	3	4	5	6	7	8	9	10	11	12	13	14	15	16
JESSinglePionHCAL	-0.1	-0.3	-0.2	+0.0	+0.2	+0.3	+0.2	-0.6	+0.2	-0.1	-0.0	+0.0	-0.1	-0.1	-0.0	+0.1
	+0.2	+0.1	-0.3	+0.4	-0.1	-0.5	+0.6	-0.4	+0.1	-0.2	+0.2	+0.6	-0.1	+0.3	-0.3	+0.9
JESTimePtEta	+0.8	-0.7	+0.6	+0.1	-0.6	-0.3	-0.4	-0.2	-0.7	+0.2	+0.3	-0.0	+0.5	+0.8	-0.5	+1.5
	-0.1	+0.2	+0.1	+0.1	+0.3	-0.4	+0.1	+0.1	-0.2	-0.5	+0.6	-0.4	+0.7	+0.0	-1.2	+1.6
E_T^{miss}	+0.7	-0.6	+0.6	-0.1	+0.2	-0.1	+0.1	-0.6	+0.3	+0.1	-0.3	-0.1	-0.6	-0.1	-0.3	+0.5
	-0.2	+0.1	+0.0	+0.5	-0.2	+0.4	-0.1	+0.1	-0.2	-0.2	+0.4	+0.2	+0.2	-0.2	+0.0	+0.4
lepton ID/ISO	-0.2	+0.1	-0.0	-0.4	-0.0	+0.2	-0.0	-0.2	-0.1	+0.2	-0.1	-0.3	-0.1	+0.3	-0.0	-0.6
	+0.2	-0.1	+0.0	+0.4	+0.0	-0.2	+0.0	+0.2	+0.1	-0.2	+0.1	+0.3	+0.1	-0.3	+0.0	+0.6
pileup	-0.1	+0.3	-0.0	-0.2	+0.1	+0.2	+0.1	-0.0	-0.1	-0.1	+0.0	-0.2	-0.1	-0.2	-0.1	-0.2
	+0.0	-0.3	+0.0	+0.3	-0.1	-0.2	-0.1	+0.0	+0.1	+0.1	+0.0	+0.1	+0.1	+0.1	+0.1	+0.2
trigger	+0.0	+0.1	+0.0	+0.0	+0.1	+0.2	+0.1	+0.2	-0.0	+0.1	+0.1	+0.1	-0.4	-0.2	-0.2	-0.2
	-0.0	-0.1	-0.0	-0.0	-0.1	-0.2	-0.1	-0.2	+0.0	-0.1	-0.1	-0.1	+0.4	+0.2	+0.2	+0.2
trigger (η)	-0.2	-0.2	-0.2	-0.2	-0.1	-0.1	-0.1	-0.1	+0.0	+0.0	+0.0	+0.0	+0.4	+0.3	+0.2	+0.2
	+0.2	+0.2	+0.2	+0.2	+0.1	+0.1	+0.1	+0.1	-0.0	-0.0	-0.0	-0.0	-0.4	-0.3	-0.2	-0.2
non-tt background	-0.9	+0.6	+0.9	+1.0	-0.8	+0.6	+0.8	+1.0	-0.7	+0.6	+0.6	+1.1	-2.0	+0.1	+1.1	+0.2
	+0.9	-0.6	-0.9	-0.9	+0.7	-0.5	-0.8	-0.9	+0.7	-0.5	-0.6	-1.0	+1.9	-0.1	-1.0	-0.2
b-tagging	-0.1	+0.1	+0.0	+0.0	-0.1	+0.0	-0.0	+0.1	-0.1	+0.0	-0.0	+0.1	-0.0	+0.1	+0.1	+0.1
	+0.1	-0.1	-0.0	-0.0	+0.1	-0.0	+0.0	-0.0	+0.1	-0.0	+0.0	-0.1	+0.0	-0.1	-0.1	-0.1
b-tagging (light jets)	-0.2	+0.2	+0.3	+0.3	-0.2	+0.2	+0.3	+0.2	-0.3	+0.1	+0.2	+0.2	-0.6	-0.0	+0.2	+0.1
	+0.2	-0.2	-0.3	-0.3	+0.2	-0.2	-0.3	-0.2	+0.3	-0.1	-0.2	-0.2	+0.6	+0.0	-0.2	-0.1
luminosity	+0.0	+0.0	+0.0	+0.0	+0.0	+0.0	+0.0	+0.0	+0.0	+0.0	+0.0	+0.0	+0.0	+0.0	+0.0	+0.0
	+0.0	+0.0	+0.0	+0.0	+0.0	+0.0	+0.0	+0.0	+0.0	+0.0	+0.0	+0.0	+0.0	+0.0	+0.0	+0.0
BR($t\bar{t} \rightarrow \ell\ell$)	+0.0	+0.0	+0.0	+0.0	+0.0	+0.0	+0.0	+0.0	+0.0	+0.0	+0.0	+0.0	+0.0	+0.0	+0.0	+0.0
	+0.0	+0.0	+0.0	+0.0	+0.0	+0.0	+0.0	+0.0	+0.0	+0.0	+0.0	+0.0	+0.0	+0.0	+0.0	+0.0
PDF eigenvector 1	-0.0	-0.0	-0.0	+0.0	-0.0	-0.0	-0.0	+0.0	-0.0	+0.0	-0.0	+0.0	+0.0	+0.0	+0.0	+0.0
	+0.0	+0.0	+0.0	+0.0	+0.0	+0.0	+0.0	+0.0	-0.0	+0.0	-0.0	+0.0	-0.0	-0.0	-0.0	+0.1
PDF eigenvector 2	-0.2	-0.1	-0.0	+0.1	-0.1	-0.0	+0.0	+0.1	+0.0	+0.0	+0.1	+0.0	+0.1	+0.1	+0.0	-0.2
	+0.1	-0.0	-0.0	-0.1	+0.0	-0.1	-0.0	-0.1	+0.0	-0.0	+0.0	-0.1	-0.0	+0.0	+0.1	-0.1
PDF eigenvector 3	+0.1	+0.1	+0.0	+0.0	+0.0	+0.0	+0.0	+0.0	+0.0	+0.0	-0.0	-0.0	-0.1	-0.1	-0.1	+0.1
	-0.0	-0.0	-0.0	-0.0	-0.0	-0.0	-0.0	-0.0	-0.0	-0.0	+0.0	+0.0	+0.0	+0.1	+0.1	-0.0
PDF eigenvector 4	-0.2	-0.0	-0.0	+0.1	-0.1	+0.0	-0.0	+0.1	-0.0	+0.0	+0.0	+0.1	+0.1	+0.1	+0.1	-0.0
	+0.1	-0.0	+0.0	-0.1	+0.0	-0.0	+0.0	-0.1	+0.0	-0.0	+0.0	-0.1	-0.0	-0.0	-0.0	-0.0
PDF eigenvector 5	+0.0	-0.1	-0.0	-0.2	+0.0	-0.1	-0.0	-0.2	+0.0	-0.0	+0.0	-0.1	+0.0	+0.1	+0.1	-0.2
	+0.1	+0.1	+0.1	+0.1	+0.1	+0.1	+0.1	+0.1	-0.0	+0.0	-0.1	-0.0	-0.1	-0.2	-0.3	+0.2
PDF eigenvector 6	-0.1	+0.0	-0.0	+0.1	-0.0	+0.1	-0.0	+0.1	-0.0	+0.0	-0.0	+0.1	-0.0	+0.0	-0.0	+0.1
	+0.1	-0.0	+0.0	-0.1	+0.0	-0.0	-0.0	-0.1	+0.0	-0.0	+0.0	-0.1	+0.0	-0.0	-0.0	-0.1
PDF eigenvector 7	+0.0	-0.1	-0.1	-0.3	+0.0	-0.1	-0.1	-0.3	+0.0	-0.0	+0.1	-0.2	+0.1	+0.2	+0.2	-0.4
	-0.0	+0.1	+0.0	+0.2	-0.0	+0.1	+0.0	+0.1	-0.0	-0.0	-0.1	+0.1	-0.1	-0.1	-0.1	+0.2
PDF eigenvector 8	-0.0	+0.0	-0.0	-0.0	+0.0	+0.0	-0.0	-0.0	-0.0	+0.0	-0.0	+0.0	-0.0	+0.1	-0.0	-0.0
	+0.0	-0.0	+0.0	+0.0	-0.0	-0.0	+0.0	+0.0	+0.0	-0.0	+0.0	+0.0	-0.1	-0.0	+0.0	+0.0
PDF eigenvector 9	+0.0	-0.0	+0.0	-0.0	-0.0	-0.1	+0.0	-0.0	+0.0	-0.0	+0.0	-0.0	+0.1	-0.0	+0.0	-0.1
	-0.0	+0.0	-0.0	+0.0	+0.0	+0.1	-0.0	+0.0	-0.0	+0.0	-0.0	+0.0	-0.1	+0.0	-0.1	+0.1
PDF eigenvector 10	-0.0	+0.1	+0.0	+0.1	-0.0	+0.1	+0.0	+0.1	-0.0	-0.0	-0.1	+0.1	-0.0	-0.1	-0.1	+0.2
	+0.0	-0.1	-0.0	-0.2	+0.0	-0.1	-0.0	-0.1	+0.0	+0.0	+0.1	-0.1	+0.0	+0.1	+0.1	-0.2
PDF eigenvector 11	-0.0	+0.0	+0.0	+0.0	-0.0	+0.0	+0.0	+0.0	-0.0	+0.0	-0.0	+0.0	-0.0	-0.0	-0.0	+0.0
	+0.0	-0.0	-0.0	-0.1	+0.0	-0.0	-0.0	-0.1	+0.0	-0.0	+0.0	-0.0	+0.0	+0.0	+0.1	-0.1
PDF eigenvector 12	+0.0	-0.0	-0.0	-0.1	+0.0	-0.0	-0.0	-0.1	+0.0	+0.0	+0.0	-0.1	-0.0	+0.1	+0.0	-0.1
	-0.0	+0.0	+0.0	+0.1	-0.0	+0.0	+0.0	+0.1	-0.0	-0.0	-0.0	+0.1	+0.0	-0.1	-0.0	+0.1
PDF eigenvector 13	+0.1	+0.0	+0.0	-0.0	+0.0	+0.0	-0.0	-0.0	-0.0	+0.0	-0.1	-0.0	-0.1	-0.0	-0.1	+0.1
	-0.1	-0.0	-0.0	+0.0	-0.0	-0.0	+0.0	+0.0	+0.0	-0.0	+0.1	+0.0	+0.1	+0.0	+0.1	-0.1
PDF eigenvector 14	+0.0	-0.0	-0.0	-0.0	+0.0	+0.0	-0.0	-0.0	+0.0	+0.0	-0.0	-0.0	+0.0	-0.0	-0.0	-0.1
	-0.0	+0.0	+0.0	+0.0	-0.0	-0.0	+0.0	+0.1	-0.0	-0.0	-0.0	+0.1	+0.0	-0.0	+0.0	+0.1

Table 30: Table 77 continued.

source / bin	1	2	3	4	5	6	7	8	9	10	11	12	13	14	15	16
PDF eigenvector 15	+0.1	-0.0	-0.0	-0.1	+0.0	-0.0	-0.0	-0.1	+0.0	+0.0	+0.0	-0.1	-0.0	-0.0	-0.0	-0.1
	-0.0	+0.0	+0.0	+0.0	-0.0	+0.0	-0.0	+0.0	-0.0	-0.0	-0.0	+0.0	+0.0	+0.0	+0.0	+0.0
PDF eigenvector 16	-0.0	+0.0	+0.0	+0.0	-0.0	+0.0	+0.0	+0.0	-0.0	+0.0	-0.0	+0.0	-0.0	-0.0	-0.0	+0.0
	+0.0	-0.0	-0.0	-0.0	+0.0	-0.0	-0.0	-0.0	+0.0	+0.0	+0.0	-0.0	+0.0	+0.0	+0.0	-0.1
PDF eigenvector 17	+0.0	-0.0	-0.0	-0.0	+0.0	-0.0	-0.0	-0.0	+0.0	+0.0	+0.0	-0.0	+0.0	+0.0	+0.0	-0.1
	-0.0	+0.0	+0.0	+0.1	-0.0	+0.0	-0.0	+0.1	-0.0	+0.0	-0.0	+0.1	-0.0	-0.0	-0.0	+0.1
PDF eigenvector 18	-0.1	-0.0	+0.0	+0.1	-0.1	-0.0	+0.0	+0.1	-0.0	-0.0	+0.0	+0.1	+0.1	+0.0	+0.2	+0.1
	+0.1	+0.0	-0.0	-0.1	+0.1	+0.0	-0.0	-0.1	+0.0	+0.0	-0.0	-0.1	-0.1	-0.0	-0.2	-0.1
PDF eigenvector 19	-0.0	+0.0	+0.0	+0.1	-0.0	+0.0	+0.0	+0.1	-0.0	-0.0	-0.0	+0.1	+0.0	-0.0	+0.0	+0.1
	+0.1	-0.0	-0.0	-0.2	+0.0	-0.0	-0.0	-0.2	+0.0	+0.0	+0.0	-0.1	-0.0	+0.1	-0.0	-0.2
PDF eigenvector 20	-0.0	+0.0	-0.0	+0.0	-0.0	+0.0	-0.0	+0.0	-0.0	-0.0	-0.0	+0.1	+0.1	-0.0	+0.1	+0.2
	+0.0	-0.0	-0.0	-0.1	+0.0	-0.0	-0.0	-0.0	+0.0	+0.0	+0.0	-0.0	-0.0	+0.0	-0.0	-0.1
PDF eigenvector 21	-0.1	-0.0	-0.0	+0.0	-0.0	-0.0	-0.0	+0.0	-0.0	+0.0	+0.0	+0.1	+0.1	+0.1	+0.1	-0.0
	+0.1	+0.1	+0.0	-0.0	+0.0	+0.0	+0.0	-0.0	+0.0	-0.0	-0.0	-0.0	-0.1	-0.1	-0.1	+0.1
PDF eigenvector 22	-0.2	-0.1	-0.1	+0.1	-0.1	-0.1	-0.0	+0.1	-0.0	-0.0	+0.1	+0.1	+0.2	+0.2	+0.4	-0.1
	+0.2	+0.1	+0.0	-0.0	+0.1	+0.1	+0.0	-0.0	-0.0	+0.0	-0.1	-0.1	-0.2	-0.1	-0.3	+0.2
PDF eigenvector 23	+0.2	+0.0	+0.0	-0.1	+0.1	+0.0	+0.0	-0.1	+0.0	+0.0	-0.0	-0.2	-0.2	-0.1	-0.3	-0.1
	-0.0	-0.0	-0.0	+0.0	-0.0	-0.0	-0.0	+0.0	-0.0	-0.0	-0.0	+0.0	+0.1	+0.0	+0.1	+0.0
PDF eigenvector 24	+0.1	-0.0	-0.0	-0.1	-0.0	-0.0	-0.0	-0.1	-0.0	-0.0	+0.0	-0.0	+0.0	+0.0	+0.1	-0.0
	-0.1	-0.1	+0.0	-0.1	+0.0	-0.0	+0.0	-0.1	+0.1	+0.0	+0.1	-0.1	+0.0	+0.0	-0.1	-0.3
PDF eigenvector 25	-0.0	-0.0	+0.0	-0.1	+0.0	-0.0	+0.0	-0.1	+0.1	+0.0	+0.1	-0.1	-0.0	+0.0	-0.1	-0.2
	+0.1	-0.1	-0.1	-0.2	-0.0	-0.1	-0.0	-0.1	+0.0	-0.0	+0.0	-0.1	+0.0	+0.1	+0.2	-0.1
PDF eigenvector 26	+0.0	+0.0	+0.0	-0.0	+0.0	+0.0	+0.0	-0.0	+0.0	+0.0	-0.0	-0.0	-0.0	-0.0	-0.0	-0.0
	-0.0	-0.0	-0.0	-0.0	-0.0	-0.0	-0.0	-0.0	-0.0	-0.0	+0.0	+0.0	+0.0	+0.0	+0.0	-0.0
PDF eigenvector 27	-0.0	-0.0	+0.1	+0.1	-0.0	-0.1	+0.0	+0.1	+0.1	-0.0	+0.0	-0.0	+0.1	-0.1	-0.0	-0.1
	-0.1	+0.0	-0.0	+0.0	-0.0	+0.0	-0.0	+0.0	-0.0	+0.0	-0.0	+0.0	-0.0	+0.0	-0.0	+0.0
PDF eigenvector 28	+0.0	-0.0	+0.0	-0.0	+0.0	-0.0	+0.0	-0.0	+0.0	-0.0	-0.0	+0.1	+0.0	+0.1	+0.0	+0.0
	-0.1	+0.0	-0.0	+0.0	-0.0	+0.0	-0.0	+0.0	-0.0	-0.0	+0.1	+0.0	+0.1	+0.0	+0.0	+0.0
α_s	+0.1	+0.0	+0.1	-0.0	+0.0	-0.0	+0.0	-0.0	+0.0	-0.0	+0.0	-0.0	+0.0	-0.1	-0.0	-0.0
	-0.1	-0.0	-0.1	-0.0	-0.0	+0.0	-0.1	-0.0	-0.0	+0.0	-0.0	+0.0	-0.0	+0.1	+0.0	+0.0
m_t	+0.4	-0.8	+0.6	+0.9	+0.4	-0.6	+0.4	+1.8	+0.2	-0.6	+0.4	+1.6	-0.8	-0.2	+0.6	+2.4
	-0.1	+0.9	-0.4	-2.1	-0.4	+0.6	-0.1	-1.2	-0.2	+0.7	-0.5	-1.7	-0.0	+0.3	-0.3	-2.2
μ_{rf}	+0.3	-0.2	+0.2	-0.5	-0.1	-0.6	+0.1	-0.2	+0.4	-0.2	+0.3	-0.0	+0.6	-0.4	+0.3	-0.0
	-0.3	+0.2	-0.1	+0.5	+0.1	+0.6	-0.1	+0.4	-0.4	+0.2	-0.2	+0.2	-0.6	+0.3	-0.5	+0.1
h_{damp}	+1.2	-0.9	+0.5	-0.8	+0.4	-0.5	+0.9	-0.3	-0.4	-0.6	+0.6	+0.1	-0.7	+0.6	-0.1	+1.8
	+0.1	+0.0	-0.2	-1.0	-1.4	+0.6	-0.2	+0.6	-0.9	+1.0	-0.5	-1.0	+0.2	+0.9	+0.2	+2.2
PS ISR	+0.2	-1.1	+1.7	-1.0	+0.4	-0.1	-0.1	+0.1	-1.0	-0.3	+0.4	+0.0	-0.0	+1.0	-0.3	+2.0
	+1.1	+0.4	-0.2	+0.3	+0.3	-0.3	-0.4	+0.8	-1.0	-0.6	+0.9	-0.5	-0.3	+0.6	+0.2	-0.1
PS FSR	-0.0	+0.7	-0.4	-1.2	+0.0	+0.4	-0.9	-0.3	+0.0	+0.8	-0.5	-1.2	-0.4	+0.5	-0.7	-0.7
	-0.2	-0.1	+0.1	+0.7	+0.3	-0.3	+0.2	+1.0	-0.2	-0.1	+0.5	+0.6	-0.6	+0.4	-0.8	+2.9
UE tune	+0.5	+0.1	-0.7	-0.8	+0.4	+0.3	-0.0	+0.2	-1.2	+0.1	-0.3	+0.0	-0.5	+0.6	+0.6	+0.9
	+2.2	+0.2	+0.2	-0.0	-1.2	+0.2	+0.2	-1.5	-1.6	-0.1	+0.5	+0.3	-0.0	+0.8	+0.0	+0.6
CR	+0.3	-0.2	+1.4	+0.2	+0.3	-0.3	-0.9	+1.5	-0.2	-0.2	-0.2	+0.7	-0.7	+0.2	+0.2	+2.8
	+0.5	+0.1	-0.0	-0.8	-0.0	-0.2	-0.2	+0.6	+0.1	+0.0	-0.4	+0.4	-0.4	+0.2	+0.5	-0.7
	+0.7	-0.2	+0.1	-0.6	-0.1	-0.4	+0.6	+0.5	-1.0	+0.2	+0.7	-0.4	-0.6	+1.0	-0.6	+0.9
$f(b \rightarrow B)$	+0.7	-0.2	-0.2	+0.3	+0.4	-0.3	-0.2	+0.6	+0.6	-0.2	-0.2	+0.5	-0.0	-0.6	-0.4	+0.7
	-0.4	+0.1	+0.1	-0.1	-0.2	+0.1	+0.2	-0.2	-0.2	+0.1	+0.1	-0.1	-0.0	+0.2	+0.3	-0.2
	+0.1	-0.0	-0.0	+0.1	+0.1	-0.1	-0.0	+0.1	+0.1	-0.0	-0.0	+0.1	-0.0	-0.1	-0.1	+0.1
	+0.7	-0.3	-0.1	+0.4	+0.4	-0.4	-0.2	+0.3	+0.5	-0.3	-0.1	+0.5	+0.2	-0.5	-0.2	+0.4
BR($B \rightarrow \mu$)	-0.1	+0.0	+0.1	-0.1	-0.0	+0.0	+0.0	-0.0	-0.1	+0.0	+0.1	-0.1	-0.0	+0.0	-0.0	-0.0
	+0.1	-0.1	-0.1	+0.1	+0.1	-0.1	-0.1	+0.1	+0.1	-0.1	-0.0	+0.1	+0.0	-0.1	-0.0	+0.2

Table 31: The measured $[M(t\bar{t}), y(t)]$ cross sections, along with their relative statistical and systematic uncertainties.

$M(t\bar{t})$ [GeV]	$y(t)$	$\frac{1}{\sigma(t\bar{t})} \frac{d\sigma}{dy(t)}$	stat. [%]	syst. [%]	bin
300–400	0.00–0.35	1.506×10^{-1}	3.1	+6.6 -5.4	1
300–400	0.35–0.85	1.511×10^{-1}	2.2	+3.5 -8.1	2
300–400	0.85–1.45	1.161×10^{-1}	2.2	+4.2 -6.2	3
300–400	1.45–2.50	4.794×10^{-2}	4.6	+19.5 -10.1	4
400–500	0.00–0.35	2.317×10^{-1}	1.9	+3.9 -3.1	5
400–500	0.35–0.85	2.181×10^{-1}	1.3	+2.2 -2.4	6
400–500	0.85–1.45	1.605×10^{-1}	1.5	+4.2 -3.0	7
400–500	1.45–2.50	7.230×10^{-2}	2.1	+6.8 -2.2	8
500–650	0.00–0.35	1.538×10^{-1}	2.2	+5.9 -2.2	9
500–650	0.35–0.85	1.438×10^{-1}	1.8	+1.7 -6.8	10
500–650	0.85–1.45	1.062×10^{-1}	1.9	+3.7 -2.5	11
500–650	1.45–2.50	5.345×10^{-2}	2.5	+3.2 -7.4	12
650–1500	0.00–0.35	6.963×10^{-2}	2.8	+4.3 -8.6	13
650–1500	0.35–0.85	7.045×10^{-2}	2.3	+6.2 -4.6	14
650–1500	0.85–1.45	6.765×10^{-2}	2.0	+3.1 -5.5	15
650–1500	1.45–2.50	4.155×10^{-2}	2.2	+4.8 -3.2	16

Table 32: The correlation matrix of statistical uncertainties for the measured $[M(t\bar{t}), y(t)]$ cross sections. The values are expressed as percentages. For bin indices see Table 80.

Table 33: Sources and values of the relative systematic uncertainties in percent of the measured $[M(t\bar{t}), y(t)]$ cross sections. For bin indices see Table 80.

source / bin	1	2	3	4	5	6	7	8	9	10	11	12	13	14	15	16	
JER	-0.6 -0.2	+0.3 -1.1	-0.3 -0.7	+2.4 +3.9	+0.3 +0.7	-0.0 -0.2	-0.2 -0.3	-0.2 +0.8	+0.4 -0.0	-0.6 -0.7	+0.6 -0.1	-0.8 -1.6	-1.1 -0.2	-0.4 +0.3	-0.2 -0.2	-0.1 +0.7	
JESAbsoluteMPFBias	-0.9 -1.3	+0.1 -0.5	-0.7 -0.8	+0.1 +1.7	+0.9 +0.7	-0.0 +0.5	-0.4 +0.2	+1.4 +0.6	+0.3 +0.1	-1.1 -0.7	-0.3 +0.2	+0.0 -1.0	+0.1 -0.4	+0.2 -0.2	+0.2 -0.1	+0.3 +0.2	
JESAbsoluteScale	-0.2 -0.5	-0.8 -1.0	+0.7 -0.4	+2.1 +3.8	+0.7 +0.4	-0.2 -0.3	-0.3 +0.1	-0.4 +0.2	+0.3 +0.4	-0.4 -0.3	-0.0 -0.2	-1.2 -1.0	+0.0 -0.9	-0.6 +0.0	-0.0 -0.1	+0.9 +0.1	
JESAbsoluteStat	+0.3 +1.2	+0.1 -1.8	-0.0 -0.3	+1.8 +0.1	-0.4 +0.1	-0.4 -0.0	-0.3 +0.1	+0.5 +1.3	+0.5 +0.2	-0.6 -0.8	+0.4 +0.1	-0.7 -0.3	-0.4 +0.1	-0.1 +0.5	+0.1 -0.0	-0.2 +0.3	
JESFlavourQCD	+1.5 -0.5	-0.1 -1.9	+0.0 -0.2	+2.5 +1.7	-0.6 +1.0	-0.8 +0.3	-0.5 +0.6	-0.0 +0.8	+0.2 +0.7	-0.6 -0.4	+0.1 -0.3	-0.7 -0.7	+0.3 -1.8	+0.7 -0.4	+0.5 -0.9	+0.3 -0.1	
JESFragmentation	-0.3 +0.5	-0.7 -0.6	+0.0 -0.6	+0.7 +3.0	+0.2 +0.0	-0.3 +0.0	-0.3 -0.2	+0.7 -0.0	+0.6 +0.5	+0.1 -0.8	+0.3 +0.3	-0.7 -0.4	-0.1 -0.6	-0.4 -0.2	+0.3 -0.1	+0.3 -0.2	
JESPileUpDataMC	+0.5 +0.8	-1.4 -0.9	+0.4 -0.3	+0.3 +3.7	+0.1 -0.2	-0.5 +0.2	+0.4 -0.3	+0.4 +0.6	+0.3 +0.8	+0.8 -0.9	+0.0 -0.3	-0.4 -1.1	+0.2 -1.0	+0.0 -0.3	+0.4 -0.6	+0.4 -0.0	
JESPileUpPtBB	-0.7 -0.4	-0.2 +0.3	-0.0 +0.0	+1.6 +1.8	+0.2 +0.0	-0.2 -0.1	-0.4 +0.1	+0.4 +0.5	+0.9 +0.7	-0.6 -1.1	-0.1 -0.0	-0.6 -1.3	-0.3 -1.0	-0.3 +0.0	+0.3 -0.1	+0.4 +0.2	
JESPileUpPtEC1	-0.1 -0.2	+0.7 -0.9	+0.0 -0.3	-1.5 +3.7	+0.8 -0.6	+0.2 -0.4	-0.5 +0.0	+0.2 +1.0	-0.5 -0.1	+0.3 -0.6	-0.1 -0.6	-0.6 -1.3	-0.3 -1.0	-0.2 -0.1	+0.4 +0.2	-0.3 +0.2	
JESPileUpPtEC2	-0.0 -0.0	+0.0 +0.0	-0.0 +0.0	+0.0 +0.0	-0.0 -0.0	-0.0 +0.0	+0.0 +0.0	+0.0 +0.0	+0.0 +0.0	+0.0 +0.0							
JESPileUpPtHF	-0.0 -0.0	+0.0 +0.0	-0.0 -0.0	+0.0 +0.0	+0.0 -0.0	-0.0 +0.0	+0.0 +0.0	+0.0 +0.0	+0.0 +0.0	+0.0 +0.0							
JESPileUpPtRef	+0.3 +0.1	+0.5 -0.6	+0.4 +0.2	+0.1 +2.1	-0.9 -0.0	+0.0 -0.1	-0.3 -0.1	+0.1 +0.8	+0.5 -0.3	-0.4 -0.2	+0.1 +0.5	-0.4 -1.2	+0.2 -0.2	+0.1 -1.0	+0.0 -0.6	+0.2 +0.2	
JESRelativeBal	+0.9 -1.7	+0.3 -0.7	+0.8 -0.7	+1.4 +1.3	-0.4 +0.4	-0.2 +0.1	-0.2 +1.0	-0.1 +0.7	+0.3 -1.9	-0.8 +0.3	-0.5 -0.3	-1.6 -1.0	+0.1 +0.4	+0.4 -0.4	+0.2 +0.6	+0.4 +0.6	
JESRelativeFSR	+0.1 +0.2	-0.4 -0.6	-0.2 +0.5	+2.3 +3.2	-0.3 +0.3	-0.2 -0.6	-0.1 -0.6	+0.6 -0.2	+1.2 +0.4	-1.0 -0.7	+1.3 +0.1	-1.4 -0.5	-0.8 -0.7	-0.4 +0.5	-0.8 -0.0	+0.3 +0.2	
JESRelativeJEREC1	-0.5 -0.6	-0.6 -0.3	+0.1 -0.3	+3.1 +1.3	+0.3 +0.0	-0.2 -0.1	-0.6 -0.1	+1.0 +0.5	-0.1 -0.0	-0.5 -0.3	-0.0 -0.6	-0.8 -0.2	-0.3 +0.0	-0.1 -0.3	-0.1 +0.2	+0.1 -0.2	
JESRelativeJEREC2	-0.0 -0.0	+0.0 +0.0	-0.0 +0.0	+0.0 +0.0	-0.0 -0.0	-0.0 +0.0	+0.0 +0.0	+0.0 +0.0	+0.0 +0.0	+0.0 +0.0							
JESRelativeJERHF	-0.0 -0.0	+0.0 +0.0	+0.0 +0.0	+0.0 +0.0	+0.0 +0.0	+0.0 +0.0	+0.0 +0.0	-0.0 +0.0	-0.0 +0.0	+0.0 +0.0	-0.0 -0.0	-0.0 +0.0	+0.0 +0.0	+0.0 +0.0	+0.0 +0.0	+0.0 +0.0	
JESRelativePtBB	+0.7 +0.9	-2.1 -1.3	-0.6 +0.3	+3.0 +1.3	+0.4 +0.4	-0.0 -0.0	+0.3 +0.3	+1.0 +0.1	-0.0 +0.5	-0.7 -0.0	-0.2 -0.0	-1.0 -0.9	-0.2 -0.3	+0.1 +0.1	-0.1 -0.3	+0.1 +0.3	+0.1 +0.3
JESRelativePtEC1	+0.6 -0.7	-0.0 -0.5	-0.2 -0.5	+1.5 +2.0	+0.1 -0.4	+0.0 -0.1	-0.3 -0.2	+0.4 +1.2	+0.2 +0.1	-0.3 -0.6	+0.1 +0.4	-1.5 +0.4	-0.3 -0.7	-0.0 +0.0	+0.3 -0.2	+0.3 +0.1	-0.3 +0.1
JESRelativePtEC2	-0.0 -0.0	+0.0 +0.0	+0.0 +0.0	+0.0 +0.0	+0.0 +0.0	+0.0 +0.0	+0.0 +0.0	-0.0 +0.0	+0.0 +0.0	+0.0 -0.0	-0.0 +0.0	-0.0 +0.0	+0.0 +0.0	+0.0 +0.0	+0.0 +0.0	+0.0 +0.0	
JESRelativePtHF	-0.0 -0.0	+0.0 +0.0	+0.0 +0.0	+0.0 +0.0	-0.0 +0.0	+0.0 +0.0	+0.0 +0.0	+0.0 +0.0	-0.0 -0.0	+0.0 +0.0	+0.0 -0.0	-0.0 +0.0	+0.0 +0.0	+0.0 +0.0	+0.0 +0.0	+0.0 +0.0	
JESRelativeStatEC	-0.1 -0.8	-0.2 +0.3	+0.1 +1.3	+1.1 -0.8	+0.6 -0.3	-0.3 -0.0	-0.8 -0.1	+1.2 +0.3	+0.2 +0.3	-0.2 -0.5	-0.2 -0.0	-0.4 +0.1	-0.5 -0.3	+0.1 +0.4	+0.1 +0.1	-0.3 -0.1	-0.3 -0.2
JESRelativeStatFSR	-0.4 -1.0	-0.8 +0.5	-0.1 +0.5	+2.7 +1.5	+0.4 -0.2	-0.1 +0.0	+0.4 -0.3	+0.3 +0.6	+0.2 +1.0	-1.5 -1.1	+0.0 -0.3	-1.0 -0.7	+0.1 -0.7	-0.2 -0.4	+0.1 +0.1	+0.1 +0.2	
JESRelativeStatHF	-0.0 -0.0	+0.0 +0.0	+0.0 +0.0	+0.0 +0.0	+0.0 +0.0	+0.0 +0.0	+0.0 +0.0	-0.0 -0.0	+0.0 +0.0	+0.0 +0.0	-0.0 +0.0	-0.0 +0.0	+0.0 +0.0	+0.0 +0.0	+0.0 +0.0	+0.0 +0.0	
JESSinglePionECAL	+0.4 -0.5	-0.8 -0.4	-0.4 -0.3	+3.4 +2.7	-0.2 +0.0	+0.2 -0.0	-0.4 -0.1	+1.1 +0.3	+0.1 +0.5	-0.7 -0.9	-0.3 +0.4	-0.8 -1.2	-0.8 -0.4	-0.1 +0.3	-0.3 -0.0	-0.2 +0.3	

Table 34: Table 82 continued.

source / bin	1	2	3	4	5	6	7	8	9	10	11	12	13	14	15	16
JESSinglePionHCAL	-0.0	-0.7	-0.1	+2.4	+0.0	+0.2	-0.4	+0.5	+0.5	-0.6	-0.0	-0.5	-0.8	-0.4	-0.0	-0.1
	+0.2	-0.1	-0.5	+2.4	-0.2	-0.1	-0.7	+0.4	+0.3	-0.5	+0.1	-0.8	-0.0	-0.3	+0.3	+0.3
JESTimePtEta	+1.4	-1.2	+0.7	+2.3	-0.5	-0.2	-0.5	+0.7	+0.8	-0.8	+0.4	-1.2	-0.4	-0.7	-0.0	+0.4
	-0.5	-0.4	+0.2	+0.7	+0.6	-0.2	-0.1	+1.2	+0.2	-0.8	-0.1	-1.2	-0.0	+0.3	+0.0	+0.3
E_T^{miss}	+0.7	-0.2	-0.5	-2.2	-0.1	+0.3	+0.5	+1.0	-0.2	-0.1	+0.2	-0.1	+0.0	-0.2	-0.2	+0.0
	-0.4	-1.0	-0.8	+3.4	+0.8	+0.1	+0.3	+0.1	-0.1	-1.0	-0.2	-0.8	-0.2	+0.2	+0.1	-0.1
lepton ID/ISO	-0.2	-0.6	-0.6	-0.2	+0.4	+0.4	+0.6	+0.5	-0.2	-0.3	-0.1	-0.4	-0.2	+0.1	-0.2	+0.1
	+0.2	+0.0	+0.1	+0.4	-0.1	-0.2	-0.1	-0.2	+0.0	-0.0	+0.1	-0.0	+0.3	+0.1	+0.1	+0.0
pileup	+0.3	+0.1	-0.0	-0.5	-0.0	+0.2	-0.2	-0.4	+0.0	+0.1	+0.0	+0.1	-0.1	+0.1	-0.0	+0.2
	-0.2	-0.7	-0.5	+0.7	+0.3	-0.0	+0.6	+0.6	-0.2	-0.5	+0.0	-0.5	+0.1	+0.0	-0.1	-0.1
trigger	+0.2	-0.1	-0.2	-0.4	+0.2	+0.2	+0.3	-0.1	-0.1	-0.1	+0.1	-0.5	-0.0	+0.2	+0.0	-0.2
	-0.1	-0.1	-0.0	+0.5	-0.1	-0.1	-0.1	+0.2	+0.0	-0.1	-0.1	+0.3	+0.0	-0.1	-0.1	+0.2
trigger (η)	-0.3	-0.2	+0.0	+1.1	-0.2	-0.1	-0.0	+0.3	-0.2	-0.1	-0.1	-0.0	-0.2	-0.1	+0.1	+0.1
	+0.3	+0.2	-0.0	-1.1	+0.2	+0.1	+0.0	-0.3	+0.2	+0.1	+0.1	+0.0	+0.2	+0.1	-0.1	-0.1
non-tt background	-0.9	-0.6	-1.0	-4.7	+0.2	+0.5	+0.4	-0.3	+0.8	+0.7	+0.5	+0.5	+1.3	+1.1	+1.1	+1.1
	+1.0	+0.2	+0.5	+4.6	+0.1	-0.4	-0.1	+0.5	-0.8	-0.9	-0.4	-0.8	-1.2	-0.9	-1.1	-1.0
b-tagging	-0.1	-0.1	-0.1	-0.1	-0.0	-0.0	+0.0	+0.1	+0.1	-0.0	-0.0	+0.0	+0.0	+0.1	+0.1	+0.1
	+0.1	+0.1	+0.1	+0.1	+0.0	-0.0	-0.0	-0.1	-0.1	+0.0	+0.0	-0.0	-0.0	-0.1	-0.1	-0.1
b-tagging (light jets)	-0.2	-0.1	-0.2	-1.2	+0.1	+0.2	+0.1	-0.2	+0.2	+0.2	+0.1	+0.1	+0.3	+0.2	+0.2	+0.1
	+0.2	-0.5	-0.3	+1.4	+0.2	-0.0	+0.4	+0.4	-0.4	-0.6	-0.0	-0.5	-0.3	-0.1	-0.3	-0.0
luminosity	+0.0	+0.0	+0.0	+0.0	+0.0	+0.0	+0.0	+0.0	+0.0	+0.0	+0.0	+0.0	+0.0	+0.0	+0.0	+0.0
	+0.0	+0.0	+0.0	+0.0	+0.0	+0.0	+0.0	+0.0	+0.0	+0.0	+0.0	+0.0	+0.0	+0.0	+0.0	+0.0
BR($t\bar{t} \rightarrow \ell\ell$)	+0.0	+0.0	+0.0	+0.0	+0.0	+0.0	+0.0	+0.0	+0.0	+0.0	+0.0	+0.0	+0.0	+0.0	+0.0	+0.0
	+0.0	+0.0	+0.0	+0.0	+0.0	+0.0	+0.0	+0.0	+0.0	+0.0	+0.0	+0.0	+0.0	+0.0	+0.0	+0.0
PDF eigenvector 1	-0.0	-0.0	+0.0	+0.0	-0.0	-0.0	-0.0	+0.0	-0.0	-0.0	-0.0	+0.0	+0.0	+0.0	+0.0	+0.0
	+0.0	+0.0	+0.0	-0.0	+0.0	+0.0	+0.0	-0.1	+0.0	-0.0	-0.0	-0.0	-0.0	-0.0	-0.0	+0.0
PDF eigenvector 2	-0.3	-0.0	+0.1	+0.2	-0.0	-0.0	+0.0	+0.0	+0.0	-0.0	-0.0	-0.1	+0.2	+0.2	+0.1	-0.0
	+0.2	+0.0	-0.1	-0.2	-0.0	-0.1	-0.0	+0.1	+0.0	+0.1	+0.1	+0.1	-0.0	-0.0	-0.0	-0.1
PDF eigenvector 3	+0.1	+0.0	+0.0	-0.1	+0.1	+0.1	+0.0	-0.1	+0.0	+0.0	-0.1	-0.0	-0.1	-0.1	-0.0	+0.1
	-0.1	-0.0	-0.0	+0.1	-0.0	-0.0	-0.0	+0.1	-0.0	-0.0	+0.0	+0.0	+0.0	+0.0	+0.0	-0.1
PDF eigenvector 4	-0.3	-0.0	+0.1	+0.3	-0.0	+0.0	-0.0	+0.1	-0.0	-0.1	-0.0	-0.0	+0.1	+0.1	+0.1	-0.0
	+0.2	-0.1	-0.2	-0.1	+0.1	+0.0	+0.1	+0.1	-0.0	-0.0	+0.1	-0.1	-0.0	+0.0	-0.1	+0.0
PDF eigenvector 5	+0.1	-0.2	-0.2	-0.0	-0.0	-0.1	+0.1	+0.3	-0.1	-0.1	+0.2	-0.0	+0.0	+0.1	-0.0	-0.1
	+0.1	-0.1	-0.1	-0.1	+0.2	+0.2	+0.2	-0.2	+0.1	-0.0	-0.2	-0.2	-0.1	-0.0	-0.1	+0.2
PDF eigenvector 6	-0.2	-0.0	+0.0	+0.1	+0.0	+0.1	+0.0	+0.0	-0.0	-0.1	-0.1	-0.0	+0.1	+0.1	+0.1	+0.1
	+0.1	+0.0	+0.0	-0.1	-0.0	-0.0	-0.0	-0.0	+0.0	+0.0	+0.1	+0.0	-0.0	-0.0	-0.0	-0.0
PDF eigenvector 7	+0.1	-0.0	-0.1	-0.2	-0.2	-0.0	+0.3	-0.0	+0.1	+0.4	+0.1	+0.0	+0.0	-0.0	-0.0	-0.3
	-0.0	+0.0	+0.0	+0.1	+0.1	+0.1	-0.0	-0.2	+0.0	-0.0	-0.2	-0.1	-0.0	-0.0	+0.0	+0.2
PDF eigenvector 8	-0.1	-0.0	-0.0	-0.0	-0.0	+0.0	+0.0	+0.1	-0.0	-0.0	+0.0	-0.0	+0.0	+0.0	-0.0	-0.0
	+0.0	+0.0	+0.0	+0.0	+0.0	-0.0	-0.0	-0.1	+0.0	+0.0	+0.0	+0.0	+0.0	+0.0	+0.0	+0.0
PDF eigenvector 9	+0.1	-0.1	-0.1	+0.1	+0.1	-0.0	+0.1	+0.0	-0.0	-0.1	+0.0	-0.1	-0.1	+0.0	-0.0	+0.0
	-0.1	-0.2	-0.2	-0.0	+0.1	+0.1	+0.2	+0.1	-0.1	-0.1	-0.0	-0.1	+0.1	+0.1	-0.0	+0.1
PDF eigenvector 10	-0.1	-0.1	-0.1	+0.2	+0.2	+0.1	+0.1	-0.1	-0.1	-0.2	-0.2	-0.1	-0.1	+0.0	+0.0	+0.2
	+0.1	-0.0	-0.1	-0.2	-0.1	-0.1	+0.0	+0.1	+0.0	+0.1	+0.2	+0.0	+0.1	+0.0	-0.0	-0.1
PDF eigenvector 11	-0.0	+0.0	+0.0	+0.0	+0.0	+0.0	+0.0	-0.0	+0.0	-0.0	-0.1	-0.0	-0.0	-0.0	+0.0	+0.0
	+0.1	-0.2	-0.2	-0.0	+0.0	-0.0	+0.1	+0.1	-0.0	-0.1	+0.1	-0.1	+0.1	+0.1	-0.0	-0.0
PDF eigenvector 12	+0.1	-0.2	-0.2	-0.1	+0.0	-0.0	+0.2	+0.2	-0.0	-0.1	+0.1	-0.1	+0.1	+0.1	-0.0	-0.0
	-0.0	+0.0	+0.0	+0.1	+0.0	+0.0	-0.0	-0.1	-0.0	-0.0	-0.1	+0.0	-0.1	-0.0	+0.0	+0.1
PDF eigenvector 13	+0.1	+0.0	-0.0	-0.0	+0.0	+0.1	+0.0	-0.0	-0.0	-0.0	-0.1	+0.0	-0.1	-0.1	-0.1	+0.0
	-0.1	-0.0	+0.0	+0.0	-0.0	-0.1	-0.0	+0.0	+0.0	+0.0	+0.1	-0.0	+0.1	+0.1	+0.1	-0.0
PDF eigenvector 14	+0.0	+0.0	-0.0	-0.1	-0.0	-0.0	+0.0	+0.0	+0.0	+0.0	+0.0	-0.0	+0.0	+0.0	-0.0	-0.0
	-0.0	-0.1	-0.1	+0.2	+0.1	+0.1	+0.1	+0.0	-0.1	-0.1	-0.0	-0.1	-0.0	+0.0	+0.0	+0.1

Table 35: Table 82 continued.

source / bin	1	2	3	4	5	6	7	8	9	10	11	12	13	14	15	16
PDF eigenvector 15	+0.1	+0.0	-0.0	-0.1	-0.0	-0.0	+0.0	+0.0	+0.0	+0.1	+0.1	-0.0	+0.0	-0.0	-0.0	-0.0
	-0.0	-0.0	+0.0	+0.0	+0.0	+0.0	-0.0	-0.0	-0.0	-0.0	-0.0	+0.0	-0.0	+0.0	+0.0	+0.0
PDF eigenvector 16	-0.0	-0.0	+0.0	+0.0	+0.0	+0.0	-0.0	-0.0	-0.0	-0.0	-0.0	+0.0	-0.0	-0.0	+0.0	+0.0
	+0.0	-0.1	-0.1	+0.0	+0.1	+0.0	+0.1	+0.1	-0.0	-0.1	+0.1	-0.1	+0.0	+0.1	-0.0	+0.0
PDF eigenvector 17	+0.1	-0.1	-0.1	-0.0	+0.1	+0.0	+0.1	+0.1	-0.0	-0.1	+0.1	-0.1	+0.0	+0.1	-0.0	+0.0
	-0.1	-0.0	+0.0	+0.1	+0.0	+0.1	-0.0	-0.0	-0.0	-0.1	-0.1	+0.0	-0.1	-0.0	+0.0	+0.1
PDF eigenvector 18	-0.1	-0.2	-0.1	+0.3	+0.1	+0.0	+0.1	+0.1	-0.1	-0.2	-0.0	-0.1	+0.0	+0.1	+0.1	+0.1
	+0.1	+0.0	-0.0	-0.2	+0.0	+0.0	+0.0	-0.0	+0.0	+0.1	+0.0	-0.0	-0.0	-0.1	-0.1	-0.0
PDF eigenvector 19	-0.1	+0.0	+0.1	+0.2	+0.0	+0.0	-0.0	-0.1	-0.0	-0.1	-0.1	+0.0	-0.0	-0.0	+0.0	+0.1
	+0.1	-0.0	-0.1	-0.3	-0.1	-0.1	+0.0	+0.1	+0.0	+0.1	+0.2	+0.0	+0.1	+0.0	-0.1	-0.1
PDF eigenvector 20	-0.0	-0.1	-0.1	+0.2	+0.1	+0.1	+0.1	+0.0	-0.1	-0.1	-0.0	-0.0	+0.0	+0.0	-0.0	+0.1
	+0.1	-0.2	-0.2	-0.1	+0.1	+0.0	+0.2	+0.1	-0.0	-0.1	+0.1	-0.1	+0.0	+0.1	-0.1	-0.0
PDF eigenvector 21	-0.1	-0.0	-0.0	+0.1	-0.0	-0.0	-0.0	+0.1	-0.0	-0.0	+0.0	+0.0	+0.1	+0.1	+0.1	-0.0
	+0.1	+0.0	+0.0	-0.1	+0.1	+0.1	+0.0	-0.1	+0.0	+0.0	-0.1	+0.0	-0.1	-0.1	-0.1	+0.1
PDF eigenvector 22	-0.3	-0.1	+0.0	+0.4	-0.1	-0.1	-0.1	+0.2	-0.1	-0.1	+0.1	+0.1	+0.1	+0.2	+0.2	-0.1
	+0.3	+0.0	-0.0	-0.2	+0.1	+0.1	+0.0	-0.2	+0.1	+0.1	-0.1	-0.0	-0.2	-0.2	-0.1	+0.1
PDF eigenvector 23	+0.3	+0.1	-0.1	-0.5	+0.0	+0.0	+0.1	-0.1	+0.1	+0.2	+0.1	-0.1	-0.0	-0.1	-0.2	-0.0
	-0.0	-0.2	-0.1	+0.2	+0.1	+0.0	+0.1	+0.2	-0.1	-0.2	+0.0	-0.0	+0.0	+0.1	+0.0	+0.0
PDF eigenvector 24	+0.1	-0.2	-0.2	+0.0	+0.0	-0.0	+0.1	+0.2	-0.1	-0.1	+0.1	-0.0	-0.0	+0.0	-0.0	-0.0
	-0.0	-0.1	-0.1	-0.2	+0.0	-0.0	+0.2	+0.1	+0.0	+0.0	+0.1	-0.3	+0.2	+0.2	-0.0	-0.1
PDF eigenvector 25	+0.0	+0.0	-0.0	-0.3	-0.0	-0.1	+0.1	-0.0	+0.1	+0.2	+0.1	-0.1	+0.2	+0.1	-0.0	-0.1
	+0.1	-0.0	-0.1	-0.1	-0.1	-0.1	-0.0	+0.2	-0.0	+0.0	+0.2	+0.2	-0.0	-0.0	-0.0	-0.1
PDF eigenvector 26	+0.0	+0.0	-0.0	-0.0	-0.0	+0.0	+0.0	-0.0	+0.0	+0.0	+0.0	-0.0	+0.0	-0.0	-0.0	-0.0
	-0.0	-0.0	-0.0	+0.0	-0.0	-0.0	-0.0	+0.0	-0.0	-0.0	+0.0	+0.0	+0.0	+0.0	+0.0	-0.0
PDF eigenvector 27	-0.1	+0.1	+0.2	+0.2	-0.0	-0.1	-0.1	-0.2	+0.1	+0.0	-0.0	+0.0	-0.1	-0.0	-0.0	+0.0
	-0.1	-0.0	-0.0	+0.0	+0.0	+0.0	+0.0	+0.0	-0.0	-0.0	-0.0	-0.0	+0.0	+0.0	+0.0	+0.0
PDF eigenvector 28	+0.1	+0.0	+0.0	-0.1	-0.0	-0.0	-0.0	-0.1	+0.0	+0.0	+0.0	+0.1	-0.0	-0.0	-0.0	+0.0
	-0.1	-0.0	-0.0	+0.1	+0.0	+0.0	-0.0	+0.1	-0.1	-0.1	-0.0	+0.0	-0.0	+0.0	+0.0	-0.0
α_s	+0.1	+0.1	+0.1	+0.0	+0.0	-0.0	-0.1	-0.2	+0.1	+0.1	+0.0	+0.0	-0.1	-0.1	-0.0	+0.0
	-0.1	-0.1	-0.1	-0.0	-0.0	+0.0	+0.1	+0.2	-0.1	-0.1	-0.0	-0.0	+0.1	+0.1	+0.0	-0.0
m_t	-1.2	-1.9	-2.1	-2.5	-0.2	+0.1	+0.3	+0.2	+1.0	+0.8	+0.8	+0.1	+1.6	+2.4	+1.5	+1.8
	+1.5	+1.5	+1.4	+0.8	+0.5	+0.2	+0.5	+0.5	-1.0	-0.9	-0.8	-0.4	-2.8	-1.9	-2.0	-1.6
μ_{rf}	+0.7	+0.4	+0.7	+0.6	-0.1	-0.4	-0.3	-0.7	+0.4	+0.2	+0.1	+0.0	-1.4	-0.8	-0.1	+0.0
	-0.8	-0.5	-0.8	-0.8	+0.1	+0.4	+0.3	+0.7	-0.4	-0.2	+0.0	-0.2	+1.8	+1.1	+0.1	-0.0
h_{damp}	+0.8	-0.6	-0.3	-0.0	+0.0	+0.1	-0.2	+0.0	+0.3	+0.3	+0.1	-0.3	-0.7	+0.4	-0.5	+0.7
	+0.1	-1.9	-1.3	-0.8	-0.6	+0.3	+1.9	+1.1	+1.1	-0.8	+0.3	-0.3	-1.7	+1.4	-1.6	+1.5
PS ISR	-0.5	+0.4	-0.9	-0.7	-0.2	+0.0	-0.4	+0.5	+1.6	-0.6	+0.4	+1.3	-1.2	+0.6	-0.1	-0.7
	+1.6	+0.0	-1.6	-1.0	-0.8	-0.2	+0.3	+0.8	+1.2	-0.4	+0.5	+0.4	-0.5	+0.6	-0.7	-0.1
PS FSR	-0.6	+0.3	-0.0	-1.0	+0.8	+0.4	+0.7	+0.6	+0.2	-0.8	+0.7	-0.3	-1.8	-0.5	-1.7	-0.3
	+0.2	+0.3	-0.7	-1.2	-0.7	-0.1	+0.3	-0.0	+0.5	-0.6	+0.6	-0.0	+0.8	+1.5	-0.1	+0.7
UE tune	-0.7	-0.0	+0.0	-2.3	+0.6	+0.6	+0.4	+0.8	-0.1	-0.7	-1.0	+1.1	-1.5	+1.0	-0.6	+0.2
	+0.8	-0.6	-1.3	-1.1	+0.3	+0.7	+0.0	+0.1	+1.1	-0.5	+0.8	+0.0	-0.4	-1.0	-0.6	+0.5
CR	-0.6	-0.2	-0.8	-1.1	+0.3	-0.1	+0.5	+0.3	+1.2	-0.7	-0.2	+1.0	+0.3	+1.1	-0.5	-0.0
	+0.3	-0.1	+0.0	-0.5	+0.0	+0.2	+0.0	-0.5	+0.2	-0.5	-0.1	+0.5	-0.9	+0.6	+0.4	+0.4
	+0.6	-0.4	-0.9	-0.6	-0.6	-0.1	+0.6	+0.2	+0.1	-0.1	+0.4	+0.2	-0.2	+1.3	-0.5	+0.3
$f(b \rightarrow B)$	+1.1	+0.4	+0.5	+0.2	+0.3	-0.2	+0.2	-0.4	-0.3	-0.4	+0.2	-0.6	-0.9	-0.4	-0.3	-0.2
	-0.5	-0.4	-0.4	-0.0	-0.1	+0.1	+0.1	+0.2	+0.1	+0.1	-0.1	+0.2	+0.5	+0.3	+0.2	+0.2
	+0.2	+0.1	+0.1	-0.0	+0.0	-0.0	-0.0	-0.1	-0.0	-0.0	+0.0	-0.1	-0.1	-0.1	-0.0	-0.1
	+1.3	+1.0	+0.9	+0.5	-0.2	-0.3	-0.3	-0.5	-0.3	-0.3	-0.1	-0.4	-0.7	-0.7	-0.2	-0.4
BR($B \rightarrow \mu$)	-0.1	-0.1	-0.1	-0.2	+0.1	+0.1	+0.1	+0.0	+0.1	+0.0	+0.1	+0.0	-0.1	-0.0	-0.1	-0.0
	+0.2	+0.1	+0.1	+0.2	-0.1	-0.1	-0.1	-0.1	-0.1	-0.0	-0.1	-0.1	+0.1	+0.0	+0.1	+0.1

Table 36: The measured $[M(t\bar{t}), y(t\bar{t})]$ cross sections, along with their relative statistical and systematic uncertainties.

$M(t\bar{t})$ [GeV]	$y(t\bar{t})$	$\frac{1}{\sigma(t\bar{t})} \frac{d\sigma}{dy(t\bar{t})}$	stat. [%]	syst. [%]	bin
300–400	0.00–0.35	1.554×10^{-1}	2.5	+6.7 -4.5	1
300–400	0.35–0.75	1.485×10^{-1}	2.3	+3.9 -9.6	2
300–400	0.75–1.15	1.320×10^{-1}	2.4	+6.3 -5.6	3
300–400	1.15–2.50	5.856×10^{-2}	2.4	+10.9 -6.9	4
400–500	0.00–0.35	2.506×10^{-1}	1.4	+3.4 -1.8	5
400–500	0.35–0.75	2.296×10^{-1}	1.3	+1.4 -3.9	6
400–500	0.75–1.15	1.889×10^{-1}	1.5	+3.9 -2.3	7
400–500	1.15–2.50	8.038×10^{-2}	1.2	+3.7 -3.9	8
500–650	0.00–0.35	1.833×10^{-1}	1.7	+3.0 -2.2	9
500–650	0.35–0.75	1.714×10^{-1}	1.6	+2.0 -5.2	10
500–650	0.75–1.15	1.340×10^{-1}	2.0	+6.7 -2.1	11
500–650	1.15–2.50	4.390×10^{-2}	2.3	+2.7 -7.7	12
650–1500	0.00–0.35	1.331×10^{-1}	1.6	+3.0 -4.5	13
650–1500	0.35–0.75	1.079×10^{-1}	2.0	+5.2 -4.2	14
650–1500	0.75–1.15	8.007×10^{-2}	2.6	+5.1 -7.9	15
650–1500	1.15–2.50	1.731×10^{-2}	4.7	+11.3 -6.3	16

Table 37: The correlation matrix of statistical uncertainties for the measured $[M(t\bar{t}), y(t\bar{t})]$ cross sections. The values are expressed as percentages. For bin indices see Table 85.

Table 38: Sources and values of the relative systematic uncertainties in percent of the measured $[M(\text{t}\bar{\text{t}}), y(\text{t}\bar{\text{t}})]$ cross sections. For bin indices see Table 85.

source / bin	1	2	3	4	5	6	7	8	9	10	11	12	13	14	15	16	
JER	+0.5 -0.3	-1.4 -1.1	+1.0 +0.1	+1.4 +1.1	+0.2 +0.2	-0.1 -0.2	+0.3 +0.1	-0.5 +0.1	+0.0 +0.0	-0.4 -0.8	+0.6 +0.1	-0.7 -0.5	-0.1 -0.1	-0.0 +0.6	-1.3 +0.2	+0.2 +1.0	
JESAbsoluteMPFBias	-0.2 -0.4	-0.8 -1.1	+0.0 -0.1	+0.5 +1.0	+0.6 +0.4	-0.1 +0.0	+0.4 +0.9	-0.2 -0.3	+0.1 +0.2	-1.0 -0.6	+0.2 +0.5	-0.8 -1.0	-0.1 -0.6	+0.9 +0.9	-0.1 -1.0	+1.2 +0.7	
JESAbsoluteScale	+0.6 -0.7	-1.0 -1.7	-0.3 +0.0	+1.4 +1.5	+0.2 +0.5	-0.0 +0.1	+0.3 +0.7	-0.2 -0.3	+0.0 -0.0	-0.4 -0.3	-0.6 +0.5	-1.0 -1.0	-0.4 -0.3	+0.1 +0.0	+0.3 -0.7	+1.6 +1.1	
JESAbsoluteStat	+0.6 -0.4	-1.0 -0.4	+0.4 +0.5	+1.4 +0.6	-0.1 +0.1	+0.2 -0.6	+0.2 +0.2	-0.5 +0.4	-0.1 -0.2	-0.0 -0.6	+0.3 +0.7	-1.4 -0.7	-0.2 +0.1	+0.5 +0.4	-0.5 -0.1	+0.2 -0.2	
JESFlavourQCD	+1.3 -0.4	-0.6 -1.9	+0.5 +0.1	+1.9 +1.8	-0.4 +0.8	-1.2 +0.4	-0.8 +0.6	-0.2 -0.0	+0.2 +0.3	-0.8 -0.2	+0.3 +0.0	-0.5 -1.4	+0.2 -0.9	+0.9 -0.0	+0.3 -1.5	+0.5 +0.6	
JESFragmentation	+0.7 +0.3	-0.5 -1.5	+0.4 +0.5	+0.2 +1.8	-0.0 +0.4	-0.6 +0.1	+0.3 +0.5	-0.3 -0.7	+0.5 +0.3	-0.6 -0.8	+0.3 +0.2	-0.5 -1.3	-0.3 -0.3	+1.0 +0.1	-1.0 -0.5	+1.5 +1.1	
JESPileUpDataMC	+1.4 -0.2	-1.4 +0.0	+0.0 +0.3	+0.5 +0.9	-0.0 +0.3	-0.1 -0.0	+0.0 +0.3	-0.1 -0.3	-0.3 +0.1	-0.3 -0.7	+0.1 +0.4	-0.8 -0.9	+0.1 -0.4	+0.8 -0.0	-0.3 -0.9	+1.8 +1.1	
JESPileUpPtBB	-0.4 -0.1	-0.7 -1.4	-0.8 +0.8	+0.7 +0.9	-0.2 +0.2	+0.1 +0.3	+0.2 +0.5	+0.7 +0.0	+0.0 -0.2	-0.1 -0.4	+0.3 +0.1	-0.6 -1.0	+0.3 -0.4	-0.2 +0.2	-0.3 -1.0	+0.5 +1.0	
JESPileUpPtEC1	+0.5 -1.1	+0.6 -0.3	+0.2 -0.2	-0.6 +2.0	+0.2 -0.5	-0.1 -0.6	+0.1 +0.4	-0.1 +0.4	+0.1 +0.1	-0.7 -0.4	-0.3 +0.2	-0.2 -0.1	-0.3 -0.1	+0.4 -0.0	+0.1 -0.3	+1.3 -0.7	
JESPileUpPtEC2	+0.0 +0.0	+0.1 +0.1	+0.2 +0.2	+0.1 +0.1	-0.0 -0.0	-0.1 -0.1	-0.1 -0.1	-0.1 -0.1	-0.0 -0.0	+0.1 +0.1	+0.1 +0.1	-0.1 -0.1	+0.0 +0.0	-0.1 +0.0	+0.0 +0.0	+0.0 +0.0	
JESPileUpPtHF	+0.0 +0.0	+0.1 +0.1	+0.2 +0.2	+0.1 +0.1	-0.0 -0.0	-0.1 -0.1	-0.1 -0.1	-0.1 -0.1	-0.0 -0.0	+0.1 +0.1	+0.1 +0.1	-0.1 -0.1	+0.0 +0.0	-0.1 -0.1	+0.0 +0.0	+0.0 +0.0	
JESPileUpPtRef	-0.7 +0.2	+0.7 -1.9	-0.3 +0.3	-0.2 +1.6	-0.2 +0.4	+0.1 -0.5	+0.3 +0.7	-0.3 +0.1	-0.2 +0.4	+0.0 -0.6	+0.2 +0.4	-0.2 -0.6	+0.4 -0.6	+0.2 +0.3	+0.0 -1.3	+0.0 -0.1	
JESRelativeBal	+0.4 -0.3	-0.5 -1.5	+1.3 -0.3	+0.7 +1.1	+0.1 +0.1	-0.4 -0.1	+0.2 +0.5	-0.7 +0.8	-0.1 -0.5	-0.1 -0.7	-0.1 +0.3	-0.6 -0.5	-0.5 -0.5	-0.1 -0.0	+1.2 +0.4	-0.8 -1.1	+1.5 +0.7
JESRelativeFSR	+0.3 +0.4	-1.3 +0.3	-0.6 +0.7	+1.4 +0.6	+0.1 -0.0	-0.1 -0.4	+0.5 +0.2	+0.0 -0.4	+0.4 +0.2	-0.3 -0.8	+0.1 -0.0	-0.7 -0.5	-0.4 -0.3	+0.3 +0.8	-0.9 -0.5	+0.5 +0.6	
JESRelativeJEREC1	-0.1 -0.7	-1.0 -0.4	-0.7 +0.7	+1.8 +1.1	-0.1 +0.1	+0.2 -0.4	+0.3 +0.2	-0.2 -0.2	+0.3 +0.2	-0.6 -0.3	+0.1 -0.2	-0.9 -0.2	-0.2 -0.2	+0.3 +0.3	-0.0 -0.1	+0.5 +0.7	
JESRelativeJEREC2	+0.0 +0.0	+0.1 +0.1	+0.2 +0.2	+0.1 +0.1	-0.0 -0.0	-0.1 -0.1	-0.1 -0.1	-0.1 -0.1	-0.0 -0.0	+0.1 +0.1	+0.1 +0.1	-0.1 -0.1	+0.0 +0.0	-0.1 -0.1	+0.0 +0.0	+0.0 +0.0	
JESRelativeJERHF	+0.0 +0.0	+0.1 +0.1	+0.2 +0.2	+0.1 +0.1	-0.0 -0.0	-0.1 -0.1	-0.1 -0.1	-0.1 -0.1	-0.0 -0.0	+0.1 +0.1	+0.1 +0.1	-0.1 -0.1	+0.0 +0.0	-0.1 -0.1	+0.0 +0.0	+0.0 +0.0	
JESRelativePtBB	+0.4 -0.0	-0.7 -1.5	+0.8 +0.4	+0.4 +0.8	+0.1 +0.6	-0.4 +0.1	-0.1 +0.1	+0.3 -0.3	-0.7 +0.1	-0.5 -0.8	+0.4 +0.4	+0.4 -0.3	+0.1 -0.4	+0.1 -0.6	-0.5 +1.1	-0.8 +1.1	
JESRelativePtEC1	-0.3 -0.1	+0.5 -1.0	+0.3 -0.5	+1.2 +1.2	+0.5 -0.4	-0.1 -0.7	-0.4 +0.4	-0.4 +0.7	+0.2 +0.0	-0.4 -0.7	-0.0 +0.2	-1.0 +0.7	-0.2 -0.2	+0.2 +0.2	-0.4 -0.6	+0.4 +0.2	
JESRelativePtEC2	+0.0 +0.0	+0.1 +0.1	+0.2 +0.2	+0.1 +0.1	-0.0 -0.0	-0.1 -0.1	-0.1 -0.1	-0.1 -0.1	-0.0 -0.0	+0.1 +0.1	+0.1 +0.1	-0.1 -0.1	+0.0 +0.0	-0.1 -0.1	+0.0 +0.0	+0.0 +0.0	
JESRelativePtHF	+0.0 +0.0	-0.0 +0.1	-0.0 +0.1	-0.0 +0.1	-0.0 -0.0	-0.0 -0.1	-0.0 -0.1	-0.0 -0.1	-0.0 -0.0	-0.0 +0.1	-0.0 +0.1	-0.0 -0.1	-0.0 +0.0	+0.0 -0.1	+0.0 +0.0	+0.0 +0.0	
JESRelativeStatEC	+0.4 +0.2	-0.8 -0.5	+0.1 +0.1	+1.3 +1.4	-0.2 -0.2	-0.0 -0.5	+0.5 +0.3	-0.3 -0.1	+0.0 +0.1	-0.3 -0.8	+0.5 +0.3	-0.9 -0.9	-0.2 -0.1	+0.1 +0.5	-1.3 -0.2	+0.7 +0.8	
JESRelativeStatFSR	-0.4 -0.7	-1.7 -1.5	+0.8 +0.7	+1.2 +1.3	+0.3 +0.4	+0.1 -0.1	+0.5 +0.5	+0.1 +0.1	+0.1 +0.1	-0.5 -0.4	+0.1 -0.4	-1.1 -0.9	+0.1 -0.2	+0.5 +0.3	-0.9 -0.9	+1.6 +0.3	
JESRelativeStatHF	+0.0 +0.0	+0.1 +0.1	+0.2 +0.2	+0.1 +0.1	-0.0 -0.0	-0.1 -0.1	-0.1 -0.1	-0.1 -0.1	-0.0 -0.0	+0.1 +0.1	+0.1 +0.1	-0.1 -0.1	+0.0 +0.0	-0.1 -0.1	+0.0 +0.0	+0.0 +0.0	
JESSinglePionECAL	+0.4 -0.5	-2.0 -0.3	+0.3 +0.2	+1.7 +1.0	+0.5 +0.1	-0.1 -0.2	+0.7 -0.3	+0.1 -0.1	-0.5 +0.3	-0.8 -0.5	-0.4 +0.6	-0.7 -0.3	-0.2 -0.1	+0.2 +0.3	-0.9 -0.3	+0.9 +0.3	

Table 39: Table 87 continued.

source / bin	1	2	3	4	5	6	7	8	9	10	11	12	13	14	15	16
JESSinglePionHCAL	-0.3	-1.3	+0.1	+1.4	+0.5	-0.1	+0.6	-0.1	-0.2	-0.3	+0.5	-1.1	-0.2	+0.2	-1.2	+0.8
	-0.4	-0.9	-0.5	+1.5	+0.3	-0.3	+0.1	+0.1	+0.1	-0.4	+0.3	-1.3	+0.1	+0.3	-0.3	+2.2
JESTimePtEta	+1.4	-1.0	-0.1	+1.4	-0.2	-0.6	+0.1	-0.0	-0.1	-0.5	+0.7	-1.2	-0.2	+0.5	-0.8	+1.2
	-0.3	+0.2	+1.4	+0.3	-0.1	-0.5	+0.4	-0.2	+0.2	-0.9	-0.0	-0.6	-0.0	+0.5	+0.1	+1.0
E_T^{miss}	+1.7	-0.3	-0.4	+0.0	-0.3	+0.4	-0.1	-0.0	-0.1	-0.3	-0.1	-0.2	+0.1	-0.1	-0.1	-0.4
	-1.0	-0.0	+0.0	+1.1	+0.1	-0.1	+0.4	-0.0	-0.3	-0.4	-0.2	-0.3	-0.0	+0.2	+0.0	+0.5
lepton ID/ISO	-0.2	+0.0	-0.3	-0.3	+0.1	+0.2	+0.0	+0.4	-0.1	+0.1	-0.0	-0.2	-0.0	-0.1	-0.1	-0.5
	+0.2	-0.0	+0.3	+0.2	-0.1	-0.2	-0.1	-0.4	+0.1	-0.1	+0.0	+0.2	+0.0	+0.1	+0.1	+0.5
pileup	+0.2	+0.0	-0.3	-0.5	+0.1	+0.2	+0.1	-0.2	+0.1	+0.2	+0.1	-0.0	+0.1	+0.1	-0.1	-0.1
	-0.1	-0.1	+0.2	+0.5	-0.1	-0.2	-0.1	+0.2	-0.0	-0.2	-0.1	+0.0	-0.1	-0.1	+0.1	+0.1
trigger	+0.1	+0.2	+0.1	-0.3	+0.2	+0.1	-0.0	-0.1	+0.1	+0.1	-0.1	-0.2	+0.1	-0.0	-0.1	-0.1
	-0.1	-0.1	+0.1	+0.4	-0.2	-0.3	-0.1	+0.0	-0.1	+0.0	+0.2	+0.2	-0.1	-0.1	+0.1	+0.2
trigger (η)	-0.3	-0.2	-0.1	+0.6	-0.2	-0.1	-0.2	+0.4	-0.2	-0.2	-0.2	+0.3	+0.1	-0.1	-0.2	+0.1
	+0.3	+0.2	+0.1	-0.6	+0.2	+0.1	+0.1	-0.4	+0.2	+0.2	+0.2	-0.3	-0.1	+0.1	+0.2	-0.1
non-tt background	-0.7	-0.1	-0.5	-3.1	+0.2	-0.2	-0.0	-0.2	+0.5	+1.1	+1.2	+0.3	+1.1	+0.8	+1.3	+0.8
	+0.9	+0.4	+1.2	+3.1	-0.3	-0.4	-0.3	-0.0	-0.5	-0.7	-0.7	-0.5	-1.0	-1.0	-1.2	-0.7
b-tagging	-0.1	-0.1	-0.2	-0.1	+0.0	+0.0	-0.0	+0.1	-0.0	-0.0	+0.0	+0.0	+0.1	+0.1	+0.1	+0.1
	+0.1	+0.1	+0.3	+0.2	-0.0	-0.2	-0.1	-0.2	+0.0	+0.1	+0.1	-0.1	-0.0	-0.2	-0.1	-0.1
b-tagging (light jets)	-0.1	+0.0	-0.2	-0.8	+0.1	+0.1	+0.1	-0.1	+0.2	+0.2	+0.2	+0.1	+0.2	+0.2	+0.2	+0.1
	+0.2	-0.0	+0.2	+0.9	-0.1	-0.1	-0.1	+0.1	-0.2	-0.2	-0.2	-0.1	-0.2	-0.2	-0.2	-0.1
luminosity	+0.0	+0.0	+0.0	+0.0	+0.0	+0.0	+0.0	+0.0	+0.0	+0.0	+0.0	+0.0	+0.0	+0.0	+0.0	+0.0
	+0.0	+0.0	+0.0	+0.0	+0.0	+0.0	+0.0	+0.0	+0.0	+0.0	+0.0	+0.0	+0.0	+0.0	+0.0	+0.0
BR($t\bar{t} \rightarrow \ell\ell$)	+0.0	+0.0	+0.0	+0.0	+0.0	+0.0	+0.0	+0.0	+0.0	+0.0	+0.0	+0.0	+0.0	+0.0	+0.0	+0.0
	+0.0	+0.0	+0.0	+0.0	+0.0	+0.0	+0.0	+0.0	+0.0	+0.0	+0.0	+0.0	+0.0	+0.0	+0.0	+0.0
PDF eigenvector 1	-0.0	-0.0	+0.0	+0.0	+0.0	+0.0	+0.0	-0.0	-0.0	-0.0	-0.0	+0.0	+0.0	+0.0	-0.0	+0.0
	+0.0	+0.0	-0.0	-0.0	+0.0	+0.0	+0.0	-0.0	+0.0	+0.0	-0.0	-0.1	+0.0	+0.0	+0.0	-0.0
PDF eigenvector 2	-0.1	-0.1	+0.1	+0.1	+0.0	-0.0	+0.0	+0.0	-0.1	-0.0	+0.1	+0.0	+0.1	+0.0	-0.1	-0.3
	+0.0	+0.0	+0.1	+0.0	-0.1	-0.1	-0.0	+0.1	+0.0	-0.0	+0.0	+0.1	-0.1	-0.1	+0.1	+0.1
PDF eigenvector 3	+0.1	+0.1	+0.1	-0.0	+0.1	-0.0	-0.0	-0.2	+0.1	+0.1	+0.0	-0.2	+0.1	+0.0	+0.1	-0.1
	-0.0	+0.0	+0.1	+0.0	-0.0	-0.1	-0.1	+0.0	+0.0	+0.0	+0.1	+0.1	-0.0	-0.1	-0.0	+0.2
PDF eigenvector 4	-0.1	-0.1	-0.0	+0.1	+0.0	+0.0	+0.0	-0.0	-0.1	-0.0	+0.0	+0.1	+0.1	+0.0	+0.0	-0.1
	+0.1	+0.1	+0.1	+0.0	-0.0	-0.1	-0.1	-0.0	+0.1	+0.1	+0.1	-0.1	-0.0	-0.1	-0.0	+0.0
PDF eigenvector 5	-0.0	-0.0	+0.1	+0.1	-0.1	-0.2	-0.1	+0.2	-0.0	+0.0	+0.1	+0.3	-0.2	-0.2	-0.1	+0.4
	+0.1	+0.1	+0.0	-0.1	+0.1	+0.1	+0.1	-0.2	+0.1	+0.1	-0.0	-0.5	+0.1	+0.1	+0.1	-0.3
PDF eigenvector 6	-0.1	+0.0	-0.0	-0.0	+0.0	+0.0	-0.0	-0.1	-0.0	+0.0	+0.0	-0.1	+0.1	+0.0	+0.1	+0.1
	+0.1	+0.0	+0.1	+0.0	-0.0	-0.1	-0.0	-0.0	+0.0	+0.0	+0.0	-0.1	-0.1	-0.1	-0.0	-0.0
PDF eigenvector 7	-0.0	-0.0	+0.1	+0.1	-0.2	-0.2	-0.1	+0.3	-0.0	-0.0	+0.0	+0.5	-0.3	-0.3	-0.2	+0.5
	+0.0	+0.0	-0.0	-0.1	+0.1	+0.1	+0.1	-0.2	+0.0	+0.0	-0.0	-0.3	+0.2	+0.2	+0.2	-0.2
PDF eigenvector 8	-0.1	+0.0	+0.0	-0.0	-0.0	-0.0	-0.1	+0.1	-0.0	+0.0	+0.0	+0.0	-0.0	-0.1	+0.0	+0.2
	+0.1	+0.0	+0.1	+0.1	-0.0	-0.1	-0.1	-0.1	+0.0	+0.1	+0.1	-0.0	+0.0	-0.0	+0.0	-0.0
PDF eigenvector 9	+0.1	+0.1	+0.2	+0.1	-0.0	-0.1	-0.1	-0.1	+0.0	+0.1	+0.1	-0.1	+0.0	-0.1	-0.1	-0.2
	-0.0	+0.0	-0.0	-0.1	+0.0	-0.0	-0.1	+0.0	-0.0	+0.0	+0.0	+0.0	-0.0	+0.1	+0.3	+0.3
PDF eigenvector 10	+0.0	+0.0	-0.1	-0.0	+0.1	+0.1	+0.1	-0.2	-0.0	+0.0	-0.0	-0.2	+0.1	+0.1	+0.1	-0.2
	-0.0	-0.0	+0.1	+0.0	-0.1	-0.1	-0.1	+0.2	+0.0	-0.0	+0.0	+0.2	-0.1	-0.2	-0.1	+0.2
PDF eigenvector 11	+0.0	+0.1	+0.1	+0.0	+0.0	-0.0	-0.0	-0.1	-0.0	+0.1	+0.1	-0.1	+0.0	-0.0	-0.0	-0.1
	-0.0	-0.0	+0.0	+0.0	-0.1	-0.1	-0.0	+0.1	-0.0	-0.0	+0.0	+0.1	-0.1	-0.1	-0.1	+0.1
PDF eigenvector 12	-0.0	-0.0	+0.0	+0.0	-0.1	-0.1	-0.0	+0.1	-0.0	-0.0	+0.0	+0.1	-0.1	-0.1	-0.1	+0.1
	+0.0	+0.1	+0.1	+0.0	+0.1	-0.0	-0.0	-0.2	+0.0	+0.1	+0.1	-0.1	+0.1	+0.0	+0.1	-0.1
PDF eigenvector 13	+0.0	+0.0	-0.1	-0.1	+0.0	+0.1	+0.0	+0.0	+0.0	+0.0	-0.1	-0.1	-0.0	+0.0	+0.1	+0.1
	-0.0	-0.0	+0.1	+0.1	-0.0	-0.1	-0.0	+0.0	-0.0	-0.0	+0.1	+0.1	+0.0	-0.0	-0.1	-0.1
PDF eigenvector 14	+0.0	+0.0	+0.1	+0.0	-0.0	-0.1	-0.1	+0.0	+0.0	+0.1	+0.1	-0.0	-0.0	-0.1	-0.0	+0.1
	+0.0	-0.0	+0.0	+0.0	+0.0	+0.0	+0.0	-0.1	-0.0	-0.0	+0.0	-0.0	+0.0	+0.0	+0.0	-0.1

Table 40: Table 87 continued.

source / bin	1	2	3	4	5	6	7	8	9	10	11	12	13	14	15	16
PDF eigenvector 15	+0.0	+0.0	+0.0	-0.0	-0.0	-0.0	+0.1	+0.0	+0.0	-0.0	+0.0	-0.1	-0.0	-0.0	+0.0	+0.0
	-0.0	-0.0	-0.0	+0.0	+0.0	+0.0	+0.0	-0.0	-0.0	-0.0	+0.0	-0.0	+0.0	+0.0	+0.0	-0.0
PDF eigenvector 16	+0.0	+0.0	+0.1	+0.0	+0.0	-0.1	-0.1	-0.0	-0.0	+0.0	+0.1	-0.0	+0.0	-0.0	+0.0	+0.0
	+0.0	-0.0	+0.0	+0.0	-0.0	-0.0	-0.0	+0.0	+0.0	+0.0	+0.0	+0.0	-0.0	-0.0	-0.0	-0.0
PDF eigenvector 17	+0.0	-0.0	+0.0	+0.0	-0.0	-0.0	-0.0	+0.0	+0.0	+0.0	+0.0	+0.0	-0.0	-0.0	-0.0	-0.0
	-0.0	+0.0	-0.1	-0.1	+0.1	+0.1	+0.0	-0.1	-0.0	-0.0	-0.1	-0.1	+0.0	+0.1	+0.1	+0.0
PDF eigenvector 18	-0.0	-0.0	+0.0	+0.1	+0.0	-0.0	+0.0	-0.1	-0.1	-0.0	+0.1	+0.1	+0.1	+0.1	+0.0	-0.0
	+0.0	+0.0	-0.0	-0.1	-0.0	+0.0	-0.0	+0.1	+0.1	+0.0	-0.1	-0.1	-0.1	-0.0	+0.0	+0.0
PDF eigenvector 19	+0.0	+0.1	+0.1	+0.0	+0.1	-0.0	-0.0	-0.2	-0.0	+0.0	+0.1	-0.1	+0.1	+0.1	+0.1	-0.2
	-0.0	-0.0	+0.0	-0.0	-0.1	-0.1	-0.1	+0.2	+0.0	-0.0	-0.0	+0.2	-0.2	-0.2	-0.1	+0.3
PDF eigenvector 20	+0.0	-0.0	+0.0	+0.0	+0.0	+0.0	+0.0	-0.1	+0.0	+0.0	-0.0	-0.0	+0.0	+0.0	+0.0	+0.0
	-0.0	+0.0	+0.0	-0.0	-0.0	-0.0	-0.0	+0.1	+0.0	-0.0	-0.0	+0.0	-0.0	-0.0	-0.0	+0.1
PDF eigenvector 21	-0.1	-0.1	-0.0	+0.0	-0.0	-0.0	-0.0	+0.1	-0.1	-0.0	+0.0	+0.2	+0.0	-0.0	-0.0	+0.1
	+0.1	+0.1	+0.1	-0.0	+0.0	-0.0	-0.0	-0.1	+0.1	+0.1	+0.0	-0.2	+0.0	-0.0	+0.0	-0.1
PDF eigenvector 22	-0.1	-0.1	-0.0	+0.1	-0.1	-0.1	-0.0	+0.1	-0.2	-0.1	+0.1	+0.4	+0.0	-0.0	-0.0	+0.1
	+0.1	+0.2	+0.1	-0.1	+0.1	+0.0	-0.0	-0.1	+0.1	+0.1	-0.0	-0.3	+0.0	+0.0	+0.1	-0.0
PDF eigenvector 23	+0.1	+0.1	+0.1	-0.1	-0.0	-0.0	-0.0	+0.1	+0.2	+0.1	-0.0	-0.3	-0.1	-0.1	-0.1	-0.1
	-0.0	-0.0	-0.0	+0.0	-0.0	-0.0	-0.0	+0.0	-0.0	-0.0	-0.0	+0.2	-0.0	-0.0	+0.0	+0.2
PDF eigenvector 24	+0.0	-0.0	+0.0	+0.0	-0.1	-0.1	-0.0	+0.1	+0.0	-0.0	+0.0	+0.2	-0.1	-0.1	-0.0	+0.2
	-0.0	+0.0	+0.2	+0.1	-0.1	-0.1	-0.1	+0.1	+0.0	+0.1	+0.2	-0.1	+0.0	-0.1	-0.1	-0.2
PDF eigenvector 25	-0.0	+0.0	+0.1	+0.1	-0.1	-0.1	-0.0	+0.1	+0.1	+0.0	+0.1	-0.1	-0.0	-0.1	-0.1	-0.2
	+0.0	-0.0	+0.0	+0.0	-0.1	-0.1	-0.1	+0.2	-0.0	-0.0	+0.0	+0.3	-0.2	-0.2	-0.1	+0.4
PDF eigenvector 26	+0.0	+0.0	+0.0	-0.0	-0.0	+0.0	-0.0	+0.0	+0.0	+0.0	-0.0	-0.0	-0.0	-0.0	+0.0	-0.0
	-0.0	-0.0	-0.0	+0.0	-0.0	-0.0	-0.0	+0.0	-0.0	-0.0	+0.0	+0.1	-0.0	-0.0	+0.0	+0.1
PDF eigenvector 27	+0.1	+0.1	+0.3	+0.2	+0.0	-0.1	-0.0	-0.3	+0.1	+0.1	+0.2	-0.1	+0.1	+0.0	-0.0	-0.4
	-0.0	+0.0	+0.0	-0.0	+0.0	-0.0	-0.1	+0.0	-0.0	+0.0	+0.0	-0.0	+0.0	+0.0	+0.0	+0.1
PDF eigenvector 28	+0.1	+0.1	+0.1	+0.0	-0.0	-0.1	-0.1	-0.1	+0.1	+0.1	+0.1	-0.0	-0.0	-0.1	-0.0	+0.0
	-0.1	-0.0	-0.1	-0.0	+0.0	+0.0	-0.0	+0.1	-0.1	-0.0	-0.0	+0.0	+0.0	+0.0	+0.0	+0.1
α_s	+0.1	+0.0	+0.2	+0.1	-0.0	-0.1	+0.0	-0.2	+0.1	+0.1	+0.1	-0.0	+0.0	-0.0	-0.0	-0.2
	-0.1	-0.0	-0.2	-0.1	-0.0	+0.1	-0.0	+0.2	-0.1	-0.1	-0.1	+0.1	-0.0	-0.0	+0.0	+0.3
m_t	-1.4	-1.6	-1.5	-2.4	-0.2	-0.3	-0.3	+0.4	+0.7	+0.6	+1.0	+0.9	+1.5	+1.6	+2.1	+2.7
	+1.4	+1.6	+1.4	+1.7	+0.6	+0.5	+0.4	-0.3	-0.4	-0.7	-0.5	-1.4	-1.7	-2.1	-1.9	-2.5
μ_{rf}	+1.0	+0.4	+1.5	+1.0	-0.1	-0.5	+0.2	-1.4	+0.6	+0.3	+0.7	-0.5	-0.0	-0.3	-1.1	-2.8
	-1.1	-0.3	-1.3	-1.1	+0.0	+0.3	-0.5	+1.3	-0.6	-0.2	-0.6	+0.6	-0.0	+0.2	+1.5	+3.9
h_{damp}	+1.0	+0.3	+0.1	-0.5	-0.5	+0.1	+0.0	-0.5	+0.1	+0.2	+1.0	-0.6	+0.0	+0.2	-1.2	+1.9
	+0.9	-1.3	-2.0	-0.4	-0.4	+0.0	+0.8	+1.1	+0.1	-0.0	+1.6	-1.0	+0.2	-0.5	+0.3	-0.5
PS ISR	+0.5	-0.6	+0.0	-0.4	+0.0	-0.6	-0.0	+0.1	+0.3	+0.0	+1.9	-0.4	-0.1	-0.4	-0.0	+0.1
	+1.0	+0.7	-1.1	-0.7	-0.2	-0.9	+0.1	+0.5	+0.7	-0.6	+1.6	-0.5	-0.6	+0.5	-0.5	+0.7
PS FSR	+0.5	-0.9	+0.9	-0.1	+0.8	+0.0	+0.8	-0.0	+0.1	-0.3	+1.9	-1.6	-1.2	-0.8	-1.5	+0.0
	+0.2	+0.6	+0.2	-1.0	-0.2	-0.6	-0.7	+0.2	+0.2	+0.0	+1.4	-0.8	+0.3	+0.6	+1.7	-0.0
UE tune	+0.5	-0.2	+0.0	-1.0	+1.0	-0.1	+0.3	+0.3	-0.4	-0.6	+1.5	-1.1	-0.1	+0.1	-0.7	+0.1
	+1.1	-0.6	-1.5	-0.3	+0.6	-0.0	-0.1	+0.3	+0.3	-0.0	+1.2	-0.6	-0.7	-0.8	+0.9	-0.2
CR	+0.1	-0.7	-0.3	-1.1	+0.5	-0.4	-0.1	+0.4	+1.0	-1.0	+0.8	+0.4	-0.5	+1.1	+0.1	+0.3
	-0.2	+0.2	-0.0	-0.1	+0.6	-0.5	-0.0	-0.2	-0.1	-0.5	+1.1	-0.8	+0.3	+0.3	-0.5	+1.8
	+0.2	+0.7	-0.6	-0.5	-0.2	-0.7	-0.6	+0.5	+0.2	+0.1	+1.4	-0.6	-0.1	+0.8	-0.2	+0.4
$f(b \rightarrow B)$	+1.2	+0.7	+1.3	+0.4	+0.1	-0.2	+0.0	-0.8	+0.2	+0.0	-0.0	-0.8	-0.0	-0.7	-0.8	-1.1
	-0.6	-0.4	-0.6	-0.3	-0.0	+0.0	-0.1	+0.3	-0.0	-0.0	+0.1	+0.4	+0.0	+0.4	+0.5	+0.6
	+0.2	+0.1	+0.2	+0.1	+0.0	-0.0	+0.0	-0.2	+0.0	+0.0	+0.0	-0.1	+0.0	-0.1	-0.1	-0.2
	+1.4	+0.8	+1.3	+0.7	-0.1	-0.2	-0.1	-0.6	-0.0	-0.2	-0.3	-0.8	-0.2	-0.5	-0.8	-1.0
BR($B \rightarrow \mu$)	-0.0	-0.0	+0.0	-0.0	+0.1	-0.1	-0.0	-0.0	+0.1	+0.1	+0.2	-0.0	-0.0	-0.1	-0.1	-0.1
	+0.1	+0.2	+0.2	+0.1	-0.1	-0.1	-0.0	-0.1	-0.1	-0.1	-0.1	+0.1	+0.1	+0.1	+0.2	+0.2

Table 41: The measured $[M(t\bar{t}), \Delta\eta(t, \bar{t})]$ cross sections, along with their relative statistical and systematic uncertainties.

$M(t\bar{t})$ [GeV]	$\Delta\eta(t, \bar{t})$	$\frac{1}{\sigma(t\bar{t})} \frac{d\sigma}{d\Delta\eta(t, \bar{t})}$	stat. [%]	syst. [%]	bin
300–400	0.0–0.4	1.874×10^{-1}	4.4	+5.0 -14.4	1
300–400	0.4–1.2	1.260×10^{-1}	1.5	+3.4 -6.0	2
300–400	1.2–6.0	1.444×10^{-2}	4.4	+17.7 -7.2	3
400–500	0.0–0.4	1.633×10^{-1}	2.7	+7.3 -6.1	4
400–500	0.4–1.2	1.587×10^{-1}	1.4	+5.2 -3.1	5
400–500	1.2–6.0	3.510×10^{-2}	1.1	+3.1 -3.4	6
500–650	0.0–0.4	5.389×10^{-2}	4.2	+5.8 -7.4	7
500–650	0.4–1.2	6.632×10^{-2}	2.6	+6.4 -4.3	8
500–650	1.2–6.0	3.601×10^{-2}	1.0	+1.4 -2.9	9
650–1500	0.0–0.4	1.803×10^{-2}	4.8	+8.5 -5.4	10
650–1500	0.4–1.2	1.991×10^{-2}	3.3	+6.0 -7.0	11
650–1500	1.2–6.0	2.575×10^{-2}	1.0	+3.9 -3.5	12

Table 42: The correlation matrix of statistical uncertainties for the measured $[M(t\bar{t}), \Delta\eta(t, \bar{t})]$ cross sections. The values are expressed as percentages. For bin indices see Table 90.

Table 43: Sources and values of the relative systematic uncertainties in percent of the measured $[M(t\bar{t}), \Delta\eta(t, \bar{t})]$ cross sections. For bin indices see Table 90.

source / bin	1	2	3	4	5	6	7	8	9	10	11	12
JER	-1.7 -0.2	-0.1 -1.3	+2.3 +0.4	+0.8 +1.6	+0.4 -0.2	-0.2 +0.1	-0.2 -0.6	+0.4 +0.3	-0.6 -0.4	-0.5 +1.1	-1.0 +0.1	+0.0 +0.6
JESAbsoluteMPFBias	-1.1 -1.5	-0.5 -0.4	+1.2 +1.0	+0.8 +0.2	-0.1 +0.7	+0.2 +0.0	-0.2 +0.1	-0.3 +0.0	-0.4 -0.3	+0.4 +0.7	+0.2 +0.1	+0.5 +0.1
JESAbsoluteScale	-0.3 -0.6	-0.5 -0.5	+2.2 +0.6	+0.4 +1.3	-0.2 -0.4	-0.3 -0.1	-0.5 -0.0	+0.5 +0.0	-0.4 +0.3	+0.6 -0.0	+0.2 +0.2	+0.1 -0.0
JESAbsoluteStat	-2.1 -1.1	+0.1 -1.1	+2.8 +0.9	+0.2 +0.7	+0.3 -0.1	-0.4 +0.5	-0.7 -0.6	+0.7 +0.4	-0.5 -0.3	+1.0 +0.3	-0.2 +0.1	+0.2 +0.5
JESFlavourQCD	-1.1 -0.7	+0.1 -1.5	+3.7 +0.6	+0.8 +2.7	-0.3 -0.1	-1.2 +0.7	+0.6 -1.3	-0.2 -0.7	-0.5 +0.0	+1.0 -0.5	+1.4 -1.1	+0.5 -0.4
JESFragmentation	-2.4 -3.1	+0.2 -0.3	+2.4 +3.0	+0.1 -0.2	+0.3 +0.5	-0.2 +0.2	+0.2 +1.5	+0.2 -0.7	-0.3 -0.2	-0.0 -0.1	+0.1 -0.2	+0.3 +0.1
JESPileUpDataMC	-2.6 +0.2	+0.5 -0.4	+0.4 +1.1	+0.2 +0.8	+0.7 -0.2	+0.0 +0.2	-1.0 -0.0	+0.2 -0.6	-0.3 -0.4	+1.2 +0.0	+0.9 -1.1	+0.4 +0.1
JESPileUpPtBB	-1.7 -1.2	-0.7 -0.5	+2.4 +1.9	+1.2 +0.8	-0.1 +0.0	-0.3 +0.1	+0.2 -0.7	+0.2 +0.1	-0.2 -0.3	+1.1 +0.0	-0.2 -0.0	+0.2 -0.1
JESPileUpPtEC1	+0.3 -0.3	-0.6 -0.0	+1.1 +0.3	-0.1 +0.0	+0.4 -0.1	-0.6 -0.2	+0.3 +0.2	+0.7 -0.1	-0.3 +0.0	-0.0 -0.6	+0.4 -1.0	+0.1 +0.5
JESPileUpPtEC2	+0.0 +0.0	+0.0 -0.0	-0.0 +0.0	-0.0 +0.0	+0.0 +0.0	+0.0 +0.0	+0.0 -0.0	-0.0 -0.0	+0.0 +0.0	+0.0 +0.0	+0.0 +0.0	+0.0 +0.0
JESPileUpPtHF	+0.0 +0.0	+0.0 -0.0	-0.0 +0.0	+0.0 +0.0	+0.0 +0.0	+0.0 +0.0	+0.0 -0.0	-0.0 -0.0	+0.0 +0.0	+0.0 +0.0	+0.0 +0.0	+0.0 +0.0
JESPileUpPtRef	-0.5 -0.7	+0.3 -0.2	+0.2 +1.2	+1.1 +1.1	-0.1 -0.2	-0.4 -0.1	+0.0 -0.5	-0.1 -0.4	-0.3 +0.1	+1.0 +0.5	+0.3 -0.9	+0.4 -0.1
JESRelativeBal	-2.5 -3.1	+0.1 -0.7	+2.9 +1.2	-0.2 +1.0	+0.5 +0.8	-0.1 +0.6	-0.5 +0.6	+0.1 -0.4	-0.6 -0.5	+1.3 -0.2	+1.2 -0.5	+0.2 +0.4
JESRelativeFSR	-1.0 -1.3	-1.0 -0.6	+1.2 +3.2	+1.9 -0.0	-0.2 -0.4	-0.1 -0.4	-0.3 +0.2	-0.0 -0.0	-0.0 -0.1	+0.3 +0.3	-0.6 +0.4	+0.1 +0.4
JESRelativeJEREC1	+1.2 -1.5	-0.3 -0.0	-0.3 +2.1	+0.1 +0.0	+0.2 +0.1	-0.3 -0.3	+0.4 +0.3	-0.3 -0.0	-0.2 -0.1	+0.0 +0.3	+0.0 -0.3	+0.2 +0.1
JESRelativeJEREC2	+0.0 +0.0	+0.0 -0.0	-0.0 +0.0	-0.0 +0.0	+0.0 +0.0	+0.0 +0.0	+0.0 -0.0	-0.0 +0.0	+0.0 +0.0	+0.0 +0.0	+0.0 +0.0	+0.0 +0.0
JESRelativeJERHF	+0.0 +0.0	+0.0 -0.0	-0.0 +0.0	+0.0 +0.0	+0.0 +0.0	+0.0 +0.0	+0.0 -0.0	-0.0 +0.0	+0.0 +0.0	+0.0 +0.0	+0.0 +0.0	+0.0 +0.0
JESRelativePtBB	-2.0 -4.2	-0.0 -0.7	+2.3 +3.5	+0.5 +0.6	+0.0 +0.5	-0.0 +0.4	+0.4 +1.3	-0.2 -0.1	-0.4 -0.4	+0.6 -0.4	-0.0 -0.1	+0.2 +0.2
JESRelativePtEC1	-1.0 -1.1	+0.2 -0.2	+1.8 -0.1	+0.1 +0.5	+0.3 +0.5	-0.4 -0.0	+0.4 +0.1	-0.2 -0.5	-0.2 +0.1	-0.2 -0.2	-0.4 -0.5	+0.4 +0.4
JESRelativePtEC2	+0.0 +0.0	+0.0 -0.0	-0.0 +0.0	+0.0 +0.0	+0.0 +0.0	+0.0 +0.0	+0.0 -0.0	-0.0 +0.0	+0.0 +0.0	+0.0 +0.0	+0.0 +0.0	+0.0 +0.0
JESRelativePtHF	+0.0 +0.0	+0.0 -0.0	+0.0 +0.0	+0.0 +0.0	+0.0 +0.0	+0.0 +0.0	+0.0 -0.0	+0.0 +0.0	+0.0 +0.0	+0.0 +0.0	+0.0 +0.0	+0.0 +0.0
JESRelativeStatEC	-0.8 -1.5	-0.1 -0.2	+1.9 +1.7	+0.5 -0.3	+0.0 +0.6	-0.4 -0.1	+0.6 +0.1	-0.0 +0.1	-0.3 -0.5	-0.4 -0.5	-0.1 -0.4	+0.1 +0.5
JESRelativeStatFSR	-0.7 -1.6	+0.1 -0.8	+0.7 +1.7	+0.5 +1.0	+0.5 +0.3	+0.3 +0.0	-0.2 -0.7	-0.7 +0.1	-0.1 -0.3	+0.3 +0.9	-0.1 -0.3	+0.3 +0.2
JESRelativeStatHF	+0.0 +0.0	+0.0 -0.0	-0.0 +0.0	+0.0 +0.0	+0.0 +0.0	+0.0 +0.0	+0.0 -0.0	-0.0 +0.0	+0.0 +0.0	+0.0 +0.0	+0.0 +0.0	+0.0 +0.0
JESSinglePionECAL	-2.4 -1.9	-0.3 -0.8	+2.3 +2.8	+1.5 +0.7	+0.4 +0.4	-0.1 -0.4	-0.5 +0.7	-0.8 +0.8	-0.3 -0.6	+0.5 +0.6	+0.2 +0.1	+0.2 +0.4

Table 44: Table 92 continued.

source / bin	1	2	3	4	5	6	7	8	9	10	11	12
JESSinglePionHCAL	-1.2	-0.6	+2.2	+0.4	+0.1	+0.1	+0.9	-0.1	-0.4	-0.6	+0.1	+0.1
	-0.3	-0.5	+1.2	+0.8	-0.3	-0.2	-0.2	-0.1	-0.2	+0.6	+0.7	+0.3
JESTimePtEta	-1.2	-0.2	+2.4	+0.8	+0.0	-0.3	+0.1	+0.1	-0.6	+0.0	-0.1	+0.3
	-1.3	-0.8	+2.2	+0.4	+0.1	+0.3	+0.9	-0.5	-0.7	+0.1	+0.7	+0.4
E_T^{miss}	-0.4	+0.0	-0.3	+0.7	-0.1	+0.2	-0.1	-0.2	+0.0	+0.4	-0.3	+0.0
	-1.0	+0.7	+0.3	-0.1	+0.1	-0.1	+0.4	-0.0	-0.2	+0.5	-0.0	+0.1
lepton ID/ISO	-0.2	+0.2	-0.6	-0.1	+0.3	+0.1	+0.0	-0.3	+0.2	-0.3	-0.4	-0.1
	+0.2	-0.2	+0.6	+0.1	-0.3	-0.1	+0.0	+0.4	-0.2	+0.4	+0.4	+0.1
pileup	+0.3	+0.2	-0.7	-0.5	+0.2	+0.0	+0.2	+0.1	-0.0	-0.3	-0.2	+0.1
	-0.4	-0.2	+0.7	+0.5	-0.1	-0.0	-0.3	-0.1	+0.0	+0.4	+0.2	-0.1
trigger	-0.1	+0.0	+0.1	+0.0	+0.1	-0.0	+0.1	+0.0	-0.0	+0.1	+0.1	-0.1
	+0.1	-0.0	-0.1	-0.0	-0.1	+0.0	-0.1	+0.0	+0.0	-0.1	-0.1	+0.1
trigger (η)	+0.3	+0.1	-0.2	+0.2	-0.0	-0.1	+0.1	-0.1	-0.1	+0.0	-0.1	+0.0
	-0.3	-0.1	+0.2	-0.2	+0.0	+0.1	-0.1	+0.1	+0.1	-0.0	+0.1	-0.0
non-tt background	-0.6	-0.3	-3.6	-0.0	+1.0	-0.3	+0.3	+1.1	+0.3	+0.8	+1.1	+0.9
	+0.5	+0.3	+3.5	+0.1	-1.0	+0.3	-0.2	-1.1	-0.3	-0.8	-1.0	-0.9
b-tagging	-0.2	+0.0	-0.1	-0.0	+0.1	-0.0	+0.1	-0.1	+0.0	+0.1	+0.0	+0.1
	+0.2	-0.0	+0.1	+0.0	-0.1	+0.0	-0.1	+0.1	-0.0	-0.1	-0.0	-0.1
b-tagging (light jets)	-0.1	-0.1	-0.9	+0.1	+0.3	-0.1	+0.2	+0.4	+0.0	+0.3	+0.2	+0.1
	+0.1	+0.1	+0.9	-0.1	-0.3	+0.1	-0.2	-0.4	-0.0	-0.3	-0.2	-0.1
luminosity	+0.0	+0.0	+0.0	+0.0	+0.0	+0.0	+0.0	+0.0	+0.0	+0.0	+0.0	+0.0
	+0.0	+0.0	+0.0	+0.0	+0.0	+0.0	+0.0	+0.0	+0.0	+0.0	+0.0	+0.0
BR($t\bar{t} \rightarrow \ell\ell$)	+0.0	+0.0	+0.0	+0.0	+0.0	+0.0	+0.0	+0.0	+0.0	+0.0	+0.0	+0.0
	+0.0	+0.0	+0.0	+0.0	+0.0	+0.0	+0.0	+0.0	+0.0	+0.0	+0.0	+0.0
PDF eigenvector 1	+0.0	+0.0	-0.0	+0.0	-0.0	-0.0	-0.0	+0.0	-0.0	+0.0	+0.0	+0.0
	+0.0	+0.0	+0.0	+0.0	-0.0	+0.0	+0.0	-0.0	-0.0	+0.0	+0.0	-0.0
PDF eigenvector 2	+0.2	-0.1	-0.4	+0.0	-0.0	-0.0	-0.1	+0.1	-0.0	+0.0	-0.0	+0.2
	-0.2	-0.1	+0.3	-0.0	-0.0	-0.0	-0.0	+0.0	+0.1	-0.1	-0.1	-0.0
PDF eigenvector 3	+0.0	+0.0	+0.1	+0.0	-0.0	+0.0	+0.0	-0.0	-0.0	+0.0	+0.1	-0.1
	-0.0	-0.0	-0.1	-0.0	+0.0	-0.0	-0.0	+0.0	+0.0	-0.0	-0.0	+0.1
PDF eigenvector 4	+0.2	+0.0	-0.4	+0.0	+0.0	-0.0	-0.0	+0.0	-0.1	+0.1	+0.1	+0.1
	-0.1	-0.1	+0.3	-0.0	-0.0	+0.0	-0.0	+0.0	+0.0	-0.0	-0.1	-0.1
PDF eigenvector 5	-0.2	-0.1	+0.2	-0.1	+0.0	-0.0	-0.0	+0.0	+0.1	-0.1	-0.2	+0.0
	-0.0	+0.0	+0.1	+0.0	-0.0	+0.1	+0.1	-0.1	-0.0	+0.1	+0.1	-0.1
PDF eigenvector 6	+0.1	+0.1	-0.3	+0.0	+0.1	-0.0	+0.0	-0.0	-0.1	+0.1	+0.2	+0.1
	-0.0	-0.1	+0.2	-0.0	-0.1	+0.0	-0.0	+0.0	+0.0	-0.1	-0.1	-0.0
PDF eigenvector 7	-0.3	-0.1	+0.4	-0.1	+0.0	-0.1	-0.0	+0.0	+0.2	-0.2	-0.4	+0.0
	+0.2	+0.1	-0.2	+0.1	+0.0	+0.0	+0.0	-0.0	-0.1	+0.2	+0.2	-0.0
PDF eigenvector 8	-0.1	+0.1	-0.1	-0.1	+0.1	-0.0	+0.0	-0.1	+0.0	-0.1	+0.0	+0.0
	+0.1	-0.1	+0.1	+0.0	-0.1	+0.0	-0.0	+0.1	-0.0	+0.1	+0.0	+0.0
PDF eigenvector 9	+0.1	-0.0	+0.1	+0.0	-0.1	-0.0	-0.0	+0.1	+0.0	-0.1	-0.1	-0.0
	-0.1	+0.1	-0.1	-0.0	+0.1	+0.0	+0.0	-0.1	-0.0	+0.1	+0.1	+0.0
PDF eigenvector 10	+0.2	+0.1	-0.3	+0.1	+0.0	+0.0	+0.0	-0.0	-0.1	+0.1	+0.2	-0.0
	-0.2	-0.1	+0.3	-0.1	-0.0	-0.0	-0.0	+0.0	+0.1	-0.2	-0.2	+0.0
PDF eigenvector 11	+0.1	+0.0	-0.1	+0.0	+0.0	+0.0	+0.0	-0.0	-0.0	+0.0	+0.1	-0.0
	-0.1	-0.1	+0.1	-0.0	-0.0	-0.0	-0.0	+0.0	+0.1	-0.1	-0.1	+0.0
PDF eigenvector 12	-0.2	-0.0	+0.1	-0.1	+0.0	-0.0	-0.0	-0.0	+0.1	-0.1	-0.1	+0.0
	+0.2	+0.0	-0.1	+0.1	-0.0	+0.0	+0.0	+0.0	-0.1	+0.1	+0.1	-0.0
PDF eigenvector 13	-0.1	+0.1	+0.1	-0.0	+0.1	+0.0	+0.0	-0.1	-0.0	+0.0	+0.1	-0.1
	+0.1	-0.1	-0.1	+0.0	-0.1	-0.0	-0.0	+0.1	+0.0	-0.0	-0.1	+0.1
PDF eigenvector 14	-0.1	-0.0	+0.1	-0.0	+0.0	+0.0	+0.0	-0.0	+0.0	-0.0	-0.1	-0.0
	+0.1	+0.0	-0.1	+0.0	-0.0	-0.0	-0.0	+0.0	-0.1	+0.0	+0.1	+0.0

Table 45: Table 92 continued.

source / bin	1	2	3	4	5	6	7	8	9	10	11	12
PDF eigenvector 15	-0.1 +0.0	-0.0 +0.0	+0.2 -0.1	-0.0 +0.0	-0.0 +0.0	+0.0 -0.0	-0.0 +0.0	-0.0 +0.0	+0.1 -0.0	-0.0 +0.0	-0.1 +0.0	-0.0 +0.0
PDF eigenvector 16	+0.0	+0.0	-0.1	+0.0	+0.0	-0.0	+0.0	-0.0	-0.0	+0.0	+0.0	-0.0
PDF eigenvector 17	-0.0	-0.0	+0.1	-0.0	-0.0	+0.0	-0.0	+0.0	+0.0	-0.0	-0.1	+0.0
PDF eigenvector 18	-0.1 +0.3 -0.3	-0.0 -0.0 +0.0	+0.1 -0.2 +0.2	-0.0 +0.1 -0.1	-0.0 +0.1 +0.0	+0.0 -0.0 +0.0	-0.0 +0.1 -0.1	+0.0 -0.1 -0.1	-0.0 +0.1 +0.1	+0.0 +0.0 -0.0	+0.1 +0.1 -0.1	+0.0 +0.1 -0.1
PDF eigenvector 19	+0.2 -0.3	+0.0 -0.1	-0.2 +0.3	+0.1 -0.1	-0.0 +0.0	-0.0 -0.0	+0.0 -0.0	+0.0 -0.0	-0.1 +0.1	+0.1 -0.2	+0.2 -0.2	+0.0 -0.0
PDF eigenvector 20	+0.1 -0.1	+0.0	-0.1	-0.0	-0.0	-0.0	+0.0	+0.0	-0.0	+0.1	+0.2	-0.0
PDF eigenvector 21	+0.0 -0.0	-0.0	-0.2	-0.0	+0.0	-0.0	-0.0	+0.0	-0.0	-0.0	-0.0	+0.1
PDF eigenvector 22	+0.3 -0.2	-0.0	-0.5	+0.0	+0.0	-0.1	-0.1	+0.2	-0.1	+0.0	+0.0	+0.2
PDF eigenvector 23	-0.4 +0.1	-0.0	+0.5	-0.1	-0.0	+0.1	+0.0	-0.2	+0.1	-0.1	-0.2	-0.2
PDF eigenvector 24	-0.1 -0.2	-0.0	+0.2	-0.0	-0.0	-0.0	-0.0	+0.1	+0.0	-0.0	-0.0	-0.0
PDF eigenvector 25	-0.2 -0.2	-0.1	+0.2	-0.1	-0.1	+0.0	-0.0	-0.0	+0.1	-0.1	-0.2	+0.0
PDF eigenvector 26	-0.0 -0.0	-0.0	+0.0	-0.0	+0.0	-0.0	+0.0	-0.0	+0.0	-0.0	-0.0	-0.0
PDF eigenvector 27	+0.4 -0.0	-0.1	+0.0	+0.1	-0.2	-0.0	-0.1	+0.2	-0.0	+0.0	+0.0	+0.0
PDF eigenvector 28	+0.0 +0.0	-0.0	+0.1	+0.0	-0.0	+0.0	+0.0	+0.0	+0.0	-0.0	+0.1	+0.0
α_s	+0.2 -0.2	-0.1	+0.1	+0.1	-0.2	+0.0	-0.0	+0.1	+0.0	+0.0	-0.0	-0.0
m_t	-2.1 +1.0	-1.8	-1.0	-0.1	+0.8	-1.0	+2.7	+2.3	+0.3	+2.5	+2.3	+1.7
μ_{rf}	+1.7 -1.9	-0.9	+1.1	+0.3	-1.1	+0.0	-0.6	+0.8	+0.1	-0.1	-1.0	-0.2
h_{damp}	-2.0 -1.4	-0.2	+2.3	-1.4	+0.6	-0.3	-1.9	+1.4	+0.3	+2.6	-0.8	-0.1
PS ISR	+2.1 -1.1	-0.4	-1.7	-1.9	+0.5	-0.3	+0.3	+2.3	+0.1	-0.9	-0.9	-0.1
PS FSR	-1.9 +0.9	-0.2	+1.1	-0.1	+0.9	+0.8	-1.8	-0.3	+0.2	-1.0	-2.1	-0.8
UE tune	-1.6 -0.7	-0.5	+1.3	-1.3	+0.8	+0.4	-2.5	-0.3	+0.4	+1.1	-0.0	-0.2
CR	-1.4 -1.9 -0.7	-0.4	+0.5	-0.5	+0.4	-0.0	-0.1	+1.0	+0.3	+0.7	+0.5	+0.0
$f(b \rightarrow B)$	-0.0 +0.1 +0.0 +0.6	-0.3	+2.5 -1.3 +0.5 +2.2	+0.0 -0.0 -0.2 -0.2	-0.9 +0.4 -0.2 +0.1	+0.4 -0.2 +0.0 +0.1	+0.1 +0.0 +0.0 -0.7	-0.6 +0.1 +0.3 -0.5	+0.0 -0.0 +0.0 -0.5	+1.6 +0.1 +0.3 +1.5	+0.5 -0.1 +0.1 +0.4	-0.7 +0.4 -0.1 -0.7
$\text{BR}(B \rightarrow \mu)$	-0.0 +0.1	-0.1	-0.2	+0.1	+0.1	+0.1	+0.1	+0.0	+0.0	-0.0	-0.2	-0.0

Table 46: The measured $[M(t\bar{t}), \Delta\phi(t, \bar{t})]$ cross sections, along with their relative statistical and systematic uncertainties.

$M(t\bar{t})$ [GeV]	$\Delta\phi(t, \bar{t})$ [rad]	$\frac{1}{\sigma(t\bar{t})} \frac{d\sigma}{d\Delta\phi(t, \bar{t})}$ [rad $^{-1}$]	stat. [%]	syst. [%]	bin
300–400	0.00–2.20	3.535×10^{-2}	3.0	$+6.3$ -16.2	1
300–400	2.20–2.95	1.249×10^{-1}	1.9	$+9.7$ -5.6	2
300–400	2.95–3.14	4.024×10^{-1}	3.2	$+20.3$ -15.5	3
400–500	0.00–2.20	2.617×10^{-2}	3.0	$+13.6$ -10.7	4
400–500	2.20–2.95	1.957×10^{-1}	1.2	$+5.7$ -6.3	5
400–500	2.95–3.14	8.082×10^{-1}	1.3	$+6.7$ -5.6	6
500–650	0.00–2.20	1.439×10^{-2}	4.0	$+4.9$ -14.4	7
500–650	2.20–2.95	1.250×10^{-1}	1.8	$+6.9$ -6.9	8
500–650	2.95–3.14	6.251×10^{-1}	1.4	$+5.9$ -6.2	9
650–1500	0.00–2.20	7.308×10^{-3}	4.8	$+12.2$ -7.6	10
650–1500	2.20–2.95	7.475×10^{-2}	2.1	$+6.9$ -6.1	11
650–1500	2.95–3.14	3.923×10^{-1}	1.5	$+5.4$ -6.2	12

Table 47: The correlation matrix of statistical uncertainties for the measured $[M(t\bar{t}), \Delta\phi(t, \bar{t})]$ cross sections. The values are expressed as percentages. For bin indices see Table 95.

Table 48: Sources and values of the relative systematic uncertainties in percent of the measured $[M(t\bar{t}), \Delta\phi(t, \bar{t})]$ cross sections. For bin indices see Table 95.

source / bin	1	2	3	4	5	6	7	8	9	10	11	12
JER	-1.8 -0.8	-0.1 -0.1	+2.7 -1.1	+0.7 +0.5	-0.4 +0.8	+0.3 +0.1	-2.1 -2.4	+0.1 +0.7	+0.1 -0.6	-0.1 +1.9	+0.2 +0.4	-0.6 +0.3
JESAbsoluteMPFBias	-3.0 -3.6	+1.1 +0.1	+1.1 +2.1	+0.9 +2.0	+0.7 +0.2	-0.1 +0.1	-2.9 +0.1	+0.0 +0.2	-0.5 -0.6	+1.7 -0.3	+0.0 +0.2	+0.3 -0.1
JESAbsoluteScale	-1.0 -1.8	+0.3 +0.4	+0.9 +0.5	-0.0 -0.9	+0.3 +0.7	-0.0 -0.0	-2.1 -0.4	+0.7 +0.8	-0.8 -0.4	-0.0 +0.4	+0.6 +0.2	+0.0 -0.2
JESAbsoluteStat	-4.8 +2.3	+0.7 +0.9	+6.8 -5.4	-4.1 +3.6	-1.8 +1.6	+2.6 +1.6	-1.9 -2.5	-2.2 +0.9	+1.8 +2.8	-1.7 -2.6	-2.8 +2.3	+1.7 +3.2
JESFlavourQCD	-0.9 -2.8	+1.6 +0.0	+1.4 +0.9	-1.8 +1.4	-0.1 +0.9	-0.7 +0.4	-2.4 +0.8	+0.4 -0.1	-0.2 -0.6	+0.1 -0.2	+0.8 +0.2	+0.7 -1.0
JESFragmentation	-0.7 -1.7	+0.8 +0.9	+0.2 +1.7	-2.5 +0.3	+0.4 +0.2	+0.0 -0.5	+0.1 -2.0	+0.4 +1.0	-0.2 -0.5	+0.5 +1.2	+0.4 +0.1	-0.0 -0.4
JESPileUpDataMC	-0.7 -1.3	+0.6 +1.4	+0.1 +0.0	-0.4 +0.2	+0.3 +0.2	-0.4 +0.1	-1.2 -0.8	+1.0 +0.4	-0.6 -0.7	-0.6 -0.7	+1.0 +0.3	+0.2 -0.3
JESPileUpPtBB	-0.9 -1.6	+0.5 +0.8	+0.0 +0.5	+0.1 +0.2	+0.1 +0.3	-0.1 +0.2	-1.6 -0.5	+0.4 -0.4	-0.1 -0.2	+1.1 -0.4	+0.4 +0.3	+0.0 -0.1
JESPileUpPtEC1	-0.7 -0.7	+0.9 +0.7	+0.2 -0.3	-1.1 -0.3	+0.0 -0.2	+0.1 +0.2	-0.3 +1.2	+0.2 -0.0	-0.1 -0.2	-0.8 +1.4	-0.1 +0.1	+0.2 -0.2
JESPileUpPtEC2	+0.0 +0.0	-0.0 -0.0	+0.0 -0.0	-0.0 -0.0	+0.0 +0.0							
JESPileUpPtHF	+0.0 +0.0	-0.0 -0.0	+0.0 -0.0	-0.0 -0.0	+0.0 +0.0							
JESPileUpPtRef	-1.6 -1.8	+0.4 +0.9	+1.1 +1.3	+0.4 +0.4	+0.1 -0.0	-0.5 -0.3	-1.2 +0.1	+0.5 +0.6	-0.2 -0.4	-0.4 +0.5	+0.7 -0.0	+0.3 -0.5
JESRelativeBal	+0.1 -2.6	+1.7 -0.8	-0.2 +1.1	-1.5 +2.5	-0.1 +0.4	-0.0 +0.4	-1.2 -1.1	-0.2 -0.1	-0.3 -0.6	-0.4 +2.0	+0.7 +0.9	+0.3 -0.4
JESRelativeFSR	-0.1 -0.7	+0.3 +0.7	+0.4 +0.9	-0.9 -1.8	-0.2 +0.4	+0.4 -0.5	-0.8 -1.4	+0.4 +0.9	-0.4 -0.5	+0.9 +1.1	+0.3 +0.2	-0.4 +0.1
JESRelativeJEREC1	-1.4 -0.8	+0.5 +1.1	+0.9 -0.6	+0.4 -1.7	+0.1 +0.3	-0.4 +0.4	-0.2 +0.3	+0.3 +0.0	-0.3 -0.2	+0.9 +0.3	-0.0 +0.3	+0.2 -0.1
JESRelativeJEREC2	+0.0 +0.0	-0.0 -0.0	+0.0 -0.0	-0.0 -0.0	+0.0 +0.0							
JESRelativeJERHF	+0.0 +0.0	-0.0 -0.0	+0.0 -0.0	-0.0 -0.0	+0.0 +0.0							
JESRelativePtBB	-2.0 -0.8	+1.1 -0.2	+0.6 +0.2	+1.0 +1.5	+0.1 +0.4	-0.1 -0.0	-0.4 -2.0	-0.2 +0.1	-0.5 -0.2	-0.5 +0.5	+0.7 +0.5	+0.0 -0.3
JESRelativePtEC1	-0.7 -0.4	+0.8 -0.4	+0.7 -0.4	-0.7 +0.2	+0.1 +0.1	+0.3 +0.4	-0.7 -0.3	+0.1 +0.3	-0.5 -0.0	-0.7 +0.8	-0.1 +0.1	+0.1 -0.1
JESRelativePtEC2	+0.0 +0.0	-0.0 -0.0	+0.0 -0.0	-0.0 -0.0	+0.0 +0.0							
JESRelativePtHF	+0.0 +0.0	+0.0 -0.0	+0.0 +0.0	+0.0 -0.0	+0.0 +0.0							
JESRelativeStatEC	-1.1 -0.3	+0.1 +0.0	+1.0 +0.5	-0.9 +0.1	+0.0 +0.1	+0.3 +0.1	+0.5 -2.3	+0.5 +0.2	-0.4 -0.3	-0.2 +1.8	-0.0 +0.3	-0.0 -0.0
JESRelativeStatFSR	-1.1 -1.5	+0.9 +1.2	+0.4 +0.7	-0.2 +0.2	+0.4 +0.1	-0.4 -0.0	-1.6 -1.1	+0.2 -0.2	-0.3 -0.3	+1.3 -0.2	+0.6 -0.2	+0.0 +0.5
JESRelativeStatHF	+0.0 +0.0	-0.0 -0.0	+0.0 +0.0	-0.0 -0.0	+0.0 +0.0							
JESSinglePionECAL	-1.1 -1.1	+0.1 +0.4	+1.4 +1.1	+0.3 -1.7	-0.2 +0.3	+0.5 +0.2	-2.0 -1.0	-0.0 +0.4	-0.5 -0.3	+0.8 +0.3	+0.5 +0.5	-0.3 +0.0

Table 49: Table 97 continued.

source / bin	1	2	3	4	5	6	7	8	9	10	11	12
JESSinglePionHCAL	-1.6	+1.0	+0.8	-0.2	+0.3	+0.1	-0.0	-0.5	-0.2	+0.5	+0.2	-0.2
	-1.3	+1.3	+0.9	-0.2	-0.3	-0.3	-1.7	-0.1	+0.2	-0.1	+0.7	+0.2
JESTimePtEta	-1.1	+0.4	+0.7	+0.3	+0.2	+0.1	-1.7	+0.1	-0.2	+1.3	+0.3	-0.2
	-1.8	+0.2	+1.8	+0.2	-0.2	+0.3	-1.7	-0.1	-0.3	+1.0	+0.6	+0.1
E_T^{miss}	-5.6	-2.7	+10.1	+0.3	-3.4	+3.3	+0.1	-3.8	+2.4	-0.3	-1.5	+0.5
	+1.6	+4.1	-6.2	-1.0	+2.3	-2.1	-1.3	+2.2	-1.7	-0.2	+1.4	-0.4
lepton ID/ISO	-0.1	-0.0	-0.4	-0.2	+0.4	+0.1	+0.2	-0.0	-0.1	+0.0	+0.0	-0.2
	+0.1	-0.0	+0.4	+0.2	-0.4	-0.1	-0.1	+0.0	+0.1	-0.0	-0.0	+0.2
pileup	-1.6	-0.7	+2.8	-0.7	-0.9	+1.0	-0.1	-1.0	+0.8	-0.1	-0.6	+0.3
	+1.5	+0.7	-2.8	+0.7	+0.9	-1.0	+0.0	+1.0	-0.8	+0.1	+0.6	-0.3
trigger	+0.0	+0.0	-0.1	-0.1	+0.1	+0.0	-0.0	-0.0	+0.0	-0.2	-0.1	-0.0
	-0.0	-0.0	+0.1	+0.1	-0.1	-0.0	+0.0	+0.0	-0.0	+0.2	+0.1	+0.0
trigger (η)	+0.0	+0.0	+0.0	-0.1	+0.0	+0.0	-0.1	-0.1	-0.0	+0.2	+0.1	-0.0
	-0.0	-0.0	-0.0	+0.1	-0.0	-0.0	+0.1	+0.1	+0.0	-0.2	-0.1	+0.0
non-tf background	-1.8	-1.4	-1.5	-0.5	+0.5	+0.3	+0.8	+0.5	+0.6	+0.7	+1.1	+1.1
	+0.9	+1.6	+0.9	+1.1	+0.1	-0.4	-1.4	-0.5	-0.7	-0.1	-1.2	-0.9
b-tagging	+0.1	-0.1	-0.3	+0.1	+0.1	-0.0	+0.1	+0.0	-0.0	+0.2	+0.1	+0.1
	-0.1	+0.1	+0.3	-0.1	-0.1	+0.0	-0.1	-0.0	+0.0	-0.2	-0.1	-0.1
b-tagging (light jets)	-0.7	-0.3	+0.0	-0.4	+0.1	+0.2	-0.1	+0.1	+0.3	-0.4	+0.2	+0.2
	+0.7	+0.3	-0.0	+0.4	-0.1	-0.2	+0.1	-0.1	-0.3	+0.4	-0.2	-0.2
luminosity	+0.0	+0.0	+0.0	+0.0	+0.0	+0.0	+0.0	+0.0	+0.0	+0.0	+0.0	+0.0
	+0.0	+0.0	+0.0	+0.0	+0.0	+0.0	+0.0	+0.0	+0.0	+0.0	+0.0	+0.0
BR($t\bar{t} \rightarrow \ell\ell$)	+0.0	+0.0	+0.0	+0.0	+0.0	+0.0	+0.0	+0.0	+0.0	+0.0	+0.0	+0.0
	+0.0	+0.0	+0.0	+0.0	+0.0	+0.0	+0.0	+0.0	+0.0	+0.0	+0.0	+0.0
PDF eigenvector 1	+0.0	-0.0	-0.0	+0.0	-0.0	-0.0	+0.0	-0.0	-0.0	+0.1	+0.0	+0.0
	+0.0	+0.0	-0.0	+0.0	+0.0	-0.0	+0.0	-0.0	-0.0	+0.0	+0.0	-0.0
PDF eigenvector 2	-0.1	-0.1	-0.1	+0.1	-0.1	-0.0	+0.1	-0.0	-0.0	+0.3	+0.2	+0.1
	-0.0	+0.0	+0.2	-0.1	-0.0	+0.0	-0.0	+0.1	+0.0	-0.2	-0.1	-0.1
PDF eigenvector 3	+0.1	+0.0	-0.0	+0.1	+0.0	+0.0	+0.1	-0.0	-0.0	-0.0	-0.0	-0.0
	-0.0	-0.0	-0.0	-0.0	+0.0	-0.0	-0.0	+0.0	+0.0	+0.0	+0.0	+0.0
PDF eigenvector 4	-0.0	-0.0	-0.1	+0.0	+0.0	-0.0	+0.0	-0.1	-0.0	+0.2	+0.1	+0.1
	+0.0	+0.0	+0.1	+0.0	-0.0	+0.0	+0.0	+0.0	+0.0	-0.1	-0.1	-0.1
PDF eigenvector 5	-0.1	+0.0	+0.1	-0.2	-0.0	-0.0	-0.1	+0.1	+0.1	-0.1	-0.1	-0.0
	+0.1	+0.0	-0.1	+0.1	+0.0	+0.0	+0.1	-0.1	-0.1	+0.0	-0.0	-0.0
PDF eigenvector 6	-0.0	-0.0	-0.2	+0.0	+0.1	-0.0	+0.0	-0.1	-0.0	+0.2	+0.0	+0.1
	+0.0	+0.0	+0.1	-0.0	-0.1	-0.0	-0.0	+0.1	+0.0	-0.1	-0.0	-0.1
PDF eigenvector 7	-0.1	+0.0	+0.2	-0.3	-0.0	-0.0	-0.2	+0.2	+0.1	-0.2	-0.1	-0.1
	+0.1	-0.0	-0.1	+0.1	+0.0	+0.0	+0.1	-0.1	-0.1	+0.1	+0.0	+0.1
PDF eigenvector 8	-0.0	+0.0	-0.1	-0.1	+0.1	-0.0	+0.0	+0.0	-0.0	+0.0	+0.0	+0.0
	+0.0	-0.0	+0.1	+0.0	-0.1	+0.0	+0.0	+0.0	+0.0	-0.0	-0.0	+0.0
PDF eigenvector 9	+0.1	+0.0	+0.1	+0.0	-0.1	-0.0	-0.0	+0.1	-0.0	-0.1	+0.0	-0.1
	-0.1	-0.0	-0.1	-0.0	+0.1	-0.0	+0.0	-0.1	+0.0	+0.1	-0.0	+0.1
PDF eigenvector 10	+0.1	+0.0	-0.1	+0.1	+0.0	+0.0	+0.0	-0.1	-0.1	+0.1	+0.0	+0.1
	-0.1	+0.0	+0.1	-0.1	-0.0	-0.0	-0.1	+0.1	+0.1	-0.1	-0.0	-0.1
PDF eigenvector 11	+0.0	-0.0	-0.0	+0.0	+0.0	+0.0	+0.0	-0.0	-0.0	+0.0	+0.0	+0.0
	-0.0	-0.0	+0.1	-0.0	-0.0	-0.0	-0.0	+0.1	+0.0	-0.0	-0.0	-0.0
PDF eigenvector 12	-0.0	+0.0	+0.0	-0.1	+0.0	-0.0	-0.0	+0.1	+0.0	-0.0	-0.0	-0.0
	+0.1	-0.0	-0.0	+0.0	-0.0	+0.0	+0.0	-0.1	-0.0	+0.0	+0.0	+0.0
PDF eigenvector 13	+0.0	+0.1	-0.0	-0.0	+0.1	+0.0	-0.0	-0.0	-0.0	-0.1	-0.1	-0.0
	-0.0	-0.1	+0.0	+0.0	-0.1	-0.0	+0.0	+0.0	+0.0	+0.1	+0.1	+0.0
PDF eigenvector 14	-0.0	+0.0	+0.0	-0.0	+0.0	-0.0	-0.0	+0.0	+0.0	-0.0	-0.0	-0.0
	+0.0	-0.0	-0.0	+0.0	-0.0	+0.0	+0.0	-0.0	-0.0	+0.0	+0.0	+0.0

Table 50: Table 97 continued.

source / bin	1	2	3	4	5	6	7	8	9	10	11	12
PDF eigenvector 15	-0.0	+0.0	+0.0	-0.0	+0.0	-0.0	-0.0	+0.0	+0.0	-0.1	-0.0	-0.0
	+0.0	-0.0	-0.0	+0.0	-0.0	+0.0	+0.0	-0.0	-0.0	+0.0	+0.0	+0.0
PDF eigenvector 16	+0.0	+0.0	-0.0	+0.0	+0.0	-0.0	+0.0	-0.0	-0.0	+0.0	+0.0	+0.0
	-0.0	+0.0	+0.0	-0.0	-0.0	+0.0	-0.0	+0.0	+0.0	-0.0	-0.0	-0.0
PDF eigenvector 17	-0.0	-0.0	+0.0	-0.0	-0.0	+0.0	-0.0	+0.0	+0.0	-0.0	+0.0	-0.0
	+0.0	+0.0	-0.1	+0.0	+0.1	-0.0	+0.0	-0.1	-0.0	+0.1	-0.0	+0.0
PDF eigenvector 18	+0.0	-0.1	-0.0	+0.1	-0.1	+0.0	+0.0	-0.0	-0.0	+0.1	+0.1	+0.1
	-0.0	+0.1	+0.0	-0.1	+0.1	-0.0	-0.0	+0.0	+0.0	-0.1	-0.1	-0.1
PDF eigenvector 19	+0.1	-0.0	-0.0	+0.1	-0.0	+0.0	+0.0	-0.1	-0.0	+0.0	+0.0	+0.0
	-0.1	+0.0	+0.1	-0.1	+0.0	-0.0	-0.0	+0.1	+0.1	-0.1	-0.1	-0.1
PDF eigenvector 20	+0.0	+0.0	+0.1	-0.1	-0.0	+0.0	+0.0	-0.0	+0.0	-0.4	-0.0	+0.1
	-0.0	+0.0	-0.0	-0.0	+0.0	+0.0	-0.0	+0.0	+0.0	-0.0	-0.0	-0.0
PDF eigenvector 21	-0.0	-0.0	-0.0	-0.0	-0.0	-0.0	+0.0	-0.0	+0.0	+0.1	+0.1	+0.1
	+0.1	+0.0	+0.0	+0.0	+0.0	-0.0	+0.0	+0.0	-0.0	-0.1	-0.1	-0.1
PDF eigenvector 22	-0.1	-0.1	-0.1	-0.0	-0.1	-0.0	-0.1	-0.0	+0.0	+0.2	+0.2	+0.2
	+0.1	+0.1	+0.0	+0.0	+0.1	+0.0	+0.0	-0.0	-0.0	-0.2	-0.2	-0.1
PDF eigenvector 23	-0.0	+0.0	+0.1	-0.1	+0.0	+0.0	+0.0	+0.1	+0.0	-0.3	-0.2	-0.2
	-0.0	-0.0	+0.0	-0.0	-0.0	+0.0	-0.1	-0.0	+0.0	-0.0	-0.0	+0.0
PDF eigenvector 24	-0.0	+0.0	+0.1	-0.1	-0.0	+0.0	-0.1	+0.0	+0.0	-0.2	-0.1	-0.0
	-0.1	-0.1	+0.1	-0.0	-0.1	+0.0	+0.1	+0.1	+0.0	+0.1	+0.1	-0.0
PDF eigenvector 25	-0.1	-0.0	+0.1	-0.0	-0.1	+0.0	+0.0	+0.1	+0.0	-0.0	+0.0	-0.0
	-0.1	+0.0	+0.2	-0.1	-0.0	+0.0	-0.1	+0.1	+0.1	-0.2	-0.1	-0.0
PDF eigenvector 26	-0.0	+0.0	+0.0	-0.0	+0.0	+0.0	-0.0	+0.0	+0.0	-0.1	-0.0	-0.0
	-0.0	-0.0	+0.0	-0.0	-0.0	+0.0	-0.0	-0.0	+0.0	-0.0	-0.0	+0.0
PDF eigenvector 27	+0.1	-0.0	+0.2	+0.1	-0.2	-0.0	+0.0	+0.0	+0.0	+0.0	+0.0	-0.0
	-0.0	-0.0	-0.1	-0.0	+0.1	-0.0	+0.0	-0.0	-0.0	+0.1	+0.0	+0.1
PDF eigenvector 28	+0.0	-0.0	+0.1	-0.0	-0.0	+0.0	+0.0	+0.0	+0.0	-0.1	-0.0	-0.0
	+0.0	+0.0	-0.1	-0.0	+0.1	-0.0	-0.0	-0.0	-0.0	+0.1	+0.0	+0.0
α_s	+0.0	-0.1	+0.2	+0.1	-0.2	-0.0	+0.1	+0.0	+0.0	+0.1	-0.0	-0.1
	-0.0	+0.1	-0.2	-0.1	+0.2	+0.0	-0.1	-0.0	-0.0	-0.1	+0.0	+0.1
m_t	-0.5	-1.7	-2.6	+0.4	+0.1	-0.5	-0.7	+0.8	+1.2	+0.8	+1.4	+2.1
	+0.2	+1.6	+2.3	+1.0	-0.0	+0.5	-0.5	-0.6	-1.1	-0.7	-1.2	-2.6
μ_{rf}	+0.5	-0.4	+1.4	+2.1	-1.4	-0.3	+2.8	-0.2	-0.3	+2.9	+0.4	-1.1
	-0.8	+0.3	-1.3	-2.7	+1.5	+0.5	-3.9	+0.3	+0.6	-3.9	-0.7	+1.4
h_{damp}	-1.3	+0.5	+2.2	-0.2	-0.6	+0.1	-1.2	-0.3	+0.9	-1.5	-1.1	+0.2
	-0.1	-1.3	-3.0	+6.2	-0.1	-0.7	-0.8	+0.9	-0.4	+3.7	+1.2	-0.3
PS ISR	+0.3	+0.1	+0.1	-1.3	-0.5	+0.2	-2.0	+0.8	+1.1	-1.8	-0.2	-0.3
	+1.9	+0.2	-2.9	+2.5	-0.4	-0.7	-0.2	+1.1	-0.1	+2.6	-0.4	-0.3
PS FSR	+1.3	-0.1	-2.5	+3.0	+1.0	-0.6	+0.1	+1.2	-1.2	+2.0	+0.5	-2.1
	-1.0	+0.9	-0.2	-1.0	+0.2	-0.3	-1.5	+0.1	+0.5	+0.9	-1.1	+1.5
UE tune	-0.6	+0.1	+0.2	+0.7	+0.4	-0.1	-0.1	+0.0	-0.3	+0.8	-0.6	-0.1
	-1.8	-0.1	+0.5	+1.8	-0.0	+0.4	-2.1	-0.0	+0.6	+1.0	-0.3	-0.8
CR	+0.1	-0.3	-0.7	+0.1	-0.3	+0.0	-0.7	+0.6	+0.4	+1.1	-0.5	+0.4
	-0.5	+0.0	+0.9	-0.8	-0.9	+1.0	-2.5	-1.1	+1.3	-0.5	-0.2	+0.4
	+0.7	+1.0	-2.3	-1.6	-0.1	+0.2	-0.6	+0.6	+0.3	+2.3	-0.7	+0.4
$f(b \rightarrow B)$	+0.7	+0.4	+1.2	+0.2	-0.3	-0.3	+0.4	+0.1	-0.6	-0.1	-0.3	-0.5
	-0.3	-0.2	-0.6	-0.1	+0.1	+0.1	-0.0	-0.0	+0.3	+0.1	+0.2	+0.3
	+0.1	+0.1	+0.2	+0.1	-0.1	-0.1	+0.1	+0.0	-0.1	-0.0	-0.0	-0.1
	+1.0	+0.8	+1.3	-0.4	-0.2	-0.4	-0.2	-0.1	-0.5	-0.7	-0.5	-0.5
BR($B \rightarrow \mu$)	-0.1	-0.1	-0.1	+0.0	+0.0	+0.1	-0.0	+0.1	+0.0	-0.1	-0.0	-0.1
	+0.3	+0.2	-0.0	-0.1	-0.1	-0.1	+0.0	-0.1	-0.1	+0.1	+0.0	+0.1

Table 51: The measured $[M(t\bar{t}), p_T(t\bar{t})]$ cross sections, along with their relative statistical and systematic uncertainties.

$M(\text{t}\bar{t})$ [GeV]	$p_T(\text{t}\bar{t})$ [GeV]	$\frac{1}{\sigma(\text{t}\bar{t})} \frac{d\sigma}{dp_T(\text{t}\bar{t})}$ [GeV $^{-1}$]	stat. [%]	syst. [%]	bin
300–400	0–30	3.671×10^{-3}	1.8	+12.4 -9.3	1
300–400	30–75	1.660×10^{-3}	2.1	+10.6 -14.1	2
300–400	75–150	5.749×10^{-4}	3.3	+9.7 -8.4	3
300–400	150–500	5.519×10^{-5}	5.1	+8.1 -9.7	4
400–500	0–30	4.915×10^{-3}	1.1	+9.8 -8.0	5
400–500	30–75	2.609×10^{-3}	1.2	+7.8 -7.8	6
400–500	75–150	8.995×10^{-4}	1.9	+7.1 -8.0	7
400–500	150–500	8.845×10^{-5}	3.8	+6.4 -10.8	8
500–650	0–30	3.107×10^{-3}	1.6	+12.1 -11.3	9
500–650	30–75	1.733×10^{-3}	1.7	+10.1 -11.2	10
500–650	75–150	6.394×10^{-4}	2.5	+6.8 -8.0	11
500–650	150–500	7.086×10^{-5}	3.6	+5.8 -5.2	12
650–1500	0–30	1.705×10^{-3}	2.6	+13.7 -12.3	13
650–1500	30–75	9.328×10^{-4}	3.3	+13.2 -15.5	14
650–1500	75–150	4.219×10^{-4}	2.9	+7.0 -6.2	15
650–1500	150–500	5.924×10^{-5}	2.7	+6.1 -5.1	16

Table 52: The correlation matrix of statistical uncertainties for the measured $[M(t\bar{t}), p_T(t\bar{t})]$ cross sections. The values are expressed as percentages. For bin indices see Table 100.

Table 53: Sources and values of the relative systematic uncertainties in percent of the measured $[M(\text{t}\bar{\text{t}}), p_T(\text{t}\bar{\text{t}})]$ cross sections. For bin indices see Table 100.

source / bin	1	2	3	4	5	6	7	8	9	10	11	12	13	14	15	16
JER	+0.4 -0.3	-0.8 -0.8	-0.1 +0.2	+0.5 +0.1	+0.7 -0.1	-0.0 +0.7	-0.4 +0.1	-1.8 -0.6	+0.9 -0.9	-0.2 +0.7	-0.8 -0.0	+0.4 +0.1	+0.2 -0.3	-1.2 +0.3	-0.1 +1.5	+0.1 +0.3
JESAbsoluteMPFBias	-0.1 +0.3	-0.1 -0.5	-0.2 -0.5	-0.1 -3.0	+0.4 +0.2	+0.5 +0.2	-0.5 -0.2	-0.9 +1.6	-0.5 -0.0	+0.0 +0.2	-0.5 -0.4	+0.0 -0.1	+0.1 -0.2	+0.4 -0.1	+0.5 +0.7	-0.4 -0.0
JESAbsoluteScale	+0.7 +0.1	-0.3 -0.1	-0.2 -0.8	-0.4 -1.9	+0.1 +0.2	+0.1 +0.3	-0.0 +0.1	-0.4 +0.5	-0.5 -0.0	+0.2 -0.1	-0.8 -0.1	-0.4 +0.3	-0.1 -0.6	+0.4 +0.2	+0.4 +0.2	-0.1 +0.0
JESAbsoluteStat	+4.4 -3.5	-3.4 +2.8	-3.0 +3.8	-2.9 +1.1	+3.7 -3.6	-1.9 +2.1	-4.2 +3.3	-2.6 +1.5	+4.0 -5.0	-2.2 +2.2	-3.5 +3.8	-1.9 +2.6	+4.8 -4.1	-2.6 +2.2	-2.7 +3.3	-2.3 +3.0
JESFlavourQCD	+1.2 -0.0	-0.3 -1.0	+0.0 -0.3	+2.6 -0.0	-0.4 +0.4	-0.2 +0.5	-1.3 +0.7	-2.6 +0.1	-0.3 -0.1	+0.9 +0.1	-0.3 +0.3	-1.2 -0.1	+0.2 -0.1	+1.2 -0.8	+0.6 -1.1	+0.5 -0.2
JESFragmentation	-0.1 +0.3	-0.2 -0.6	+0.4 +0.5	+1.5 +0.4	+0.1 +0.3	+0.5 -0.1	-1.2 -0.3	-2.4 -0.8	-0.2 +0.0	+0.7 +0.1	+0.2 -0.2	+0.6 +0.5	-0.3 -0.6	+0.1 -0.2	+0.6 +0.5	+0.0 -0.1
JESPileUpDataMC	+0.5 +0.1	-0.5 -0.0	-0.9 +0.2	-0.4 -0.6	-0.1 +0.4	+0.2 +0.5	-0.1 -0.2	-0.7 -0.4	-0.1 -0.5	+0.1 -0.1	-0.3 -0.2	-0.2 +0.4	-0.1 -0.4	+0.6 -0.2	+0.7 +0.3	+0.4 +0.3
JESPileUpPtBB	-0.3 +0.4	-0.6 +0.3	+0.0 -0.3	+0.3 -0.0	+0.1 +0.1	+0.6 +0.3	-0.6 -0.0	-0.5 -0.7	-0.3 -0.2	+0.5 -0.1	-0.1 -0.9	+0.5 +0.1	+0.3 -0.3	-0.2 -0.1	+0.5 +0.2	-0.0 -0.2
JESPileUpPtEC1	+0.9 +0.3	-0.2 -0.1	-0.6 +0.1	+1.0 +0.5	-0.1 +0.0	+0.2 -0.2	-0.7 -0.1	-1.9 -0.5	-0.7 -0.3	+0.5 -0.1	+0.1 -0.1	+1.0 +0.8	+0.1 +0.1	+0.1 -0.1	+0.2 +0.2	-0.2 +0.2
JESPileUpPtEC2	-0.0 -0.0	+0.0 +0.0	-0.0 -0.0	+0.0 +0.0	-0.0 +0.0	+0.0 +0.0	-0.0 -0.0	+0.0 +0.0	-0.0 -0.0	+0.0 +0.0	-0.0 -0.0	+0.0 +0.0	-0.0 -0.0	+0.0 +0.0	-0.0 +0.0	+0.0 +0.0
JESPileUpPtHF	-0.0 -0.0	+0.0 +0.0	-0.0 -0.0	+0.0 +0.0	-0.0 +0.0	+0.0 +0.0	-0.0 -0.0	+0.0 +0.0	-0.0 -0.0	+0.0 +0.0	-0.0 -0.0	+0.0 +0.0	-0.0 -0.0	+0.0 +0.0	-0.0 +0.0	+0.0 +0.0
JESPileUpPtRef	+0.2 +0.7	-0.1 +0.2	-0.5 -0.5	+0.6 -1.6	-0.0 +0.3	+0.1 +0.3	-0.5 -0.3	-1.4 -0.3	-0.3 -0.8	+0.3 +0.2	+0.2 +0.3	+0.9 +0.7	+0.2 -0.4	+0.4 -0.2	+0.4 -0.5	+0.1 -0.5
JESRelativeBal	+0.8 -0.5	+0.1 -1.6	+1.2 -0.6	+1.1 -1.4	-0.4 +0.6	+0.3 +0.9	-0.7 +0.8	-1.7 +0.7	-0.7 -0.4	+0.3 -0.0	-0.7 -0.4	-0.6 -0.2	+0.4 -0.0	+0.1 -0.5	+0.7 +0.6	+0.3 +0.3
JESRelativeFSR	+0.2 +0.5	-0.7 -0.4	+0.4 +0.1	+1.4 +2.3	+0.1 -0.0	+0.3 +0.2	-0.6 -0.5	-1.5 -2.7	-0.3 -0.2	+0.6 +0.2	+0.1 -0.5	+1.0 +0.9	+0.0 -0.4	-0.5 +0.5	+0.2 +0.8	+0.1 +0.0
JESRelativeJEREC1	+0.0 -0.1	-0.2 +0.0	-0.3 -0.1	-0.1 +0.3	+0.3 +0.2	+0.3 +0.3	-0.6 -0.7	-0.4 -0.5	-0.2 -0.4	+0.1 +0.4	+0.2 +0.1	-0.1 -0.0	-0.1 -0.0	+0.3 -0.1	+0.2 +0.3	+0.1 -0.1
JESRelativeJEREC2	-0.0 -0.0	+0.0 +0.0	-0.0 -0.0	+0.0 +0.0	-0.0 +0.0	+0.0 +0.0	-0.0 -0.0	+0.0 +0.0	-0.0 -0.0	+0.0 +0.0	-0.0 -0.0	+0.0 +0.0	-0.0 -0.0	+0.0 +0.0	-0.0 +0.0	+0.0 +0.0
JESRelativeJERHF	-0.0 -0.0	+0.0 +0.0	-0.0 +0.0	+0.0 +0.0												
JESRelativePtBB	+0.0 -0.1	-0.2 +0.2	-0.7 +0.1	+0.5 -1.2	+0.3 +0.2	+0.2 +0.3	-0.3 -0.4	-0.4 +0.5	+0.2 -0.2	-0.3 -0.1	-0.4 -0.6	+0.1 +0.1	+0.2 -0.3	-0.3 -0.2	+1.0 +0.6	-0.3 +0.3
JESRelativePtEC1	+0.5 -0.3	-0.2 -0.5	+0.1 -0.6	+1.2 +0.3	+0.2 +0.1	+0.2 +0.6	-0.7 -0.5	-0.8 -0.7	-0.6 -0.1	+0.2 +0.4	+0.2 +0.7	+0.3 +0.2	-0.5 -0.1	+0.4 -0.0	+0.1 +0.3	-0.6 +0.1
JESRelativePtEC2	-0.0 -0.0	+0.0 +0.0	-0.0 -0.0	+0.0 -0.0	-0.0 +0.0	+0.0 +0.0	-0.0 -0.0	+0.0 +0.0	-0.0 -0.0	+0.0 +0.0	-0.0 -0.0	+0.0 +0.0	-0.0 -0.0	+0.0 +0.0	-0.0 +0.0	+0.0 +0.0
JESRelativePtHF	+0.0 -0.0	+0.0 +0.0	-0.0 -0.0	+0.0 +0.0	+0.0 +0.0	+0.0 +0.0										
JESRelativeStatEC	+0.9 +0.7	+0.6 -0.4	-1.5 -0.6	+1.3 -0.4	-0.4 +0.0	+0.2 +0.1	-0.5 -0.1	-1.0 +0.4	-0.4 -0.6	+0.1 +0.5	+0.4 -0.1	+0.6 -0.8	-0.2 -0.3	+0.2 +0.4	-0.3 +0.1	-0.2 +0.6
JESRelativeStatFSR	+0.5 +0.0	-0.6 -0.1	-0.6 -0.0	+0.6 +0.1	-0.0 +0.3	+0.6 +0.6	-0.1 -1.2	-0.3 +0.3	-0.3 -0.5	+0.0 +0.4	-0.1 +0.1	-0.6 -0.9	+0.0 -0.1	+0.5 -0.5	+0.2 +0.3	+0.4 +0.4
JESRelativeStatHF	-0.0 -0.0	+0.0 +0.0	-0.0 +0.0	+0.0 +0.0												
JESSinglePionECAL	-0.1 +0.4	-0.3 -0.6	+1.1 +0.1	+0.0 +0.5	+0.4 +0.1	+0.4 +0.1	-0.3 -0.6	-0.9 -1.5	-0.4 +0.1	+0.0 +0.5	-0.7 -0.6	-0.1 +0.9	-0.4 +0.2	+0.0 +0.2	+0.3 +0.2	+0.0 -0.1

Table 54: Table 102 continued.

source / bin	1	2	3	4	5	6	7	8	9	10	11	12	13	14	15	16
JESSinglePionHCAL	+0.5	-0.4	-1.2	-1.0	+0.3	+0.2	-0.1	+0.7	-0.3	+0.4	-0.2	-0.9	-0.3	-0.3	+0.5	+0.1
	+0.5	+0.4	-1.0	+0.2	-0.0	+0.1	-0.7	-0.4	-0.1	+0.1	-0.5	-0.6	+0.6	-0.4	+0.7	+0.5
JESTimePtEta	+0.2	+0.4	-0.1	-0.4	+0.2	+0.4	-0.8	-0.4	-0.5	+0.2	-0.2	-0.7	+0.1	-0.3	+0.2	+0.5
	-0.1	-0.1	-0.6	-0.2	+0.4	+0.6	-0.5	-0.7	-0.3	-0.1	-0.9	+0.8	-0.0	+0.2	+0.9	+0.2
E_T^{miss}	+6.5	-7.8	-3.1	-0.8	+5.2	-4.8	-1.4	-0.2	+6.7	-7.2	-1.9	-0.5	+7.5	-9.9	+0.2	-0.6
	-4.0	+5.6	+1.0	+0.4	-3.6	+4.2	+0.3	+0.1	-5.0	+5.7	-0.4	-0.3	-4.8	+6.7	-0.2	+0.5
lepton ID/ISO	-0.2	-0.3	-0.1	+0.0	+0.2	+0.3	+0.1	+0.0	-0.1	-0.0	-0.0	-0.0	-0.1	-0.1	-0.1	-0.2
	+0.1	+0.4	+0.0	-0.0	-0.2	-0.2	-0.2	+0.0	+0.1	+0.1	-0.0	+0.1	+0.0	+0.3	+0.0	+0.2
pileup	+1.7	-2.0	-1.1	-0.1	+1.6	-1.4	-1.1	-0.1	+2.0	-1.9	-0.8	-0.0	+2.1	-2.2	-0.3	-0.5
	-1.9	+2.1	+1.0	+0.2	-1.7	+1.5	+1.0	+0.2	-2.1	+2.0	+0.7	-0.0	-2.1	+2.2	+0.3	+0.6
trigger	-0.0	-0.0	-0.0	+0.1	+0.0	+0.1	+0.0	+0.0	-0.0	-0.0	-0.0	+0.0	-0.0	-0.0	-0.0	-0.0
	+0.0	+0.0	+0.0	-0.1	-0.0	-0.1	-0.0	-0.0	+0.0	+0.0	+0.0	-0.0	+0.0	+0.0	+0.0	+0.0
trigger (η)	+0.0	+0.0	+0.0	+0.1	-0.0	+0.0	-0.0	-0.0	-0.1	-0.0	-0.1	-0.1	+0.0	+0.1	+0.0	+0.0
	-0.1	+0.0	-0.1	-0.1	-0.0	+0.0	-0.0	+0.0	+0.0	+0.1	+0.0	+0.1	-0.1	-0.0	-0.1	+0.0
non-tt background	-1.3	-2.1	-1.0	+0.3	+0.4	+0.0	+0.4	+0.1	+0.5	+0.2	+0.7	+0.5	+0.8	+0.9	+1.3	+0.9
	+0.9	+2.4	+0.7	-0.3	-0.4	+0.3	-0.5	+0.0	-0.6	-0.0	-0.8	-0.4	-0.9	-0.6	-1.4	-0.8
b-tagging	-0.2	-0.2	+0.2	-0.2	-0.0	-0.0	+0.2	+0.1	-0.0	-0.1	+0.1	+0.1	+0.1	+0.0	+0.2	+0.2
	+0.1	+0.2	-0.3	+0.2	+0.0	+0.1	-0.2	-0.1	-0.0	+0.1	-0.1	-0.1	-0.1	+0.0	-0.2	-0.1
b-tagging (light jets)	-0.1	-0.5	-0.7	+0.1	+0.2	+0.1	-0.2	-0.1	+0.2	+0.1	-0.0	-0.0	+0.2	+0.2	+0.1	+0.0
	+0.0	+0.6	+0.6	-0.1	-0.2	-0.0	+0.2	+0.1	-0.3	-0.1	-0.0	+0.0	-0.2	-0.2	-0.1	-0.0
luminosity	+0.0	+0.0	+0.0	+0.0	+0.0	+0.0	+0.0	+0.0	+0.0	+0.0	+0.0	+0.0	+0.0	+0.0	+0.0	+0.0
	+0.0	+0.0	+0.0	+0.0	+0.0	+0.0	+0.0	+0.0	+0.0	+0.0	+0.0	+0.0	+0.0	+0.0	+0.0	+0.0
BR($t\bar{t} \rightarrow \ell\ell$)	+0.0	+0.0	+0.0	+0.0	+0.0	+0.0	+0.0	+0.0	+0.0	+0.0	+0.0	+0.0	+0.0	+0.0	+0.0	+0.0
	+0.0	+0.0	+0.0	+0.0	+0.0	+0.0	+0.0	+0.0	+0.0	+0.0	+0.0	+0.0	+0.0	+0.0	+0.0	+0.0
PDF eigenvector 1	-0.0	+0.0	-0.0	+0.0	-0.0	+0.0	-0.0	+0.0	-0.0	+0.0	-0.0	+0.0	-0.0	+0.0	+0.0	+0.0
	-0.0	+0.0	+0.0	+0.0	-0.0	+0.0	+0.0	+0.0	-0.0	-0.0	-0.0	+0.0	-0.0	+0.0	-0.0	+0.0
PDF eigenvector 2	-0.1	-0.1	-0.1	-0.0	-0.0	-0.0	-0.0	+0.0	+0.0	-0.0	-0.0	-0.0	+0.2	+0.2	+0.2	+0.1
	+0.1	+0.0	-0.0	-0.1	+0.0	-0.0	-0.0	-0.1	+0.1	+0.0	+0.0	-0.0	-0.1	-0.1	-0.1	-0.1
PDF eigenvector 3	+0.0	+0.0	+0.0	+0.1	-0.0	+0.0	+0.0	+0.1	-0.0	-0.0	-0.0	+0.0	-0.1	-0.0	-0.0	+0.0
	-0.0	+0.0	-0.0	-0.0	-0.0	+0.0	-0.0	-0.0	-0.0	+0.0	-0.0	-0.0	+0.0	+0.1	+0.0	+0.0
PDF eigenvector 4	-0.1	-0.0	-0.1	+0.0	-0.0	+0.0	-0.0	+0.1	-0.0	-0.0	-0.1	+0.0	+0.1	+0.2	+0.1	+0.1
	+0.1	+0.0	+0.0	-0.0	+0.0	-0.0	-0.0	-0.1	+0.0	+0.0	+0.0	-0.0	-0.1	-0.1	-0.1	-0.1
PDF eigenvector 5	+0.0	+0.0	-0.1	-0.1	+0.0	+0.0	-0.1	-0.2	+0.1	+0.1	+0.1	-0.0	+0.0	-0.0	-0.1	-0.1
	-0.0	+0.0	+0.0	+0.1	+0.0	+0.0	+0.0	+0.1	-0.1	-0.1	-0.0	+0.0	-0.1	-0.0	-0.0	+0.0
PDF eigenvector 6	-0.1	-0.0	-0.1	+0.1	+0.0	+0.1	-0.0	+0.1	-0.1	-0.0	-0.1	+0.0	+0.1	+0.1	+0.1	+0.1
	+0.1	+0.1	+0.0	-0.0	-0.0	-0.0	-0.0	-0.1	+0.0	+0.0	+0.0	-0.0	-0.1	-0.0	-0.0	-0.1
PDF eigenvector 7	+0.0	+0.0	-0.1	-0.2	+0.0	-0.0	-0.1	-0.3	+0.1	+0.2	+0.1	-0.1	+0.0	-0.1	-0.1	-0.2
	-0.0	+0.0	+0.0	+0.1	+0.0	+0.0	+0.0	+0.2	-0.1	-0.1	-0.1	+0.0	-0.0	+0.0	+0.1	+0.1
PDF eigenvector 8	-0.1	+0.0	-0.1	+0.0	+0.0	+0.1	-0.0	-0.0	-0.1	+0.0	-0.1	+0.0	+0.0	+0.1	-0.0	+0.0
	+0.0	+0.0	+0.0	-0.0	-0.0	-0.1	-0.0	+0.0	+0.0	-0.0	+0.0	-0.0	+0.0	-0.0	+0.0	+0.0
PDF eigenvector 9	+0.1	+0.1	+0.1	-0.0	-0.0	-0.1	+0.0	-0.0	-0.0	+0.0	+0.0	-0.0	-0.1	+0.0	-0.0	-0.0
	-0.1	-0.0	-0.1	+0.0	+0.0	+0.1	-0.0	+0.1	-0.0	-0.0	-0.1	+0.0	+0.1	+0.0	-0.0	+0.0
PDF eigenvector 10	-0.1	+0.0	+0.0	+0.1	-0.0	+0.1	+0.0	+0.2	-0.1	-0.1	-0.1	+0.0	-0.0	+0.1	+0.1	+0.2
	+0.0	+0.0	-0.1	-0.1	+0.0	-0.0	-0.1	-0.2	+0.1	+0.1	+0.1	-0.0	+0.0	-0.0	-0.1	-0.2
PDF eigenvector 11	-0.0	+0.0	+0.0	+0.0	+0.0	+0.0	+0.0	+0.0	-0.0	-0.0	-0.0	+0.0	-0.0	+0.0	+0.0	+0.0
	-0.0	+0.0	-0.0	-0.1	-0.0	-0.0	-0.0	-0.1	+0.0	+0.0	+0.0	-0.0	+0.0	+0.0	-0.0	-0.1
PDF eigenvector 12	-0.0	+0.0	-0.1	-0.1	+0.0	+0.0	-0.0	-0.1	+0.0	+0.1	+0.0	-0.0	+0.0	+0.0	-0.0	-0.1
	-0.0	+0.0	+0.0	+0.1	-0.0	+0.0	+0.0	+0.1	-0.0	-0.0	-0.0	+0.0	-0.0	+0.0	+0.0	+0.1
PDF eigenvector 13	-0.0	+0.0	+0.0	+0.0	+0.0	+0.1	+0.0	+0.0	-0.1	-0.0	-0.0	+0.0	-0.1	-0.1	-0.1	-0.0
	-0.0	+0.0	-0.1	-0.0	-0.0	-0.0	-0.0	-0.0	+0.0	+0.0	+0.0	-0.0	+0.0	+0.1	+0.1	+0.0
PDF eigenvector 14	-0.0	+0.0	-0.0	-0.0	+0.0	+0.0	-0.0	-0.0	+0.0	+0.0	+0.0	-0.0	-0.0	-0.0	-0.0	-0.0
	-0.0	+0.0	+0.0	+0.0	-0.0	+0.0	+0.0	+0.0	-0.0	-0.0	-0.0	+0.0	+0.0	+0.0	+0.0	+0.1

Table 55: Table 102 continued.

source / bin	1	2	3	4	5	6	7	8	9	10	11	12	13	14	15	16
PDF eigenvector 15	-0.0	+0.0	-0.0	-0.0	+0.0	+0.0	-0.0	-0.1	+0.0	+0.0	+0.0	+0.0	-0.0	-0.0	-0.1	-0.1
	-0.0	+0.0	+0.0	+0.0	-0.0	+0.0	+0.0	+0.0	-0.0	-0.0	-0.0	+0.0	+0.0	+0.0	+0.0	+0.0
PDF eigenvector 16	-0.0	+0.0	-0.0	+0.0	-0.0	+0.0	+0.0	+0.0	-0.0	+0.0	-0.0	+0.0	-0.0	+0.0	-0.0	+0.0
	+0.0	+0.0	-0.0	-0.0	+0.0	-0.0	-0.0	-0.0	+0.0	+0.0	+0.0	-0.0	-0.0	+0.0	-0.0	-0.0
PDF eigenvector 17	+0.0	+0.0	-0.0	-0.0	+0.0	-0.0	-0.0	-0.0	+0.0	+0.0	+0.0	-0.0	-0.0	+0.0	-0.0	-0.0
	-0.1	+0.0	+0.0	+0.1	-0.0	+0.1	+0.0	+0.1	-0.1	-0.0	-0.1	+0.0	-0.0	+0.0	+0.0	+0.1
PDF eigenvector 18	-0.0	+0.0	-0.0	+0.0	-0.0	-0.0	-0.0	+0.1	-0.0	-0.0	-0.0	-0.0	+0.0	+0.1	+0.1	+0.1
	-0.0	+0.0	-0.0	-0.0	+0.0	+0.1	-0.0	-0.1	-0.0	+0.0	+0.0	+0.0	-0.1	-0.1	-0.1	-0.1
PDF eigenvector 19	-0.0	+0.0	+0.0	+0.1	-0.0	+0.0	+0.0	+0.1	-0.1	-0.1	-0.0	+0.0	-0.0	+0.1	+0.1	+0.1
	-0.0	+0.0	-0.1	-0.1	+0.0	+0.0	-0.1	-0.2	+0.1	+0.1	+0.0	-0.0	+0.0	-0.0	-0.1	-0.2
PDF eigenvector 20	+0.0	+0.0	+0.0	+0.1	-0.0	-0.0	-0.0	-0.1	-0.0	-0.0	+0.0	+0.1	+0.0	-0.0	+0.0	-0.1
	-0.0	-0.0	-0.0	+0.0	+0.0	+0.0	-0.0	-0.1	+0.0	+0.0	+0.0	+0.0	-0.0	-0.0	-0.0	-0.0
PDF eigenvector 21	-0.0	-0.0	-0.1	-0.0	-0.0	+0.0	-0.0	-0.0	+0.0	+0.0	-0.0	-0.0	+0.1	+0.1	+0.1	+0.1
	+0.0	+0.1	+0.1	+0.1	-0.0	+0.0	+0.0	+0.0	-0.0	-0.0	+0.0	+0.0	-0.1	-0.1	-0.1	-0.0
PDF eigenvector 22	-0.1	-0.0	-0.1	-0.1	-0.0	-0.0	-0.1	-0.0	+0.0	+0.0	-0.0	-0.0	+0.2	+0.2	+0.2	+0.1
	+0.0	+0.1	+0.1	+0.1	+0.0	+0.1	+0.0	+0.1	-0.1	-0.0	-0.0	+0.1	-0.2	-0.2	-0.2	-0.1
PDF eigenvector 23	+0.1	+0.0	+0.0	-0.0	+0.0	+0.0	-0.0	-0.1	+0.1	+0.1	+0.1	+0.0	-0.2	-0.2	-0.2	-0.2
	-0.0	+0.0	-0.0	-0.0	-0.0	+0.0	-0.0	-0.0	+0.0	+0.0	-0.0	-0.0	+0.0	+0.0	+0.0	+0.0
PDF eigenvector 24	+0.0	+0.0	-0.0	-0.0	+0.0	-0.0	-0.0	-0.1	+0.1	+0.0	+0.0	-0.0	+0.0	-0.0	-0.1	-0.1
	+0.0	-0.0	-0.1	-0.1	+0.0	-0.0	-0.1	-0.1	+0.1	+0.0	+0.0	-0.0	+0.1	+0.0	+0.0	-0.1
PDF eigenvector 25	+0.1	-0.1	-0.1	-0.1	+0.0	-0.1	-0.0	-0.1	+0.1	+0.0	+0.1	-0.0	+0.0	-0.0	-0.0	-0.1
	+0.0	+0.0	-0.0	-0.1	+0.0	-0.0	-0.1	-0.2	+0.1	+0.1	+0.1	-0.0	-0.0	-0.1	-0.2	-0.2
PDF eigenvector 26	-0.0	+0.0	-0.0	+0.0	+0.0	+0.0	-0.0	-0.0	+0.0	+0.0	-0.0	-0.0	-0.0	-0.0	-0.0	-0.0
	-0.0	+0.0	-0.0	-0.0	+0.0	+0.0	-0.0	-0.0	+0.0	+0.0	-0.0	-0.0	+0.0	-0.0	-0.0	-0.0
PDF eigenvector 27	+0.1	+0.1	+0.1	+0.1	-0.1	-0.2	-0.0	+0.0	+0.0	-0.0	+0.1	+0.0	-0.1	+0.0	+0.0	+0.1
	-0.1	-0.0	-0.0	+0.0	+0.0	+0.1	-0.0	+0.0	-0.0	+0.0	-0.0	+0.0	+0.1	+0.0	+0.0	+0.0
PDF eigenvector 28	+0.0	+0.0	+0.0	-0.1	-0.0	-0.0	-0.0	-0.0	+0.0	+0.0	+0.0	+0.0	-0.0	-0.0	-0.0	-0.1
	-0.1	+0.0	-0.0	+0.0	+0.0	+0.1	-0.0	+0.0	-0.1	+0.0	-0.1	+0.0	+0.0	+0.1	+0.0	+0.1
α_s	+0.1	+0.1	+0.1	+0.1	-0.1	-0.1	-0.0	+0.0	+0.1	+0.0	+0.0	+0.1	-0.1	-0.0	-0.1	+0.0
	-0.1	-0.0	-0.1	-0.1	+0.0	+0.2	-0.0	-0.0	-0.1	+0.0	-0.1	-0.1	+0.1	+0.1	+0.0	-0.0
m_t	-1.4	-2.0	-1.8	-0.9	-0.2	+0.1	-0.1	-0.9	+0.8	+1.1	+0.6	+0.3	+2.0	+2.3	+1.3	+0.9
	+1.1	+1.6	+2.1	+1.1	+0.2	+0.2	+0.6	+1.1	-0.7	-1.0	-0.9	-0.2	-2.3	-2.3	-1.5	-1.2
μ_{rf}	+1.1	+0.8	+0.5	+1.2	-0.3	-0.8	-0.5	+1.1	+0.3	-0.2	-0.5	+0.6	-1.2	-0.5	-0.9	+0.8
	-1.3	-1.0	-0.7	-1.8	+0.3	+0.8	+0.6	-1.4	-0.1	+0.3	+0.7	-1.2	+1.4	+0.9	+1.2	-1.0
h_{damp}	-0.2	-0.3	+1.0	-2.7	-0.2	-0.2	+0.4	-0.8	+0.9	+0.0	-0.1	+0.2	-0.9	+2.2	-0.7	-0.6
	-0.9	-0.8	+1.6	-2.9	-0.4	+0.3	+1.4	+2.2	+0.0	+0.7	-0.6	-0.6	-1.1	+1.2	+0.0	-0.1
PS ISR	-0.4	-0.7	+0.3	+0.5	-0.4	+0.4	+0.2	-0.8	+0.8	+1.0	-0.7	+0.1	-1.2	+1.6	-0.7	-0.9
	-1.3	-0.2	+3.3	-0.1	-1.3	+0.3	+1.3	+0.7	-1.1	+1.5	+0.8	+0.6	-0.3	-0.4	-0.1	+1.5
PS FSR	-1.2	+0.2	+2.0	+1.0	-0.8	+0.6	+2.4	+2.1	-1.1	+0.1	+1.1	+1.0	-3.4	+0.7	-1.0	+0.6
	+0.3	-0.1	-0.1	-2.1	-0.6	+0.1	-0.5	-1.1	-0.1	+0.9	+0.5	-0.6	+0.2	+2.3	-0.3	-0.5
UE tune	+0.2	-1.0	+0.5	-0.9	-0.2	+0.3	+1.0	+1.1	+0.2	-0.3	-0.8	+0.3	-0.8	+1.7	-1.5	-0.3
	-0.6	-0.6	-1.0	+1.3	-0.1	+0.6	+1.1	-0.8	-0.1	+1.0	+0.6	+0.2	-1.8	+0.8	+0.2	-0.7
CR	-0.2	-1.4	+0.8	+0.8	+0.1	-0.3	+0.2	-1.0	+0.1	+0.3	+1.4	-0.7	+0.0	+0.8	-0.8	+1.1
	+0.7	-1.5	-0.2	-0.2	+1.2	-0.6	-0.6	-1.3	+1.8	-0.5	-2.2	-1.2	+0.1	+1.9	-0.9	-0.9
	-0.5	-0.6	+0.6	-0.1	-0.2	+0.3	+0.4	-2.2	+0.4	+0.3	-0.0	+1.1	+0.4	+0.3	-0.0	+0.1
$f(b \rightarrow B)$	+0.5	+0.7	+1.2	+0.6	-0.3	-0.2	-0.0	+0.2	-0.5	-0.1	+0.1	+0.3	-1.2	-0.3	-0.3	+0.2
	-0.3	-0.3	-0.6	-0.3	+0.1	+0.1	+0.0	-0.1	+0.2	+0.1	-0.1	-0.1	+0.6	+0.3	+0.2	+0.0
	+0.1	+0.1	+0.2	+0.1	-0.1	-0.0	-0.0	+0.1	-0.1	+0.0	+0.0	+0.1	-0.2	-0.0	-0.0	+0.1
	+0.7	+1.0	+1.2	+1.4	-0.4	-0.2	-0.0	-0.2	-0.5	-0.2	-0.0	-0.1	-1.0	-0.6	-0.2	-0.0
BR($B \rightarrow \mu$)	-0.1	-0.1	-0.1	-0.2	+0.1	+0.1	+0.0	+0.1	+0.0	+0.1	+0.1	-0.0	-0.1	-0.1	-0.1	+0.0
	+0.1	+0.2	+0.1	+0.2	-0.1	-0.1	-0.1	-0.0	-0.1	-0.1	-0.1	-0.0	+0.1	+0.1	+0.1	+0.1

Table 56: The measured $[M(t\bar{t}), p_T(t)]$ cross sections, along with their relative statistical and systematic uncertainties.

$M(\text{t}\bar{\text{t}})$ [GeV]	$p_T(\text{t})$ [GeV]	$\frac{1}{\sigma(\text{t}\bar{\text{t}})} \frac{d\sigma}{dp_T(\text{t})}$ [GeV $^{-1}$]	stat. [%]	syst. [%]	bin
300–450	0–100	3.173×10^{-3}	0.6	+2.7 -2.5	1
300–450	100–180	1.440×10^{-3}	1.2	+5.5 -5.7	2
300–450	180–600	1.956×10^{-5}	6.5	+27.8 -28.8	3
450–600	0–100	1.199×10^{-3}	1.2	+4.9 -4.6	4
450–600	100–180	2.104×10^{-3}	0.7	+4.4 -4.6	5
450–600	180–600	1.424×10^{-4}	1.9	+2.6 -3.4	6
600–1500	0–100	5.409×10^{-4}	2.5	+5.4 -5.1	7
600–1500	100–180	8.166×10^{-4}	1.9	+5.4 -4.6	8
600–1500	180–600	2.187×10^{-4}	1.0	+4.4 -4.4	9

Table 57: The correlation matrix of statistical uncertainties for the measured $[M(t\bar{t}), p_T(t)]$ cross sections. The values are expressed as percentages. For bin indices see Table 105.

Table 58: Sources and values of the relative systematic uncertainties in percent of the measured $[M(t\bar{t}), p_T(t)]$ cross sections. For bin indices see Table 105.

source / bin	1	2	3	4	5	6	7	8	9
JER	+0.3 -0.2	+0.1 +0.0	-3.7 -0.9	-0.3 -0.1	-0.0 +0.1	+0.2 +0.1	+0.5 +0.8	-0.7 +0.0	-0.2 +0.3
JESAbsoluteMPFBias	+0.0 -0.2	+0.3 +0.6	-1.7 -0.4	-0.1 +0.0	-0.2 -0.1	-0.0 -0.0	+0.3 -0.1	-0.2 +0.0	+0.3 +0.1
JESAbsoluteScale	+0.2 +0.1	-0.2 -0.3	-0.1 -1.0	-0.0 +0.5	-0.2 -0.2	+0.1 +0.2	+0.1 -0.4	-0.0 -0.3	+0.1 +0.1
JESAbsoluteStat	+0.6 -0.4	-0.8 +0.5	-8.2 +6.6	-0.3 +0.2	+0.4 -0.6	-0.5 +0.4	-0.0 +1.5	-0.4 -0.4	+0.1 +0.2
JESFlavourQCD	+0.3 -0.4	-0.7 +1.0	-0.9 -1.2	-0.9 +1.0	+0.1 -0.2	+0.3 +0.1	-0.2 +0.5	+0.5 -0.3	+0.6 -0.8
JESFragmentation	+0.1 +0.1	-0.3 -0.0	+0.2 -1.3	-0.2 +0.2	-0.1 -0.3	+0.3 +0.1	+0.5 +0.5	-0.2 -0.2	+0.2 -0.1
JESPileUpDataMC	-0.1 +0.2	+0.1 +0.4	-1.8 -2.9	-0.4 +0.2	+0.0 -0.3	-0.2 +0.4	+0.6 -0.9	+0.1 -0.1	+0.3 -0.3
JESPileUpPtBB	-0.1 +0.1	-0.2 +0.2	-2.5 +0.1	-0.1 +0.1	+0.0 -0.2	+0.5 +0.2	+0.7 +0.3	-0.1 -0.4	+0.1 -0.2
JESPileUpPtEC1	+0.1 -0.2	+0.2 +0.1	-3.5 +0.4	-0.3 +0.2	+0.2 -0.3	+0.3 -0.1	-1.3 +1.8	-0.1 +0.1	+0.4 -0.3
JESPileUpPtEC2	+0.0 +0.0	+0.0 -0.0	+0.0 +0.0	+0.0 -0.0	+0.0 -0.0	+0.0 +0.0	+0.0 +0.0	+0.0 +0.0	+0.0 -0.0
JESPileUpPtHF	+0.0 +0.0	-0.0 +0.0	+0.0 +0.0	-0.0 +0.0	-0.0 +0.0	+0.0 +0.0	+0.0 +0.0	+0.0 +0.0	-0.0 +0.0
JESPileUpPtRef	-0.0 +0.1	-0.3 +0.1	+0.6 -1.2	-0.3 +0.1	-0.1 +0.1	+0.7 -0.4	-0.3 +0.2	+0.4 -0.0	+0.4 -0.4
JESRelativeBal	+0.3 -0.4	+0.3 +0.8	-2.0 +1.6	-0.6 +0.2	-0.1 -0.3	-0.3 -0.2	-0.4 +1.0	-0.5 +0.0	+0.6 -0.1
JESRelativeFSR	+0.0 +0.1	-0.1 -0.1	-0.4 -0.8	+0.1 -0.3	+0.1 -0.2	-0.1 +0.1	+0.4 -0.1	-0.2 +0.3	-0.2 +0.2
JESRelativeJEREC1	-0.0 +0.0	+0.1 -0.3	+0.1 +1.3	-0.1 +0.2	-0.1 -0.1	-0.1 -0.2	+0.2 -0.0	-0.0 +0.1	+0.1 +0.1
JESRelativeJEREC2	+0.0 +0.0	+0.0 -0.0	+0.0 +0.0	+0.0 -0.0	+0.0 -0.0	+0.0 +0.0	+0.0 +0.0	+0.0 +0.0	+0.0 -0.0
JESRelativeJERHF	+0.0 +0.0	+0.0 -0.0	+0.0 +0.0	+0.0 -0.0	+0.0 -0.0	+0.0 +0.0	+0.0 +0.0	+0.0 +0.0	+0.0 -0.0
JESRelativePtBB	-0.0 +0.0	-0.2 +0.3	-0.7 -1.0	+0.4 -0.1	-0.2 -0.0	+0.0 -0.0	+0.5 +0.2	-0.4 -0.3	+0.2 -0.1
JESRelativePtEC1	+0.3 -0.2	+0.0 -0.1	-2.4 +0.5	-0.5 +0.1	-0.2 -0.1	+0.6 +0.0	-0.7 +1.2	-0.2 +0.2	+0.1 -0.2
JESRelativePtEC2	+0.0 +0.0								
JESRelativePtHF	+0.0 +0.0								
JESRelativeStatEC	+0.2 -0.0	-0.0 -0.2	-2.2 -0.8	-0.2 +0.1	+0.0 -0.1	+0.4 +0.2	-0.5 +0.3	-0.3 +0.1	+0.1 -0.0
JESRelativeStatFSR	+0.0 +0.1	+0.0 -0.0	-0.1 +0.5	+0.0 -0.0	-0.1 +0.0	-0.4 -0.2	+0.3 -0.4	-0.1 +0.2	+0.2 -0.1
JESRelativeStatHF	+0.0 +0.0	-0.0 +0.0	+0.0 +0.0	-0.0 +0.0	-0.0 +0.0	+0.0 +0.0	+0.0 +0.0	+0.0 +0.0	-0.0 +0.0
JESSinglePionECAL	+0.0 +0.0	+0.1 +0.0	-0.8 -2.4	+0.2 -0.5	-0.3 +0.0	+0.1 +0.4	+0.4 +0.3	-0.0 -0.0	-0.2 +0.2

Table 59: Table 107 continued.

source / bin	1	2	3	4	5	6	7	8	9
JESSinglePionHCAL	-0.1	+0.3	-0.2	+0.4	-0.1	-0.2	+0.7	-0.5	-0.1
	+0.1	-0.3	-0.1	-0.2	-0.2	-0.3	+0.3	+0.1	+0.4
JESTimePtEta	+0.0	+0.1	-1.6	-0.1	-0.0	+0.0	+0.2	-0.2	+0.2
	+0.1	-0.1	-1.4	+0.1	-0.3	+0.4	+0.0	+0.0	+0.2
E_T^{miss}	+0.2	-0.6	-1.3	+0.2	+0.1	-0.6	-0.1	-0.2	+0.0
	-0.0	+0.4	+0.7	-0.3	-0.2	+0.1	-0.2	+0.4	+0.1
lepton ID/ISO	+0.2	-0.7	+0.5	-0.7	+0.6	-0.3	+0.7	-0.0	-0.3
	-0.2	+0.7	-0.5	+0.7	-0.7	+0.3	-0.7	+0.1	+0.3
pileup	-0.0	-0.2	-0.7	-0.1	+0.1	-0.1	+0.0	+0.2	+0.0
	-0.0	+0.2	+0.7	+0.1	-0.1	+0.1	-0.1	-0.2	+0.0
trigger	+0.1	-0.1	+0.2	-0.2	+0.1	+0.0	-0.1	-0.2	+0.0
	-0.0	+0.1	-0.2	+0.2	-0.2	-0.0	+0.1	+0.2	-0.0
trigger (η)	+0.0	-0.0	+0.1	-0.2	-0.0	+0.0	+0.3	+0.0	-0.1
	-0.0	+0.0	-0.1	+0.2	-0.0	+0.0	-0.3	-0.0	+0.1
non-tt background	-1.0	-0.4	+0.9	-0.8	+1.2	+0.5	+0.9	+1.2	+1.1
	+1.1	+0.2	-0.8	+0.7	-1.2	-0.4	-0.9	-1.1	-1.1
b-tagging	-0.0	-0.1	+0.2	-0.1	+0.1	-0.0	+0.2	+0.1	+0.0
	+0.0	+0.1	-0.2	+0.1	-0.1	+0.0	-0.2	-0.0	-0.0
b-tagging (light jets)	-0.2	+0.0	-0.2	-0.3	+0.3	+0.3	-0.2	+0.2	+0.3
	+0.2	-0.0	+0.2	+0.3	-0.3	-0.3	+0.2	-0.2	-0.3
luminosity	+0.0	+0.0	+0.0	+0.0	+0.0	+0.0	+0.0	+0.0	+0.0
	+0.0	+0.0	+0.0	+0.0	+0.0	+0.0	+0.0	+0.0	+0.0
BR($t\bar{t} \rightarrow \ell\ell$)	+0.0	+0.0	+0.0	+0.0	+0.0	+0.0	+0.0	+0.0	+0.0
	+0.0	+0.0	+0.0	+0.0	+0.0	+0.0	+0.0	+0.0	+0.0
PDF eigenvector 1	+0.0	-0.0	+0.1	-0.0	-0.0	-0.0	+0.0	+0.0	+0.0
	+0.0	-0.0	+0.2	-0.0	-0.0	+0.0	-0.0	-0.0	-0.0
PDF eigenvector 2	-0.1	-0.0	+0.2	-0.0	-0.1	-0.0	+0.3	+0.4	+0.1
	-0.0	+0.1	-0.4	+0.2	-0.1	-0.0	-0.1	+0.0	-0.1
PDF eigenvector 3	+0.0	+0.0	+0.3	+0.0	-0.0	+0.0	-0.1	-0.1	-0.0
	-0.0	-0.0	-0.1	-0.0	+0.0	-0.0	+0.1	+0.1	+0.0
PDF eigenvector 4	+0.0	-0.1	+0.3	-0.2	+0.0	+0.0	+0.1	+0.1	+0.1
	-0.0	+0.1	-0.2	+0.2	-0.1	-0.0	-0.1	+0.0	-0.1
PDF eigenvector 5	-0.0	-0.0	-0.7	+0.1	+0.0	-0.0	+0.1	+0.0	-0.1
	+0.0	+0.0	+0.5	-0.0	-0.0	+0.0	-0.1	-0.1	-0.0
PDF eigenvector 6	+0.0	-0.1	+0.4	-0.2	+0.1	+0.0	+0.0	-0.1	+0.1
	-0.0	+0.1	-0.2	+0.1	-0.1	+0.0	-0.0	+0.1	-0.1
PDF eigenvector 7	-0.1	-0.0	-1.2	+0.2	+0.1	-0.1	+0.2	+0.1	-0.1
	+0.1	-0.0	+0.6	-0.1	-0.0	+0.1	-0.1	-0.1	+0.1
PDF eigenvector 8	+0.1	-0.2	+0.2	-0.2	+0.2	-0.1	+0.1	-0.1	-0.0
	-0.0	+0.1	-0.1	+0.1	-0.2	+0.1	-0.1	+0.1	+0.0
PDF eigenvector 9	-0.0	+0.1	-0.0	+0.1	-0.2	+0.0	-0.0	+0.2	-0.0
	+0.0	-0.1	+0.1	-0.2	+0.2	-0.0	+0.1	-0.2	+0.0
PDF eigenvector 10	+0.1	-0.0	+0.6	-0.2	+0.0	+0.1	-0.1	-0.1	+0.1
	-0.1	+0.0	-0.7	+0.2	-0.0	-0.0	+0.1	+0.1	-0.1
PDF eigenvector 11	+0.0	-0.0	+0.2	-0.1	+0.0	+0.0	-0.0	-0.0	+0.0
	-0.0	+0.0	-0.3	+0.1	-0.0	-0.0	+0.1	+0.1	-0.0
PDF eigenvector 12	-0.0	-0.0	-0.2	+0.1	+0.0	-0.1	+0.1	+0.1	-0.0
	+0.0	+0.0	+0.3	-0.1	-0.0	+0.1	-0.1	-0.0	+0.0
PDF eigenvector 13	+0.1	-0.1	-0.0	-0.1	+0.1	+0.0	-0.1	-0.3	-0.0
	-0.1	+0.1	+0.0	+0.1	-0.2	-0.0	+0.1	+0.3	+0.0
PDF eigenvector 14	+0.0	-0.0	-0.1	+0.0	+0.0	-0.0	+0.0	+0.0	-0.0
	+0.0	+0.0	+0.2	-0.0	-0.0	+0.0	-0.1	+0.0	+0.0

Table 60: Table 107 continued.

source / bin	1	2	3	4	5	6	7	8	9
PDF eigenvector 15	+0.0	-0.0	-0.2	+0.0	+0.0	-0.0	+0.0	-0.0	-0.0
	+0.0	-0.0	+0.1	-0.0	-0.0	+0.0	-0.0	+0.0	+0.0
PDF eigenvector 16	+0.0	-0.0	+0.1	-0.1	+0.0	+0.0	-0.0	-0.0	+0.0
	-0.0	+0.0	-0.1	+0.1	-0.0	-0.0	+0.0	+0.0	-0.0
PDF eigenvector 17	-0.0	+0.0	-0.1	+0.1	-0.1	-0.0	+0.0	+0.1	-0.0
	+0.1	-0.1	+0.3	-0.2	+0.1	+0.0	-0.1	-0.2	+0.0
PDF eigenvector 18	-0.0	+0.1	+0.3	+0.0	-0.1	+0.0	-0.0	+0.2	+0.1
	+0.0	-0.1	-0.2	-0.0	+0.1	-0.0	-0.0	-0.2	-0.1
PDF eigenvector 19	+0.0	+0.0	+0.3	-0.1	-0.0	+0.1	-0.1	-0.0	+0.1
	-0.0	-0.1	-0.5	+0.1	+0.1	-0.1	+0.1	+0.0	-0.1
PDF eigenvector 20	+0.0	+0.0	-0.4	-0.0	-0.0	+0.1	-0.1	-0.0	+0.0
	+0.0	-0.1	-0.1	+0.0	+0.0	-0.0	+0.1	+0.0	-0.0
PDF eigenvector 21	-0.0	-0.0	+0.0	-0.0	-0.0	-0.0	+0.1	+0.2	+0.0
	+0.0	+0.0	+0.1	-0.0	+0.0	+0.0	-0.1	-0.2	-0.0
PDF eigenvector 22	-0.1	-0.0	-0.0	-0.1	-0.0	+0.0	+0.1	+0.3	+0.1
	+0.1	+0.0	+0.1	-0.0	+0.1	+0.0	-0.2	-0.3	-0.1
PDF eigenvector 23	+0.0	-0.0	-0.5	+0.2	+0.0	-0.1	+0.0	-0.1	-0.2
	+0.0	-0.0	-0.1	-0.0	+0.0	+0.0	-0.1	-0.0	+0.0
PDF eigenvector 24	-0.0	+0.0	-0.4	+0.1	-0.0	+0.0	-0.1	-0.0	-0.0
	-0.1	-0.0	-0.3	+0.2	-0.1	-0.1	+0.3	+0.3	-0.1
PDF eigenvector 25	-0.1	+0.0	-0.4	+0.2	-0.1	-0.1	+0.2	+0.3	-0.1
	-0.0	+0.0	-0.7	+0.1	-0.0	-0.0	-0.0	+0.0	-0.0
PDF eigenvector 26	+0.0	-0.0	-0.1	+0.0	+0.0	+0.0	-0.0	-0.0	-0.0
	-0.0	+0.0	-0.2	+0.0	+0.0	+0.0	-0.0	-0.0	+0.0
PDF eigenvector 27	-0.1	+0.3	-0.0	+0.2	-0.3	+0.1	-0.2	+0.2	+0.0
	+0.0	-0.1	+0.1	-0.1	+0.1	-0.0	+0.1	-0.1	+0.0
PDF eigenvector 28	-0.0	+0.1	-0.3	+0.1	-0.1	+0.1	-0.1	+0.0	-0.0
	+0.0	-0.1	+0.3	-0.2	+0.1	-0.0	+0.1	-0.1	+0.0
α_s	-0.1	+0.3	+0.2	+0.3	-0.2	+0.1	-0.2	+0.1	-0.0
	+0.1	-0.3	-0.2	-0.2	+0.2	-0.1	+0.2	-0.1	+0.0
m_t	-0.5	-2.7	-1.7	+0.5	+0.9	-0.2	+0.4	+1.4	+2.1
	+0.5	+2.5	+3.6	-0.2	-0.8	+0.1	-1.1	-1.2	-2.1
$\mu_{r,f}$	-0.7	+1.7	+10.2	+2.1	-2.2	+0.0	-0.4	+1.8	-0.3
	+0.9	-1.8	-14.6	-2.2	+2.3	+0.2	+0.1	-2.0	+0.5
h_{damp}	+0.2	-0.4	-6.7	-0.1	-0.0	+0.7	-0.4	+0.7	+0.1
	-0.5	-0.1	+11.3	+0.3	+0.4	-0.8	-0.6	+1.1	-0.3
PS ISR	-0.1	-0.6	+1.1	+0.1	+0.5	+0.1	-0.7	+0.1	+0.1
	-0.0	-0.6	+3.8	+0.2	+0.3	-0.5	-1.4	+1.2	-0.1
PS FSR	-0.4	+1.3	+7.4	+1.4	-0.4	-0.8	+0.0	-0.0	-1.4
	+0.2	-1.2	-0.7	-0.5	+0.5	-0.4	-0.6	+0.3	+1.0
UE tune	+0.1	-0.1	+4.3	+0.4	+0.2	-1.4	-1.8	+0.7	+0.0
	-0.2	+0.0	+2.7	+0.2	+0.3	-0.1	-0.5	+0.3	-0.2
CR	-0.2	-0.4	+1.1	+0.2	+0.3	-0.2	+0.9	-0.9	+0.6
	+0.1	-0.3	-0.3	-0.3	+0.2	-0.7	+0.2	+0.6	+0.1
	-0.1	-0.2	-1.4	-0.6	+0.3	-0.1	-0.1	+1.4	+0.0
$f(b \rightarrow B)$	-0.1	+0.7	-0.6	+0.9	-0.7	-0.3	-0.2	-0.1	+0.2
	+0.0	-0.3	+0.3	-0.4	+0.3	+0.2	+0.0	+0.1	-0.0
	-0.0	+0.1	-0.1	+0.2	-0.2	-0.0	-0.1	+0.0	+0.0
	+0.2	+0.5	-1.3	+0.3	-0.6	-0.2	-0.5	-0.3	+0.2
$\text{BR}(B \rightarrow \mu)$	-0.0	-0.0	-0.2	+0.1	+0.0	+0.1	-0.1	+0.0	-0.1
	+0.1	-0.1	+0.2	-0.1	-0.1	-0.1	+0.0	-0.0	+0.1

Table 61: The measured $[N_{\text{jet}}^{0,1,2+}, M(\text{t}\bar{\text{t}}), y(\text{t}\bar{\text{t}})]$ cross sections, along with their relative statistical and systematic uncertainties, and NP corrections (see Section 8).

N_{jet}	$M(\text{t}\bar{\text{t}})$ [GeV]	$y(\text{t}\bar{\text{t}})$	$\frac{1}{\sigma(\text{t}\bar{\text{t}})} \frac{d\sigma}{dy(\text{t}\bar{\text{t}})}$	stat. [%]	syst. [%]	\mathcal{C}_{NP}	bin
0	300–400	0.00–0.35	8.224×10^{-2}	4.6	$^{+12.9}_{-8.5}$	0.973	1
0	300–400	0.35–0.75	8.712×10^{-2}	3.7	$^{+6.9}_{-12.6}$	0.974	2
0	300–400	0.75–1.15	7.671×10^{-2}	4.1	$^{+6.3}_{-14.5}$	0.973	3
0	300–400	1.15–2.50	3.590×10^{-2}	4.0	$^{+8.4}_{-9.4}$	0.975	4
0	400–500	0.00–0.35	1.368×10^{-1}	2.7	$^{+2.4}_{-3.6}$	0.971	5
0	400–500	0.35–0.75	1.234×10^{-1}	2.4	$^{+5.5}_{-2.2}$	0.971	6
0	400–500	0.75–1.15	1.032×10^{-1}	2.9	$^{+5.3}_{-1.4}$	0.972	7
0	400–500	1.15–2.50	4.739×10^{-2}	2.3	$^{+4.8}_{-3.3}$	0.974	8
0	500–1500	0.00–0.35	1.625×10^{-1}	1.8	$^{+3.7}_{-5.5}$	0.976	9
0	500–1500	0.35–0.75	1.422×10^{-1}	2.0	$^{+6.3}_{-3.5}$	0.978	10
0	500–1500	0.75–1.15	1.123×10^{-1}	2.4	$^{+3.7}_{-6.4}$	0.977	11
0	500–1500	1.15–2.50	3.223×10^{-2}	3.5	$^{+7.0}_{-7.0}$	0.982	12
≥ 1	300–400	0.00–0.35	6.493×10^{-2}	5.9	$^{+12.9}_{-4.8}$	1.033	13
≥ 1	300–400	0.35–0.75	6.231×10^{-2}	5.1	$^{+10.6}_{-5.0}$	1.031	14
≥ 1	300–400	0.75–1.15	5.557×10^{-2}	5.5	$^{+8.1}_{-7.4}$	1.035	15
≥ 1	300–400	1.15–2.50	2.482×10^{-2}	5.2	$^{+5.8}_{-14.6}$	1.037	16
≥ 1	400–500	0.00–0.35	1.220×10^{-1}	3.1	$^{+4.4}_{-9.2}$	1.036	17
≥ 1	400–500	0.35–0.75	1.083×10^{-1}	2.7	$^{+4.3}_{-8.5}$	1.034	18
≥ 1	400–500	0.75–1.15	8.512×10^{-2}	3.5	$^{+9.0}_{-5.4}$	1.036	19
≥ 1	400–500	1.15–2.50	3.283×10^{-2}	3.1	$^{+9.0}_{-4.6}$	1.037	20
≥ 1	500–1500	0.00–0.35	1.556×10^{-1}	1.7	$^{+7.6}_{-4.9}$	1.024	21
≥ 1	500–1500	0.35–0.75	1.362×10^{-1}	2.0	$^{+3.7}_{-8.2}$	1.024	22
≥ 1	500–1500	0.75–1.15	9.834×10^{-2}	2.5	$^{+7.3}_{-5.4}$	1.025	23
≥ 1	500–1500	1.15–2.50	2.700×10^{-2}	3.6	$^{+9.7}_{-8.1}$	1.022	24

Table 62: The correlation matrix of statistical uncertainties for the measured $[N_{\text{jet}}^{0,1,2+}, M(\text{t}\bar{\text{t}}), y(\text{t}\bar{\text{t}})]$ cross sections. The values are expressed as percentages. For bin indices see Table 110.

Table 63: Sources and values of the relative systematic uncertainties in percent of the measured $[N_{\text{jet}}^{0,1,2+}, M(\text{t}\bar{\text{t}}), y(\text{t}\bar{\text{t}})]$ cross sections. For bin indices see Table 110.

source / bin	1	2	3	4	5	6	7	8	9	10	11	12	13	14	15	16	17	18	19	20	21	22	23	24	
JER	+0.2 -0.4	+0.6 -1.0	+0.4 -2.1	+0.8 -0.8	+0.1 -0.7	+0.7 +0.2	+0.5 -0.2	+0.8 +0.1	+0.1 -0.3	+0.5 -0.4	+0.2 +0.1	+0.9 +2.1	-0.6 +0.0	-0.1 +0.0	+0.1 +0.7	-0.8 -0.4	-0.5 +0.4	-0.6 -0.2	+0.3 +0.5	-1.0 +1.2	-0.6 +0.6	-0.6 +0.6	-0.5 +0.1	-1.8 +0.4	
JESAbsoluteMPFBias	+0.8 -0.8	+0.4 -0.9	-0.1 -1.5	+0.7 -0.3	-0.1 -0.1	+0.1 +0.1	+0.4 +0.1	+0.4 +0.1	+0.3 -0.1	-0.0 +0.2	+0.2 +0.0	-0.5 -0.0	+1.2 -0.3	+0.7 -0.8	+0.3 +0.2	-0.2 -0.8	-0.4 -0.8	-0.6 +0.5	-0.6 +0.3	-0.2 +0.5	-0.5 +0.4	-0.4 +0.5	-0.3 +0.2	-1.0 +0.7	
JESAbsoluteScale	+0.6 -0.7	+0.0 -0.7	+0.0 -1.1	+0.6 -1.4	-0.1 -0.4	+0.1 -0.1	+0.4 -0.0	+0.3 +0.3	+0.1 +0.2	-0.1 -0.1	+0.1 +0.1	+0.2 -0.3	-0.0 -0.4	+0.5 +0.2	+0.7 +0.2	+0.0 -0.2	+0.1 -0.4	-0.2 +0.4	-0.4 +0.3	-0.5 -0.1	+0.2 +0.2	-0.3 +0.3	-0.4 +0.3	-1.3 +0.3	
JESAbsoluteStat	+0.4 -1.2	+1.0 -0.4	-1.1 -0.3	-0.3 -0.3	-0.4 +0.4	-0.0 +0.1	-0.2 +0.4	+0.5 +0.3	+0.2 -0.4	+0.2 -0.3	+0.2 -0.5	+0.7 +0.6	+0.5 -0.6	+1.0 -0.6	+0.1 -0.1	+0.1 +1.4	+0.6 -0.0	-0.7 +0.3	-0.6 +0.3	-0.7 +0.3	-0.6 +0.2	+0.1 +0.2	+0.3 -0.2	+0.0 -0.7	
JESFlavourQCD	+3.0 -3.3	+2.9 -3.7	+1.4 -3.4	+2.0 -2.1	+0.0 -0.2	+0.9 -0.4	+0.3 -0.1	+1.1 -1.4	+1.2 -1.4	+1.3 -0.8	+1.1 -0.9	+1.3 -0.6	+1.0 -0.2	+1.9 +0.8	+0.0 +0.5	-0.8 +0.5	-2.5 +1.9	-2.7 +1.9	-2.4 +2.4	-1.3 +2.7	-1.3 +1.8	-1.6 +1.4	-1.4 +1.4	-2.3 +1.5	
JESFragmentation	+0.2 -0.4	-0.2 -0.6	-0.1 -1.2	+0.4 -0.1	+0.2 -0.1	+0.5 -0.0	+0.6 +0.0	+0.5 +0.2	+0.3 -0.2	+0.3 -0.2	-0.2 -0.2	-0.4 -0.2	+0.4 -0.2	+0.4 -0.2	+0.4 +0.1	+0.1 +0.1	-0.7 +0.4	-0.5 +0.3	-0.6 +0.3	-0.6 +0.2	-0.2 +0.2	-0.1 +0.1	+0.2 +0.0	-0.7 +0.2	
JESPileUpDataMC	+0.6 -0.6	+0.1 -1.0	-0.5 -1.1	-0.0 -0.5	+0.0 +0.1	+0.5 +0.2	+0.5 -0.1	+0.8 -0.3	+0.3 -0.3	+0.4 -0.4	+0.3 -0.2	+0.6 -0.5	+0.0 +0.4	-0.2 +0.7	-0.1 +0.9	-0.1 +0.0	-0.4 +0.6	-0.5 +0.4	-0.6 +0.4	-0.3 +0.0	-0.6 +0.2	-0.2 +0.4	-0.3 +0.1	+0.1 -0.1	-1.2 +0.4
JESPileUpPtBB	+0.1 -0.2	-0.3 -0.5	-0.5 -0.5	+0.2 -0.2	+0.5 -0.0	+0.6 -0.1	+0.4 -0.3	+0.5 -0.3	+0.2 -0.2	+0.2 -0.2	-0.2 -0.2	-0.2 -0.1	+0.5 +0.5	+0.4 +1.7	+0.4 +1.9	-0.7 -0.0	-0.2 +0.2	-1.0 -0.1	-0.2 -0.2	-0.4 -0.1	-0.5 +0.3	-0.0 +0.0	-0.1 -0.2	-0.0 +0.0	
JESPileUpPtEC1	+1.1 -0.9	+1.5 -1.2	-0.1 -1.3	+0.2 -0.2	+0.2 -0.7	+0.5 -0.4	+0.4 -0.1	+0.4 -0.3	+0.5 -0.6	+0.6 -0.7	+0.9 -0.7	+0.7 -0.4	+0.4 -0.1	+0.4 -0.1	+0.5 +0.9	+0.5 +1.8	-0.2 +0.4	-2.4 +0.4	-0.4 +0.4	-0.8 +0.4	-0.8 +0.9	-1.0 +1.3	-0.5 +0.5	-0.3 +0.5	-1.3 +0.5
JESPileUpPtEC2	+0.0 +0.0																								
JESPileUpPtHF	+0.0 +0.0																								
JESPileUpPtRef	+0.2 -0.2	-0.0 -1.0	-0.4 -1.1	+0.4 +0.0	+0.3 -0.3	+0.3 -0.2	-0.6 -0.6	-0.7 -0.7	-0.7 -0.7	-0.4 -0.4	-0.1 -0.3	-0.3 +0.9	-0.1 +1.6	-0.6 +0.7	-0.7 +0.4	-0.5 +0.3	-0.5 +0.3	-0.1 +0.3	-0.6 +0.5	-0.1 +0.1	-0.6 +0.3	-0.1 +0.3	-0.8 +0.0		
JESRelativeBal	+2.0 -2.8	+2.4 -2.9	+1.7 -2.9	+2.0 -2.9	+0.0 -2.9	+0.5 -1.8	-0.1 -1.8	+0.5 -0.2	-0.1 -0.3	+0.1 -0.2	+0.2 -0.2	+0.6 -0.2	+0.4 -0.2	+0.4 -0.2	+0.5 -0.3	+0.5 +0.5	+0.6 +1.2	+0.6 +1.5	-2.2 -1.5	-1.0 -0.5	-0.8 -0.8	-0.8 -0.9	-0.9 -0.9	-1.0 -1.1	
JESRelativeFSR	-0.6 +0.2	-0.9 +0.6	-0.8 +0.3	-0.3 +0.1	+0.2 +0.3	+0.1 +0.1	+0.2 +0.3	+0.2 +0.2	+0.0 +0.3	+0.0 +0.0															
JESRelativeJEREC1	-0.0 -0.0	+0.0 -0.7	-0.2 +0.2	+0.2 +0.0	+0.0 +0.0	+0.0 +0.0	+0.1 +0.4	+0.1 +0.0	-0.2 -0.2	-0.2 -0.2	-0.3 -0.3	+0.1 +0.1	-0.0 -0.0	+0.3 +0.3	-0.4 -0.6	-0.1 -0.1	+0.0 +0.0	-0.2 -0.2	+0.0 +0.1	-0.0 +0.0	+0.0 +0.1	-0.4 -0.1	+0.2 +0.8		
JESRelativeJEREC2	+0.0 +0.0																								
JESRelativeJERHF	+0.0 +0.0																								
JESRelativePtBB	+0.3 -0.4	+0.3 -1.6	+0.1 -0.8	+0.2 +0.3	+0.2 +0.3	+0.1 +0.5	+0.1 -0.1	+0.1 -0.1	+0.1 -0.1	-0.0 -0.0	+0.0 -0.5	+0.5 +0.8	+0.1 +0.3	+0.3 -0.9	-0.3 +0.5	-0.5 +0.0	-0.1 -0.1	+0.1 +0.2	+0.1 +0.1	+0.1 +0.1	+0.1 +0.1	+0.1 +0.1	+0.1 +0.1	+0.1 +0.1	
JESRelativePtEC1	+0.0 -0.6	+1.2 -0.8	+0.3 -1.1	+0.5 -1.1	+0.3 -0.5	+0.4 -0.5	+0.4 -0.4	+0.1 -0.3	+0.3 -0.3	+0.3 -0.4	+0.2 -0.1	+0.3 -0.7	+0.1 -0.7	-0.7 -0.7	-0.8 -0.8	+0.5 +0.5	-0.1 -0.1	+0.2 +0.2	+0.5 +0.5	+0.7 +0.7	+0.3 +0.3	+0.5 +0.5	+0.4 +0.6		
JESRelativePtEC2	+0.0 +0.0																								
JESRelativePtHF	+0.0 +0.0																								
JESRelativeStatEC	+0.0 -0.2	+0.3 -0.4	-0.0 -1.0	+0.2 +0.1	+0.1 -0.1	+0.1 +0.1	+0.1 +0.4	+0.4 -0.1	-0.1 -0.1	+0.1 +0.1	+0.2 +0.2	+0.1 +0.3	+0.3 -0.8	-0.4 -0.2	-0.5 -0.2	-0.1 -0.2	-0.1 -0.2	-0.1 -0.1							
JESRelativeStatFSR	+0.0 -0.0	+0.1 +0.8	-0.3 -0.8	+0.1 -0.2	+0.1 +0.1	+0.3 +0.3	+0.2 +0.3	+0.2 +0.3	-0.1 -0.1	+0.1 +0.1	-0.1 -0.2	-0.2 -0.2	-0.1 -0.2	-0.2 -0.2											
JESRelativeStatHF	+0.0 +0.0																								
JESSinglePionECAL	-0.7 +0.3	-1.1 -0.0	-0.8 +0.3	-0.0 +0.0	+0.1 +0.6	+0.2 +0.5	+0.0 +0.7	+0.6 +0.6	+0.0 +0.2	+0.0 -0.2	-0.2 -0.2	+0.5 +0.3	+0.3 +0.7	+0.7 +0.2	+0.2 +0.3	+0.3 +0.3	+0.4 +0.4	+0.2 +0.2	+0.1 +0.1	+0.4 +0.4	+0.2 +0.2	+0.3 +0.3	+0.3 +0.3	+0.3 +0.3	

Table 64: Table 112 continued.

source / bin	1	2	3	4	5	6	7	8	9	10	11	12	13	14	15	16	17	18	19	20	21	22	23	24
JESSinglePionHCAL	-0.3	-0.9	-0.6	-0.1	-0.4	+0.1	+0.2	-0.1	-0.3	-0.2	-0.6	+0.2	+0.2	-0.3	+0.1	+0.2	+0.6	+0.5	+0.5	+0.2	+0.2	+0.2	+0.0	
	+0.3	-0.1	-0.5	+0.5	+0.2	+0.6	+0.5	+0.6	+0.5	+0.1	-0.1	-0.3	+0.3	+0.7	+0.2	-0.7	-0.6	-0.6	-0.6	-0.1	-0.3	-0.1	+0.1	-0.8
JESTimePtEta	-0.1	-0.1	-0.4	-0.1	-0.2	-0.1	+0.3	+0.0	+0.3	-0.1	+0.1	+0.0	-0.0	-0.1	+0.0	+0.3	+0.2	+0.1	-0.4	+0.0	-0.3	+0.0	-0.1	+0.3
	-0.2	+0.2	+0.0	+0.1	+0.0	+0.3	-0.0	-0.1	+0.1	-0.2	+0.1	+0.4	+0.4	+0.1	+0.1	+0.2	+0.0	-0.1	+0.0	+0.0	-0.1	+0.1	-0.1	-1.6
E_T^{miss}	-2.4	-0.3	-1.1	-0.2	+0.3	+0.3	-0.3	-0.2	+0.1	+0.1	+0.6	+0.3	+1.2	+0.3	+0.2	+0.5	-0.4	-0.0	+0.1	+0.0	+0.3	+0.1	+0.2	-0.1
	-0.1	-0.2	+0.8	+0.4	-0.1	-0.3	+0.2	+0.8	-0.1	+0.1	-0.5	-0.6	-0.4	+0.5	-0.4	+0.8	-0.1	+0.1	+0.0	-0.2	-0.2	-0.3	-0.2	+0.1
lepton ID/ISO	-0.3	+0.0	-0.5	-0.3	+0.1	+0.2	+0.1	+0.6	-0.1	-0.1	-0.7	-0.0	+0.1	-0.0	+0.1	+0.3	+0.4	+0.3	+0.6	-0.1	-0.1	-0.2	-0.7	
	+0.3	-0.0	+0.5	+0.3	-0.1	-0.2	-0.1	-0.6	+0.1	+0.1	+0.7	+0.0	-0.1	+0.0	-0.1	-0.3	-0.4	-0.3	-0.6	+0.2	+0.1	+0.2	+0.7	
pileup	+0.6	-0.4	-0.5	-0.5	+0.0	+0.2	+0.4	+0.2	+0.3	+0.4	+0.2	+0.2	-0.4	+0.6	-0.1	-1.0	+0.4	-0.3	-0.5	-0.0	+0.0	-0.4	+0.1	-0.3
	-0.7	+0.3	+0.6	+0.5	-0.0	-0.2	-0.4	-0.3	-0.3	-0.2	-0.2	+0.4	-0.5	+0.2	+1.1	-0.5	+0.2	+0.4	+0.0	+0.0	+0.3	-0.1	+0.3	
trigger	+0.1	+0.2	+0.1	-0.4	+0.2	+0.1	-0.0	-0.1	+0.1	-0.0	-0.1	-0.3	+0.1	+0.2	+0.2	-0.3	+0.2	+0.2	+0.1	-0.2	+0.1	+0.0	-0.1	-0.2
	-0.1	-0.2	-0.1	+0.4	-0.2	-0.1	+0.0	+0.1	-0.1	+0.0	+0.1	+0.3	-0.1	-0.2	-0.2	+0.3	-0.2	-0.2	-0.1	+0.2	-0.1	-0.0	+0.1	+0.2
trigger (η)	-0.3	-0.2	-0.3	+0.7	-0.3	-0.2	-0.2	+0.4	+0.0	-0.1	-0.2	+0.3	-0.2	-0.1	-0.3	+0.8	-0.3	-0.2	-0.2	+0.5	-0.0	-0.1	-0.3	+0.2
	+0.3	+0.2	+0.3	-0.7	+0.3	+0.2	+0.2	-0.4	-0.0	+0.1	+0.2	-0.3	+0.2	+0.1	+0.3	-0.8	+0.3	+0.2	+0.2	-0.5	+0.0	+0.1	+0.3	-0.2
non-tt background	-1.0	-1.0	-2.0	-4.3	-0.3	-0.1	+0.3	-0.3	+0.5	+0.4	+0.5	-0.2	+1.6	+1.8	+1.7	-1.2	+0.4	+0.6	+0.5	+0.8	+1.0	+0.8	+0.8	-0.1
	+1.5	-0.1	+2.0	+4.1	+0.2	+0.6	+0.2	-0.2	-0.5	-0.1	-1.0	+0.7	-1.0	-1.2	-1.3	+1.1	-0.9	-0.8	-0.6	-0.5	-0.8	-0.7	-0.8	-0.0
b-tagging	-0.0	+0.0	-0.1	-0.1	-0.1	-0.1	+0.0	-0.1	-0.1	-0.1	-0.1	-0.5	-0.5	-0.6	-0.2	+0.2	+0.2	+0.2	+0.3	+0.2	+0.3	+0.3	+0.3	+0.3
	+0.0	-0.0	+0.1	+0.1	+0.1	+0.1	-0.0	+0.1	+0.1	+0.1	+0.1	+0.5	+0.5	+0.6	+0.2	-0.2	-0.2	-0.2	-0.2	-0.3	-0.2	-0.3	-0.3	-0.3
b-tagging (light jets)	-0.3	-0.3	-0.6	-1.0	+0.1	+0.2	+0.4	+0.2	+0.2	+0.2	+0.2	+0.1	+0.5	+0.6	+0.3	-1.0	+0.1	+0.1	+0.2	+0.1	+0.0	-0.0	-0.1	-0.2
	+0.3	+0.3	+0.6	+1.0	-0.1	-0.2	-0.4	-0.2	-0.2	-0.2	-0.2	-0.1	-0.5	-0.5	-0.2	+1.0	-0.1	-0.1	-0.2	-0.1	-0.0	+0.0	+0.1	+0.2
luminosity	+0.0	+0.0	+0.0	+0.0	+0.0	+0.0	+0.0	+0.0	+0.0	+0.0	+0.0	+0.0	+0.0	+0.0	+0.0	+0.0	+0.0	+0.0	+0.0	+0.0	+0.0	+0.0	+0.0	+0.0
	+0.0	+0.0	+0.0	+0.0	+0.0	+0.0	+0.0	+0.0	+0.0	+0.0	+0.0	+0.0	+0.0	+0.0	+0.0	+0.0	+0.0	+0.0	+0.0	+0.0	+0.0	+0.0	+0.0	+0.0
BR($t\bar{t} \rightarrow \ell\ell$)	+0.0	+0.0	+0.0	+0.0	+0.0	+0.0	+0.0	+0.0	+0.0	+0.0	+0.0	+0.0	+0.0	+0.0	+0.0	+0.0	+0.0	+0.0	+0.0	+0.0	+0.0	+0.0	+0.0	+0.0
	+0.0	+0.0	+0.0	+0.0	+0.0	+0.0	+0.0	+0.0	+0.0	+0.0	+0.0	+0.0	+0.0	+0.0	+0.0	+0.0	+0.0	+0.0	+0.0	+0.0	+0.0	+0.0	+0.0	+0.0
PDF eigenvector 1	+0.0	+0.0	-0.0	-0.0	-0.0	-0.0	-0.1	+0.0	+0.0	+0.0	-0.0	+0.0	+0.1	+0.0	-0.0	+0.0	-0.0	-0.0	-0.1	-0.1	+0.0	+0.0	+0.1	+0.0
	+0.0	+0.0	+0.0	-0.0	+0.0	-0.0	-0.1	+0.0	+0.0	+0.0	-0.0	+0.0	+0.1	+0.0	-0.0	+0.0	-0.0	-0.0	-0.1	-0.1	+0.0	+0.0	+0.1	+0.0
PDF eigenvector 2	-0.0	-0.1	+0.1	+0.1	-0.3	-0.1	+0.0	+0.2	+0.1	-0.0	-0.1	+0.1	-0.0	+0.1	+0.1	-0.4	-0.2	+0.1	+0.0	+0.3	+0.1	-0.0	-0.1	-0.1
	-0.0	-0.0	+0.0	+0.0	+0.1	+0.0	+0.1	+0.1	-0.1	-0.1	-0.0	+0.1	-0.1	-0.1	-0.0	+0.0	+0.2	+0.1	+0.1	-0.2	-0.1	-0.1	+0.0	-0.0
PDF eigenvector 3	+0.1	+0.1	+0.0	-0.1	+0.1	+0.0	-0.1	-0.2	+0.0	+0.0	+0.1	-0.2	+0.1	+0.1	-0.1	+0.1	+0.0	-0.1	-0.2	+0.1	+0.1	+0.1	+0.1	+0.1
	-0.0	-0.0	-0.0	+0.0	-0.0	-0.0	+0.0	+0.1	-0.0	-0.0	+0.0	+0.2	-0.0	-0.1	-0.0	+0.0	-0.0	+0.1	+0.1	-0.0	-0.0	-0.1	-0.0	-0.0
PDF eigenvector 4	+0.0	-0.0	-0.0	+0.1	-0.2	-0.1	-0.0	+0.0	+0.1	+0.1	-0.0	-0.0	+0.1	+0.0	-0.0	-0.3	-0.1	-0.0	+0.1	+0.2	+0.1	+0.0	-0.1	-0.1
	-0.0	+0.0	+0.0	-0.0	+0.1	+0.0	+0.0	-0.0	-0.0	-0.0	-0.0	-0.0	-0.0	-0.0	-0.0	+0.1	+0.0	+0.0	-0.0	-0.1	-0.0	-0.1	-0.0	-0.0
PDF eigenvector 5	-0.1	-0.3	-0.1	+0.1	+0.1	+0.1	+0.2	+0.2	-0.2	-0.1	-0.3	+0.5	-0.1	-0.2	-0.1	+0.1	+0.1	+0.1	+0.3	+0.4	-0.3	-0.2	-0.3	-0.1
	+0.1	+0.2	+0.1	-0.1	+0.1	+0.1	-0.1	-0.3	+0.1	+0.1	+0.1	+0.1	-0.4	+0.1	+0.3	+0.1	-0.1	+0.0	-0.3	-0.5	+0.2	+0.2	+0.1	+0.1
PDF eigenvector 6	+0.0	+0.0	-0.0	-0.1	-0.0	-0.1	-0.0	+0.0	-0.1	-0.0	-0.0	-0.0	-0.0	-0.0	-0.0	-0.0	-0.2	-0.1	-0.1	-0.0	-0.0	-0.1	-0.0	-0.0
	-0.0	-0.0	+0.0	+0.0	+0.0	+0.0	+0.0	-0.0	-0.1	-0.0	-0.0	-0.0	-0.0	-0.0	-0.0	-0.0	-0.0	-0.1	-0.0	-0.1	-0.0	-0.1	-0.0	-0.0
PDF eigenvector 7	-0.2	-0.2	-0.0	+0.1	+0.1	+0.1	+0.3	+0.5	-0.3	-0.2	-0.2	+0.5	-0.3	-0.4	-0.1	+0.2	+0.3	+0.3	+0.5	-0.5	-0.4	-0.5	-0.2	
	+0.1	+0.1	+0.0	-0.1	-0.0	-0.2	-0.3	+0.1	+0.2	+0.1	-0.3	+0.2	+0.3	+0.1	-0.1	-0.1	-0.1	-0.3	-0.3	+0.3	+0.2	+0.3	+0.1	
PDF eigenvector 8	-0.1	-0.0	-0.1	-0.0	+0.0	+0.1	+0.0	-0.1	-0.1	-0.0	-0.1	-0.0	-0.0	-0.0	-0.0	-0.0	-0.0	-0.0	-0.1	-0.0	-0.1	-0.0	-0.1	-0.0
	+0.1	+0.0	+0.1	-0.0	-0.1	-0.0	-0.1	-0.0	-0.1	-0.0	-0.0	-0.0	-0.0	-0.0	-0.0	-0.0	-0.0	-0.1	-0.0	-0.1	-0.0	-0.1	-0.0	-0.0
PDF eigenvector 9	+0.0	-0.0	+0.1	-0.0	-0.0	-0.0	-0.0	-0.0	-0.0	-0.0	-0.2	+0.1	-0.0	-0.0	-0.0	-0.0	-0.0	-0.0	-0.1	-0.0	-0.0	-0.0	-0.0	-0.1
	-0.0	+0.0	-0.1	-0.1	-0.0	-0.0	-0.0	-0.0	-0.0	-0.0	-0.0	-0.0	-0.0	-0.0	-0.0	-0.0	-0.0	-0.0	-0.0	-0.0	-0.0	-0.0	-0.0	-0.1
PDF eigenvector 10	+0.1	+0.1	-0.0	-0.1	-0.0	-0.2	+0.1	+0.1	-0.1	-0.2	-0.2	+0.2	+0.0	-0.1	-0.2	-0.1	-0.3	-0.3	+0.2	+0.2	+0.2	+0.1	+0.0	
	-0.1	-0.1	+0.0	+0.1	+0.1	+0.0	+0.1	-0.1	-0.1	-0.2	-0.2	-0.0	+0.1	+0.2	+0.1	+0.3	+0.3	+0.2	+0.2	-0.3	-0.1	-0.1	-0.1	-0.1
PDF eigenvector 11	+0.0	+0.0	-0.0	-0.0	-0.0	-0.1	-0.0	-0.0	-0.0	-0.1	-0.0	-0.0	-0.0	-0.0	-0.0	-0.0	-0.0	-0.0	-0.0	-0.1	-0.1	-0.1	-0.1	-0.0
	-0.0	-0.1	+0.0	+0.0	+0.0	-0.0	-0.1	-0.1	-0.0	-0.2	-0.1	-0.1	-0.0	-0.0	-0.0	-0.1	-0.0	-0.0	-0.1	-0.1	-0.1	-0.1	-0.0	-0.0
PDF eigenvector 12	-0.1	-0.1	-0.0	+0.0	+0.0	+0.1	+0.2	-0.1	-0.1	-0.1	-0.1	-0.1	-0.1	-0.0	-0.0	-0.1	-0.1	-0.1	-0.1	-0.2	+0.1	-0.1	-0.1	-0.0
	+0.1	+0.1	+0.0	-0.0	-0.0	-0.1	-0.1	-0.1	-0.1	-0.1	-0.1	-0.1	-0.1	-0.0	-0.0	-0.1	-0.1	-0.1	-0.1	-0.2	+0.1	+0.1	+0.0	+0.0
PDF eigenvector 13	+0.0	+0.1	-0.0	+0.1	+0.1	-0.0	-0.0	-0.1	-0.0	-0.0	-0.0	-0.0	-0.0	-0.0	-0.0	-0.1	+0.2	+0.1	-0.0	-0.1	-0.1	-0.1	-0.0	-0.0
	-0.0	-0.0	+0.0	+0.1	-0.1	-0.1	+0.0	+0.0	-0.0	-0.0	-0.0	-0.0	-0.0	-0.0	-0.0	-0.1	-0.2	-0.1	+0.0	+0.1	+0.1	+0.0	+0.0	-0.0
PDF eigenvector 14	-0.0	-0.0	+0.0	+0.0	+0.0	-0.0	-0.0	-0.1	-0.1	-0.0	-0.0	-0.0	-0.1	-0.1	-0.1	-0.1	-0.0	-0.1	-0.1	-0.1	-0.1	-0.1	-0.1	-0.0
	+0.0	+0.0	+0.0	-0.0	-0.0	-0.0	-0.0	-0.1	-0.1	-0.0	-0.0	-0.1	-0.1	-0.1	-0.0	-0.1	-0.1	-0.1	-					

Table 65: Table 112 continued.

source / bin	1	2	3	4	5	6	7	8	9	10	11	12	13	14	15	16	17	18	19	20	21	22	23	24
PDF eigenvector 15	-0.0	-0.0	+0.0	-0.0	+0.1	+0.1	+0.0	+0.1	-0.0	-0.0	-0.0	+0.0	-0.1	-0.1	-0.0	-0.0	+0.1	+0.1	+0.1	+0.1	-0.1	-0.1	-0.0	
	+0.0	+0.0	-0.0	+0.0	-0.0	-0.0	-0.0	-0.0	+0.0	+0.0	+0.0	-0.0	+0.0	+0.0	-0.0	-0.0	-0.0	-0.0	-0.0	+0.0	+0.0	+0.0	+0.0	
PDF eigenvector 16	+0.0	+0.0	-0.0	-0.0	-0.0	-0.0	-0.0	-0.0	+0.0	+0.0	+0.0	+0.0	+0.0	+0.0	-0.0	-0.0	-0.0	-0.0	-0.0	-0.0	+0.0	+0.0	+0.0	
	+0.1	-0.2	-0.0	+0.1	-0.0	+0.1	+0.1	-0.0	-0.0	+0.0	-0.1	+0.1	+0.1	+0.0	-0.0	-0.0	-0.1	-0.0	+0.0	+0.1	-0.0	-0.0	-0.0	
PDF eigenvector 17	-0.0	-0.0	+0.0	+0.0	-0.0	-0.0	+0.0	+0.0	-0.0	-0.0	-0.0	+0.0	-0.0	-0.1	+0.0	+0.0	+0.0	+0.1	+0.0	-0.0	-0.0	-0.0	-0.0	
	+0.0	+0.0	-0.0	-0.1	+0.0	+0.0	-0.1	+0.0	+0.0	+0.0	+0.0	+0.1	+0.1	-0.0	-0.1	-0.0	-0.0	-0.1	+0.0	+0.1	+0.1	+0.1	+0.1	
PDF eigenvector 18	+0.1	-0.0	+0.0	+0.0	-0.2	-0.1	-0.1	+0.1	+0.1	+0.1	+0.0	+0.1	+0.1	+0.0	+0.1	-0.3	-0.2	-0.1	-0.0	+0.2	+0.2	+0.2	+0.0	
	-0.1	+0.0	-0.0	-0.0	+0.2	+0.1	+0.1	-0.1	-0.1	-0.1	-0.0	-0.1	-0.0	-0.0	-0.1	+0.3	+0.2	+0.1	+0.0	-0.2	-0.1	-0.2	-0.0	
PDF eigenvector 19	+0.1	+0.1	+0.0	-0.0	-0.1	-0.1	-0.1	-0.2	+0.1	+0.1	+0.1	-0.2	+0.1	+0.1	+0.0	-0.0	-0.1	-0.1	-0.2	-0.2	+0.2	+0.2	+0.0	
	-0.1	-0.1	-0.0	+0.0	+0.1	+0.1	+0.1	+0.3	-0.2	-0.2	-0.1	+0.3	-0.2	-0.2	-0.0	+0.0	+0.2	+0.2	+0.3	+0.3	-0.3	-0.3	-0.1	
PDF eigenvector 20	+0.0	+0.0	+0.0	+0.0	-0.0	-0.0	-0.0	-0.1	+0.0	+0.0	+0.1	+0.0	+0.0	-0.0	-0.1	+0.0	-0.0	-0.0	-0.0	+0.1	+0.0	+0.1	-0.2	
	-0.0	-0.0	-0.0	-0.0	+0.0	+0.0	+0.0	+0.1	-0.0	-0.1	-0.1	+0.0	-0.1	-0.0	+0.0	+0.0	+0.1	+0.1	+0.1	-0.1	-0.1	-0.1	-0.0	
PDF eigenvector 21	-0.0	-0.1	-0.0	+0.0	-0.1	-0.1	-0.0	+0.1	+0.0	+0.0	-0.0	+0.2	+0.0	-0.1	-0.0	+0.1	-0.2	-0.1	+0.0	+0.1	+0.1	+0.0	-0.0	
	+0.0	+0.1	+0.0	-0.1	+0.1	+0.1	-0.0	-0.1	-0.0	+0.0	-0.0	-0.1	+0.0	+0.1	+0.0	-0.1	+0.2	+0.1	-0.1	-0.2	-0.0	+0.0	+0.0	
PDF eigenvector 22	-0.0	-0.1	-0.1	+0.1	-0.3	-0.2	+0.0	+0.2	+0.0	+0.0	-0.0	+0.3	+0.1	-0.1	-0.1	+0.2	-0.4	-0.3	+0.1	+0.3	+0.1	+0.1	-0.0	
	+0.0	+0.1	+0.0	-0.1	+0.3	+0.2	-0.0	-0.2	-0.0	+0.0	+0.0	-0.2	-0.0	+0.1	+0.0	-0.1	+0.3	+0.2	-0.1	-0.3	-0.1	-0.0	+0.1	
PDF eigenvector 23	-0.1	+0.0	+0.1	-0.1	+0.3	+0.2	+0.1	+0.0	-0.1	-0.1	-0.1	-0.2	-0.2	-0.1	+0.1	-0.1	+0.5	+0.3	+0.2	-0.1	-0.2	-0.2	-0.1	
	+0.0	-0.0	-0.0	+0.0	-0.0	-0.0	-0.0	+0.0	-0.0	-0.0	+0.0	+0.2	-0.0	-0.0	-0.1	+0.0	-0.0	-0.1	-0.0	+0.1	-0.0	-0.0	+0.0	
PDF eigenvector 24	-0.0	-0.0	-0.0	+0.0	+0.1	+0.0	+0.0	+0.1	-0.1	-0.1	-0.0	+0.2	-0.1	-0.1	-0.1	+0.0	+0.1	+0.0	+0.1	-0.2	-0.1	-0.1	+0.0	
	-0.1	-0.1	+0.1	+0.1	-0.1	+0.0	+0.1	+0.1	+0.1	-0.0	-0.1	-0.1	-0.2	-0.2	-0.1	+0.1	-0.1	+0.2	+0.1	+0.0	-0.1	-0.2	-0.2	
PDF eigenvector 25	-0.1	-0.1	+0.1	+0.1	-0.0	+0.0	+0.1	+0.1	+0.0	-0.0	-0.1	-0.1	-0.2	-0.2	-0.1	+0.0	+0.1	+0.1	+0.2	+0.0	-0.0	-0.1	-0.2	
	-0.1	-0.1	-0.1	+0.0	+0.1	+0.1	+0.2	-0.2	-0.2	-0.1	+0.4	-0.2	-0.2	-0.1	+0.1	+0.2	+0.1	+0.2	+0.3	-0.3	-0.2	-0.2	+0.0	
PDF eigenvector 26	-0.0	+0.0	+0.0	-0.0	+0.0	+0.0	+0.0	+0.0	-0.0	-0.0	-0.0	-0.0	-0.0	-0.0	-0.0	+0.0	-0.0	+0.1	+0.0	+0.0	-0.0	-0.0	-0.0	
	-0.0	-0.0	-0.0	+0.0	+0.0	-0.0	+0.0	+0.0	-0.0	-0.0	+0.0	+0.1	-0.0	-0.0	-0.0	+0.0	-0.0	+0.0	+0.0	-0.0	-0.0	-0.0	-0.0	
PDF eigenvector 27	+0.1	+0.0	+0.2	+0.1	-0.1	+0.1	-0.2	+0.1	+0.1	+0.0	-0.3	+0.1	+0.0	+0.1	+0.1	-0.1	-0.1	+0.0	-0.2	+0.2	+0.1	+0.1	-0.1	
	-0.0	-0.0	-0.0	-0.0	-0.0	+0.0	-0.0	+0.0	-0.0	+0.0	-0.0	+0.1	-0.0	-0.0	-0.0	-0.0	-0.0	-0.0	+0.0	+0.0	-0.0	-0.0	-0.0	
PDF eigenvector 28	+0.0	+0.0	-0.0	-0.0	+0.0	+0.0	-0.0	-0.0	-0.0	-0.0	+0.0	-0.0	-0.0	-0.0	-0.0	+0.0	+0.0	+0.1	-0.0	-0.0	+0.0	+0.0	+0.0	
	-0.0	-0.0	-0.1	-0.0	-0.0	-0.0	-0.0	+0.1	-0.0	-0.0	-0.0	-0.0	-0.0	-0.0	-0.0	-0.0	-0.0	-0.0	-0.0	+0.1	+0.0	+0.0	+0.0	
α_s	+0.1	+0.0	+0.1	+0.0	-0.0	+0.0	-0.2	+0.0	-0.0	+0.0	-0.1	+0.0	+0.0	+0.1	+0.0	+0.0	+0.0	-0.2	+0.1	+0.0	+0.1	-0.0	-0.0	
	-0.1	-0.0	-0.1	-0.0	-0.0	+0.0	-0.0	+0.2	-0.0	-0.0	-0.0	+0.2	-0.0	-0.0	-0.1	-0.0	-0.0	+0.0	+0.2	-0.1	-0.0	-0.1	+0.0	
m_t	+1.8	-0.1	+0.6	-0.7	-0.8	-0.1	-0.4	-0.6	+0.2	+0.5	+0.0	+0.1	+1.0	+0.2	-1.2	-1.1	-0.6	+0.3	+0.5	+0.3	+0.6	-0.1	-0.0	
	+0.5	-1.9	-1.1	+0.8	+0.5	+1.0	+0.7	-0.4	-0.6	+0.1	-0.8	-0.3	-0.2	+1.2	-0.6	+0.1	-0.1	-0.1	+0.4	+0.8	+0.3	-0.7	+0.1	
$\mu_{r,f}$	+0.6	+0.2	+1.1	+0.5	-0.4	-0.5	+0.0	-1.3	-0.1	-0.5	-0.6	-2.2	+0.9	+0.2	+1.0	+0.8	-0.4	-0.4	-0.1	-0.8	+1.6	+1.1	+0.2	
	-0.7	-0.2	-1.2	-0.6	+0.5	+0.6	+0.1	+1.4	+0.3	+0.7	+1.2	+3.5	-1.0	-0.2	-1.1	-1.0	+0.4	+0.3	-0.1	+0.5	-2.1	-1.5	-1.7	
h_{damp}	+1.3	+0.6	-1.4	-0.5	-0.9	+0.4	-0.1	-0.4	+0.1	+1.8	-0.4	+1.8	+3.8	+3.5	+0.7	-2.1	-2.6	-1.1	+0.7	-0.4	+0.7	-2.3	-1.6	
	+2.5	-2.5	-3.5	-1.6	-1.1	+1.0	+0.8	-0.2	-2.1	-0.5	-2.2	-2.7	-2.3	+0.0	-0.6	-1.4	+0.2	+0.8	+3.6	+1.8	+3.3	-0.6	+2.4	
PS ISR	+0.5	-0.6	-0.9	+1.4	+0.9	+1.1	+1.3	+1.0	+1.1	+1.8	+1.0	-0.0	+3.7	-2.4	+0.8	-6.2	-2.1	-1.3	+0.4	+0.8	-0.6	-2.5	+0.2	
	+0.4	-1.7	-2.4	-1.6	-0.6	+0.5	+0.1	-0.5	-1.5	-1.3	-1.7	-1.0	+1.5	+1.0	-0.0	-1.7	+0.8	+0.2	+1.8	+2.3	+2.1	-0.4	+3.1	
PS FSR	-1.7	-4.5	-4.0	-2.5	-0.4	+0.5	+0.9	-0.5	-1.5	-0.9	-1.4	-0.3	+2.7	+2.6	+2.9	+1.3	+0.8	+1.4	+3.1	+1.9	+1.1	-0.1	+0.9	
	+4.4	+1.3	+1.6	+0.8	-0.5	-0.4	-0.1	-0.6	+0.7	+0.9	+0.1	-0.5	-0.9	-1.0	-0.9	-2.9	-1.0	-1.7	+0.1	-0.3	+0.2	-1.1	+0.6	
UE tune	+3.9	-1.7	-4.2	+0.2	-1.0	+1.2	+0.9	-0.5	+0.0	-0.2	-0.9	-1.8	+3.7	+3.3	+2.8	-2.9	-2.0	-1.6	+1.8	+1.8	+0.7	-1.0	+0.5	
	+2.8	-0.2	-2.9	-1.0	+0.2	+0.4	+1.1	-0.4	-0.6	+1.0	-1.5	+0.5	-0.7	+1.4	-3.2	-2.5	+0.2	+0.3	+0.1	+2.4	+0.2	-0.7	+1.2	
CR	+1.3	+0.5	+0.0	-0.7	-0.6	+0.1	-0.5	+0.1	+0.3	-1.2	-0.7	+2.6	+2.0	-1.5	-2.2	-0.3	-1.0	+0.3	+1.5	+0.9	-0.9	+0.8	+2.3	
	+3.0	+0.4	+1.0	+0.6	+0.0	+1.7	+1.8	+0.6	+0.6	+2.1	+0.2	+0.6	+2.6	+0.6	-2.3	-3.1	-2.8	-3.0	-2.1	-0.6	+0.1	-2.6	+0.7	
	+2.8	-1.9	-1.1	+0.0	+0.1	+0.5	+0.9	+0.6	-0.5	+1.7	-0.7	-0.1	+1.2	+0.6	-0.0	-1.6	-2.2	-1.5	-0.3	+0.1	+0.6	-0.3	+0.8	
$f(b \rightarrow B)$	+1.3	+0.8	+1.3	+0.6	+0.4	+0.2	+0.4	-0.5	+0.2	-0.4	-0.3	-1.0	+0.0	+0.8	+0.2	-0.3	+0.1	+0.2	+0.1	-0.8	-0.1	-0.4	-0.7	
	-0.6	-0.6	-0.7	-0.3	-0.2	+0.0	-0.0	+0.2	-0.1	+0.2	+0.1	+0.6	+0.0	-0.5	-0.3	-0.0	-0.2	-0.1	+0.0	+0.4	+0.1	+0.3	+0.4	
	+0.2	+0.2	+0.2	+0.1	+0.1	+0.0	+0.0	-0.1	+0.0	-0.0	-0.2	-0.1	+0.1	-0.0	-0.1	+0.0	+0.0	+0.0	-0.2	+0.0	-0.1	-0.1	-0.1	
	+1.5	+0.9	+1.2	+0.8	+0.3	+0.2	+0.3	-0.4	-0.1	-0.4	-0.5	-1.0	+1.2	+1.2	+1.0	+0.6	+0.1	+0.0	-0.5	-0.5	-0.8	-1.1	-1.0	
BR($B \rightarrow \mu$)	-0.2	-0.2	-0.2	-0.2	+0.1	+0.1	+0.2	+0.0	+0.1	+0.0	+0.1	-0.4	-0.4	-0.2	-0.1	+0.2	+0.0	+0.1	+0.0	+0.0	+0.1	+0.0	+0.0	
	+0.4	+0.4	+0.4	+0.2	-0.1	-0.2	-0.2	-0.1	-0.1	-0.1	-0.2	+0.6	+0.5	+0.4	+0.2	-0.1	-0.2	-0.1	-0.1	-0.1	-0.1	-0.1	-0.1	

Table 66: The measured $[N_{\text{jet}}^{0,1+}, M(\text{t}\bar{\text{t}}), y(\text{t}\bar{\text{t}})]$ cross sections, along with their relative statistical and systematic uncertainties, and NP corrections (see Section 8).

N_{jet}	$M(\text{t}\bar{\text{t}})$ [GeV]	$y(\text{t}\bar{\text{t}})$	$\frac{1}{\sigma(\text{t}\bar{\text{t}})} \frac{d\sigma}{dy(\text{t}\bar{\text{t}})}$	stat. [%]	syst. [%]	\mathcal{C}_{NP}	bin
0	300–400	0.00–0.35	8.235×10^{-2}	4.2	$^{+12.1}_{-8.0}$	0.973	1
0	300–400	0.35–0.75	8.580×10^{-2}	3.3	$^{+6.6}_{-10.7}$	0.974	2
0	300–400	0.75–1.15	7.629×10^{-2}	3.7	$^{+6.0}_{-12.6}$	0.973	3
0	300–400	1.15–2.50	3.578×10^{-2}	3.5	$^{+6.9}_{-8.2}$	0.975	4
0	400–500	0.00–0.35	1.361×10^{-1}	2.5	$^{+1.8}_{-3.1}$	0.971	5
0	400–500	0.35–0.75	1.231×10^{-1}	2.2	$^{+5.2}_{-1.8}$	0.971	6
0	400–500	0.75–1.15	1.030×10^{-1}	2.6	$^{+5.3}_{-1.5}$	0.972	7
0	400–500	1.15–2.50	4.724×10^{-2}	2.0	$^{+4.2}_{-3.0}$	0.974	8
0	500–1500	0.00–0.35	1.598×10^{-1}	1.7	$^{+2.6}_{-4.2}$	0.976	9
0	500–1500	0.35–0.75	1.402×10^{-1}	1.9	$^{+4.9}_{-2.6}$	0.978	10
0	500–1500	0.75–1.15	1.102×10^{-1}	2.3	$^{+2.7}_{-4.5}$	0.977	11
0	500–1500	1.15–2.50	3.225×10^{-2}	3.3	$^{+5.5}_{-6.4}$	0.982	12
1	300–400	0.00–0.35	4.219×10^{-2}	7.0	$^{+13.9}_{-6.0}$	1.031	13
1	300–400	0.35–0.75	4.211×10^{-2}	5.9	$^{+11.9}_{-5.3}$	1.031	14
1	300–400	0.75–1.15	3.709×10^{-2}	6.5	$^{+5.1}_{-13.3}$	1.035	15
1	300–400	1.15–2.50	1.619×10^{-2}	5.7	$^{+9.1}_{-14.9}$	1.034	16
1	400–500	0.00–0.35	7.864×10^{-2}	3.7	$^{+2.8}_{-9.7}$	1.036	17
1	400–500	0.35–0.75	7.203×10^{-2}	3.2	$^{+2.5}_{-7.0}$	1.033	18
1	400–500	0.75–1.15	5.572×10^{-2}	4.1	$^{+6.0}_{-3.7}$	1.034	19
1	400–500	1.15–2.50	2.186×10^{-2}	3.6	$^{+10.8}_{-2.8}$	1.034	20
1	500–1500	0.00–0.35	1.003×10^{-1}	2.5	$^{+7.8}_{-2.7}$	1.029	21
1	500–1500	0.35–0.75	8.991×10^{-2}	2.5	$^{+1.9}_{-8.1}$	1.032	22
1	500–1500	0.75–1.15	6.298×10^{-2}	3.5	$^{+8.0}_{-3.2}$	1.033	23
1	500–1500	1.15–2.50	1.796×10^{-2}	4.7	$^{+10.8}_{-8.7}$	1.027	24
≥ 2	300–400	0.00–0.35	2.241×10^{-2}	13.4	$^{+24.6}_{-8.9}$	1.037	25
≥ 2	300–400	0.35–0.75	2.132×10^{-2}	12.2	$^{+14.6}_{-12.7}$	1.031	26
≥ 2	300–400	0.75–1.15	1.872×10^{-2}	12.8	$^{+27.3}_{-6.2}$	1.035	27
≥ 2	300–400	1.15–2.50	8.949×10^{-3}	10.0	$^{+11.2}_{-20.8}$	1.045	28
≥ 2	400–500	0.00–0.35	4.412×10^{-2}	6.7	$^{+8.1}_{-12.6}$	1.036	29
≥ 2	400–500	0.35–0.75	3.703×10^{-2}	6.5	$^{+7.9}_{-14.4}$	1.035	30
≥ 2	400–500	0.75–1.15	2.985×10^{-2}	8.1	$^{+12.6}_{-10.9}$	1.040	31
≥ 2	400–500	1.15–2.50	1.069×10^{-2}	8.1	$^{+10.3}_{-15.6}$	1.044	32
≥ 2	500–1500	0.00–0.35	5.843×10^{-2}	3.2	$^{+8.0}_{-7.5}$	1.017	33
≥ 2	500–1500	0.35–0.75	4.772×10^{-2}	4.3	$^{+9.0}_{-9.1}$	1.013	34
≥ 2	500–1500	0.75–1.15	3.761×10^{-2}	4.9	$^{+9.7}_{-8.6}$	1.012	35
≥ 2	500–1500	1.15–2.50	9.239×10^{-3}	7.0	$^{+10.9}_{-8.1}$	1.014	36

Table 67: The correlation matrix of statistical uncertainties for the measured $[N_{\text{jet}}^{0,1+}, M(\bar{t}\bar{t}), y(\bar{t}\bar{t})]$ cross sections. The values are expressed as percentages. For bin indices see Table 115.

bin	2	3	4	5	6	7	8	9	10	11	12	13	14	15	16	17	18	19	20	21	22	23	24	25	26	27	28	29	30	31	32	33	34	35	36
1	-14	-18	+1	-33	-22	+6	+2	-8	+5	+1	-5	-5	-10	+1	+0	-14	+1	+7	-2	+6	+1	-3	-2	-10	+3	+2	-1	+9	+3	-3	-1	-3	-3	-0	+1
2	+20	-23	-20	-6	-28	-6	+7	-12	+1	+4	-10	+6	-9	-1	+2	-10	-7	+6	+2	+2	+5	-1	+4	-11	-1	+2	+2	+4	+6	-2	-3	+0	-2	-2	
3	+2	+5	-28	-14	-25	+1	+0	-11	-1	+1	-9	+4	-13	+6	-9	-12	-10	-3	+4	+5	+5	+2	-2	-9	+0	-3	+5	+6	+5	-0	-2	-2	-4		
4	-1	-4	-22	+3	-9	-1	-2	-29	-1	-1	-11	+7	-4	+4	-7	-24	-5	-6	+2	-1	-2	+1	+1	-17	-2	-4	+3	+6	-2	-3	-5	+3			
5	+5	-9	-5	-16	-10	+2	-1	-20	-2	+6	-3	+5	-5	-0	-1	-5	+2	+2	-1	+10	+3	-2	-1	-12	-1	+1	+1	+5	+1	-1	-1				
6	+24	-13	-10	-3	-14	-3	-2	-14	-11	+4	-5	+10	-3	-1	+2	-5	-1	+1	+4	+3	+6	-1	-1	-10	-2	+1	+2	+2	+3	-1					
7	+13	+3	-12	-6	-10	+7	-11	-16	-12	-1	-2	+10	-3	+2	-0	-6	-3	-3	+6	+6	+5	+1	-3	-10	-2	-1	+2	+3	+2						
8	-4	-4	-14	+3	-2	+6	-13	-28	-3	-2	-1	+12	-4	-1	-2	-16	-2	-1	+5	+2	-0	-1	-3	-11	-2	-3	+1	+3							
9	-19	-6	-1	+8	+3	-2	-4	-11	-1	+3	-1	-21	-6	+5	-1	-0	-2	+0	+0	+4	+2	+0	-0	-3	+4	-1	-1								
10	-3	-12	+3	+2	+5	-3	-0	-9	-3	+1	-5	-9	-13	+3	-2	+1	-1	-2	+2	+1	+3	+0	+4	-7	+4	-0									
11	-7	-2	+6	+4	+2	+2	-4	-9	-5	+5	-11	-12	-12	-1	-1	+0	-2	-0	+2	+2	+3	-1	+4	-6	+3										
12	-2	-1	+5	-6	-1	+1	-2	-19	-3	+3	-8	-16	+1	-2	-2	+6	-1	-1	+1	-0	-2	-2	+3	-10											
13	-10	-13	+3	-30	-22	+5	+3	-8	+4	+2	-1	-6	-7	+3	+0	-6	-6	+4	-2	+7	+1	-3	+1												
14	+16	-17	-21	-4	-25	-0	+4	-10	+0	+4	-8	+3	-9	+1	+6	-9	-1	+6	+1	+3	+4	+4	-4												
15	+7	+4	-26	-11	-19	+2	+1	-10	+0	+3	-9	-1	-6	+4	-1	-7	-0	-3	+5	+5	+4														
16	+2	-1	-18	+4	-3	+1	-0	-21	-0	+1	-6	+5	-3	+5	-0	-21	-1	-4	+2	+9															
17	+5	-7	+0	-12	-9	+2	+1	-16	+3	+4	-2	+4	-4	-1	+1	-2	+3	+1	-1																
18	+22	-9	-10	-1	-11	+1	+3	-13	-4	+5	-4	+7	-2	-2	+4	-5	+2	+1																	
19	+11	+3	-10	-5	-9	+6	-4	-12	-2	-1	-2	+6	-1	+2	+1	-3	+1																		
20	+1	+1	-10	-0	-3	+7	-1	-27	+0	-2	-1	+15	-1	+1	+3	-10																			
21	-20	-5	+2	+7	+1	-3	-0	-7	+1	+2	+0	-20	-2	+5	-2																				
22	-5	-8	+2	+3	+4	-2	+1	-7	-1	+2	+0	-11	-7	+3																					
23	-7	-3	+5	+4	+3	+2	-0	-7	-1	+5	-5	-13	-6																						
24	-0	-2	+4	+5	-0	+1	+0	-12	-1	+4	-2	-16																							
25	-24	-7	+3	-60	-17	+15	-1	+4	+9	-2	-2																								
26	-4	-9	-13	-29	-32	+12	+9	-6	+9	-1																									
27	-8	+12	-30	-40	-19	-3	+10	-3	+10																										
28	-1	+12	-18	-50	-1	-2	+9	-10																											
29	-2	-7	+0	-28	-8	+5	+0																												
30	+11	-9	-8	-17	-13	+4																													
31	+8	+5	-14	-20	-10																														
32	-0	+4	-9	-27																															
33	-35	+4	+1																																
34	-25	+0																																	
35	-24																																		

Table 68: Sources and values of the relative systematic uncertainties in percent of the measured $[N_{\text{jet}}^{0,1+}, M(\text{t}\bar{\text{t}}), y(\text{t}\bar{\text{t}})]$ cross sections. For bin indices see Table 115.

source / bin	1	2	3	4	5	6	7	8	9	10	11	12	13	14	15	16	17	18	19	20	21	22	23	24	25	26	27	28	29	30	31	32	33	34	35	36	
JER	+0.2	+0.6	+0.3	+0.6	+0.0	+0.5	+0.4	+0.8	-0.0	+0.3	+0.2	+0.9	-0.8	+0.9	-0.6	-0.5	-0.2	+0.8	-0.6	-0.0	+0.1	+0.1	-2.9	+0.3	-0.2	-0.5	-1.1	-0.2	-2.3	-0.9	-1.4	-1.3	+0.3				
JESAbsoluteMPFBias	-0.3	-1.1	-1.9	-0.6	-0.6	+0.2	-0.1	+0.2	-0.2	-0.2	+0.2	+0.0	+0.22	+0.4	+0.3	-2.0	-0.5	-0.3	-0.1	+0.7	+0.6	+0.3	+0.1	+0.7	+2.4	-1.3	+0.5	+1.1	+1.5	-0.3	+2.0	+1.8	+0.3	+1.2	-0.4	-0.3	
JESAbsoluteScale	+0.7	+0.4	-0.1	+0.5	-0.1	+0.3	+0.3	+0.4	+0.1	-0.1	-0.05	+0.14	+1.3	-0.0	+0.4	-0.4	-0.4	-0.5	+0.5	+0.1	-0.1	+0.2	-1.0	+1.1	-0.6	+1.4	-0.3	-0.7	-0.5	-1.8	-1.0	-0.8	-0.8	-0.6			
JESAbsoluteStat	-0.7	-0.8	-1.4	-0.3	-0.0	+0.2	+0.1	+0.2	-0.2	+0.2	+0.1	-0.0	-0.3	-0.7	-0.2	-1.4	-0.0	-0.0	+0.3	+0.2	+0.8	+0.1	+0.4	+0.3	-0.1	-1.7	+1.3	-0.5	+1.2	+1.1	+0.4	+0.8	+0.1	+0.4	+0.3		
JESFavourQCD	+0.5	+0.0	-0.1	+0.5	-0.2	+0.3	+0.3	+0.0	-0.1	+0.2	+0.0	-0.4	-0.4	-0.5	+0.3	+0.2	+0.1	+0.1	+0.1	+0.3	+1.2	+0.5	-0.0	+0.2	+0.4	-0.1	-1.1	+2.7	+0.4	+0.8	+0.4	-1.4	-2.1	-0.2	+1.3	-0.3	+0.9
JESFrag	+0.3	+0.9	-1.1	-0.4	-0.4	+0.0	-0.2	+0.4	+0.1	+0.1	+0.06	+0.4	+1.1	+0.8	-0.6	+1.3	-0.5	-0.5	-0.4	+0.6	+0.2	+0.2	+0.7	-2.2	-0.2	+1.8	+1.7	+0.8	-1.0	-1.1	-1.5	-3.7	-0.1	+0.9	-0.8	+0.7	
JESProfileUpDataMC	-3.0	-3.4	-3.1	-1.8	+0.0	-0.1	-0.1	-0.1	-0.3	-0.2	-0.6	-0.5	-0.3	-1.9	-0.5	-0.9	-1.2	+1.1	+1.0	+1.4	+2.1	+1.1	+0.1	+0.5	+0.3	+2.8	+1.9	+1.6	+1.7	+2.4	+2.3	+3.5	+3.8	+1.8	+3.5	+1.6	+2.3
JESProfileUpPBB	-0.1	-0.2	-0.2	+0.2	+0.1	+0.4	+0.5	+0.4	+0.2	+0.2	-0.4	+0.7	+0.8	+0.1	-0.2	-0.6	-0.4	-0.4	-0.7	+0.3	+0.4	+0.3	-1.1	+0.1	-0.4	+0.8	-0.5	-0.2	-1.3	-0.9	-0.2	-0.7	-0.2	+0.3	+0.4		
JESProfileUpPHEC1	-0.4	-0.6	-1.1	-0.2	-0.0	-0.0	-0.0	-0.1	-0.3	-0.2	-0.2	-0.3	-0.1	-0.1	-0.1	+0.3	+0.1	+0.1	+0.3	+1.4	+0.3	-0.1	+0.1	+0.3	+1.1	-0.5	+3.1	-0.1	+0.5	+0.9	-1.6	+0.0	-0.1	+0.6	-0.0	+0.4	
JESProfileUpPHEC2	+0.5	+0.0	-0.5	-0.0	-0.1	+0.4	+0.4	+0.7	+0.2	+0.2	+0.1	+0.5	+0.4	+0.5	+0.1	-0.7	-0.5	-0.3	-0.1	-0.3	+0.3	+0.1	+1.0	-1.1	-0.5	-1.1	-0.2	+0.4	-0.4	-1.0	-0.2	-1.4	-0.5	-0.8	-0.9	-0.9	
JESProfileUpPtHF	-0.0	-0.3	-0.4	+0.1	-0.2	+0.4	+0.5	+0.3	+0.4	+0.2	+0.3	-0.3	-0.2	-0.1	-1.1	-0.0	-0.2	-0.2	-0.2	-0.1	-0.4	-0.1	+0.1	+0.3	+0.4	-1.1	-1.7	-0.0	-0.6	-0.4	-0.3	-0.8	-0.5	-0.2	-0.0	-0.8	-0.5
JESRelativeBal	-0.2	-0.4	-0.4	-0.1	+0.0	-0.1	-0.3	+0.0	-0.3	-0.2	-0.2	-0.0	-0.1	-1.9	+2.3	-0.6	-0.0	-0.2	-0.2	-0.1	-0.2	-0.2	-0.1	-0.1	+1.7	+0.8	+1.0	-0.1	+0.5	+0.6	-0.0	+1.9	-0.1	+1.0	-0.5	-0.3	
JESRelativeFSR	+1.9	+2.2	+1.5	+1.6	-0.1	+0.3	-0.2	+0.0	+0.3	+0.4	+0.2	-1.1	+1.6	+1.4	+0.7	+0.1	-0.7	-0.5	-0.6	-0.2	+0.2	-0.2	-0.5	-0.8	+2.5	-0.7	+1.5	-4.7	-1.9	-2.5	-0.9	-0.8	-1.8	-1.8	-1.7	-1.7	
JESRelativeJEREC1	-2.6	-2.7	-2.8	-1.7	-0.1	-0.2	-0.2	+0.7	-0.7	-0.4	-0.1	-1.1	-0.8	-0.1	-0.6	-1.7	+0.2	-0.0	+1.1	+2.0	+0.9	+0.2	+1.5	+0.9	+0.2	+0.7	+1.4	+1.4	-0.3	+1.1	+2.1	+1.2	+1.4	+1.4			

Table 69: Table 117 continued.

source / bin	1	2	3	4	5	6	7	8	9	10	11	12	13	14	15	16	17	18	19	20	21	22	23	24	25	26	27	28	29	30	31	32	33	34	35	36
JESrelativeJERFC2	+0.0	+0.0	+0.0	+0.0	+0.0	+0.0	+0.0	+0.0	+0.0	+0.0	+0.0	+0.0	+0.0	+0.0	+0.0	+0.0	+0.0	+0.0	+0.0	+0.0	+0.0	+0.0	+0.0	+0.0	+0.0	+0.0	+0.0	+0.0	+0.0	+0.0	+0.0	+0.0	+0.0	+0.0	+0.0	+0.0
JESrelativeJERHF	+0.0	+0.0	+0.0	+0.0	+0.0	+0.0	+0.0	+0.0	+0.0	+0.0	+0.0	+0.0	+0.0	+0.0	+0.0	+0.0	+0.0	+0.0	+0.0	+0.0	+0.0	+0.0	+0.0	+0.0	+0.0	+0.0	+0.0	+0.0	+0.0	+0.0	+0.0	+0.0	+0.0	+0.0	+0.0	+0.0
JESrelativePtBB	+0.2	+0.2	+0.2	-0.2	-0.1	+0.2	+0.2	+0.1	+0.1	+0.1	-0.2	+0.6	+0.2	+0.1	-0.5	-0.3	-0.2	-0.4	+0.1	+0.0	-0.3	+0.4	+0.7	+0.9	+0.1	+1.0	+0.3	-1.0	-0.4	-1.0	-0.6	-0.6	+0.9	-1.2	-0.4	
JESrelativePtFC1	+0.0	+1.1	+0.2	+0.3	+0.3	+0.4	+0.0	-0.0	+0.3	+0.2	+0.2	-0.1	+0.3	+1.1	-0.1	+1.0	+0.2	-0.0	-0.2	-0.1	-0.1	+0.1	-0.2	-2.3	+0.3	-0.3	+1.6	-4.6	-0.0	-1.1	-0.6	+0.5	-0.5	-0.5	-1.5	
JESrelativePtFC2	+0.0	+0.0	+0.0	+0.0	+0.0	+0.0	+0.0	+0.0	+0.0	+0.0	+0.0	+0.0	+0.0	+0.0	+0.0	+0.0	+0.0	+0.0	+0.0	+0.0	+0.0	+0.0	+0.0	+0.0	+0.0	+0.0	+0.0	+0.0	+0.0	+0.0	+0.0	+0.0	+0.0	+0.0	+0.0	
JESrelativePtHF	+0.0	+0.0	+0.0	+0.0	+0.0	+0.0	+0.0	+0.0	+0.0	+0.0	+0.0	+0.0	+0.0	+0.0	+0.0	+0.0	+0.0	+0.0	+0.0	+0.0	+0.0	+0.0	+0.0	+0.0	+0.0	+0.0	+0.0	+0.0	+0.0	+0.0	+0.0	+0.0	+0.0	+0.0	+0.0	
JESrelativeStatEC	+0.0	+0.3	-0.1	+0.1	+0.0	+0.2	+0.3	+0.2	+0.2	+0.1	+0.2	-0.5	+0.1	+0.4	-0.1	+1.0	-0.0	+0.1	-0.2	+0.6	+0.1	-0.1	+0.2	-1.3	-0.1	-0.4	+1.9	+0.4	+0.1	-0.1	-1.5	-3.0	-0.4	+0.2	-0.6	+0.2
JESrelativeStatHF	-0.1	-0.4	-1.0	-0.0	-0.0	+0.0	+0.3	-0.1	-0.1	+0.0	+0.0	+0.1	-0.3	-0.8	-0.2	-0.1	+0.1	+1.3	+0.2	-0.1	+0.2	+1.3	+0.7	-0.2	+0.2	-0.1	-0.3	+0.2	-0.7	-1.5	-0.3	+0.5	-0.0	-0.5		
JESrelativeStatFSR	-0.0	+0.1	-0.2	+0.1	-0.2	+0.0	+0.2	+0.2	+0.2	-0.2	+0.2	-0.1	+0.5	+0.1	-0.5	+0.0	+0.0	-0.1	-0.0	-0.2	+0.3	+0.0	+0.3	-0.5	-1.0	+1.0	-0.1	+0.4	+0.3	-1.1	+0.4	-0.3	-0.1	-0.8	-0.3	
JESSinglePionFCAL	-0.0	+0.0	-0.0	-0.07	+0.0	-0.1	+0.0	+0.0	+0.02	+0.0	-0.1	-0.0	+0.1	-0.1	-0.0	-0.2	-0.4	+0.1	-0.0	+0.1	+0.0	+0.3	+0.1	+0.9	-0.2	-0.7	+1.2	-0.7	+0.3	+0.3	-0.9	+1.0	-0.0	-0.1	-0.6	-0.7
JESSinglePionHCAL	+0.3	-0.0	-0.1	+0.3	-0.0	+0.5	+0.4	+0.6	+0.5	+0.1	-0.3	-0.3	+0.3	+0.5	-0.4	-0.7	-0.2	-0.3	-0.1	+0.5	+0.0	+0.0	+0.6	-0.7	+0.3	+0.3	+0.0	-0.8	-0.9	-1.4	-1.3	-0.4	-0.7	-0.5	-0.2	-0.8
JESTimePTEta	-0.1	-0.1	-0.4	-0.1	-0.2	-0.0	+0.3	+0.0	+0.3	-0.1	+0.1	+0.0	+0.3	-0.2	-0.0	-0.3	-0.1	-0.0	+0.2	-0.2	+0.0	+0.1	+0.3	-1.0	-0.3	+1.0	+1.0	+1.2	+0.7	-1.6	-0.6	-0.5	+0.0	-0.3	+0.4	
E_T^{miss}	-0.2	+0.2	-0.0	+0.0	-0.0	+0.3	-0.1	-0.1	+0.1	-0.2	+0.0	+0.2	+0.8	+0.2	-0.5	+1.0	-0.1	+0.0	+0.1	+0.8	-0.0	+0.3	+0.3	-1.4	-0.2	+2.5	-0.4	+0.4	-0.5	+0.1	-1.6	-0.1	-0.6	-1.1		
lepton ID/ISO	-0.2	-0.1	-0.5	-0.2	+0.1	+0.3	+0.2	+0.6	-0.1	-0.0	-0.2	-0.6	-0.1	-0.1	-0.3	+0.2	+0.3	+0.3	+0.5	-0.1	-0.1	-0.2	-0.7	+0.1	-0.2	-0.7	+0.1	+0.4	-0.1	-0.2	-0.1	-0.9				
pileup	+0.6	-0.3	-0.5	-0.1	+0.2	+0.3	+0.1	+0.3	+0.3	+0.2	+0.2	-0.5	+0.3	-0.3	-0.5	+0.2	-0.1	-0.2	+0.1	-0.2	-0.1	-0.1	-0.4	+1.7	+0.4	-2.1	+0.9	-0.9	-0.9	+0.8	+0.2	-0.6	+0.2	-0.7		
trigger	-0.7	+0.2	+0.6	+0.5	-0.1	-0.2	-0.3	-0.1	-0.3	-0.2	-0.1	+0.4	-0.1	-0.6	+0.3	-0.2	+0.1	+0.3	-0.1	+0.2	+0.0	-0.2	+0.1	+0.8	-1.8	-0.2	+2.4	-1.0	+0.8	+0.7	-0.9	-0.1	+0.5	-0.1	+0.7	
	+0.1	+0.2	+0.1	-0.3	+0.2	+0.1	+0.0	-0.1	+0.1	-0.2	+0.1	+0.2	-0.4	+0.2	+0.1	+0.0	-0.2	+0.1	+0.0	-0.1	+0.2	+0.1	+0.0	+0.0	-0.1	+0.2	+0.1	+0.0	-0.1	-0.2	+0.2	+0.1	+0.0	-0.1	+0.2	

Table 70: Table 117 continued.

source / bin	1	2	3	4	5	6	7	8	9	10	11	12	13	14	15	16	17	18	19	20	21	22	23	24	25	26	27	28	29	30	31	32	33	34	35	36
trigger (η)	-0.3	-0.2	-0.3	+0.7	-0.2	-0.2	+0.4	+0.0	-0.1	-0.2	+0.3	-0.2	-0.1	-0.3	-0.2	+0.5	-0.0	-0.1	-0.3	+0.2	-0.2	+0.0	-0.4	+0.7	-0.3	-0.2	-0.2	+0.6	-0.0	-0.1	-0.3	+0.2				
b-tagging	+0.3	+0.2	+0.3	-0.6	+0.2	+0.2	-0.4	-0.0	+0.1	+0.2	-0.3	+0.2	+0.1	+0.3	-0.9	+0.3	+0.2	-0.5	+0.0	+0.1	+0.3	-0.2	+0.2	+0.0	+0.4	-0.7	+0.3	+0.2	+0.2	-0.6	+0.0	+0.1	+0.3	+0.2		
non-tt background	-0.9	-0.7	-1.8	-3.9	-0.2	-0.2	+0.2	+0.0	+0.6	+0.3	+0.7	-0.3	+0.7	+1.1	+1.2	-3.7	-0.0	+0.5	+0.3	+0.8	+0.8	+0.6	+0.2	+2.9	+2.4	+3.0	+0.6	+0.9	+0.5	+0.3	+1.0	+1.2	+0.4	+1.3	-0.6	
b-tagging (light jets)	+1.1	+0.5	+2.0	+3.7	+0.1	+0.1	-0.3	-0.2	-0.5	-0.3	-0.6	+0.3	-0.6	-0.8	-0.8	+3.4	-0.1	-0.5	-0.6	-0.8	-0.5	-0.1	-3.0	-2.5	-2.9	-0.1	-0.8	-0.4	-0.3	-1.0	-1.2	-0.3	-1.2	+0.5		
b-tagging	-0.0	-0.0	-0.1	-0.1	-0.1	-0.1	-0.1	-0.0	-0.0	-0.0	-0.0	-0.0	-0.0	-0.0	-0.0	-0.0	-0.0	-0.0	-0.0	-0.0	-0.0	-0.0	-0.0	-0.0	-0.0	-0.0	-0.0	-0.0	-0.0	-0.0	-0.0	-0.0	-0.0	-0.0	-0.0	
luminosity	+0.0	+0.0	+0.0	+0.0	+0.0	+0.0	+0.0	+0.0	+0.0	+0.0	+0.0	+0.0	+0.0	+0.0	+0.0	+0.0	+0.0	+0.0	+0.0	+0.0	+0.0	+0.0	+0.0	+0.0	+0.0	+0.0	+0.0	+0.0	+0.0	+0.0	+0.0	+0.0	+0.0	+0.0	+0.0	
$\text{BR}(t\bar{t} \rightarrow \ell\ell)$	+0.0	+0.0	+0.0	+0.0	+0.0	+0.0	+0.0	+0.0	+0.0	+0.0	+0.0	+0.0	+0.0	+0.0	+0.0	+0.0	+0.0	+0.0	+0.0	+0.0	+0.0	+0.0	+0.0	+0.0	+0.0	+0.0	+0.0	+0.0	+0.0	+0.0	+0.0	+0.0	+0.0	+0.0	+0.0	
PDF eigenvector 1	+0.0	+0.0	-0.0	-0.0	-0.0	-0.0	-0.0	-0.0	-0.0	-0.0	-0.0	-0.0	-0.0	-0.0	-0.0	-0.0	-0.0	-0.0	-0.0	-0.0	-0.0	-0.0	-0.0	-0.0	-0.0	-0.0	-0.0	-0.0	-0.0	-0.0	-0.0	-0.0	-0.0	-0.0	-0.0	
PDF eigenvector 2	-0.0	-0.1	+0.1	-0.3	-0.1	-0.0	+0.0	+0.0	+0.0	+0.0	+0.0	+0.0	+0.0	+0.0	+0.0	+0.0	+0.0	+0.0	+0.0	+0.0	+0.0	+0.0	+0.0	+0.0	+0.0	+0.0	+0.0	+0.0	+0.0	+0.0	+0.0	+0.0	+0.0	+0.0	+0.0	
PDF eigenvector 3	+0.1	+0.0	-0.1	+0.1	+0.0	-0.0	-0.0	-0.2	+0.1	+0.1	+0.1	-0.2	+0.1	+0.1	+0.1	+0.1	-0.1	-0.3	+0.1	+0.1	+0.1	-0.0	+0.1	+0.2	+0.1	+0.1	-0.3	-0.4	+0.1	+0.1	+0.1	+0.1	+0.1	+0.2		
PDF eigenvector 4	-0.0	-0.0	+0.1	-0.2	-0.1	-0.0	-0.0	+0.1	+0.0	+0.0	+0.1	-0.0	-0.0	-0.3	-0.2	-0.0	+0.1	+0.1	+0.1	+0.0	-0.1	+0.3	+0.1	+0.0	-0.4	-0.2	+0.2	+0.0	+0.2	+0.0	+0.0	+0.0	+0.0	+0.0		
PDF eigenvector 5	-0.1	-0.1	-0.0	+0.1	+0.0	+0.1	+0.3	-0.2	-0.2	+0.4	-0.2	-0.2	-0.1	+0.1	+0.2	+0.2	+0.3	+0.4	-0.2	-0.2	+0.1	-0.4	-0.3	-0.1	+0.3	+0.5	+0.5	-0.3	-0.4	-0.3	-0.3	-0.3	-0.3	-0.3		
PDF eigenvector 6	+0.0	+0.0	-0.0	-0.1	-0.0	-0.1	-0.0	-0.1	-0.0	-0.0	-0.0	-0.0	-0.0	-0.0	-0.0	-0.0	-0.0	-0.0	-0.0	-0.0	-0.0	-0.0	-0.0	-0.0	-0.0	-0.0	-0.0	-0.0	-0.0	-0.0	-0.0	-0.0	-0.0	-0.0	-0.0	
PDF eigenvector 7	-0.2	-0.2	-0.0	+0.2	+0.1	+0.1	-0.1	-0.3	+0.2	+0.1	+0.1	-0.2	+0.2	+0.1	+0.0	-0.3	-0.5	+0.2	+0.1	+0.1	+0.1	+0.0	+0.2	+0.1	+0.0	-0.2	-0.1	-0.1	-0.1	-0.1	-0.1	-0.0	-0.0	-0.0	-0.5	
PDF eigenvector 8	-0.1	+0.1	+0.0	-0.1	-0.0	-0.1	-0.0	-0.1	-0.0	-0.0	-0.0	-0.0	-0.0	-0.0	-0.0	-0.0	-0.0	-0.0	-0.0	-0.0	-0.0	-0.0	-0.0	-0.0	-0.0	-0.0	-0.0	-0.0	-0.0	-0.0	-0.0	-0.0	-0.0	-0.0	-0.0	
PDF eigenvector 9	-0.0	+0.0	+0.1	+0.1	-0.0	-0.0	-0.0	-0.0	-0.0	-0.0	-0.0	-0.0	-0.0	-0.0	-0.0	-0.0	-0.0	-0.0	-0.0	-0.0	-0.0	-0.0	-0.0	-0.0	-0.0	-0.0	-0.0	-0.0	-0.0	-0.0	-0.0	-0.0	-0.0	-0.0	-0.0	
PDF eigenvector 10	-0.1	-0.1	+0.0	+0.1	+0.0	+0.0	+0.0	+0.1	+0.1	+0.1	+0.1	+0.1	+0.2	+0.2	+0.2	+0.2	+0.2	+0.2	+0.2	+0.2	+0.2	+0.3	+0.3	+0.4	+0.4	+0.3	+0.3	+0.3	+0.2	+0.2	+0.2	+0.2	+0.2	+0.2		

Table 71: Table 117 continued

Table 72: Table 117 continued.

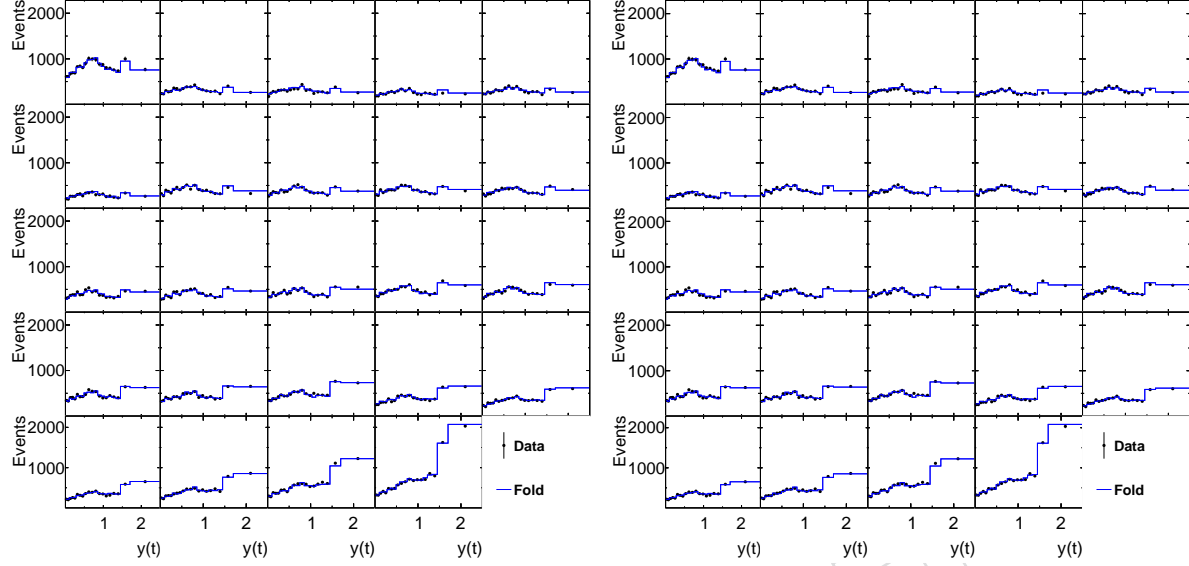


Figure 145: The folded $[M(\bar{t}t), y(t)]$ cross sections compared to the data for the unregularised (left) and regularised (right) unfolding shown as a function of $y(t)$ in different $M(\bar{t}t)$ ranges.

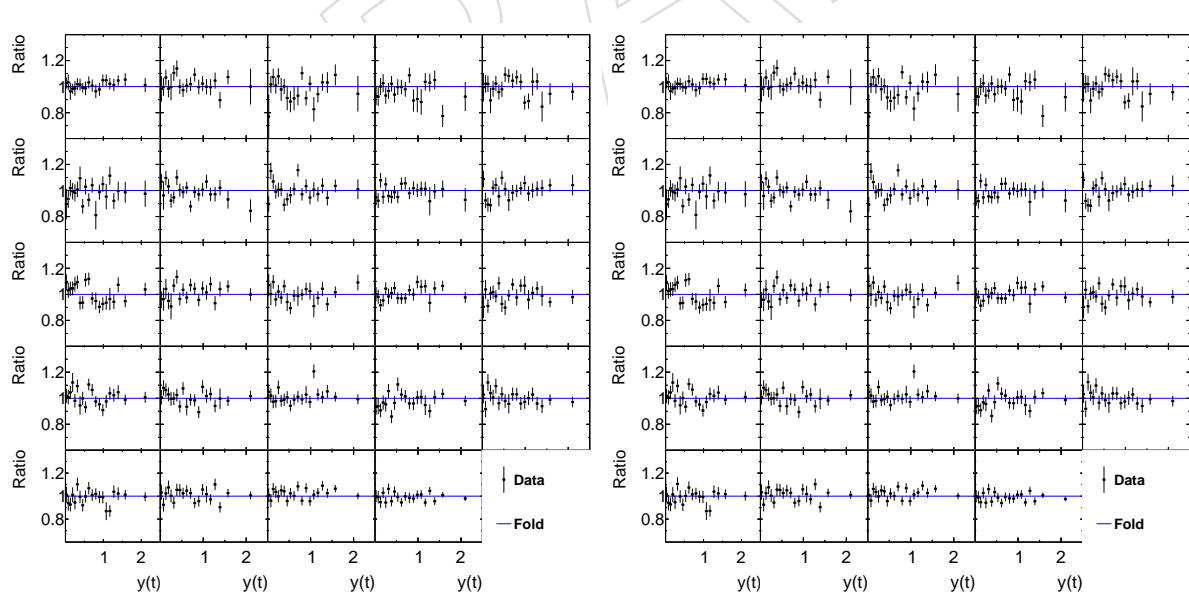


Figure 146: Ratio of the folded $[M(\bar{t}t), y(t)]$ cross sections to the data for the unregularised (left) and regularised (right) unfolding shown as a function of $y(t)$ in different $M(\bar{t}t)$ ranges.

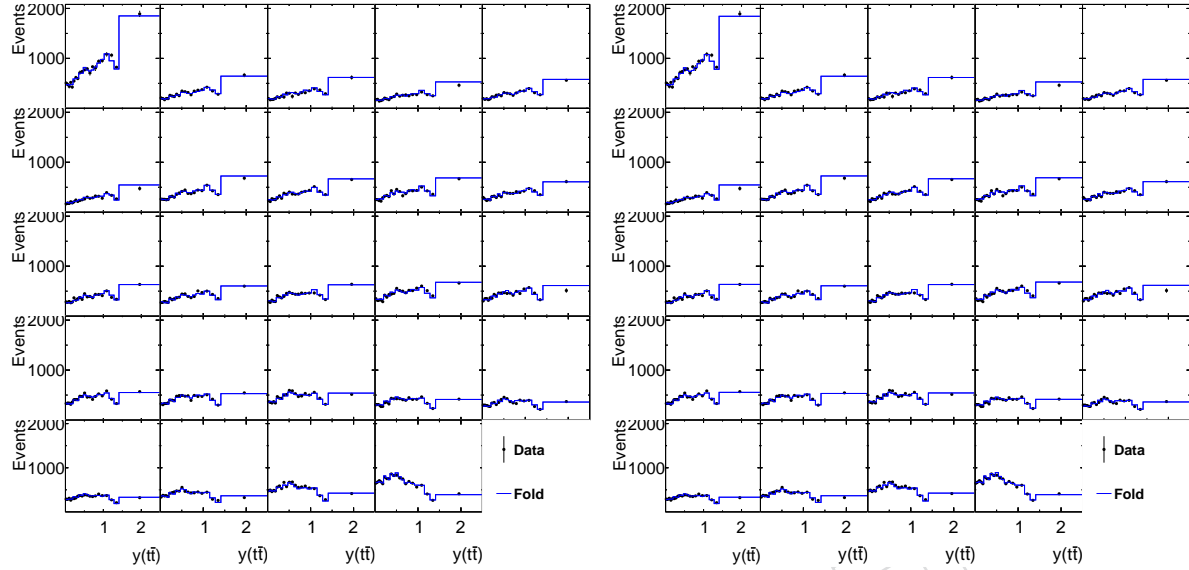


Figure 147: The folded $[M(\bar{t}), y(\bar{t})]$ cross sections compared to the data for the unregularised (left) and regularised (right) unfolding shown as a function of $y(\bar{t})$ in different $M(\bar{t})$ ranges.

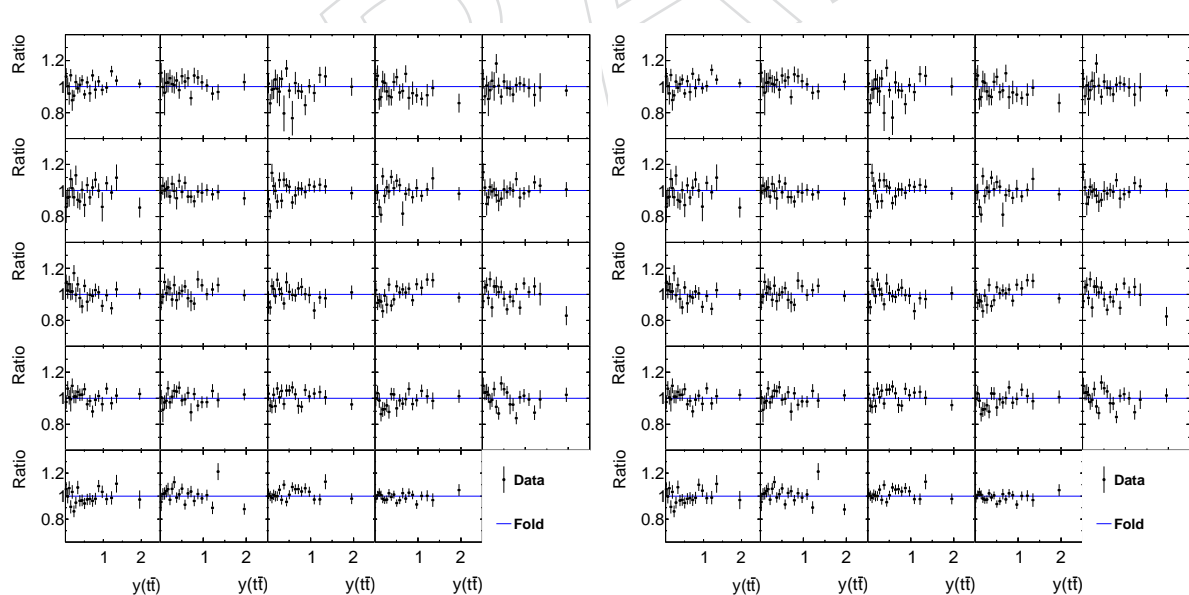


Figure 148: Ratio of the folded $[M(\bar{t}), y(\bar{t})]$ cross sections to the data for the unregularised (left) and regularised (right) unfolding shown as a function of $y(\bar{t})$ in different $M(\bar{t})$ ranges.

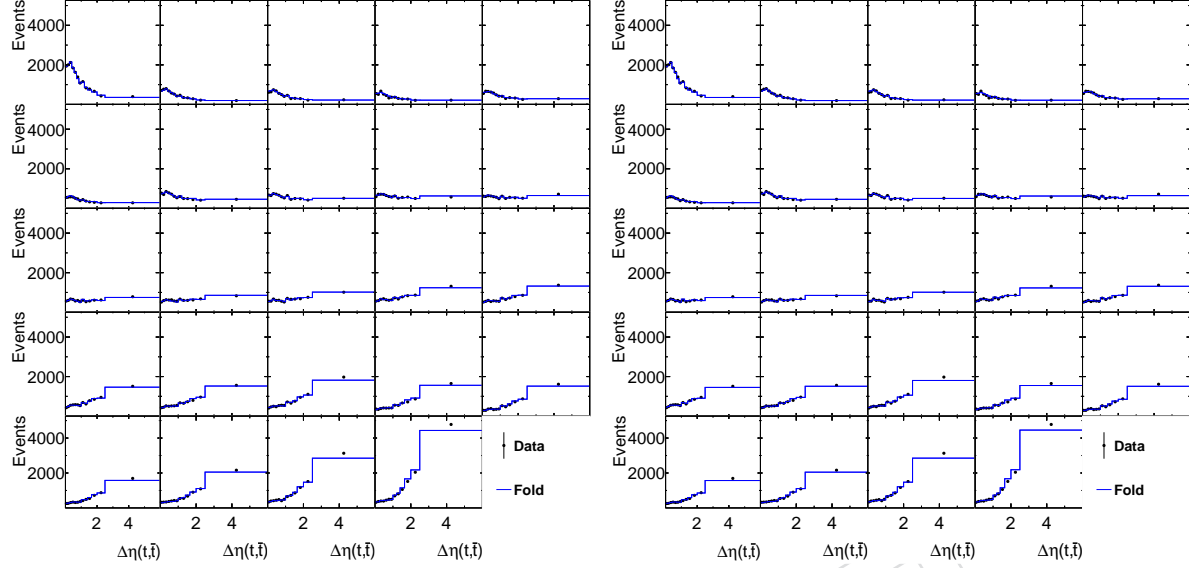


Figure 149: The folded $[M(t\bar{t}), \Delta\eta(t, \bar{t})]$ cross sections compared to the data for the unregularised (left) and regularised (right) unfolding shown as a function of $\Delta\eta(t, \bar{t})$ in different $M(t\bar{t})$ ranges.

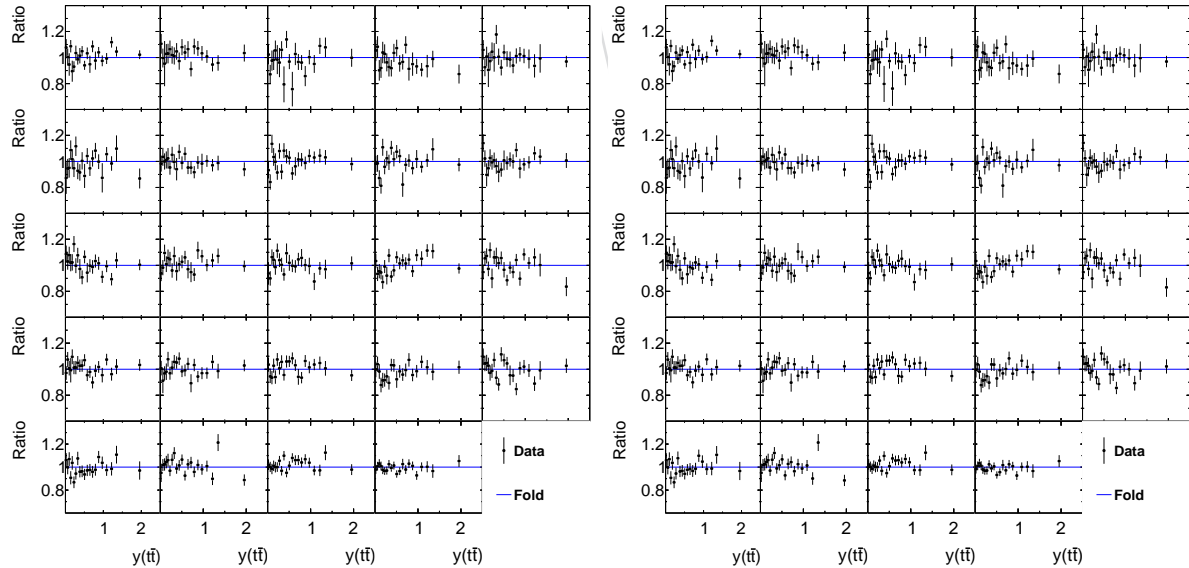


Figure 150: Ratio of the folded $[M(t\bar{t}), \Delta\eta(t, \bar{t})]$ cross sections to the data for the unregularised (left) and regularised (right) unfolding shown as a function of $\Delta\eta(t, \bar{t})$ in different $M(t\bar{t})$ ranges.

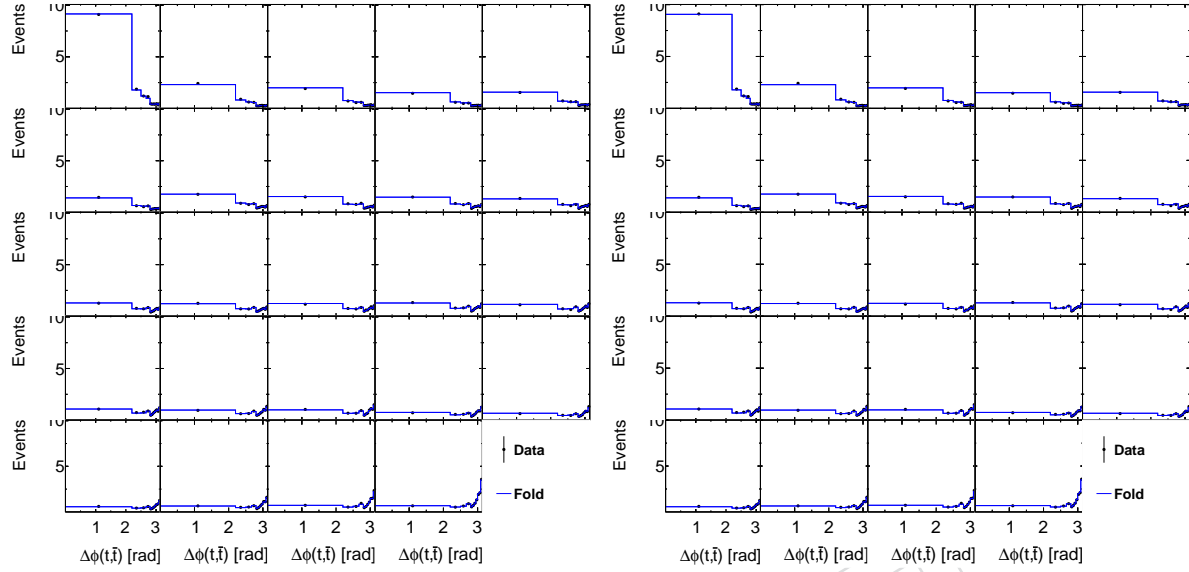


Figure 151: The folded $[M(t\bar{t}), \Delta\phi(t, \bar{t})]$ cross sections compared to the data for the unregularised (left) and regularised (right) unfolding shown as a function of $\Delta\phi(t, \bar{t})$ in different $M(t\bar{t})$ ranges.

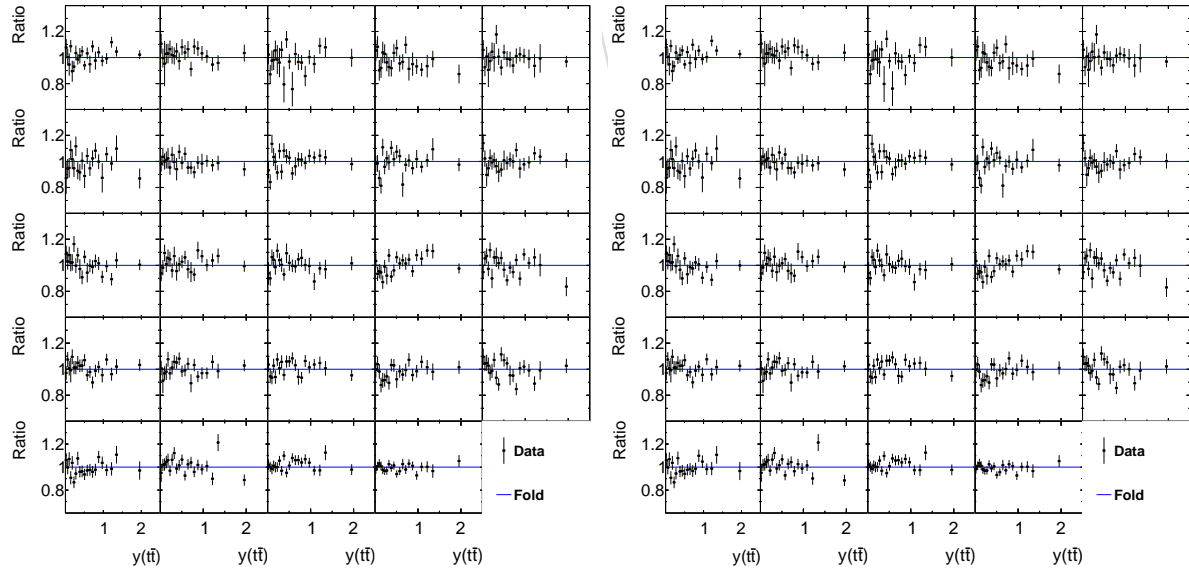


Figure 152: Ratio of the folded $[M(t\bar{t}), \Delta\phi(t, \bar{t})]$ cross sections to the data for the unregularised (left) and regularised (right) unfolding shown as a function of $\Delta\phi(t, \bar{t})$ in different $M(t\bar{t})$ ranges.

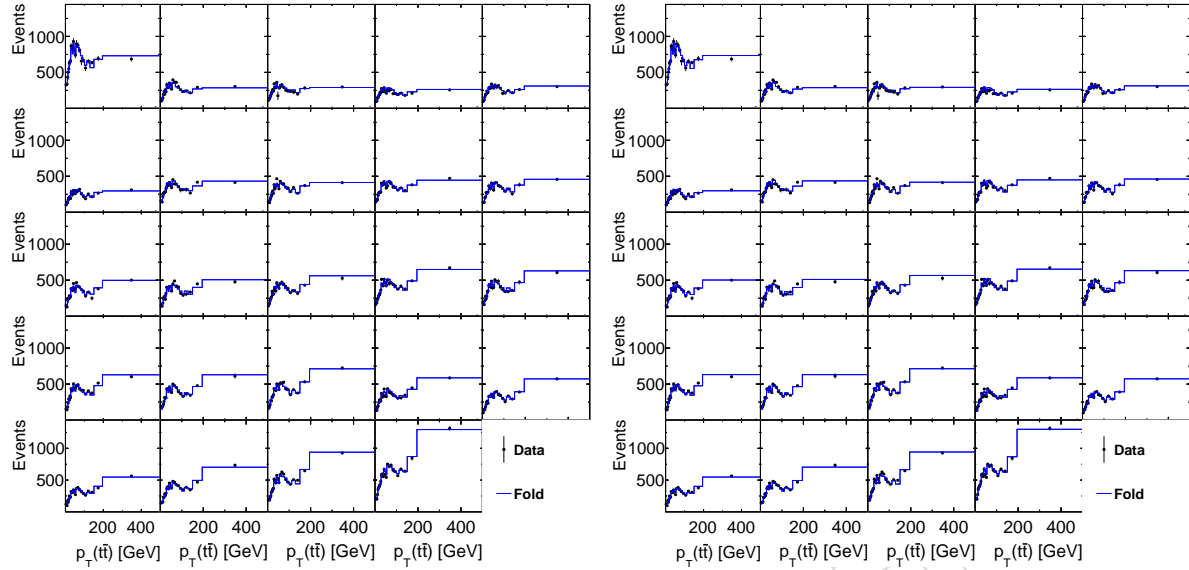


Figure 153: The folded $[M(t\bar{t}), p_T(t\bar{t})]$ cross sections compared to the data for the unregularised (left) and regularised (right) unfolding shown as a function of $p_T(t\bar{t})$ in different $M(t\bar{t})$ ranges.

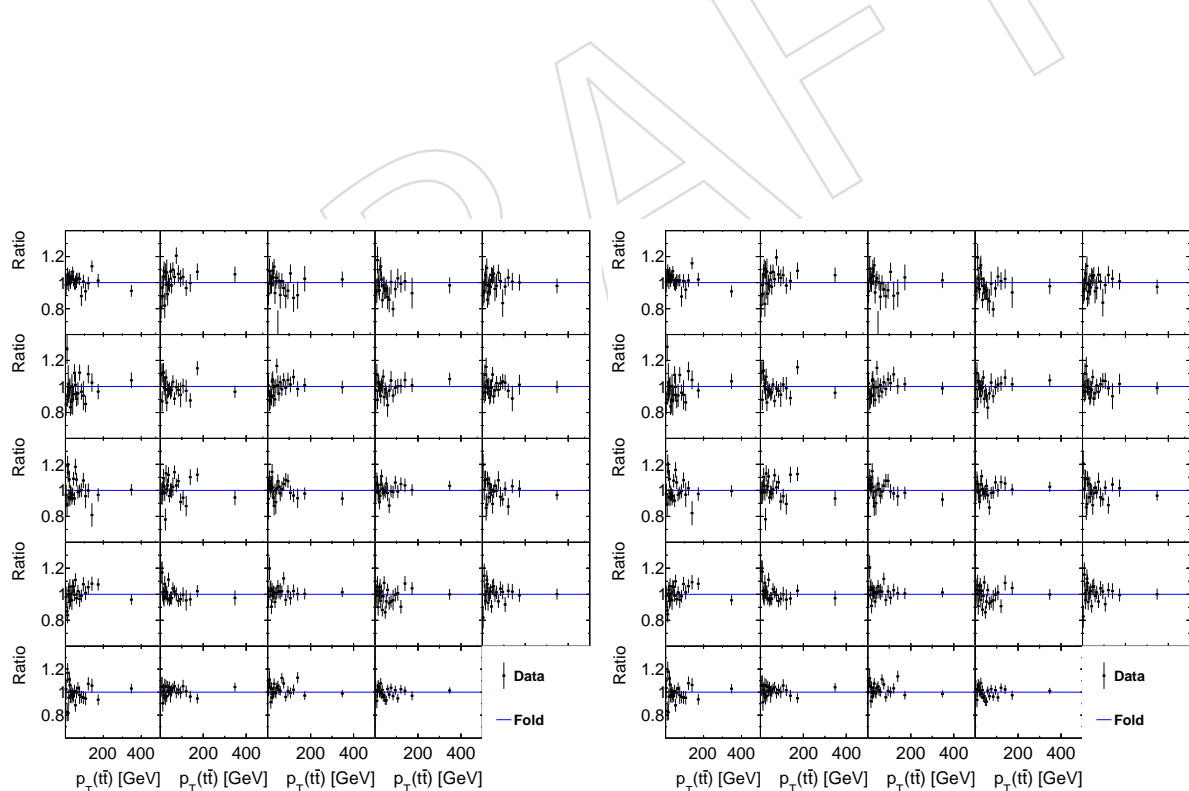


Figure 154: Ratio of the folded $[M(t\bar{t}), p_T(t\bar{t})]$ cross sections to the data for the unregularised (left) and regularised (right) unfolding shown as a function of $p_T(t\bar{t})$ in different $M(t\bar{t})$ ranges.

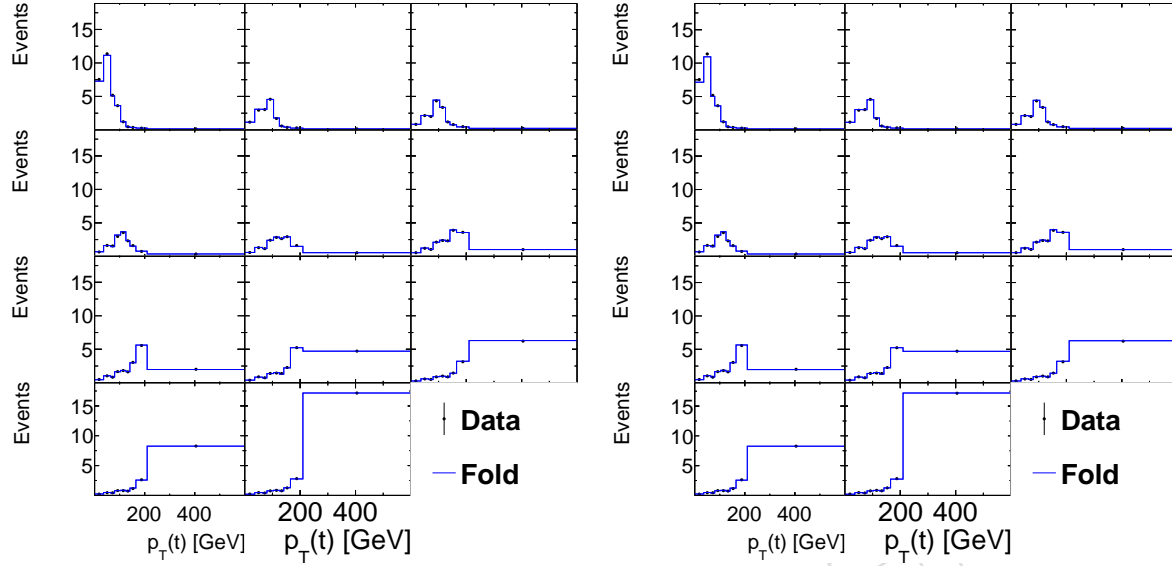


Figure 155: The folded $[M(t\bar{t}), p_T(t)]$ cross sections compared to the data for the unregularised (left) and regularised (right) unfolding shown as a function of $p_T(t)$ in different $M(t\bar{t})$ ranges.

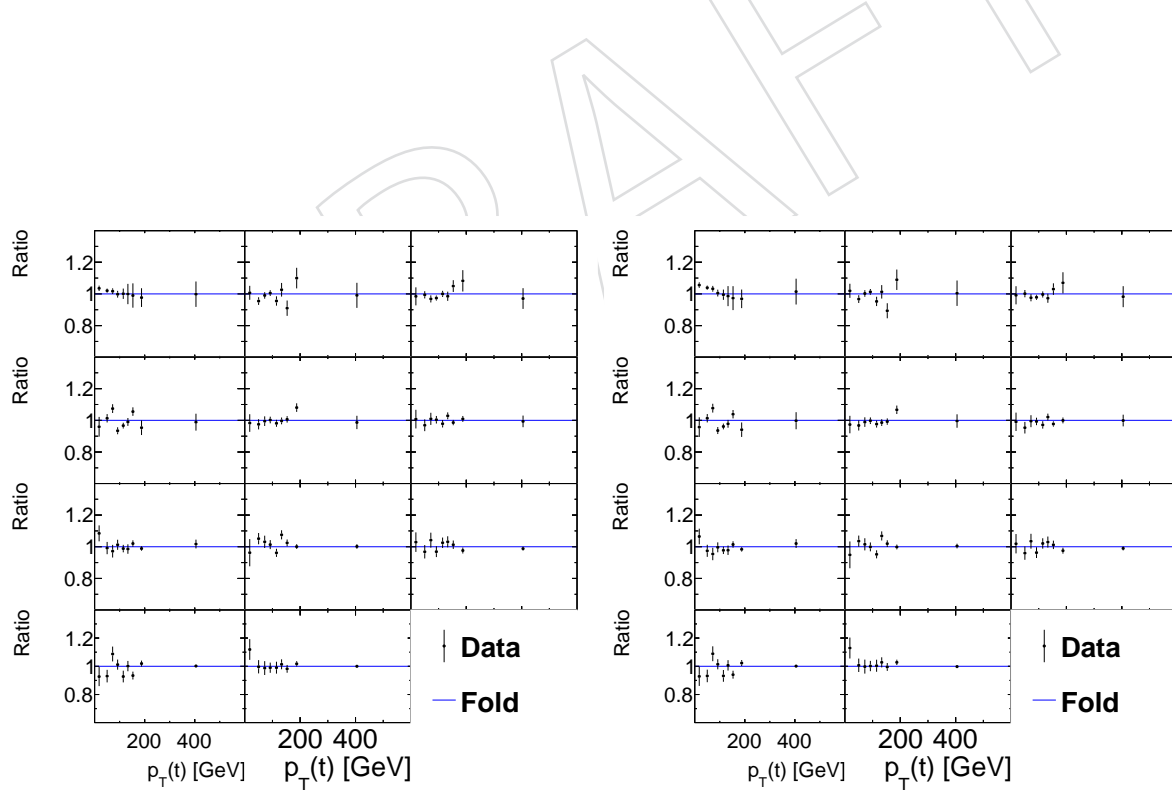


Figure 156: Ratio of the folded $[M(t\bar{t}), p_T(t)]$ cross sections to the data for the unregularised (left) and regularised (right) unfolding shown as a function of $p_T(t)$ in different $M(t\bar{t})$ ranges.

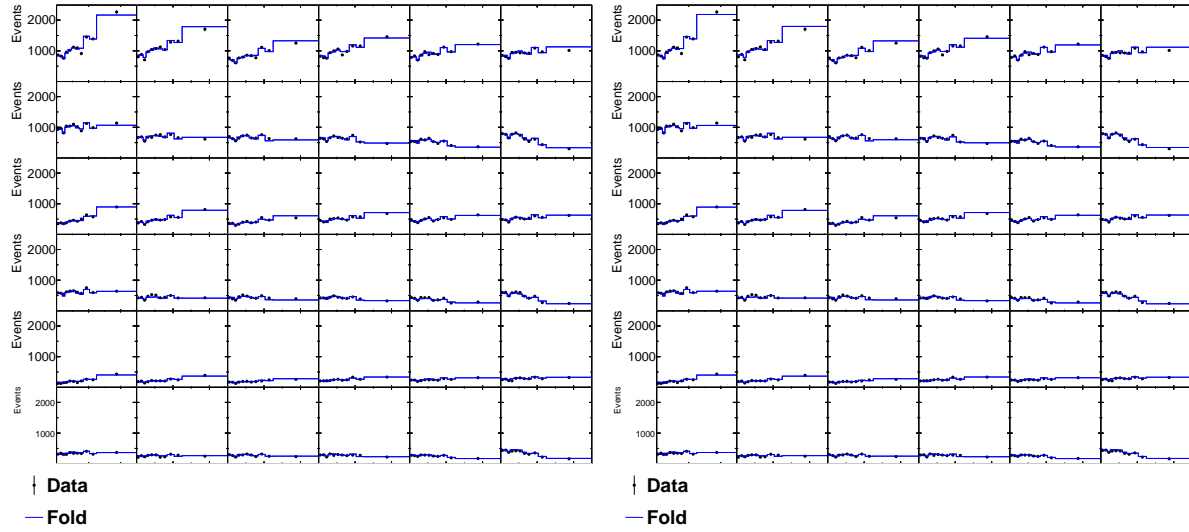


Figure 157: The folded $[N_{jet}, M(t\bar{t}), y(t\bar{t})]$ cross sections (with 2 N_{jet} bins) compared to the data for the unregularised (left) and regularised (right) unfolding shown as a function of $y(t\bar{t})$ in different $[N_{jet}, M(t\bar{t})]$ ranges.

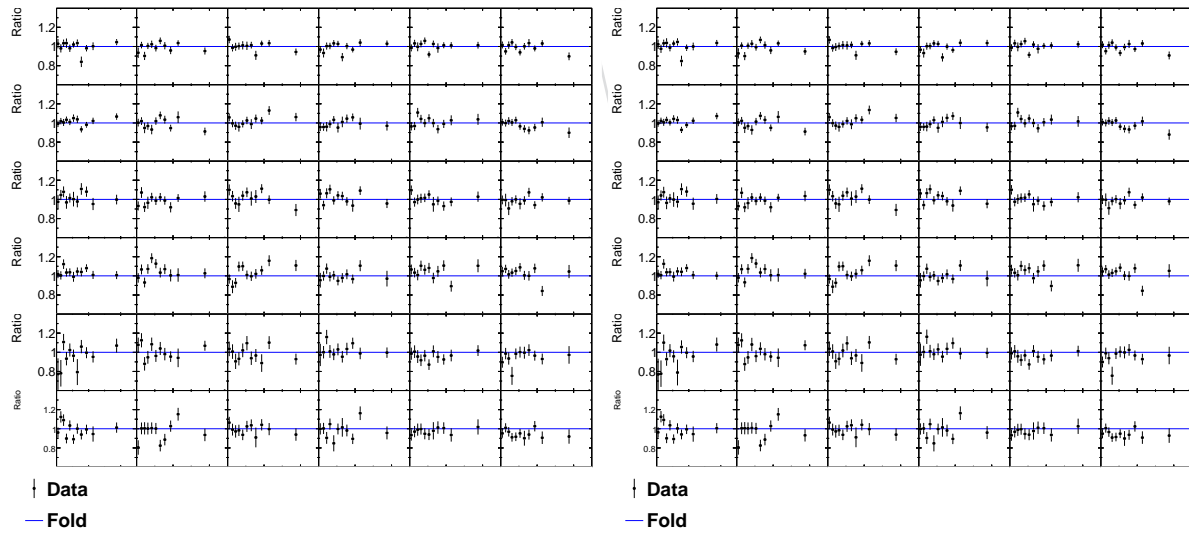


Figure 158: Ratio of the folded $[N_{jet}, M(t\bar{t}), y(t\bar{t})]$ cross sections (with 2 N_{jet} bins) to the data for the unregularised (left) and regularised (right) unfolding shown as a function of $y(t\bar{t})$ in different $[N_{jet}, M(t\bar{t})]$ ranges.

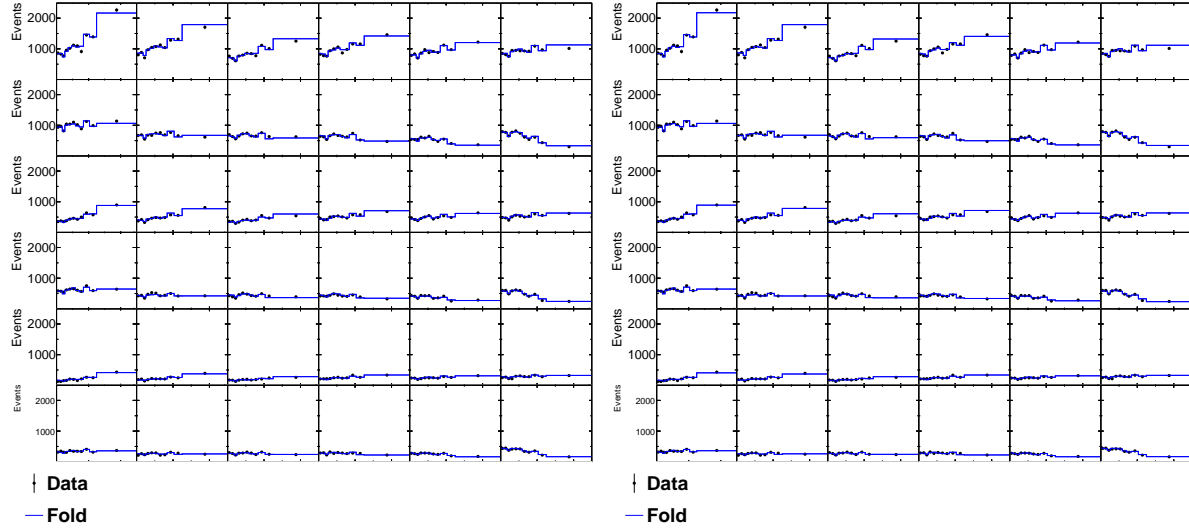


Figure 159: The folded $[N_{\text{jet}}, M(\bar{t}t), y(\bar{t}t)]$ cross sections (with 3 N_{jet} bins) compared to the data for the unregularised (left) and regularised (right) unfolding shown as a function of $y(\bar{t}t)$ in different $[N_{\text{jet}}, M(\bar{t}t)]$ ranges.

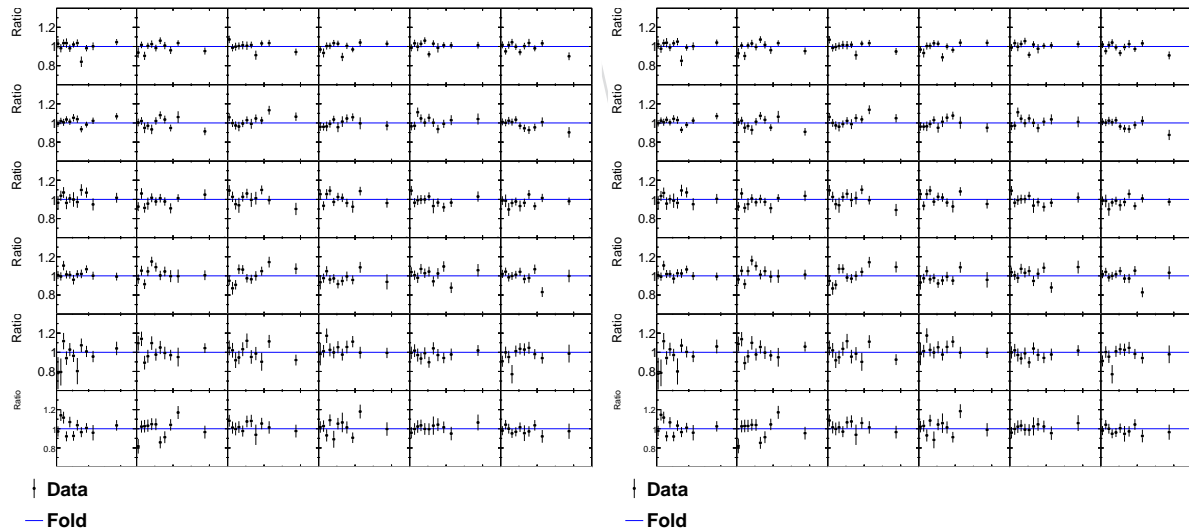


Figure 160: Ratio of the folded $[N_{\text{jet}}, M(\bar{t}t), y(\bar{t}t)]$ cross sections (with 3 N_{jet} bins) to the data for the unregularised (left) and regularised (right) unfolding shown as a function of $y(\bar{t}t)$ in different $[N_{\text{jet}}, M(\bar{t}t)]$ ranges.

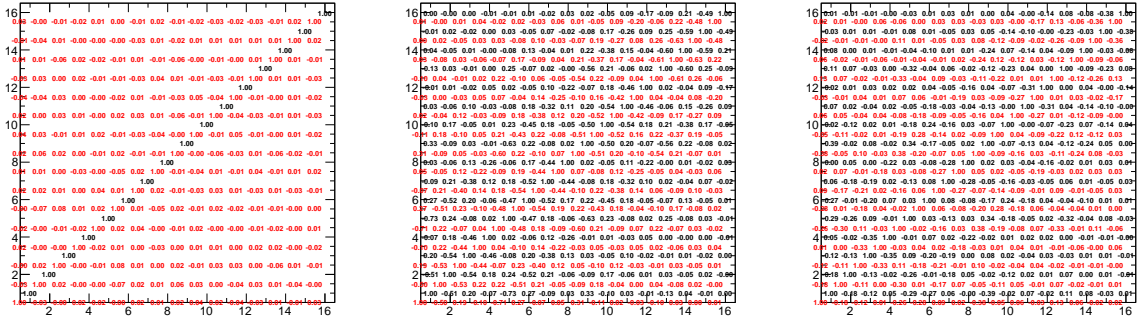


Figure 161: The correlation matrices for the unfolded $[y(t), p_T(t)]$ cross sections using the bin-by-bin (top left), unregularised (top right) and regularised (bottom) unfolding. Black numbers show the values of $\langle (\mathbf{Cov}_{\hat{\mathbf{M}}_{\text{avg}}^{\text{unf}} \hat{\mathbf{M}}_{\text{avg}}^{\text{unf}}})_{ij} \rangle$, while red numbers (displaced for each element to the bottom right for better visibility) show the values of $\langle (\hat{\mathbf{M}}_i^{\text{unf}} - \hat{\mathbf{M}}_{\text{avg},i}^{\text{unf}})(\hat{\mathbf{M}}_j^{\text{unf}} - \hat{\mathbf{M}}_{\text{avg},j}^{\text{unf}}) \rangle$ (see text for further details). No black off-diagonal numbers are shown for the bin-by-bin unfolding, because all such elements are 0.

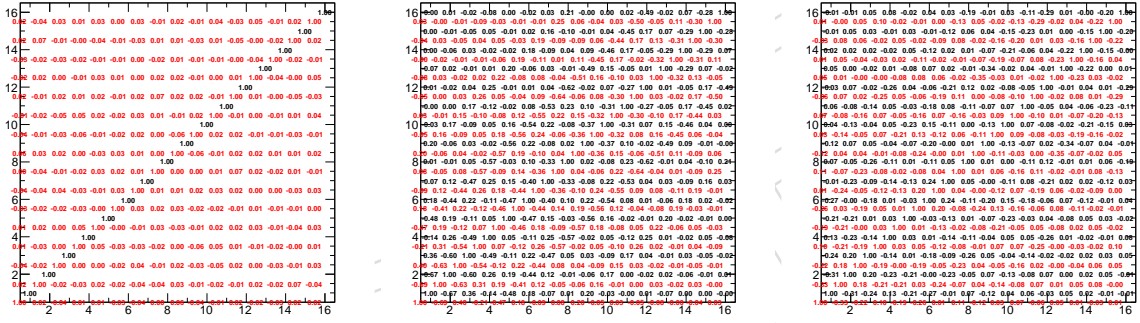
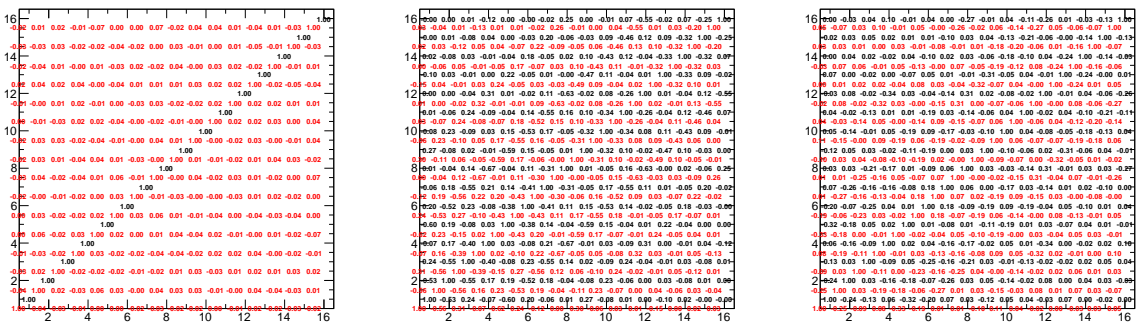
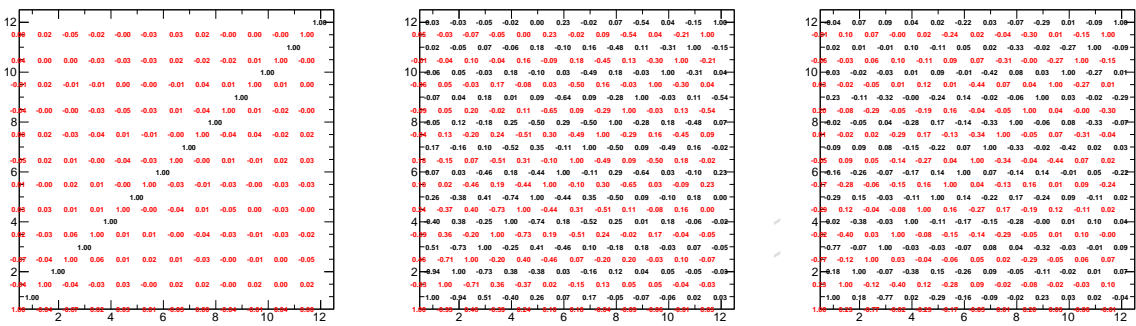
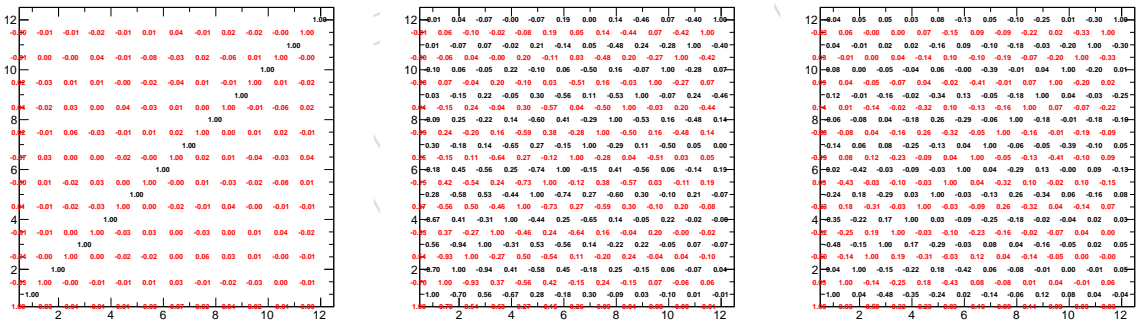
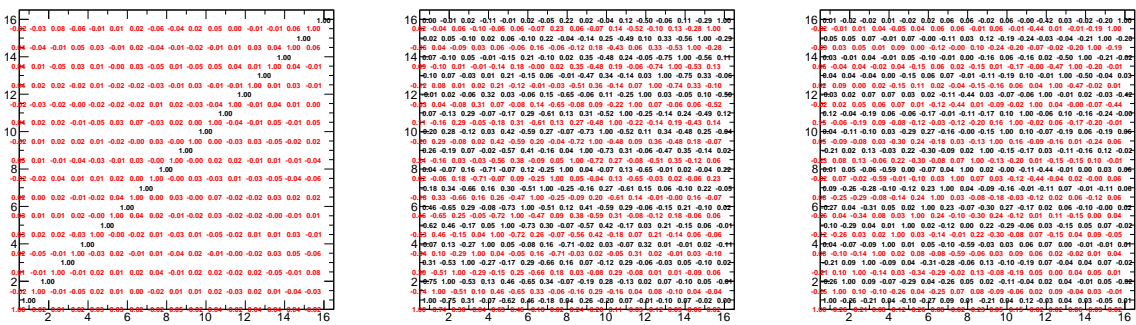


Figure 162: Same as in Fig. 161 for the $[M(t\bar{t}), y(t)]$ cross sections.

1374 B.2 Toy tests

1375 Figures 161–173 compare the correlation coefficients returned by the unfolding algorithms to
1376 the ones estimated from the set of toys.

Figure 163: Same as in Fig. 161 for the $[M(\bar{t}), y(\bar{t})]$ cross sections.Figure 164: Same as in Fig. 161 for the $[M(\bar{t}), \Delta\eta(\bar{t}, \bar{t})]$ cross sections.Figure 165: Same as in Fig. 161 for the $[M(\bar{t}), \Delta\phi(\bar{t}, \bar{t})]$ cross sections.Figure 166: Same as in Fig. 166 for the $[M(\bar{t}), p_T(\bar{t})]$ cross sections.

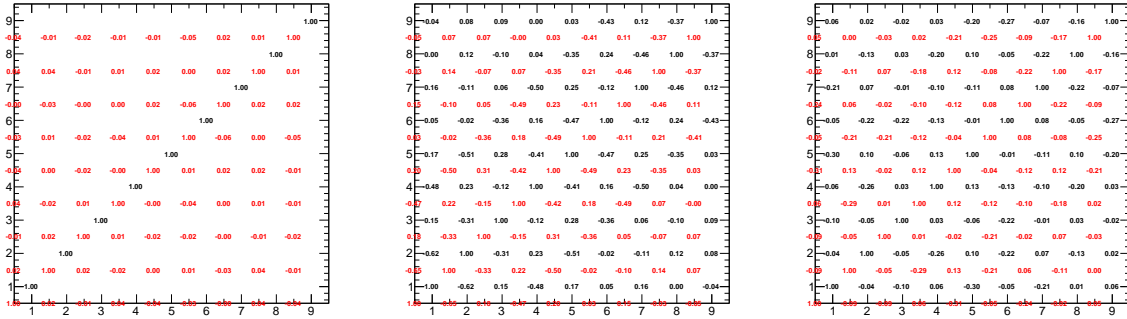


Figure 167: Same as in Fig. 161 for the $[M(\bar{t}), p_T(t)]$ cross sections.

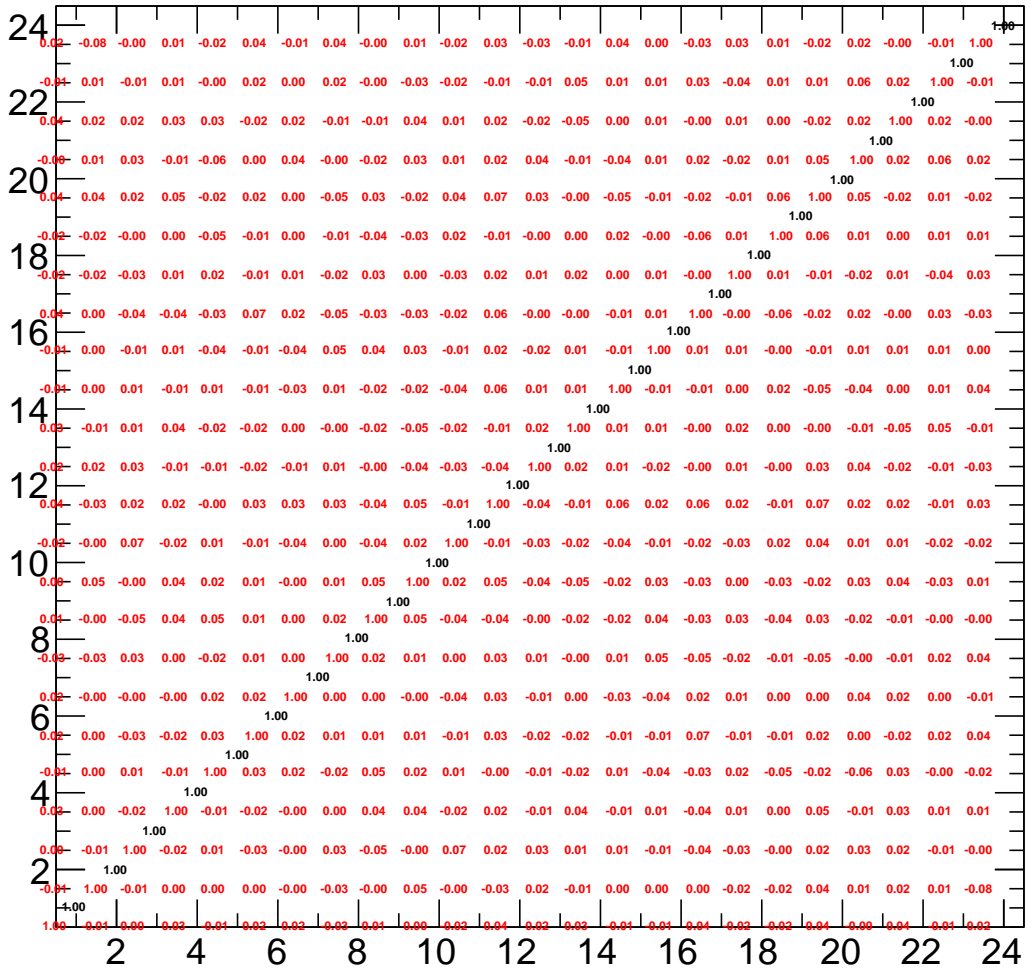


Figure 168: Same as in Fig. 161 for the $[N_{\text{jet}}, M(\bar{t}), y(t)]$ cross sections (2 N_{jet} bins) and bin-by-bin unfolding (see next figures for another algorithms).

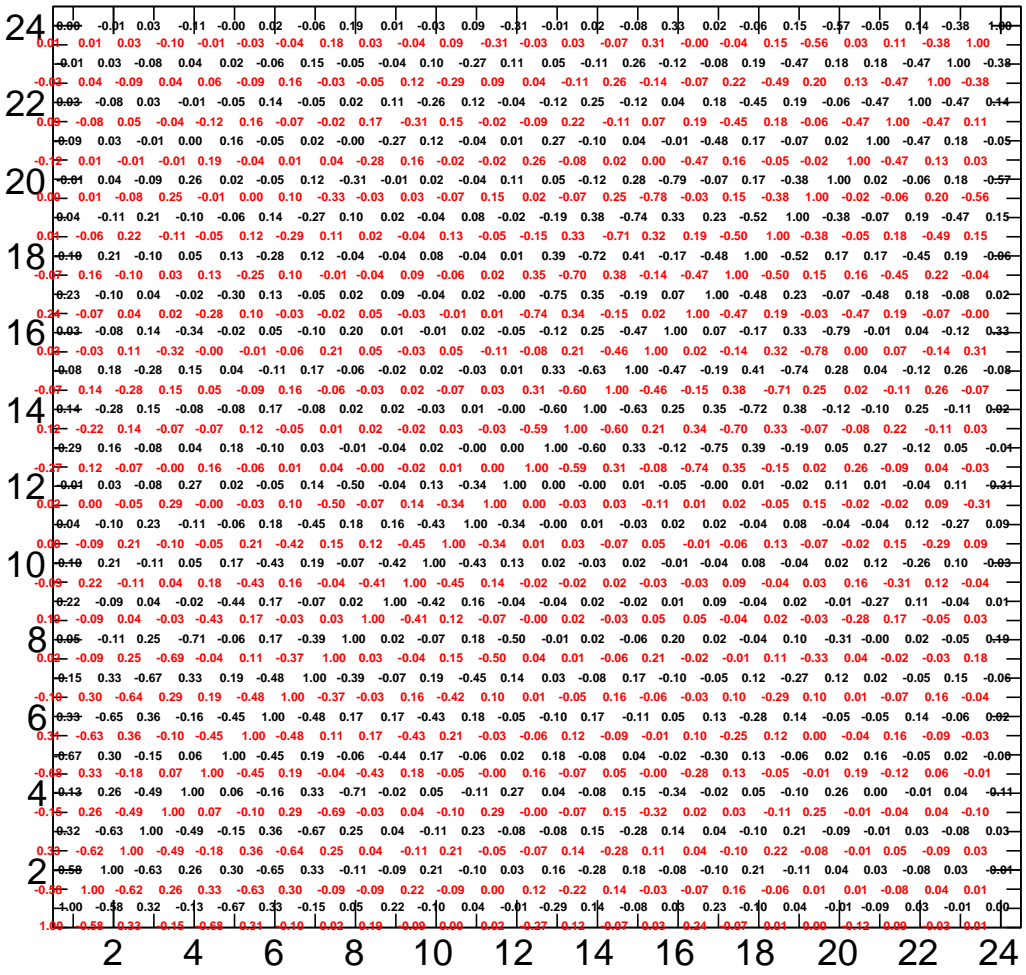


Figure 169: Same as in Fig. 161 for the $[N_{\text{jet}}, M(\bar{t}), y(t)]$ cross sections (2 N_{jet} bins) and unregularised unfolding (see previous and next figures for another algorithms).

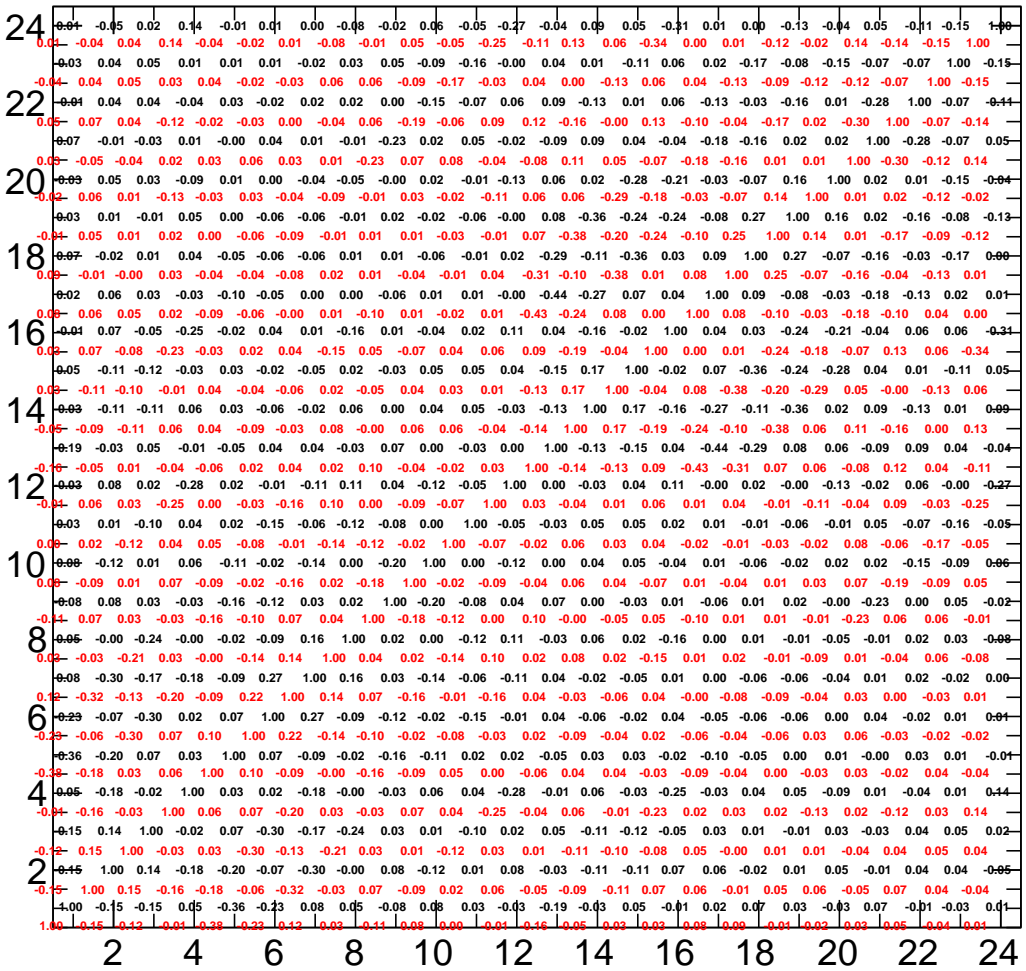


Figure 170: Same as in Fig. 161 for the $[N_{\text{jet}}, M(t\bar{t}), y(t)]$ cross sections (2 N_{jet} bins) and regularised unfolding (see previous figures for another algorithms).

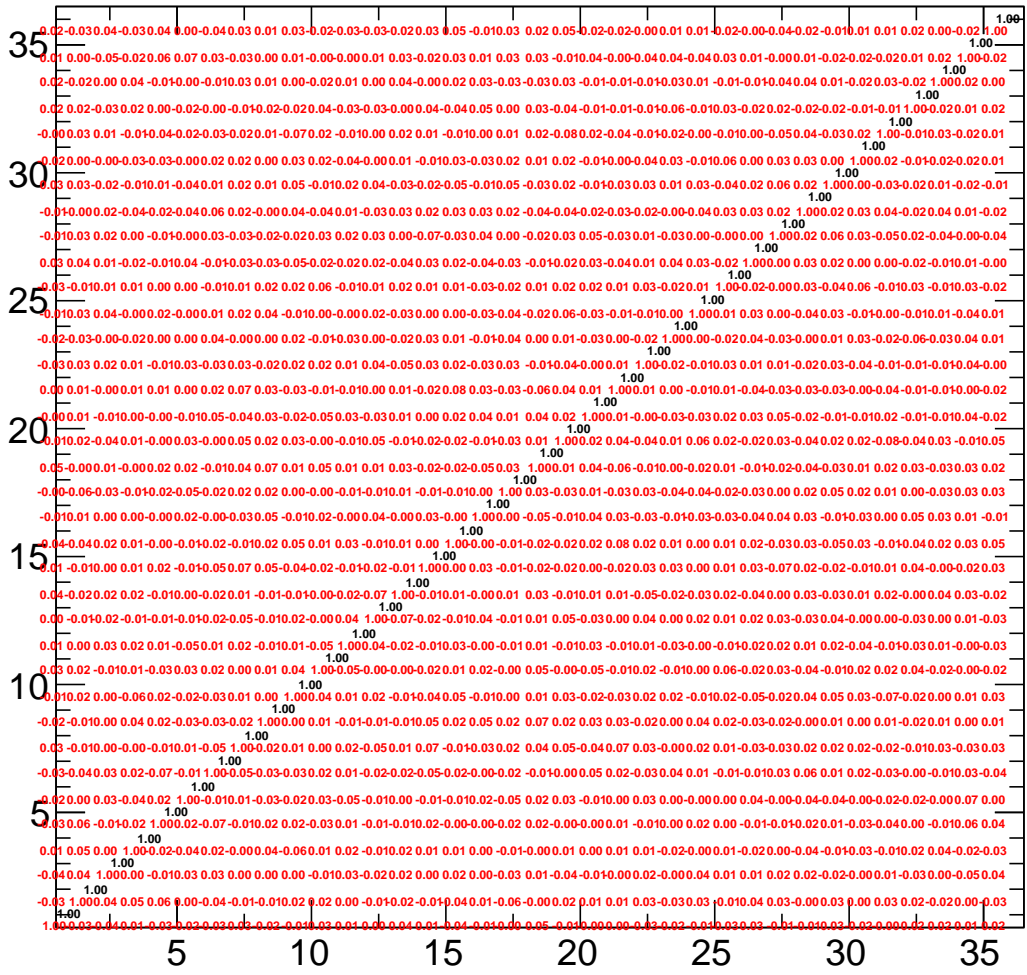


Figure 171: Same as in Fig. 161 for the $[N_{\text{jet}}, M(t\bar{t}), y(t)]$ cross sections (3 N_{jet} bins) and bin-by-bin unfolding (see next figures for another algorithms).

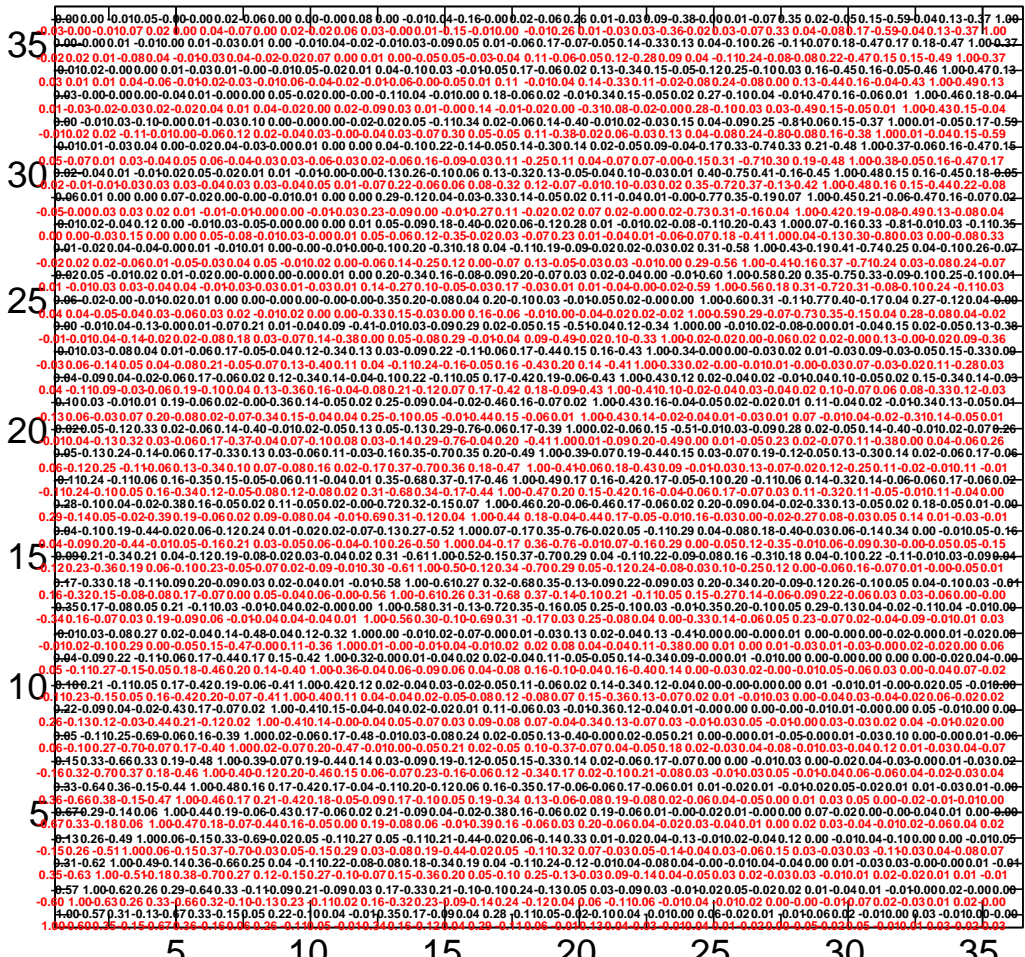


Figure 172: Same as in Fig. 161 for the $[N_{\text{jet}}, M(t\bar{t}), y(t)]$ cross sections (3 N_{jet} bins) and unregularised unfolding (see previous and next figures for another algorithms).

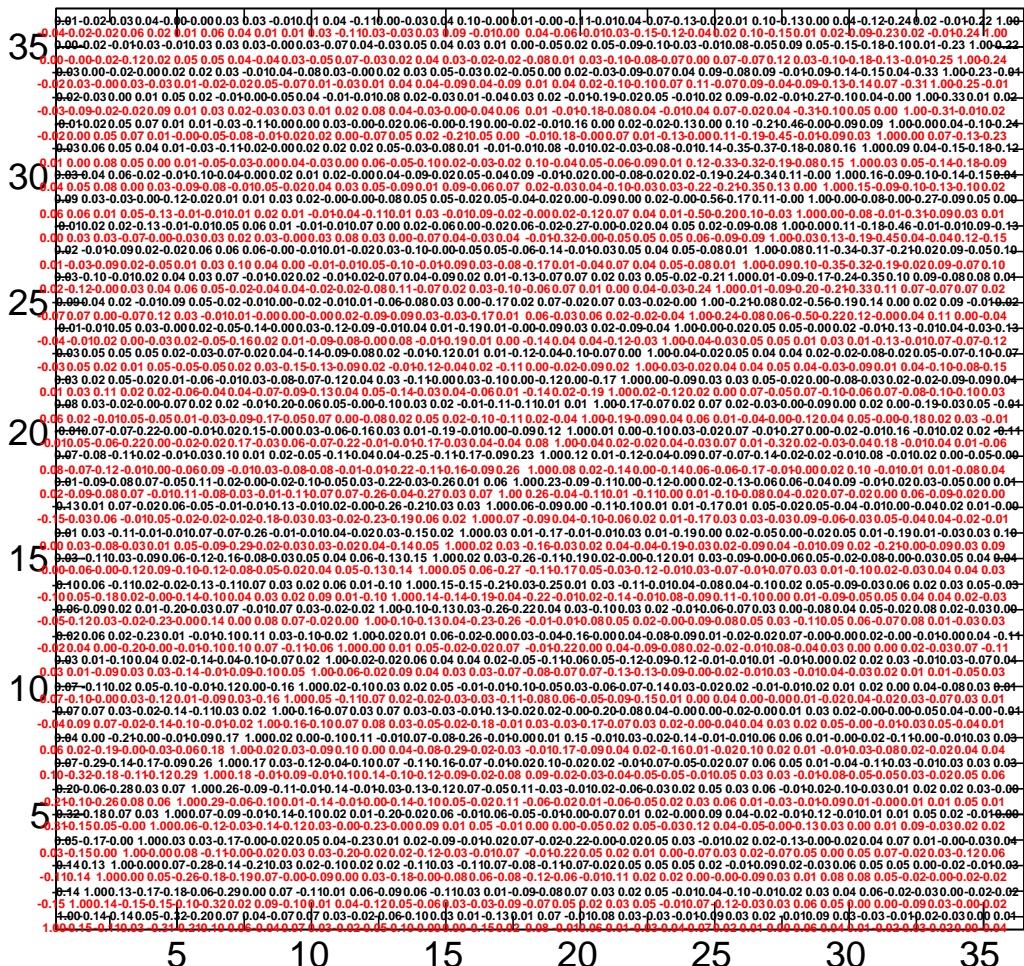


Figure 173: Same as in Fig. 161 for the $[N_{\text{jet}}, M(t), y(t)]$ cross sections (3 N_{jet} bins) and regularised unfolding (see previous figures for another algorithms).

1377 **B.3 Reweighting tests**

1378 Figures 174–182 present the reweighting tests (see Section 6.4.4) for all distributions.

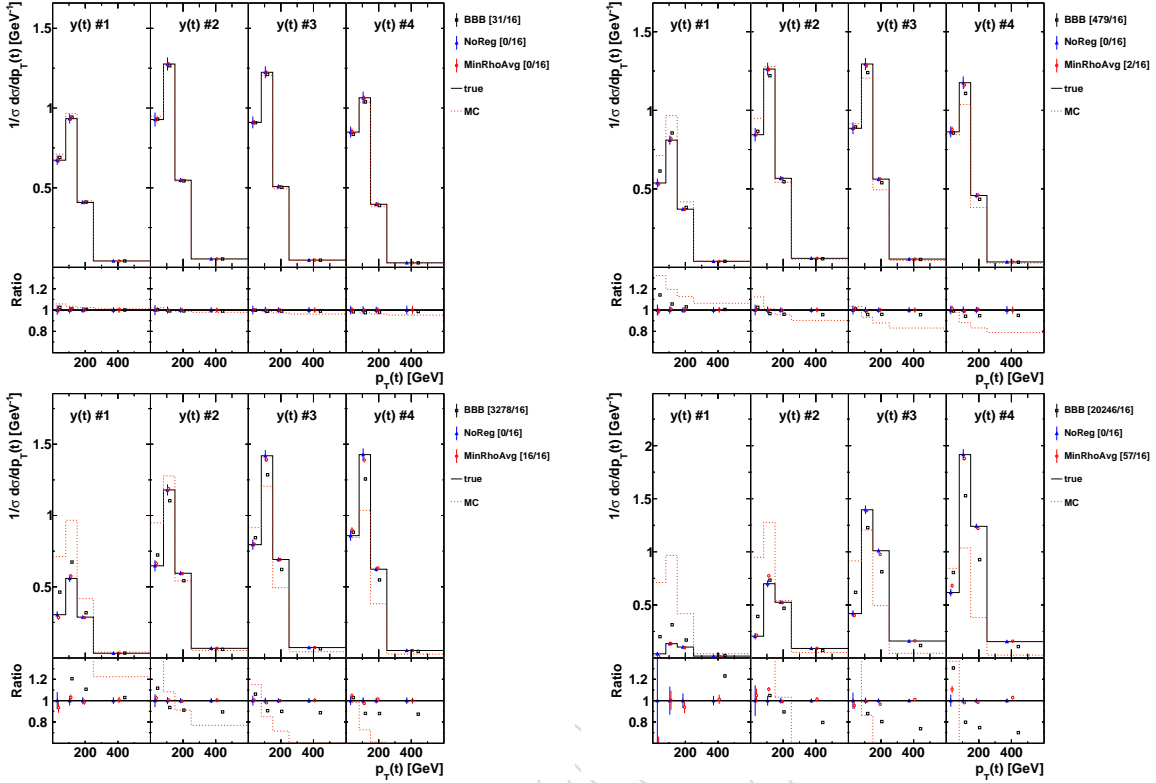


Figure 174: The unfolded $[y(t), p_T(t)]$ cross sections obtained using differently reweighted MC models. The value of χ^2/dof is reported (in quadratic brackets) for each algorithm.

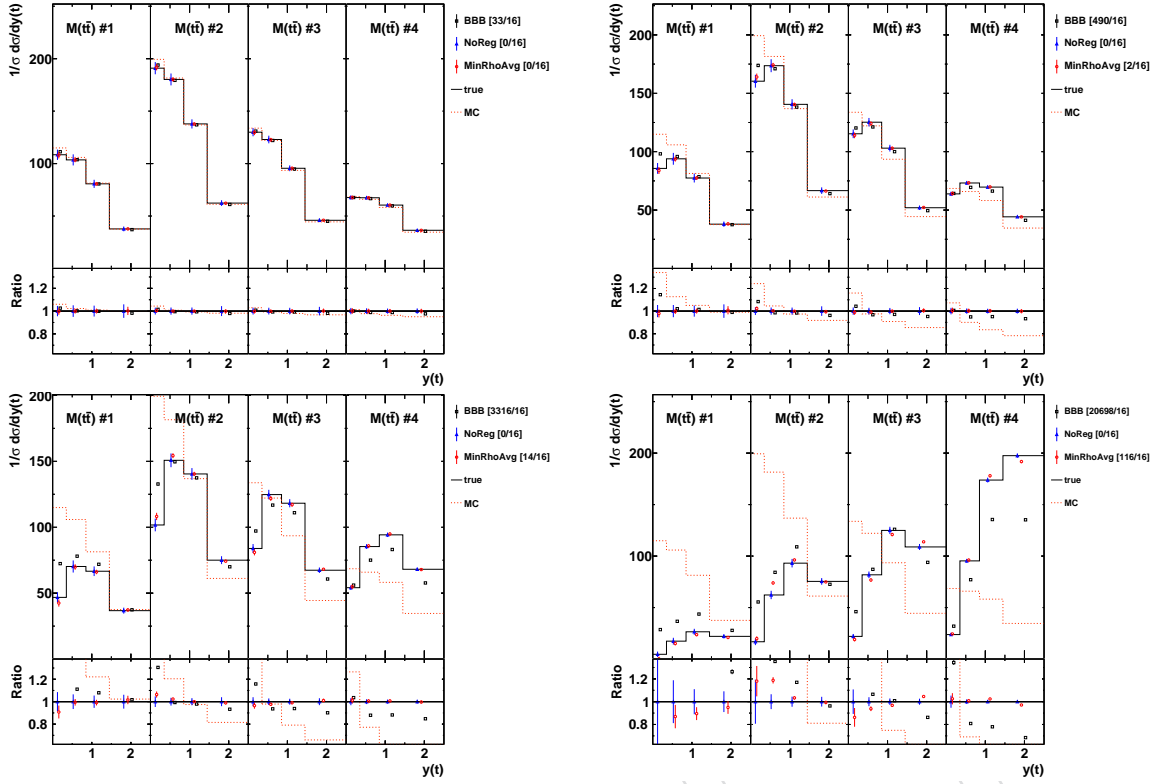


Figure 175: The unfolded $[M(\bar{t}\bar{t}), y(t)]$ cross sections obtained using differently reweighted MC models. The value of χ^2/dof is reported (in quadratic brackets) for each algorithm.

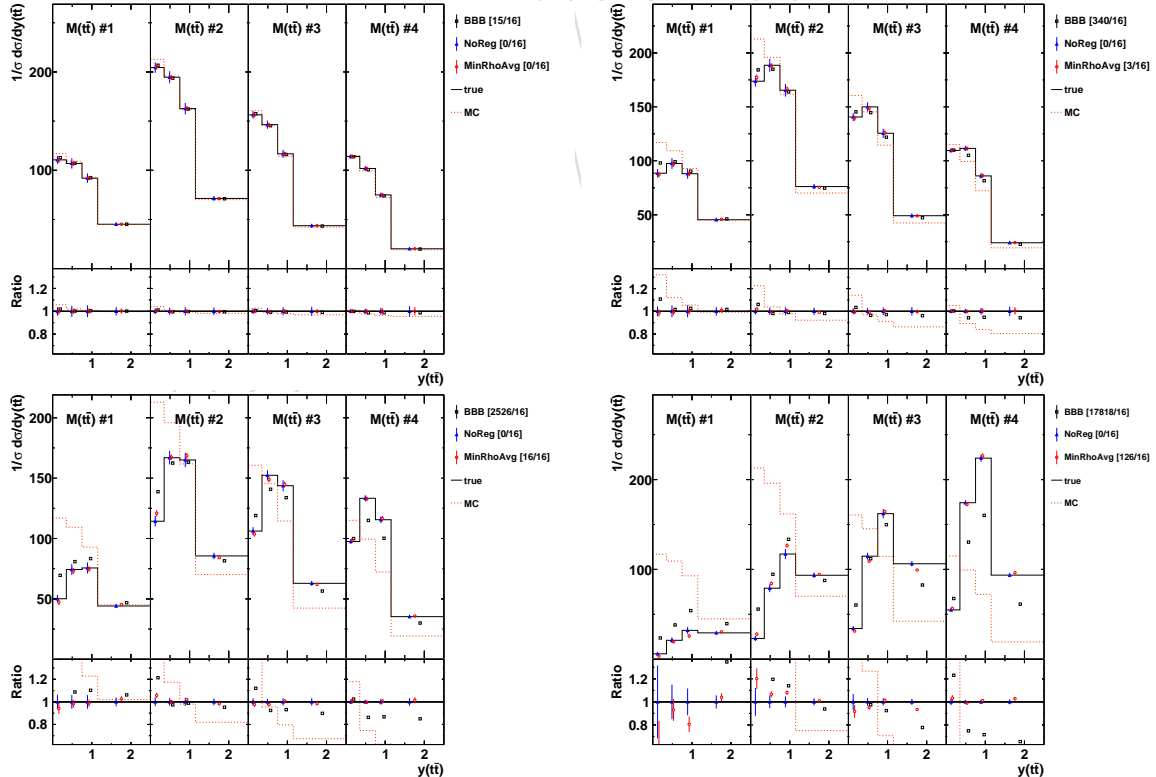


Figure 176: The unfolded $[M(\bar{t}\bar{t}), y(\bar{t}\bar{t})]$ cross sections obtained using differently reweighted MC models. The value of χ^2/dof is reported (in quadratic brackets) for each algorithm.

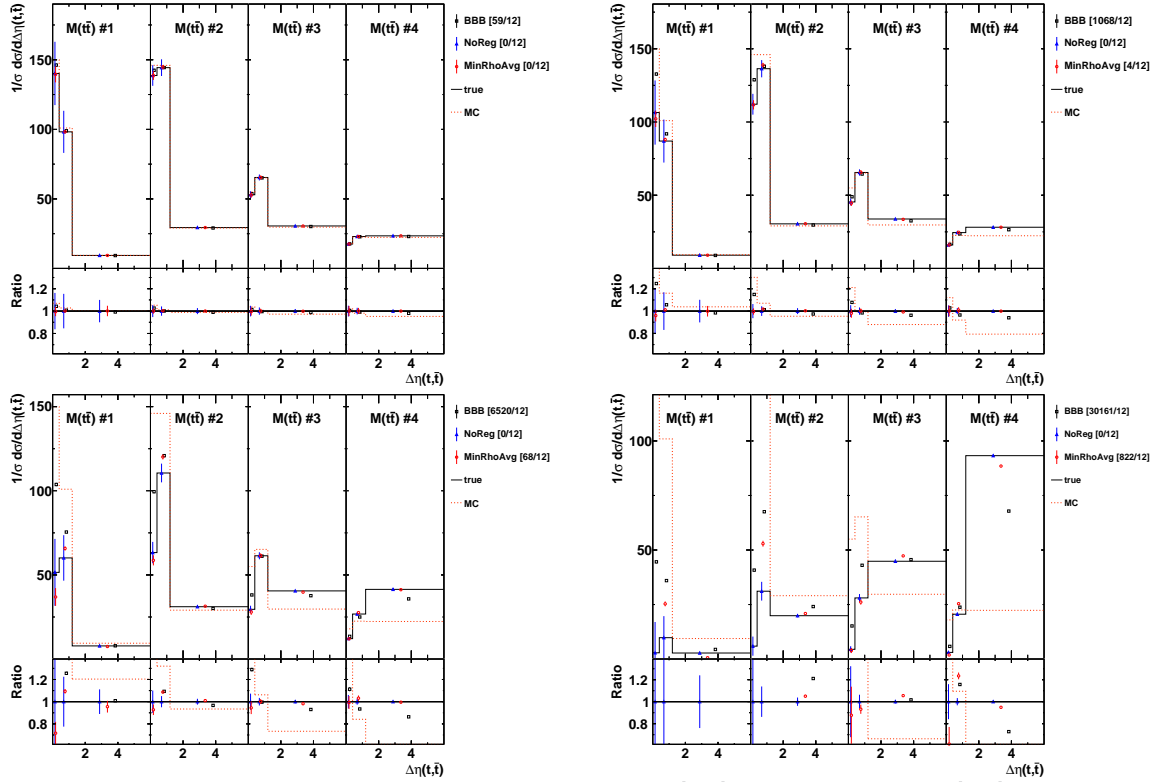


Figure 177: The unfolded $[M(t\bar{t}), \Delta\eta(t, \bar{t})]$ cross sections obtained using differently reweighted MC models. The value of χ^2/dof is reported (in quadratic brackets) for each algorithm.

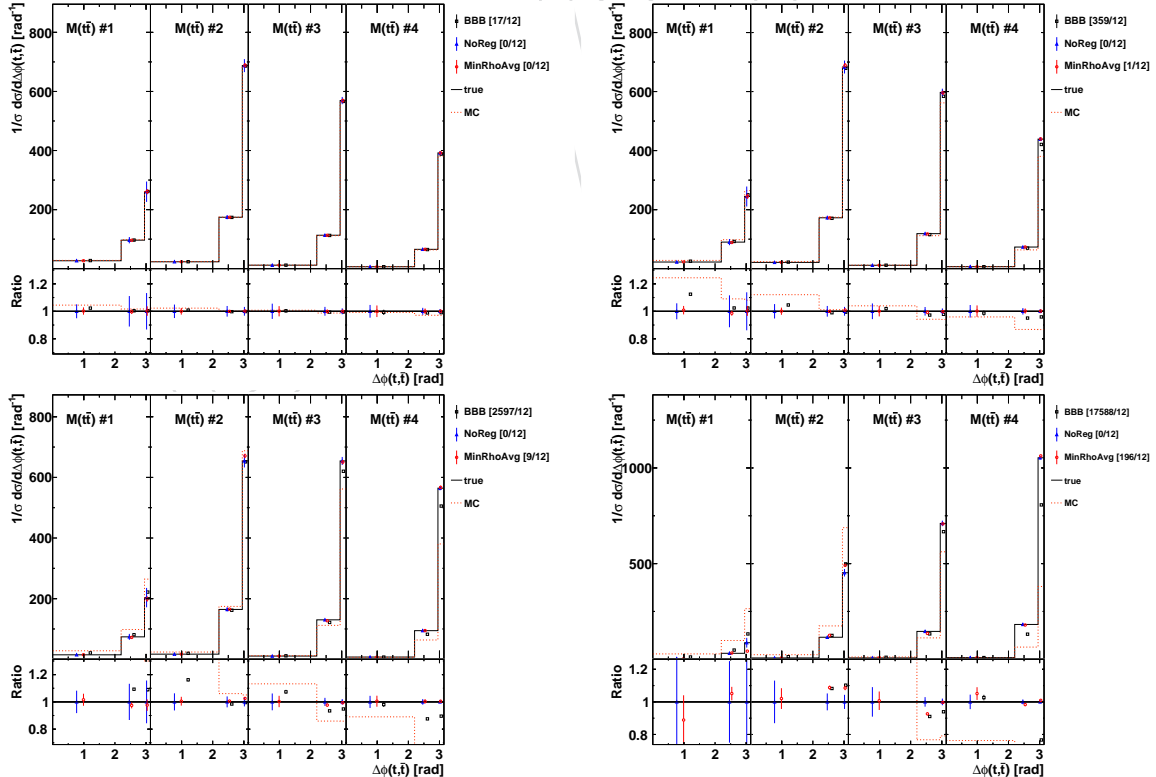


Figure 178: The unfolded $[M(t\bar{t}), \Delta\phi(t, \bar{t})]$ cross sections obtained using differently reweighted MC models. The value of χ^2/dof is reported (in quadratic brackets) for each algorithm.

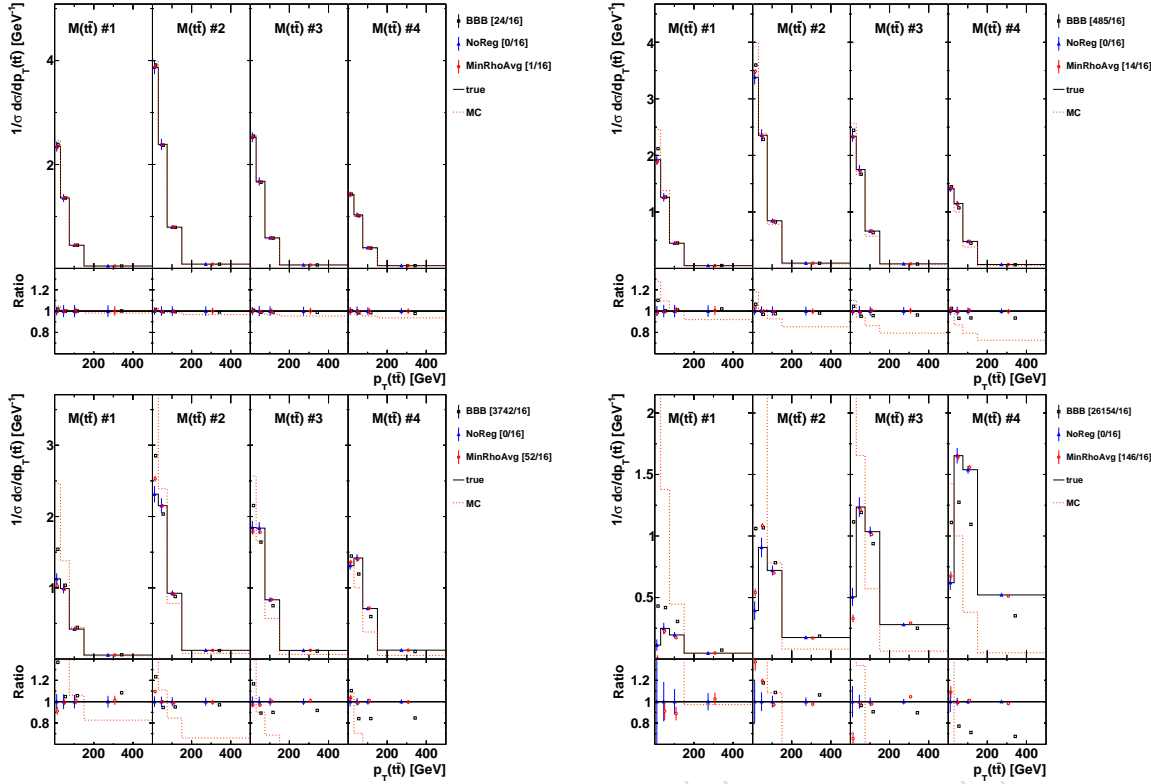


Figure 179: The unfolded $[M(t\bar{t}), p_T(t\bar{t})]$ cross sections obtained using differently reweighted MC models. The value of χ^2/dof is reported (in quadratic brackets) for each algorithm.

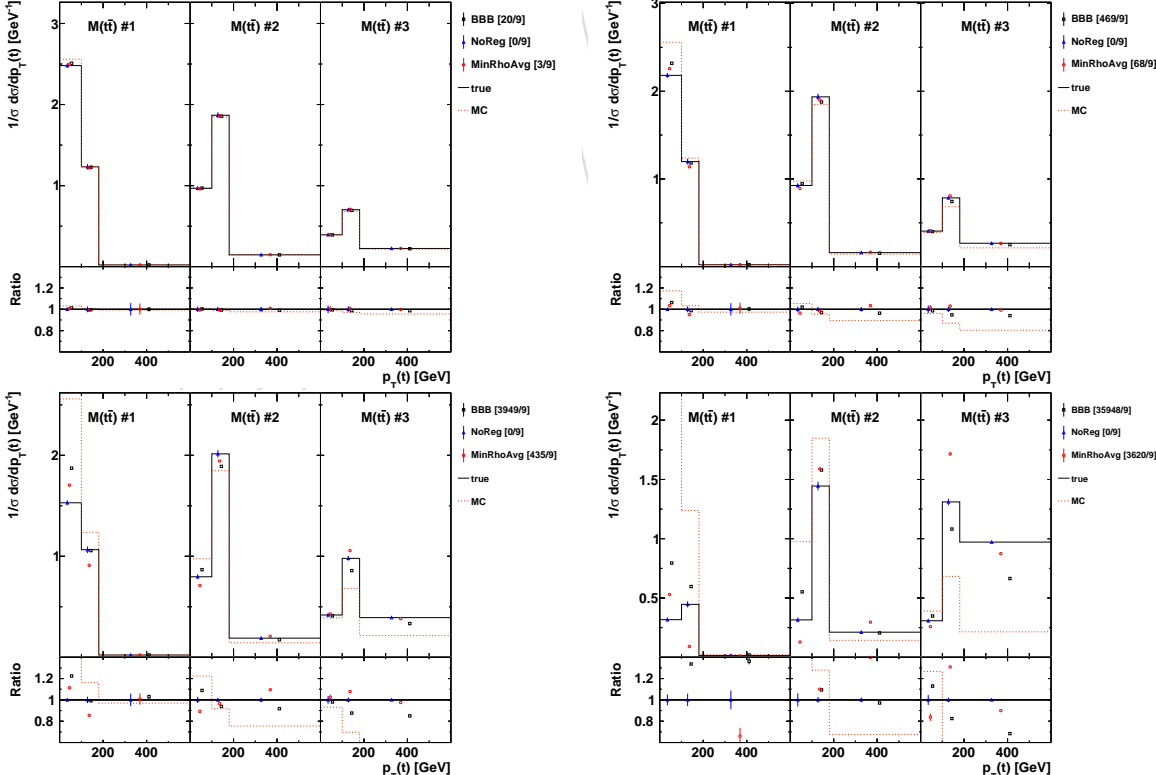


Figure 180: The unfolded $[M(t\bar{t}), p_T(t)]$ cross sections obtained using differently reweighted MC models. The value of χ^2/dof is reported (in quadratic brackets) for each algorithm.

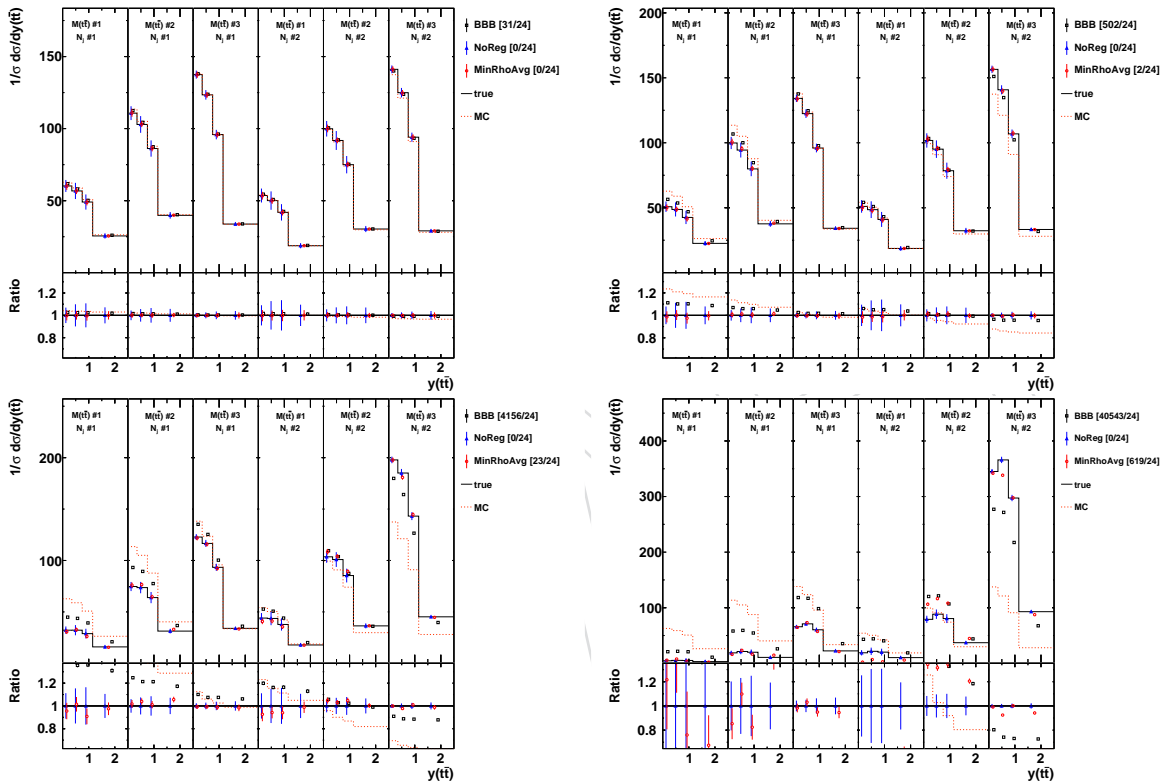


Figure 181: The unfolded $[N_{jet}, M(t\bar{t}), y(t\bar{t})]$ cross sections (2 N_{jet} bins) obtained using differently reweighted MC models. The value of χ^2/dof is reported (in quadratic brackets) for each algorithm.

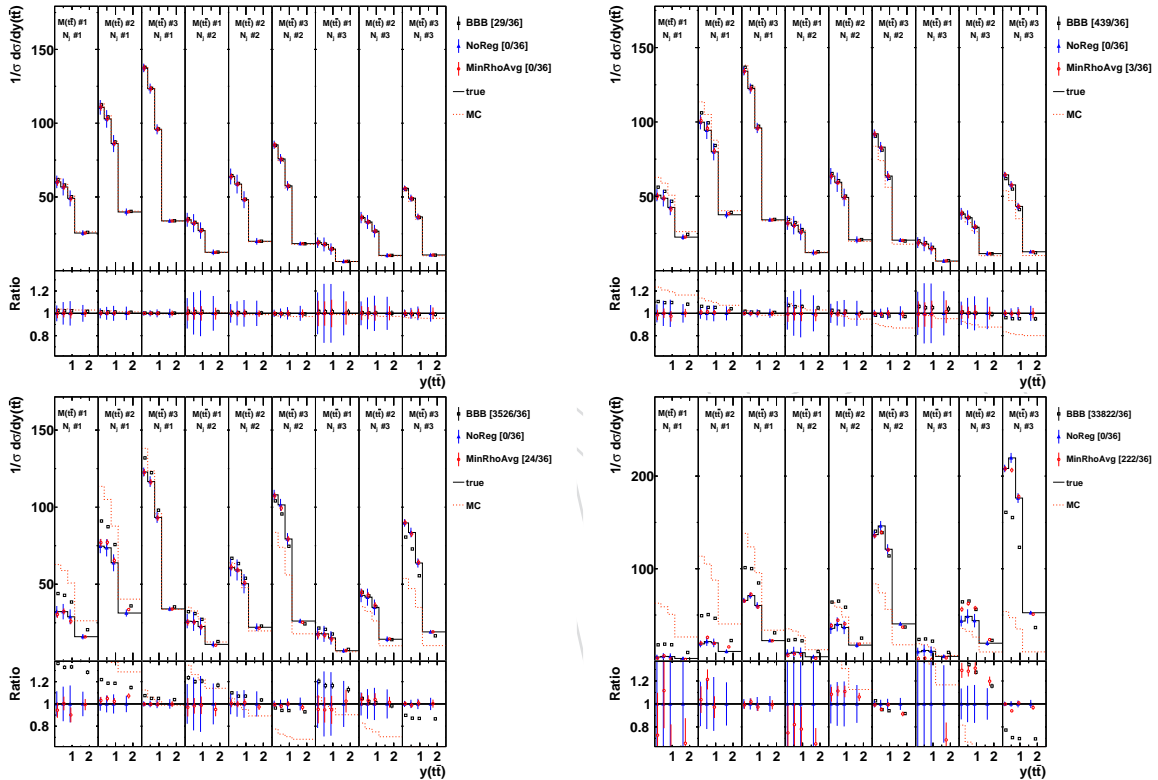


Figure 182: The unfolded $[N_{\text{jet}}, M(t\bar{t}), y(t\bar{t})]$ cross sections (3 N_{jet} bins) obtained using differently reweighted MC models. The value of χ^2/dof is reported (in quadratic brackets) for each algorithm.

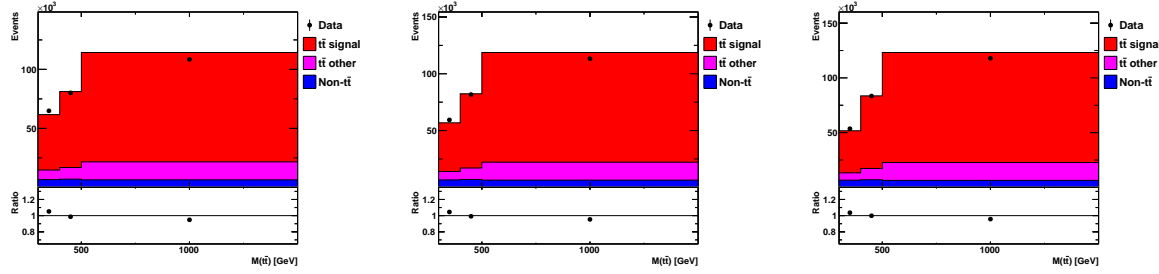


Figure 183: Distributions of $t\bar{t}$ $M(t\bar{t})$ in bins of $y(t\bar{t})$ using in the kinematic reconstruction $m_t = 169.5$ GeV (top), $m_t = 172.5$ GeV (middle) and $m_t = 175.5$ GeV (bottom).

C Study of m_t sensitivity of full kinematic reconstruction

The apparent sensitivity of the $M(t\bar{t})$ cross section to the value of m_t^{pole} (see Fig. 102) suggests to use the data to extract m_t^{pole} . It is noticeable that this sensitivity is largest at low $M(t\bar{t})$ where $M(t\bar{t}) \approx 2m_t^{\text{pole}}$, while the effect is propagated to a higher $M(t\bar{t})$ because of cross section normalisation. However, it is important to verify that the measured cross section does not have significant sensitivity to m_t which can be introduced when reconstructing $t\bar{t}$ and applying m_t kinematic constraints. A dedicated study of the sensitivity to m_t was performed therefore. As a result, an alternative, so called loose, kinematic reconstruction algorithm was developed (see Section 4.2) and employed to measure the triple-differential cross sections which are used to extract the QCD parameters and PDFs.

The kinematic reconstruction procedure described in Section 4 is referred to as full kinematic reconstruction. It is used to restore the top quark and antiquark kinematics from the measured leptons, jets and p_T^{miss} (see Section 4), which at first place recovers the momenta of the top and antitop quarks, while their energies are calculated after assigning an external value of m_t . This reduces a lot the sensitivity to the genuine m_t after applying the kinematic reconstruction. The detector-level distribution of $M(t\bar{t})$ (see Fig. 19) appears to be driven to a large extent by the value of m_t used in the kinematic reconstruction, especially at low values of $M(t\bar{t})$. This is demonstrated in Fig. 183 where the control distribution for $[M(t\bar{t}), y(t\bar{t})]$ is shown for $m_t = 171.5$ GeV, $m_t = 172.5$ GeV (nominal) and $m_t = 173.5$ GeV. The changes of the shape in the data and MC are mostly identical (because the m_t in the kinematic reconstruction is varied simultaneously in both), and the ratio data/MC is essentially not sensitive to the variations.

The next step is the variation of m_t in MC at true level. The corresponding distributions are shown in Fig. 184. In these comparisons, m_t is varied by ± 3 GeV both in MC and in the kinematic reconstruction (the variation by ± 3 GeV is chosen in order to use the MC samples generated for $m_t = 169.5$ GeV and $m_t = 175.5$ GeV which are available with a large statistics, while further this variation is scaled to ± 1 GeV to assess the systematic uncertainties). Note that the distributions with m_t variations are normalised to the cross section of the nominal MC. Similarly to the previous observation, a large part of the changes appear to be the same in the data and MC and cancel in their ratio. However, once the m_t parameter is changed in MC at true level, the opposite is expected for the impact on the measured cross section after unfolding: it is expected to be mostly correlated with the MC true-level cross section. This is shown in Fig. 185: the change of the detector-level MC distribution mostly follows the change of the true-level distribution, and since the data distribution is changed similar to the MC detector-level distribution, the measured cross sections is highly sensitive to the MC m_t parameter. Since the m_t MC parameter is somehow related, but not identical to the physical pole top-quark mass, such dependence will introduce a systematic uncertainty which is hard to have under control

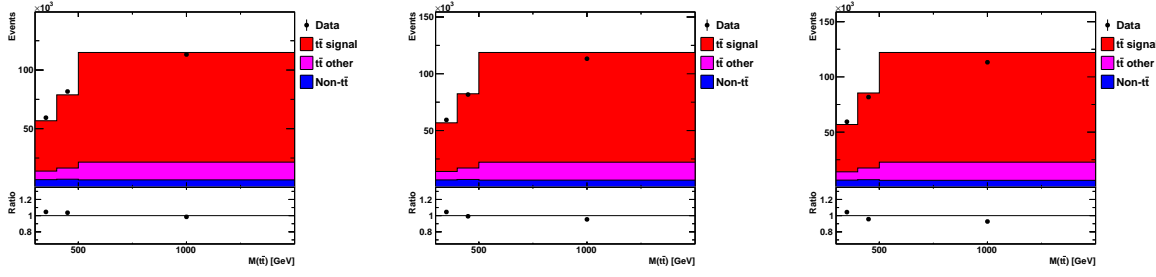


Figure 184: Distributions of $t\bar{t}$ $M(t\bar{t})$ in bins of $y(t\bar{t})$ using MC simulations with $m_t = 169.5$ GeV (top), $m_t = 172.5$ GeV (middle) and $m_t = 175.5$ GeV (bottom).

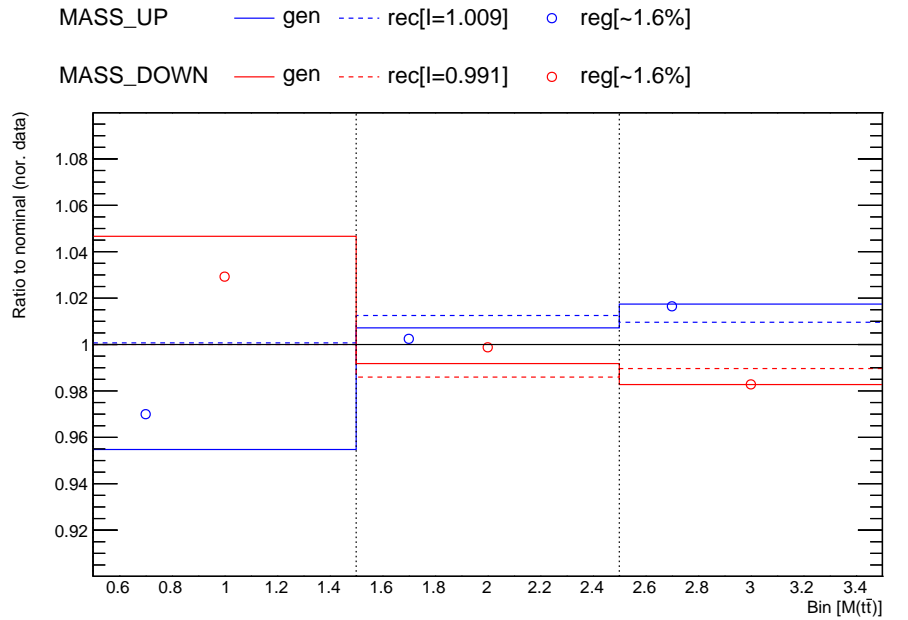


Figure 185: The impact of m_t variation by ± 1 GeV in MC and kinematic reconstruction at generator level ('gen'), reconstructed level ('rec') and measured cross-section ('reg', for the regularised unfolding). For each variation, the average effect is reported in quadratic brackets (at true level, the distributions with m_t variations are normalised to the cross section of the nominal MC).

- 1415 if extracting m_t from the measured cross sections. The same conclusions apply to the triple-
 1416 differential $[N_{\text{jet}}, M(t\bar{t}), y(t\bar{t})]$ cross sections.
 1417 To summarise, the data from the present analysis obtained using the full kinematic reconstruction
 1418 (the double-differential cross sections) should not be used to compare to predictions ob-
 1419 tained using m_t which is significantly different from the range $m_t = 172.5 \pm 1$ GeV because
 1420 there is potentially a high but not precisely known correlation between the measured cross sec-
 1421 tions and m_t^{pole} . Instead, the triple cross sections measured using loose kinematic reconstruc-
 1422 tion (see Section 4.2) have negligible sensitivity to m_t and can be used for m_t^{pole} extraction.

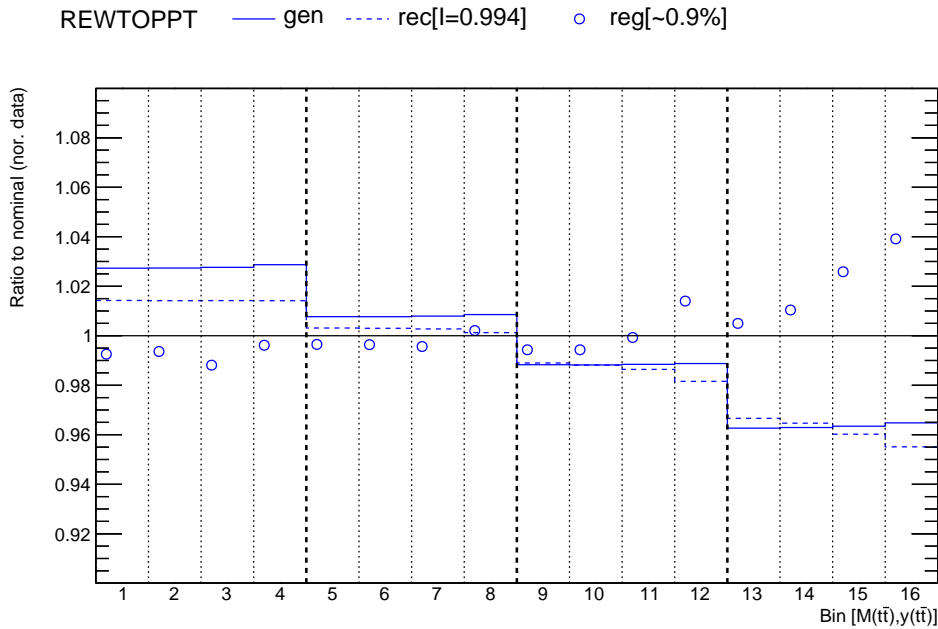


Figure 186: The impact of $p_T(t)$ reweighting at generator level ('gen'), reconstructed level ('rec') and measured cross-section ('reg', for the regularised unfolding), for the double-differential cross section as a function of $M(t\bar{t})$ and $y(t\bar{t})$. The average effect is reported in quadratic brackets. At true level, the distribution after $p_T(t)$ reweighting is normalised to the cross section of the nominal MC.

1423 D Study of cross sections sensitivity to $p_T(t)$ reweighting

1424 Since the $p_T(t)$ distribution predicted by POWHEG2 + PYTHIA8 is harder than the one in the
 1425 data (see Figs. 16, 91, according to recommendations [104] a cross check was done to estimate
 1426 the possible uncertainty arising due to the mismodelling of $p_T(t)$ by reweighting the $p_T(t)$
 1427 distribution in POWHEG2 + PYTHIA8. The reweighting function [104] was determined as
 1428 the ratio of the $p_T(t)$ distribution in the data to the one POWHEG2 + PYTHIA8. The effect
 1429 was checked for the double-differential cross section as a function of $M(t\bar{t})$ and $y(t\bar{t})$. The
 1430 variation of the measured cross section is shown in Fig. 186. It is well within the total systematic
 1431 uncertainties (see Fig. 84), thus the possible uncertainty arising due to the mismodelling of
 1432 $p_T(t)$ is already covered by the assigned systematic uncertainties described in Section 5, and
 1433 no extra uncertainty is assigned.

1434 E Study of scale choice for NLO calculations

1435 For normalised differential $t\bar{t}$ cross sections as a function of $t\bar{t}$ kinematic variables, scale variations
 1436 have very little impact ($\lesssim 1\%$), but for the cross section as a function of N_{jet} scale variations
 1437 reach a few % and more (see Fig. 102). A dedicated study was done in order to find the most
 1438 reasonable scale choice for $t\bar{t}$ production with various N_{jet} considered in this analysis. This
 1439 study aims to find the scale choice which minimises the dependence of the cross section on the
 1440 scale, following the principle of minimal sensitivity [105–107].

The predictions were generated as described in I.1. The CT14 PDF set and $m_t^{\text{pole}} = 172.5 \text{ GeV}$
 were used (the results are not expected to be sensitive to these settings). Several scale choices
 were studied [74]:

$$\begin{aligned} \mu_r = \mu_f &= H/2, H = \sum_i m_{T,i}, \quad i = t, \bar{t}, \\ \mu_r = \mu_f &= H'/2, H' = \sum_i m_{T,i}, \quad i = t, \bar{t} \text{ and light partons}, \\ \mu_r = \mu_f &= H''/2, H'' = \sum_i m_{T,i}, \quad i = t, \bar{t} \text{ and jets clustered from light partons}, \\ \mu_r = \mu_f &= m_t. \end{aligned} \tag{17}$$

1441 where m_T is transverse mass $m_T = \sqrt{m^2 + p_T^2}$. Scales μ_r and μ_f were varied in a wide range
 1442 with respect to their nominal values, both simultaneously or independently. The study was
 1443 done for inclusive $t\bar{t}$ and $t\bar{t} + 1$ jet production.

1444 The results for $\sigma(t\bar{t})$, $\sigma(t\bar{t}j)$ and their ratio $R = \sigma(t\bar{t}j)/\sigma(t\bar{t})$ are shown in Figs. 187 and 188.
 1445 Several conclusions have been drawn:

- 1446 1. Over a large range of μ/μ_{ref} , the impact of μ_r variation is greater than the impact of μ_f
 1447 variation. Furthermore, in the bulk of the considered μ/μ_{ref} range both μ_r and μ_f scale
 1448 variations lead to the cross section changes in the same direction, and the simultaneous
 1449 $\mu_r = \mu_f$ variation leads to the largest cross section change.
- 1450 2. The first 3 functional forms from Eq. 17 (dynamical scales which depend not only on m_t^{pole}
 1451 but also on $p_T(t)$) behave similar, while the static scale $\mu_r = \mu_f = m_t$ leads to a somewhat
 1452 larger cross section variation for $t\bar{t} + 1$ jet cross section and R .
- 1453 3. For the ratio of $t\bar{t}$ and $t\bar{t} + 1$ jet cross sections the scale choice which minimises its variation
 1454 is when any scale is set to its reference value, i.e. $\mu/m_t \sim 1$.

1455 Based on these observations, the nominal scale is chosen to be $\mu_{\text{ref}} = H'/2$. To estimate scale
 1456 uncertainties, μ_r and μ_f are varied independently up and down by a factor of 2, subject to
 1457 the additional restriction that the ratio μ_r/μ_f be between 0.5 and 2. However, by construction
 1458 of the principle of minimal sensitivity, scale variations around this nominal value result in
 1459 asymmetric (always negative) scale uncertainties for the ratio of $t\bar{t} + 1$ jet over $t\bar{t}$ cross sections
 1460 (see Fig. 188). Therefore, in order to be on the safe side, an alternative scale choice $\mu_{\text{ref}} = H/2$ is
 1461 considered when estimating scale uncertainties. As can be seen from Fig. 188, this prescription
 1462 results in the scale uncertainty $\approx 1.5\%$ for R .

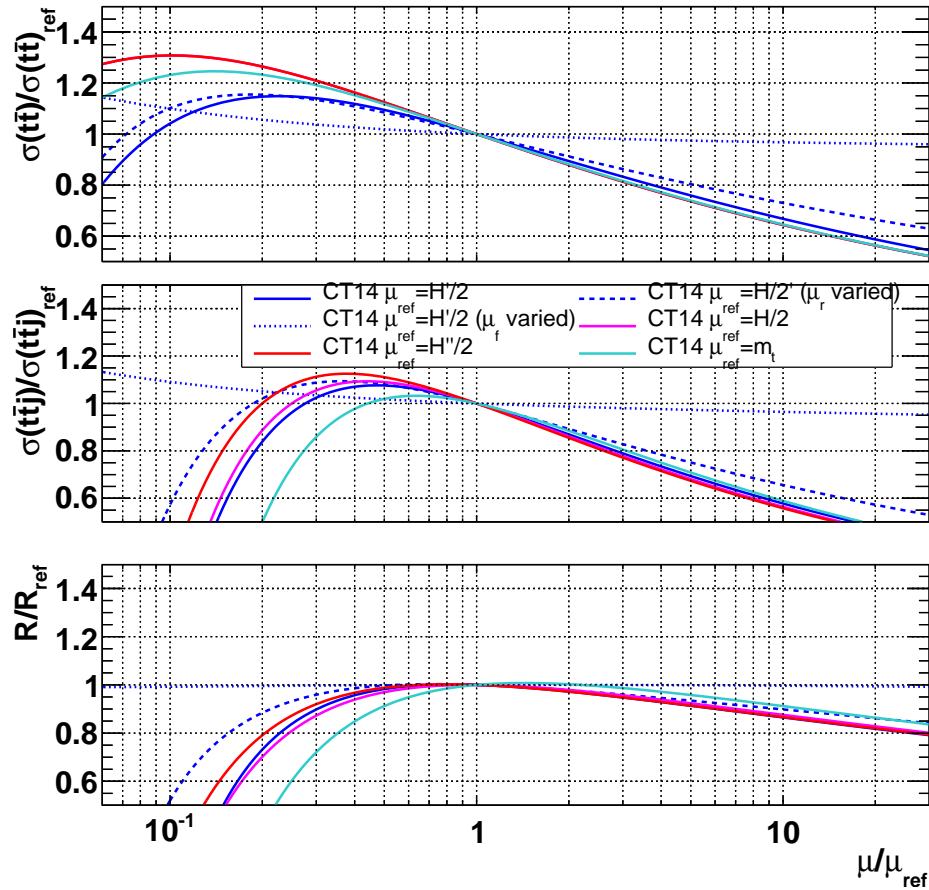


Figure 187: Theoretical predictions for the total $t\bar{t}$ (up panel) and $t\bar{t} + 1 \text{ jet}$ (middle panel) cross section as a function of μ_r and μ_f . Both the scales and the predicted cross sections are shown as the ratios over their nominal values corresponding to the scale choice μ_{ref} . Predictions obtained using different functional forms for μ_{ref} (see Eq. 17) are shown in different colors. Predictions obtained when varying only μ_r or μ_f are shown as dashed or dotted lines, respectively. The bottom panel shows the predicted ratio (R) of $t\bar{t} + 1 \text{ jet}$ over $t\bar{t}$ cross section.

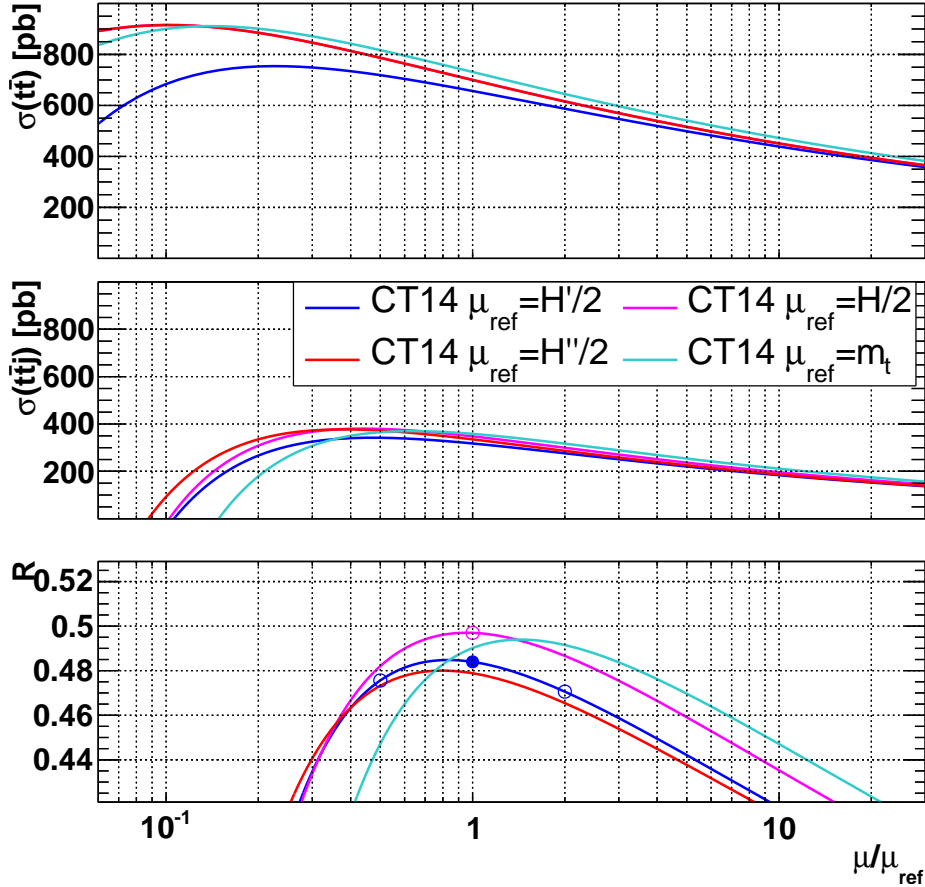


Figure 188: Theoretical predictions for the total $t\bar{t}$ and $t\bar{t} + 1$ jet cross section as a function of μ_r and μ_f . Predictions obtained using different functional forms for μ_{ref} (see Eq. 17) are shown in different colors. The bottom panel shows the predicted ratio (R) of $t\bar{t} + 1$ jet over $t\bar{t}$ cross section. The nominal scale choice is shown as a full marker, while the values used as scale variations are shown as empty markers.

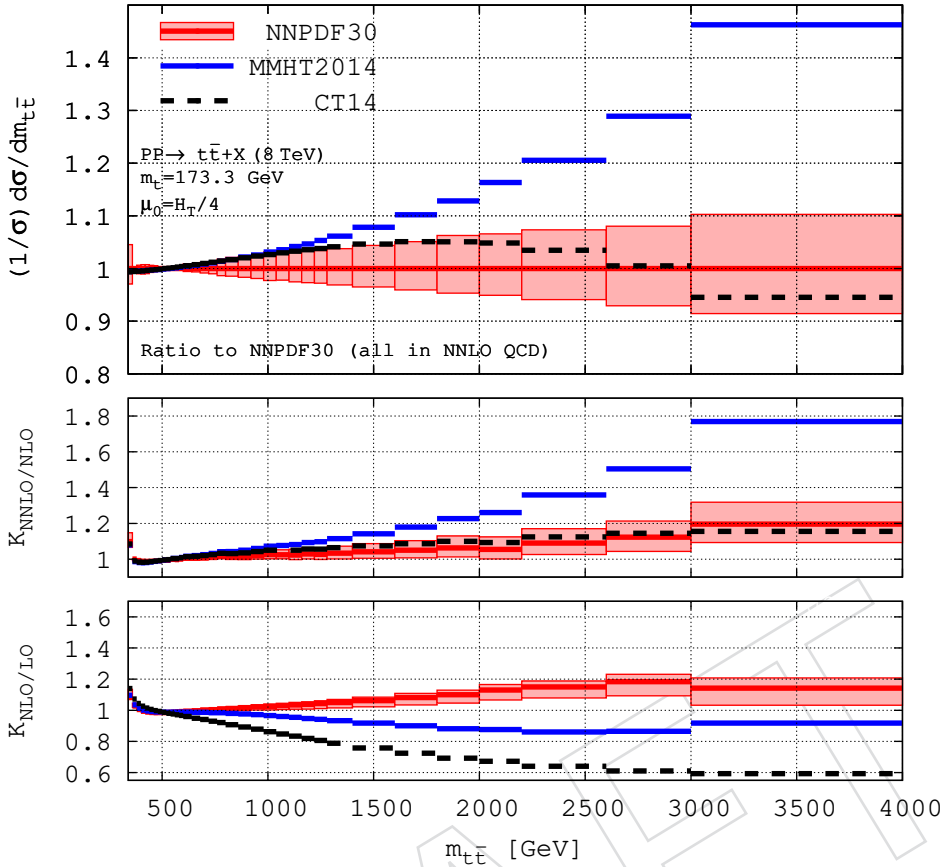


Figure 189: The ratios of NNLO over NLO calculations for normalised cross sections as a function of $M(t\bar{t})$ from Ref. [74].

F NNLO corrections to the $M(t\bar{t})$ distribution

When estimating NLO scale uncertainties, the scales are varied simultaneously in all $M(t\bar{t})$, $y(t\bar{t})$ and N_{jet} bins. In order to check if these variations estimate missing higher-order corrections reliably, NNLO/NLO correction factors (so called K factors) from Ref. [74] are applied as function of $M(t\bar{t})$ only, assuming they are independent of $y(t\bar{t})$ and N_{jet} . Note, that for normalised cross section only the shape of NNLO/NLO factors as functions of kinematic variables, but not their normalisation.

The ratios of NNLO over NLO calculations from Ref. [74] displayed in Fig. 189 are used to multiply the NLO calculations. The NNLO/NLO corrections are obtained with the CT14, MMHT2014 and NNPDF3.0 PDF sets and $m_t^{\text{pole}} = 173.1$ GeV and applied independently of $y(t\bar{t})$ or N_{jet} (note that NNLO/NLO corrections for the $y(t\bar{t})$ distribution are generally smaller than for $M(t\bar{t})$, and no NNLO corrections for the N_{jet} distribution are available; for the latter see also Section G). The NNLO/NLO corrections for the $M(t\bar{t})$ bins used in this analysis are tabulated in Table 73 together with the impact on extracted α_s and m_t^{pole} . They do not exceed 2%, and the impact on the extracted m_t^{pole} and α_s values is -0.2 GeV, -0.4 GeV, $+0.01$ GeV, and -0.0005 , -0.0006 , -0.0004 using the CT14, MMHT2014, NNPDF3.0 PDFs, respectively, which is compatible with the uncertainties assigned to the NLO results. Because of the several assumptions explained above, this study should not be interpreted as an extraction of m_t^{pole} and α_s at NNLO, but only as a check of the uncertainties assigned to the NLO results.

$M(t\bar{t})$ [GeV]	NNLO/NLO		
	CT	MMHT	NNPDF
[300, 400]	1.006	1.000	1.012
[400, 500]	0.984	0.979	0.985
[500, 1500]	1.011	1.015	1.006
Δm_t^{pole} [GeV]	-0.2	-0.4	+0.01
$\Delta \alpha_s$	-0.0005	-0.0006	-0.0004

Table 73: NNLO/NLO corrections for the $M(t\bar{t})$ bins obtained with the CT14, MMHT2014 and NNPDF3.0 PDF sets and $m_t^{\text{pole}} = 173.1$ GeV, together with the impact on extracted α_s and m_t^{pole} .

G Study of scale variation in bins with different N_{jet}

Similarly to what is described in Section F, it is not apriori clear that scale varied simultaneously in bins with different N_{jet} would cover missing higher-order corrections. However, no NNLO correactions are available for bins with higher N_{jet} . Thus today this question can be tackled only by considering different assumptions about scale correlations. Four different scenarios are considered: scales in bins $N_{\text{jet}} \geq 0$ and $N_{\text{jet}} \geq 1$ are uncorrelated by 0% (the nominal approach), by 25%, by 50% and by 100%. However, since events in the $N_{\text{jet}} \geq 0$ and $N_{\text{jet}} \geq 1$ samples overlap by about 50%, the most conservative option is that the scales ar uncorrelated by 50%. the results are given in Table 74. One conclude that the nominal approach (the fully correlated scale variations) is compatible also with the ‘25% uncorrelated’ scenario (which is half of the most conservative among reasonable scenarios that the scales are 50% uncorrelated). Furthermore, the alternative scale choice ($\mu = H/2$) partially mimics decorrelated scale variations.

DRAFT

Scale $\mu^{t\bar{t}}/\mu_0 \mu^{t\bar{t}j}/\mu_0 \Delta\alpha_s \Delta m_t^{\text{pole}}/\text{GeV}$	0% uncorrelated			25% uncorrelated			50% uncorrelated			100% uncorrelated							
	$\mu^{t\bar{t}}/\mu_0 \mu^{t\bar{t}j}/\mu_0$	$\Delta\alpha_s$	$\Delta m_t^{\text{pole}}/\text{GeV}$														
μ_r	0.5	0.5	+0.0007	+0.1	$\sqrt[4]{0.5}$	1	+0.0006	-0.1	$\sqrt{0.5}$	1	+0.0012	-0.2	0.5	1	+0.0024	-0.5	
	2	2	+0.0004	-0.2	$\sqrt[4]{2}$	1	-0.0006	+0.1	$\sqrt[4]{0.5}$	1	$\sqrt{0.5}$	-0.0010	+0.3	1	0.5	-0.0018	+0.5
μ_f	0.5	0.5	+0.0001	-0.3	$\sqrt[4]{0.5}$	1	+0.0003	-0.1	$\sqrt[4]{0.5}$	1	$\sqrt{0.5}$	+0.0006	-0.3	0.5	1	+0.0010	-0.6
	2	2	-0.0001	+0.3	$\sqrt[4]{2}$	1	-0.0003	+0.1	$\sqrt[4]{0.5}$	1	$\sqrt{0.5}$	-0.0005	+0.1	1	0.5	-0.0009	+0.2
$\mu_{r,f}$	0.5	0.5	+0.0011	-0.2	$\sqrt[4]{0.5}$	1	+0.0009	-0.3	$\sqrt[4]{0.5}$	1	$\sqrt{0.5}$	+0.0016	-0.5	0.5	1	+0.0029	-0.8
	2	2	+0.0004	+0.1	$\sqrt[4]{2}$	1	-0.0009	+0.3	$\sqrt[4]{0.5}$	1	$\sqrt{0.5}$	-0.0014	+0.4	1	0.5	-0.0020	+0.6
alt. μ			-0.0005	+0.1													
Total			+0.0011 -0.0005	+0.3 -0.3			+0.0009 -0.0009	+0.3 -0.3		+0.0019 -0.0019	+0.6 -0.5		+0.0040 -0.0042	+1.1 -1.2			

Table 74: Scale uncertainties obtained using four different scenarios on scale variations in bins with different N_{jet} .

1495 H Comparison of measured $[N_{\text{jet}}, M(t\bar{t}), y(t\bar{t})]$ cross sections to 1496 fixed-order calculations: additional plots

1497 The α_s scans for different PDF sets (including MMHT2014 and NNPDF3.1 not shown in
1498 Fig. 106) are shown in Fig. 190. It can be seen that the scan using NNPDF3.1 possibly suf-
1499 fers from the limited number of PDF sets with different α_s values ($0.116 < \alpha_s(M_Z) < 0.120$),
1500 while for MMHT2014 the χ^2 on $\alpha_s(M_Z)$ is not parabolic, implying that the cross section depen-
1501 dence on $\alpha_s(M_Z)$ is significantly non-linear. This is related to the dependence of the gluon PDF
1502 on $\alpha_s(M_Z)$ at high values of x in the MMHT2014 PDF set shown in Fig. 191.

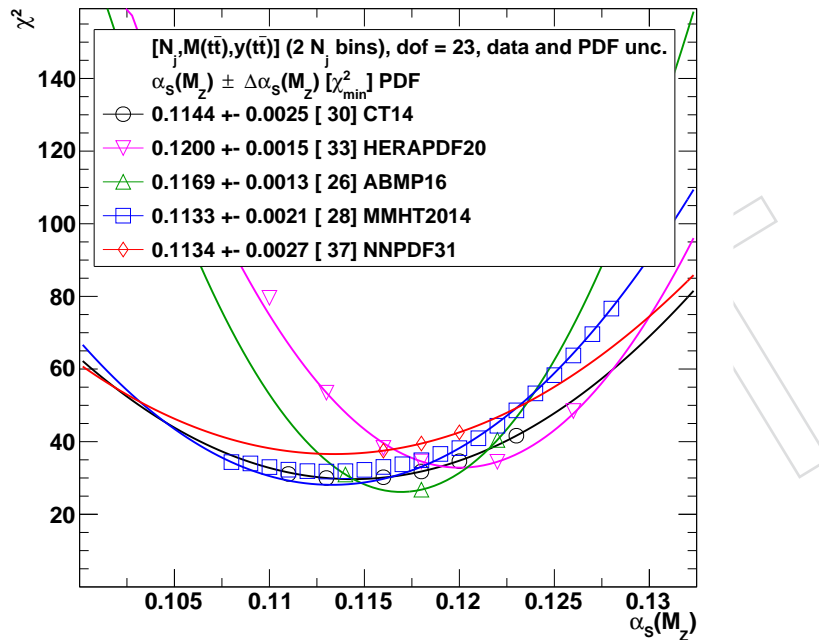


Figure 190: The α_s extraction from the measured $N_{\text{jet}}, M(t\bar{t}), y(t\bar{t})$ cross sections with 2 N_{jet} bins using different PDF sets. The extracted α_s values are reported for each PDF set, and the estimated minimum χ^2 value is shown in brackets. See text for further details.

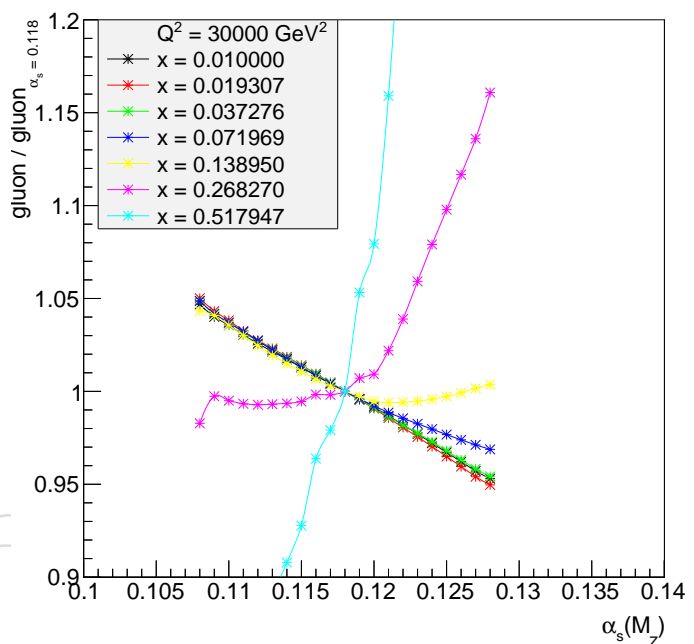


Figure 191: The gluon PDF in MMHT2014 for different values of x as a function of $\alpha_s(M_Z)$. The results are shown normalised to the reference gluon PDF obtained using $\alpha_s(M_Z) = 0.118$.

I Comparison of absolute cross sections to NLO predictions and extraction of α_s and m_t^{pole}

In this section, the extraction of α_s and m_t^{pole} from the measured unnormalised (also referred to as absolute) cross sections is described, which is used as a cross check. Unnormalised $[N_{\text{jet}}, M(\bar{t}\bar{t}), y(\bar{t}\bar{t})]$ cross sections are measured using the same procedure as the normalised cross sections, but they are defined as not divided by the integrated cross section:

$$\frac{d\sigma}{\prod dx_i} = \frac{1}{\prod \Delta x_i} \frac{\hat{M}^{\text{unf}}}{\mathcal{B} \mathcal{L}}, \quad (18)$$

(cf. Eq. 11).

I.1 Comparison of unnormalised $[N_{\text{jet}}, M(\bar{t}\bar{t}), y(\bar{t}\bar{t})]$ cross sections to fixed-order calculations

The NLO QCD predictions are obtained as described in Section 8. The theoretical uncertainties for the $[N_{\text{jet}}, M(\bar{t}\bar{t}), y(\bar{t}\bar{t})]$ cross sections with 2 N_{jet} bins are shown in Fig. 192. The CT14 PDF set with $\alpha_s(M_Z) = 0.118$, $m_t^{\text{pole}} = 172.5$ GeV is used. The contributions arising from the PDF, $\alpha_s \pm 0.005$ and $m_t^{\text{pole}} \pm 1$ GeV uncertainties are shown separately. On average, the total theory uncertainties are 15% and are dominated by the scale uncertainties.

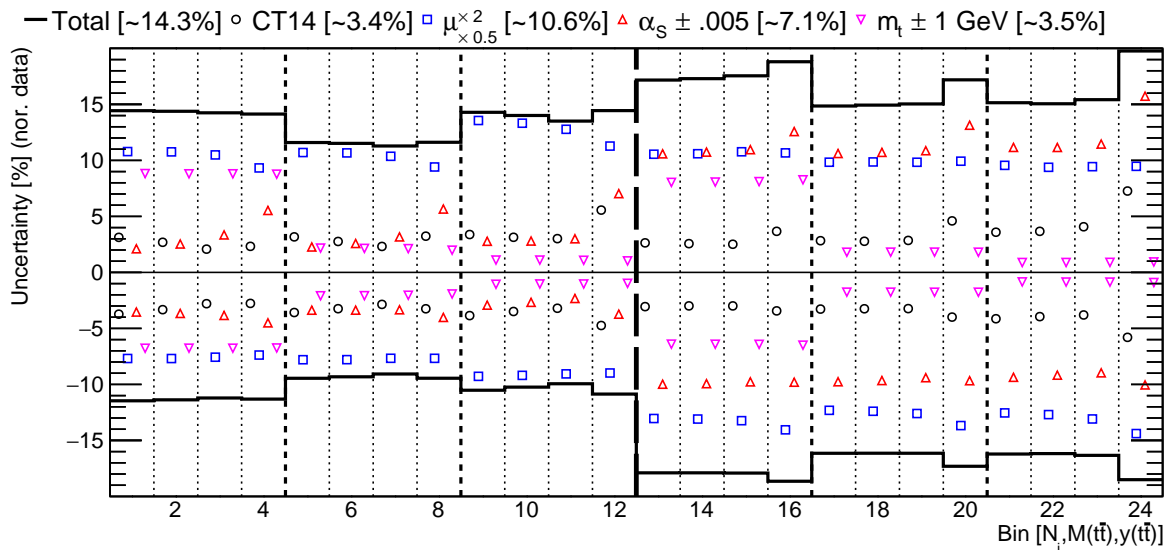


Figure 192: The theoretical uncertainties for the unnormalised $[N_{\text{jet}}, M(\bar{t}\bar{t}), y(\bar{t}\bar{t})]$ cross sections with 2 N_{jet} bins.

Further investigation of the theoretical uncertainties is shown in Figs. 193 and 195, which present the individual scale variations and the PDF uncertainties obtained using different PDF sets, respectively. The cross section changes arising from the scale variations are similar in all bins and largely cancel for the normalised cross sections (see Fig. 102) if the scale variations are assumed to be fully correlated between the bins. Figure 194 shows ratios of NLO over LO cross sections (so called K factors). The NLO corrections are about factor 1.5 on average.

The sensitivity of the unnormalised $[N_{\text{jet}}, M(\bar{t}\bar{t}), y(\bar{t}\bar{t})]$ cross sections with 2 N_{jet} bins to the different PDFs, α_s and m_t^{pole} values is further demonstrated by comparing the measured cross

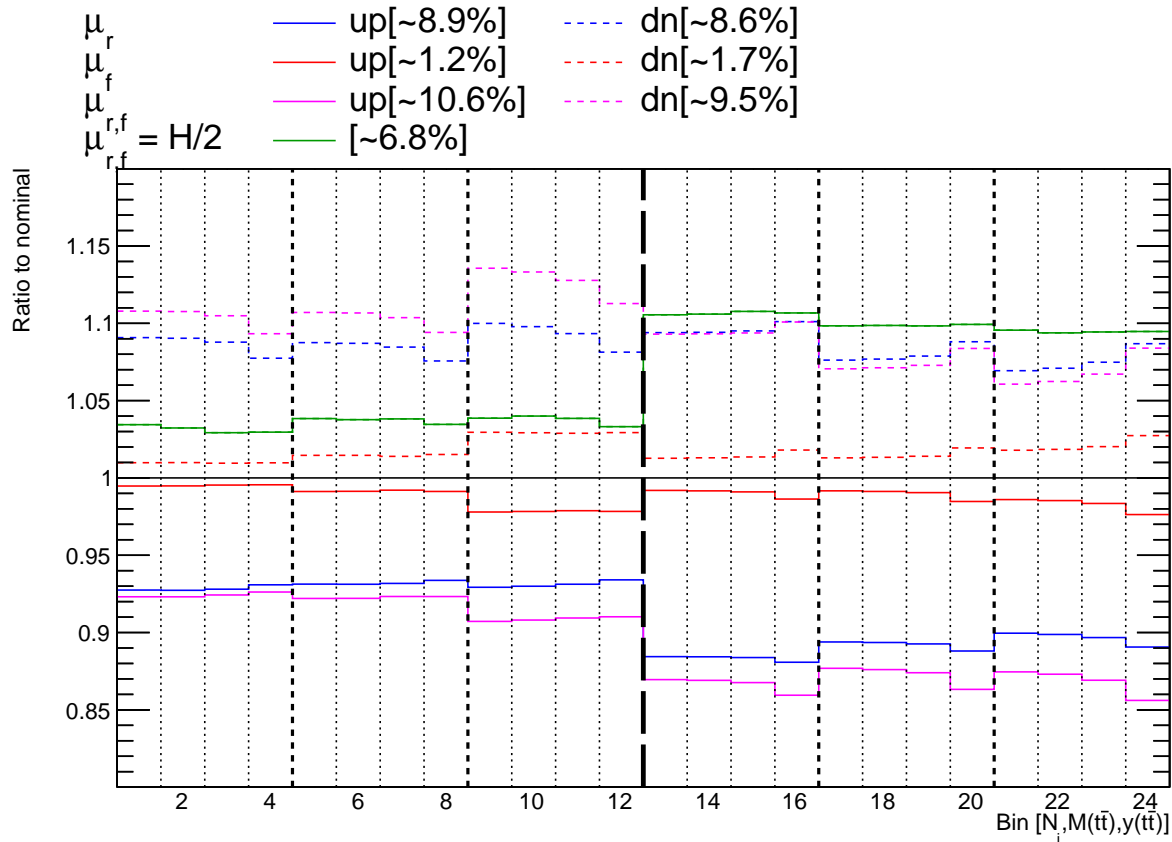


Figure 193: The individual scale variations for the unnormalised $[N_{\text{jet}}, M(t\bar{t}), y(t\bar{t})]$ cross sections with 2 N_{jet} bins.

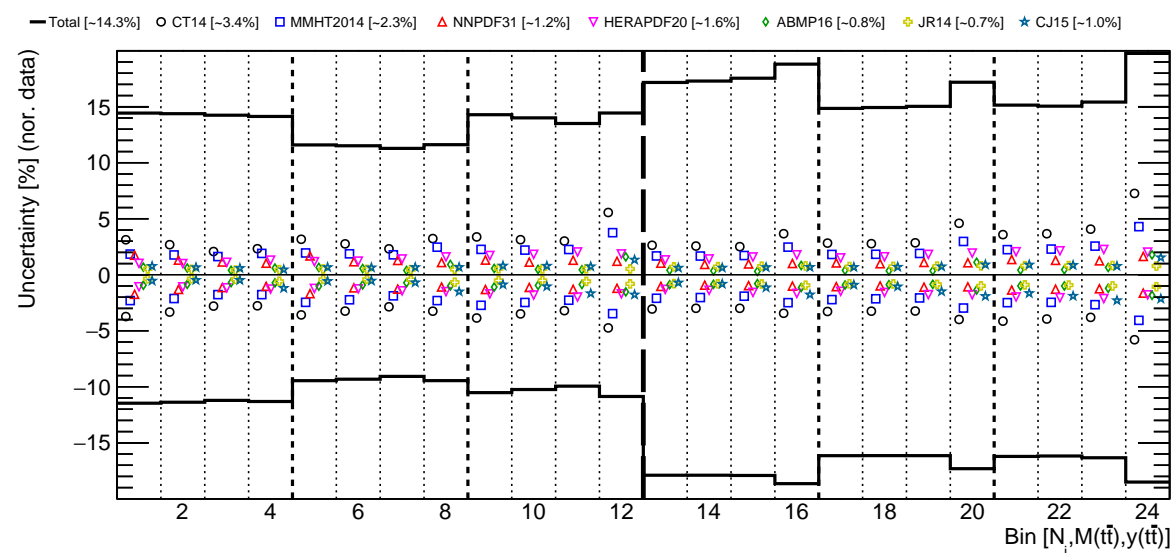


Figure 194: The PDF uncertainties obtained using different PDF sets for the unnormalised $[N_{\text{jet}}, M(t\bar{t}), y(t\bar{t})]$ cross sections with 2 N_{jet} bins.

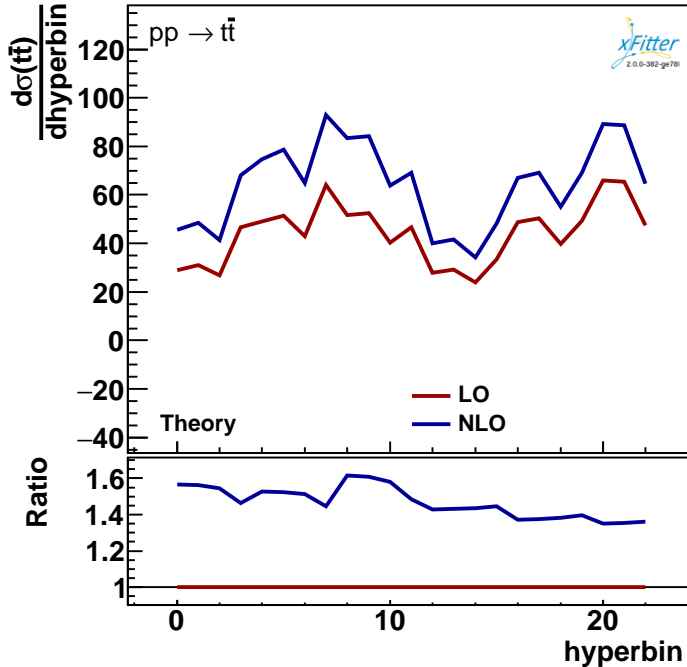


Figure 195: The ratios of NLO over LO predictions (K factors) for the unnormalised $[N_{\text{jet}}, M(t\bar{t}), y(t\bar{t})]$ cross sections with 2 N_{jet} bins. The ‘hyperbin’ indices refer to the bin indices in Table 16.

sections to the predictions obtained with their altered values. In Fig. 196 the data are compared to the predictions calculated using various PDF sets, α_s and m_t^{pole} . For each comparison, χ^2 is calculated which takes into account data only or data and PDF uncertainties, i.e. Eq. (13) becomes $\mathbf{Cov} = \mathbf{Cov}^{\text{unf}} + \mathbf{Cov}^{\text{syst}} + \mathbf{Cov}^{\text{PDF}}$, where $\mathbf{Cov}^{\text{PDF}}$ is a covariance matrix that accounts for the PDF uncertainties. Theoretical uncertainties from scale, α_s and m_t^{pole} variations are not included in this χ^2 calculation.

I.2 Extraction of α_s and m_t^{pole} from unnormalised $[N_{\text{jet}}, M(t\bar{t}), y(t\bar{t})]$ cross sections

The values of α_s and m_t^{pole} are extracted from the comparison of the unnormalised data and NLO predictions calculated using different input values of α_s and m_t^{pole} . The procedure is described in Section 8.

The α_s scans for different PDF sets are shown in Fig. 197. The extracted α_s values are reported on the plots. Furthermore, the α_s scans performed using altered scale and m_t^{pole} settings and CT14, HERAPDF2.0 and ABMP16 PDF sets are shown in Fig. 198. Independent of the input PDF set, the impact of the scale variations is larger than for the normalised cross sections, especially for m_t^{pole} (see Figs. 106, 107). There is a positive correlation of α_s and m_t^{pole} which is slightly smaller than when using the normalised cross sections. Similarly, the m_t^{pole} scans for different PDF sets, scale choices and α_s values are shown in Fig. 199 and 200, respectively.

The extracted α_s and m_t^{pole} values are compared in Fig. 201. The results are consistent with those obtained using the normalised cross sections (see Figs. 108 and 111). The total uncertainties are larger than those obtained using the normalised cross sections due to several effects leading to this:

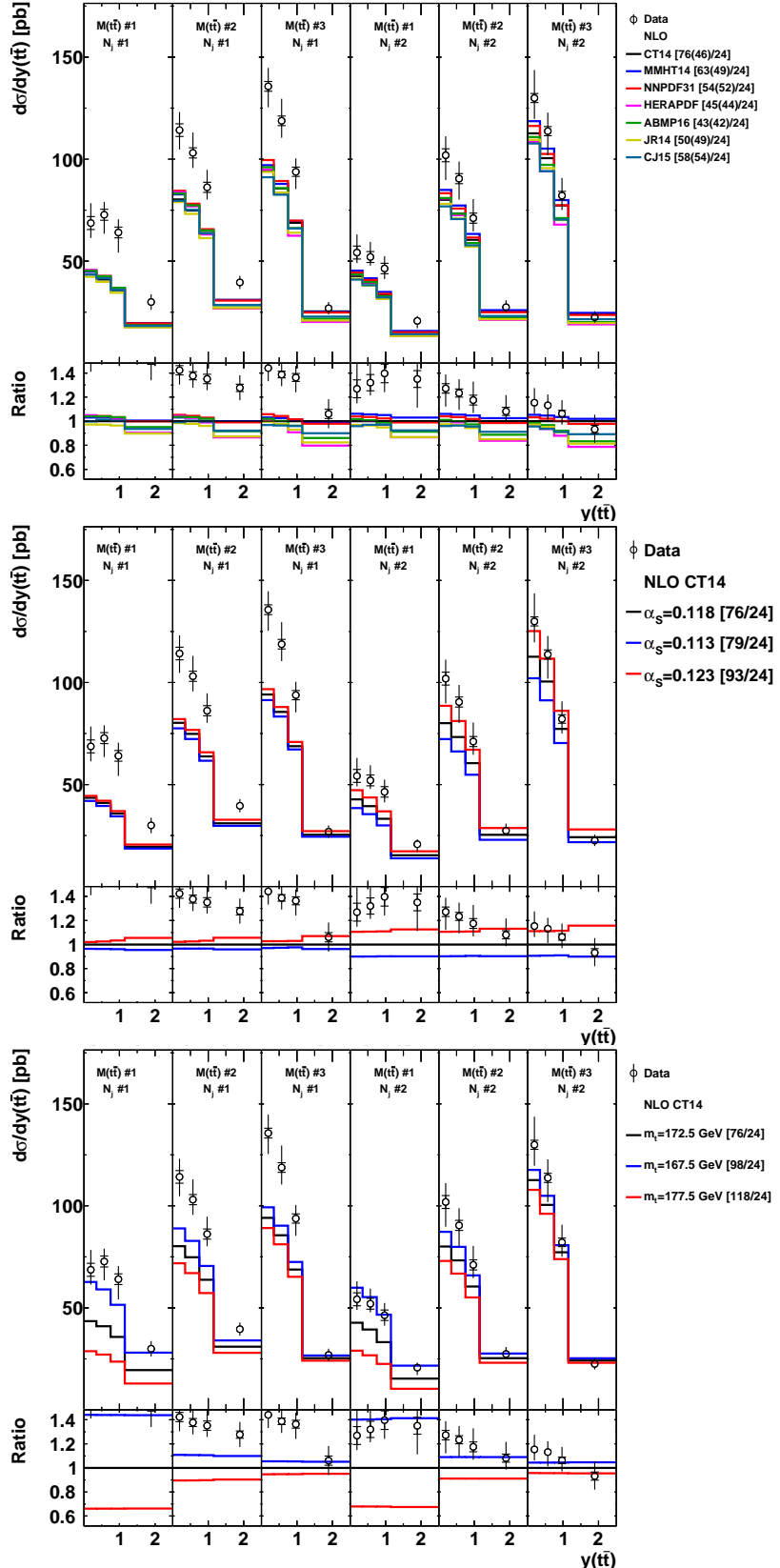


Figure 196: Comparison of the unnormalised $[N_{\text{jet}}, M(\bar{t}\bar{t}), y(\bar{t}\bar{t})]$ cross sections to NLO predictions obtained using different PDF sets (top), α_s (middle) and m_t^{pole} (bottom) values.

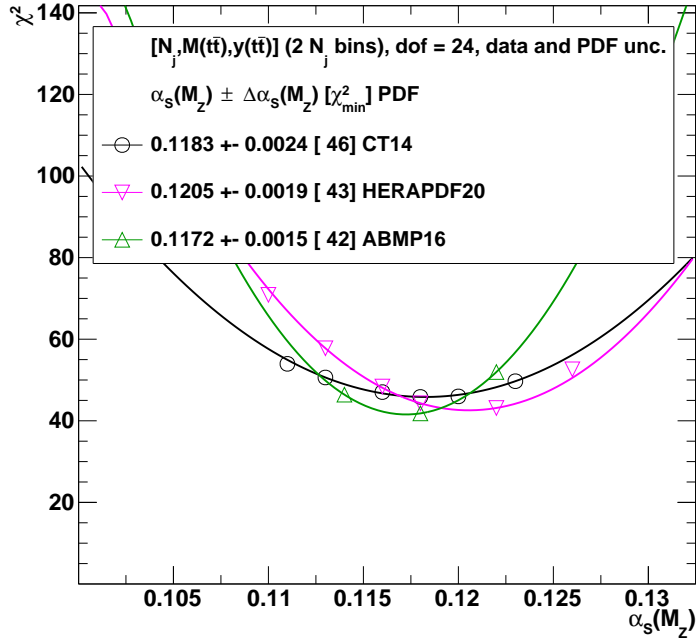


Figure 197: The α_s extraction from the unnormalised $N_{\text{jet}}, M(\text{t}\bar{\text{t}}), y(\text{t}\bar{\text{t}})$ cross sections with $2 N_{\text{jet}}$ bins using different PDF sets. The extracted α_s values are reported for each PDF set, and the estimated minimum χ^2 value is shown in brackets. See text for further details.

- theoretical scale uncertainties are significantly larger for the unnormalised cross sections,
- experimental systematic uncertainties are larger for the unnormalised cross sections (no cancellation of the luminosity and normalisation components of other uncertainties).

The α_s and m_t^{pole} values are differently affected by the increased scale uncertainties of the unnormalised cross sections: a larger impact is observed on m_t^{pole} than on α_s . This is explained by the different origins of the sensitivities:

- m_t^{pole} is constrained by the $M(\text{t}\bar{\text{t}})$ shape (near the threshold) and the total $\text{t}\bar{\text{t}}$ cross section,
- α_s is constrained (with the PDFs) by the $y(\text{t}\bar{\text{t}})$ and $M(\text{t}\bar{\text{t}})$ shapes, the N_{jet} distribution and the total $\text{t}\bar{\text{t}}$ cross section.

In summary, more precise determination of α_s and m_t^{pole} in this analysis with NLO calculations is obtained using the normalised $\text{t}\bar{\text{t}}$ cross sections, while the results extracted using the unnormalised cross sections are in agreement with those extracted using the normalised cross sections.

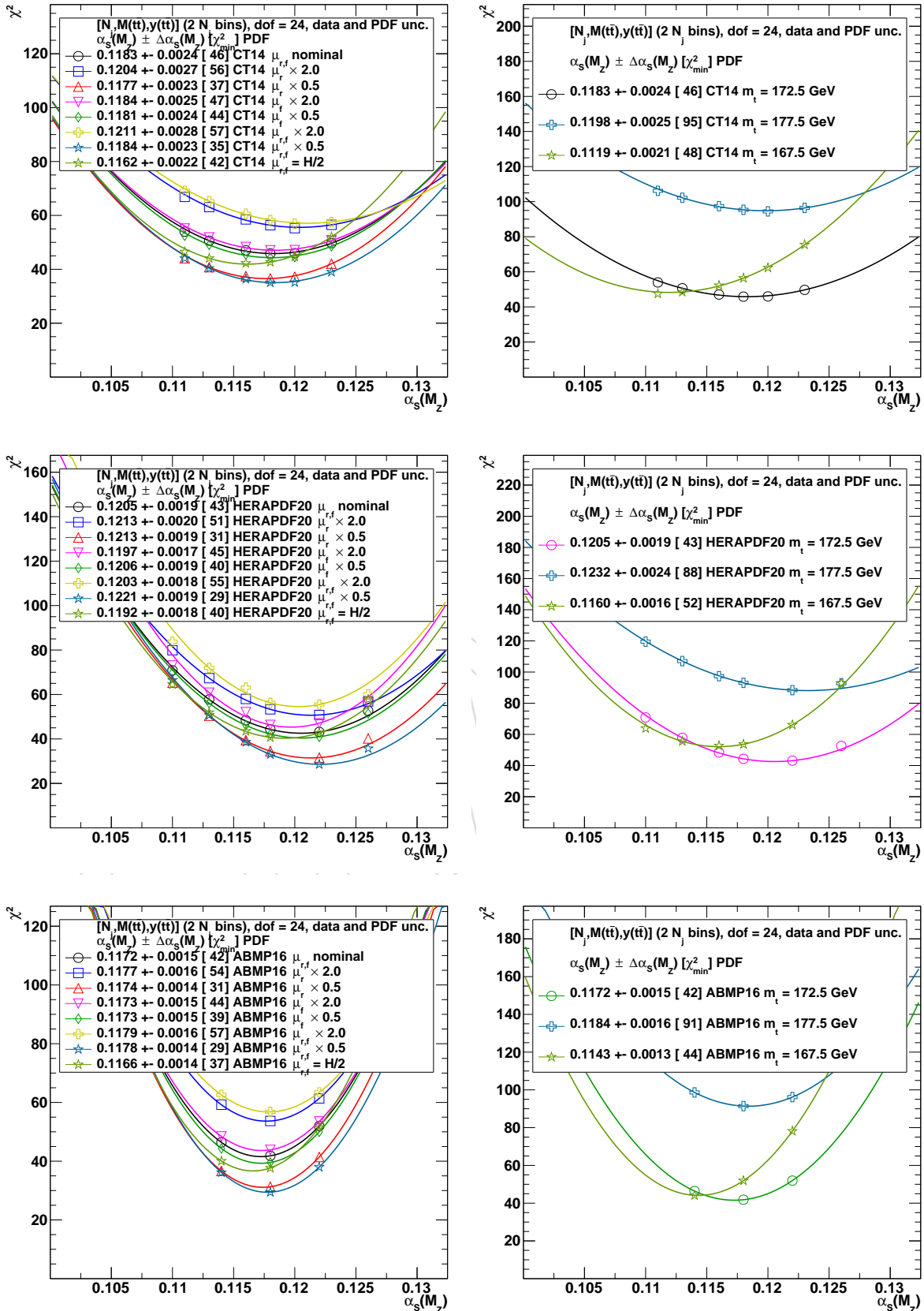


Figure 198: The α_s extraction from the unnormalised $N_{\text{jet}}, M(\bar{t}\bar{t}), y(\bar{t}\bar{t})$ cross sections with 2 N_{jet} bins using varied scale and m_t^{pole} settings and CT14 (top), HERAPDF2.0 (middle) and ABMP16 (bottom) PDF sets.

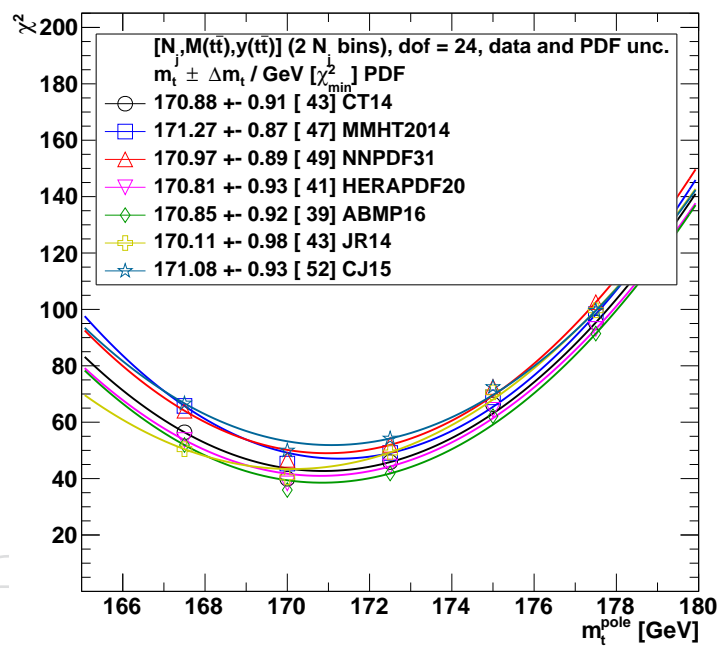


Figure 199: The m_t^{pole} extraction from the measured $N_{jet}, M(t\bar{t}), y(t\bar{t})$ cross sections with 2 N_{jet} bins using different PDF sets. The extracted m_t^{pole} values are reported for each PDF set, and the estimated minimum χ^2 value is shown in brackets. See text for further details.

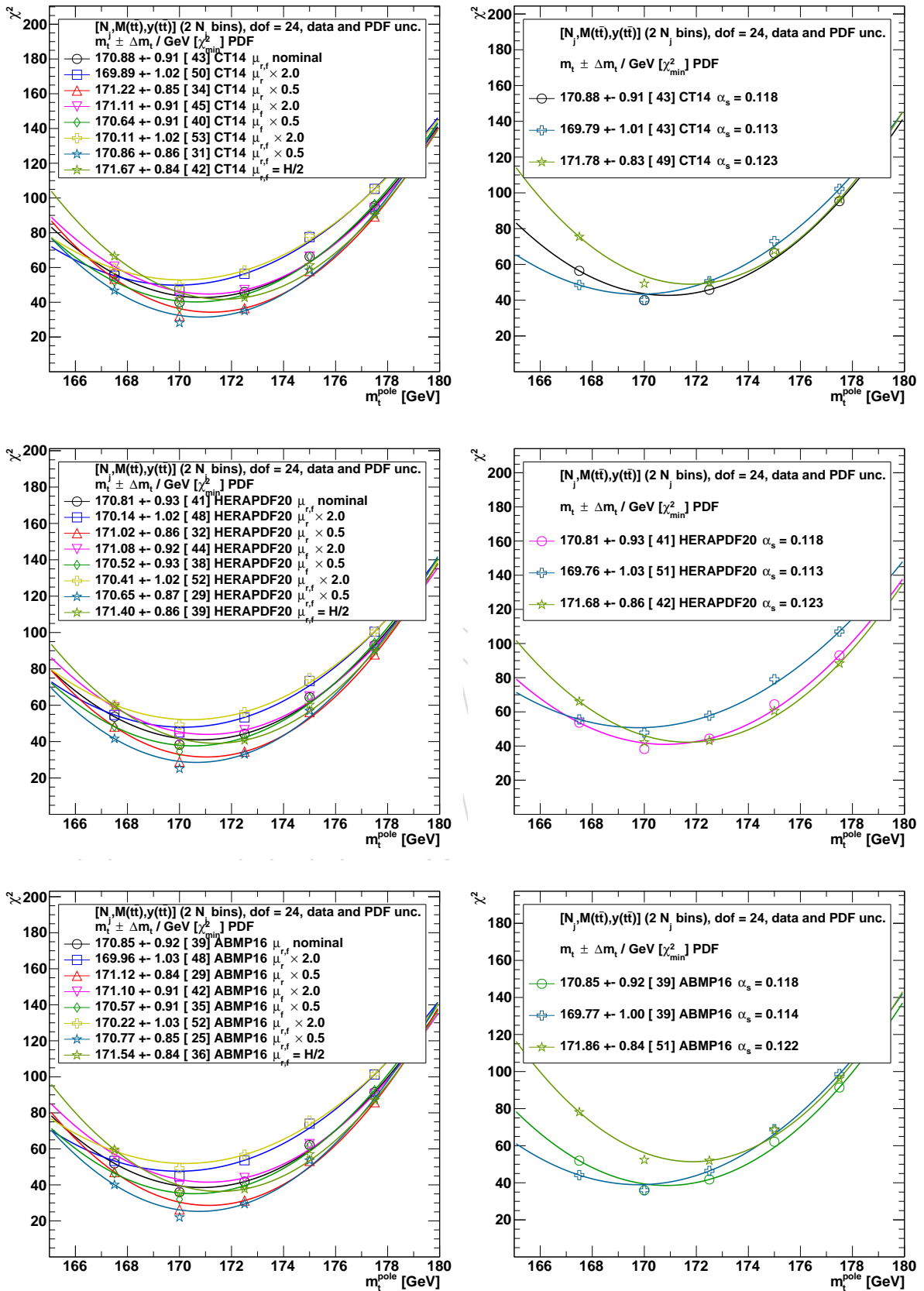


Figure 200: The m_t^{pole} extraction from the unnormalised $N_{\text{jet}}, M(\bar{t}\bar{t}), y(\bar{t}\bar{t})$ cross sections with 2 N_{jet} bins using varied scale and α_s settings and CT14 (top), HERAPDF2.0 (middle) and ABMP16 (bottom) PDF sets.

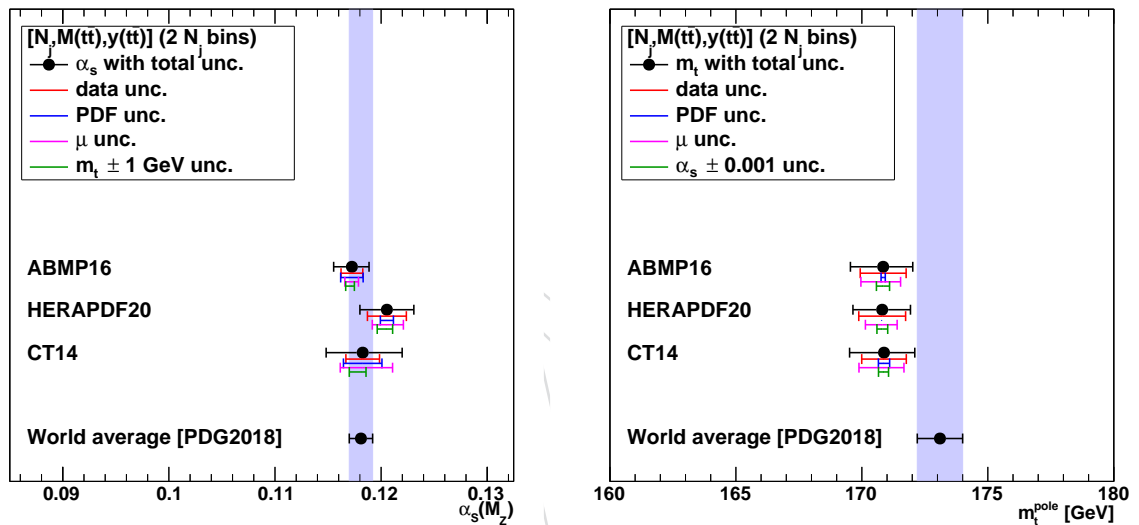


Figure 201: The α_s (left) and m_t^{pole} (right) values extracted from the unnormalised $N_{\text{jet}}, M(t\bar{t}), y(t\bar{t})$ cross sections with $2 N_{\text{jet}}$ bins using different PDFs. The contributions to the total uncertainty arising from the data, PDF, scale and m_t^{pole} uncertainties are shown separately. The world average α_s value is also shown.

1559 **J Full kinematic reconstruction: performance studies related to**
 1560 **minimum $M(t\bar{t})$ choice**

1561 In this section some studies on the full kinematic reconstruction are presented. They were
 1562 already performed when the reconstruction was developed and used for the two RUN I pa-
 1563 pers [51, 52] and are documented in the PhD thesis [54]. In particular the question is addressed
 1564 if the choice of the solution of the quartic equations yielding the minimum reconstructed $M(t\bar{t})$
 1565 value is a reasonable one.

1566 Figure 202 shows the fraction of correct solutions as function of the $M(t\bar{t})$ ranking of the (up to
 1567 four) solutions. The results were obtained with the $t\bar{t}$ signal MC on the generator level. Correct
 1568 solutions are defined by a χ^2 -matching criterion between the true neutrino and anti-neutrino
 1569 kinematics and the kinematics obtained from each solution. One can see in Fig. 202 that for
 1570 about 60% of the events the minimum $M(t\bar{t})$ solution is the correct one.

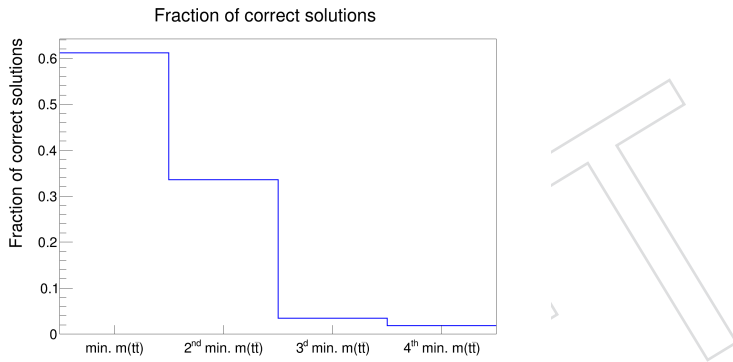


Figure 202: Fractions of correct solutions of the quartic equations used for the full kinematic recon-
 struction versus the $M(t\bar{t})$ ordering of the solutions.

1571 A related question is if one could improve the kinematic reconstruction by choosing an average
 1572 of the solutions. Figure 203 shows that the choice of the minimum $M(t\bar{t})$ solutions yields much
 1573 better resolutions for the reconstructed top transverse momentum and top-pair invariant mass
 1574 compared to taking an average of the solutions (unweighted or using the expected fractions of
 1575 correct solutions, shown in Fig. 202, as weights).

1576 A further question is if the choice of the minimum $M(t\bar{t})$ solution could bias the reconstruction
 1577 towards too small values of $M(t\bar{t})$. The studies of correlations between true and reconstructed
 1578 $M(t\bar{t})$ values and the mean value of the difference between the two (see Fig. 25, left panels)
 1579 indicate that biases are at a small level. Mean and RMS values of the differences between true
 1580 and reconstructed $M(t\bar{t})$ values as a function of the true $M(t\bar{t})$ are shown in Fig. 26 (right)).
 1581 Below 1 TeV there is a small bias towards too high reconstructed $M(t\bar{t})$ values. Above 1 TeV
 1582 the bias starts to grow slowly towards too small reconstructed $M(t\bar{t})$ values, however, it stays
 1583 well below the resolutions.

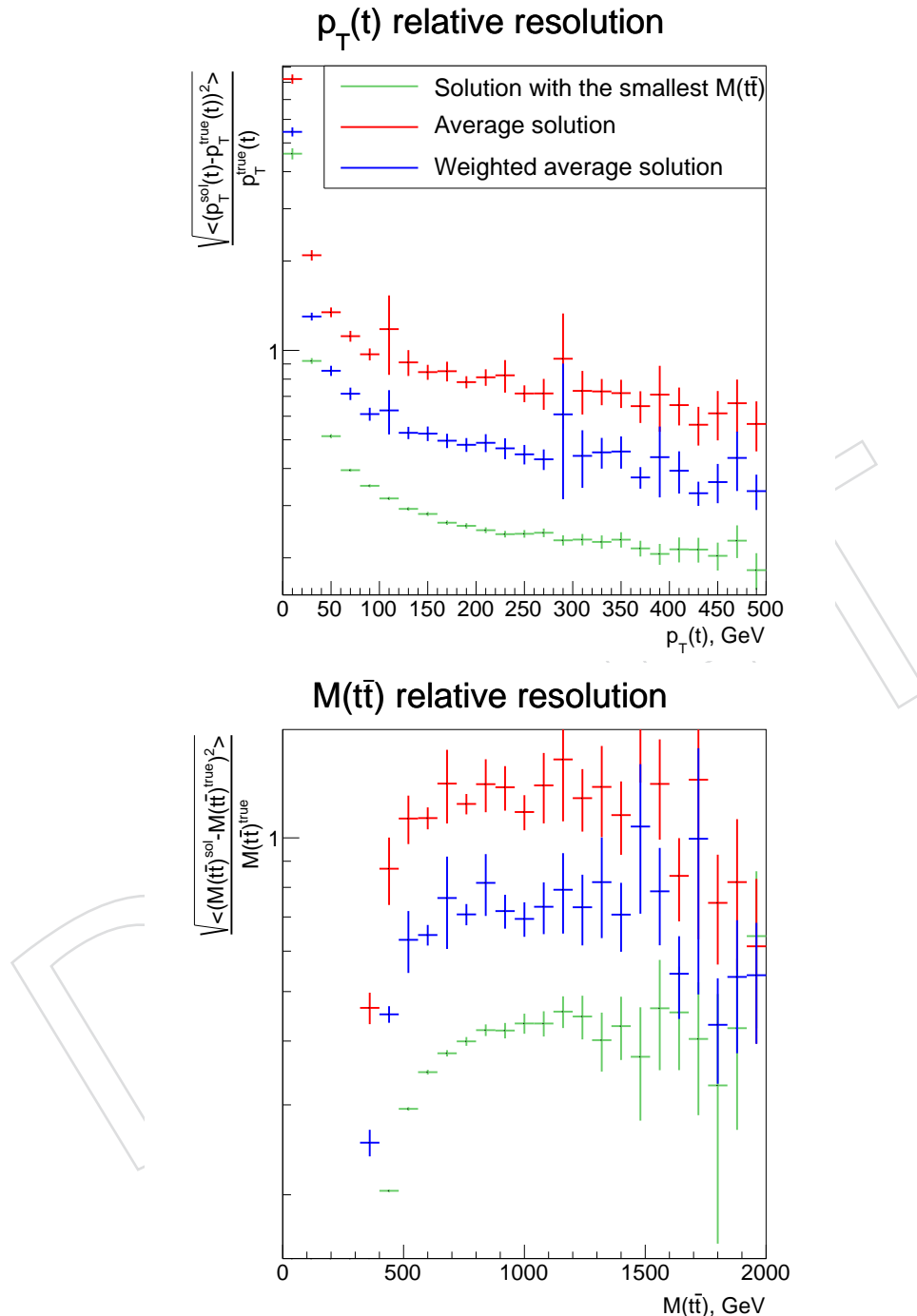


Figure 203: Fractional resolutions of the transverse momentum of the top (upper panel) and $M(t\bar{t})$ (lower panel) as a function of the respective variable. The results for the solution with the smallest $M(t\bar{t})$ are compared to the ones using the average and weighted average solutions.

1584 K Values of the measured cross sections

1585 Tables 75 to 121 provide the measured cross sections, including their correlation matrices of
 1586 statistical uncertainties and detailed breakdown of systematic uncertainties.

Table 75: The measured $[y(t), p_T(t)]$ cross sections, along with their relative statistical and systematic uncertainties.

$y(t)$	$p_T(t)$ [GeV]	$\frac{1}{\sigma(\text{t}\bar{\text{t}})} \frac{d\sigma}{dp_T(t)}$ [GeV $^{-1}$]	stat. [%]	syst. [%]	bin
0.00–0.35	0–80	9.251×10^{-4}	2.5	+6.6 −5.2	1
0.00–0.35	80–150	1.118×10^{-3}	1.8	+2.4 −4.6	2
0.00–0.35	150–250	4.596×10^{-4}	2.1	+4.6 −2.7	3
0.00–0.35	250–600	3.993×10^{-5}	2.9	+3.7 −5.6	4
0.35–0.85	0–80	1.279×10^{-3}	1.6	+3.6 −3.4	5
0.35–0.85	80–150	1.503×10^{-3}	1.3	+2.5 −2.8	6
0.35–0.85	150–250	6.206×10^{-4}	1.7	+3.7 −2.6	7
0.35–0.85	250–600	5.097×10^{-5}	2.8	+4.9 −4.7	8
0.85–1.45	0–80	1.248×10^{-3}	1.6	+2.1 −4.4	9
0.85–1.45	80–150	1.435×10^{-3}	1.3	+2.6 −2.7	10
0.85–1.45	150–250	5.328×10^{-4}	2.0	+4.6 −2.0	11
0.85–1.45	250–600	4.516×10^{-5}	2.9	+4.0 −5.4	12
1.45–2.50	0–80	1.128×10^{-3}	2.4	+4.2 −5.8	13
1.45–2.50	80–150	1.284×10^{-3}	1.6	+4.0 −2.5	14
1.45–2.50	150–250	4.238×10^{-4}	2.5	+2.7 −5.6	15
1.45–2.50	250–600	2.430×10^{-5}	4.9	+12.7 −4.2	16

Table 76: The correlation matrix of statistical uncertainties for the measured $[y(t), p_T(t)]$ cross sections. The values are expressed as percentages. For bin indices see Table 75.

Table 77: Sources and values of the relative systematic uncertainties in percent of the measured $[y(t), p_T(t)]$ cross sections. For bin indices see Table 75.

source / bin	1	2	3	4	5	6	7	8	9	10	11	12	13	14	15	16
JER	+0.4	-0.9	-0.3	+0.0	+0.1	+0.2	+0.2	-0.5	-0.7	-0.1	+0.4	-0.7	+0.7	+0.4	-0.2	-0.3
	+0.7	-0.3	-0.2	+0.8	+0.2	+0.1	+0.3	-0.2	-0.6	-0.1	+0.7	-0.1	-0.9	+0.3	-0.3	+1.0
JESAbsoluteMPFBias	+0.6	-0.3	+0.2	+0.2	+0.3	-0.0	+0.0	-0.3	+0.0	+0.1	+0.1	-0.0	-1.2	+0.3	+0.1	+0.8
	+1.0	-0.5	+0.1	-0.1	+0.7	-0.4	+0.3	+0.0	-0.6	+0.1	+0.4	-0.4	-0.9	+0.3	-0.1	+0.2
JESAbsoluteScale	-0.5	-0.5	+0.4	+0.0	+0.7	-0.1	+0.1	-0.1	+0.4	-0.5	+0.1	-0.5	+0.2	+0.1	-0.9	+2.1
	-0.0	-0.2	+0.2	-0.3	+0.2	-0.2	+0.4	-0.2	-0.4	-0.1	+0.4	+0.2	+0.3	-0.0	-0.5	+1.7
JESAbsoluteStat	+1.2	-0.1	-0.8	-0.2	+0.1	+0.0	+0.1	-0.8	+0.3	-0.0	-0.3	-0.1	+0.1	-0.3	-0.8	-0.5
	-2.1	+0.5	+0.1	+0.6	-0.4	+0.2	+0.8	+0.4	-0.2	-0.2	+0.4	+0.1	+0.6	+0.2	-0.3	+1.5
JESFlavourQCD	+0.4	-0.2	+0.3	+0.7	+0.5	-0.3	-0.1	+0.6	-0.3	-0.2	+0.5	+0.8	-1.1	+0.3	+0.2	+0.7
	+0.4	+0.2	+0.3	-1.5	-0.3	+0.3	+0.3	-0.8	-0.6	+0.2	+0.0	-1.5	-0.1	+0.3	+0.1	-0.8
JESFragmentation	-0.4	-0.4	+0.6	-0.0	+0.0	+0.2	+0.6	-0.8	-0.2	+0.2	-0.3	+0.7	+0.2	-0.1	-0.5	+1.0
	-0.3	-0.3	+0.4	-0.0	+0.5	-0.3	+0.2	-0.5	+0.1	-0.2	+0.4	-0.4	+0.1	+0.4	-0.9	+0.7
JESPileUpDataMC	-0.5	+0.4	+0.3	+0.4	-1.0	-0.2	-0.1	+0.0	-0.1	-0.1	+0.2	+0.1	+0.8	+0.4	-0.3	+2.5
	+0.8	-0.3	+0.4	-0.4	-0.4	+0.2	+0.4	-0.6	-0.1	-0.1	+0.3	-1.0	+0.3	-0.4	-0.5	+0.9
JESPileUpPtBB	+0.5	-0.6	+0.2	+0.1	+0.4	-0.4	+0.0	+0.3	-0.1	-0.3	+0.6	+0.0	+0.3	-0.3	-0.3	+1.2
	+1.0	-0.5	+0.1	-0.3	+0.1	-0.2	-0.1	-0.6	-0.1	-0.1	+0.3	-0.2	+0.8	-0.7	-0.4	+0.4
JESPileUpPtEC1	+0.8	+0.1	+0.5	+0.0	+0.4	+0.4	+0.9	+0.3	-0.4	+0.2	-0.1	+0.7	-1.7	-0.6	-0.3	+1.2
	-0.1	-0.9	-0.2	-0.6	+0.1	-0.0	-0.3	-0.5	+0.3	+0.2	-0.1	-0.1	+0.9	-0.2	+0.4	-0.8
JESPileUpPtEC2	-0.0	+0.0	-0.0	+0.0	+0.0	+0.0	-0.0	+0.0	+0.0	+0.0	+0.0	+0.0	-0.0	+0.0	+0.0	+0.0
	+0.0	+0.0	-0.0	+0.0	+0.0	+0.0	-0.0	+0.0	-0.0	+0.0	+0.0	+0.0	+0.0	+0.0	+0.0	+0.0
JESPileUpPtHF	+0.0	-0.0	-0.0	+0.0	-0.0	-0.0	-0.0	-0.0	-0.0	+0.0	+0.0	+0.0	+0.0	+0.0	+0.0	-0.0
	+0.0	+0.0	+0.0	+0.0	+0.0	+0.0	+0.0	+0.0	+0.0	+0.0	+0.0	+0.0	+0.0	+0.0	+0.0	+0.0
JESPileUpPtRef	+0.6	-0.8	+0.3	+0.2	+0.4	-0.2	+0.8	-0.0	+0.1	-0.5	+1.4	-0.2	-1.0	-0.1	+0.0	+1.4
	-0.3	+0.3	-0.7	+0.4	+0.2	+0.1	+0.0	-1.1	-0.0	-0.4	+0.8	-0.9	+0.4	+0.1	-0.6	+0.4
JESRelativeBal	+0.1	-0.7	-0.1	+0.9	+1.1	+0.1	+0.2	+0.1	-0.2	-0.0	+0.4	-0.2	+0.1	-0.4	-1.7	+1.9
	-0.5	-0.6	+0.1	-0.5	+0.1	+0.0	-0.0	-0.5	-0.3	+0.2	+0.4	-1.0	+0.1	+0.7	-0.0	+1.7
JESRelativeFSR	-1.1	-0.3	+0.5	-0.0	+0.4	+0.1	+0.0	-0.4	-0.3	+0.2	+0.2	-0.4	-0.1	+0.7	-0.5	+1.1
	+1.4	-0.9	+0.3	-0.3	+0.2	-0.2	-0.1	+0.6	-0.5	-0.1	+1.0	-0.6	+0.2	-0.3	-1.0	+2.6
JESRelativeJEREC1	-0.6	-0.1	+0.1	-0.2	+0.2	+0.3	+0.0	+0.0	-0.0	-0.3	-0.1	-0.0	-0.0	+0.4	-0.1	+0.4
	-0.2	-0.2	+0.2	-0.3	+0.3	+0.3	-0.1	-0.1	+0.2	+0.1	+0.0	+0.2	-0.1	-0.5	-0.3	+1.0
JESRelativeJEREC2	-0.0	+0.0	-0.0	+0.0	+0.0	+0.0	-0.0	+0.0	+0.0	+0.0	+0.0	+0.0	-0.0	+0.0	+0.0	+0.0
	+0.0	-0.0	-0.0	+0.0	-0.0	-0.0	-0.0	-0.0	-0.0	+0.0	+0.0	+0.0	+0.0	+0.0	+0.0	-0.0
JESRelativeJERHF	-0.0	+0.0	-0.0	+0.0	+0.0	+0.0	-0.0	+0.0	+0.0	+0.0	+0.0	+0.0	-0.0	+0.0	+0.0	+0.0
	+0.0	+0.0	-0.0	+0.0	+0.0	+0.0	-0.0	+0.0	-0.0	+0.0	+0.0	+0.0	+0.0	+0.0	+0.0	+0.0
JESRelativePtBB	+1.2	-0.4	+0.2	-0.2	-0.2	-0.7	+0.1	-0.2	-0.3	-0.3	+1.2	-0.3	+0.3	+0.0	-0.4	+0.7
	-0.6	+0.1	+0.5	+0.0	+0.2	+0.2	-0.2	-0.1	+0.2	+0.0	+0.1	-0.2	-0.4	+0.1	-0.6	+2.2
JESRelativePtEC1	-0.1	-0.1	+0.4	-0.1	+0.4	+0.3	+0.7	-0.1	+0.3	-0.4	+0.1	+0.2	-0.2	-0.5	-1.2	+0.0
	-0.2	-0.2	-0.3	-0.5	+0.3	+0.0	-0.1	-0.1	-0.3	+0.3	-0.0	+0.1	-0.3	+0.3	+0.5	+0.7
JESRelativePtEC2	-0.0	+0.0	-0.0	+0.0	+0.0	+0.0	-0.0	+0.0	+0.0	+0.0	+0.0	+0.0	-0.0	+0.0	+0.0	+0.0
	+0.0	+0.0	+0.0	+0.0	+0.0	+0.0	-0.0	+0.0	-0.0	+0.0	+0.0	+0.0	+0.0	+0.0	+0.0	+0.0
JESRelativePtHF	-0.0	+0.0	-0.0	+0.0	+0.0	+0.0	-0.0	+0.0	+0.0	+0.0	+0.0	+0.0	-0.0	+0.0	+0.0	+0.0
	-0.0	+0.0	-0.0	+0.0	+0.0	+0.0	-0.0	+0.0	-0.0	+0.0	+0.0	+0.0	-0.0	+0.0	+0.0	+0.0
JESRelativeStatEC	-0.3	+0.2	-0.0	-0.4	+0.4	+0.0	+0.5	-0.2	-0.1	-0.5	-0.1	+0.2	-0.1	+0.4	-0.4	-0.1
	-0.7	-0.4	+0.2	-0.4	+0.5	+0.1	+0.1	-0.0	+0.4	+0.1	+0.2	-0.2	-0.5	-0.1	+0.2	+0.4
JESRelativeStatFSR	-1.1	+0.1	+0.1	+0.2	+0.0	-0.1	+0.1	-0.4	+0.1	-0.1	+0.5	-0.4	+0.4	+0.3	-0.5	+0.8
	+0.6	-0.8	+0.5	+0.2	+0.5	-0.3	-0.3	-0.2	-0.5	+0.2	+0.3	-0.1	-0.1	+0.6	-1.1	+1.5
JESRelativeStatHF	+0.0	-0.0	-0.0	+0.0	-0.0	-0.0	-0.0	-0.0	-0.0	+0.0	+0.0	+0.0	+0.0	+0.0	+0.0	-0.0
	-0.0	+0.0	-0.0	+0.0	+0.0	+0.0	-0.0	+0.0	+0.0	+0.0	+0.0	+0.0	-0.0	+0.0	+0.0	+0.0
JESSinglePionECAL	+0.1	-0.2	-0.1	-0.5	+0.4	-0.0	-0.0	-0.3	-0.1	-0.1	-0.1	-0.5	+0.2	+0.2	-0.2	+0.5
	-1.6	-0.0	+0.0	+0.4	+0.6	+0.6	-0.1	+0.4	+0.2	+0.3	+0.4	-0.1	-0.9	-0.2	+0.1	+0.6

Table 78: Table 77 continued.

source / bin	1	2	3	4	5	6	7	8	9	10	11	12	13	14	15	16
JESSinglePionHCAL	-0.1	-0.3	-0.2	+0.0	+0.2	+0.3	+0.2	-0.6	+0.2	-0.1	-0.0	+0.0	-0.1	-0.1	-0.0	+0.1
	+0.2	+0.1	-0.3	+0.4	-0.1	-0.5	+0.6	-0.4	+0.1	-0.2	+0.2	+0.6	-0.1	+0.3	-0.3	+0.9
JESTimePtEta	+0.8	-0.7	+0.6	+0.1	-0.6	-0.3	-0.4	-0.2	-0.7	+0.2	+0.3	-0.0	+0.5	+0.8	-0.5	+1.5
	-0.1	+0.2	+0.1	+0.1	+0.3	-0.4	+0.1	+0.1	-0.2	-0.5	+0.6	-0.4	+0.7	+0.0	-1.2	+1.6
E_T^{miss}	+0.7	-0.6	+0.6	-0.1	+0.2	-0.1	+0.1	-0.6	+0.3	+0.1	-0.3	-0.1	-0.6	-0.1	-0.3	+0.5
	-0.2	+0.1	+0.0	+0.5	-0.2	+0.4	-0.1	+0.1	-0.2	-0.2	+0.4	+0.2	+0.2	-0.2	+0.0	+0.4
lepton ID/ISO	-0.2	+0.1	-0.0	-0.4	-0.0	+0.2	-0.0	-0.2	-0.1	+0.2	-0.1	-0.3	-0.1	+0.3	-0.0	-0.6
	+0.2	-0.1	+0.0	+0.4	+0.0	-0.2	+0.0	+0.2	+0.1	-0.2	+0.1	+0.3	+0.1	-0.3	+0.0	+0.6
pileup	-0.1	+0.3	-0.0	-0.2	+0.1	+0.2	+0.1	-0.0	-0.1	-0.1	+0.0	-0.2	-0.1	-0.2	-0.1	-0.2
	+0.0	-0.3	+0.0	+0.3	-0.1	-0.2	-0.1	+0.0	+0.1	+0.1	+0.0	+0.1	+0.1	+0.1	+0.1	+0.2
trigger	+0.0	+0.1	+0.0	+0.0	+0.1	+0.2	+0.1	+0.2	-0.0	+0.1	+0.1	+0.1	-0.4	-0.2	-0.2	-0.2
	-0.0	-0.1	-0.0	-0.0	-0.1	-0.2	-0.1	-0.2	+0.0	-0.1	-0.1	-0.1	+0.4	+0.2	+0.2	+0.2
trigger (η)	-0.2	-0.2	-0.2	-0.2	-0.1	-0.1	-0.1	-0.1	+0.0	+0.0	+0.0	+0.0	+0.4	+0.3	+0.2	+0.2
	+0.2	+0.2	+0.2	+0.2	+0.1	+0.1	+0.1	+0.1	-0.0	-0.0	-0.0	-0.0	-0.4	-0.3	-0.2	-0.2
non-tt background	-0.9	+0.6	+0.9	+1.0	-0.8	+0.6	+0.8	+1.0	-0.7	+0.6	+0.6	+1.1	-2.0	+0.1	+1.1	+0.2
	+0.9	-0.6	-0.9	-0.9	+0.7	-0.5	-0.8	-0.9	+0.7	-0.5	-0.6	-1.0	+1.9	-0.1	-1.0	-0.2
b-tagging	-0.1	+0.1	+0.0	+0.0	-0.1	+0.0	-0.0	+0.1	-0.1	+0.0	-0.0	+0.1	-0.0	+0.1	+0.1	+0.1
	+0.1	-0.1	-0.0	-0.0	+0.1	-0.0	+0.0	-0.0	+0.1	-0.0	+0.0	-0.1	+0.0	-0.1	-0.1	-0.1
b-tagging (light jets)	-0.2	+0.2	+0.3	+0.3	-0.2	+0.2	+0.3	+0.2	-0.3	+0.1	+0.2	+0.2	-0.6	-0.0	+0.2	+0.1
	+0.2	-0.2	-0.3	-0.3	+0.2	-0.2	-0.3	-0.2	+0.3	-0.1	-0.2	-0.2	+0.6	+0.0	-0.2	-0.1
luminosity	+0.0	+0.0	+0.0	+0.0	+0.0	+0.0	+0.0	+0.0	+0.0	+0.0	+0.0	+0.0	+0.0	+0.0	+0.0	+0.0
	+0.0	+0.0	+0.0	+0.0	+0.0	+0.0	+0.0	+0.0	+0.0	+0.0	+0.0	+0.0	+0.0	+0.0	+0.0	+0.0
BR($t\bar{t} \rightarrow \ell\ell$)	+0.0	+0.0	+0.0	+0.0	+0.0	+0.0	+0.0	+0.0	+0.0	+0.0	+0.0	+0.0	+0.0	+0.0	+0.0	+0.0
	+0.0	+0.0	+0.0	+0.0	+0.0	+0.0	+0.0	+0.0	+0.0	+0.0	+0.0	+0.0	+0.0	+0.0	+0.0	+0.0
PDF eigenvector 1	-0.0	-0.0	-0.0	+0.0	-0.0	-0.0	-0.0	+0.0	-0.0	+0.0	-0.0	+0.0	+0.0	+0.0	+0.0	+0.0
	+0.0	+0.0	+0.0	+0.0	+0.0	+0.0	+0.0	+0.0	-0.0	+0.0	-0.0	+0.0	-0.0	-0.0	-0.0	+0.1
PDF eigenvector 2	-0.2	-0.1	-0.0	+0.1	-0.1	-0.0	+0.0	+0.1	+0.0	+0.0	+0.1	+0.0	+0.1	+0.1	+0.0	-0.2
	+0.1	-0.0	-0.0	-0.1	+0.0	-0.1	-0.0	-0.1	+0.0	-0.0	+0.0	-0.1	-0.0	+0.0	+0.1	-0.1
PDF eigenvector 3	+0.1	+0.1	+0.0	+0.0	+0.0	+0.0	+0.0	+0.0	+0.0	+0.0	-0.0	-0.0	-0.1	-0.1	-0.1	+0.1
	-0.0	-0.0	-0.0	-0.0	-0.0	-0.0	-0.0	-0.0	-0.0	-0.0	+0.0	+0.0	+0.0	+0.1	+0.1	-0.0
PDF eigenvector 4	-0.2	-0.0	-0.0	+0.1	-0.1	+0.0	-0.0	+0.1	-0.0	+0.0	+0.0	+0.1	+0.1	+0.1	+0.1	-0.0
	+0.1	-0.0	+0.0	-0.1	+0.0	-0.0	+0.0	-0.1	+0.0	-0.0	+0.0	-0.1	-0.0	-0.0	-0.0	-0.0
PDF eigenvector 5	+0.0	-0.1	-0.0	-0.2	+0.0	-0.1	-0.0	-0.2	+0.0	-0.0	+0.0	-0.1	+0.0	+0.1	+0.1	-0.2
	+0.1	+0.1	+0.1	+0.1	+0.1	+0.1	+0.1	+0.1	-0.0	+0.0	-0.1	-0.0	-0.1	-0.2	-0.3	+0.2
PDF eigenvector 6	-0.1	+0.0	-0.0	+0.1	-0.0	+0.1	-0.0	+0.1	-0.0	+0.0	-0.0	+0.1	-0.0	+0.0	-0.0	+0.1
	+0.1	-0.0	+0.0	-0.1	+0.0	-0.0	-0.0	-0.1	+0.0	-0.0	+0.0	-0.1	+0.0	-0.0	-0.0	-0.1
PDF eigenvector 7	+0.0	-0.1	-0.1	-0.3	+0.0	-0.1	-0.1	-0.3	+0.0	-0.0	+0.1	-0.2	+0.1	+0.2	+0.2	-0.4
	-0.0	+0.1	+0.0	+0.2	-0.0	+0.1	+0.0	+0.1	-0.0	-0.0	-0.1	+0.1	-0.1	-0.1	-0.1	+0.2
PDF eigenvector 8	-0.0	+0.0	-0.0	-0.0	+0.0	+0.0	-0.0	-0.0	-0.0	+0.0	-0.0	+0.0	-0.0	+0.1	-0.0	-0.0
	+0.0	-0.0	+0.0	+0.0	-0.0	-0.0	+0.0	+0.0	+0.0	-0.0	+0.0	+0.0	-0.1	-0.0	+0.0	+0.0
PDF eigenvector 9	+0.0	-0.0	+0.0	-0.0	-0.0	-0.1	+0.0	-0.0	+0.0	-0.0	+0.0	-0.0	+0.1	-0.0	+0.0	-0.1
	-0.0	+0.0	-0.0	+0.0	+0.0	+0.1	-0.0	+0.0	-0.0	+0.0	-0.0	+0.0	-0.1	+0.0	-0.1	+0.1
PDF eigenvector 10	-0.0	+0.1	+0.0	+0.1	-0.0	+0.1	+0.0	+0.1	-0.0	-0.0	-0.1	+0.1	-0.0	-0.1	-0.1	+0.2
	+0.0	-0.1	-0.0	-0.2	+0.0	-0.1	-0.0	-0.1	+0.0	+0.0	+0.1	-0.1	+0.0	+0.1	+0.1	-0.2
PDF eigenvector 11	-0.0	+0.0	+0.0	+0.0	-0.0	+0.0	+0.0	+0.0	-0.0	+0.0	-0.0	+0.0	-0.0	-0.0	-0.0	+0.0
	+0.0	-0.0	-0.0	-0.1	+0.0	-0.0	-0.0	-0.1	+0.0	-0.0	+0.0	-0.0	+0.0	+0.0	+0.1	-0.1
PDF eigenvector 12	+0.0	-0.0	-0.0	-0.1	+0.0	-0.0	-0.0	-0.1	+0.0	+0.0	+0.0	-0.1	-0.0	+0.1	+0.0	-0.1
	-0.0	+0.0	+0.0	+0.1	-0.0	+0.0	+0.0	+0.1	-0.0	-0.0	-0.0	+0.1	+0.0	-0.1	-0.0	+0.1
PDF eigenvector 13	+0.1	+0.0	+0.0	-0.0	+0.0	+0.0	-0.0	-0.0	-0.0	+0.0	-0.1	-0.0	-0.1	-0.0	-0.1	+0.1
	-0.1	-0.0	-0.0	+0.0	-0.0	-0.0	+0.0	+0.0	+0.0	-0.0	+0.1	+0.0	+0.1	+0.0	+0.1	-0.1
PDF eigenvector 14	+0.0	-0.0	-0.0	-0.0	+0.0	+0.0	-0.0	-0.0	+0.0	+0.0	-0.0	-0.0	+0.0	-0.0	-0.0	-0.1
	-0.0	+0.0	+0.0	+0.0	-0.0	-0.0	+0.0	+0.1	-0.0	-0.0	-0.0	+0.1	+0.0	-0.0	+0.0	+0.1

Table 79: Table 77 continued.

source / bin	1	2	3	4	5	6	7	8	9	10	11	12	13	14	15	16
PDF eigenvector 15	+0.1	-0.0	-0.0	-0.1	+0.0	-0.0	-0.0	-0.1	+0.0	+0.0	+0.0	-0.1	-0.0	-0.0	-0.0	-0.1
	-0.0	+0.0	+0.0	+0.0	-0.0	+0.0	-0.0	+0.0	-0.0	-0.0	-0.0	+0.0	+0.0	+0.0	+0.0	+0.0
PDF eigenvector 16	-0.0	+0.0	+0.0	+0.0	-0.0	+0.0	+0.0	+0.0	-0.0	+0.0	-0.0	+0.0	-0.0	-0.0	-0.0	+0.0
	+0.0	-0.0	-0.0	-0.0	+0.0	-0.0	-0.0	-0.0	+0.0	+0.0	+0.0	-0.0	+0.0	+0.0	+0.0	-0.1
PDF eigenvector 17	+0.0	-0.0	-0.0	-0.0	+0.0	-0.0	-0.0	-0.0	+0.0	+0.0	+0.0	-0.0	+0.0	+0.0	+0.0	-0.1
	-0.0	+0.0	+0.0	+0.1	-0.0	+0.0	-0.0	+0.1	-0.0	+0.0	-0.0	+0.1	-0.0	-0.0	-0.0	+0.1
PDF eigenvector 18	-0.1	-0.0	+0.0	+0.1	-0.1	-0.0	+0.0	+0.1	-0.0	-0.0	+0.0	+0.1	+0.1	+0.0	+0.2	+0.1
	+0.1	+0.0	-0.0	-0.1	+0.1	+0.0	-0.0	-0.1	+0.0	+0.0	-0.0	-0.1	-0.1	-0.0	-0.2	-0.1
PDF eigenvector 19	-0.0	+0.0	+0.0	+0.1	-0.0	+0.0	+0.0	+0.1	-0.0	-0.0	-0.0	+0.1	+0.0	-0.0	+0.0	+0.1
	+0.1	-0.0	-0.0	-0.2	+0.0	-0.0	-0.0	-0.2	+0.0	+0.0	+0.0	-0.1	-0.0	+0.1	-0.0	-0.2
PDF eigenvector 20	-0.0	+0.0	-0.0	+0.0	-0.0	+0.0	-0.0	+0.0	-0.0	-0.0	-0.0	+0.1	+0.1	-0.0	+0.1	+0.2
	+0.0	-0.0	-0.0	-0.1	+0.0	-0.0	-0.0	-0.0	+0.0	+0.0	+0.0	-0.0	-0.0	+0.0	-0.0	-0.1
PDF eigenvector 21	-0.1	-0.0	-0.0	+0.0	-0.0	-0.0	-0.0	+0.0	-0.0	+0.0	+0.0	+0.1	+0.1	+0.1	+0.1	-0.0
	+0.1	+0.1	+0.0	-0.0	+0.0	+0.0	+0.0	-0.0	+0.0	-0.0	-0.0	-0.0	-0.1	-0.1	-0.1	+0.1
PDF eigenvector 22	-0.2	-0.1	-0.1	+0.1	-0.1	-0.1	-0.0	+0.1	-0.0	-0.0	+0.1	+0.1	+0.2	+0.2	+0.4	-0.1
	+0.2	+0.1	+0.0	-0.0	+0.1	+0.1	+0.0	-0.0	-0.0	+0.0	-0.1	-0.1	-0.2	-0.1	-0.3	+0.2
PDF eigenvector 23	+0.2	+0.0	+0.0	-0.1	+0.1	+0.0	+0.0	-0.1	+0.0	+0.0	-0.0	-0.2	-0.2	-0.1	-0.3	-0.1
	-0.0	-0.0	-0.0	+0.0	-0.0	-0.0	-0.0	+0.0	-0.0	-0.0	-0.0	+0.0	+0.1	+0.0	+0.1	+0.0
PDF eigenvector 24	+0.1	-0.0	-0.0	-0.1	-0.0	-0.0	-0.0	-0.1	-0.0	-0.0	+0.0	-0.0	+0.0	+0.0	+0.1	-0.0
	-0.1	-0.1	+0.0	-0.1	+0.0	-0.0	+0.0	-0.1	+0.1	+0.0	+0.1	-0.1	+0.0	+0.0	-0.1	-0.3
PDF eigenvector 25	-0.0	-0.0	+0.0	-0.1	+0.0	-0.0	+0.0	-0.1	+0.1	+0.0	+0.1	-0.1	-0.0	+0.0	-0.1	-0.2
	+0.1	-0.1	-0.1	-0.2	-0.0	-0.1	-0.0	-0.1	+0.0	-0.0	+0.0	-0.1	+0.0	+0.1	+0.2	-0.1
PDF eigenvector 26	+0.0	+0.0	+0.0	-0.0	+0.0	+0.0	+0.0	-0.0	+0.0	+0.0	-0.0	-0.0	-0.0	-0.0	-0.0	-0.0
	-0.0	-0.0	-0.0	-0.0	-0.0	-0.0	-0.0	-0.0	-0.0	-0.0	+0.0	+0.0	+0.0	+0.0	+0.0	-0.0
PDF eigenvector 27	-0.0	-0.0	+0.1	+0.1	-0.0	-0.1	+0.0	+0.1	+0.1	-0.0	+0.0	-0.0	+0.1	-0.1	-0.0	-0.1
	-0.1	+0.0	-0.0	+0.0	-0.0	+0.0	-0.0	+0.0	-0.0	+0.0	-0.0	+0.0	-0.0	+0.0	-0.0	+0.0
PDF eigenvector 28	+0.0	-0.0	+0.0	-0.0	+0.0	-0.0	+0.0	-0.0	+0.0	-0.0	-0.0	+0.1	+0.0	+0.1	+0.0	+0.0
	-0.1	+0.0	-0.0	+0.0	-0.0	+0.0	-0.0	+0.0	-0.0	-0.0	+0.1	+0.0	+0.1	+0.0	+0.0	+0.0
α_s	+0.1	+0.0	+0.1	-0.0	+0.0	-0.0	+0.0	-0.0	+0.0	-0.0	+0.0	-0.0	+0.0	-0.1	-0.0	-0.0
	-0.1	-0.0	-0.1	-0.0	-0.0	+0.0	-0.1	-0.0	-0.0	+0.0	-0.0	+0.0	-0.0	+0.1	+0.0	+0.0
m_t	+0.4	-0.8	+0.6	+0.9	+0.4	-0.6	+0.4	+1.8	+0.2	-0.6	+0.4	+1.6	-0.8	-0.2	+0.6	+2.4
	-0.1	+0.9	-0.4	-2.1	-0.4	+0.6	-0.1	-1.2	-0.2	+0.7	-0.5	-1.7	-0.0	+0.3	-0.3	-2.2
μ_{rf}	+0.3	-0.2	+0.2	-0.5	-0.1	-0.6	+0.1	-0.2	+0.4	-0.2	+0.3	-0.0	+0.6	-0.4	+0.3	-0.0
	-0.3	+0.2	-0.1	+0.5	+0.1	+0.6	-0.1	+0.4	-0.4	+0.2	-0.2	+0.2	-0.6	+0.3	-0.5	+0.1
h_{damp}	+1.2	-0.9	+0.5	-0.8	+0.4	-0.5	+0.9	-0.3	-0.4	-0.6	+0.6	+0.1	-0.7	+0.6	-0.1	+1.8
	+0.1	+0.0	-0.2	-1.0	-1.4	+0.6	-0.2	+0.6	-0.9	+1.0	-0.5	-1.0	+0.2	+0.9	+0.2	+2.2
PS ISR	+0.2	-1.1	+1.7	-1.0	+0.4	-0.1	-0.1	+0.1	-1.0	-0.3	+0.4	+0.0	-0.0	+1.0	-0.3	+2.0
	+1.1	+0.4	-0.2	+0.3	+0.3	-0.3	-0.4	+0.8	-1.0	-0.6	+0.9	-0.5	-0.3	+0.6	+0.2	-0.1
PS FSR	-0.0	+0.7	-0.4	-1.2	+0.0	+0.4	-0.9	-0.3	+0.0	+0.8	-0.5	-1.2	-0.4	+0.5	-0.7	-0.7
	-0.2	-0.1	+0.1	+0.7	+0.3	-0.3	+0.2	+1.0	-0.2	-0.1	+0.5	+0.6	-0.6	+0.4	-0.8	+2.9
UE tune	+0.5	+0.1	-0.7	-0.8	+0.4	+0.3	-0.0	+0.2	-1.2	+0.1	-0.3	+0.0	-0.5	+0.6	+0.6	+0.9
	+2.2	+0.2	+0.2	-0.0	-1.2	+0.2	+0.2	-1.5	-1.6	-0.1	+0.5	+0.3	-0.0	+0.8	+0.0	+0.6
CR	+0.3	-0.2	+1.4	+0.2	+0.3	-0.3	-0.9	+1.5	-0.2	-0.2	-0.2	+0.7	-0.7	+0.2	+0.2	+2.8
	+0.5	+0.1	-0.0	-0.8	-0.0	-0.2	-0.2	+0.6	+0.1	+0.0	-0.4	+0.4	-0.4	+0.2	+0.5	-0.7
	+0.7	-0.2	+0.1	-0.6	-0.1	-0.4	+0.6	+0.5	-1.0	+0.2	+0.7	-0.4	-0.6	+1.0	-0.6	+0.9
$f(b \rightarrow B)$	+0.7	-0.2	-0.2	+0.3	+0.4	-0.3	-0.2	+0.6	+0.6	-0.2	-0.2	+0.5	-0.0	-0.6	-0.4	+0.7
	-0.4	+0.1	+0.1	-0.1	-0.2	+0.1	+0.2	-0.2	-0.2	+0.1	+0.1	-0.1	-0.0	+0.2	+0.3	-0.2
	+0.1	-0.0	-0.0	+0.1	+0.1	-0.1	-0.0	+0.1	+0.1	-0.0	-0.0	+0.1	-0.0	-0.1	-0.1	+0.1
	+0.7	-0.3	-0.1	+0.4	+0.4	-0.4	-0.2	+0.3	+0.5	-0.3	-0.1	+0.5	+0.2	-0.5	-0.2	+0.4
BR($B \rightarrow \mu$)	-0.1	+0.0	+0.1	-0.1	-0.0	+0.0	+0.0	-0.0	-0.1	+0.0	+0.1	-0.1	-0.0	+0.0	-0.0	-0.0
	+0.1	-0.1	-0.1	+0.1	+0.1	-0.1	-0.1	+0.1	+0.1	-0.1	-0.0	+0.1	+0.0	-0.1	-0.0	+0.2

Table 80: The measured $[M(t\bar{t}), y(t)]$ cross sections, along with their relative statistical and systematic uncertainties.

$M(t\bar{t})$ [GeV]	$y(t)$	$\frac{1}{\sigma(t\bar{t})} \frac{d\sigma}{dy(t)}$	stat. [%]	syst. [%]	bin
300–400	0.00–0.35	1.506×10^{-1}	3.1	+6.6 -5.4	1
300–400	0.35–0.85	1.511×10^{-1}	2.2	+3.5 -8.1	2
300–400	0.85–1.45	1.161×10^{-1}	2.2	+4.2 -6.2	3
300–400	1.45–2.50	4.794×10^{-2}	4.6	+19.5 -10.1	4
400–500	0.00–0.35	2.317×10^{-1}	1.9	+3.9 -3.1	5
400–500	0.35–0.85	2.181×10^{-1}	1.3	+2.2 -2.4	6
400–500	0.85–1.45	1.605×10^{-1}	1.5	+4.2 -3.0	7
400–500	1.45–2.50	7.230×10^{-2}	2.1	+6.8 -2.2	8
500–650	0.00–0.35	1.538×10^{-1}	2.2	+5.9 -2.2	9
500–650	0.35–0.85	1.438×10^{-1}	1.8	+1.7 -6.8	10
500–650	0.85–1.45	1.062×10^{-1}	1.9	+3.7 -2.5	11
500–650	1.45–2.50	5.345×10^{-2}	2.5	+3.2 -7.4	12
650–1500	0.00–0.35	6.963×10^{-2}	2.8	+4.3 -8.6	13
650–1500	0.35–0.85	7.045×10^{-2}	2.3	+6.2 -4.6	14
650–1500	0.85–1.45	6.765×10^{-2}	2.0	+3.1 -5.5	15
650–1500	1.45–2.50	4.155×10^{-2}	2.2	+4.8 -3.2	16

Table 81: The correlation matrix of statistical uncertainties for the measured $[M(t\bar{t}), y(t)]$ cross sections. The values are expressed as percentages. For bin indices see Table 80.

Table 82: Sources and values of the relative systematic uncertainties in percent of the measured $[M(t\bar{t}), y(t)]$ cross sections. For bin indices see Table 80.

source / bin	1	2	3	4	5	6	7	8	9	10	11	12	13	14	15	16
JER	-0.6 -0.2	+0.3 -1.1	-0.3 -0.7	+2.4 +3.9	+0.3 +0.7	-0.0 -0.2	-0.2 -0.3	-0.2 +0.8	+0.4 -0.0	-0.6 -0.7	+0.6 -0.1	-0.8 -1.6	-1.1 -0.2	-0.4 +0.3	-0.2 -0.2	-0.1 +0.7
JESAbsoluteMPFBias	-0.9 -1.3	+0.1 -0.5	-0.7 -0.8	+0.1 +1.7	+0.9 +0.7	-0.0 +0.5	-0.4 +0.2	+1.4 +0.6	+0.3 +0.1	-1.1 -0.7	-0.3 +0.2	+0.0 -1.0	+0.1 -0.4	+0.2 -0.2	+0.2 -0.1	+0.3 +0.2
JESAbsoluteScale	-0.2 -0.5	-0.8 -1.0	+0.7 -0.4	+2.1 +3.8	+0.7 +0.4	-0.2 -0.3	-0.3 +0.1	-0.4 +0.2	+0.3 +0.4	-0.4 -0.3	-0.0 -0.2	-1.2 -1.0	+0.0 -0.9	-0.6 +0.0	-0.0 -0.1	+0.9 +0.1
JESAbsoluteStat	+0.3 +1.2	+0.1 -1.8	-0.0 -0.3	+1.8 +0.1	-0.4 +0.1	-0.4 -0.0	-0.3 +0.1	+0.5 +1.3	+0.5 +0.2	-0.6 -0.8	+0.4 +0.1	-0.7 -0.3	-0.4 +0.1	-0.1 +0.5	+0.1 -0.0	-0.2 +0.3
JESFlavourQCD	+1.5 -0.5	-0.1 -1.9	+0.0 -0.2	+2.5 +1.7	-0.6 +1.0	-0.8 +0.3	-0.5 +0.6	-0.0 +0.8	+0.2 +0.7	-0.6 -0.4	+0.1 -0.3	-0.7 -0.7	+0.3 -1.8	+0.7 -0.4	+0.5 -0.9	+0.3 -0.1
JESFragmentation	-0.3 +0.5	-0.7 -0.6	+0.0 -0.6	+0.7 +3.0	+0.2 +0.0	-0.3 +0.0	-0.3 -0.2	+0.7 -0.0	+0.6 +0.5	+0.1 -0.8	+0.3 +0.3	-0.7 -0.4	-0.1 -0.6	-0.4 -0.2	+0.3 -0.1	+0.3 -0.2
JESPileUpDataMC	+0.5 +0.8	-1.4 -0.9	+0.4 -0.3	+0.3 +3.7	+0.1 -0.2	-0.5 +0.2	+0.4 -0.3	+0.4 +0.6	+0.3 +0.8	+0.8 -0.9	+0.0 -0.3	-0.4 -1.1	+0.2 -1.0	+0.0 -0.3	+0.4 -0.6	+0.4 -0.0
JESPileUpPtBB	-0.7 -0.4	-0.2 +0.3	-0.0 +0.0	+1.6 +1.8	+0.2 +0.0	-0.2 -0.1	-0.4 +0.1	+0.4 +0.5	+0.9 +0.7	-0.6 -1.1	-0.1 -0.0	-0.6 -1.3	-0.3 -1.0	-0.3 +0.0	+0.3 -0.1	+0.4 +0.2
JESPileUpPtEC1	-0.1 -0.2	+0.7 -0.9	+0.0 -0.3	-1.5 +3.7	+0.8 -0.6	+0.2 -0.4	-0.5 +0.0	+0.2 +1.0	-0.5 -0.1	+0.3 -0.6	-0.1 -0.6	-0.6 -1.3	-0.3 -1.0	-0.3 -0.1	+0.4 -0.2	-0.3 +0.2
JESPileUpPtEC2	-0.0 -0.0	+0.0 +0.0	-0.0 +0.0	+0.0 +0.0	-0.0 -0.0	-0.0 +0.0	+0.0 +0.0	+0.0 +0.0	+0.0 +0.0	+0.0 +0.0						
JESPileUpPtHF	-0.0 -0.0	+0.0 +0.0	-0.0 -0.0	+0.0 +0.0	+0.0 -0.0	-0.0 +0.0	+0.0 +0.0	+0.0 +0.0	+0.0 +0.0	+0.0 +0.0						
JESPileUpPtRef	+0.3 +0.1	+0.5 -0.6	+0.4 +0.2	+0.1 +2.1	-0.9 -0.0	+0.0 -0.1	-0.3 -0.1	+0.1 +0.8	+0.5 -0.3	-0.4 -0.2	+0.1 +0.5	-0.4 -1.2	+0.2 -0.2	+0.1 -1.0	+0.0 -0.6	+0.2 +0.2
JESRelativeBal	+0.9 -1.7	+0.3 -0.7	+0.8 -0.7	+1.4 +1.3	-0.4 +0.4	-0.2 +0.1	-0.2 +1.0	-0.1 +0.7	+0.3 -1.9	-0.8 +0.3	-0.5 -0.3	-1.6 -1.0	+0.1 +0.4	+0.4 -0.4	+0.2 +0.6	+0.4 +0.6
JESRelativeFSR	+0.1 +0.2	-0.4 -0.6	-0.2 +0.5	+2.3 +3.2	-0.3 +0.3	-0.2 -0.6	-0.1 -0.6	+0.6 -0.2	+1.2 +0.4	-1.0 -0.7	+1.3 +0.1	-1.4 -0.5	-0.8 -0.7	-0.4 +0.5	-0.8 -0.0	+0.3 +0.2
JESRelativeJEREC1	-0.5 -0.6	-0.6 -0.3	+0.1 -0.3	+3.1 +1.3	+0.3 +0.0	-0.2 -0.1	-0.6 -0.1	+1.0 +0.5	-0.1 -0.0	-0.5 -0.3	-0.0 +0.6	-0.8 -0.2	-0.3 +0.0	-0.1 -0.3	-0.1 +0.2	+0.1 -0.2
JESRelativeJEREC2	-0.0 -0.0	+0.0 +0.0	-0.0 +0.0	+0.0 +0.0	-0.0 -0.0	-0.0 +0.0	+0.0 +0.0	+0.0 +0.0	+0.0 +0.0	+0.0 +0.0						
JESRelativeJERHF	-0.0 -0.0	+0.0 +0.0	+0.0 +0.0	+0.0 +0.0	+0.0 +0.0	+0.0 +0.0	+0.0 +0.0	-0.0 +0.0	-0.0 +0.0	+0.0 +0.0	-0.0 +0.0	-0.0 +0.0	+0.0 +0.0	+0.0 +0.0	+0.0 +0.0	+0.0 +0.0
JESRelativePtBB	+0.7 +0.9	-2.1 -1.3	-0.6 +0.3	+3.0 +1.3	+0.4 +0.4	-0.0 -0.0	+0.3 +0.3	+1.0 +0.1	-0.0 +0.5	-0.7 -0.0	-0.2 -0.0	-1.0 -0.9	-0.2 -0.3	+0.1 +0.1	-0.1 -0.3	+0.1 +0.3
JESRelativePtEC1	+0.6 -0.7	-0.0 -0.5	-0.2 -0.5	+1.5 +2.0	+0.1 -0.4	+0.0 -0.1	-0.3 -0.2	+0.4 +1.2	+0.2 +0.1	-0.3 -0.6	+0.1 +0.4	-1.5 +0.4	-0.3 -0.7	-0.0 +0.0	+0.3 -0.2	-0.3 +0.1
JESRelativePtEC2	-0.0 -0.0	+0.0 +0.0	+0.0 +0.0	+0.0 +0.0	+0.0 +0.0	+0.0 +0.0	+0.0 +0.0	-0.0 +0.0	+0.0 +0.0	+0.0 -0.0	-0.0 +0.0	-0.0 +0.0	+0.0 +0.0	+0.0 +0.0	+0.0 +0.0	+0.0 +0.0
JESRelativePtHF	-0.0 -0.0	+0.0 +0.0	+0.0 +0.0	+0.0 +0.0	-0.0 +0.0	+0.0 +0.0	+0.0 +0.0	+0.0 +0.0	+0.0 -0.0	+0.0 +0.0	+0.0 -0.0	-0.0 +0.0	+0.0 +0.0	+0.0 +0.0	+0.0 +0.0	+0.0 +0.0
JESRelativeStatEC	-0.1 -0.8	-0.2 +0.3	+0.1 +1.3	+1.1 -0.8	+0.6 -0.3	-0.3 -0.0	-0.8 -0.1	+1.2 +0.3	+0.2 +0.3	-0.2 -0.5	-0.2 -0.0	-0.4 +0.1	-0.5 -0.3	+0.1 +0.4	+0.1 +0.1	-0.3 -0.1
JESRelativeStatFSR	-0.4 -1.0	-0.8 +0.5	-0.1 +0.5	+2.7 +1.5	+0.4 -0.2	-0.1 +0.0	+0.4 -0.3	+0.3 +0.6	+0.2 +1.0	-1.5 -1.1	+0.0 -0.3	-1.0 -0.7	+0.1 -0.7	-0.2 -0.4	+0.1 +0.1	+0.3 +0.2
JESRelativeStatHF	-0.0 -0.0	+0.0 +0.0	+0.0 +0.0	+0.0 +0.0	+0.0 +0.0	+0.0 +0.0	+0.0 +0.0	-0.0 +0.0	-0.0 +0.0	+0.0 +0.0	-0.0 -0.0	-0.0 +0.0	+0.0 +0.0	+0.0 +0.0	+0.0 +0.0	+0.0 +0.0
JESSinglePionECAL	+0.4 -0.5	-0.8 -0.4	-0.4 -0.3	+3.4 +2.7	-0.2 +0.0	+0.2 -0.0	-0.4 -0.1	+1.1 +0.3	+0.1 +0.5	-0.7 -0.9	-0.3 +0.4	-0.8 -1.2	-0.8 -0.4	-0.1 +0.3	-0.3 -0.0	-0.2 +0.3

Table 83: Table 82 continued.

source / bin	1	2	3	4	5	6	7	8	9	10	11	12	13	14	15	16
JESSinglePionHCAL	-0.0	-0.7	-0.1	+2.4	+0.0	+0.2	-0.4	+0.5	+0.5	-0.6	-0.0	-0.5	-0.8	-0.4	-0.0	-0.1
	+0.2	-0.1	-0.5	+2.4	-0.2	-0.1	-0.7	+0.4	+0.3	-0.5	+0.1	-0.8	-0.0	-0.3	+0.3	+0.3
JESTimePtEta	+1.4	-1.2	+0.7	+2.3	-0.5	-0.2	-0.5	+0.7	+0.8	-0.8	+0.4	-1.2	-0.4	-0.7	-0.0	+0.4
	-0.5	-0.4	+0.2	+0.7	+0.6	-0.2	-0.1	+1.2	+0.2	-0.8	-0.1	-1.2	-0.0	+0.3	+0.0	+0.3
E_T^{miss}	+0.7	-0.2	-0.5	-2.2	-0.1	+0.3	+0.5	+1.0	-0.2	-0.1	+0.2	-0.1	+0.0	-0.2	-0.2	+0.0
	-0.4	-1.0	-0.8	+3.4	+0.8	+0.1	+0.3	+0.1	-0.1	-1.0	-0.2	-0.8	-0.2	+0.2	+0.1	-0.1
lepton ID/ISO	-0.2	-0.6	-0.6	-0.2	+0.4	+0.4	+0.6	+0.5	-0.2	-0.3	-0.1	-0.4	-0.2	+0.1	-0.2	+0.1
	+0.2	+0.0	+0.1	+0.4	-0.1	-0.2	-0.1	-0.2	+0.0	-0.0	+0.1	-0.0	+0.3	+0.1	+0.1	+0.0
pileup	+0.3	+0.1	-0.0	-0.5	-0.0	+0.2	-0.2	-0.4	+0.0	+0.1	+0.0	+0.1	-0.1	+0.1	-0.0	+0.2
	-0.2	-0.7	-0.5	+0.7	+0.3	-0.0	+0.6	+0.6	-0.2	-0.5	+0.0	-0.5	+0.1	+0.0	-0.1	-0.1
trigger	+0.2	-0.1	-0.2	-0.4	+0.2	+0.2	+0.3	-0.1	-0.1	-0.1	+0.1	-0.5	-0.0	+0.2	+0.0	-0.2
	-0.1	-0.1	-0.0	+0.5	-0.1	-0.1	-0.1	+0.2	+0.0	-0.1	-0.1	+0.3	+0.0	-0.1	-0.1	+0.2
trigger (η)	-0.3	-0.2	+0.0	+1.1	-0.2	-0.1	-0.0	+0.3	-0.2	-0.1	-0.1	-0.0	-0.2	-0.1	+0.1	+0.1
	+0.3	+0.2	-0.0	-1.1	+0.2	+0.1	+0.0	-0.3	+0.2	+0.1	+0.1	+0.0	+0.2	+0.1	-0.1	-0.1
non-tt background	-0.9	-0.6	-1.0	-4.7	+0.2	+0.5	+0.4	-0.3	+0.8	+0.7	+0.5	+0.5	+1.3	+1.1	+1.1	+1.1
	+1.0	+0.2	+0.5	+4.6	+0.1	-0.4	-0.1	+0.5	-0.8	-0.9	-0.4	-0.8	-1.2	-0.9	-1.1	-1.0
b-tagging	-0.1	-0.1	-0.1	-0.1	-0.0	-0.0	+0.0	+0.1	+0.1	-0.0	-0.0	+0.0	+0.0	+0.1	+0.1	+0.1
	+0.1	+0.1	+0.1	+0.1	+0.0	-0.0	-0.0	-0.1	-0.1	+0.0	+0.0	-0.0	-0.0	-0.1	-0.1	-0.1
b-tagging (light jets)	-0.2	-0.1	-0.2	-1.2	+0.1	+0.2	+0.1	-0.2	+0.2	+0.2	+0.1	+0.1	+0.3	+0.2	+0.2	+0.1
	+0.2	-0.5	-0.3	+1.4	+0.2	-0.0	+0.4	+0.4	-0.4	-0.6	-0.0	-0.5	-0.3	-0.1	-0.3	-0.0
luminosity	+0.0	+0.0	+0.0	+0.0	+0.0	+0.0	+0.0	+0.0	+0.0	+0.0	+0.0	+0.0	+0.0	+0.0	+0.0	+0.0
	+0.0	+0.0	+0.0	+0.0	+0.0	+0.0	+0.0	+0.0	+0.0	+0.0	+0.0	+0.0	+0.0	+0.0	+0.0	+0.0
BR($t\bar{t} \rightarrow \ell\ell$)	+0.0	+0.0	+0.0	+0.0	+0.0	+0.0	+0.0	+0.0	+0.0	+0.0	+0.0	+0.0	+0.0	+0.0	+0.0	+0.0
	+0.0	+0.0	+0.0	+0.0	+0.0	+0.0	+0.0	+0.0	+0.0	+0.0	+0.0	+0.0	+0.0	+0.0	+0.0	+0.0
PDF eigenvector 1	-0.0	-0.0	+0.0	+0.0	-0.0	-0.0	-0.0	+0.0	-0.0	-0.0	-0.0	+0.0	+0.0	+0.0	+0.0	+0.0
	+0.0	+0.0	+0.0	-0.0	+0.0	+0.0	+0.0	-0.1	+0.0	-0.0	-0.0	-0.0	-0.0	-0.0	-0.0	+0.0
PDF eigenvector 2	-0.3	-0.0	+0.1	+0.2	-0.0	-0.0	+0.0	+0.0	+0.0	-0.0	-0.0	-0.1	+0.2	+0.2	+0.1	-0.0
	+0.2	+0.0	-0.1	-0.2	-0.0	-0.1	-0.0	+0.1	+0.0	+0.1	+0.1	+0.1	-0.0	-0.0	-0.0	-0.1
PDF eigenvector 3	+0.1	+0.0	+0.0	-0.1	+0.1	+0.1	+0.0	-0.1	+0.0	+0.0	-0.1	-0.0	-0.1	-0.1	-0.0	+0.1
	-0.1	-0.0	-0.0	+0.1	-0.0	-0.0	-0.0	+0.1	-0.0	-0.0	+0.0	+0.0	+0.0	+0.0	+0.0	-0.1
PDF eigenvector 4	-0.3	-0.0	+0.1	+0.3	-0.0	+0.0	-0.0	+0.1	-0.0	-0.1	-0.0	-0.0	+0.1	+0.1	+0.1	-0.0
	+0.2	-0.1	-0.2	-0.1	+0.1	+0.0	+0.1	+0.1	-0.0	-0.0	+0.1	-0.1	-0.0	+0.0	-0.1	+0.0
PDF eigenvector 5	+0.1	-0.2	-0.2	-0.0	-0.0	-0.1	+0.1	+0.3	-0.1	-0.1	+0.2	-0.0	+0.0	+0.1	-0.0	-0.1
	+0.1	-0.1	-0.1	-0.1	+0.2	+0.2	+0.2	-0.2	+0.1	-0.0	-0.2	-0.2	-0.1	-0.0	-0.1	+0.2
PDF eigenvector 6	-0.2	-0.0	+0.0	+0.1	+0.0	+0.1	+0.0	+0.0	-0.0	-0.1	-0.1	-0.0	+0.1	+0.1	+0.1	+0.1
	+0.1	+0.0	+0.0	-0.1	-0.0	-0.0	-0.0	-0.0	+0.0	+0.0	+0.1	+0.0	-0.0	-0.0	-0.0	-0.0
PDF eigenvector 7	+0.1	-0.0	-0.1	-0.2	-0.2	-0.0	+0.3	-0.0	+0.1	+0.4	+0.1	+0.0	+0.0	-0.0	-0.0	-0.3
	-0.0	+0.0	+0.0	+0.1	+0.1	+0.1	-0.0	-0.2	+0.0	-0.0	-0.2	-0.1	-0.0	-0.0	+0.0	+0.2
PDF eigenvector 8	-0.1	-0.0	-0.0	-0.0	-0.0	+0.0	+0.0	+0.1	-0.0	-0.0	+0.0	-0.0	+0.0	+0.0	-0.0	-0.0
	+0.0	+0.0	+0.0	+0.0	+0.0	-0.0	-0.0	-0.1	+0.0	+0.0	+0.0	+0.0	+0.0	+0.0	+0.0	+0.0
PDF eigenvector 9	+0.1	-0.1	-0.1	+0.1	+0.1	-0.0	+0.1	+0.0	-0.0	-0.1	+0.0	-0.1	-0.1	+0.0	-0.0	+0.0
	-0.1	-0.2	-0.2	-0.0	+0.1	+0.1	+0.2	+0.1	-0.1	-0.1	-0.0	-0.1	+0.1	+0.1	-0.0	+0.1
PDF eigenvector 10	-0.1	-0.1	-0.1	+0.2	+0.2	+0.1	+0.1	-0.1	-0.1	-0.2	-0.2	-0.1	-0.1	+0.0	+0.0	+0.2
	+0.1	-0.0	-0.1	-0.2	-0.1	-0.1	+0.0	+0.1	+0.0	+0.1	+0.2	+0.0	+0.1	+0.0	-0.0	-0.1
PDF eigenvector 11	-0.0	+0.0	+0.0	+0.0	+0.0	+0.0	+0.0	-0.0	+0.0	-0.0	-0.1	-0.0	-0.0	-0.0	+0.0	+0.0
	+0.1	-0.2	-0.2	-0.0	+0.0	-0.0	+0.1	+0.1	-0.0	-0.1	+0.1	-0.1	+0.1	+0.1	-0.0	-0.0
PDF eigenvector 12	+0.1	-0.2	-0.2	-0.1	+0.0	-0.0	+0.2	+0.2	-0.0	-0.1	+0.1	-0.1	+0.1	+0.1	-0.0	-0.0
	-0.0	+0.0	+0.0	+0.1	+0.0	+0.0	-0.0	-0.1	-0.0	-0.0	-0.1	+0.0	-0.1	-0.0	+0.0	+0.1
PDF eigenvector 13	+0.1	+0.0	-0.0	-0.0	+0.0	+0.1	+0.0	-0.0	-0.0	-0.0	-0.1	+0.0	-0.1	-0.1	-0.1	+0.0
	-0.1	-0.0	+0.0	+0.0	-0.0	-0.1	-0.0	+0.0	+0.0	+0.0	+0.1	-0.0	+0.1	+0.1	+0.1	-0.0
PDF eigenvector 14	+0.0	+0.0	-0.0	-0.1	-0.0	-0.0	+0.0	+0.0	+0.0	+0.0	+0.0	-0.0	+0.0	+0.0	-0.0	-0.0
	-0.0	-0.1	-0.1	+0.2	+0.1	+0.1	+0.1	+0.0	-0.1	-0.1	-0.0	-0.1	-0.0	+0.0	+0.0	+0.1

Table 84: Table 82 continued.

source / bin	1	2	3	4	5	6	7	8	9	10	11	12	13	14	15	16
PDF eigenvector 15	+0.1	+0.0	-0.0	-0.1	-0.0	-0.0	+0.0	+0.0	+0.0	+0.1	+0.1	-0.0	+0.0	-0.0	-0.0	-0.0
	-0.0	-0.0	+0.0	+0.0	+0.0	+0.0	-0.0	-0.0	-0.0	-0.0	-0.0	+0.0	-0.0	+0.0	+0.0	+0.0
PDF eigenvector 16	-0.0	-0.0	+0.0	+0.0	+0.0	+0.0	-0.0	-0.0	-0.0	-0.0	-0.0	+0.0	-0.0	-0.0	+0.0	+0.0
	+0.0	-0.1	-0.1	+0.0	+0.1	+0.0	+0.1	+0.1	-0.0	-0.1	+0.1	-0.1	+0.0	+0.1	-0.0	+0.0
PDF eigenvector 17	+0.1	-0.1	-0.1	-0.0	+0.1	+0.0	+0.1	+0.1	-0.0	-0.1	+0.1	-0.1	+0.0	+0.1	-0.0	+0.0
	-0.1	-0.0	+0.0	+0.1	+0.0	+0.1	-0.0	-0.0	-0.0	-0.1	-0.1	+0.0	-0.1	-0.0	+0.0	+0.1
PDF eigenvector 18	-0.1	-0.2	-0.1	+0.3	+0.1	+0.0	+0.1	+0.1	-0.1	-0.2	-0.0	-0.1	+0.0	+0.1	+0.1	+0.1
	+0.1	+0.0	-0.0	-0.2	+0.0	+0.0	+0.0	-0.0	+0.0	+0.1	+0.0	-0.0	-0.0	-0.1	-0.1	-0.0
PDF eigenvector 19	-0.1	+0.0	+0.1	+0.2	+0.0	+0.0	-0.0	-0.1	-0.0	-0.1	-0.1	+0.0	-0.0	-0.0	+0.0	+0.1
	+0.1	-0.0	-0.1	-0.3	-0.1	-0.1	+0.0	+0.1	+0.0	+0.1	+0.2	+0.0	+0.1	+0.0	-0.1	-0.1
PDF eigenvector 20	-0.0	-0.1	-0.1	+0.2	+0.1	+0.1	+0.1	+0.0	-0.1	-0.1	-0.0	-0.0	+0.0	+0.0	-0.0	+0.1
	+0.1	-0.2	-0.2	-0.1	+0.1	+0.0	+0.2	+0.1	-0.0	-0.1	+0.1	-0.1	+0.0	+0.1	-0.1	-0.0
PDF eigenvector 21	-0.1	-0.0	-0.0	+0.1	-0.0	-0.0	-0.0	+0.1	-0.0	-0.0	+0.0	+0.0	+0.1	+0.1	+0.1	-0.0
	+0.1	+0.0	+0.0	-0.1	+0.1	+0.1	+0.0	-0.1	+0.0	+0.0	-0.1	+0.0	-0.1	-0.1	-0.1	+0.1
PDF eigenvector 22	-0.3	-0.1	+0.0	+0.4	-0.1	-0.1	-0.1	+0.2	-0.1	-0.1	+0.1	+0.1	+0.1	+0.2	+0.2	-0.1
	+0.3	+0.0	-0.0	-0.2	+0.1	+0.1	+0.0	-0.2	+0.1	+0.1	-0.1	-0.0	-0.2	-0.2	-0.1	+0.1
PDF eigenvector 23	+0.3	+0.1	-0.1	-0.5	+0.0	+0.0	+0.1	-0.1	+0.1	+0.2	+0.1	-0.1	-0.0	-0.1	-0.2	-0.0
	-0.0	-0.2	-0.1	+0.2	+0.1	+0.0	+0.1	+0.2	-0.1	-0.2	+0.0	-0.0	+0.0	+0.1	+0.0	+0.0
PDF eigenvector 24	+0.1	-0.2	-0.2	+0.0	+0.0	-0.0	+0.1	+0.2	-0.1	-0.1	+0.1	-0.0	-0.0	+0.0	-0.0	-0.0
	-0.0	-0.1	-0.1	-0.2	+0.0	-0.0	+0.2	+0.1	+0.0	+0.0	+0.1	-0.3	+0.2	+0.2	-0.0	-0.1
PDF eigenvector 25	+0.0	+0.0	-0.0	-0.3	-0.0	-0.1	+0.1	-0.0	+0.1	+0.2	+0.1	-0.1	+0.2	+0.1	-0.0	-0.1
	+0.1	-0.0	-0.1	-0.1	-0.1	-0.1	-0.0	+0.2	-0.0	+0.0	+0.2	+0.2	-0.0	-0.0	-0.0	-0.1
PDF eigenvector 26	+0.0	+0.0	-0.0	-0.0	-0.0	+0.0	+0.0	-0.0	+0.0	+0.0	+0.0	-0.0	+0.0	-0.0	-0.0	-0.0
	-0.0	-0.0	-0.0	+0.0	-0.0	-0.0	-0.0	+0.0	-0.0	-0.0	+0.0	+0.0	+0.0	+0.0	+0.0	-0.0
PDF eigenvector 27	-0.1	+0.1	+0.2	+0.2	-0.0	-0.1	-0.1	-0.2	+0.1	+0.0	-0.0	+0.0	-0.1	-0.0	-0.0	+0.0
	-0.1	-0.0	-0.0	+0.0	+0.0	+0.0	+0.0	+0.0	-0.0	-0.0	-0.0	-0.0	+0.0	+0.0	+0.0	+0.0
PDF eigenvector 28	+0.1	+0.0	+0.0	-0.1	-0.0	-0.0	-0.0	-0.1	+0.0	+0.0	+0.0	+0.1	-0.0	-0.0	-0.0	+0.0
	-0.1	-0.0	-0.0	+0.1	+0.0	+0.0	-0.0	+0.1	-0.1	-0.1	-0.0	+0.0	-0.0	+0.0	+0.0	-0.0
α_s	+0.1	+0.1	+0.1	+0.0	+0.0	-0.0	-0.1	-0.2	+0.1	+0.1	+0.0	+0.0	-0.1	-0.1	-0.0	+0.0
	-0.1	-0.1	-0.1	-0.0	-0.0	+0.0	+0.1	+0.2	-0.1	-0.1	-0.0	-0.0	+0.1	+0.1	+0.0	-0.0
m_t	-1.2	-1.9	-2.1	-2.5	-0.2	+0.1	+0.3	+0.2	+1.0	+0.8	+0.8	+0.1	+1.6	+2.4	+1.5	+1.8
	+1.5	+1.5	+1.4	+0.8	+0.5	+0.2	+0.5	+0.5	-1.0	-0.9	-0.8	-0.4	-2.8	-1.9	-2.0	-1.6
μ_{rf}	+0.7	+0.4	+0.7	+0.6	-0.1	-0.4	-0.3	-0.7	+0.4	+0.2	+0.1	+0.0	-1.4	-0.8	-0.1	+0.0
	-0.8	-0.5	-0.8	-0.8	+0.1	+0.4	+0.3	+0.7	-0.4	-0.2	+0.0	-0.2	+1.8	+1.1	+0.1	-0.0
h_{damp}	+0.8	-0.6	-0.3	-0.0	+0.0	+0.1	-0.2	+0.0	+0.3	+0.3	+0.1	-0.3	-0.7	+0.4	-0.5	+0.7
	+0.1	-1.9	-1.3	-0.8	-0.6	+0.3	+1.9	+1.1	+1.1	-0.8	+0.3	-0.3	-1.7	+1.4	-1.6	+1.5
PS ISR	-0.5	+0.4	-0.9	-0.7	-0.2	+0.0	-0.4	+0.5	+1.6	-0.6	+0.4	+1.3	-1.2	+0.6	-0.1	-0.7
	+1.6	+0.0	-1.6	-1.0	-0.8	-0.2	+0.3	+0.8	+1.2	-0.4	+0.5	+0.4	-0.5	+0.6	-0.7	-0.1
PS FSR	-0.6	+0.3	-0.0	-1.0	+0.8	+0.4	+0.7	+0.6	+0.2	-0.8	+0.7	-0.3	-1.8	-0.5	-1.7	-0.3
	+0.2	+0.3	-0.7	-1.2	-0.7	-0.1	+0.3	-0.0	+0.5	-0.6	+0.6	-0.0	+0.8	+1.5	-0.1	+0.7
UE tune	-0.7	-0.0	+0.0	-2.3	+0.6	+0.6	+0.4	+0.8	-0.1	-0.7	-1.0	+1.1	-1.5	+1.0	-0.6	+0.2
	+0.8	-0.6	-1.3	-1.1	+0.3	+0.7	+0.0	+0.1	+1.1	-0.5	+0.8	+0.0	-0.4	-1.0	-0.6	+0.5
CR	-0.6	-0.2	-0.8	-1.1	+0.3	-0.1	+0.5	+0.3	+1.2	-0.7	-0.2	+1.0	+0.3	+1.1	-0.5	-0.0
	+0.3	-0.1	+0.0	-0.5	+0.0	+0.2	+0.0	-0.5	+0.2	-0.5	-0.1	+0.5	-0.9	+0.6	+0.4	+0.4
$f(b \rightarrow B)$	+1.1	+0.4	+0.5	+0.2	+0.3	-0.2	+0.2	-0.4	-0.3	-0.4	+0.2	-0.6	-0.9	-0.4	-0.3	-0.2
	-0.5	-0.4	-0.4	-0.0	-0.1	+0.1	+0.1	+0.2	+0.1	+0.1	-0.1	+0.2	+0.5	+0.3	+0.2	+0.2
$\text{BR}(B \rightarrow \mu)$	+0.2	+0.1	+0.1	+0.2	-0.1	-0.1	-0.1	-0.1	-0.0	-0.0	-0.1	-0.1	+0.1	+0.0	+0.1	+0.1
	-0.1	-0.1	-0.1	-0.2	+0.1	+0.1	+0.1	+0.0	+0.1	+0.0	+0.1	+0.0	-0.1	-0.0	-0.1	-0.0

Table 85: The measured $[M(t\bar{t}), y(t\bar{t})]$ cross sections, along with their relative statistical and systematic uncertainties.

$M(t\bar{t})$ [GeV]	$y(t\bar{t})$	$\frac{1}{\sigma(t\bar{t})} \frac{d\sigma}{dy(t\bar{t})}$	stat. [%]	syst. [%]	bin
300–400	0.00–0.35	1.554×10^{-1}	2.5	+6.7 -4.5	1
300–400	0.35–0.75	1.485×10^{-1}	2.3	+3.9 -9.6	2
300–400	0.75–1.15	1.320×10^{-1}	2.4	+6.3 -5.6	3
300–400	1.15–2.50	5.856×10^{-2}	2.4	+10.9 -6.9	4
400–500	0.00–0.35	2.506×10^{-1}	1.4	+3.4 -1.8	5
400–500	0.35–0.75	2.296×10^{-1}	1.3	+1.4 -3.9	6
400–500	0.75–1.15	1.889×10^{-1}	1.5	+3.9 -2.3	7
400–500	1.15–2.50	8.038×10^{-2}	1.2	+3.7 -3.9	8
500–650	0.00–0.35	1.833×10^{-1}	1.7	+3.0 -2.2	9
500–650	0.35–0.75	1.714×10^{-1}	1.6	+2.0 -5.2	10
500–650	0.75–1.15	1.340×10^{-1}	2.0	+6.7 -2.1	11
500–650	1.15–2.50	4.390×10^{-2}	2.3	+2.7 -7.7	12
650–1500	0.00–0.35	1.331×10^{-1}	1.6	+3.0 -4.5	13
650–1500	0.35–0.75	1.079×10^{-1}	2.0	+5.2 -4.2	14
650–1500	0.75–1.15	8.007×10^{-2}	2.6	+5.1 -7.9	15
650–1500	1.15–2.50	1.731×10^{-2}	4.7	+11.3 -6.3	16

Table 86: The correlation matrix of statistical uncertainties for the measured $[M(t\bar{t}), y(t\bar{t})]$ cross sections. The values are expressed as percentages. For bin indices see Table 85.

Table 87: Sources and values of the relative systematic uncertainties in percent of the measured $[M(\text{t}\bar{\text{t}}), y(\text{t}\bar{\text{t}})]$ cross sections. For bin indices see Table 85.

source / bin	1	2	3	4	5	6	7	8	9	10	11	12	13	14	15	16	
JER	+0.5 -0.3	-1.4 -1.1	+1.0 +0.1	+1.4 +1.1	+0.2 +0.2	-0.1 -0.2	+0.3 +0.1	-0.5 +0.1	+0.0 +0.0	-0.4 -0.8	+0.6 +0.1	-0.7 -0.5	-0.1 -0.1	-0.0 +0.6	-1.3 +0.2	+0.2 +1.0	
JESAbsoluteMPFBias	-0.2 -0.4	-0.8 -1.1	+0.0 -0.1	+0.5 +1.0	+0.6 +0.4	-0.1 +0.0	+0.4 +0.9	-0.2 -0.3	+0.1 +0.2	-1.0 -0.6	+0.2 +0.5	-0.8 -1.0	-0.1 -0.6	+0.9 +0.9	-0.1 -1.0	+1.2 +0.7	
JESAbsoluteScale	+0.6 -0.7	-1.0 -1.7	-0.3 +0.0	+1.4 +1.5	+0.2 +0.5	-0.0 +0.1	+0.3 +0.7	-0.2 -0.3	+0.0 -0.0	-0.4 -0.3	-0.6 +0.5	-1.0 -1.0	-0.4 -0.3	+0.1 +0.0	+0.3 -0.7	+1.6 +1.1	
JESAbsoluteStat	+0.6 -0.4	-1.0 -0.4	+0.4 +0.5	+1.4 +0.6	-0.1 +0.1	+0.2 -0.6	+0.2 +0.2	-0.5 +0.4	-0.1 -0.2	-0.0 -0.6	+0.3 +0.7	-1.4 -0.7	-0.2 +0.1	+0.5 +0.4	-0.5 -0.1	+0.2 -0.2	
JESFlavourQCD	+1.3 -0.4	-0.6 -1.9	+0.5 +0.1	+1.9 +1.8	-0.4 +0.8	-1.2 +0.4	-0.8 +0.6	-0.2 -0.0	+0.2 +0.3	-0.8 -0.2	+0.3 +0.0	-0.5 -1.4	+0.2 -0.9	+0.9 -0.0	+0.3 -1.5	+0.5 +0.6	
JESFragmentation	+0.7 +0.3	-0.5 -1.5	+0.4 +0.5	+0.2 +1.8	-0.0 +0.4	-0.6 +0.1	+0.3 +0.5	-0.3 -0.7	+0.5 +0.3	-0.6 -0.8	+0.3 +0.2	-0.5 -1.3	-0.3 -0.3	+1.0 +0.1	-1.0 -0.5	+1.5 +1.1	
JESPileUpDataMC	+1.4 -0.2	-1.4 +0.0	+0.0 +0.3	+0.5 +0.9	-0.0 +0.3	-0.1 -0.0	+0.0 +0.3	-0.1 -0.3	-0.3 +0.1	-0.3 -0.7	+0.1 +0.4	-0.8 -0.9	+0.1 -0.4	+0.8 -0.0	-0.3 -0.9	+1.8 +1.1	
JESPileUpPtBB	-0.4 -0.1	-0.7 -1.4	-0.8 +0.8	+0.7 +0.9	-0.2 +0.2	+0.1 +0.3	+0.2 +0.5	+0.7 +0.0	+0.0 -0.2	-0.1 -0.4	+0.3 +0.1	-0.6 -1.0	+0.3 -0.4	+0.9 +0.2	-0.2 -1.0	+0.5 +1.0	
JESPileUpPtEC1	+0.5 -1.1	+0.6 -0.3	+0.2 -0.2	+2.0 -0.5	-0.6 -0.6	+0.2 +0.4	+0.4 +0.4	+0.1 +0.1	-0.7 -0.4	+0.4 -0.4	+0.0 +0.2	-0.2 -0.1	-0.3 -0.0	+0.4 +0.0	+0.1 -0.3	+1.3 -0.7	
JESPileUpPtEC2	+0.0 +0.0	+0.1 +0.1	+0.2 +0.2	+0.1 +0.1	-0.0 -0.0	-0.1 -0.1	-0.1 -0.1	-0.1 -0.1	-0.0 -0.0	+0.1 +0.1	+0.1 +0.1	-0.1 -0.1	+0.0 +0.0	-0.1 +0.0	+0.0 +0.0	+0.0 +0.0	
JESPileUpPtHF	+0.0 +0.0	+0.1 +0.1	+0.2 +0.2	+0.1 +0.1	-0.0 -0.0	-0.1 -0.1	-0.1 -0.1	-0.1 -0.1	-0.0 -0.0	+0.1 +0.1	+0.1 +0.1	-0.1 -0.1	+0.0 +0.0	-0.1 -0.1	+0.0 +0.0	+0.0 +0.0	
JESPileUpPtRef	-0.7 +0.2	+0.7 -1.9	-0.3 +0.3	-0.2 +1.6	-0.2 +0.4	+0.1 -0.5	+0.3 +0.7	-0.3 +0.1	-0.2 +0.4	+0.0 -0.6	+0.2 +0.4	-0.2 -0.6	+0.4 -0.6	+0.2 -0.6	+0.0 +0.3	+0.0 -1.3	+1.1 -0.1
JESRelativeBal	+0.4 -0.3	-0.5 -1.5	+1.3 -0.3	+0.7 +1.1	+0.1 +0.1	-0.4 -0.1	+0.2 +0.5	-0.7 +0.8	-0.1 -0.5	-0.1 -0.7	-0.1 +0.3	-0.6 -0.5	-0.5 -0.5	-0.1 -0.0	+1.2 +0.4	-0.8 -1.1	+1.5 +0.7
JESRelativeFSR	+0.3 +0.4	-1.3 +0.3	-0.6 +0.7	+1.4 +0.6	+0.1 -0.0	-0.1 -0.4	+0.5 +0.2	+0.0 -0.4	+0.4 +0.2	-0.3 -0.8	+0.1 -0.0	-0.7 -0.5	-0.4 -0.3	+0.3 +0.8	-0.9 -0.5	+0.5 +0.6	
JESRelativeJEREC1	-0.1 -0.7	-1.0 -0.4	-0.7 +0.7	+1.8 +1.1	-0.1 +0.1	+0.2 -0.4	+0.3 +0.2	-0.2 -0.2	+0.3 +0.2	-0.6 -0.3	+0.1 -0.2	-0.9 -0.2	-0.2 -0.2	+0.3 +0.3	-0.0 -0.1	+0.5 +0.7	
JESRelativeJEREC2	+0.0 +0.0	+0.1 +0.1	+0.2 +0.2	+0.1 +0.1	-0.0 -0.0	-0.1 -0.1	-0.1 -0.1	-0.1 -0.1	-0.0 -0.0	+0.1 +0.1	+0.1 +0.1	-0.1 -0.1	+0.0 +0.0	-0.1 -0.1	+0.0 +0.0	+0.0 +0.0	
JESRelativeJERHF	+0.0 +0.0	+0.1 +0.1	+0.2 +0.2	+0.1 +0.1	-0.0 -0.0	-0.1 -0.1	-0.1 -0.1	-0.1 -0.1	-0.0 -0.0	+0.1 +0.1	+0.1 +0.1	-0.1 -0.1	+0.0 +0.0	-0.1 -0.1	+0.0 +0.0	+0.0 +0.0	
JESRelativePtBB	+0.4 -0.0	-0.7 -1.5	+0.8 +0.4	+0.4 +0.8	+0.1 +0.6	-0.4 +0.1	-0.1 +0.1	+0.3 -0.3	-0.7 +0.1	-0.5 -0.8	+0.4 +0.4	+0.4 -0.3	+0.1 -0.4	+0.1 -0.6	-0.5 +1.1	-0.8 +1.1	
JESRelativePtEC1	-0.3 -0.1	+0.5 -1.0	+0.3 -0.5	+1.2 +1.2	+0.5 -0.4	-0.1 -0.7	-0.4 +0.4	-0.4 +0.7	+0.2 +0.0	-0.4 -0.7	-0.0 +0.2	-1.0 +0.7	-0.2 -0.2	+0.2 +0.2	-0.4 -0.6	+0.4 +0.2	
JESRelativePtEC2	+0.0 +0.0	+0.1 +0.1	+0.2 +0.2	+0.1 +0.1	-0.0 -0.0	-0.1 -0.1	-0.1 -0.1	-0.1 -0.1	-0.0 -0.0	+0.1 +0.1	+0.1 +0.1	-0.1 -0.1	+0.0 +0.0	-0.1 -0.1	+0.0 +0.0	+0.0 +0.0	
JESRelativePtHF	+0.0 +0.0	-0.0 +0.1	-0.0 +0.1	-0.0 +0.1	-0.0 -0.0	-0.0 -0.1	-0.0 -0.1	-0.0 -0.1	-0.0 -0.0	-0.0 +0.1	-0.0 +0.1	-0.0 -0.1	-0.0 +0.0	+0.0 -0.1	+0.0 +0.0	+0.0 +0.0	
JESRelativeStatEC	+0.4 +0.2	-0.8 -0.5	+0.1 +0.1	+1.3 +1.4	-0.2 -0.2	-0.0 -0.5	+0.5 +0.3	-0.3 -0.1	+0.0 +0.1	-0.3 -0.8	+0.5 +0.3	-0.9 -0.9	-0.2 -0.1	+0.1 +0.5	-1.3 -0.2	+0.7 +0.8	
JESRelativeStatFSR	-0.4 -0.7	-1.7 -1.5	+0.8 +0.7	+1.2 +1.3	+0.3 +0.4	+0.1 -0.1	+0.5 +0.5	+0.1 +0.1	+0.1 +0.1	-0.5 -0.4	+0.1 +0.1	-1.1 -0.9	+0.1 -0.2	+0.1 +0.3	+0.5 -0.9	+1.6 +0.3	
JESRelativeStatHF	+0.0 +0.0	+0.1 +0.1	+0.2 +0.2	+0.1 +0.1	-0.0 -0.0	-0.1 -0.1	-0.1 -0.1	-0.1 -0.1	-0.0 -0.0	+0.1 +0.1	+0.1 +0.1	-0.1 -0.1	+0.0 +0.0	-0.1 +0.0	+0.0 +0.0	+0.0 +0.0	
JESSinglePionECAL	+0.4 -0.5	-2.0 -0.3	+0.3 +0.2	+1.7 +1.0	+0.5 +0.1	-0.1 -0.2	+0.7 -0.3	+0.1 -0.1	-0.5 +0.3	-0.8 -0.5	-0.4 +0.6	-0.7 -0.3	-0.2 -0.1	+0.2 +0.3	-0.9 -0.3	+0.9 +0.3	

Table 88: Table 87 continued.

source / bin	1	2	3	4	5	6	7	8	9	10	11	12	13	14	15	16
JESSinglePionHCAL	-0.3	-1.3	+0.1	+1.4	+0.5	-0.1	+0.6	-0.1	-0.2	-0.3	+0.5	-1.1	-0.2	+0.2	-1.2	+0.8
	-0.4	-0.9	-0.5	+1.5	+0.3	-0.3	+0.1	+0.1	+0.1	-0.4	+0.3	-1.3	+0.1	+0.3	-0.3	+2.2
JESTimePtEta	+1.4	-1.0	-0.1	+1.4	-0.2	-0.6	+0.1	-0.0	-0.1	-0.5	+0.7	-1.2	-0.2	+0.5	-0.8	+1.2
	-0.3	+0.2	+1.4	+0.3	-0.1	-0.5	+0.4	-0.2	+0.2	-0.9	-0.0	-0.6	-0.0	+0.5	+0.1	+1.0
E_T^{miss}	+1.7	-0.3	-0.4	+0.0	-0.3	+0.4	-0.1	-0.0	-0.1	-0.3	-0.1	-0.2	+0.1	-0.1	-0.1	-0.4
	-1.0	-0.0	+0.0	+1.1	+0.1	-0.1	+0.4	-0.0	-0.3	-0.4	-0.2	-0.3	-0.0	+0.2	+0.0	+0.5
lepton ID/ISO	-0.2	+0.0	-0.3	-0.3	+0.1	+0.2	+0.0	+0.4	-0.1	+0.1	-0.0	-0.2	-0.0	-0.1	-0.1	-0.5
	+0.2	-0.0	+0.3	+0.2	-0.1	-0.2	-0.1	-0.4	+0.1	-0.1	+0.0	+0.2	+0.0	+0.1	+0.1	+0.5
pileup	+0.2	+0.0	-0.3	-0.5	+0.1	+0.2	+0.1	-0.2	+0.1	+0.2	+0.1	-0.0	+0.1	+0.1	-0.1	-0.1
	-0.1	-0.1	+0.2	+0.5	-0.1	-0.2	-0.1	+0.2	-0.0	-0.2	-0.1	+0.0	-0.1	-0.1	+0.1	+0.1
trigger	+0.1	+0.2	+0.1	-0.3	+0.2	+0.1	-0.0	-0.1	+0.1	+0.1	-0.1	-0.2	+0.1	-0.0	-0.1	-0.1
	-0.1	-0.1	+0.1	+0.4	-0.2	-0.3	-0.1	+0.0	-0.1	+0.0	+0.2	+0.2	-0.1	-0.1	+0.1	+0.2
trigger (η)	-0.3	-0.2	-0.1	+0.6	-0.2	-0.1	-0.2	+0.4	-0.2	-0.2	-0.2	+0.3	+0.1	-0.1	-0.2	+0.1
	+0.3	+0.2	+0.1	-0.6	+0.2	+0.1	+0.1	-0.4	+0.2	+0.2	+0.2	-0.3	-0.1	+0.1	+0.2	-0.1
non-tt background	-0.7	-0.1	-0.5	-3.1	+0.2	-0.2	-0.0	-0.2	+0.5	+1.1	+1.2	+0.3	+1.1	+0.8	+1.3	+0.8
	+0.9	+0.4	+1.2	+3.1	-0.3	-0.4	-0.3	-0.0	-0.5	-0.7	-0.7	-0.5	-1.0	-1.0	-1.2	-0.7
b-tagging	-0.1	-0.1	-0.2	-0.1	+0.0	+0.0	-0.0	+0.1	-0.0	-0.0	+0.0	+0.0	+0.1	+0.1	+0.1	+0.1
	+0.1	+0.1	+0.3	+0.2	-0.0	-0.2	-0.1	-0.2	+0.0	+0.1	+0.1	-0.1	-0.0	-0.2	-0.1	-0.1
b-tagging (light jets)	-0.1	+0.0	-0.2	-0.8	+0.1	+0.1	+0.1	-0.1	+0.2	+0.2	+0.2	+0.1	+0.2	+0.2	+0.2	+0.1
	+0.2	-0.0	+0.2	+0.9	-0.1	-0.1	-0.1	+0.1	-0.2	-0.2	-0.2	-0.1	-0.2	-0.2	-0.2	-0.1
luminosity	+0.0	+0.0	+0.0	+0.0	+0.0	+0.0	+0.0	+0.0	+0.0	+0.0	+0.0	+0.0	+0.0	+0.0	+0.0	+0.0
	+0.0	+0.0	+0.0	+0.0	+0.0	+0.0	+0.0	+0.0	+0.0	+0.0	+0.0	+0.0	+0.0	+0.0	+0.0	+0.0
BR($t\bar{t} \rightarrow \ell\ell$)	+0.0	+0.0	+0.0	+0.0	+0.0	+0.0	+0.0	+0.0	+0.0	+0.0	+0.0	+0.0	+0.0	+0.0	+0.0	+0.0
	+0.0	+0.0	+0.0	+0.0	+0.0	+0.0	+0.0	+0.0	+0.0	+0.0	+0.0	+0.0	+0.0	+0.0	+0.0	+0.0
PDF eigenvector 1	-0.0	-0.0	+0.0	+0.0	+0.0	+0.0	+0.0	-0.0	-0.0	-0.0	-0.0	+0.0	+0.0	+0.0	-0.0	+0.0
	+0.0	+0.0	-0.0	-0.0	+0.0	+0.0	+0.0	-0.0	+0.0	+0.0	-0.0	-0.1	+0.0	+0.0	+0.0	-0.0
PDF eigenvector 2	-0.1	-0.1	+0.1	+0.1	+0.0	-0.0	+0.0	+0.0	-0.1	-0.0	+0.1	+0.0	+0.1	+0.0	-0.1	-0.3
	+0.0	+0.0	+0.1	+0.0	-0.1	-0.1	-0.0	+0.1	+0.0	-0.0	+0.0	+0.1	-0.1	-0.1	+0.1	+0.1
PDF eigenvector 3	+0.1	+0.1	+0.1	-0.0	+0.1	-0.0	-0.0	-0.2	+0.1	+0.1	+0.0	-0.2	+0.1	+0.0	+0.1	-0.1
	-0.0	+0.0	+0.1	+0.0	-0.0	-0.1	-0.1	+0.0	+0.0	+0.0	+0.1	+0.1	-0.0	-0.1	-0.0	+0.2
PDF eigenvector 4	-0.1	-0.1	-0.0	+0.1	+0.0	+0.0	+0.0	-0.0	-0.1	-0.0	+0.0	+0.1	+0.1	+0.0	+0.0	-0.1
	+0.1	+0.1	+0.1	+0.0	-0.0	-0.1	-0.1	-0.0	+0.1	+0.1	+0.1	-0.1	-0.0	-0.1	-0.0	+0.0
PDF eigenvector 5	-0.0	-0.0	+0.1	+0.1	-0.1	-0.2	-0.1	+0.2	-0.0	+0.0	+0.1	+0.3	-0.2	-0.2	-0.1	+0.4
	+0.1	+0.1	+0.0	-0.1	+0.1	+0.1	+0.1	-0.2	+0.1	+0.1	-0.0	-0.5	+0.1	+0.1	+0.1	-0.3
PDF eigenvector 6	-0.1	+0.0	-0.0	-0.0	+0.0	+0.0	-0.0	-0.1	-0.0	+0.0	+0.0	-0.1	+0.1	+0.0	+0.1	+0.1
	+0.1	+0.0	+0.1	+0.0	-0.0	-0.1	-0.0	-0.0	+0.0	+0.0	+0.0	-0.1	-0.1	-0.1	-0.0	-0.0
PDF eigenvector 7	-0.0	-0.0	+0.1	+0.1	-0.2	-0.2	-0.1	+0.3	-0.0	-0.0	+0.0	+0.5	-0.3	-0.3	-0.2	+0.5
	+0.0	+0.0	-0.0	-0.1	+0.1	+0.1	+0.1	-0.2	+0.0	+0.0	-0.0	-0.3	+0.2	+0.2	+0.2	-0.2
PDF eigenvector 8	-0.1	+0.0	+0.0	-0.0	-0.0	-0.0	-0.1	+0.1	-0.0	+0.0	+0.0	+0.0	-0.0	-0.1	+0.0	+0.2
	+0.1	+0.0	+0.1	+0.1	-0.0	-0.1	-0.1	-0.1	+0.0	+0.1	+0.1	-0.0	+0.0	-0.0	+0.0	-0.0
PDF eigenvector 9	+0.1	+0.1	+0.2	+0.1	-0.0	-0.1	-0.1	-0.1	+0.0	+0.1	+0.1	-0.1	+0.0	-0.1	-0.1	-0.2
	-0.0	+0.0	-0.0	-0.1	+0.0	-0.0	-0.1	+0.0	-0.0	+0.0	+0.0	+0.0	-0.0	+0.1	+0.3	+0.3
PDF eigenvector 10	+0.0	+0.0	-0.1	-0.0	+0.1	+0.1	+0.1	-0.2	-0.0	+0.0	-0.0	-0.2	+0.1	+0.1	+0.1	-0.2
	-0.0	-0.0	+0.1	+0.0	-0.1	-0.1	-0.1	+0.2	+0.0	-0.0	+0.0	+0.2	-0.1	-0.2	-0.1	+0.2
PDF eigenvector 11	+0.0	+0.1	+0.1	+0.0	+0.0	-0.0	-0.0	-0.1	-0.0	+0.1	+0.1	-0.1	+0.0	-0.0	-0.0	-0.1
	-0.0	-0.0	+0.0	+0.0	-0.1	-0.1	-0.0	+0.1	-0.0	-0.0	+0.0	+0.1	-0.1	-0.1	-0.1	+0.1
PDF eigenvector 12	-0.0	-0.0	+0.0	+0.0	-0.1	-0.1	-0.0	+0.1	-0.0	-0.0	+0.0	+0.1	-0.1	-0.1	-0.1	+0.1
	+0.0	+0.1	+0.1	+0.0	+0.1	-0.0	-0.0	-0.2	+0.0	+0.1	+0.1	-0.1	+0.1	+0.0	+0.1	-0.1
PDF eigenvector 13	+0.0	+0.0	-0.1	-0.1	+0.0	+0.1	+0.0	+0.0	+0.0	+0.0	-0.1	-0.1	-0.0	+0.0	+0.1	+0.1
	-0.0	-0.0	+0.1	+0.1	-0.0	-0.1	-0.0	+0.0	-0.0	-0.0	+0.1	+0.1	+0.0	-0.0	-0.1	-0.1
PDF eigenvector 14	+0.0	+0.0	+0.1	+0.0	-0.0	-0.1	-0.1	+0.0	+0.0	+0.1	+0.1	-0.0	-0.0	-0.1	-0.0	+0.1
	+0.0	-0.0	+0.0	+0.0	+0.0	+0.0	+0.0	-0.1	-0.0	-0.0	+0.0	-0.0	+0.0	+0.0	+0.0	-0.1

Table 89: Table 87 continued.

source / bin	1	2	3	4	5	6	7	8	9	10	11	12	13	14	15	16
PDF eigenvector 15	+0.0	+0.0	+0.0	-0.0	-0.0	-0.0	-0.0	+0.1	+0.0	+0.0	-0.0	+0.0	-0.1	-0.0	-0.0	+0.0
	-0.0	-0.0	-0.0	+0.0	+0.0	+0.0	+0.0	-0.0	-0.0	-0.0	+0.0	-0.0	+0.0	+0.0	+0.0	-0.0
PDF eigenvector 16	+0.0	+0.0	+0.1	+0.0	+0.0	-0.1	-0.1	-0.0	-0.0	+0.0	+0.1	-0.0	+0.0	-0.0	+0.0	+0.0
	+0.0	-0.0	+0.0	+0.0	-0.0	-0.0	-0.0	+0.0	+0.0	+0.0	+0.0	+0.0	-0.0	-0.0	-0.0	-0.0
PDF eigenvector 17	+0.0	-0.0	+0.0	+0.0	-0.0	-0.0	-0.0	+0.0	+0.0	+0.0	+0.0	+0.0	-0.0	-0.0	-0.0	-0.0
	-0.0	+0.0	-0.1	-0.1	+0.1	+0.1	+0.0	-0.1	-0.0	-0.0	-0.1	-0.1	+0.0	+0.1	+0.1	+0.0
PDF eigenvector 18	-0.0	-0.0	+0.0	+0.1	+0.0	-0.0	+0.0	-0.1	-0.1	-0.0	+0.1	+0.1	+0.1	+0.1	+0.0	-0.0
	+0.0	+0.0	-0.0	-0.1	-0.0	+0.0	-0.0	+0.1	+0.1	+0.0	-0.1	-0.1	-0.1	-0.0	+0.0	+0.0
PDF eigenvector 19	+0.0	+0.1	+0.1	+0.0	+0.1	-0.0	-0.0	-0.2	-0.0	+0.0	+0.1	-0.1	+0.1	+0.1	+0.1	-0.2
	-0.0	-0.0	+0.0	-0.0	-0.1	-0.1	-0.1	+0.2	+0.0	-0.0	-0.0	+0.2	-0.2	-0.2	-0.1	+0.3
PDF eigenvector 20	+0.0	-0.0	+0.0	+0.0	+0.0	+0.0	+0.0	-0.1	+0.0	+0.0	-0.0	-0.0	+0.0	+0.0	+0.0	+0.0
	-0.0	+0.0	+0.0	-0.0	-0.0	-0.0	-0.0	+0.1	+0.0	-0.0	-0.0	+0.0	-0.0	-0.0	-0.0	+0.1
PDF eigenvector 21	-0.1	-0.1	-0.0	+0.0	-0.0	-0.0	-0.0	+0.1	-0.1	-0.0	+0.0	+0.2	+0.0	-0.0	-0.0	+0.1
	+0.1	+0.1	+0.1	-0.0	+0.0	-0.0	-0.0	-0.1	+0.1	+0.1	+0.0	-0.2	+0.0	-0.0	+0.0	-0.1
PDF eigenvector 22	-0.1	-0.1	-0.0	+0.1	-0.1	-0.1	-0.0	+0.1	-0.2	-0.1	+0.1	+0.4	+0.0	-0.0	-0.0	+0.1
	+0.1	+0.2	+0.1	-0.1	+0.1	+0.0	-0.0	-0.1	+0.1	+0.1	-0.0	-0.3	+0.0	+0.0	+0.1	-0.0
PDF eigenvector 23	+0.1	+0.1	+0.1	-0.1	-0.0	-0.0	-0.0	+0.1	+0.2	+0.1	-0.0	-0.3	-0.1	-0.1	-0.1	-0.1
	-0.0	-0.0	-0.0	+0.0	-0.0	-0.0	-0.0	+0.0	-0.0	-0.0	-0.0	+0.2	-0.0	-0.0	+0.0	+0.2
PDF eigenvector 24	+0.0	-0.0	+0.0	+0.0	-0.1	-0.1	-0.0	+0.1	+0.0	-0.0	+0.0	+0.2	-0.1	-0.1	-0.0	+0.2
	-0.0	+0.0	+0.2	+0.1	-0.1	-0.1	-0.1	+0.1	+0.0	+0.1	+0.2	-0.1	+0.0	-0.1	-0.1	-0.2
PDF eigenvector 25	-0.0	+0.0	+0.1	+0.1	-0.1	-0.1	-0.0	+0.1	+0.1	+0.0	+0.1	-0.1	-0.0	-0.1	-0.1	-0.2
	+0.0	-0.0	+0.0	+0.0	-0.1	-0.1	-0.1	+0.2	-0.0	-0.0	+0.0	+0.3	-0.2	-0.2	-0.1	+0.4
PDF eigenvector 26	+0.0	+0.0	+0.0	-0.0	-0.0	+0.0	-0.0	+0.0	+0.0	+0.0	-0.0	-0.0	-0.0	+0.0	-0.0	-0.0
	-0.0	-0.0	-0.0	+0.0	-0.0	-0.0	-0.0	+0.0	-0.0	-0.0	+0.0	+0.1	-0.0	-0.0	+0.0	+0.1
PDF eigenvector 27	+0.1	+0.1	+0.3	+0.2	+0.0	-0.1	-0.0	-0.3	+0.1	+0.1	+0.2	-0.1	+0.1	+0.0	-0.0	-0.4
	-0.0	+0.0	+0.0	-0.0	+0.0	-0.0	-0.1	+0.0	-0.0	+0.0	+0.0	-0.0	+0.0	+0.0	+0.0	+0.1
PDF eigenvector 28	+0.1	+0.1	+0.1	+0.0	-0.0	-0.1	-0.1	-0.1	+0.1	+0.1	+0.1	-0.0	-0.0	-0.1	-0.0	+0.0
	-0.1	-0.0	-0.1	-0.0	+0.0	+0.0	-0.0	+0.1	-0.1	-0.0	-0.0	+0.0	+0.0	+0.0	+0.0	+0.1
α_s	+0.1	+0.0	+0.2	+0.1	-0.0	-0.1	+0.0	-0.2	+0.1	+0.1	+0.1	-0.0	+0.0	-0.0	-0.0	-0.2
	-0.1	-0.0	-0.2	-0.1	-0.0	+0.1	-0.0	+0.2	-0.1	-0.1	-0.1	+0.1	-0.0	-0.0	+0.0	+0.3
m_t	-1.4	-1.6	-1.5	-2.4	-0.2	-0.3	-0.3	+0.4	+0.7	+0.6	+1.0	+0.9	+1.5	+1.6	+2.1	+2.7
	+1.4	+1.6	+1.4	+1.7	+0.6	+0.5	+0.4	-0.3	-0.4	-0.7	-0.5	-1.4	-1.7	-2.1	-1.9	-2.5
μ_{rf}	+1.0	+0.4	+1.5	+1.0	-0.1	-0.5	+0.2	-1.4	+0.6	+0.3	+0.7	-0.5	-0.0	-0.3	-1.1	-2.8
	-1.1	-0.3	-1.3	-1.1	+0.0	+0.3	-0.5	+1.3	-0.6	-0.2	-0.6	+0.6	-0.0	+0.2	+1.5	+3.9
h_{damp}	+1.0	+0.3	+0.1	-0.5	-0.5	+0.1	+0.0	-0.5	+0.1	+0.2	+1.0	-0.6	+0.0	+0.2	-1.2	+1.9
	+0.9	-1.3	-2.0	-0.4	-0.4	+0.0	+0.8	+1.1	+0.1	-0.0	+1.6	-1.0	+0.2	-0.5	+0.3	-0.5
PS ISR	+0.5	-0.6	+0.0	-0.4	+0.0	-0.6	-0.0	+0.1	+0.3	+0.0	+1.9	-0.4	-0.1	-0.4	-0.0	+0.1
	+1.0	+0.7	-1.1	-0.7	-0.2	-0.9	+0.1	+0.5	+0.7	-0.6	+1.6	-0.5	-0.6	+0.5	-0.5	+0.7
PS FSR	+0.5	-0.9	+0.9	-0.1	+0.8	+0.0	+0.8	-0.0	+0.1	-0.3	+1.9	-1.6	-1.2	-0.8	-1.5	+0.0
	+0.2	+0.6	+0.2	-1.0	-0.2	-0.6	-0.7	+0.2	+0.2	+0.0	+1.4	-0.8	+0.3	+0.6	+1.7	-0.0
UE tune	+0.5	-0.2	+0.0	-1.0	+1.0	-0.1	+0.3	+0.3	-0.4	-0.6	+1.5	-1.1	-0.1	+0.1	-0.7	+0.1
	+1.1	-0.6	-1.5	-0.3	+0.6	-0.0	-0.1	+0.3	+0.3	-0.0	+1.2	-0.6	-0.7	-0.8	+0.9	-0.2
CR	+0.1	-0.7	-0.3	-1.1	+0.5	-0.4	-0.1	+0.4	+1.0	-1.0	+0.8	+0.4	-0.5	+1.1	+0.1	+0.3
	-0.2	+0.2	-0.0	-0.1	+0.6	-0.5	-0.0	-0.2	-0.1	-0.5	+1.1	-0.8	+0.3	+0.3	-0.5	+1.8
	+0.2	+0.7	-0.6	-0.5	-0.2	-0.7	-0.6	+0.5	+0.2	+0.1	+1.4	-0.6	-0.1	+0.8	-0.2	+0.4
$f(b \rightarrow B)$	+1.2	+0.7	+1.3	+0.4	+0.1	-0.2	+0.0	-0.8	+0.2	+0.0	-0.0	-0.8	-0.0	-0.7	-0.8	-1.1
	-0.6	-0.4	-0.6	-0.3	-0.0	+0.0	-0.1	+0.3	-0.0	-0.0	+0.1	+0.4	+0.0	+0.4	+0.5	+0.6
	+0.2	+0.1	+0.2	+0.1	+0.0	-0.0	+0.0	-0.2	+0.0	+0.0	+0.0	-0.1	+0.0	-0.1	-0.1	-0.2
	+1.4	+0.8	+1.3	+0.7	-0.1	-0.2	-0.1	-0.6	-0.0	-0.2	-0.3	-0.8	-0.2	-0.5	-0.8	-1.0
BR($B \rightarrow \mu$)	-0.0	-0.0	+0.0	-0.0	+0.1	-0.1	-0.0	-0.0	+0.1	+0.1	+0.2	-0.0	-0.0	-0.1	-0.1	-0.1
	+0.1	+0.2	+0.2	+0.1	-0.1	-0.1	-0.0	-0.1	-0.1	-0.1	-0.1	+0.1	+0.1	+0.1	+0.2	+0.2

Table 90: The measured $[M(t\bar{t}), \Delta\eta(t, \bar{t})]$ cross sections, along with their relative statistical and systematic uncertainties.

$M(t\bar{t})$ [GeV]	$\Delta\eta(t, \bar{t})$	$\frac{1}{\sigma(t\bar{t})} \frac{d\sigma}{d\Delta\eta(t, \bar{t})}$	stat. [%]	syst. [%]	bin
300–400	0.0–0.4	1.874×10^{-1}	4.4	+5.0 -14.4	1
300–400	0.4–1.2	1.260×10^{-1}	1.5	+3.4 -6.0	2
300–400	1.2–6.0	1.444×10^{-2}	4.4	+17.7 -7.2	3
400–500	0.0–0.4	1.633×10^{-1}	2.7	+7.3 -6.1	4
400–500	0.4–1.2	1.587×10^{-1}	1.4	+5.2 -3.1	5
400–500	1.2–6.0	3.510×10^{-2}	1.1	+3.1 -3.4	6
500–650	0.0–0.4	5.389×10^{-2}	4.2	+5.8 -7.4	7
500–650	0.4–1.2	6.632×10^{-2}	2.6	+6.4 -4.3	8
500–650	1.2–6.0	3.601×10^{-2}	1.0	+1.4 -2.9	9
650–1500	0.0–0.4	1.803×10^{-2}	4.8	+8.5 -5.4	10
650–1500	0.4–1.2	1.991×10^{-2}	3.3	+6.0 -7.0	11
650–1500	1.2–6.0	2.575×10^{-2}	1.0	+3.9 -3.5	12

Table 91: The correlation matrix of statistical uncertainties for the measured $[M(t\bar{t}), \Delta\eta(t, \bar{t})]$ cross sections. The values are expressed as percentages. For bin indices see Table 90.

Table 92: Sources and values of the relative systematic uncertainties in percent of the measured $[M(t\bar{t}), \Delta\eta(t, \bar{t})]$ cross sections. For bin indices see Table 90.

source / bin	1	2	3	4	5	6	7	8	9	10	11	12
JER	-1.7	-0.1	+2.3	+0.8	+0.4	-0.2	-0.2	+0.4	-0.6	-0.5	-1.0	+0.0
	-0.2	-1.3	+0.4	+1.6	-0.2	+0.1	-0.6	+0.3	-0.4	+1.1	+0.1	+0.6
JESAbsoluteMPFBias	-1.1	-0.5	+1.2	+0.8	-0.1	+0.2	-0.2	-0.3	-0.4	+0.4	+0.2	+0.5
	-1.5	-0.4	+1.0	+0.2	+0.7	+0.0	+0.1	+0.0	-0.3	+0.7	+0.1	+0.1
JESAbsoluteScale	-0.3	-0.5	+2.2	+0.4	-0.2	-0.3	-0.5	+0.5	-0.4	+0.6	+0.2	+0.1
	-0.6	-0.5	+0.6	+1.3	-0.4	-0.1	-0.0	+0.0	+0.3	-0.0	+0.2	-0.0
JESAbsoluteStat	-2.1	+0.1	+2.8	+0.2	+0.3	-0.4	-0.7	+0.7	-0.5	+1.0	-0.2	+0.2
	-1.1	-1.1	+0.9	+0.7	-0.1	+0.5	-0.6	+0.4	-0.3	+0.3	+0.1	+0.5
JESFlavourQCD	-1.1	+0.1	+3.7	+0.8	-0.3	-1.2	+0.6	-0.2	-0.5	+1.0	+1.4	+0.5
	-0.7	-1.5	+0.6	+2.7	-0.1	+0.7	-1.3	-0.7	+0.0	-0.5	-1.1	-0.4
JESFragmentation	-2.4	+0.2	+2.4	+0.1	+0.3	-0.2	+0.2	+0.2	-0.3	-0.0	+0.1	+0.3
	-3.1	-0.3	+3.0	-0.2	+0.5	+0.2	+1.5	-0.7	-0.2	-0.1	-0.2	+0.1
JESPileUpDataMC	-2.6	+0.5	+0.4	+0.2	+0.7	+0.0	-1.0	+0.2	-0.3	+1.2	+0.9	+0.4
	+0.2	-0.4	+1.1	+0.8	-0.2	+0.2	-0.0	-0.6	-0.4	+0.0	-1.1	+0.1
JESPileUpPtBB	-1.7	-0.7	+2.4	+1.2	-0.1	-0.3	+0.2	+0.2	-0.2	+1.1	-0.2	+0.2
	-1.2	-0.5	+1.9	+0.8	+0.0	+0.1	-0.7	+0.1	-0.3	+0.0	-0.0	-0.1
JESPileUpPtEC1	+0.3	-0.6	+1.1	-0.1	+0.4	-0.6	+0.3	+0.7	-0.3	-0.0	+0.4	+0.1
	-0.3	-0.0	+0.3	+0.0	-0.1	-0.2	+0.2	-0.1	+0.0	-0.6	-1.0	+0.5
JESPileUpPtEC2	+0.0	+0.0	-0.0	-0.0	+0.0	+0.0	+0.0	-0.0	+0.0	+0.0	+0.0	+0.0
	+0.0	+0.0	-0.0	+0.0	+0.0	+0.0	+0.0	-0.0	+0.0	+0.0	+0.0	+0.0
JESPileUpPtHF	+0.0	+0.0	-0.0	+0.0	+0.0	+0.0	+0.0	-0.0	+0.0	+0.0	+0.0	+0.0
	+0.0	+0.0	-0.0	-0.0	+0.0	+0.0	+0.0	-0.0	+0.0	+0.0	+0.0	+0.0
JESPileUpPtRef	-0.5	+0.3	+0.2	+1.1	-0.1	-0.4	+0.0	-0.1	-0.3	+1.0	+0.3	+0.4
	-0.7	-0.2	+1.2	+1.1	-0.2	-0.1	-0.5	-0.4	+0.1	+0.5	-0.9	-0.1
JESRelativeBal	-2.5	+0.1	+2.9	-0.2	+0.5	-0.1	-0.5	+0.1	-0.6	+1.3	+1.2	+0.2
	-3.1	-0.7	+1.2	+1.0	+0.8	+0.6	+0.6	-0.4	-0.5	-0.2	-0.5	+0.4
JESRelativeFSR	-1.0	-1.0	+1.2	+1.9	-0.2	-0.1	-0.3	-0.0	-0.0	+0.3	-0.6	+0.1
	-1.3	-0.6	+3.2	-0.0	-0.4	-0.4	+0.2	-0.0	-0.1	+0.3	+0.4	+0.4
JESRelativeJEREC1	+1.2	-0.3	-0.3	+0.1	+0.2	-0.3	+0.4	-0.3	-0.2	+0.0	+0.0	+0.2
	-1.5	-0.0	+2.1	+0.0	+0.1	-0.3	+0.3	-0.0	-0.1	+0.3	-0.3	+0.1
JESRelativeJEREC2	+0.0	+0.0	-0.0	-0.0	+0.0	+0.0	+0.0	-0.0	+0.0	+0.0	+0.0	+0.0
	+0.0	+0.0	-0.0	-0.0	+0.0	+0.0	+0.0	-0.0	+0.0	+0.0	+0.0	+0.0
JESRelativeJERHF	+0.0	+0.0	-0.0	+0.0	+0.0	+0.0	+0.0	-0.0	+0.0	+0.0	+0.0	+0.0
	+0.0	+0.0	-0.0	+0.0	+0.0	+0.0	+0.0	-0.0	+0.0	+0.0	+0.0	+0.0
JESRelativePtBB	-2.0	-0.0	+2.3	+0.5	+0.0	-0.0	+0.4	-0.2	-0.4	+0.6	-0.0	+0.2
	-4.2	-0.7	+3.5	+0.6	+0.5	+0.4	+1.3	-0.1	-0.4	-0.4	-0.1	+0.2
JESRelativePtEC1	-1.0	+0.2	+1.8	+0.1	+0.3	-0.4	+0.4	-0.2	-0.2	-0.2	+0.4	-0.1
	-1.1	-0.2	-0.1	+0.5	+0.5	-0.0	+0.1	-0.5	+0.1	-0.2	-0.5	+0.4
JESRelativePtEC2	+0.0	+0.0	-0.0	-0.0	+0.0	+0.0	+0.0	-0.0	+0.0	+0.0	+0.0	+0.0
	+0.0	+0.0	-0.0	-0.0	+0.0	+0.0	+0.0	-0.0	+0.0	+0.0	+0.0	+0.0
JESRelativePtHF	+0.0	+0.0	+0.0	+0.0	+0.0	+0.0	+0.0	+0.0	+0.0	+0.0	+0.0	+0.0
	+0.0	+0.0	-0.0	+0.0	+0.0	+0.0	+0.0	-0.0	+0.0	+0.0	+0.0	+0.0
JESRelativeStatEC	-0.8	-0.1	+1.9	+0.5	+0.0	-0.4	+0.6	-0.0	-0.3	-0.4	-0.1	+0.1
	-1.5	-0.2	+1.7	-0.3	+0.6	-0.1	+0.1	+0.1	-0.5	-0.0	-0.4	+0.5
JESRelativeStatFSR	-0.7	+0.1	+0.7	+0.5	+0.3	-0.2	-0.7	-0.1	-0.3	+0.3	-0.1	+0.3
	-1.6	-0.8	+1.7	+1.0	+0.3	+0.0	-0.7	+0.1	-0.3	+0.9	-0.3	+0.2
JESRelativeStatHF	+0.0	+0.0	-0.0	+0.0	+0.0	+0.0	+0.0	-0.0	+0.0	+0.0	+0.0	+0.0
	+0.0	+0.0	-0.0	-0.0	+0.0	+0.0	+0.0	-0.0	+0.0	+0.0	+0.0	+0.0
JESSinglePionECAL	-2.4	-0.3	+2.3	+1.5	+0.4	-0.1	-0.5	-0.8	-0.3	+0.5	+0.2	+0.2
	-1.9	-0.8	+2.8	+0.7	+0.4	-0.4	+0.7	+0.8	-0.6	-0.6	+0.1	+0.4

Table 93: Table 92 continued.

source / bin	1	2	3	4	5	6	7	8	9	10	11	12
JESSinglePionHCAL	-1.2 -0.3	-0.6 +0.5	+2.2 +1.2	+0.4 +0.8	+0.1 -0.3	+0.1 -0.2	+0.9 -0.2	-0.1 -0.1	-0.4 -0.2	-0.6 +0.6	+0.1 +0.7	+0.1 +0.3
JESTimePtEta	-1.2 -1.3	-0.2 -0.8	+2.4 +2.2	+0.8 +0.4	+0.0 +0.1	-0.3 +0.3	+0.1 +0.9	+0.1 -0.5	-0.6 -0.7	+0.0 +0.1	-0.1 +0.7	+0.3 +0.4
E_T^{miss}	-0.4 -1.0	+0.0 +0.7	-0.3 +0.3	+0.7 -0.1	-0.1 +0.1	+0.2 -0.1	-0.1 +0.4	-0.2 -0.0	+0.0 -0.2	+0.4 +0.5	-0.3 -0.0	+0.0 +0.1
lepton ID/ISO	-0.2 +0.2	+0.2 -0.2	-0.6 +0.6	-0.1 +0.1	+0.3 -0.3	+0.1 -0.1	+0.0 +0.0	-0.3 +0.4	+0.2 -0.2	-0.3 +0.4	-0.4 +0.4	-0.1 +0.1
pileup	+0.3 -0.4	+0.2 -0.2	-0.7 +0.7	-0.5 +0.5	+0.2 -0.1	+0.0 -0.0	+0.2 -0.3	+0.1 -0.1	-0.0 +0.0	-0.3 +0.4	-0.2 +0.2	+0.1 -0.1
trigger	-0.1 +0.1	+0.0 -0.0	+0.1 -0.1	+0.0 -0.0	+0.1 -0.1	-0.0 +0.0	+0.1 -0.1	+0.0 +0.0	-0.0 +0.0	+0.1 -0.1	+0.1 -0.1	-0.1 +0.1
trigger (η)	+0.3 -0.3	+0.1 -0.1	-0.2 +0.2	+0.2 -0.2	-0.0 +0.0	-0.1 +0.1	+0.1 -0.1	-0.1 +0.1	-0.1 +0.1	+0.0 -0.0	-0.1 +0.1	+0.0 -0.0
non-tt background	-0.6 +0.5	-0.3 +0.3	-3.6 +3.5	-0.0 +0.1	+1.0 -1.0	-0.3 +0.3	+0.3 -0.2	+1.1 -1.1	+0.3 -0.3	+0.8 -0.8	+1.1 -1.0	+0.9 -0.9
b-tagging	-0.2 +0.2	+0.0 -0.0	-0.1 +0.1	-0.0 +0.0	+0.1 -0.1	-0.0 +0.0	+0.1 -0.1	-0.1 +0.1	+0.0 -0.0	+0.1 -0.1	+0.0 -0.0	+0.1 -0.1
b-tagging (light jets)	-0.1 +0.1	-0.1 +0.1	-0.9 +0.9	+0.1 -0.1	+0.3 -0.3	-0.1 +0.1	+0.2 -0.2	+0.4 -0.4	+0.0 -0.0	+0.3 -0.3	+0.2 -0.2	+0.1 -0.1
luminosity	+0.0 +0.0											
$\text{BR}(\bar{t}t \rightarrow \ell\ell)$	+0.0 +0.0											
PDF eigenvector 1	+0.0 +0.0	+0.0 +0.0	-0.0 +0.0	+0.0 +0.0	-0.0 +0.0	-0.0 +0.0	+0.0 -0.0	+0.0 -0.0	-0.0 -0.0	+0.0 +0.0	+0.0 +0.0	+0.0 -0.0
PDF eigenvector 2	+0.2 -0.2	-0.1 -0.1	-0.4 +0.3	+0.0 -0.0	-0.0 -0.0	-0.0 -0.0	-0.1 -0.0	+0.1 +0.0	-0.0 +0.1	+0.0 -0.1	-0.0 -0.1	+0.2 -0.0
PDF eigenvector 3	+0.0 -0.0	+0.0 -0.0	+0.1 -0.1	+0.0 -0.0	-0.0 -0.0	+0.0 -0.0	+0.0 -0.0	-0.0 +0.0	-0.0 +0.0	+0.0 -0.0	+0.1 -0.0	-0.1 +0.1
PDF eigenvector 4	+0.2 -0.1	+0.0 -0.1	-0.4 +0.3	+0.0 -0.0	+0.0 -0.0	-0.0 -0.0	-0.0 -0.0	+0.0 +0.0	-0.1 +0.0	+0.1 -0.0	+0.1 -0.1	+0.1 -0.1
PDF eigenvector 5	-0.2 -0.0	-0.1 +0.0	+0.2 +0.1	-0.1 +0.0	+0.0 +0.1	-0.0 +0.1	-0.0 -0.1	+0.0 -0.0	+0.1 -0.0	-0.1 +0.1	-0.2 +0.1	+0.0 -0.1
PDF eigenvector 6	+0.1 -0.0	+0.1 -0.1	-0.3 +0.2	+0.0 -0.0	+0.1 -0.1	-0.0 +0.0	+0.0 -0.0	-0.0 +0.0	-0.1 +0.0	+0.1 -0.1	+0.2 -0.1	+0.1 -0.0
PDF eigenvector 7	-0.3 +0.2	-0.1 +0.1	+0.4 -0.2	-0.1 +0.1	+0.0 +0.0	-0.1 +0.0	-0.0 +0.0	+0.0 -0.0	+0.2 -0.1	-0.2 +0.2	-0.4 +0.2	+0.0 -0.0
PDF eigenvector 8	-0.1 +0.1	+0.1 -0.1	-0.1 +0.1	-0.1 +0.0	+0.1 -0.1	-0.0 +0.0	+0.0 -0.0	-0.1 +0.1	+0.0 -0.0	-0.1 +0.1	+0.0 +0.0	+0.0 +0.0
PDF eigenvector 9	+0.1 -0.1	-0.0 +0.1	+0.1 -0.1	+0.0 -0.0	-0.1 +0.1	-0.0 +0.0	-0.0 +0.0	+0.1 -0.1	+0.0 -0.0	-0.1 +0.1	-0.1 +0.1	-0.0 +0.0
PDF eigenvector 10	+0.2 -0.2	+0.1 -0.1	-0.3 +0.3	+0.1 -0.1	+0.0 -0.0	+0.0 -0.0	+0.0 -0.0	-0.0 +0.0	-0.1 +0.1	+0.1 -0.2	+0.2 -0.2	-0.0 +0.0
PDF eigenvector 11	+0.1 -0.1	+0.0 -0.1	-0.1 +0.1	+0.0 -0.0	+0.0 -0.0	+0.0 -0.0	+0.0 +0.0	-0.0 +0.0	-0.0 +0.1	+0.0 -0.1	+0.1 -0.1	-0.0 +0.0
PDF eigenvector 12	-0.2 +0.2	-0.0 +0.0	+0.1 -0.1	-0.1 +0.1	+0.0 -0.0	-0.0 +0.0	-0.0 +0.0	-0.0 +0.0	+0.1 -0.1	-0.1 +0.1	-0.1 +0.1	+0.0 -0.0
PDF eigenvector 13	-0.1 +0.1	+0.1 -0.1	+0.1 +0.0	-0.0 -0.1	+0.1 -0.0	+0.0 -0.0	+0.0 -0.0	-0.1 +0.1	+0.0 +0.0	+0.0 -0.0	+0.1 -0.1	-0.1 +0.1
PDF eigenvector 14	-0.1 +0.1	-0.0 +0.0	+0.1 -0.1	-0.0 +0.0	+0.0 -0.0	-0.0 -0.0	-0.0 -0.0	+0.0 +0.0	+0.0 -0.1	-0.0 +0.0	-0.1 +0.1	-0.0 +0.0

Table 94: Table 92 continued.

source / bin	1	2	3	4	5	6	7	8	9	10	11	12
PDF eigenvector 15	-0.1	-0.0	+0.2	-0.0	-0.0	+0.0	-0.0	-0.0	+0.1	-0.0	-0.1	-0.0
	+0.0	+0.0	-0.1	+0.0	+0.0	-0.0	+0.0	+0.0	-0.0	+0.0	+0.0	+0.0
PDF eigenvector 16	+0.0	+0.0	-0.1	+0.0	+0.0	-0.0	+0.0	-0.0	-0.0	+0.0	+0.0	-0.0
	-0.0	-0.0	+0.1	-0.0	-0.0	+0.0	-0.0	+0.0	+0.0	-0.0	-0.1	+0.0
PDF eigenvector 17	-0.1	-0.0	+0.1	-0.0	-0.0	+0.0	-0.0	+0.0	+0.0	-0.0	-0.1	+0.0
	+0.1	+0.1	-0.2	+0.0	+0.1	-0.0	+0.0	-0.0	-0.1	+0.1	+0.1	-0.0
PDF eigenvector 18	+0.3	-0.0	-0.2	+0.1	-0.1	-0.0	-0.0	+0.1	-0.1	+0.0	+0.1	+0.1
	-0.3	+0.0	+0.2	-0.1	+0.0	+0.0	+0.0	-0.1	+0.1	-0.0	-0.1	-0.1
PDF eigenvector 19	+0.2	+0.0	-0.2	+0.1	-0.0	-0.0	+0.0	+0.0	-0.1	+0.1	+0.2	+0.0
	-0.3	-0.1	+0.3	-0.1	+0.0	-0.0	-0.0	-0.0	+0.1	-0.2	-0.2	-0.0
PDF eigenvector 20	+0.1	+0.0	-0.1	-0.0	-0.0	-0.0	+0.0	+0.0	-0.0	+0.1	+0.2	-0.0
	-0.1	-0.0	+0.1	-0.0	+0.0	+0.0	+0.0	-0.0	+0.0	-0.1	-0.1	-0.0
PDF eigenvector 21	+0.0	-0.0	-0.2	-0.0	+0.0	-0.0	-0.0	+0.0	-0.0	-0.0	-0.0	+0.1
	-0.0	+0.0	+0.1	+0.0	-0.0	+0.0	+0.0	-0.0	-0.0	+0.0	+0.0	-0.1
PDF eigenvector 22	+0.3	-0.0	-0.5	+0.0	+0.0	-0.1	-0.1	+0.2	-0.1	+0.0	+0.0	+0.2
	-0.2	+0.1	+0.3	-0.0	+0.0	+0.1	+0.1	-0.1	+0.0	+0.0	+0.1	-0.2
PDF eigenvector 23	-0.4	-0.0	+0.5	-0.1	-0.0	+0.1	+0.0	-0.2	+0.1	-0.1	-0.2	-0.2
	+0.1	+0.0	-0.1	+0.0	+0.0	-0.0	-0.0	+0.1	-0.0	+0.0	+0.0	+0.0
PDF eigenvector 24	-0.1	-0.0	+0.2	-0.0	-0.0	-0.0	-0.0	+0.1	+0.0	-0.0	-0.0	-0.0
	-0.2	-0.1	+0.1	-0.1	-0.1	+0.0	-0.0	-0.0	+0.1	-0.1	-0.2	+0.1
PDF eigenvector 25	-0.2	-0.1	+0.2	-0.1	-0.1	+0.0	-0.0	-0.0	+0.1	-0.1	-0.2	+0.0
	-0.2	-0.1	+0.3	-0.0	+0.0	-0.0	-0.0	+0.1	+0.1	-0.2	-0.2	-0.0
PDF eigenvector 26	-0.0	+0.0	+0.0	-0.0	+0.0	+0.0	+0.0	-0.0	+0.0	-0.0	-0.0	-0.0
	-0.0	-0.0	+0.0	+0.0	+0.0	-0.0	+0.0	+0.0	+0.0	+0.0	+0.0	+0.0
PDF eigenvector 27	+0.4	-0.1	+0.0	+0.1	-0.2	-0.0	-0.1	+0.2	-0.0	+0.0	+0.0	+0.0
	-0.0	+0.0	-0.2	-0.0	+0.1	-0.0	+0.0	-0.0	-0.0	+0.0	+0.0	+0.0
PDF eigenvector 28	+0.0	-0.0	+0.1	+0.0	-0.0	+0.0	+0.0	+0.0	+0.0	-0.0	-0.0	-0.0
	+0.0	+0.1	-0.2	-0.0	+0.1	-0.0	+0.0	-0.0	-0.0	+0.0	+0.1	+0.0
α_s	+0.2	-0.1	+0.1	+0.1	-0.2	+0.0	-0.0	+0.1	+0.0	+0.0	-0.0	-0.0
	-0.2	+0.1	-0.1	-0.1	+0.2	-0.0	+0.0	-0.1	-0.0	-0.0	+0.0	+0.0
m_t	-2.1	-1.8	-1.0	-0.1	+0.8	-1.0	+2.7	+2.3	+0.3	+2.5	+2.3	+1.7
	+1.0	+1.8	+1.3	-1.1	-0.1	+1.3	-2.3	-1.8	-0.3	-2.5	-2.9	-1.8
μ_{rf}	+1.7	-0.9	+1.1	+0.3	-1.1	+0.0	-0.6	+0.8	+0.1	-0.1	-1.0	-0.2
	-1.9	+0.9	-1.2	-0.2	+1.1	-0.0	+1.0	-0.9	-0.1	+0.1	+1.4	+0.2
h_{damp}	-2.0	-0.2	+2.3	-1.4	+0.6	-0.3	-1.9	+1.4	+0.3	+2.6	-0.8	-0.1
	-1.4	-0.9	-1.0	-0.9	+1.5	+0.4	-2.5	+1.5	+0.3	-0.1	-0.3	-0.0
PS ISR	+2.1	-0.4	-1.7	-1.9	+0.5	-0.3	+0.3	+2.3	+0.1	-0.9	-0.9	-0.1
	-1.1	+0.5	+0.1	-1.9	+0.8	-0.4	+0.1	+1.3	+0.2	+0.9	-1.2	+0.1
PS FSR	-1.9	-0.2	+1.1	-0.1	+0.9	+0.8	-1.8	-0.3	+0.2	-1.0	-2.1	-0.8
	+0.9	+0.4	-0.5	-1.8	+0.0	-0.7	+0.9	+0.8	+0.2	+1.6	+1.2	+0.4
UE tune	-1.6	-0.5	+1.3	-1.3	+0.8	+0.4	-2.5	-0.3	+0.4	+1.1	-0.0	-0.2
	-0.7	-0.9	-0.1	-0.6	+0.9	+0.3	-0.4	+1.1	+0.3	-0.1	-0.1	-0.5
CR	-1.4	-0.4	+0.5	-0.5	+0.4	-0.0	-0.1	+1.0	+0.3	+0.7	+0.5	+0.0
	-1.9	+0.1	+1.3	-2.0	+1.2	-0.0	+0.3	+0.6	-0.3	-1.2	+0.8	+0.4
	-0.7	+0.1	-0.0	-0.3	+0.5	-0.5	-0.0	+0.1	+0.2	-0.5	-0.1	+0.5
$f(b \rightarrow B)$	-0.0	-0.3	+2.5	+0.0	-0.9	+0.4	+0.1	-0.6	+0.0	+1.6	+0.5	-0.7
	+0.1	+0.1	-1.3	-0.0	+0.4	-0.2	+0.0	+0.3	-0.0	-0.6	-0.1	+0.4
	+0.0	-0.1	+0.5	+0.0	-0.2	+0.1	+0.0	-0.1	+0.0	+0.3	+0.1	-0.1
	+0.6	+0.2	+2.2	-0.2	-0.7	+0.1	-0.0	-0.5	-0.2	+1.5	+0.4	-0.7
BR($B \rightarrow \mu$)	-0.0	-0.1	-0.2	+0.1	+0.1	+0.1	+0.1	+0.0	+0.0	-0.0	-0.2	-0.0
	+0.1	+0.2	+0.3	-0.2	-0.1	-0.1	+0.0	-0.1	-0.1	+0.2	+0.2	+0.0

Table 95: The measured $[M(t\bar{t}), \Delta\phi(t, \bar{t})]$ cross sections, along with their relative statistical and systematic uncertainties.

$M(t\bar{t})$ [GeV]	$\Delta\phi(t, \bar{t})$ [rad]	$\frac{1}{\sigma(t\bar{t})} \frac{d\sigma}{d\Delta\phi(t, \bar{t})}$ [rad $^{-1}$]	stat. [%]	syst. [%]	bin
300–400	0.00–2.20	3.535×10^{-2}	3.0	+6.3 -16.2	1
300–400	2.20–2.95	1.249×10^{-1}	1.9	+9.7 -5.6	2
300–400	2.95–3.14	4.024×10^{-1}	3.2	+20.3 -15.5	3
400–500	0.00–2.20	2.617×10^{-2}	3.0	+13.6 -10.7	4
400–500	2.20–2.95	1.957×10^{-1}	1.2	+5.7 -6.3	5
400–500	2.95–3.14	8.082×10^{-1}	1.3	+6.7 -5.6	6
500–650	0.00–2.20	1.439×10^{-2}	4.0	+4.9 -14.4	7
500–650	2.20–2.95	1.250×10^{-1}	1.8	+6.9 -6.9	8
500–650	2.95–3.14	6.251×10^{-1}	1.4	+5.9 -6.2	9
650–1500	0.00–2.20	7.308×10^{-3}	4.8	+12.2 -7.6	10
650–1500	2.20–2.95	7.475×10^{-2}	2.1	+6.9 -6.1	11
650–1500	2.95–3.14	3.923×10^{-1}	1.5	+5.4 -6.2	12

Table 96: The correlation matrix of statistical uncertainties for the measured $[M(t\bar{t}), \Delta\phi(t, \bar{t})]$ cross sections. The values are expressed as percentages. For bin indices see Table 95.

Table 97: Sources and values of the relative systematic uncertainties in percent of the measured $[M(t\bar{t}), \Delta\phi(t, \bar{t})]$ cross sections. For bin indices see Table 95.

source / bin	1	2	3	4	5	6	7	8	9	10	11	12
JER	-1.8	-0.1	+2.7	+0.7	-0.4	+0.3	-2.1	+0.1	+0.1	-0.1	+0.2	-0.6
	-0.8	-0.1	-1.1	+0.5	+0.8	+0.1	-2.4	+0.7	-0.6	+1.9	+0.4	+0.3
JESAbsoluteMPFBias	-3.0	+1.1	+1.1	+0.9	+0.7	-0.1	-2.9	+0.0	-0.5	+1.7	+0.0	+0.3
	-3.6	+0.1	+2.1	+2.0	+0.2	+0.1	+0.1	+0.2	-0.6	-0.3	+0.2	-0.1
JESAbsoluteScale	-1.0	+0.3	+0.9	-0.0	+0.3	-0.0	-2.1	+0.7	-0.8	-0.0	+0.6	+0.0
	-1.8	+0.4	+0.5	-0.9	+0.7	-0.0	-0.4	+0.8	-0.4	+0.4	+0.2	-0.2
JESAbsoluteStat	-4.8	+0.7	+6.8	-4.1	-1.8	+2.6	-1.9	-2.2	+1.8	-1.7	-2.8	+1.7
	+2.3	+0.9	-5.4	+3.6	+1.6	-2.5	+0.9	+2.8	-2.6	+2.3	+3.2	-1.3
JESFlavourQCD	-0.9	+1.6	+1.4	-1.8	-0.1	-0.7	-2.4	+0.4	-0.2	+0.1	+0.8	+0.7
	-2.8	+0.0	+0.9	+1.4	+0.9	+0.4	+0.8	-0.1	-0.6	-0.2	+0.2	-1.0
JESFragmentation	-0.7	+0.8	+0.2	-2.5	+0.4	+0.0	+0.1	+0.4	-0.2	+0.5	+0.4	-0.0
	-1.7	+0.9	+1.7	+0.3	+0.2	-0.5	-2.0	+1.0	-0.5	+1.2	+0.1	-0.4
JESPileUpDataMC	-0.7	+0.6	+0.1	-0.4	+0.3	-0.4	-1.2	+1.0	-0.6	-0.6	+1.0	+0.2
	-1.3	+1.4	+0.0	+0.2	+0.2	+0.1	-0.8	+0.4	-0.7	-0.7	+0.3	-0.3
JESPileUpPtBB	-0.9	+0.5	+0.0	+0.1	+0.1	-0.1	-1.6	+0.4	-0.1	+1.1	+0.4	+0.0
	-1.6	+0.8	+0.5	+0.2	+0.3	+0.2	-0.5	-0.4	-0.2	-0.4	+0.3	-0.1
JESPileUpPtEC1	-0.7	+0.9	+0.2	-1.1	+0.0	+0.1	-0.3	+0.2	-0.1	-0.8	-0.1	+0.2
	-0.7	+0.7	-0.3	-0.3	-0.2	+0.2	+1.2	-0.0	-0.2	+1.4	+0.1	-0.2
JESPileUpPtEC2	+0.0	-0.0	+0.0	-0.0	+0.0	+0.0	+0.0	+0.0	+0.0	+0.0	+0.0	+0.0
	+0.0	-0.0	-0.0	-0.0	+0.0	+0.0	+0.0	+0.0	+0.0	+0.0	+0.0	+0.0
JESPileUpPtHF	+0.0	-0.0	+0.0	-0.0	+0.0	+0.0	+0.0	+0.0	+0.0	+0.0	+0.0	+0.0
	+0.0	-0.0	-0.0	-0.0	+0.0	+0.0	+0.0	+0.0	+0.0	+0.0	+0.0	+0.0
JESPileUpPtRef	-1.6	+0.4	+1.1	+0.4	+0.1	-0.5	-1.2	+0.5	-0.2	-0.4	+0.7	+0.3
	-1.8	+0.9	+1.3	+0.4	-0.0	-0.3	+0.1	+0.6	-0.4	+0.5	-0.0	-0.5
JESRelativeBal	+0.1	+1.7	-0.2	-1.5	-0.1	-0.0	-1.2	-0.2	-0.3	-0.4	+0.7	+0.3
	-2.6	-0.8	+1.1	+2.5	+0.4	+0.4	-1.1	-0.1	-0.6	+2.0	+0.9	-0.4
JESRelativeFSR	-0.1	+0.3	+0.4	-0.9	-0.2	+0.4	-0.8	+0.4	-0.4	+0.9	+0.3	-0.4
	-0.7	+0.7	+0.9	-1.8	+0.4	-0.5	-1.4	+0.9	-0.5	+1.1	+0.2	+0.1
JESRelativeJEREC1	-1.4	+0.5	+0.9	+0.4	+0.1	-0.4	-0.2	+0.3	-0.3	+0.9	-0.0	+0.2
	-0.8	+1.1	-0.6	-1.7	+0.3	+0.4	+0.3	+0.0	-0.2	+0.3	+0.3	-0.1
JESRelativeJEREC2	+0.0	-0.0	+0.0	-0.0	+0.0	+0.0	+0.0	+0.0	+0.0	+0.0	+0.0	+0.0
	+0.0	-0.0	-0.0	-0.0	+0.0	+0.0	+0.0	+0.0	+0.0	+0.0	+0.0	+0.0
JESRelativeJERHF	+0.0	-0.0	+0.0	-0.0	+0.0	+0.0	+0.0	+0.0	+0.0	+0.0	+0.0	+0.0
	+0.0	-0.0	-0.0	-0.0	+0.0	+0.0	+0.0	+0.0	+0.0	+0.0	+0.0	+0.0
JESRelativePtBB	-2.0	+1.1	+0.6	+1.0	+0.1	-0.1	-0.4	-0.2	-0.5	-0.5	+0.7	+0.0
	-0.8	-0.2	+0.2	+1.5	+0.4	-0.0	-2.0	+0.1	-0.2	+0.5	+0.5	-0.3
JESRelativePtEC1	-0.7	+0.8	+0.7	-0.7	+0.1	+0.3	-0.7	+0.1	-0.5	-0.7	-0.1	+0.1
	-0.4	-0.4	-0.4	+0.2	+0.1	+0.4	-0.3	+0.3	-0.0	+0.8	+0.1	-0.1
JESRelativePtEC2	+0.0	-0.0	+0.0	-0.0	+0.0	+0.0	+0.0	+0.0	+0.0	+0.0	+0.0	+0.0
	+0.0	-0.0	-0.0	-0.0	+0.0	+0.0	+0.0	+0.0	+0.0	+0.0	+0.0	+0.0
JESRelativePtHF	+0.0	+0.0	+0.0	+0.0	+0.0	+0.0	+0.0	+0.0	+0.0	+0.0	+0.0	+0.0
	+0.0	-0.0	+0.0	-0.0	+0.0	+0.0	+0.0	+0.0	+0.0	+0.0	+0.0	+0.0
JESRelativeStatEC	-1.1	+0.1	+1.0	-0.9	+0.0	+0.3	+0.5	+0.5	-0.4	-0.2	-0.0	-0.0
	-0.3	+0.0	+0.5	+0.1	+0.1	+0.1	-2.3	+0.2	-0.3	+1.8	+0.3	-0.0
JESRelativeStatFSR	-1.1	+0.9	+0.4	-0.2	+0.4	-0.4	-1.6	+0.2	-0.3	+1.3	+0.6	+0.0
	-1.5	+1.2	+0.7	+0.2	+0.1	-0.0	-1.1	-0.2	-0.3	-0.2	+0.5	-0.1
JESRelativeStatHF	+0.0	-0.0	+0.0	-0.0	+0.0	+0.0	+0.0	+0.0	+0.0	+0.0	+0.0	+0.0
	+0.0	-0.0	+0.0	-0.0	+0.0	+0.0	+0.0	+0.0	+0.0	+0.0	+0.0	+0.0
JESSinglePionECAL	-1.1	+0.1	+1.4	+0.3	-0.2	+0.5	-2.0	-0.0	-0.5	+0.8	+0.5	-0.3
	-1.1	+0.4	+1.1	-1.7	+0.3	+0.2	-1.0	+0.4	-0.3	+0.3	+0.5	+0.0

Table 98: Table 97 continued.

source / bin	1	2	3	4	5	6	7	8	9	10	11	12
JESSinglePionHCAL	-1.6	+1.0	+0.8	-0.2	+0.3	+0.1	-0.0	-0.5	-0.2	+0.5	+0.2	-0.2
	-1.3	+1.3	+0.9	-0.2	-0.3	-0.3	-1.7	-0.1	+0.2	-0.1	+0.7	+0.2
JESTimePtEta	-1.1	+0.4	+0.7	+0.3	+0.2	+0.1	-1.7	+0.1	-0.2	+1.3	+0.3	-0.2
	-1.8	+0.2	+1.8	+0.2	-0.2	+0.3	-1.7	-0.1	-0.3	+1.0	+0.6	+0.1
E_T^{miss}	-5.6	-2.7	+10.1	+0.3	-3.4	+3.3	+0.1	-3.8	+2.4	-0.3	-1.5	+0.5
	+1.6	+4.1	-6.2	-1.0	+2.3	-2.1	-1.3	+2.2	-1.7	-0.2	+1.4	-0.4
lepton ID/ISO	-0.1	-0.0	-0.4	-0.2	+0.4	+0.1	+0.2	-0.0	-0.1	+0.0	+0.0	-0.2
	+0.1	-0.0	+0.4	+0.2	-0.4	-0.1	-0.1	+0.0	+0.1	-0.0	-0.0	+0.2
pileup	-1.6	-0.7	+2.8	-0.7	-0.9	+1.0	-0.1	-1.0	+0.8	-0.1	-0.6	+0.3
	+1.5	+0.7	-2.8	+0.7	+0.9	-1.0	+0.0	+1.0	-0.8	+0.1	+0.6	-0.3
trigger	+0.0	+0.0	-0.1	-0.1	+0.1	+0.0	-0.0	-0.0	+0.0	-0.2	-0.1	-0.0
	-0.0	-0.0	+0.1	+0.1	-0.1	-0.0	+0.0	+0.0	-0.0	+0.2	+0.1	+0.0
trigger (η)	+0.0	+0.0	+0.0	-0.1	+0.0	+0.0	-0.1	-0.1	-0.0	+0.2	+0.1	-0.0
	-0.0	-0.0	-0.0	+0.1	-0.0	-0.0	+0.1	+0.1	+0.0	-0.2	-0.1	+0.0
non-tf background	-1.8	-1.4	-1.5	-0.5	+0.5	+0.3	+0.8	+0.5	+0.6	+0.7	+1.1	+1.1
	+0.9	+1.6	+0.9	+1.1	+0.1	-0.4	-1.4	-0.5	-0.7	-0.1	-1.2	-0.9
b-tagging	+0.1	-0.1	-0.3	+0.1	+0.1	-0.0	+0.1	+0.0	-0.0	+0.2	+0.1	+0.1
	-0.1	+0.1	+0.3	-0.1	-0.1	+0.0	-0.1	-0.0	+0.0	-0.2	-0.1	-0.1
b-tagging (light jets)	-0.7	-0.3	+0.0	-0.4	+0.1	+0.2	-0.1	+0.1	+0.3	-0.4	+0.2	+0.2
	+0.7	+0.3	-0.0	+0.4	-0.1	-0.2	+0.1	-0.1	-0.3	+0.4	-0.2	-0.2
luminosity	+0.0	+0.0	+0.0	+0.0	+0.0	+0.0	+0.0	+0.0	+0.0	+0.0	+0.0	+0.0
	+0.0	+0.0	+0.0	+0.0	+0.0	+0.0	+0.0	+0.0	+0.0	+0.0	+0.0	+0.0
BR($t\bar{t} \rightarrow \ell\ell$)	+0.0	+0.0	+0.0	+0.0	+0.0	+0.0	+0.0	+0.0	+0.0	+0.0	+0.0	+0.0
	+0.0	+0.0	+0.0	+0.0	+0.0	+0.0	+0.0	+0.0	+0.0	+0.0	+0.0	+0.0
PDF eigenvector 1	+0.0	-0.0	-0.0	+0.0	-0.0	-0.0	+0.0	-0.0	-0.0	+0.1	+0.0	+0.0
	+0.0	+0.0	-0.0	+0.0	+0.0	-0.0	+0.0	-0.0	-0.0	+0.0	+0.0	-0.0
PDF eigenvector 2	-0.1	-0.1	-0.1	+0.1	-0.1	-0.0	+0.1	-0.0	-0.0	+0.3	+0.2	+0.1
	-0.0	+0.0	+0.2	-0.1	-0.0	+0.0	-0.0	+0.1	+0.0	-0.2	-0.1	-0.1
PDF eigenvector 3	+0.1	+0.0	-0.0	+0.1	+0.0	+0.0	+0.1	-0.0	-0.0	-0.0	-0.0	-0.0
	-0.0	-0.0	-0.0	-0.0	+0.0	-0.0	-0.0	+0.0	+0.0	+0.0	+0.0	+0.0
PDF eigenvector 4	-0.0	-0.0	-0.1	+0.0	+0.0	-0.0	+0.0	-0.1	-0.0	+0.2	+0.1	+0.1
	+0.0	+0.0	+0.1	+0.0	-0.0	+0.0	+0.0	+0.0	+0.0	-0.1	-0.1	-0.1
PDF eigenvector 5	-0.1	+0.0	+0.1	-0.2	-0.0	-0.0	-0.1	+0.1	+0.1	-0.1	-0.1	-0.0
	+0.1	+0.0	-0.1	+0.1	+0.0	+0.0	+0.1	-0.1	-0.1	+0.0	-0.0	-0.0
PDF eigenvector 6	-0.0	-0.0	-0.2	+0.0	+0.1	-0.0	+0.0	-0.1	-0.0	+0.2	+0.0	+0.1
	+0.0	+0.0	+0.1	-0.0	-0.1	-0.0	-0.0	+0.1	+0.0	-0.1	-0.0	-0.1
PDF eigenvector 7	-0.1	+0.0	+0.2	-0.3	-0.0	-0.0	-0.2	+0.2	+0.1	-0.2	-0.1	-0.1
	+0.1	-0.0	-0.1	+0.1	+0.0	+0.0	+0.1	-0.1	-0.1	+0.1	+0.0	+0.1
PDF eigenvector 8	-0.0	+0.0	-0.1	-0.1	+0.1	-0.0	+0.0	-0.0	-0.0	+0.0	+0.0	+0.0
	+0.0	-0.0	+0.1	+0.0	-0.1	+0.0	+0.0	+0.0	+0.0	-0.0	-0.0	+0.0
PDF eigenvector 9	+0.1	+0.0	+0.1	+0.0	-0.1	-0.0	-0.0	+0.1	-0.0	-0.1	+0.0	-0.1
	-0.1	-0.0	-0.1	-0.0	+0.1	-0.0	+0.0	-0.1	+0.0	+0.1	-0.0	+0.1
PDF eigenvector 10	+0.1	+0.0	-0.1	+0.1	+0.0	+0.0	+0.0	-0.1	-0.1	+0.1	+0.0	+0.1
	-0.1	+0.0	+0.1	-0.1	-0.0	-0.0	-0.1	+0.1	+0.1	-0.1	-0.0	-0.1
PDF eigenvector 11	+0.0	-0.0	-0.0	+0.0	+0.0	+0.0	+0.0	-0.0	-0.0	+0.0	+0.0	+0.0
	-0.0	-0.0	+0.1	-0.0	-0.0	-0.0	-0.0	+0.1	+0.0	-0.0	-0.0	-0.0
PDF eigenvector 12	-0.0	+0.0	+0.0	-0.1	+0.0	-0.0	-0.0	+0.1	+0.0	-0.0	-0.0	-0.0
	+0.1	-0.0	-0.0	+0.0	-0.0	+0.0	+0.0	-0.1	-0.0	+0.0	+0.0	+0.0
PDF eigenvector 13	+0.0	+0.1	-0.0	-0.0	+0.1	+0.0	-0.0	-0.0	-0.0	-0.1	-0.1	-0.0
	-0.0	-0.1	+0.0	+0.0	-0.1	-0.0	+0.0	+0.0	+0.0	+0.1	+0.1	+0.0
PDF eigenvector 14	-0.0	+0.0	+0.0	-0.0	+0.0	-0.0	-0.0	+0.0	+0.0	-0.0	-0.0	-0.0
	+0.0	-0.0	-0.0	+0.0	-0.0	+0.0	+0.0	-0.0	-0.0	+0.0	+0.0	+0.0

Table 99: Table 97 continued.

source / bin	1	2	3	4	5	6	7	8	9	10	11	12
PDF eigenvector 15	-0.0	+0.0	+0.0	-0.0	+0.0	-0.0	-0.0	+0.0	+0.0	-0.1	-0.0	-0.0
	+0.0	-0.0	-0.0	+0.0	-0.0	+0.0	+0.0	-0.0	-0.0	+0.0	+0.0	+0.0
PDF eigenvector 16	+0.0	+0.0	-0.0	+0.0	+0.0	-0.0	+0.0	-0.0	-0.0	+0.0	+0.0	+0.0
	-0.0	+0.0	+0.0	-0.0	-0.0	+0.0	-0.0	+0.0	+0.0	-0.0	-0.0	-0.0
PDF eigenvector 17	-0.0	-0.0	+0.0	-0.0	-0.0	+0.0	-0.0	+0.0	+0.0	-0.0	+0.0	-0.0
	+0.0	+0.0	-0.1	+0.0	+0.1	-0.0	+0.0	-0.1	-0.0	+0.1	-0.0	+0.0
PDF eigenvector 18	+0.0	-0.1	-0.0	+0.1	-0.1	+0.0	+0.0	-0.0	-0.0	+0.1	+0.1	+0.1
	-0.0	+0.1	+0.0	-0.1	+0.1	-0.0	-0.0	+0.0	+0.0	-0.1	-0.1	-0.1
PDF eigenvector 19	+0.1	-0.0	-0.0	+0.1	-0.0	+0.0	+0.0	-0.1	-0.0	+0.0	+0.0	+0.0
	-0.1	+0.0	+0.1	-0.1	+0.0	-0.0	-0.0	+0.1	+0.1	-0.1	-0.1	-0.1
PDF eigenvector 20	+0.0	+0.0	+0.1	-0.1	-0.0	+0.0	+0.0	-0.0	+0.0	-0.4	-0.0	+0.1
	-0.0	+0.0	-0.0	-0.0	+0.0	+0.0	-0.0	+0.0	+0.0	-0.0	-0.0	-0.0
PDF eigenvector 21	-0.0	-0.0	-0.0	-0.0	-0.0	-0.0	+0.0	-0.0	+0.0	+0.1	+0.1	+0.1
	+0.1	+0.0	+0.0	+0.0	+0.0	-0.0	+0.0	+0.0	-0.0	-0.1	-0.1	-0.1
PDF eigenvector 22	-0.1	-0.1	-0.1	-0.0	-0.1	-0.0	-0.1	-0.0	+0.0	+0.2	+0.2	+0.2
	+0.1	+0.1	+0.0	+0.0	+0.1	+0.0	+0.0	-0.0	-0.0	-0.2	-0.2	-0.1
PDF eigenvector 23	-0.0	+0.0	+0.1	-0.1	+0.0	+0.0	+0.0	+0.1	+0.0	-0.3	-0.2	-0.2
	-0.0	-0.0	+0.0	-0.0	-0.0	+0.0	-0.1	-0.0	+0.0	-0.0	-0.0	+0.0
PDF eigenvector 24	-0.0	+0.0	+0.1	-0.1	-0.0	+0.0	-0.1	+0.0	+0.0	-0.2	-0.1	-0.0
	-0.1	-0.1	+0.1	-0.0	-0.1	+0.0	+0.1	+0.1	+0.0	+0.1	+0.1	-0.0
PDF eigenvector 25	-0.1	-0.0	+0.1	-0.0	-0.1	+0.0	+0.0	+0.1	+0.0	-0.0	+0.0	-0.0
	-0.1	+0.0	+0.2	-0.1	-0.0	+0.0	-0.1	+0.1	+0.1	-0.2	-0.1	-0.0
PDF eigenvector 26	-0.0	+0.0	+0.0	-0.0	+0.0	+0.0	-0.0	+0.0	+0.0	-0.1	-0.0	-0.0
	-0.0	-0.0	+0.0	-0.0	-0.0	+0.0	-0.0	-0.0	+0.0	-0.0	-0.0	+0.0
PDF eigenvector 27	+0.1	-0.0	+0.2	+0.1	-0.2	-0.0	+0.0	+0.0	+0.0	+0.0	+0.0	-0.0
	-0.0	-0.0	-0.1	-0.0	+0.1	-0.0	+0.0	-0.0	-0.0	+0.1	+0.0	+0.1
PDF eigenvector 28	+0.0	-0.0	+0.1	-0.0	-0.0	+0.0	+0.0	+0.0	+0.0	-0.1	-0.0	-0.0
	+0.0	+0.0	-0.1	-0.0	+0.1	-0.0	-0.0	-0.0	-0.0	+0.1	+0.0	+0.0
α_s	+0.0	-0.1	+0.2	+0.1	-0.2	-0.0	+0.1	+0.0	+0.0	+0.1	-0.0	-0.1
	-0.0	+0.1	-0.2	-0.1	+0.2	+0.0	-0.1	-0.0	-0.0	-0.1	+0.0	+0.1
m_t	-0.5	-1.7	-2.6	+0.4	+0.1	-0.5	-0.7	+0.8	+1.2	+0.8	+1.4	+2.1
	+0.2	+1.6	+2.3	+1.0	-0.0	+0.5	-0.5	-0.6	-1.1	-0.7	-1.2	-2.6
μ_{rf}	+0.5	-0.4	+1.4	+2.1	-1.4	-0.3	+2.8	-0.2	-0.3	+2.9	+0.4	-1.1
	-0.8	+0.3	-1.3	-2.7	+1.5	+0.5	-3.9	+0.3	+0.6	-3.9	-0.7	+1.4
h_{damp}	-1.3	+0.5	+2.2	-0.2	-0.6	+0.1	-1.2	-0.3	+0.9	-1.5	-1.1	+0.2
	-0.1	-1.3	-3.0	+6.2	-0.1	-0.7	-0.8	+0.9	-0.4	+3.7	+1.2	-0.3
PS ISR	+0.3	+0.1	+0.1	-1.3	-0.5	+0.2	-2.0	+0.8	+1.1	-1.8	-0.2	-0.3
	+1.9	+0.2	-2.9	+2.5	-0.4	-0.7	-0.2	+1.1	-0.1	+2.6	-0.4	-0.3
PS FSR	+1.3	-0.1	-2.5	+3.0	+1.0	-0.6	+0.1	+1.2	-1.2	+2.0	+0.5	-2.1
	-1.0	+0.9	-0.2	-1.0	+0.2	-0.3	-1.5	+0.1	+0.5	+0.9	-1.1	+1.5
UE tune	-0.6	+0.1	+0.2	+0.7	+0.4	-0.1	-0.1	+0.0	-0.3	+0.8	-0.6	-0.1
	-1.8	-0.1	+0.5	+1.8	-0.0	+0.4	-2.1	-0.0	+0.6	+1.0	-0.3	-0.8
CR	+0.1	-0.3	-0.7	+0.1	-0.3	+0.0	-0.7	+0.6	+0.4	+1.1	-0.5	+0.4
	-0.5	+0.0	+0.9	-0.8	-0.9	+1.0	-2.5	-1.1	+1.3	-0.5	-0.2	+0.4
	+0.7	+1.0	-2.3	-1.6	-0.1	+0.2	-0.6	+0.6	+0.3	+2.3	-0.7	+0.4
$f(b \rightarrow B)$	+0.7	+0.4	+1.2	+0.2	-0.3	-0.3	+0.4	+0.1	-0.6	-0.1	-0.3	-0.5
	-0.3	-0.2	-0.6	-0.1	+0.1	+0.1	-0.0	-0.0	+0.3	+0.1	+0.2	+0.3
	+0.1	+0.1	+0.2	+0.1	-0.1	-0.1	+0.1	+0.0	-0.1	-0.0	-0.0	-0.1
	+1.0	+0.8	+1.3	-0.4	-0.2	-0.4	-0.2	-0.1	-0.5	-0.7	-0.5	-0.5
BR($B \rightarrow \mu$)	-0.1	-0.1	-0.1	+0.0	+0.0	+0.1	-0.0	+0.1	+0.0	-0.1	-0.0	-0.1
	+0.3	+0.2	-0.0	-0.1	-0.1	-0.1	+0.0	-0.1	-0.1	+0.1	+0.0	+0.1

Table 100: The measured $[M(t\bar{t}), p_T(t\bar{t})]$ cross sections, along with their relative statistical and systematic uncertainties.

$M(\text{t}\bar{t})$ [GeV]	$p_T(\text{t}\bar{t})$ [GeV]	$\frac{1}{\sigma(\text{t}\bar{t})} \frac{d\sigma}{dp_T(\text{t}\bar{t})}$ [GeV $^{-1}$]	stat. [%]	syst. [%]	bin
300–400	0–30	3.671×10^{-3}	1.8	$+12.4$ -9.3	1
300–400	30–75	1.660×10^{-3}	2.1	$+10.6$ -14.1	2
300–400	75–150	5.749×10^{-4}	3.3	$+9.7$ -8.4	3
300–400	150–500	5.519×10^{-5}	5.1	$+8.1$ -9.7	4
400–500	0–30	4.915×10^{-3}	1.1	$+9.8$ -8.0	5
400–500	30–75	2.609×10^{-3}	1.2	$+7.8$ -7.8	6
400–500	75–150	8.995×10^{-4}	1.9	$+7.1$ -8.0	7
400–500	150–500	8.845×10^{-5}	3.8	$+6.4$ -10.8	8
500–650	0–30	3.107×10^{-3}	1.6	$+12.1$ -11.3	9
500–650	30–75	1.733×10^{-3}	1.7	$+10.1$ -11.2	10
500–650	75–150	6.394×10^{-4}	2.5	$+6.8$ -8.0	11
500–650	150–500	7.086×10^{-5}	3.6	$+5.8$ -5.2	12
650–1500	0–30	1.705×10^{-3}	2.6	$+13.7$ -12.3	13
650–1500	30–75	9.328×10^{-4}	3.3	$+13.2$ -15.5	14
650–1500	75–150	4.219×10^{-4}	2.9	$+7.0$ -6.2	15
650–1500	150–500	5.924×10^{-5}	2.7	$+6.1$ -5.1	16

Table 101: The correlation matrix of statistical uncertainties for the measured $[M(t\bar{t}), p_T(t\bar{t})]$ cross sections. The values are expressed as percentages. For bin indices see Table 100.

Table 102: Sources and values of the relative systematic uncertainties in percent of the measured $[M(\text{t}\bar{\text{t}}), p_{\text{T}}(\text{t}\bar{\text{t}})]$ cross sections. For bin indices see Table 100.

source / bin	1	2	3	4	5	6	7	8	9	10	11	12	13	14	15	16
JER	+0.4 -0.3	-0.8 -0.8	-0.1 +0.2	+0.5 +0.1	+0.7 -0.1	-0.0 +0.7	-0.4 +0.1	-1.8 -0.6	+0.9 -0.9	-0.2 +0.7	-0.8 -0.0	+0.4 +0.1	+0.2 -0.3	-1.2 +0.3	-0.1 +1.5	+0.1 +0.3
JESAbsoluteMPFBias	-0.1 +0.3	-0.1 -0.5	-0.2 -0.5	-0.1 -3.0	+0.4 +0.2	+0.5 +0.2	-0.5 -0.2	-0.9 +1.6	-0.5 -0.0	+0.0 +0.2	-0.5 -0.4	+0.0 -0.1	+0.1 -0.2	+0.4 -0.1	+0.5 +0.7	-0.4 -0.0
JESAbsoluteScale	+0.7 +0.1	-0.3 -0.1	-0.2 -0.8	-0.4 -1.9	+0.1 +0.2	+0.1 +0.3	-0.0 +0.1	-0.4 +0.5	-0.5 -0.0	+0.2 -0.1	-0.8 -0.1	-0.4 +0.3	-0.1 -0.6	+0.4 +0.2	+0.4 +0.2	-0.1 +0.0
JESAbsoluteStat	+4.4 -3.5	-3.4 +2.8	-3.0 +3.8	-2.9 +1.1	+3.7 -3.6	-1.9 +2.1	-4.2 +3.3	-2.6 +1.5	+4.0 -5.0	-2.2 +2.2	-3.5 +3.8	-1.9 +2.6	+4.8 -4.1	-2.6 +2.2	-2.7 +3.3	-2.3 +3.0
JESFlavourQCD	+1.2 -0.0	-0.3 -1.0	+0.0 -0.3	+2.6 -0.0	-0.4 +0.4	-0.2 +0.5	-1.3 +0.7	-2.6 +0.1	-0.3 -0.1	+0.9 +0.1	-0.3 +0.3	-1.2 -0.1	+0.2 -0.1	+1.2 -0.8	+0.6 -1.1	+0.5 -0.2
JESFragmentation	-0.1 +0.3	-0.2 -0.6	+0.4 +0.5	+1.5 +0.4	+0.1 +0.3	+0.5 -0.1	-1.2 -0.3	-2.4 -0.8	-0.2 +0.0	+0.7 +0.1	+0.2 -0.2	+0.6 +0.5	-0.3 -0.6	+0.1 -0.2	+0.6 +0.5	+0.0 -0.1
JESPileUpDataMC	+0.5 +0.1	-0.5 -0.0	-0.9 +0.2	-0.4 -0.6	-0.1 +0.4	+0.2 +0.5	-0.1 -0.2	-0.7 -0.4	-0.1 -0.5	+0.1 -0.1	-0.3 -0.2	-0.2 +0.4	-0.1 -0.4	+0.6 -0.2	+0.7 +0.3	+0.4 +0.3
JESPileUpPtBB	-0.3 +0.4	-0.6 +0.3	+0.0 -0.3	+0.3 -0.0	+0.1 +0.1	+0.6 +0.3	-0.6 -0.0	-0.5 -0.7	-0.3 -0.2	+0.5 -0.1	-0.1 -0.9	+0.5 +0.1	+0.3 -0.3	-0.2 -0.1	+0.5 +0.2	-0.0 -0.2
JESPileUpPtEC1	+0.9 +0.3	-0.2 -0.1	-0.6 +0.1	+1.0 +0.5	-0.1 +0.0	+0.2 -0.2	-0.7 -0.1	-1.9 -0.5	-0.7 -0.3	+0.5 -0.1	+0.5 -0.1	+1.0 +0.8	+0.1 +0.1	+0.1 -0.1	+0.2 +0.2	-0.2 +0.2
JESPileUpPtEC2	-0.0 -0.0	+0.0 +0.0	-0.0 -0.0	+0.0 +0.0	-0.0 +0.0	+0.0 +0.0	-0.0 -0.0	+0.0 +0.0	-0.0 -0.0	+0.0 +0.0	-0.0 -0.0	+0.0 +0.0	-0.0 -0.0	+0.0 +0.0	-0.0 +0.0	+0.0 +0.0
JESPileUpPtHF	-0.0 -0.0	+0.0 +0.0	-0.0 -0.0	+0.0 +0.0	-0.0 +0.0	+0.0 +0.0	-0.0 -0.0	+0.0 +0.0	-0.0 -0.0	+0.0 +0.0	-0.0 -0.0	+0.0 +0.0	-0.0 -0.0	+0.0 +0.0	-0.0 +0.0	+0.0 +0.0
JESPileUpPtRef	+0.2 +0.7	-0.1 +0.2	-0.5 -0.5	+0.6 -1.6	-0.0 +0.3	+0.1 +0.3	-0.5 -0.3	-1.4 -0.3	-0.3 -0.8	+0.3 +0.2	+0.2 +0.3	+0.9 +0.7	+0.2 -0.4	+0.4 -0.2	+0.4 -0.5	+0.1 -0.5
JESRelativeBal	+0.8 -0.5	+0.1 -1.6	+1.2 -0.6	+1.1 -1.4	-0.4 +0.6	+0.3 +0.9	-0.7 +0.8	-1.7 +0.7	-0.7 -0.4	+0.3 -0.0	-0.7 -0.4	-0.6 -0.2	+0.4 -0.0	+0.1 -0.5	+0.7 +0.6	+0.3 +0.6
JESRelativeFSR	+0.2 +0.5	-0.7 -0.4	+0.4 +0.1	+1.4 +2.3	+0.1 -0.0	+0.3 +0.2	-0.6 -0.5	-1.5 -2.7	-0.3 -0.2	+0.6 +0.2	+0.1 -0.5	+1.0 +0.9	+0.0 -0.4	-0.5 +0.5	+0.2 +0.8	+0.1 +0.0
JESRelativeJEREC1	+0.0 -0.1	-0.2 +0.0	-0.3 -0.1	-0.1 +0.3	+0.3 +0.2	+0.3 +0.3	-0.6 -0.7	-0.4 -0.5	-0.2 -0.4	+0.1 +0.4	+0.2 +0.1	-0.1 -0.0	-0.1 -0.0	+0.3 -0.1	+0.2 +0.3	+0.1 -0.1
JESRelativeJEREC2	-0.0 -0.0	+0.0 +0.0	-0.0 -0.0	+0.0 +0.0	-0.0 +0.0	+0.0 +0.0	-0.0 -0.0	+0.0 +0.0	-0.0 -0.0	+0.0 +0.0	-0.0 -0.0	+0.0 +0.0	-0.0 -0.0	+0.0 +0.0	-0.0 +0.0	+0.0 +0.0
JESRelativeJERHF	-0.0 -0.0	+0.0 +0.0	-0.0 +0.0	+0.0 +0.0												
JESRelativePtBB	+0.0 -0.1	-0.2 +0.2	-0.7 +0.1	+0.5 -1.2	+0.3 +0.2	+0.2 -0.4	-0.3 -0.4	-0.4 +0.5	+0.2 -0.2	-0.3 -0.1	-0.4 -0.6	+0.1 +0.1	+0.2 -0.3	-0.3 -0.2	+1.0 +0.6	-0.3 +0.3
JESRelativePtEC1	+0.5 -0.3	-0.2 -0.5	+0.1 -0.6	+1.2 +0.3	+0.2 +0.1	+0.2 +0.6	-0.7 -0.5	-0.8 -0.7	-0.6 -0.1	+0.2 +0.4	+0.2 +0.7	+0.3 +0.2	-0.5 -0.1	+0.4 -0.0	+0.1 +0.3	-0.6 +0.1
JESRelativePtEC2	-0.0 -0.0	+0.0 +0.0	-0.0 -0.0	+0.0 -0.0	-0.0 +0.0	+0.0 +0.0	-0.0 -0.0	+0.0 +0.0	-0.0 -0.0	+0.0 +0.0	-0.0 -0.0	+0.0 +0.0	-0.0 -0.0	+0.0 +0.0	-0.0 +0.0	+0.0 +0.0
JESRelativePtHF	+0.0 -0.0	+0.0 +0.0	-0.0 -0.0	+0.0 +0.0	+0.0 +0.0	+0.0 +0.0										
JESRelativeStatEC	+0.9 +0.7	+0.6 -0.4	-1.5 -0.6	+1.3 -0.4	-0.4 +0.0	+0.2 +0.1	-0.5 -0.1	-1.0 +0.4	-0.4 -0.6	+0.1 +0.5	+0.4 -0.1	+0.6 -0.8	-0.2 -0.3	+0.2 +0.4	+0.1 +0.1	-0.2 +0.6
JESRelativeStatFSR	+0.5 +0.0	-0.6 -0.1	-0.6 -0.0	+0.6 +0.1	-0.0 +0.3	+0.6 +0.6	-0.1 -1.2	-0.3 +0.3	-0.3 -0.5	+0.0 +0.4	-0.1 +0.1	-0.6 -0.9	+0.0 -0.1	+0.5 -0.5	+0.2 +0.3	+0.4 +0.4
JESRelativeStatHF	-0.0 -0.0	+0.0 +0.0	-0.0 +0.0	+0.0 +0.0												
JESSinglePionECAL	-0.1 +0.4	-0.3 -0.6	+1.1 +0.1	+0.0 +0.5	+0.4 +0.1	+0.4 +0.1	-0.3 -0.6	-0.9 -1.5	-0.4 +0.1	+0.0 +0.5	-0.7 -0.6	-0.1 +0.9	-0.4 +0.2	+0.0 +0.2	+0.3 +0.2	+0.0 -0.1

Table 103: Table 102 continued.

source / bin	1	2	3	4	5	6	7	8	9	10	11	12	13	14	15	16
JESSinglePionHCAL	+0.5	-0.4	-1.2	-1.0	+0.3	+0.2	-0.1	+0.7	-0.3	+0.4	-0.2	-0.9	-0.3	-0.3	+0.5	+0.1
	+0.5	+0.4	-1.0	+0.2	-0.0	+0.1	-0.7	-0.4	-0.1	+0.1	-0.5	-0.6	+0.6	-0.4	+0.7	+0.5
JESTimePtEta	+0.2	+0.4	-0.1	-0.4	+0.2	+0.4	-0.8	-0.4	-0.5	+0.2	-0.2	-0.7	+0.1	-0.3	+0.2	+0.5
	-0.1	-0.1	-0.6	-0.2	+0.4	+0.6	-0.5	-0.7	-0.3	-0.1	-0.9	+0.8	-0.0	+0.2	+0.9	+0.2
E_T^{miss}	+6.5	-7.8	-3.1	-0.8	+5.2	-4.8	-1.4	-0.2	+6.7	-7.2	-1.9	-0.5	+7.5	-9.9	+0.2	-0.6
	-4.0	+5.6	+1.0	+0.4	-3.6	+4.2	+0.3	+0.1	-5.0	+5.7	-0.4	-0.3	-4.8	+6.7	-0.2	+0.5
lepton ID/ISO	-0.2	-0.3	-0.1	+0.0	+0.2	+0.3	+0.1	+0.0	-0.1	-0.0	-0.0	-0.0	-0.1	-0.1	-0.1	-0.2
	+0.1	+0.4	+0.0	-0.0	-0.2	-0.2	-0.2	+0.0	+0.1	+0.1	-0.0	+0.1	+0.0	+0.3	+0.0	+0.2
pileup	+1.7	-2.0	-1.1	-0.1	+1.6	-1.4	-1.1	-0.1	+2.0	-1.9	-0.8	-0.0	+2.1	-2.2	-0.3	-0.5
	-1.9	+2.1	+1.0	+0.2	-1.7	+1.5	+1.0	+0.2	-2.1	+2.0	+0.7	-0.0	-2.1	+2.2	+0.3	+0.6
trigger	-0.0	-0.0	-0.0	+0.1	+0.0	+0.1	+0.0	+0.0	-0.0	-0.0	-0.0	+0.0	-0.0	-0.0	-0.0	-0.0
	+0.0	+0.0	+0.0	-0.1	-0.0	-0.1	-0.0	-0.0	+0.0	+0.0	+0.0	-0.0	+0.0	+0.0	+0.0	+0.0
trigger (η)	+0.0	+0.0	+0.0	+0.1	-0.0	+0.0	-0.0	-0.0	-0.1	-0.0	-0.1	-0.1	+0.0	+0.1	+0.0	+0.0
	-0.1	+0.0	-0.1	-0.1	-0.0	+0.0	-0.0	+0.0	+0.0	+0.1	+0.0	+0.1	-0.1	-0.0	-0.1	+0.0
non-tt background	-1.3	-2.1	-1.0	+0.3	+0.4	+0.0	+0.4	+0.1	+0.5	+0.2	+0.7	+0.5	+0.8	+0.9	+1.3	+0.9
	+0.9	+2.4	+0.7	-0.3	-0.4	+0.3	-0.5	+0.0	-0.6	-0.0	-0.8	-0.4	-0.9	-0.6	-1.4	-0.8
b-tagging	-0.2	-0.2	+0.2	-0.2	-0.0	-0.0	+0.2	+0.1	-0.0	-0.1	+0.1	+0.1	+0.1	+0.0	+0.2	+0.2
	+0.1	+0.2	-0.3	+0.2	+0.0	+0.1	-0.2	-0.1	-0.0	+0.1	-0.1	-0.1	-0.1	+0.0	-0.2	-0.1
b-tagging (light jets)	-0.1	-0.5	-0.7	+0.1	+0.2	+0.1	-0.2	-0.1	+0.2	+0.1	-0.0	-0.0	+0.2	+0.2	+0.1	+0.0
	+0.0	+0.6	+0.6	-0.1	-0.2	-0.0	+0.2	+0.1	-0.3	-0.1	-0.0	+0.0	-0.2	-0.2	-0.1	-0.0
luminosity	+0.0	+0.0	+0.0	+0.0	+0.0	+0.0	+0.0	+0.0	+0.0	+0.0	+0.0	+0.0	+0.0	+0.0	+0.0	+0.0
	+0.0	+0.0	+0.0	+0.0	+0.0	+0.0	+0.0	+0.0	+0.0	+0.0	+0.0	+0.0	+0.0	+0.0	+0.0	+0.0
BR($t\bar{t} \rightarrow \ell\ell$)	+0.0	+0.0	+0.0	+0.0	+0.0	+0.0	+0.0	+0.0	+0.0	+0.0	+0.0	+0.0	+0.0	+0.0	+0.0	+0.0
	+0.0	+0.0	+0.0	+0.0	+0.0	+0.0	+0.0	+0.0	+0.0	+0.0	+0.0	+0.0	+0.0	+0.0	+0.0	+0.0
PDF eigenvector 1	-0.0	+0.0	-0.0	+0.0	-0.0	+0.0	-0.0	+0.0	-0.0	+0.0	-0.0	+0.0	-0.0	+0.0	+0.0	+0.0
	-0.0	+0.0	+0.0	+0.0	-0.0	+0.0	+0.0	+0.0	-0.0	-0.0	-0.0	+0.0	-0.0	+0.0	-0.0	+0.0
PDF eigenvector 2	-0.1	-0.1	-0.1	-0.0	-0.0	-0.0	-0.0	+0.0	+0.0	-0.0	-0.0	-0.0	+0.2	+0.2	+0.2	+0.1
	+0.1	+0.0	-0.0	-0.1	+0.0	-0.0	-0.0	-0.1	+0.1	+0.0	+0.0	-0.0	-0.1	-0.1	-0.1	-0.1
PDF eigenvector 3	+0.0	+0.0	+0.0	+0.1	-0.0	+0.0	+0.0	+0.1	-0.0	-0.0	-0.0	+0.0	-0.1	-0.0	-0.0	+0.0
	-0.0	+0.0	-0.0	-0.0	-0.0	+0.0	-0.0	-0.0	-0.0	+0.0	-0.0	-0.0	+0.0	+0.1	+0.0	+0.0
PDF eigenvector 4	-0.1	-0.0	-0.1	+0.0	-0.0	+0.0	-0.0	+0.1	-0.0	-0.0	-0.1	+0.0	+0.1	+0.2	+0.1	+0.1
	+0.1	+0.0	+0.0	-0.0	+0.0	-0.0	-0.0	-0.1	+0.0	+0.0	+0.0	-0.0	-0.1	-0.1	-0.1	-0.1
PDF eigenvector 5	+0.0	+0.0	-0.1	-0.1	+0.0	+0.0	-0.1	-0.2	+0.1	+0.1	+0.1	-0.0	+0.0	-0.0	-0.1	-0.1
	-0.0	+0.0	+0.0	+0.1	+0.0	+0.0	+0.0	+0.1	-0.1	-0.1	-0.0	+0.0	-0.1	-0.0	-0.0	+0.0
PDF eigenvector 6	-0.1	-0.0	-0.1	+0.1	+0.0	+0.1	-0.0	+0.1	-0.1	-0.0	-0.1	+0.0	+0.1	+0.1	+0.1	+0.1
	+0.1	+0.1	+0.0	-0.0	-0.0	-0.0	-0.0	-0.1	+0.0	+0.0	+0.0	-0.0	-0.1	-0.0	-0.0	-0.1
PDF eigenvector 7	+0.0	+0.0	-0.1	-0.2	+0.0	-0.0	-0.1	-0.3	+0.1	+0.2	+0.1	-0.1	+0.0	-0.1	-0.1	-0.2
	-0.0	+0.0	+0.0	+0.1	+0.0	+0.0	+0.0	+0.2	-0.1	-0.1	-0.1	+0.0	-0.0	+0.0	+0.1	+0.1
PDF eigenvector 8	-0.1	+0.0	-0.1	+0.0	+0.0	+0.1	-0.0	-0.0	-0.1	+0.0	-0.1	+0.0	+0.0	+0.1	-0.0	+0.0
	+0.0	+0.0	+0.0	-0.0	-0.0	-0.1	-0.0	+0.0	+0.0	-0.0	+0.0	-0.0	+0.0	-0.0	+0.0	+0.0
PDF eigenvector 9	+0.1	+0.1	+0.1	-0.0	-0.0	-0.1	+0.0	-0.0	-0.0	+0.0	+0.0	-0.0	-0.1	+0.0	-0.0	-0.0
	-0.1	-0.0	-0.1	+0.0	+0.0	+0.1	-0.0	+0.1	-0.0	-0.0	-0.1	+0.0	+0.1	+0.0	-0.0	+0.0
PDF eigenvector 10	-0.1	+0.0	+0.0	+0.1	-0.0	+0.1	+0.0	+0.2	-0.1	-0.1	-0.1	+0.0	-0.0	+0.1	+0.1	+0.2
	+0.0	+0.0	-0.1	-0.1	+0.0	-0.0	-0.1	-0.2	+0.1	+0.1	+0.1	-0.0	+0.0	-0.0	-0.1	-0.2
PDF eigenvector 11	-0.0	+0.0	+0.0	+0.0	+0.0	+0.0	+0.0	+0.0	-0.0	-0.0	-0.0	+0.0	-0.0	+0.0	+0.0	+0.0
	-0.0	+0.0	-0.0	-0.1	-0.0	-0.0	-0.0	-0.1	+0.0	+0.0	+0.0	-0.0	+0.0	+0.0	-0.0	-0.1
PDF eigenvector 12	-0.0	+0.0	-0.1	-0.1	+0.0	+0.0	-0.0	-0.1	+0.0	+0.1	+0.0	-0.0	+0.0	+0.0	-0.0	-0.1
	-0.0	+0.0	+0.0	+0.1	-0.0	+0.0	+0.0	+0.1	-0.0	-0.0	-0.0	+0.0	-0.0	+0.0	+0.0	+0.1
PDF eigenvector 13	-0.0	+0.0	+0.0	+0.0	+0.0	+0.1	+0.0	+0.0	-0.1	-0.0	-0.0	+0.0	-0.1	-0.1	-0.1	-0.0
	-0.0	+0.0	-0.1	-0.0	-0.0	-0.0	-0.0	-0.0	+0.0	+0.0	+0.0	-0.0	+0.0	+0.1	+0.1	+0.0
PDF eigenvector 14	-0.0	+0.0	-0.0	-0.0	+0.0	+0.0	-0.0	-0.0	+0.0	+0.0	+0.0	-0.0	-0.0	-0.0	-0.0	-0.0
	-0.0	+0.0	+0.0	+0.0	-0.0	+0.0	+0.0	+0.0	-0.0	-0.0	-0.0	+0.0	+0.0	+0.0	+0.0	+0.1

Table 104: Table 102 continued.

source / bin	1	2	3	4	5	6	7	8	9	10	11	12	13	14	15	16
PDF eigenvector 15	-0.0	+0.0	-0.0	-0.0	+0.0	+0.0	-0.0	-0.1	+0.0	+0.0	+0.0	+0.0	-0.0	-0.0	-0.1	-0.1
	-0.0	+0.0	+0.0	+0.0	-0.0	+0.0	+0.0	+0.0	-0.0	-0.0	-0.0	+0.0	+0.0	+0.0	+0.0	+0.0
PDF eigenvector 16	-0.0	+0.0	-0.0	+0.0	-0.0	+0.0	+0.0	+0.0	-0.0	+0.0	-0.0	+0.0	-0.0	+0.0	-0.0	+0.0
	+0.0	+0.0	-0.0	-0.0	+0.0	-0.0	-0.0	-0.0	+0.0	+0.0	+0.0	-0.0	-0.0	+0.0	-0.0	-0.0
PDF eigenvector 17	+0.0	+0.0	-0.0	-0.0	+0.0	-0.0	-0.0	-0.0	+0.0	+0.0	+0.0	-0.0	-0.0	+0.0	-0.0	-0.0
	-0.1	+0.0	+0.0	+0.1	-0.0	+0.1	+0.0	+0.1	-0.1	-0.0	-0.1	+0.0	-0.0	+0.0	+0.0	+0.1
PDF eigenvector 18	-0.0	+0.0	-0.0	+0.0	-0.0	-0.0	-0.0	+0.1	-0.0	-0.0	-0.0	-0.0	+0.0	+0.1	+0.1	+0.1
	-0.0	+0.0	-0.0	-0.0	+0.0	+0.1	-0.0	-0.1	-0.0	+0.0	+0.0	+0.0	-0.1	-0.1	-0.1	-0.1
PDF eigenvector 19	-0.0	+0.0	+0.0	+0.1	-0.0	+0.0	+0.0	+0.1	-0.1	-0.1	-0.0	+0.0	-0.0	+0.1	+0.1	+0.1
	-0.0	+0.0	-0.1	-0.1	+0.0	+0.0	-0.1	-0.2	+0.1	+0.1	+0.0	-0.0	+0.0	-0.0	-0.1	-0.2
PDF eigenvector 20	+0.0	+0.0	+0.0	+0.1	-0.0	-0.0	-0.0	-0.1	-0.0	-0.0	+0.0	+0.1	+0.0	-0.0	+0.0	-0.1
	-0.0	-0.0	-0.0	+0.0	+0.0	+0.0	-0.0	-0.1	+0.0	+0.0	+0.0	+0.0	-0.0	-0.0	-0.0	-0.0
PDF eigenvector 21	-0.0	-0.0	-0.1	-0.0	-0.0	+0.0	-0.0	-0.0	+0.0	+0.0	-0.0	-0.0	+0.1	+0.1	+0.1	+0.1
	+0.0	+0.1	+0.1	+0.1	-0.0	+0.0	+0.0	+0.0	-0.0	-0.0	+0.0	+0.0	-0.1	-0.1	-0.1	-0.0
PDF eigenvector 22	-0.1	-0.0	-0.1	-0.1	-0.0	-0.0	-0.1	-0.0	+0.0	+0.0	-0.0	-0.0	+0.2	+0.2	+0.2	+0.1
	+0.0	+0.1	+0.1	+0.1	+0.0	+0.1	+0.0	+0.1	-0.1	-0.0	-0.0	+0.1	-0.2	-0.2	-0.2	-0.1
PDF eigenvector 23	+0.1	+0.0	+0.0	-0.0	+0.0	+0.0	-0.0	-0.1	+0.1	+0.1	+0.1	+0.0	-0.2	-0.2	-0.2	-0.2
	-0.0	+0.0	-0.0	-0.0	-0.0	+0.0	-0.0	-0.0	+0.0	+0.0	-0.0	-0.0	+0.0	+0.0	+0.0	+0.0
PDF eigenvector 24	+0.0	+0.0	-0.0	-0.0	+0.0	-0.0	-0.0	-0.1	+0.1	+0.0	+0.0	-0.0	+0.0	-0.0	-0.1	-0.1
	+0.0	-0.0	-0.1	-0.1	+0.0	-0.0	-0.1	-0.1	+0.1	+0.0	+0.0	-0.0	+0.1	+0.0	+0.0	-0.1
PDF eigenvector 25	+0.1	-0.1	-0.1	-0.1	+0.0	-0.1	-0.0	-0.1	+0.1	+0.0	+0.1	-0.0	+0.0	-0.0	-0.0	-0.1
	+0.0	+0.0	-0.0	-0.1	+0.0	-0.0	-0.1	-0.2	+0.1	+0.1	+0.1	-0.0	-0.0	-0.1	-0.1	-0.2
PDF eigenvector 26	-0.0	+0.0	-0.0	+0.0	+0.0	+0.0	-0.0	-0.0	+0.0	+0.0	-0.0	-0.0	-0.0	-0.0	-0.0	-0.0
	-0.0	+0.0	-0.0	-0.0	+0.0	+0.0	-0.0	-0.0	+0.0	+0.0	-0.0	-0.0	+0.0	-0.0	-0.0	-0.0
PDF eigenvector 27	+0.1	+0.1	+0.1	+0.1	-0.1	-0.2	-0.0	+0.0	+0.0	-0.0	+0.1	+0.0	-0.1	+0.0	+0.0	+0.1
	-0.1	-0.0	-0.0	+0.0	+0.0	+0.1	-0.0	+0.0	-0.0	+0.0	-0.0	+0.0	+0.1	+0.0	+0.0	+0.0
PDF eigenvector 28	+0.0	+0.0	+0.0	-0.1	-0.0	-0.0	-0.0	-0.0	+0.0	+0.0	+0.0	+0.0	-0.0	-0.0	-0.0	-0.1
	-0.1	+0.0	-0.0	+0.0	+0.0	+0.1	-0.0	+0.0	-0.1	+0.0	-0.1	+0.0	+0.0	+0.1	+0.0	+0.1
α_s	+0.1	+0.1	+0.1	+0.1	-0.1	-0.1	-0.0	+0.0	+0.1	+0.0	+0.0	+0.1	-0.1	-0.0	-0.1	+0.0
	-0.1	-0.0	-0.1	-0.1	+0.0	+0.2	-0.0	-0.0	-0.1	+0.0	-0.1	-0.1	+0.1	+0.1	+0.0	-0.0
m_t	-1.4	-2.0	-1.8	-0.9	-0.2	+0.1	-0.1	-0.9	+0.8	+1.1	+0.6	+0.3	+2.0	+2.3	+1.3	+0.9
	+1.1	+1.6	+2.1	+1.1	+0.2	+0.2	+0.6	+1.1	-0.7	-1.0	-0.9	-0.2	-2.3	-2.3	-1.5	-1.2
μ_{rf}	+1.1	+0.8	+0.5	+1.2	-0.3	-0.8	-0.5	+1.1	+0.3	-0.2	-0.5	+0.6	-1.2	-0.5	-0.9	+0.8
	-1.3	-1.0	-0.7	-1.8	+0.3	+0.8	+0.6	-1.4	-0.1	+0.3	+0.7	-1.2	+1.4	+0.9	+1.2	-1.0
h_{damp}	-0.2	-0.3	+1.0	-2.7	-0.2	-0.2	+0.4	-0.8	+0.9	+0.0	-0.1	+0.2	-0.9	+2.2	-0.7	-0.6
	-0.9	-0.8	+1.6	-2.9	-0.4	+0.3	+1.4	+2.2	+0.0	+0.7	-0.6	-0.6	-1.1	+1.2	+0.0	-0.1
PS ISR	-0.4	-0.7	+0.3	+0.5	-0.4	+0.4	+0.2	-0.8	+0.8	+1.0	-0.7	+0.1	-1.2	+1.6	-0.7	-0.9
	-1.3	-0.2	+3.3	-0.1	-1.3	+0.3	+1.3	+0.7	-1.1	+1.5	+0.8	+0.6	-0.3	-0.4	-0.1	+1.5
PS FSR	-1.2	+0.2	+2.0	+1.0	-0.8	+0.6	+2.4	+2.1	-1.1	+0.1	+1.1	+1.0	-3.4	+0.7	-1.0	+0.6
	+0.3	-0.1	-0.1	-2.1	-0.6	+0.1	-0.5	-1.1	-0.1	+0.9	+0.5	-0.6	+0.2	+2.3	-0.3	-0.5
UE tune	+0.2	-1.0	+0.5	-0.9	-0.2	+0.3	+1.0	+1.1	+0.2	-0.3	-0.8	+0.3	-0.8	+1.7	-1.5	-0.3
	-0.6	-0.6	-1.0	+1.3	-0.1	+0.6	+1.1	-0.8	-0.1	+1.0	+0.6	+0.2	-1.8	+0.8	+0.2	-0.7
CR	-0.2	-1.4	+0.8	+0.8	+0.1	-0.3	+0.2	-1.0	+0.1	+0.3	+1.4	-0.7	+0.0	+0.8	-0.8	+1.1
	+0.7	-1.5	-0.2	-0.2	+1.2	-0.6	-0.6	-1.3	+1.8	-0.5	-2.2	-1.2	+0.1	+1.9	-0.9	-0.9
	-0.5	-0.6	+0.6	-0.1	-0.2	+0.3	+0.4	-2.2	+0.4	+0.3	-0.0	+1.1	+0.4	+0.3	-0.0	+0.1
$f(b \rightarrow B)$	+0.5	+0.7	+1.2	+0.6	-0.3	-0.2	-0.0	+0.2	-0.5	-0.1	+0.1	+0.3	-1.2	-0.3	-0.3	+0.2
	-0.3	-0.3	-0.6	-0.3	+0.1	+0.1	+0.0	-0.1	+0.2	+0.1	-0.1	-0.1	+0.6	+0.3	+0.2	+0.0
	+0.1	+0.1	+0.2	+0.1	-0.1	-0.0	-0.0	+0.1	-0.1	+0.0	+0.0	+0.1	-0.2	-0.0	-0.0	+0.1
	+0.7	+1.0	+1.2	+1.4	-0.4	-0.2	-0.0	-0.2	-0.5	-0.2	-0.0	-0.1	-1.0	-0.6	-0.2	-0.0
$\text{BR}(B \rightarrow \mu)$	-0.1	-0.1	-0.1	-0.2	+0.1	+0.1	+0.0	+0.1	+0.0	+0.1	+0.1	-0.0	-0.1	-0.1	-0.1	+0.0
	+0.1	+0.2	+0.1	+0.2	-0.1	-0.1	-0.1	-0.0	-0.1	-0.1	-0.1	-0.0	+0.1	+0.1	+0.1	+0.1

Table 105: The measured $[M(t\bar{t}), p_T(t)]$ cross sections, along with their relative statistical and systematic uncertainties.

$M(\text{t}\bar{\text{t}})$ [GeV]	$p_T(\text{t})$ [GeV]	$\frac{1}{\sigma(\text{t}\bar{\text{t}})} \frac{d\sigma}{dp_T(\text{t})}$ [GeV $^{-1}$]	stat. [%]	syst. [%]	bin
300–450	0–100	3.173×10^{-3}	0.6	+2.7 -2.5	1
300–450	100–180	1.440×10^{-3}	1.2	+5.5 -5.7	2
300–450	180–600	1.956×10^{-5}	6.5	+27.8 -28.8	3
450–600	0–100	1.199×10^{-3}	1.2	+4.9 -4.6	4
450–600	100–180	2.104×10^{-3}	0.7	+4.4 -4.6	5
450–600	180–600	1.424×10^{-4}	1.9	+2.6 -3.4	6
600–1500	0–100	5.409×10^{-4}	2.5	+5.4 -5.1	7
600–1500	100–180	8.166×10^{-4}	1.9	+5.4 -4.6	8
600–1500	180–600	2.187×10^{-4}	1.0	+4.4 -4.4	9

Table 106: The correlation matrix of statistical uncertainties for the measured $[M(t\bar{t}), p_T(t)]$ cross sections. The values are expressed as percentages. For bin indices see Table 105.

Table 107: Sources and values of the relative systematic uncertainties in percent of the measured $[M(t\bar{t}), p_T(t)]$ cross sections. For bin indices see Table 105.

source / bin	1	2	3	4	5	6	7	8	9
JER	+0.3 -0.2	+0.1 +0.0	-3.7 -0.9	-0.3 -0.1	-0.0 +0.1	+0.2 +0.1	+0.5 +0.8	-0.7 +0.0	-0.2 +0.3
JESAbsoluteMPFBias	+0.0 -0.2	+0.3 +0.6	-1.7 -0.4	-0.1 +0.0	-0.2 -0.1	-0.0 -0.0	+0.3 -0.1	-0.2 +0.0	+0.3 +0.1
JESAbsoluteScale	+0.2 +0.1	-0.2 -0.3	-0.1 -1.0	-0.0 +0.5	-0.2 -0.2	+0.1 +0.2	+0.1 -0.4	-0.0 -0.3	+0.1 +0.1
JESAbsoluteStat	+0.6 -0.4	-0.8 +0.5	-8.2 +6.6	-0.3 +0.2	+0.4 -0.6	-0.5 +0.4	-0.0 +1.5	-0.4 -0.4	+0.1 +0.2
JESFlavourQCD	+0.3 -0.4	-0.7 +1.0	-0.9 -1.2	-0.9 +1.0	+0.1 -0.2	+0.3 +0.1	-0.2 +0.5	+0.5 -0.3	+0.6 -0.8
JESFragmentation	+0.1 +0.1	-0.3 -0.0	+0.2 -1.3	-0.2 +0.2	-0.1 -0.3	+0.3 +0.1	+0.5 +0.5	-0.2 -0.2	+0.2 -0.1
JESPileUpDataMC	-0.1 +0.2	+0.1 +0.4	-1.8 -2.9	-0.4 +0.2	+0.0 -0.3	-0.2 +0.4	+0.6 -0.9	+0.1 -0.1	+0.3 -0.3
JESPileUpPtBB	-0.1 +0.1	-0.2 +0.2	-2.5 +0.1	-0.1 +0.1	+0.0 -0.2	+0.5 +0.2	+0.7 +0.3	-0.1 -0.4	+0.1 -0.2
JESPileUpPtEC1	+0.1 -0.2	+0.2 +0.1	-3.5 +0.4	-0.3 +0.2	+0.2 -0.3	+0.3 -0.1	-1.3 +1.8	-0.1 +0.1	+0.4 -0.3
JESPileUpPtEC2	+0.0 +0.0	+0.0 -0.0	+0.0 +0.0	+0.0 -0.0	+0.0 -0.0	+0.0 +0.0	+0.0 +0.0	+0.0 +0.0	+0.0 -0.0
JESPileUpPtHF	+0.0 +0.0	-0.0 +0.0	+0.0 +0.0	-0.0 +0.0	-0.0 +0.0	+0.0 +0.0	+0.0 +0.0	+0.0 +0.0	-0.0 +0.0
JESPileUpPtRef	-0.0 +0.1	-0.3 +0.1	+0.6 -1.2	-0.3 +0.1	-0.1 +0.1	+0.7 -0.4	-0.3 +0.2	+0.4 -0.0	+0.4 -0.4
JESRelativeBal	+0.3 -0.4	+0.3 +0.8	-2.0 +1.6	-0.6 +0.2	-0.1 -0.3	-0.3 -0.2	-0.4 +1.0	-0.5 +0.0	+0.6 -0.1
JESRelativeFSR	+0.0 +0.1	-0.1 -0.1	-0.4 -0.8	+0.1 -0.3	+0.1 -0.2	-0.1 +0.1	+0.4 -0.1	-0.2 +0.3	-0.2 +0.2
JESRelativeJEREC1	-0.0 +0.0	+0.1 -0.3	+0.1 +1.3	-0.1 +0.2	-0.1 -0.1	-0.1 -0.2	+0.2 -0.0	-0.0 +0.1	+0.1 +0.1
JESRelativeJEREC2	+0.0 +0.0	+0.0 -0.0	+0.0 +0.0	+0.0 -0.0	+0.0 -0.0	+0.0 +0.0	+0.0 +0.0	+0.0 +0.0	+0.0 -0.0
JESRelativeJERHF	+0.0 +0.0	+0.0 -0.0	+0.0 +0.0	+0.0 -0.0	+0.0 -0.0	+0.0 +0.0	+0.0 +0.0	+0.0 +0.0	+0.0 -0.0
JESRelativePtBB	-0.0 +0.0	-0.2 +0.3	-0.7 -1.0	+0.4 -0.1	-0.2 -0.0	+0.0 -0.0	+0.5 +0.2	-0.4 -0.3	+0.2 -0.1
JESRelativePtEC1	+0.3 -0.2	+0.0 -0.1	-2.4 +0.5	-0.5 +0.1	-0.2 -0.1	+0.6 +0.0	-0.7 +1.2	-0.2 +0.2	+0.1 -0.2
JESRelativePtEC2	+0.0 +0.0								
JESRelativePtHF	+0.0 +0.0								
JESRelativeStatEC	+0.2 -0.0	-0.0 -0.2	-2.2 -0.8	-0.2 +0.1	+0.0 -0.1	+0.4 +0.2	-0.5 +0.3	-0.3 +0.1	+0.1 -0.0
JESRelativeStatFSR	+0.0 +0.1	+0.0 -0.0	-0.1 +0.5	+0.0 -0.0	-0.1 +0.0	-0.4 -0.2	+0.3 -0.4	-0.1 +0.2	+0.2 -0.1
JESRelativeStatHF	+0.0 +0.0	-0.0 +0.0	+0.0 +0.0	-0.0 +0.0	-0.0 +0.0	+0.0 +0.0	+0.0 +0.0	+0.0 +0.0	-0.0 +0.0
JESSinglePionECAL	+0.0 +0.0	+0.1 +0.0	-0.8 -2.4	+0.2 -0.5	-0.3 +0.0	+0.1 +0.4	+0.4 +0.3	-0.0 -0.0	-0.2 +0.2

Table 108: Table 107 continued.

source / bin	1	2	3	4	5	6	7	8	9
JESSinglePionHCAL	-0.1	+0.3	-0.2	+0.4	-0.1	-0.2	+0.7	-0.5	-0.1
	+0.1	-0.3	-0.1	-0.2	-0.2	-0.3	+0.3	+0.1	+0.4
JESTimePtEta	+0.0	+0.1	-1.6	-0.1	-0.0	+0.0	+0.2	-0.2	+0.2
	+0.1	-0.1	-1.4	+0.1	-0.3	+0.4	+0.0	+0.0	+0.2
E_T^{miss}	+0.2	-0.6	-1.3	+0.2	+0.1	-0.6	-0.1	-0.2	+0.0
	-0.0	+0.4	+0.7	-0.3	-0.2	+0.1	-0.2	+0.4	+0.1
lepton ID/ISO	+0.2	-0.7	+0.5	-0.7	+0.6	-0.3	+0.7	-0.0	-0.3
	-0.2	+0.7	-0.5	+0.7	-0.7	+0.3	-0.7	+0.1	+0.3
pileup	-0.0	-0.2	-0.7	-0.1	+0.1	-0.1	+0.0	+0.2	+0.0
	-0.0	+0.2	+0.7	+0.1	-0.1	+0.1	-0.1	-0.2	+0.0
trigger	+0.1	-0.1	+0.2	-0.2	+0.1	+0.0	-0.1	-0.2	+0.0
	-0.0	+0.1	-0.2	+0.2	-0.2	-0.0	+0.1	+0.2	-0.0
trigger (η)	+0.0	-0.0	+0.1	-0.2	-0.0	+0.0	+0.3	+0.0	-0.1
	-0.0	+0.0	-0.1	+0.2	-0.0	+0.0	-0.3	-0.0	+0.1
non-tt background	-1.0	-0.4	+0.9	-0.8	+1.2	+0.5	+0.9	+1.2	+1.1
	+1.1	+0.2	-0.8	+0.7	-1.2	-0.4	-0.9	-1.1	-1.1
b-tagging	-0.0	-0.1	+0.2	-0.1	+0.1	-0.0	+0.2	+0.1	+0.0
	+0.0	+0.1	-0.2	+0.1	-0.1	+0.0	-0.2	-0.0	-0.0
b-tagging (light jets)	-0.2	+0.0	-0.2	-0.3	+0.3	+0.3	-0.2	+0.2	+0.3
	+0.2	-0.0	+0.2	+0.3	-0.3	-0.3	+0.2	-0.2	-0.3
luminosity	+0.0	+0.0	+0.0	+0.0	+0.0	+0.0	+0.0	+0.0	+0.0
	+0.0	+0.0	+0.0	+0.0	+0.0	+0.0	+0.0	+0.0	+0.0
BR($t\bar{t} \rightarrow \ell\ell$)	+0.0	+0.0	+0.0	+0.0	+0.0	+0.0	+0.0	+0.0	+0.0
	+0.0	+0.0	+0.0	+0.0	+0.0	+0.0	+0.0	+0.0	+0.0
PDF eigenvector 1	+0.0	-0.0	+0.1	-0.0	-0.0	-0.0	+0.0	+0.0	+0.0
	+0.0	-0.0	+0.2	-0.0	-0.0	+0.0	-0.0	-0.0	-0.0
PDF eigenvector 2	-0.1	-0.0	+0.2	-0.0	-0.1	-0.0	+0.3	+0.4	+0.1
	-0.0	+0.1	-0.4	+0.2	-0.1	-0.0	-0.1	+0.0	-0.1
PDF eigenvector 3	+0.0	+0.0	+0.3	+0.0	-0.0	+0.0	-0.1	-0.1	-0.0
	-0.0	-0.0	-0.1	-0.0	+0.0	-0.0	+0.1	+0.1	+0.0
PDF eigenvector 4	+0.0	-0.1	+0.3	-0.2	+0.0	+0.0	+0.1	+0.1	+0.1
	-0.0	+0.1	-0.2	+0.2	-0.1	-0.0	-0.1	+0.0	-0.1
PDF eigenvector 5	-0.0	-0.0	-0.7	+0.1	+0.0	-0.0	+0.1	+0.0	-0.1
	+0.0	+0.0	+0.5	-0.0	-0.0	+0.0	-0.1	-0.1	-0.0
PDF eigenvector 6	+0.0	-0.1	+0.4	-0.2	+0.1	+0.0	+0.0	-0.1	+0.1
	-0.0	+0.1	-0.2	+0.1	-0.1	+0.0	-0.0	+0.1	-0.1
PDF eigenvector 7	-0.1	-0.0	-1.2	+0.2	+0.1	-0.1	+0.2	+0.1	-0.1
	+0.1	-0.0	+0.6	-0.1	-0.0	+0.1	-0.1	-0.1	+0.1
PDF eigenvector 8	+0.1	-0.2	+0.2	-0.2	+0.2	-0.1	+0.1	-0.1	-0.0
	-0.0	+0.1	-0.1	+0.1	-0.2	+0.1	-0.1	+0.1	+0.0
PDF eigenvector 9	-0.0	+0.1	-0.0	+0.1	-0.2	+0.0	-0.0	+0.2	-0.0
	+0.0	-0.1	+0.1	-0.2	+0.2	-0.0	+0.1	-0.2	+0.0
PDF eigenvector 10	+0.1	-0.0	+0.6	-0.2	+0.0	+0.1	-0.1	-0.1	+0.1
	-0.1	+0.0	-0.7	+0.2	-0.0	-0.0	+0.1	+0.1	-0.1
PDF eigenvector 11	+0.0	-0.0	+0.2	-0.1	+0.0	+0.0	-0.0	-0.0	+0.0
	-0.0	+0.0	-0.3	+0.1	-0.0	-0.0	+0.1	+0.1	-0.0
PDF eigenvector 12	-0.0	-0.0	-0.2	+0.1	+0.0	-0.1	+0.1	+0.1	-0.0
	+0.0	+0.0	+0.3	-0.1	-0.0	+0.1	-0.1	-0.0	+0.0
PDF eigenvector 13	+0.1	-0.1	-0.0	-0.1	+0.1	+0.0	-0.1	-0.3	-0.0
	-0.1	+0.1	+0.0	+0.1	-0.2	-0.0	+0.1	+0.3	+0.0
PDF eigenvector 14	+0.0	-0.0	-0.1	+0.0	+0.0	-0.0	+0.0	+0.0	-0.0
	+0.0	+0.0	+0.2	-0.0	-0.0	+0.0	-0.1	+0.0	+0.0

Table 109: Table 107 continued.

source / bin	1	2	3	4	5	6	7	8	9
PDF eigenvector 15	+0.0	-0.0	-0.2	+0.0	+0.0	-0.0	+0.0	-0.0	-0.0
	+0.0	-0.0	+0.1	-0.0	-0.0	+0.0	-0.0	+0.0	+0.0
PDF eigenvector 16	+0.0	-0.0	+0.1	-0.1	+0.0	+0.0	-0.0	-0.0	+0.0
	-0.0	+0.0	-0.1	+0.1	-0.0	-0.0	+0.0	+0.0	-0.0
PDF eigenvector 17	-0.0	+0.0	-0.1	+0.1	-0.1	-0.0	+0.0	+0.1	-0.0
	+0.1	-0.1	+0.3	-0.2	+0.1	+0.0	-0.1	-0.2	+0.0
PDF eigenvector 18	-0.0	+0.1	+0.3	+0.0	-0.1	+0.0	-0.0	+0.2	+0.1
	+0.0	-0.1	-0.2	-0.0	+0.1	-0.0	-0.0	-0.2	-0.1
PDF eigenvector 19	+0.0	+0.0	+0.3	-0.1	-0.0	+0.1	-0.1	-0.0	+0.1
	-0.0	-0.1	-0.5	+0.1	+0.1	-0.1	+0.1	+0.0	-0.1
PDF eigenvector 20	+0.0	+0.0	-0.4	-0.0	-0.0	+0.1	-0.1	-0.0	+0.0
	+0.0	-0.1	-0.1	+0.0	+0.0	-0.0	+0.1	+0.0	-0.0
PDF eigenvector 21	-0.0	-0.0	+0.0	-0.0	-0.0	-0.0	+0.1	+0.2	+0.0
	+0.0	+0.0	+0.1	-0.0	+0.0	+0.0	-0.1	-0.2	-0.0
PDF eigenvector 22	-0.1	-0.0	-0.0	-0.1	-0.0	+0.0	+0.1	+0.3	+0.1
	+0.1	+0.0	+0.1	-0.0	+0.1	+0.0	-0.2	-0.3	-0.1
PDF eigenvector 23	+0.0	-0.0	-0.5	+0.2	+0.0	-0.1	+0.0	-0.1	-0.2
	+0.0	-0.0	-0.1	-0.0	+0.0	+0.0	-0.1	-0.0	+0.0
PDF eigenvector 24	-0.0	+0.0	-0.4	+0.1	-0.0	+0.0	-0.1	-0.0	-0.0
	-0.1	-0.0	-0.3	+0.2	-0.1	-0.1	+0.3	+0.3	-0.1
PDF eigenvector 25	-0.1	+0.0	-0.4	+0.2	-0.1	-0.1	+0.2	+0.3	-0.1
	-0.0	+0.0	-0.7	+0.1	-0.0	-0.0	-0.0	+0.0	-0.0
PDF eigenvector 26	+0.0	-0.0	-0.1	+0.0	+0.0	+0.0	-0.0	-0.0	-0.0
	-0.0	+0.0	-0.2	+0.0	+0.0	+0.0	-0.0	-0.0	+0.0
PDF eigenvector 27	-0.1	+0.3	-0.0	+0.2	-0.3	+0.1	-0.2	+0.2	+0.0
	+0.0	-0.1	+0.1	-0.1	+0.1	-0.0	+0.1	-0.1	+0.0
PDF eigenvector 28	-0.0	+0.1	-0.3	+0.1	-0.1	+0.1	-0.1	+0.0	-0.0
	+0.0	-0.1	+0.3	-0.2	+0.1	-0.0	+0.1	-0.1	+0.0
α_s	-0.1	+0.3	+0.2	+0.3	-0.2	+0.1	-0.2	+0.1	-0.0
	+0.1	-0.3	-0.2	-0.2	+0.2	-0.1	+0.2	-0.1	+0.0
m_t	-0.5	-2.7	-1.7	+0.5	+0.9	-0.2	+0.4	+1.4	+2.1
	+0.5	+2.5	+3.6	-0.2	-0.8	+0.1	-1.1	-1.2	-2.1
$\mu_{r,f}$	-0.7	+1.7	+10.2	+2.1	-2.2	+0.0	-0.4	+1.8	-0.3
	+0.9	-1.8	-14.6	-2.2	+2.3	+0.2	+0.1	-2.0	+0.5
h_{damp}	+0.2	-0.4	-6.7	-0.1	-0.0	+0.7	-0.4	+0.7	+0.1
	-0.5	-0.1	+11.3	+0.3	+0.4	-0.8	-0.6	+1.1	-0.3
PS ISR	-0.1	-0.6	+1.1	+0.1	+0.5	+0.1	-0.7	+0.1	+0.1
	-0.0	-0.6	+3.8	+0.2	+0.3	-0.5	-1.4	+1.2	-0.1
PS FSR	-0.4	+1.3	+7.4	+1.4	-0.4	-0.8	+0.0	-0.0	-1.4
	+0.2	-1.2	-0.7	-0.5	+0.5	-0.4	-0.6	+0.3	+1.0
UE tune	+0.1	-0.1	+4.3	+0.4	+0.2	-1.4	-1.8	+0.7	+0.0
	-0.2	+0.0	+2.7	+0.2	+0.3	-0.1	-0.5	+0.3	-0.2
CR	-0.2	-0.4	+1.1	+0.2	+0.3	-0.2	+0.9	-0.9	+0.6
	+0.1	-0.3	-0.3	-0.3	+0.2	-0.7	+0.2	+0.6	+0.1
	-0.1	-0.2	-1.4	-0.6	+0.3	-0.1	-0.1	+1.4	+0.0
$f(b \rightarrow B)$	-0.1	+0.7	-0.6	+0.9	-0.7	-0.3	-0.2	-0.1	+0.2
	+0.0	-0.3	+0.3	-0.4	+0.3	+0.2	+0.0	+0.1	-0.0
	-0.0	+0.1	-0.1	+0.2	-0.2	-0.0	-0.1	+0.0	+0.0
	+0.2	+0.5	-1.3	+0.3	-0.6	-0.2	-0.5	-0.3	+0.2
$\text{BR}(B \rightarrow \mu)$	-0.0	-0.0	-0.2	+0.1	+0.0	+0.1	-0.1	+0.0	-0.1
	+0.1	-0.1	+0.2	-0.1	-0.1	-0.1	+0.0	-0.0	+0.1

Table 110: The measured $[N_{\text{jet}}^{0,1,2+}, M(\text{t}\bar{\text{t}}), y(\text{t}\bar{\text{t}})]$ cross sections, along with their relative statistical and systematic uncertainties, and NP corrections (see Section 8).

N_{jet}	$M(\text{t}\bar{\text{t}})$ [GeV]	$y(\text{t}\bar{\text{t}})$	$\frac{1}{\sigma(\text{t}\bar{\text{t}})} \frac{d\sigma}{dy(\text{t}\bar{\text{t}})}$	stat. [%]	syst. [%]	\mathcal{C}_{NP}	bin
0	300–400	0.00–0.35	8.224×10^{-2}	4.6	$^{+12.9}_{-8.5}$	0.973	1
0	300–400	0.35–0.75	8.712×10^{-2}	3.7	$^{+6.9}_{-12.6}$	0.974	2
0	300–400	0.75–1.15	7.671×10^{-2}	4.1	$^{+6.3}_{-14.5}$	0.973	3
0	300–400	1.15–2.50	3.590×10^{-2}	4.0	$^{+8.4}_{-9.4}$	0.975	4
0	400–500	0.00–0.35	1.368×10^{-1}	2.7	$^{+2.4}_{-3.6}$	0.971	5
0	400–500	0.35–0.75	1.234×10^{-1}	2.4	$^{+5.5}_{-2.2}$	0.971	6
0	400–500	0.75–1.15	1.032×10^{-1}	2.9	$^{+5.3}_{-1.4}$	0.972	7
0	400–500	1.15–2.50	4.739×10^{-2}	2.3	$^{+4.8}_{-3.3}$	0.974	8
0	500–1500	0.00–0.35	1.625×10^{-1}	1.8	$^{+3.7}_{-5.5}$	0.976	9
0	500–1500	0.35–0.75	1.422×10^{-1}	2.0	$^{+6.3}_{-3.5}$	0.978	10
0	500–1500	0.75–1.15	1.123×10^{-1}	2.4	$^{+3.7}_{-6.4}$	0.977	11
0	500–1500	1.15–2.50	3.223×10^{-2}	3.5	$^{+7.0}_{-7.0}$	0.982	12
≥ 1	300–400	0.00–0.35	6.493×10^{-2}	5.9	$^{+12.9}_{-4.8}$	1.033	13
≥ 1	300–400	0.35–0.75	6.231×10^{-2}	5.1	$^{+10.6}_{-5.0}$	1.031	14
≥ 1	300–400	0.75–1.15	5.557×10^{-2}	5.5	$^{+8.1}_{-7.4}$	1.035	15
≥ 1	300–400	1.15–2.50	2.482×10^{-2}	5.2	$^{+5.8}_{-14.6}$	1.037	16
≥ 1	400–500	0.00–0.35	1.220×10^{-1}	3.1	$^{+4.4}_{-9.2}$	1.036	17
≥ 1	400–500	0.35–0.75	1.083×10^{-1}	2.7	$^{+4.3}_{-8.5}$	1.034	18
≥ 1	400–500	0.75–1.15	8.512×10^{-2}	3.5	$^{+9.0}_{-5.4}$	1.036	19
≥ 1	400–500	1.15–2.50	3.283×10^{-2}	3.1	$^{+9.0}_{-4.6}$	1.037	20
≥ 1	500–1500	0.00–0.35	1.556×10^{-1}	1.7	$^{+7.6}_{-4.9}$	1.024	21
≥ 1	500–1500	0.35–0.75	1.362×10^{-1}	2.0	$^{+3.7}_{-8.2}$	1.024	22
≥ 1	500–1500	0.75–1.15	9.834×10^{-2}	2.5	$^{+7.3}_{-5.4}$	1.025	23
≥ 1	500–1500	1.15–2.50	2.700×10^{-2}	3.6	$^{+9.7}_{-8.1}$	1.022	24

Table 111: The correlation matrix of statistical uncertainties for the measured $[N_{\text{jet}}^{0,1,2+}, M(t\bar{t}), y(t\bar{t})]$ cross sections. The values are expressed as percentages. For bin indices see Table 110.

bin	2	3	4	5	6	7	8	9	10	11	12	13	14	15	16	17	18	19	20	21	22	23	24
1	-17	-17	+2	-40	-23	+9	+3	-6	+7	+0	-5	-20	-4	+4	-2	+4	+7	+1	-4	+3	-3	-4	+0
2		+16	-23	-20	-10	-31	-4	+9	-12	+3	+5	-3	-12	-10	+5	+7	-2	+3	+4	-2	+3	+3	-5
3		-2	+8	-31	-20	-29	+1	+2	-9	+1	+4	-10	-12	-6	+1	+2	+0	+3	-3	+2	+3	+1	
4			-1	-2	-24	+1	-9	-1	-0	-31	-3	+3	-5	-25	-6	-0	+2	-13	-5	-9	-4	+10	
5				+3	-9	-5	-21	-10	+3	-1	-2	+4	+2	-3	-12	-4	+1	+1	+2	+4	+0	-1	
6					+22	-13	-10	-6	-15	-1	+5	-5	+0	+3	-4	-7	-6	-0	+5	-1	+3	-0	
7						+11	+4	-13	-10	-12	+3	+1	-4	+0	+1	-5	-7	-4	+1	+4	-0	+1	
8							-4	-3	-15	-2	-5	+4	+1	-20	-2	-3	-3	-8	-5	-4	+0	-8	
9								-25	-4	-0	+6	-1	-3	-0	-4	+2	+2	-0	-22	+2	+4	-2	
10									-10	-11	-1	+4	+4	-5	+2	-5	+1	+1	+3	-17	-6	+4	
11										-13	-3	+3	+4	+1	+1	+0	-4	+0	+4	-4	-17	-3	
12											-0	-4	+2	+9	-2	-1	-0	-12	-5	+2	+0	-29	
13												-16	-13	+3	-50	-26	+12	+4	-3	+9	+1	-4	
14													+11	-16	-24	-17	-36	+6	+10	-11	+5	+6	
15														-1	+10	-37	-28	-28	+1	+5	-7	+8	
16															+3	+5	-26	-23	-4	+3	+7	-29	
17																+6	-8	-2	-22	-10	+4	+1	
18																	+23	-7	-12	-8	-16	+2	
19																		+14	+5	-14	-12	-10	
20																		+2	+2	-13	-13		
21																			-31	-1	+3		
22																				-16	-6		
23																					-21		

Table 112: Sources and values of the relative systematic uncertainties in percent of the measured $[N_{\text{jet}}^{0,1,2+}, M(\text{t}\bar{\text{t}}), y(\text{t}\bar{\text{t}})]$ cross sections. For bin indices see Table 110.

source / bin	1	2	3	4	5	6	7	8	9	10	11	12	13	14	15	16	17	18	19	20	21	22	23	24
JER	+0.2 -0.4	+0.6 -1.0	+0.4 -2.1	+0.8 -0.8	+0.1 -0.2	+0.7 +0.2	+0.5 -0.2	+0.8 +0.1	+0.1 -0.3	+0.5 -0.4	+0.2 +0.1	+0.9 +2.1	-0.6 +0.0	-0.1 +0.0	+0.1 +0.7	-0.8 -0.4	-0.5 +0.4	-0.6 -0.2	+0.3 +0.5	-1.0 +1.2	-0.6 +0.6	-0.6 +0.6	-0.5 +0.1	-1.8 +0.4
JESAbsoluteMPFBias	+0.8 -0.8	+0.4 -0.9	-0.1 -1.5	+0.7 -0.3	-0.1 -0.1	+0.4 +0.1	+0.4 +0.1	+0.4 +0.1	+0.3 -0.1	-0.0 +0.2	+0.2 +0.0	-0.5 -0.0	+1.2 -0.3	+0.7 -0.8	+0.3 +0.2	-0.2 -0.8	-0.4 -0.8	-0.6 +0.5	-0.6 +0.3	-0.2 +0.5	-0.5 +0.4	-0.4 +0.5	-0.3 +0.2	-1.0 +0.7
JESAbsoluteScale	+0.6 -0.7	+0.0 -0.7	+0.0 -1.1	+0.6 -1.4	-0.1 -0.4	+0.4 -0.1	+0.3 -0.0	+0.3 +0.3	+0.1 -0.1	-0.1 +0.1	+0.2 +0.2	-0.0 -0.1	+0.5 -0.3	+0.7 -0.4	+0.0 +0.2	+0.1 -0.2	-0.2 -0.0	-0.4 +0.4	-0.5 +0.3	+0.2 -0.1	-0.3 +0.2	-0.4 +0.3	-1.3 -0.0	
JESAbsoluteStat	+0.4 -1.2	+1.0 -0.4	-1.1 -0.3	-0.3 -0.3	-0.4 +0.4	-0.0 +0.1	-0.2 +0.4	+0.5 +0.3	+0.2 -0.4	+0.2 -0.3	+0.2 -0.5	+0.7 +0.6	+0.5 -0.6	+1.0 -0.6	+0.1 -0.1	+0.1 +1.4	-0.7 -0.0	-0.6 +0.3	-0.7 +0.3	-0.6 +0.3	+0.1 -0.2	+0.3 -0.2	+0.0 -0.7	
JESFlavourQCD	+3.0 -3.3	+2.9 -3.7	+1.4 -3.4	+2.0 -2.1	+0.0 -0.2	+0.9 -0.4	+0.3 -0.1	+1.1 -1.4	+1.2 -0.6	+1.3 -0.8	+1.1 -0.9	+1.3 -0.6	+1.0 -0.2	+1.9 +0.8	+0.0 +0.5	-0.8 +0.5	-2.5 +1.9	-2.7 +2.4	-1.3 +1.9	-1.3 +2.4	-1.6 +2.7	-1.4 +1.8	-2.3 +1.4	+1.5 +1.5
JESFragmentation	+0.2 -0.4	-0.2 -0.6	-0.1 -1.2	+0.4 -0.1	+0.2 -0.1	+0.5 -0.0	+0.6 +0.0	+0.5 +0.2	+0.3 -0.2	+0.3 -0.2	-0.2 -0.2	-0.4 -0.2	+0.4 +0.2	+0.4 +0.2	+0.1 +0.7	-0.7 +0.1	-0.5 +0.4	-0.6 +0.3	-0.6 -0.1	-0.6 +0.8	-0.2 +0.2	-0.2 +0.1	-0.1 +0.0	-0.7 +0.2
JESPileUpDataMC	+0.6 -0.6	+0.1 -1.0	-0.5 -1.1	-0.0 -0.5	+0.0 +0.1	+0.5 +0.2	+0.5 -0.1	+0.8 -0.3	+0.3 -0.4	+0.4 -0.2	+0.6 -0.2	+0.0 -0.5	+0.6 +0.4	+0.6 +0.7	+0.0 +0.9	-0.2 +0.0	-0.4 +0.6	-0.6 +0.4	-0.3 +0.0	-0.6 +0.8	-0.2 +0.2	-0.3 +0.4	+0.1 -0.0	-1.2 +0.4
JESPileUpPtBB	+0.1 -0.2	-0.5 -0.5	+0.2 -0.2	-0.2 -0.0	+0.5 -0.1	+0.6 -0.3	+0.4 -0.4	+0.4 -0.2	+0.5 -0.2	+0.2 -0.2	+0.2 -0.1	+0.5 +0.5	+0.4 +1.7	+0.4 +1.9	-0.7 -0.0	-0.2 +0.2	-0.2 -0.1	-0.4 +0.3	-0.5 +0.3	-0.0 +0.0	-0.1 -0.2	-0.0 -0.0	-0.2 +0.0	-0.0 +0.0
JESPileUpPtEC1	+1.1 -0.9	+1.5 -1.2	-0.1 -1.3	+0.2 -0.2	+0.2 -0.7	+0.5 -0.4	+0.4 -0.1	+0.4 -0.3	+0.5 -0.6	+0.6 -0.7	+0.9 -0.7	+0.4 -0.4	+0.4 -0.1	+0.1 -0.1	-0.7 +0.9	-0.5 +1.8	-0.4 +0.4	-0.5 +0.3	-0.0 +0.9	-0.5 +1.3	-0.3 +0.5	-0.3 +0.5	-1.3 +0.5	
JESPileUpPtEC2	+0.0 +0.0																							
JESPileUpPtHF	+0.0 +0.0																							
JESPileUpPtRef	+0.2 -0.2	-0.0 -1.0	-0.4 -1.1	+0.4 +0.0	+0.3 -0.3	+0.3 -0.2	-0.6 -0.6	-0.7 -0.7	-0.7 -0.7	-0.4 -0.4	-0.1 -0.1	-0.3 -0.3	+0.9 +0.9	+1.8 +1.8	+0.4 +0.4	+0.3 +0.3	+0.9 +0.9	+1.3 +1.3	+0.5 +0.5	+0.5 +0.5	+0.5 +0.5	+0.5 +0.5	+0.5 +0.5	
JESRelativeBal	+2.0 -2.8	+2.4 -2.9	+1.7 -2.9	+2.0 -2.9	+0.0 -2.9	+0.5 -1.8	-0.1 -0.2	+0.2 -0.3	+0.5 -0.2	-0.1 -0.3	+0.1 -0.3	+0.6 -0.6	+0.6 -0.6	+0.4 -0.2	+0.4 -0.2	+0.5 -0.3	-0.2 +0.5	-2.4 +1.2	-1.0 +1.2	-1.3 +1.1	-0.8 +1.0	-0.8 +1.4	-0.9 +1.3	-1.1 +1.3
JESRelativeFSR	-0.6 +0.2	-0.9 +0.6	-0.8 +0.3	-0.3 +0.1	+0.2 +0.3	+0.1 +0.1	+0.2 +0.3	+0.2 +0.3	+0.0 +0.0															
JESRelativeJEREC1	-0.0 -0.0	+0.0 -0.7	-0.2 +0.2	+0.2 +0.0	+0.0 +0.0	+0.0 +0.0	+0.1 +0.4	+0.1 +0.0	-0.0 -0.2	-0.2 -0.2	-0.3 -0.3	+0.1 -0.1	-0.0 -0.0	+0.3 -0.3	-0.4 -0.6	-0.1 -0.1	+0.0 +0.0	-0.2 -0.2	+0.0 +0.1	-0.0 +0.0	+0.0 +0.1	-0.4 -0.1	+0.2 +0.8	
JESRelativeJEREC2	+0.0 +0.0																							
JESRelativeJERHF	+0.0 +0.0																							
JESRelativePtBB	+0.3 -0.4	+0.3 -1.6	+0.1 -0.8	+0.2 +0.3	+0.3 +0.3	+0.2 +0.5	+0.2 -0.1	+0.1 -0.1	+0.1 -0.1	+0.1 -0.0	+0.1 -0.0	+0.5 -0.5	+0.1 -0.8	+0.1 +0.3	+0.3 -0.9	-0.3 +0.5	+0.0 +0.0	-0.2 -0.1	-0.5 +0.1	-0.1 +0.2	-0.6 +0.1	-0.1 +0.1	-0.2 +0.1	-0.3 +0.1
JESRelativePtEC1	+0.0 -0.6	+1.2 -0.8	+0.3 -1.1	+0.5 -1.1	+0.3 -0.5	+0.4 -0.5	+0.4 -0.4	+0.1 -0.3	+0.7 -0.3	-0.3 -0.4	-0.1 -0.7	+0.7 +0.1	-0.7 -0.7	-0.8 -0.8	+0.5 +0.5	-0.1 -0.1	+0.2 +0.2	-0.4 +0.5	-0.5 +0.3	-0.4 +0.3	-0.2 +0.3	-0.3 +0.4	-2.0 +0.6	
JESRelativePtEC2	+0.0 +0.0																							
JESRelativePtHF	+0.0 +0.0																							
JESRelativeStatEC	+0.0 -0.2	+0.3 -0.4	-0.0 -1.0	+0.2 +0.1	+0.1 -0.1	+0.4 +0.4	-0.1 -0.1	-0.1 +0.1	+0.3 +0.2	-0.1 +0.2	+0.1 +0.1	+0.2 +0.2	+0.1 +0.3	+0.3 -0.8	-0.4 -0.2	+0.0 -0.2	-0.1 -0.2	-0.5 -0.2	-0.2 -0.1	-0.5 -0.1	-0.1 -0.1	-0.2 -0.2	-0.1 -0.3	-1.0 +0.3
JESRelativeStatFSR	+0.0 -0.0	+0.1 -0.8	-0.3 -0.8	+0.1 -0.2	+0.1 -0.1	+0.3 +0.3	+0.2 -0.0	-0.1 +0.1	+0.3 -0.1	-0.1 +0.2	-0.2 +0.2	-0.2 -0.2	-0.2 +0.1	-0.1 -0.4	-0.1 -0.4	-0.2 +0.2	-0.2 +0.2	-0.3 -0.3	-0.0 -0.1	-0.3 -0.1	-0.1 -0.1	-0.4 -0.3	-0.1 +0.4	
JESRelativeStatHF	+0.0 +0.0																							
JESSinglePionECAL	-0.7 +0.3	-1.1 -0.0	-0.8 +0.3	-0.0 +0.0	+0.1 +0.6	+0.2 +0.5	+0.0 +0.7	+0.0 +0.6	+0.0 +0.6	+0.0 +0.2	+0.0 -0.2	-0.2 -0.2	-0.3 -0.3	+0.5 +0.3	+0.3 -0.4	+0.7 +0.7	+0.2 +0.2	+0.3 +0.3	+0.3 +0.4	+0.4 +0.2	+0.2 +0.1	+0.4 +0.4	+0.2 +0.3	+0.3 +0.3

Table 113: Table 112 continued.

Table 114: Table 112 continued.

source / bin	1	2	3	4	5	6	7	8	9	10	11	12	13	14	15	16	17	18	19	20	21	22	23	24
PDF eigenvector 15	-0.0	-0.0	+0.0	-0.0	+0.1	+0.1	+0.0	+0.1	-0.0	-0.0	-0.0	+0.0	-0.1	-0.1	-0.0	-0.0	+0.1	+0.1	+0.1	+0.1	-0.1	-0.1	-0.0	
	+0.0	+0.0	-0.0	+0.0	-0.0	-0.0	-0.0	-0.0	+0.0	+0.0	+0.0	-0.0	+0.0	+0.0	-0.0	-0.0	-0.0	-0.0	-0.0	+0.0	+0.0	+0.0	+0.0	
PDF eigenvector 16	+0.0	+0.0	-0.0	-0.0	-0.0	-0.0	-0.0	-0.0	+0.0	+0.0	+0.0	+0.0	+0.0	+0.0	-0.0	-0.0	-0.0	-0.0	-0.0	-0.0	+0.0	+0.0	+0.0	
	+0.1	-0.2	-0.0	+0.1	-0.0	+0.1	+0.1	-0.0	-0.0	+0.0	-0.1	+0.1	+0.1	+0.0	-0.0	-0.0	-0.1	-0.0	+0.0	+0.1	-0.0	-0.0	-0.0	
PDF eigenvector 17	-0.0	-0.0	+0.0	+0.0	-0.0	-0.0	+0.0	+0.0	-0.0	-0.0	-0.0	+0.0	-0.0	-0.1	+0.0	+0.0	+0.0	+0.1	+0.0	-0.0	-0.0	-0.0	-0.0	
	+0.0	+0.0	-0.0	-0.1	+0.0	+0.0	-0.1	+0.0	+0.0	+0.0	+0.1	+0.1	+0.0	-0.0	-0.1	-0.0	-0.0	-0.1	+0.0	+0.1	+0.1	+0.1	+0.1	
PDF eigenvector 18	+0.1	-0.0	+0.0	+0.0	-0.2	-0.1	-0.1	+0.1	+0.1	+0.0	+0.1	+0.1	+0.1	+0.0	+0.1	-0.3	-0.2	-0.1	-0.0	+0.2	+0.2	+0.2	+0.0	
	-0.1	+0.0	-0.0	-0.0	+0.2	+0.1	+0.1	-0.1	-0.1	-0.1	-0.0	-0.1	-0.0	-0.0	-0.1	+0.3	+0.2	+0.1	+0.0	-0.2	-0.1	-0.2	-0.0	
PDF eigenvector 19	+0.1	+0.1	+0.0	-0.0	-0.1	-0.1	-0.1	-0.2	+0.1	+0.1	+0.1	-0.2	+0.1	+0.1	+0.0	-0.0	-0.1	-0.1	-0.2	-0.2	+0.2	+0.2	+0.0	
	-0.1	-0.1	-0.0	+0.0	+0.1	+0.1	+0.1	+0.3	-0.2	-0.2	-0.1	+0.3	-0.2	-0.2	-0.0	+0.0	+0.2	+0.2	+0.3	+0.3	-0.3	-0.3	-0.1	
PDF eigenvector 20	+0.0	+0.0	+0.0	+0.0	-0.0	-0.0	-0.0	-0.1	+0.0	+0.0	+0.1	+0.0	+0.0	-0.0	-0.1	+0.0	-0.0	-0.0	-0.0	+0.1	+0.0	+0.1	-0.2	
	-0.0	-0.0	-0.0	-0.0	+0.0	+0.0	+0.0	+0.1	-0.0	-0.1	-0.1	+0.0	-0.1	-0.0	+0.0	+0.0	+0.1	+0.1	+0.1	-0.1	-0.1	-0.1	-0.0	
PDF eigenvector 21	-0.0	-0.1	-0.0	+0.0	-0.1	-0.1	-0.0	+0.1	+0.0	+0.0	-0.0	+0.2	+0.0	-0.1	-0.0	+0.1	-0.2	-0.1	+0.0	+0.1	+0.1	+0.0	-0.0	
	+0.0	+0.1	+0.0	-0.1	+0.1	+0.1	-0.0	-0.1	-0.0	+0.0	-0.1	+0.0	+0.1	+0.0	-0.1	+0.2	+0.1	-0.1	-0.2	-0.0	+0.0	+0.0	+0.0	
PDF eigenvector 22	-0.0	-0.1	-0.1	+0.1	-0.3	-0.2	+0.0	+0.2	+0.0	+0.0	-0.0	+0.3	+0.1	-0.1	-0.1	+0.2	-0.4	-0.3	+0.1	+0.3	+0.1	+0.1	-0.0	
	+0.0	+0.1	+0.0	-0.1	+0.3	+0.2	-0.0	-0.2	-0.0	+0.0	+0.0	-0.2	-0.0	+0.1	+0.0	-0.1	+0.3	+0.2	-0.1	-0.3	-0.1	-0.0	+0.1	
PDF eigenvector 23	-0.1	+0.0	+0.1	-0.1	+0.3	+0.2	+0.1	+0.0	-0.1	-0.1	-0.1	-0.2	-0.2	-0.1	+0.1	-0.1	+0.5	+0.3	+0.2	-0.1	-0.2	-0.2	-0.1	
	+0.0	-0.0	-0.0	+0.0	-0.0	-0.0	-0.0	+0.0	-0.0	-0.0	+0.0	+0.2	-0.0	-0.0	-0.1	+0.0	-0.0	-0.1	-0.0	+0.1	-0.0	-0.0	+0.0	
PDF eigenvector 24	-0.0	-0.0	-0.0	+0.0	+0.1	+0.0	+0.0	+0.1	-0.1	-0.1	-0.0	+0.2	-0.1	-0.1	-0.1	+0.0	+0.1	+0.0	+0.1	-0.2	-0.1	-0.1	+0.0	
	-0.1	-0.1	+0.1	+0.1	-0.1	+0.0	+0.1	+0.1	+0.1	-0.0	-0.1	-0.1	-0.2	-0.2	-0.1	+0.1	-0.1	+0.2	+0.1	+0.0	-0.1	-0.2	-0.2	
PDF eigenvector 25	-0.1	-0.1	+0.1	+0.1	-0.0	+0.0	+0.1	+0.1	+0.0	-0.0	-0.1	-0.1	-0.2	-0.2	-0.1	+0.0	+0.1	+0.1	+0.2	+0.0	-0.0	-0.1	-0.2	
	-0.1	-0.1	-0.1	+0.0	+0.1	+0.1	+0.2	-0.2	-0.2	-0.1	-0.1	+0.4	-0.2	-0.2	-0.1	+0.1	+0.2	+0.1	+0.2	+0.3	-0.3	-0.2	-0.2	
PDF eigenvector 26	-0.0	+0.0	+0.0	-0.0	+0.0	+0.0	+0.0	+0.0	-0.0	-0.0	-0.0	-0.0	-0.0	-0.0	-0.0	+0.0	+0.1	+0.0	+0.0	-0.0	-0.0	-0.0	-0.0	
	-0.0	-0.0	-0.0	+0.0	+0.0	-0.0	+0.0	+0.0	-0.0	-0.0	-0.0	+0.0	+0.1	-0.0	-0.0	-0.0	+0.0	+0.0	+0.0	-0.0	-0.0	-0.0	-0.0	
PDF eigenvector 27	+0.1	+0.0	+0.2	+0.1	-0.1	+0.1	-0.2	+0.1	+0.1	+0.0	-0.3	+0.1	+0.0	+0.1	+0.1	-0.1	-0.1	-0.1	-0.2	+0.1	+0.1	-0.1	-0.1	
	-0.0	-0.0	-0.0	-0.0	-0.0	+0.0	-0.0	+0.0	-0.0	-0.0	+0.0	-0.0	+0.1	-0.0	-0.0	-0.0	-0.0	-0.0	+0.0	+0.0	-0.0	-0.0	-0.0	
PDF eigenvector 28	+0.0	+0.0	-0.0	-0.0	+0.0	+0.0	-0.0	-0.0	-0.0	-0.0	-0.0	-0.0	-0.0	-0.0	-0.0	-0.0	-0.0	-0.0	-0.0	-0.0	-0.0	-0.0	-0.0	
	-0.0	-0.0	-0.1	-0.0	-0.0	-0.0	-0.0	+0.1	-0.0	-0.0	-0.0	-0.0	-0.0	-0.0	-0.0	-0.0	-0.0	-0.0	-0.0	+0.1	+0.0	+0.0	+0.0	
α_s	+0.1	+0.0	+0.1	+0.0	-0.0	+0.0	-0.2	+0.0	-0.0	+0.0	-0.1	+0.0	+0.0	+0.1	+0.0	+0.0	+0.0	-0.2	+0.1	+0.0	+0.1	-0.0	-0.0	
	-0.1	-0.0	-0.1	-0.0	-0.0	+0.0	-0.0	+0.2	-0.0	-0.0	-0.0	+0.2	-0.0	-0.0	-0.1	-0.0	-0.0	+0.0	+0.2	-0.1	-0.0	-0.1	+0.0	
m_t	+1.8	-0.1	+0.6	-0.7	-0.8	-0.1	-0.4	-0.6	+0.2	+0.5	+0.0	+0.1	+1.0	+0.2	-1.2	-1.1	-0.6	+0.3	+0.5	+0.6	-0.1	-0.0	+0.3	
	+0.5	-1.9	-1.1	+0.8	+0.5	+1.0	+0.7	-0.4	-0.6	+0.1	-0.8	-0.3	-0.2	+1.2	-0.6	+0.1	-0.1	-0.1	+0.4	+0.8	+0.3	-0.7	+0.1	
$\mu_{r,f}$	+0.6	+0.2	+1.1	+0.5	-0.4	-0.5	+0.0	-1.3	-0.1	-0.5	-0.6	-2.2	+0.9	+0.2	+1.0	+0.8	-0.4	-0.4	-0.1	-0.8	+1.6	+1.1	+0.2	
	-0.7	-0.2	-1.2	-0.6	+0.5	+0.6	+0.1	+1.4	+0.3	+0.7	+1.2	+3.5	-1.0	-0.2	-1.1	-1.0	+0.4	+0.3	-0.1	+0.5	-2.1	-1.5	-1.7	
h_{damp}	+1.3	+0.6	-1.4	-0.5	-0.9	+0.4	-0.1	-0.4	+0.1	+1.8	-0.4	+1.8	+3.8	+3.5	+0.7	-2.1	-2.6	-1.1	+0.7	-0.4	+0.7	-2.3	-1.6	
	+2.5	-2.5	-3.5	-1.6	-1.1	+1.0	+0.8	-0.2	-2.1	-0.5	-2.2	-2.7	-2.3	+0.0	-0.6	-1.4	+0.2	+0.8	+3.6	+1.8	+3.3	-0.6	+2.4	
PS ISR	+0.5	-0.6	-0.9	+1.4	+0.9	+1.1	+1.3	+1.0	+1.1	+1.8	+1.0	-0.0	+3.7	-2.4	+0.8	-6.2	-2.1	-1.3	+0.4	+0.8	-0.6	-2.5	+0.2	
	+0.4	-1.7	-2.4	-1.6	-0.6	+0.5	+0.1	-0.5	-1.5	-1.3	-1.7	-1.0	+1.5	+1.0	-0.0	-1.7	+0.8	+0.2	+1.8	+2.3	+2.1	-0.4	+3.1	
PS FSR	-1.7	-4.5	-4.0	-2.5	-0.4	+0.5	+0.9	-0.5	-1.5	-0.9	-1.4	-0.3	+2.7	+2.6	+2.9	+1.3	+0.8	+1.4	+3.1	+1.9	+1.1	-0.1	+0.9	
	+4.4	+1.3	+1.6	+0.8	-0.5	-0.4	-0.1	-0.6	+0.7	+0.9	+0.1	-0.5	-0.9	+1.0	-0.9	-2.9	-1.0	-1.7	+0.1	-0.3	+0.2	-1.1	+0.4	
UE tune	+3.9	-1.7	-4.2	+0.2	-1.0	+1.2	+0.9	-0.5	+0.0	-0.2	-0.9	-1.8	+3.7	+3.3	+2.8	-2.9	-2.0	-1.6	+1.8	+1.8	+0.7	-1.0	+0.5	
	+2.8	-0.2	-2.9	-1.0	+0.2	+0.4	+1.1	-0.4	-0.6	+1.0	-1.5	+0.5	-0.7	+1.4	-3.2	-2.5	+0.2	+0.3	+0.1	+2.4	+0.2	-0.7	+1.2	
CR	+1.3	+0.5	+0.0	-0.7	-0.6	+0.1	-0.5	+0.1	+0.3	-1.2	-0.7	+2.6	+2.0	-1.5	-2.2	-0.3	-1.0	+0.3	+1.5	+0.9	-0.9	+0.8	+2.3	
	+3.0	+0.4	+1.0	+0.6	+0.0	+1.7	+1.8	+0.6	+0.6	+2.1	+0.2	+0.6	+2.6	+0.6	-2.3	-3.1	-2.8	-3.0	-2.1	-0.6	+0.1	-2.6	+0.7	
	+2.8	-1.9	-1.1	+0.0	+0.1	+0.5	+0.9	+0.6	-0.5	+1.7	-0.7	-0.1	+1.2	+0.6	-0.0	-1.6	-2.2	-1.5	-0.3	+0.1	+0.6	-0.3	+0.8	
$f(b \rightarrow B)$	+1.3	+0.8	+1.3	+0.6	+0.4	+0.2	+0.4	-0.5	+0.2	-0.4	-0.3	-1.0	+0.0	+0.8	+0.2	-0.3	+0.1	+0.2	+0.1	-0.8	-0.1	-0.4	-0.7	
	-0.6	-0.6	-0.7	-0.3	-0.2	+0.0	-0.0	+0.2	-0.1	+0.2	+0.1	+0.6	+0.0	-0.5	-0.3	-0.0	-0.2	-0.1	+0.0	+0.4	+0.1	+0.3	+0.4	
	+0.2	+0.2	+0.2	+0.1	+0.0	+0.0	-0.1	+0.0	-0.0	-0.2	-0.1	+0.1	-0.0	-0.1	+0.0	+0.0	+0.0	-0.2	+0.0	-0.1	-0.1	-0.1	-0.1	
	+1.5	+0.9	+1.2	+0.8	+0.3	+0.2	+0.3	-0.4	-0.1	-0.4	-0.5	-1.0	+1.2	+1.2	+1.0	+0.6	+0.1	+0.0	-0.5	-0.5	-0.8	-1.1	-1.0	
BR($B \rightarrow \mu$)	-0.2	-0.2	-0.2	-0.2	+0.1	+0.1	+0.2	+0.0	+0.1	+0.1	+0.1	-0.4	-0.4	-0.2	-0.1	+0.2	+0.0	+0.1	+0.0	+0.0	+0.1	+0.0	+0.0	
	+0.4	+0.4	+0.4	+0.2	-0.1	-0.2	-0.2	-0.1	-0.1	-0.1	-0.2	+0.6	+0.5	+0.4	+0.2	-0.1	-0.2	-0.1	-0.1	-0.1	-0.0	-0.1	-0.1	

Table 115: The measured $[N_{\text{jet}}^{0,1+}, M(\bar{t}t), y(\bar{t}t)]$ cross sections, along with their relative statistical and systematic uncertainties, and NP corrections (see Section 8).

N_{jet}	$M(\bar{t}t)$ [GeV]	$y(\bar{t}t)$	$\frac{1}{\sigma(\bar{t}t)} \frac{d\sigma}{dy(\bar{t}t)}$	stat. [%]	syst. [%]	\mathcal{C}_{NP}	bin
0	300–400	0.00–0.35	8.235×10^{-2}	4.2	$+12.1$ -8.0	0.973	1
0	300–400	0.35–0.75	8.580×10^{-2}	3.3	$+6.6$ -10.7	0.974	2
0	300–400	0.75–1.15	7.629×10^{-2}	3.7	$+6.0$ -12.6	0.973	3
0	300–400	1.15–2.50	3.578×10^{-2}	3.5	$+6.9$ -8.2	0.975	4
0	400–500	0.00–0.35	1.361×10^{-1}	2.5	$+1.8$ -3.1	0.971	5
0	400–500	0.35–0.75	1.231×10^{-1}	2.2	$+5.2$ -1.8	0.971	6
0	400–500	0.75–1.15	1.030×10^{-1}	2.6	$+5.3$ -1.5	0.972	7
0	400–500	1.15–2.50	4.724×10^{-2}	2.0	$+4.2$ -3.0	0.974	8
0	500–1500	0.00–0.35	1.598×10^{-1}	1.7	$+2.6$ -4.2	0.976	9
0	500–1500	0.35–0.75	1.402×10^{-1}	1.9	$+4.9$ -2.6	0.978	10
0	500–1500	0.75–1.15	1.102×10^{-1}	2.3	$+2.7$ -4.5	0.977	11
0	500–1500	1.15–2.50	3.225×10^{-2}	3.3	$+5.5$ -6.4	0.982	12
1	300–400	0.00–0.35	4.219×10^{-2}	7.0	$+13.9$ -6.0	1.031	13
1	300–400	0.35–0.75	4.211×10^{-2}	5.9	$+11.9$ -5.3	1.031	14
1	300–400	0.75–1.15	3.709×10^{-2}	6.5	$+5.1$ -13.3	1.035	15
1	300–400	1.15–2.50	1.619×10^{-2}	5.7	$+9.1$ -14.9	1.034	16
1	400–500	0.00–0.35	7.864×10^{-2}	3.7	$+2.8$ -9.7	1.036	17
1	400–500	0.35–0.75	7.203×10^{-2}	3.2	$+2.5$ -7.0	1.033	18
1	400–500	0.75–1.15	5.572×10^{-2}	4.1	$+6.0$ -3.7	1.034	19
1	400–500	1.15–2.50	2.186×10^{-2}	3.6	$+10.8$ -2.8	1.034	20
1	500–1500	0.00–0.35	1.003×10^{-1}	2.5	$+7.8$ -2.7	1.029	21
1	500–1500	0.35–0.75	8.991×10^{-2}	2.5	$+1.9$ -8.1	1.032	22
1	500–1500	0.75–1.15	6.298×10^{-2}	3.5	$+8.0$ -3.2	1.033	23
1	500–1500	1.15–2.50	1.796×10^{-2}	4.7	$+10.8$ -8.7	1.027	24
≥ 2	300–400	0.00–0.35	2.241×10^{-2}	13.4	$+24.6$ -8.9	1.037	25
≥ 2	300–400	0.35–0.75	2.132×10^{-2}	12.2	$+14.6$ -12.7	1.031	26
≥ 2	300–400	0.75–1.15	1.872×10^{-2}	12.8	$+27.3$ -6.2	1.035	27
≥ 2	300–400	1.15–2.50	8.949×10^{-3}	10.0	$+11.2$ -20.8	1.045	28
≥ 2	400–500	0.00–0.35	4.412×10^{-2}	6.7	$+8.1$ -12.6	1.036	29
≥ 2	400–500	0.35–0.75	3.703×10^{-2}	6.5	$+7.9$ -14.4	1.035	30
≥ 2	400–500	0.75–1.15	2.985×10^{-2}	8.1	$+12.6$ -10.9	1.040	31
≥ 2	400–500	1.15–2.50	1.069×10^{-2}	8.1	$+10.3$ -15.6	1.044	32
≥ 2	500–1500	0.00–0.35	5.843×10^{-2}	3.2	$+8.0$ -7.5	1.017	33
≥ 2	500–1500	0.35–0.75	4.772×10^{-2}	4.3	$+9.0$ -9.1	1.013	34
≥ 2	500–1500	0.75–1.15	3.761×10^{-2}	4.9	$+9.7$ -8.6	1.012	35
≥ 2	500–1500	1.15–2.50	9.239×10^{-3}	7.0	$+10.9$ -8.1	1.014	36

Table 116: The correlation matrix of statistical uncertainties for the measured $[N_{\text{jet}}^{0,1+}, M(\bar{t}\bar{t}), y(\bar{t}\bar{t})]$ cross sections. The values are expressed as percentages. For bin indices see Table 115.

bin	2	3	4	5	6	7	8	9	10	11	12	13	14	15	16	17	18	19	20	21	22	23	24	25	26	27	28	29	30	31	32	33	34	35	36
1	-14	-18	+1	-33	-22	+6	+2	-8	+5	+1	-5	-5	-10	+1	+0	-14	+1	+7	-2	+6	+1	-3	-2	-10	+3	+2	-1	+9	+3	-3	-1	-3	-3	-0	+1
2	+20	-23	-20	-6	-28	-6	+7	-12	+1	+4	-10	+6	-9	-1	+2	-10	-7	+6	+2	+2	+5	-1	+4	-11	-1	+2	+2	+4	+6	-2	-3	+0	-2	-2	
3	+2	+5	-28	-14	-25	+1	+0	-11	-1	+1	-9	+4	-13	+6	-9	-12	-10	-3	+4	+5	+5	+2	-2	-9	+0	-3	+5	+6	+5	-0	-2	-2	-4		
4	-1	-4	-22	+3	-9	-1	-2	-29	-1	-1	-11	+7	-4	+4	-7	-24	-5	-6	+2	-1	-2	+1	+1	-17	-2	-4	+3	+6	-2	-3	-5	+3			
5	+5	-9	-5	-16	-10	+2	-1	-20	-2	+6	-3	+5	-5	-0	-1	-5	+2	+2	-1	+10	+3	-2	-1	-12	-1	+1	+1	+5	+1	-1	-1				
6	+24	-13	-10	-3	-14	-3	-2	-14	-11	+4	-5	+10	-3	-1	+2	-5	-1	+1	+4	+3	+6	-1	-1	-10	-2	+1	+2	+2	+3	-1					
7	+13	+3	-12	-6	-10	+7	-11	-16	-12	-1	-2	+10	-3	+2	-0	-6	-3	-3	+6	+6	+5	+1	-3	-10	-2	-1	+2	+3	+2						
8	-4	-4	-14	+3	-2	+6	-13	-28	-3	-2	-1	+12	-4	-1	-2	-16	-2	-1	+5	+2	-0	-1	-3	-11	-2	-3	+1	+3							
9	-19	-6	-1	+8	+3	-2	-4	-11	-1	+3	-1	-21	-6	+5	-1	-0	-2	+0	+0	+4	+2	+0	-0	-3	+4	-1	-1								
10	-3	-12	+3	+2	+5	-3	-0	-9	-3	+1	-5	-9	-13	+3	-2	+1	-1	-2	+2	+1	+3	+0	+4	-7	+4	-0									
11	-7	-2	+6	+4	+2	+2	-4	-9	-5	+5	-11	-12	-12	-1	-1	+0	-2	-0	+2	+2	+3	-1	+4	-6	+3										
12	-2	-1	+5	-6	-1	+1	-2	-19	-3	+3	-8	-16	+1	-2	-2	+6	-1	-1	+1	-0	-2	-2	+3	-10											
13	-10	-13	+3	-30	-22	+5	+3	-8	+4	+2	-1	-6	-7	+3	+0	-6	+6	+4	-2	+7	+1	-3	+1												
14	+16	-17	-21	-4	-25	-0	+4	-10	+0	+4	-8	+3	-9	+1	+6	-9	-1	+6	+1	+3	+4	+4	-4												
15	+7	+4	-26	-11	-19	+2	+1	-10	+0	+3	-9	-1	-6	+4	-1	-7	-0	-3	+5	+5	+4														
16	+2	-1	-18	+4	-3	+1	-0	-21	-0	+1	-6	+5	-3	+5	-0	-21	-1	-4	+2	+9															
17	+5	-7	+0	-12	-9	+2	+1	-16	+3	+4	-2	+4	-4	-1	+1	-2	+3	+1	-1																
18	+22	-9	-10	-1	-11	+1	+3	-13	-4	+5	-4	+7	-2	-2	+4	-5	+2	+1																	
19	+11	+3	-10	-5	-9	+6	-4	-12	-2	-1	-2	+6	-1	+2	+1	-3	+1																		
20	+1	+1	-10	-0	-3	+7	-1	-27	+0	-2	-1	+15	-1	+1	+3	-10																			
21	-20	-5	+2	+7	+1	-3	-0	-7	+1	+2	+0	-20	-2	+5	-2																				
22	-5	-8	+2	+3	+4	-2	+1	-7	-1	+2	+0	-11	-7	+3																					
23	-7	-3	+5	+4	+3	+2	-0	-7	-1	+5	-5	-13	-6																						
24	-0	-2	+4	+5	-0	+1	+0	-12	-1	+4	-2	-16																							
25	-24	-7	+3	-60	-17	+15	-1	+4	+9	-2	-2																								
26	-4	-9	-13	-29	-32	+12	+9	-6	+9	-1																									
27	-8	+12	-30	-40	-19	-3	+10	-3	+10																										
28	-1	+12	-18	-50	-1	-2	+9	-10																											
29	-2	-7	+0	-28	-8	+5	+0																												
30	+11	-9	-8	-17	-13	+4																													
31	+8	+5	-14	-20	-10																														
32	-0	+4	-9	-27																															
33	-35	+4	+1																																
34	-25	+0																																	
35	-24																																		

Table 117: Sources and values of the relative systematic uncertainties in percent of the measured [$N_{\text{jet}}^{0,1+}, M(\text{t}\bar{\text{t}}), \gamma(\text{t}\bar{\text{t}})$] cross sections. For bin indices see Table 115.

source / bin	1	2	3	4	5	6	7	8	9	10	11	12	13	14	15	16	17	18	19	20	21	22	23	24	25	26	27	28	29	30	31	32	33	34	35	36
JER	+0.2	+0.6	+0.3	+0.6	+0.0	+0.5	+0.4	+0.8	-0.0	+0.3	+0.2	+0.9	-0.8	+0.9	+0.3	-0.6	-0.5	-0.2	+0.8	-0.6	-0.0	+0.1	+0.1	-2.9	+0.3	-0.2	-0.5	-1.1	-0.2	-2.3	-0.9	-1.4	-1.3	+0.3		
JES	-0.3	-1.1	-1.9	-0.6	-0.6	+0.2	-0.1	+0.2	-0.2	-0.2	+0.0	+0.2	+0.3	-0.2	-0.0	-0.5	-0.3	-0.1	+0.7	+0.6	+0.3	+0.1	+0.7	+2.4	-1.3	+0.5	+1.1	+1.5	-0.3	+2.0	+1.8	+0.3	+1.2	-0.4	-0.3	
JESAbsoluteMPFBias	+0.7	+0.4	-0.1	+0.5	-0.1	+0.3	+0.3	+0.4	+0.1	-0.1	-0.05	+1.4	+1.3	-0.0	+0.4	-0.4	-0.4	-0.5	+0.5	+0.1	-0.1	+0.2	-1.0	+1.1	-0.6	+1.4	-0.3	-0.7	-0.5	-1.8	-1.0	-0.8	-0.8	-0.6		
JESAbsoluteScale	-0.7	-0.8	-1.4	-0.3	-0.0	+0.2	+0.1	+0.2	-0.2	+0.2	+0.1	-0.3	-0.7	-0.2	-1.4	-0.0	-0.0	+0.3	+0.2	+0.8	+0.1	+0.4	+0.3	-0.1	-1.7	+1.3	-0.5	+1.2	+1.1	+0.4	+0.8	+0.1	+0.4	+0.3		
JESAbsoluteStat	+0.5	+0.0	-0.1	+0.5	-0.2	+0.3	+0.2	+0.3	+0.0	-0.1	+0.2	+0.1	+0.8	+0.9	-0.3	+0.8	-0.3	-0.4	-0.4	+0.6	-0.1	-0.4	+0.2	-1.5	-0.2	+0.3	+0.9	-1.2	+0.1	-0.5	-0.7	+0.0	-0.6	-0.2	-1.0	-0.6
JESAbsoluteSyst	-0.7	-0.7	-1.1	-0.5	-0.1	-0.0	+0.2	+0.1	-0.1	+0.1	+0.2	+0.0	-0.4	-0.4	-0.5	+0.3	+0.2	+0.1	+0.3	+1.2	+0.5	-0.0	+0.2	+0.4	-0.1	-1.1	+2.7	+0.4	+0.8	+0.4	-1.4	-2.1	-0.2	+1.3	-0.3	+0.9
JESFrag	+0.3	+0.9	-1.1	-0.4	-0.4	+0.0	-0.2	+0.4	+0.1	+0.1	+0.6	+0.4	+1.1	+0.8	-0.6	+1.3	-0.5	-0.5	-0.4	+0.6	+0.2	+0.2	+0.7	-2.2	-0.2	+1.8	+1.7	+0.8	-1.0	-1.1	-1.5	-3.7	-0.1	+0.9	-0.8	+0.7
JESFrag	-1.0	-0.3	-0.4	-0.3	+0.1	+0.4	+0.2	-0.4	-0.3	-0.5	+0.3	-0.4	-0.3	-1.2	+2.4	-0.1	+0.2	+0.6	+1.4	+0.1	-0.0	+0.1	-0.4	+2.9	-2.7	+2.2	+0.4	-0.2	+0.6	-0.1	-2.1	-0.6	+0.7	-0.7	-0.1	
JESFavourQCD	+2.9	+2.6	+1.2	+1.4	-0.2	+0.6	+0.1	+0.7	+0.8	+1.0	+0.9	+0.7	+2.3	+1.1	-0.1	+0.4	-1.7	-1.0	-0.9	-0.1	-0.0	-0.3	-0.7	-1.6	+2.8	-0.2	-1.0	-5.7	-4.8	-5.1	-1.1	-2.4	-2.5	-2.2	-2.2	-2.4
JESFavourQCD	-3.0	-3.4	-3.1	-1.8	+0.0	-0.1	-0.1	-0.3	-1.2	-0.6	-0.5	-0.3	-1.9	-0.5	-0.9	-1.2	+1.1	+1.0	+1.4	+2.1	+1.1	+0.1	+0.5	+0.3	+2.8	+1.9	+1.6	+1.7	+2.4	+2.3	+3.5	+3.8	+1.8	+3.5	+1.6	
JESFrag	+0.1	-0.2	-0.2	+0.2	+0.1	+0.4	+0.5	+0.4	+0.2	+0.2	-0.2	-0.4	+0.7	+0.8	+0.1	-0.2	-0.6	-0.4	-0.4	+0.7	+0.3	+0.4	+0.3	-1.1	+0.1	-0.4	+0.8	-0.5	-0.2	-1.3	-0.9	-0.2	-0.7	-0.2	+0.3	+0.4
JESFrag	-0.4	-0.6	-1.1	-0.2	-0.0	-0.0	-0.0	-0.1	-0.3	-0.2	-0.2	-0.3	-0.1	-0.1	-0.1	+0.3	+0.1	+0.1	+0.3	+1.4	+0.3	-0.1	+0.1	+0.3	+1.1	-0.5	+3.1	-0.1	+0.5	+0.9	-1.6	+0.0	-0.1	+0.6	-0.0	+0.4
JESProfileUpDataMC	+0.5	+0.0	-0.5	-0.0	-0.1	+0.4	+0.4	+0.7	+0.2	+0.2	+0.1	+0.5	+0.4	+0.5	+0.1	-0.7	-0.5	-0.3	-0.1	-0.3	+0.3	+0.1	+1.0	-1.1	-0.5	-1.1	-0.2	+0.4	-0.4	-1.0	-0.2	-1.4	-0.5	-0.8	-0.9	-0.9
JESProfileUpPtBB	-0.5	-0.9	-1.0	-0.5	+0.1	+0.1	+0.1	-0.1	-0.2	-0.4	-0.3	-0.6	+0.0	+0.3	+0.4	-0.1	+0.4	+0.1	+0.4	+1.4	-0.0	-0.0	+0.5	+0.3	+12	+0.3	+2.3	+0.3	+0.7	+0.9	-0.9	-1.1	-0.9	+0.9		
JESProfileUpPtBB	-0.2	-0.4	-0.4	-0.1	+0.0	-0.1	-0.3	+0.0	-0.3	-0.2	-0.2	-0.1	-0.1	-0.2	-0.2	-0.1	-0.2	-0.2	-0.2	-0.1	-0.4	-0.1	-0.1	+1.7	+0.8	+1.0	-0.1	+0.5	+0.6	-0.0	+1.9	-0.1	+1.0	-0.5	-0.3	
JESProfileUpPtEC1	-0.2	-0.4	-0.4	-0.1	+0.0	-0.1	-0.3	+0.0	-0.3	-0.2	-0.2	-0.1	-0.2	-0.2	-0.2	-0.1	-0.2	-0.2	-0.2	-0.1	-0.2	-0.1	-0.1	-0.1	-0.1	-0.4	+1.2	-5.9	-0.8	-1.9	-0.7	-2.1	-0.9	-0.5	-0.6	-0.8
JESProfileUpPtEC2	+0.0	+0.0	+0.0	+0.0	+0.0	+0.0	+0.0	+0.0	+0.0	+0.0	+0.0	+0.0	+0.0	+0.0	+0.0	+0.0	+0.0	+0.0	+0.0	+0.0	+0.0	+0.0	+0.0	+0.0	+0.0	+0.0	+0.0	+0.0	+0.0	+0.0	+0.0	+0.0	+0.0	+0.0	+0.0	
JESProfileUpPtHF	+0.0	+0.0	+0.0	+0.0	+0.0	+0.0	+0.0	+0.0	+0.0	+0.0	+0.0	+0.0	+0.0	+0.0	+0.0	+0.0	+0.0	+0.0	+0.0	+0.0	+0.0	+0.0	+0.0	+0.0	+0.0	+0.0	+0.0	+0.0	+0.0	+0.0	+0.0	+0.0	+0.0	+0.0	+0.0	
JESProfileUpPtHF	+0.0	+0.0	+0.0	+0.0	+0.0	+0.0	+0.0	+0.0	+0.0	+0.0	+0.0	+0.0	+0.0	+0.0	+0.0	+0.0	+0.0	+0.0	+0.0	+0.0	+0.0	+0.0	+0.0	+0.0	+0.0	+0.0	+0.0	+0.0	+0.0	+0.0	+0.0	+0.0	+0.0	+0.0	+0.0	
JESProfileUpPtRef	+0.1	-0.1	-0.3	+0.3	+0.2	+0.5	+0.1	+0.5	+0.5	+0.1	+0.3	-0.3	-0.6	-0.9	-0.4	-0.1	-0.2	-0.4	+0.2	+0.5	+0.7	-0.7	-1.1	-1.2	-1.2	-0.9	-0.8	+0.5	-0.8	-0.1	-1.2	-0.4	-0.6			
JESRelativeBal	-0.2	-0.6	-1.0	-0.0	-0.2	+0.1	-0.2	-0.3	-0.6	-0.4	-0.7	+0.1	+0.7	+0.8	+2.3	+0.1	-0.0	+0.9	+0.1	-0.1	-0.6	+1.3	+1.1	+1.7	+1.4	+1.0	-0.6	+0.2	+0.6	-0.4	-0.6	-0.8				
JESRelativeBal	+1.9	+2.2	+1.5	+1.6	-0.1	+0.3	-0.2	+0.0	+0.3	+0.4	+0.2	-1.1	+1.6	+1.4	+0.7	+0.1	-0.7	-0.5	-0.6	-0.2	+0.2	-0.5	-0.8	+2.5	-0.7	+1.5	-4.7	-1.9	-2.5	-0.9	-0.8	-1.8	-1.8	-1.7		
JESRelativeBal	-2.6	-2.7	-2.8	-1.7	-0.1	-0.2	+0.2	+0.7	-0.7	-0.4	-0.1	-0.8	-0.1	-0.6	-1.7	+0.2	-0.0	+1.1	+2.0	+0.9	+0.2	+1.5	+0.9	+0.2	+0.7	+1.4	+1.4	+1.3	+1.1	+1.2	+1.4	+1.4	+1.2	+1.4		
JESRelativeFSR	-0.6	-0.9	-0.7	-0.1	+0.2	+0.2	-0.2	-0.2	-0.2	-0.2	-0.2	-0.5	-0.8	-0.5	-0.7	-0.8	-0.5	-0.1	-0.5	-0.1	-0.5	-0.1	-0.1	-0.4	-0.4	-0.9	+0.5	+0.7	+0.8	-0.7	+0.8	-0.5	-0.5	-0.5		
JESRelativeFSR	+0.2	+0.5	+0.2	+0.0	+0.1	+0.2	+0.1	+0.2	-0.1	+0.3	+0.0	+1.0	+0.8	+0.1	+0.7	-0.8	-0.5	-0.1	+0.9	+0.3	-0.0	-0.0	-0.9	-0.2	-0.1	-0.6	-0.5	-1.5	-0.9	-0.6	-0.4	-0.9	-1.0			
JESRelativeJEREC1	-0.0	+0.0	-0.2	-0.0	+0.1	-0.0	+0.0	+0.1	-0.0	-0.0	+0.2	-0.4	+0.1	-0.1	-0.1	-0.2	+0.4	+0.0	+0.1	+0.2	+0.1	+0.3	+0.2	-0.0	+0.1	+1.8	+1.0	-1.0	+2.1	-0.1	-0.6	-0.2	+0.1			
JESRelativeJEREC1	-0.0	+0.0	-0.7	-0.1	+0.0	+0.0	-0.1	+0.2	-0.0	-0.2	-0.3	-0.6	-0.1	-0.1	-0.2	-0.3	-0.0	-0.1	-0.2	-0.1	-0.1	-0.1	-0.1	-0.1	-0.1	-0.1	-0.8	-3.1	-0.2	+0.6	-0.2	+0.1				

Table 118: Table 117 continued.

source / bin	1	2	3	4	5	6	7	8	9	10	11	12	13	14	15	16	17	18	19	20	21	22	23	24	25	26	27	28	29	30	31	32	33	34	35	36
JESrelativeJERFC2	+0.0	+0.0	+0.0	+0.0	+0.0	+0.0	+0.0	+0.0	+0.0	+0.0	+0.0	+0.0	+0.0	+0.0	+0.0	+0.0	+0.0	+0.0	+0.0	+0.0	+0.0	+0.0	+0.0	+0.0	+0.0	+0.0	+0.0	+0.0	+0.0	+0.0	+0.0	+0.0	+0.0	+0.0	+0.0	+0.0
JESrelativeJERHF	+0.0	+0.0	+0.0	+0.0	+0.0	+0.0	+0.0	+0.0	+0.0	+0.0	+0.0	+0.0	+0.0	+0.0	+0.0	+0.0	+0.0	+0.0	+0.0	+0.0	+0.0	+0.0	+0.0	+0.0	+0.0	+0.0	+0.0	+0.0	+0.0	+0.0	+0.0	+0.0	+0.0	+0.0	+0.0	+0.0
JESrelativePtBB	+0.2	+0.2	+0.2	-0.2	-0.1	+0.2	+0.2	+0.1	+0.1	+0.1	-0.2	+0.6	+0.2	+0.1	-0.5	-0.3	-0.2	-0.4	+0.1	+0.0	-0.3	+0.4	+0.7	+0.9	+0.1	+1.0	+0.3	-1.0	-0.4	-1.0	-0.6	-0.6	+0.9	-1.2	-0.4	
JESrelativePtFC1	-0.5	-1.5	-0.8	+0.2	+0.3	+0.4	+0.4	-0.0	-0.1	+0.0	+0.0	-0.4	+1.0	+0.4	-1.1	+0.4	-0.0	-0.1	-0.1	+0.5	-0.1	+0.2	+0.1	-0.7	-0.3	-0.1	-0.8	+0.9	+0.2	+0.4	+0.7	-0.3	+0.6	-0.3	-0.1	
JESrelativePtFC2	+0.0	+1.1	+0.2	+0.3	+0.3	+0.4	+0.0	-0.0	+0.3	+0.2	+0.2	-0.1	+0.3	+1.1	-0.1	+1.0	+0.2	-0.0	-0.2	-0.1	-0.1	+0.1	-0.2	-2.3	+0.3	-0.3	+1.6	-4.6	-0.0	-1.1	-0.6	+0.5	-0.5	-0.5	-1.5	
JESrelativePtHF	-0.6	-0.8	-1.0	-0.4	-0.4	+0.1	+0.7	-0.3	-0.4	-0.1	+0.7	-0.2	-0.9	-1.8	-0.3	-0.2	+0.2	+0.6	+0.8	+0.3	+0.2	+0.6	+0.5	+1.1	-0.8	+1.0	+1.6	-0.2	+0.1	-0.1	-0.1	+0.3	+0.9	+0.1	+0.9	
JESrelativeStatEC	+0.0	+0.0	+0.0	+0.0	+0.0	+0.0	+0.0	+0.0	+0.0	+0.0	+0.0	+0.0	+0.0	+0.0	+0.0	+0.0	+0.0	+0.0	+0.0	+0.0	+0.0	+0.0	+0.0	+0.0	+0.0	+0.0	+0.0	+0.0	+0.0	+0.0	+0.0	+0.0	+0.0	+0.0	+0.0	
JESrelativeStatHF	-0.1	-0.4	-1.0	-0.0	-0.0	+0.0	+0.3	-0.1	-0.1	+0.0	+0.0	+0.1	-0.0	-0.3	-0.8	-0.2	-0.1	+0.1	+1.3	+0.2	-0.1	+0.2	+1.3	+0.7	-0.2	+0.0	-0.3	+0.2	-0.7	-1.5	-0.3	+0.5	-0.0	-0.5		
JESrelativeStatFSR	-0.0	+0.1	-0.2	+0.1	-0.2	+0.0	+0.2	+0.2	-0.2	+0.2	-0.1	+0.5	+0.1	-0.5	+0.0	+0.0	-0.1	-0.0	-0.2	+0.3	+0.0	+0.3	-0.5	-1.0	+1.0	-0.1	+0.4	+0.3	-1.1	+0.4	-0.3	-0.1	-0.8	-0.3		
JESSinglePionFCAL	+0.0	+0.3	-0.1	+0.1	+0.0	+0.2	+0.3	+0.2	-0.1	+0.2	-0.5	+0.1	+0.4	-0.1	+1.0	-0.0	+0.1	-0.2	+0.6	+0.1	-0.1	+0.2	-1.3	-0.1	-0.4	+1.9	+0.4	+0.1	-0.1	-1.5	-3.0	-0.4	+0.2	-0.6	+0.2	
JESSinglePionHCAL	+0.3	-0.0	+0.1	+0.3	-0.0	+0.5	+0.4	+0.6	+0.5	+0.1	-0.3	+0.3	+0.5	-0.4	-0.7	-0.2	-0.1	-0.0	-0.1	-0.0	-0.2	+0.3	+0.0	-0.5	-1.0	+1.0	-0.1	+0.4	+0.3	-1.1	+0.4	-0.3	-0.1	-0.8	-0.3	
JESTimePTEta	-0.1	-0.1	-0.4	-0.1	-0.2	-0.0	+0.3	+0.0	+0.3	-0.1	+0.1	+0.0	+0.3	-0.2	-0.0	-0.3	-0.1	-0.0	-0.2	-0.0	+0.1	+0.3	-1.0	-0.3	+1.0	+1.0	+1.2	+0.7	-1.6	-0.6	-0.5	+0.0	-0.3	+0.4		
E_T^{miss}	-0.2	+0.2	-0.0	+0.0	-0.0	+0.3	-0.1	-0.1	+0.1	-0.2	+0.0	+0.2	+0.8	+0.2	-0.5	+1.0	-0.1	+0.0	+0.1	+0.8	-0.0	+0.3	+0.3	-1.4	-0.2	+2.5	-0.4	+0.4	-0.5	+0.1	-1.6	-0.1	-0.6	-1.1		
lepton ID/ISO	-0.2	-0.1	-0.5	-0.2	+0.1	+0.3	+0.2	+0.6	-0.1	-0.0	-0.2	-0.6	-0.1	-0.1	-0.3	+0.2	+0.3	+0.5	-0.1	-0.1	-0.2	-0.7	+0.1	-0.2	-0.7	+0.1	-0.4	-0.5	-0.1	-0.9	-0.2	-0.1	-0.9			
pileup	+0.6	-0.3	-0.5	-0.1	+0.2	+0.3	+0.1	+0.3	+0.3	+0.2	+0.2	-0.5	-0.3	-0.5	+0.2	-0.1	-0.2	+0.1	-0.2	-0.1	-0.1	-0.4	+1.7	+0.4	-2.1	+0.9	-0.9	-0.9	+0.8	+0.2	-0.6	+0.2	-0.7			
trigger	-0.7	+0.2	+0.6	+0.5	-0.1	-0.2	-0.3	-0.1	-0.3	-0.2	-0.1	+0.4	-0.1	-0.6	+0.3	-0.2	+0.1	+0.3	-0.1	+0.2	+0.0	-0.2	+0.1	+0.8	-1.8	-0.2	+2.4	-1.0	+0.8	+0.7	-0.9	-0.1	+0.5	-0.1	+0.7	
	+0.1	+0.2	+0.1	-0.3	+0.2	+0.1	+0.0	-0.1	+0.1	-0.2	+0.1	+0.2	-0.4	+0.2	+0.1	+0.0	-0.2	+0.1	+0.0	-0.1	+0.2	+0.1	+0.0	-0.1	+0.2	+0.1	+0.0	-0.1	-0.2	+0.2	+0.1	+0.0	-0.1	-0.2		

Table 119: Table 117 continued.

Table 120: Table 117 continued.

Table 121: Table 117 continued.

L Change Logs

- 1588 • v1
- 1589 • v2
 - 1590 • All plots in Sections about kinematic reconstruction and scale factors /
1591 systematic uncertainties are currently from 1D note: need to be checked
1592 and updated if needed.
- 1593 • v3,v4
 - 1594 • Added results.
- 1595 • v5
 - 1596 • Extended PDF fit section.
- 1597 • v5,v6
 - 1598 • Extended results and PDF fit sections.
- 1599 • v7
 - 1600 • Addressed first comments from Top Cross Section group
 - 1601 • Some other analysis details added
- 1602 • v8
 - 1603 • Major update: analysis extended to fit also m_t^{pole} from measured cross
1604 sections, required new loose kinematic reconstruciton and number of ad-
1605 dditional plots and text in data interpretation part
 - 1606 • Also some analysis updates: new JER scale factors, slight tuning of un-
1607 folding etc.
- 1608 • v10
 - 1609 • Added remark on resummation effects on mt extraction.
- 1610 • v12
 - 1611 • After preapproval: improved description of extra jets definition, more NP
1612 correction uncertainties, some other minor changes
- 1613 • v13
 - 1614 • Addressed first set of comments from ARC:
 - 1615 • Added details on kinematic reconstruciton (more resolution
1616 plots and estimation of event fractions with correct input b jets)
 - 1617 • Added unnormalised data to NLO comparison
- 1618 • v14
 - 1619 • Further addressing ARC comments:
 - 1620 • Added uncertainty bands for Powheg+Pythia predictions
 - 1621 • Added $p_T(t)$ reweighting cross check
 - 1622 • Added comparison data vs fitted NLO
 - 1623 • Some further minor corrections
- 1624 • v15
 - 1625 • Added description of perfomance studies of full kinematic reconstruction
1626 related to minimum $M(t\bar{t})$ choice
- 1627 • v16
 - 1628 • Added comparison of NLO vs NLO+PS predictions

-
- 1629 • v17
- 1630 • Updated NLO fits (improved precision)
- 1631 • Updated figure cosmetics
- 1632 • Included cross check using ratio cross sections calculated in each $M(t\bar{t})$,
- 1633 $y(t\bar{t})$ bin
- 1634 • Included tables with measured cross sections
- 1635 • v18
- 1636 • Study of NNLO/NLO correction to $M(t\bar{t})$
- 1637 • Study of uncorrelated scale variations in different N_{jet} bins
- 1638 • More plots for unnormalised theory prediction (NLO/LO)
- 1639 • Minor corrections (typos etc.)

DRAFT

References

- [1] M. Czakon, M. L. Mangano, A. Mitov, and J. Rojo, "Constraints on the gluon PDF from top quark pair production at hadron colliders", *JHEP* **07** (2013) 167, doi:10.1007/JHEP07(2013)167, arXiv:1303.7215.
- [2] M. Guzzi, K. Lipka, and S. Moch, "Top-quark pair production at hadron colliders: differential cross section and phenomenological applications with DIFFTOP", *JHEP* **01** (2015) 082, doi:10.1007/JHEP01(2015)082, arXiv:1406.0386.
- [3] M. Czakon et al., "Pinning down the large-x gluon with NNLO top-quark pair differential distributions", *JHEP* **04** (2017) 044, doi:10.1007/JHEP04(2017)044, arXiv:1611.08609.
- [4] S. Alioli et al., "A new observable to measure the top-quark mass at hadron colliders", *Eur. Phys. J.* **C73** (2013) 2438, doi:10.1140/epjc/s10052-013-2438-2, arXiv:1303.6415.
- [5] CDF Collaboration, "First measurement of the $t\bar{t}$ differential cross section $d\sigma/dM_{t\bar{t}}$ in $p\bar{p}$ collisions at $\sqrt{s} = 1.96$ TeV", *Phys. Rev. Lett.* **102** (2009) 222003, doi:10.1103/PhysRevLett.102.222003, arXiv:0903.2850.
- [6] D0 Collaboration, "Measurement of differential $t\bar{t}$ production cross sections in $p\bar{p}$ collisions", *Phys. Rev. D* **90** (2014) 092006, doi:10.1103/PhysRevD.90.092006, arXiv:1401.5785.
- [7] ATLAS Collaboration, "Measurements of top quark pair relative differential cross-sections with ATLAS in pp collisions at $\sqrt{s} = 7$ TeV", *Eur. Phys. J. C* **73** (2013) 2261, doi:10.1140/epjc/s10052-012-2261-1, arXiv:1207.5644.
- [8] CMS Collaboration, "Measurement of differential top-quark pair production cross sections in pp collisions at $\sqrt{s} = 7$ TeV", *Eur. Phys. J. C* **73** (2013) 2339, doi:10.1140/epjc/s10052-013-2339-4, arXiv:1211.2220.
- [9] ATLAS Collaboration, "Measurements of normalized differential cross-sections for $t\bar{t}$ production in pp collisions at $\sqrt{s} = 7$ TeV using the ATLAS detector", *Phys. Rev. D* **90** (2014) 072004, doi:10.1103/PhysRevD.90.072004, arXiv:1407.0371.
- [10] ATLAS Collaboration, "Measurement of top quark pair differential cross-sections in the dilepton channel in pp collisions at $\sqrt{s} = 7$ and 8 TeV with ATLAS", *Phys. Rev. D* **94** (2016) 092003, doi:10.1103/PhysRevD.94.092003, arXiv:1607.07281.
- [11] CMS Collaboration, "Measurement of the differential cross section for top quark pair production in pp collisions at $\sqrt{s} = 8$ TeV", *Eur. Phys. J. C* **75** (2015) 542, doi:10.1140/epjc/s10052-015-3709-x, arXiv:1505.04480.
- [12] ATLAS Collaboration, "Measurements of top-quark pair differential cross-sections in the lepton+jets channel in pp collisions at $\sqrt{s} = 8$ TeV using the ATLAS detector", *Eur. Phys. J. C* **76** (2016) 538, doi:10.1140/epjc/s10052-016-4366-4, arXiv:1511.04716.
- [13] CMS Collaboration, "Measurement of differential cross sections for top quark pair production using the lepton+jets final state in proton-proton collisions at 13 TeV", (2016). arXiv:1610.04191. Submitted to Phys. Rev. D.

- [14] CMS Collaboration, "Measurement of differential cross sections for the production of top quark pairs and of additional jets in lepton+jets events from pp collisions at $\sqrt{s} = 13$ TeV", arXiv:1803.08856.
- [15] CMS Collaboration, "Measurement of double-differential cross sections for top quark pair production in pp collisions at $\sqrt{s} = 8$ TeV and impact on parton distribution functions", *Eur. Phys. J.* **C77** (2017), no. 7, 459, doi:10.1140/epjc/s10052-017-4984-5, arXiv:1703.01630.
- [16] S. Frixione, P. Nason, and C. Oleari, "Matching NLO QCD computations with parton shower simulations: the POWHEG method", *JHEP* **11** (2007) 070, doi:10.1088/1126-6708/2007/11/070, arXiv:0709.2092.
- [17] E. Re, "Single-top Wt-channel production matched with parton showers using the POWHEG method", *Eur. Phys. J. C* **71** (2011) 1547, doi:10.1140/epjc/s10052-011-1547-z, arXiv:1009.2450.
- [18] J. Alwall et al., "The automated computation of tree-level and next-to-leading order differential cross sections, and their matching to parton shower simulations", *JHEP* **07** (2014) 079, doi:10.1007/JHEP07(2014)079, arXiv:1405.0301.
- [19] T. Sjöstrand, S. Mrenna, and P. Z. Skands, "PYTHIA 6.4 Physics and Manual", *JHEP* **05** (2006) 026, doi:10.1088/1126-6708/2006/05/026, arXiv:hep-ph/0603175.
- [20] T. Sjöstrand et al., "An introduction to PYTHIA 8.2", *Comput. Phys. Commun.* **191** (2015) 159, doi:10.1016/j.cpc.2015.01.024, arXiv:1410.3012.
- [21] JSON file /afs/cern.ch/cms/CAF/CMSCOMM/COMM_DQM/certification/Collisions16/13TeV/ReReco/Final/Cert_271036-284044_13TeV_23Sep2016ReReco_Collisions16_JSON.txt.
- [22] CMS Collaboration, "CMS Luminosity 2016", CMS PAS LUM-17-001.
- [23] S. Alioli et al., "A general framework for implementing NLO calculations in shower Monte Carlo programs: the POWHEG BOX", *JHEP* **06** (2010) 043, doi:10.1007/JHEP06(2010)043, arXiv:1002.2581.
- [24] NNPDF Collaboration, "Unbiased global determination of parton distributions and their uncertainties at NNLO and LO", *Nucl. Phys. B* **855** (2012) 153, doi:10.1016/j.nuclphysb.2011.09.024, arXiv:1107.2652.
- [25] GEANT4 Collaboration, "GEANT4—a simulation toolkit", *Nucl. Instrum. Meth. A* **506** (2003) 250, doi:10.1016/S0168-9002(03)01368-8.
- [26] P. Artoisenet et al., "Automatic spin-entangled decays of heavy resonances in Monte Carlo simulations", *JHEP* **03** (2013) 015, doi:10.1007/JHEP03(2013)015, arXiv:1212.3460.
- [27] R. Frederix and S. Frixione, "Merging meets matching in MC@NLO", *JHEP* **12** (2012) 061, doi:10.1007/JHEP12(2012)061, arXiv:1209.6215.
- [28] M. Bahr et al., "Herwig++ Physics and Manual", *Eur. Phys. J.* **C58** (2008) 639–707, doi:10.1140/epjc/s10052-008-0798-9, arXiv:0803.0883.

- [29] S. Alioli et al., "NLO single-top production matched with shower in POWHEG: s - and t -channel contributions", *JHEP* **09** (2009) 111, doi:10.1088/1126-6708/2009/09/111, arXiv:0907.4076.
- [30] CMS Collaboration, "Underlying event tunes and double parton scattering", CMS Physics Analysis Summary CMS-PAS-GEN-14-001, CERN, 2014.
- [31] P. Skands, S. Carrazza, and J. Rojo, "Tuning PYTHIA 8.1: the Monash 2013 Tune", *Eur. Phys. J.* **C74** (2014), no. 8, 3024, doi:10.1140/epjc/s10052-014-3024-y, arXiv:1404.5630.
- [32] N. Kidonakis, "Two-loop soft anomalous dimensions for single top quark associated production with W^- or H^- ", *Phys. Rev. D* **82** (2010) 054018, doi:10.1103/PhysRevD.82.054018, arXiv:hep-ph/1005.4451.
- [33] J. M. Campbell, R. K. Ellis, and C. Williams, "Vector boson pair production at the LHC", *JHEP* **07** (2011) 018, doi:10.1007/JHEP07(2011)018, arXiv:1105.0020.
- [34] M. Cacciari et al., "Top-pair production at hadron colliders with next-to-next-to-leading logarithmic soft-gluon resummation", *Phys. Lett. B* **710** (2012) 612, arXiv:1111.5869.
- [35] P. Baernreuther et al., "Percent level precision physics at the tevatron: First genuine nnlo qcd corrections to $q\bar{q} \rightarrow t\bar{t} + x$ ", *Phys. Rev. Lett.* **109** (2012) 132001, doi:10.1103/PhysRevLett.109.132001, arXiv:1204.5201.
- [36] M. Czakon and A. Mitov, "Nnlo corrections to top-pair production at hadron colliders: the all-fermionic scattering channels", *JHEP* **12** (2012) 054, arXiv:1207.0236.
- [37] M. Czakon and A. Mitov, "Nnlo corrections to top-pair production at hadron colliders: the quark-gluon reaction", *JHEP* **01** (2013) 080, arXiv:1210.6832.
- [38] M. Beneke et al., "Hadronic top-quark pair production with nnll threshold resummation", *Nucl. Phys. B* **855** (2012) 695, doi:10.1016/j.nuclphysb.2011.10.021, arXiv:1109.1536.
- [39] M. Czakon, P. Fiedler, and A. Mitov, "Total Top-Quark Pair-Production Cross Section at Hadron Colliders Through $O(\alpha_S^4)$ ", *Phys.Rev.Lett.* **110** (2013) 252004, doi:10.1103/PhysRevLett.110.252004, arXiv:1303.6254.
- [40] M. Czakon and A. Mitov, "Top++: A Program for the Calculation of the Top-Pair Cross-Section at Hadron Colliders", *Comput.Phys.Commun.* **185** (2014) 2930, doi:10.1016/j.cpc.2014.06.021, arXiv:1112.5675.
- [41] <https://twiki.cern.ch/twiki/bin/view/CMS/TopEventSelection>.
- [42] <https://twiki.cern.ch/twiki/bin/viewauth/CMS/PileupJSONFileforData>.
- [43] CMS Collaboration, "Commissioning of the particle-flow reconstruction in minimum-bias and jet events from pp collisions at 7 tev", CMS Physics Analysis Summary CMS-PAS-PFT-10-002, CERN, 2010.
- [44] <https://twiki.cern.ch/twiki/bin/viewauth/CMS/CutBasedElectronIdentificationRun2>.

- [45] CMS Collaboration, "Determination of the jet energy scale in CMS with pp Collisions at $\sqrt{s} = 7 \text{ TeV}$ ", *CMS Physics Analysis Summary JME-10-010* (2010).
- [46] CMS collaboration, "Identification of b-quark jets with the CMS experiment", *Journal of Instrumentation* **8** (2013), no. 04, P04013.
- [47] CMS Collaboration, "Performance of b tagging at $\sqrt{s}=8 \text{ TeV}$ in multijet, ttbar and boosted topology events", Technical Report CMS-PAS-BTV-13-001, CERN, Geneva, 2013.
- [48] https://twiki.cern.ch/twiki/bin/view/CMS/BTagSFMethods#1a_Event_reweighting_using_scale.
- [49] CMS Collaboration, "CMS MET performance in events containing electroweak bosons from pp collisions at $\sqrt{s} = 7 \text{ TeV}$ ", CMS Physics Analysis Summary CMS-PAS-PFT-10-002, CERN, 2010.
- [50] <https://twiki.cern.ch/twiki/bin/viewauth/CMS/MissingETOptionalFiltersRun2>.
- [51] CMS Collaboration, "Measurement of differential cross section for top quark pair production in pp collisions at $\sqrt{s} = 8 \text{ TeV}$ ", (2015). arXiv:hep-ex/1505.04480. Submitted to EPJC.
- [52] CMS Collaboration, "Measurement of double-differential cross sections for top quark pair production in pp collisions at $\sqrt{s} = 8 \text{ TeV}$ and impact on parton distribution functions", *Eur. Phys. J.* **C77** (2017), no. 7, 459, doi:10.1140/epjc/s10052-017-4984-5, arXiv:hep-ex/1703.01630.
- [53] CMS Collaboration, "First measurement of the differential cross section for $t\bar{t}$ production in the dilepton final state at $\sqrt{s} = 13 \text{ TeV}$ ", CMS Physics Analysis Summary CMS-PAS-TOP-15-010, CERN, 2015.
- [54] I. Korol, "Measurement of Double Differential $t\bar{t}$ Production Cross Sections with the CMS Detector". PhD thesis, Universität Hamburg, 2016. DESY-THESIS-2016-011 (2016). doi:10.3204/DESY-THESIS-2016-011.
- [55] O. Behnke, I. Korol, O. Zenaiev, "Measurement of double differential cross sections for top quark pair production in pp collisions at $\sqrt(s) = 8 \text{ TeV}$ ", CMS AN-15-141.
- [56] J. Kieseler and C. Diez Pardos, "Dilepton trigger and lepton identification efficiencies for the top quark pair production cross section measurement at 8 TeV in the dilepton decay channel", CMS AN-12-389.
- [57] M. Aldaya et al., "First Measurement of the Top-Quark Pair Production Cross Section in Proton-Proton Collisions at $\sqrt(s) = 13 \text{ TeV}$ ", CMS AN-15-022.
- [58] Till Arndt, Carmen Diez Pardos, Andreas Meyer, "Measurement of the 2016 Trigger Efficiencies for a dilepton selection for a ttbar analysis", CMS AN-16-392.
- [59] "Uncertainty on the differential shapes" in BTWIKI https://twiki.cern.ch/twiki/bin/viewauth/CMS/BtagPOG#2012_Data_and_MC_EPS13_prescript.
- [60] M. Aldaya et al., "Measurement of differential top-quark pair production cross sections in the dilepton final state at $\sqrt{s} = 8 \text{ TeV}$ ", AN-13-266 (2013).

- [61] CMS Collaboration, "Determination of the Jet Energy Scale in CMS with pp collisions at $\sqrt{s} = 7 \text{ TeV}$ ", *PAS JME-10-010* (2010).
- [62] https://twiki.cern.ch/twiki/bin/view/CMS/JetResolution#JER_Scaling_factors.
- [63] CMS Collaboration, "Investigations of the impact of the parton shower tuning in Pythia 8 in the modelling of ttbar at sqrt(s)= 8 and 13 TeV", *CMS PAS TOP-16-021*.
- [64] S. Schmitt, "TUnfold: an algorithm for correcting migration effects in high energy physics", *JINST* **7** (2012) T10003, doi:10.1088/1748-0221/7/10/T10003, arXiv:1205.6201.
- [65] A. N. Tikhonov, "Solution of incorrectly formulated problems and the regularization method", *Soviet Math. Dokl.* **4** (1963) 1035.
- [66] S. Schmitt, "Data Unfolding Methods in High Energy Physics", *EPJ Web Conf.* **137** (2017) 11008, doi:10.1051/epjconf/201713711008, arXiv:1611.01927.
- [67] Particle Data Group Collaboration, "Review of Particle Physics", *Phys. Rev.* **D98** (2018), no. 3, 030001, doi:10.1103/PhysRevD.98.030001.
- [68] M. L. Mangano, P. Nason, and G. Ridolfi, "Heavy quark correlations in hadron collisions at next-to-leading order", *Nucl. Phys. B* **373** (1992) 295, doi:10.1016/0550-3213(92)90435-E.
- [69] S. Dittmaier, P. Uwer, and S. Weinzierl, "NLO QCD corrections to t anti-t + jet production at hadron colliders", *Phys. Rev. Lett.* **98** (2007) 262002, doi:10.1103/PhysRevLett.98.262002, arXiv:hep-ph/0703120.
- [70] G. Bevilacqua, M. Czakon, C. G. Papadopoulos, and M. Worek, "Dominant QCD Backgrounds in Higgs Boson Analyses at the LHC: A Study of pp -> t anti-t + 2 jets at Next-To-Leading Order", *Phys. Rev. Lett.* **104** (2010) 162002, doi:10.1103/PhysRevLett.104.162002, arXiv:1002.4009.
- [71] G. Bevilacqua, M. Czakon, C. G. Papadopoulos, and M. Worek, "Hadronic top-quark pair production in association with two jets at Next-to-Leading Order QCD", *Phys. Rev.* **D84** (2011) 114017, doi:10.1103/PhysRevD.84.114017, arXiv:1108.2851.
- [72] S. Höche et al., "Next-to-leading order QCD predictions for top-quark pair production with up to three jets", *Eur. Phys. J.* **C77** (2017), no. 3, 145, doi:10.1140/epjc/s10052-017-4715-y, arXiv:1607.06934.
- [73] M. Czakon, D. Heymes, and A. Mitov, "High-precision differential predictions for top-quark pairs at the LHC", *Phys. Rev. Lett.* **116** (2016) 082003, doi:10.1103/PhysRevLett.116.082003, arXiv:1511.00549.
- [74] M. Czakon, D. Heymes, and A. Mitov, "Dynamical scales for multi-TeV top-pair production at the LHC", *JHEP* **04** (2017) 071, doi:10.1007/JHEP04(2017)071, arXiv:1606.03350.
- [75] S. Alekhin, J. Blümlein, and S. Moch, "NLO PDFs from the ABMP16 fit", arXiv:1803.07537.

- [76] A. Accardi et al., "Constraints on large- x parton distributions from new weak boson production and deep-inelastic scattering data", *Phys. Rev. D* **93** (2016) 114017, doi:10.1103/PhysRevD.93.114017, arXiv:1602.03154.
- [77] S. Dulat et al., "New parton distribution functions from a global analysis of quantum chromodynamics", *Phys. Rev. D* **93** (2016) 033006, doi:10.1103/PhysRevD.93.033006, arXiv:1506.07443.
- [78] H1 and ZEUS Collaborations, "Combination of measurements of inclusive deep inelastic $e^\pm p$ scattering cross sections and QCD analysis of HERA data", *Eur. Phys. J. C* **75** (2015) 580, doi:10.1140/epjc/s10052-015-3710-4, arXiv:1506.06042.
- [79] P. Jimenez-Delgado and E. Reya, "Delineating parton distributions and the strong coupling", *Phys. Rev. D* **89** (2014) 074049, doi:10.1103/PhysRevD.89.074049, arXiv:1403.1852.
- [80] L. A. Harland-Lang, A. D. Martin, P. Motylinski, and R. S. Thorne, "Parton distributions in the LHC era: MMHT 2014 PDFs", *Eur. Phys. J. C* **75** (2015) 204, doi:10.1140/epjc/s10052-015-3397-6, arXiv:1412.3989.
- [81] NNPDF Collaboration, "Parton distributions from high-precision collider data", *Eur. Phys. J. C* **77** (2017), no. 10, 663, doi:10.1140/epjc/s10052-017-5199-5, arXiv:1706.00428.
- [82] A. Buckley et al., "LHAPDF6: parton density access in the LHC precision era", *Eur. Phys. J. C* **75** (2015) 132, doi:10.1140/epjc/s10052-015-3318-8, arXiv:1412.7420.
- [83] M. Cacciari et al., "Updated predictions for the total production cross sections of top and of heavier quark pairs at the Tevatron and at the LHC", *JHEP* **09** (2008) 127, doi:10.1088/1126-6708/2008/09/127, arXiv:0804.2800.
- [84] Y. Kiyo et al., "Top-quark pair production near threshold at LHC", *Eur. Phys. J. C* **60** (2009) 375–386, doi:10.1140/epjc/s10052-009-0892-7, arXiv:0812.0919.
- [85] S. Alekhin et al., "HERAFitter", *Eur. Phys. J. C* **75** (2015) 304, doi:10.1140/epjc/s10052-015-3480-z, arXiv:1410.4412. xFITTER web site, <https://www.xfitter.org>.
- [86] Y. L. Dokshitzer, "Calculation of the structure functions for deep inelastic scattering and $e+e-$ annihilation by perturbation theory in quantum chromodynamics", *Sov. Phys. JETP* **46** (1977) 641.
- [87] V. N. Gribov and L. N. Lipatov, "Deep inelastic ep scattering in perturbation theory", *Sov. J. Nucl. Phys.* **15** (1972) 438.
- [88] G. Altarelli and G. Parisi, "Asymptotic freedom in parton language", *Nucl. Phys. B* **126** (1977) 298, doi:10.1016/0550-3213(77)90384-4.
- [89] G. Curci, W. Furmanski, and R. Petronzio, "Evolution of parton densities beyond leading order: the nonsinglet case", *Nucl. Phys. B* **175** (1980) 27, doi:10.1016/0550-3213(80)90003-6.
- [90] W. Furmanski and R. Petronzio, "Singlet parton densities beyond leading order", *Phys. Lett. B* **97** (1980) 437, doi:10.1016/0370-2693(80)90636-X.

- [91] S. Moch, J. A. M. Vermaseren, and A. Vogt, “The three-loop splitting functions in QCD: the nonsinglet case”, *Nucl. Phys. B* **688** (2004) 101,
doi:10.1016/j.nuclphysb.2004.03.030, arXiv:hep-ph/0403192.
- [92] A. Vogt, S. Moch, and J. A. M. Vermaseren, “The three-loop splitting functions in QCD: the singlet case”, *Nucl. Phys. B* **691** (2004) 129,
doi:10.1016/j.nuclphysb.2004.04.024, arXiv:hep-ph/0404111.
- [93] M. Botje, “QCDNUM: Fast QCD evolution and convolution”, *Comput. Phys. Commun.* **182** (2011) 490, doi:10.1016/j.cpc.2010.10.020, arXiv:1005.1481.
- [94] R. S. Thorne and R. G. Roberts, “An ordered analysis of heavy flavor production in deep inelastic scattering”, *Phys. Rev. D* **57** (1998) 6871, doi:10.1103/PhysRevD.57.6871, arXiv:hep-ph/9709442.
- [95] R. S. Thorne, “A variable-flavor number scheme for NNLO”, *Phys. Rev. D* **73** (2006) 054019, doi:10.1103/PhysRevD.73.054019, arXiv:hep-ph/0601245.
- [96] R. S. Thorne, “Effect of changes of variable flavor number scheme on parton distribution functions and predicted cross sections”, *Phys. Rev. D* **86** (2012) 074017,
doi:10.1103/PhysRevD.86.074017, arXiv:1201.6180.
- [97] V. Bertone et al., “aMCfast: automation of fast NLO computations for PDF fits”, *JHEP* **08** (2014) 166, doi:10.1007/JHEP08(2014)166, arXiv:1406.7693.
- [98] T. Carli et al., “A posteriori inclusion of parton density functions in NLO QCD final-state calculations at hadron colliders: The APPLGRID project”, *Eur. Phys. J. C* **66** (2010) 503, doi:10.1140/epjc/s10052-010-1255-0, arXiv:0911.2985.
- [99] A. D. Martin, W. J. Stirling, R. S. Thorne, and G. Watt, “Parton distributions for the LHC”, *Eur. Phys. J. C* **63** (2009) 189, doi:10.1140/epjc/s10052-009-1072-5, arXiv:0901.0002.
- [100] CMS Collaboration, “Measurement of the muon charge asymmetry in inclusive $\text{pp} \rightarrow W + X$ production at $\sqrt{s} = 7 \text{ TeV}$ and an improved determination of light parton distribution functions”, *Phys. Rev. D* **90** (2014) 032004, doi:10.1103/PhysRevD.90.032004, arXiv:1312.6283.
- [101] H1 Collaboration, “Inclusive deep inelastic scattering at high Q^2 with longitudinally polarised lepton beams at HERA”, *JHEP* **09** (2012) 061,
doi:10.1007/JHEP09(2012)061, arXiv:1206.7007.
- [102] W. T. Giele and S. Keller, “Implications of hadron collider observables on parton distribution function uncertainties”, *Phys. Rev. D* **58** (1998) 094023,
doi:10.1103/PhysRevD.58.094023, arXiv:hep-ph/9803393.
- [103] W. T. Giele, S. A. Keller, and D. A. Kosower, “Parton distribution function uncertainties”, arXiv:hep-ph/0104052.
- [104] CMS Collaboration, “pt(top-quark) based reweighting of ttbar MC”,
<https://twiki.cern.ch/twiki/bin/view/CMS/TopPtReweighting>. [Unpublished. Online] (2018).
- [105] P. M. Stevenson, “Resolution of the Renormalization Scheme Ambiguity in Perturbative QCD”, *Phys. Lett.* **100B** (1981) 61–64, doi:10.1016/0370-2693(81)90287-2.

- 1918 [106] P. M. Stevenson, "Optimized Perturbation Theory", *Phys. Rev.* **D23** (1981) 2916,
1919 doi:10.1103/PhysRevD.23.2916.
- 1920 [107] P. M. Stevenson, "Optimization of QCD Perturbation Theory: Results for R(e+e-) at
1921 fourth order", *Nucl. Phys.* **B868** (2013) 38–64,
1922 doi:10.1016/j.nuclphysb.2012.11.005, arXiv:1210.7001.

DRAFT